REPORT CUMENTATION PAGE

AFRL-SR-AR-TR-04-

0476

Public reporting burden for this collection of information is estimated to average 1 hour per response, i... sources, gathering and maintaining the data needed, and completing and reviewing the collection of information ...ct of this collection of information, including suggestions for reducing this burden, to Washington Headquarters ... Jefferson Davis Highway, Suite 1204, Arlington, VA 22202-4302, and to the Office of Management and Budget, ...3.

1. AGENCY USE ONLY (Leave blank)	2. REPORT DATE	3. REPORT TYPE AND DA... 01 Aug 2003 - 31 Dec 2003 FINAL
4. TITLE AND SUBTITLE Plantoms Travel Grant: Trends in Nanotechnology Conference (TNTC2003)		5. FUNDING NUMBERS 61102F 2305/DX
6. AUTHOR(S) Dr Landman		
7. PERFORMING ORGANIZATION NAME(S) AND ADDRESS(ES) GEORGIA TECH RESEARCH CORP GEORGIA INSTITUTE OF TECHNOLOGY 505 TENTH STREET NW ATLANTA GA 30332-0420		8. PERFORMING ORGANIZATION REPORT NUMBER
9. SPONSORING/MONITORING AGENCY NAME(S) AND ADDRESS(ES) AFOSR/NE 4015 WILSON BLVD SUITE 713 ARLINGTON VA 22203		10. SPONSORING/MONITORING AGENCY REPORT NUMBER F49620-03-1-0411
11. SUPPLEMENTARY NOTES		
12a. DISTRIBUTION AVAILABILITY STATEMENT DISTRIBUTION STATEMENT A: Unlimited		12b. DISTRIBUTION CODE

13. ABSTRACT (Maximum 200 words)

In response to the growing awareness of the importance of nanotechnology, "Trends in Nanotechnology" (TNT) has become a key meeting in the nanoteclmology field since it brings fresh ideas on organization, first level speakers, and an environment suitable to keep discussions, ideas exchange and enhance scientific and personal relations among participants. 1NT2003 was held in large part due to the overwhelming success of earlier Nanotechnology Conferences, TNT2000, TNT200I and TNT2002. The aim of the "Trends in Nanotechnology" conference (TNT2003) was focused on the applications of Nanotechnology and to bring together in a scientific Forum various groups throughout the world working in this field. This granted supported (in part) the participation of nine US speakers at TNT2003 held during the period of 15 Sep and 19 Sep 2003 in Salamanca, Spain.

20040921 038

14. SUBJECT TERMS			15. NUMBER OF PAGES
			16. PRICE CODE
17. SECURITY CLASSIFICATION OF REPORT	18. SECURITY CLASSIFICATION OF THIS PAGE	19. SECURITY CLASSIFICATION OF ABSTRACT	20. LIMITATION OF ABSTRACT
Unclassified	Unclassified	Unclassified	UL

BEST AVAILABLE COPY

TNT 2003
Trends in Nanotechnology

Salamanca (Spain), 15-19 September 2003

BEST AVAILABLE COPY

Posters Abstracts

DISTRIBUTION STATEMENT A
Approved for Public Release
Distribution Unlimited

CMP científica

UNIVERSITY OF CAMBRIDGE

UAM
UNIVERSIDAD AUTONOMA DE MADRID

NRI

Purdue University

Georgia Tech

CSIC

Universidad de Salamanca

NIMS
Nanomaterials Laboratory

Phantoms Travel Grant: Trends in Nanotechnology Conference

Grant Number: F49620 – 03 – 1 -0411

Uzi Landman

School of Physics
Georgia Institute of Technology
Atlanta, Georgia 30332-0430

Final Report prepared for the

Air Force Office of Scientific Research

Period covered: August 1, 2003–December 31, 2003

Summary of Activities Supported by the Grant

This grant supported (in part) the participation of nine US speakers at the Trends in Nano Technology Conference (TNT 2003), held in the Period September 15 to September 19, in Salamanca, Spain. In the Program that is shown in the following the names of the US scientists that received support from this grant, and the titles of their key-note talks are highlighted (in green).

The financial support has been distributed as follows:

1. Phaedon Avouris (IBM, Yorktown Heights)	$1,250
2. Franz Himpsel (University of Wisconsin)	$ 740
3. Clifford Kubiak (UCSD)	$1,120
4. Uzi Landman (Georgia Institute of Technology)	$1,250
5. Elisa Riedo (Georgia Institute of Technology)	$1,250
6. Miguel Salmeron (Lawrence Berkeley Laboratories)	$1,250
7. Ivan Schuller (UCSD)	$1,250
8. Gary Schuster (Georgia Institute of Technology)	$1,250
9. Joseph Strocio (NIST, Maryland)	$ 520
Copying Machine /communications	$ 120
TOTAL	$10,000

The program of the TNT 2003 Conference is displayed below:

TNT 2003 Conference Programme

SCIENTIFIC PROGRAM - TNT2003				
Sunday, 14 th September 2003				
17h00-20h00	**REGISTRATION**			
20h00	**WELCOME RECEPTION** **At Faculty of Science, Faculty of Physics Building** In front of the Faculty of Chemistry Building (Conference location) Sponsored by NIMS (Japan)			
Week Schedule				
Monday, 15 th	**Tuesday, 16 th**	**Wednesday, 17 th**	**Thursday, 18 th**	**Friday, 19 th**

K: Keynote Lecture / O: Oral presentation

SCIENTIFIC PROGRAM - TNT2003	
Monday, 15 th September 2003	
08h00 - 09h00	**REGISTRATION**
09h00 -	Welcome and Introduction

09h15	·	
Chairman: Ron Reifenberger		
09h15-09h45	Masakazu Aono (Nanomaterials Laboratory-NIMS, Japan) "Control of atomic and Molecular Dynamic Processes on the Nanoscale"	K
09h45-10h15	Catherine Brechignac (Laboratoire Aime Cotton-CNRS, France) "Self-Alignment of Silver Nano-Chains from Cluster Deposition on Starined Surface"	K
10h15-10h45	Joseph A. Strocio (National Institute of Standards and Technology, USA) "Atomic Scale Measurement and Fabrication"	K
10h45-11h00	Peter M. Albrecht (University of Illinois, USA) "Atomic-scale Characterisation of Single-walled Carbon Nanotubes on H-passivated Silicon Surfaces using a UHV-STM"	O
11h00-11h30	**Coffee Break / Poster Session A - Instrument Exhibition**	
Chairman: Catherine Brechignac		
11h30-12h00	Jose Ignacio Pascual (ICMAB-CSIC, Spain) "Control of a Single-Bond Cleavage with Mode-Specific Strategies"	K
12h00-12h30	Clifford Kubiak (Dep. of Chemistry and Biochemistry-UCSD, USA) "Chemical Control of Conductance: "Doping" Molecules, CHEM- RESISTORS and CHEM-FETs"	K
12h30-12h45	Jascha Repp (IBM Zurich Research Laboratory, Switzerland) "LTSTM Investigations on Ultrathin Insulating Films: NACL/CU Interface States and Adsorption of Metal Atoms"	O
12h45-13h00	Thomas A. Jung (Paul Scherrer Institute, Switzerland) "Self Intermixed Monolayer Phases: Fullerenes Self-intermixed with Phthalocyanines"	O
13h00-13h15	Roberto Otero (University of Aarhus, iNANO, Denmark) "Controlling the diffusion of large organic molecules by means of STM manipulation"	O
13h15-13h30	Walter Arnold (University of Saarbrücken - FhG-IZFP, Germany) "Quantitative Measurement of Elastic Constants of Anisotropic Materials by Atomic Force Acoustic Microscopy"	O
13h30-15h15	**Lunch**	
Chairman: Joseph A. Strocio		
15h15-15h45	Denis Koltsov (University of Cambridge / Nanoscience, UK) "Nanometre and Nanosecond Properties of Ferromagnets"	K
15h45-16h15	David Walton (University of Sussex, UK) "Nanoscience Research at Sussex"	K
Chairman: Masakazu Aono		
16h15-16h45	Uzi Landman (Georgia Tech School of Physics, USA) "Emergent Materials in the Non- Scalable Size Regime"	K

16h45-17h15	Kazuhiko Matsumoto (Osaka University, Japan) "Defective Carbon Nanotube Channel Single Electron Transistor with Ultra-High Coulomb Energy of 5000 K"	K
17h15-17h45	Phaedon Avouris (IBM Research Division, USA) "Carbon Nanotube Electronics and Opto-Electronics"	K
17h45-20h30	**Poster Session A / Refreshments**	**PS**

SCIENTIFIC PROGRAM - TNT2003		
Tuesday, 16 th September 2003		
Chairman: Flemming Besenbacher		
08h45-09h15	Ivan Schuller (University of California, USA) "25 Years of Metallic Superlattices"	K
09h15-09h45	Ron Reifenberger (Purdue University, USA) "Measuring Molecular Conductance: A Review of Experimental Approaches"	K
09h45-10h00	Toyo Kazu Yamada (NSRIM University of Nijmegen, Netherlands) "Observation of Spin-polarised Surface States on Ultra-thin bct Mn(001) Films by Spin-polarised Scanning Tunneling Spectroscopy"	O
10h00-10h15	Jaume Veciana (Instituto de Ciencia de Materiales de Barcelona, CSIC, Spain) "Deposition and Nanopatterning of Mn12 Single-Molecule Magnets on Surfaces with Size and Positional Control at Multiple Length Scales"	O
10h15-11h15	**Coffee Break - Poster Session A - Instrument Exhibition**	
Chairman: Rodolfo Miranda		
11h15-11h45	Dieter Kern (Tuebingen University, Germany) "Materials Issues in Nanolithography"	K
11h45-12h15	Urs Duerig (IBM Zurich Research Laboratory, Switzerland) "'Millipede' - Integrating Nanotechnology into a Working Storage devices"	K
12h15-12h45	Satoshi Kawata (Osaka University, Japan) "Near Field Raman Microscopy for Nanostructure Imaging and Analysis"	K
12h45-13h15	Giyuu Kido (Nanomaterials Laboratory-NIMS, Japan) "Fabrication of nano-Films for Solid-States Quantum Computer"	K
13h15-13h30	Enrique Calleja (UPM, Spain) "Self-Organized AlgaN/GaN Nanostructures Grown by MBE"	O
13h30-15h15	**Lunch**	
Chairman: Angel Rubio		

15h15-15h45	Miquel Salmeron (Lawrence Berkeley National Laboratory, USA) "The Ensemble Effect in Chemisorption and Catalysis"	K
15h45-16h15	Flemming Besenbacher (Aarhus University, Denmark) "Diffusion Adatoms and Vacancies on metal and Oxide Surfaces Revealed by High-Resolution, Fast-Scanning STM"	K
16h15-16h45	Paulo Freitas (INESC, Portugal)	K
16h45-17h00	Danny Porath (The Hebrew University, Israel) "Novel DNA-based Molecular Nanowires"	O
17h00-18h00	**Coffee Break - Poster Session A - Instrument Exhibition**	
Chairman: Juan Jose Saenz		
18h00-18h15	Patrick Van-Hove (European Commission / IST-FET, Belgium) "Nanotechnology Information Devices Proactive Initiative in FP6"	O
18h15-18h30	Jason J. Davis (University of Oxford, UK) "Metalloprotein Biomolecular Electronics"	O
18h30-19h00	Martin Hegner (NCCR Nanoscale Science, University of Basel, Switzerland) "Multifunctional Cantilever Arrays for Label-Free Detection"	K
19h00-19h30	Rodolfo Miranda (Universidad Autonoma de Madrid, Spain) "Observing the electronic states of Room-Temperature-stable Metallic nanostructrured"	K
21h00	**GUIDED TOUR OF SALAMANCA**	

SCIENTIFIC PROGRAM - TNT2003		
Wednesday, 17 th September 2003		
Chairman: Erio Tosatti		
08h30-09h00	Angel Rubio (DIPC, Spain) "Optical, Infrared and STM Spectroscopies of Carbon and BN Nanotubes"	K
09h00-09h30	Inder P. Batra (University of Illinois at Chicago, USA) "Electronic Properties of Free and Supported Nanowires"	K
09h30-10h00	Tord Claeson (Chalmers University of Technology, Sweden) "Transport and charging of single molecules between 2 nm spaced electrodes: influence of distinctly different charged states of the conjugate molecule and of the image charge in the electrodes"	K
10h00-10h15	Daniel Sanchez-Portal (DIPC, Spain) "First-principles Calculations of Charge Transfer Rates from Photoexcited Adsorbates into Metal Substrates"	O
10h15-10h30	Juan Jose Palacios (University of Alicante, Spain) "Electronic Transport and vibrational modes in the smallest molecular bridge: H2 in Pt nanocontacs"	O

10h30-11h00	**Coffee Break - Instrument Exhibition**	
	Chairman: Uzi Landman	
11h00-11h30	Jose-Luis Martins (INESC MN, Portugal) "Mesoscopic simulation of magnetic thin films"	**K**
11h30-12h00	Erio Tosatti (SISSA-ISAS, Italy) "Magnetic Phenomena in Monatomic Transition Metal Nanowires"	**K**
12h00-12h30	Jean-Jacques Greffet (Ecole Centrale Paris – CNRS, France) "Coherent Emission of Thermal Light by Microstructures"	**K**
12h30-12h45	Xavier Oriols (Universidad Autonoma de Barcelona, Spain) "Non-universal Conductance Quantisation for Long Quantum Wires: the Role of the Exchange Interaction"	**O**
12h45-13h00	**TNT2003 CONFERENCE GROUP PHOTOGRAPH**	
13h00-14h45	**Lunch**	
	Chairman: Tord Claeson	
14h45-15h15	Christian Joachim (CEMES-CNRS, France) "An Intramolecular Quantum Hamiltonian Logic Gate"	**K**
15h15-15h30	Paolo Visconti (University of Lecce, Italy) "Fabrication of Nanodevices with sub 10 nm Scale for Transport Experiments on Molecules"	**O**
15h30-15h45	Andrea Camposeo (University of Pisa, Italy) "Fabrication of Ordered Nanosized Structures by Laser Manipulated Neutral Atoms"	**O**
15h45-16h00	Yann Kervennic (Delft University of Technology, Netherlands) "Contacting and Measuring Small Conjugated Organic Molecules"	**O**
16h00-16h15	Robert Stadler (CEMES-CNRS, France) "Integrating Logic Functions Inside a Single Molecule"	**O**
16h15-16h30	Chris Mills (Barcelona Science Park, Spain) "Nanofabrication with Polymers for Biomedical Applications"	**O**
16h30-16h45	Patrick Carlberg (Lund University, Sweden) "Structure for Life Applications Fabricated by Nanoimprint Lithography"	**O**
16h45 -17h15	Ramon Compaño (European Commission) "Open Questions to Nanotechnology"	**K**
17h15-18h45	**Coffee Break - Poster Session B - Instrument Exhibition**	
19h30	**RECEPTION AT "PATIO DE ESCUELAS"**	

	SCIENTIFIC PROGRAM - TNT2003	
	Thursday, 18 th September 2003	
	Chairman: Clivia Sotomayor Torres	
08h30-08h45	Michael Forshaw (University College London, UK) "A Review of Nanoarchitecture"	**O**
	Jouni Ahopelto (VTT Centre for Microelectronics, Finland)	

TNT 2003
Trends in Nanotechnology

ABSTRACTS

Posters - Session A

Poster

EFFECTIVE ELECTRON MICROREFRIGERATION BY SIN TUNNEL JUNCTIONS WITH ADVANCED GEOMETRY OF ELECTRODES

Ian Jasper Agulo[1], Leonid Kuzmin[2], Michael Fominsky[3] and Michael Tarasov[4]
Department of Microtechnology and Nanoscience, Quantum Device Physics Laboratory
Chalmers University of Technology, SE-412 96 Göteborg, Sweden
E-mail: [1]agulo@fy.chalmers.se, [2]kuzmin@fy.chalmers.se, [3]fominsky@fy.chalmers.se, [4]tarasov@fy.chalmers.se

We demonstrate effective electron cooling of normal strip by superconductor-insulator-normal metal (SIN) tunnel junctions. This was achieved by two methods: first, by using an advanced geometry of the superconducting electrode; and, second, by adding a normal metal metal trap near the cooling junctions. With simple cross geometry and no metal traps, the decrease in electron temperature is 56 mK. With the improvement of the geometry of superconducting electrodes, the decrease in electron temperature is 129 mK. With the addition of normal metal traps, the electron temperature decreased by 197 mK. This is the best electron cooling ever achieved (Fig.1).

We attribute this effective electron cooling to the reduction of the number of quasiparticles in the superconducting electrode. At voltages slightly below the superconducting gap, hot electrons in the normal metal tunnel through the barrier and appear as quasiparticles in the superconducting electrode. In order to achieve effective electron cooling by SIN tunnel junctions, quasiparticle density in the superconductor must be reduced. To do this, previous articles [1,2] have suggested increasing electrode thickness and adding normal metal traps. Both methods of electrode enhancement facilitate the removal of quasiparticles from the electrode (Fig.2).

Figure 3 shows an atomic force microscopy image of our device. There are four junctions. The outer pair of junctions is used for cooling junctions, while the inner pair for temperature sensing. The edges of the cooling junctions are equidistant to the edge of the gold traps separated by a distance of about 750 nm. They are electrically connected through the superconducting electrode.

Figure 4 shows the schematic diagram of the bolometer structure both with advanced geometry, one with (b) and the other without (b) normal metal traps. In both diagrams, the geometry of the aluminum electrodes around the cooling junctions gives more space for quasiparticle diffusion from the tunnel junctions than those at the middle junctions. This decreases the probability of quasiparticles accumulating at the junction region. Adding a normal metal trap, as shown in figure 2b, leads to more effective cooling since it removes and traps quasiparticles.

Our results were compared to theoretical calculations developed by Golubev and Kuzmin [3]. Comparison reveals good coincidence between experimental results and theory as bias is increased. At temperatures of about 300-400 mK, the cooling of normal metal electrons is the dominant process. Going down to 20 mK, the effect of heating due to bias current and quasiparticle back absorption effects begins to be evident.

Comparison of experimental results to theory also shows some discrepancy. At temperatures greater than 150 mK, our experiments show even better cooling than theory predicts. In the theory, only the heat flow from the electron subsystem to the phonon one in the normal metal is analyzed, since the Kapitza resistance is negligible compared to the electron-phonon thermal resistance in the normal metal. However, if the normal electrode is thermally isolated, such as probably in our case where we use SiO_2 as substrate, refrigeration of the lattice

becomes possible. The decoupling between the two phonon subsystems should therefore be also considered in the theory. This revision, which includes this particular decoupling for better fitting with experimental data, is in progress.

References:

[1] J. P. Pekola, D. V. Anghel, T. I. Suppula, J. K. Suoknuuti, A. J. Manninen, Appl. Phys. Lett., **76** (2000) 2782.

[2] J. N. Ullom, P. A. Fisher, M. Nahum, Physical Review B, **61** (2000) 14839.

[3] D. Golubev, L. Kuzmin, J. of Appl. Phys., **89** (2001) 6464.

Figures:

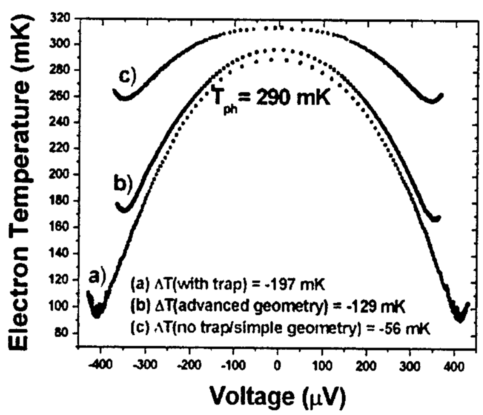

FIGURE 1. The dependence of electron temperature on voltage for different superconducting electrode configurations. The best electron cooling was observed for the electrode with normal metal trap, displaying a temperature drop of 197 mK.

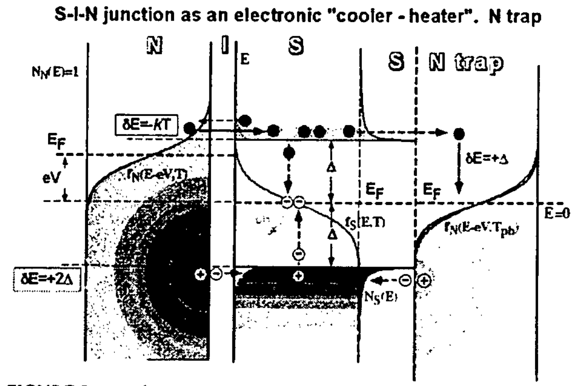

FIGURE 2. At voltage near the superconducting gap voltage, hot electrons tunnel through the barrier and appear as quasiparticles in the superconductor. These quasiparticles may back tunnel or combine with other quasiparticles to form Cooper pairs emitting a phonon in the process, which can also proceed back to the normal metal. Both processes contribute to the heating of the absorber. To remove quasiparticles, a normal metal trap is added near the tunnel junction to minimize the probability of quasiparticle back tunneling and recombination.

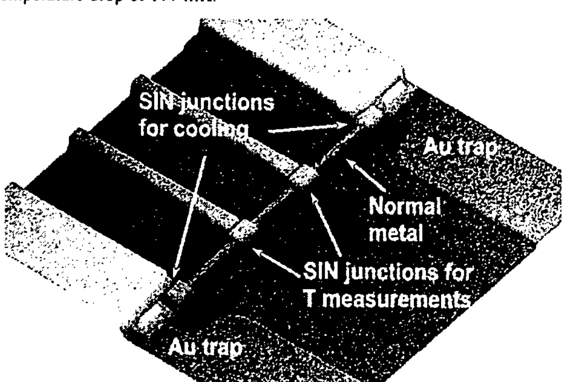

FIGURE 3. AFM picture of the tunnel junctions with the normal metal trap. The two outer tunnel junctions are the cooling junctions, while the two inner junctions were used for temperature measurements. Gold was used as the normal metal trap. It has a rounded edge around the cooling junctions in order to achieve uniform junction-to-trap distances. Aluminum was used as the superconducting electrode. It was evaporated on gold with a thickness of about 65 nm, followed by oxidization to form the tunnel barrier. A bi-layer of chromium/copper was subsequently evaporated to form the normal metal, with a thickness of about 70 nm. The junctions were fabricated using shadow evaporation technique.

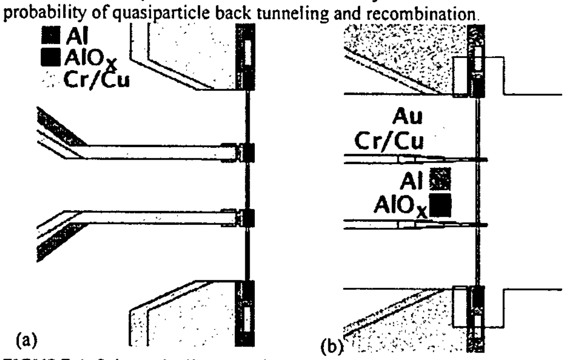

FIGURE 4. Schematic diagram of our device showing advanced geometry of outer junctions (a) without and (b) with normal metal traps. The grainy areas in (b) indicate metal regions with gold underneath it.

MAGNETO-OPTICS AND MAGNETIC INTERACTIONS IN CO NANOSTRUCTURE ARRAYS

R. Alvarez-Sánchez , J.L. Costa-Krämer, P. García-Mochales, A. Bengoechea, F. Torres, and F. Briones

Instituto de Microelectrónica de Madrid, IMM (CNM-CSIC)
Isaac Newton 8, PTM, 28760 Tres Cantos, Spain

Proximity effects between micron and sub-micron size magnetic elements in a planar array determine the integration limits of magnetic memories and nano-patterned recording media. Magneto-optic techniques and, in particular Diffraction Magneto-Optic Kerr Effect (DMOKE), are most suited to experimentally investigate such effects as showing the high sensitivity needed to monitor the magnetization changes of thin films and very small elements. We have previously shown also that DMOKE supplies valuable information also on the magnetization distribution ([i]) and anisotropy ([ii]). On the other hand, micro-magnetic modelling is not only highly valuable interpreting and calculating magnetic interactions, but permits also to set the basis for an extended model in which electromagnetic fields interact with the array. In this way, DMOKE effects can be modelled and interpreted.

In this work the magnetic properties of arrays of micro-squares of polycrystalline Co are studied, as a first step on the way of analysing sub-micron magnetic elements. The square arrays are fabricated by e-beam lithography and Co triode sputtering on glass substrates, and the magnetic response of the arrays is measured by magneto optics (MO) focussing a He-Ne laser within the array (**fig. 1**). The MO response is measured at both reflected and diffracted beams. This magnetic response is measured exciting the array with uniaxial magnetic fields. These reflected and diffracted beams MO dependencies are analysed in detail for Co arrays with elements of the same size and different inter element separation in the same range. This allows to discern the relative relevance of the magnetic interaction between adjacent tiles, and the effect it has on the measured MO dependencies. The experimental results are correlated with micromagnetic simulations, that are also used to calculate the expected MO dependencies at the different diffracted beams.

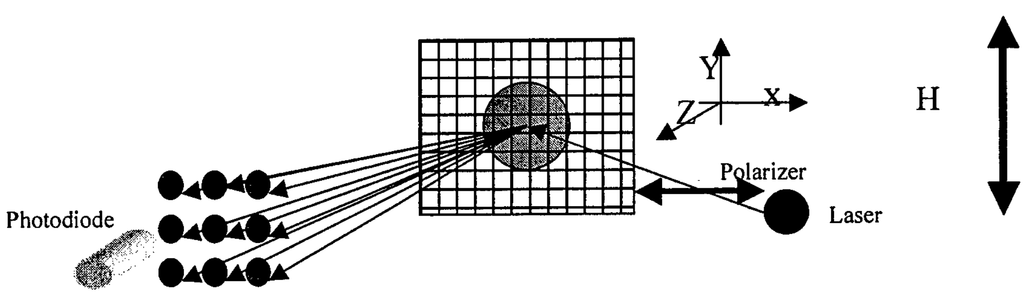

Fig. 1: Magneto-optic setup for tile arrays measurements.

Arrays of 2 μm tiles with the uniaxial Co anisotropy easy axis parallel to one of the square edges at 2.0, 1.0, 0.5 and 0.2 μm separation are studied. **Fig. 2** shows the hysteresis loops for tiles separated 2 μm, 0.2 μm and for the continuous film. As the distance between tiles decreases, the hysteresis loop trends to the continuous film one as expected.

In addition, the evolution of the diffracted beams MO dependencies (diffracted X -in the polarization plane- and diffracted Y -perpendicular to the polarization plane-, see **fig. 1**) is also studied with the magnetic field applied along both Co hard and easy axes, correlating these measurements with micromagnetic simulations. As an example, in **fig. 3** a comparison is carried out between the experimental loops and micromagnetic simulations in the particular case of 0.2 μm separation between tiles with H parallel to the Co easy axis.

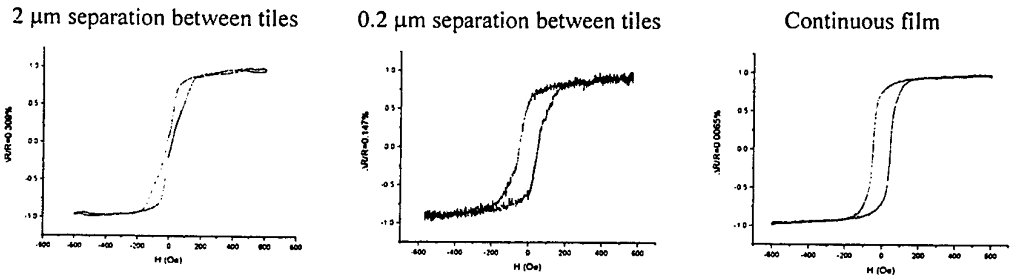

Fig. 2: Hysteresis loops for arrays of 2 μm separated 2 μm, 0.2 μm and the continuous film with H parallel to the Co uniaxial anisotropy hard axis.

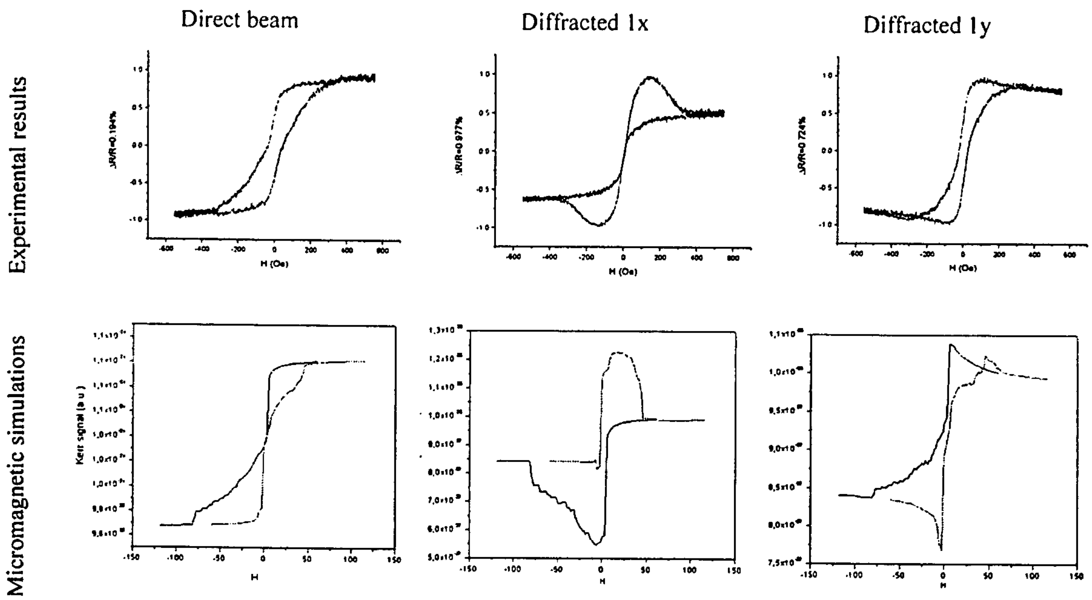

Fig. 3: Comparison between experiments and simulations for arrays of 2μm tiles separated 0.2μm with H parallel to Co easy axis

References:

[1] P. García-Mochales, J.L. Costa-Krämer, G. Armelles J.I. Martín , F. Briones, D. Jaque y J.L. Vicent, *App. Phys. Lett.* **81** (2002) 3206

[2] D. Jaque, J.I. Martín, G. Armelles, J.L. Costa-Krämer, F. Briones, J.L. Vicent, *J. of Appl. Phys.* **91** (2002)

NEAR-FIELD OPTICAL MICROSCOPY OF POLYMER-BASED FILMS WITH DISPERSED TERTHIOPHENE CHROMOPHORES FOR POLARIZER APPLICATIONS

A. Ambrosio, M. Alderighi, M.Labardi, L.Pardi, F.Fuso, M. Allegrini
INFM, Dipartimento di Fisica "E. Fermi", Università di Pisa, Via F. Buonarroti 2, I-56127 Pisa, Italy
S. Nannizzi, A. Pucci, G. Ruggeri
Dipartimento di Chimica e Chimica Industriale, Università di Pisa, Via Risorgimento 35, I-56126 Pisa, Italy
e-mail: ambrosio@df.unipi.it ;
http://www.df.unipi.it/gruppi/struttura/ma/page.htm

The recent developments of near-field scanning optical microscopy (NSOM) open the way to investigate the optical properties of samples with a space resolution well below the diffraction limit. Such capabilities make NSOM a unique tool for the assessment of sample performance in the sub-micron range while providing valuable information for a deep understanding of the physical processes involved at the local scale. In particular, by combining NSOM with techniques aimed at controlling the polarization state of the light coupled to the near-field probe, optical activity can be successfully investigated provided that suitable tapered optical fibers are used as probes [1].

We have studied optical activity of polymer-based films with potential applications in a variety of fields, ranging from high-tech packaging to liquid crystal colour display fabrication [2]. The films are produced starting from a toluene solution of a terthiophene derivative chromophore (3% wt) and a high-density polyethylene, the ultra high molecular weight polyethylene (UHMWPE). A casting process with solvent evaporation is used to obtain a bulk sample, followed by drawing to fabricate films with polymer chains aligned along the drawing direction; the dispersed chromophore molecules turn out to align along the same direction, with a larger concentration close to the upper surface of the cast. So-produced films turn out to exhibit remarkable optical activity due to their dichroic behavior.

We have analyzed bulk samples and films produced with different drawing ratios. Furthermore, since the chromophore can be synthesized in both right- and left-handed isomers, we have explored the associated effects by investigating samples containing only right-handed isomers, and samples with the same concentration of the two isomers. Studies have been carried out by using radiation from an Ar^+ laser operated at 488 nm, a wavelength weakly absorbed by the chromophore. NSOM fluorescence measurements have been carried out by exciting the samples with the violet radiation (417 nm) from an external-cavity coupled diode laser.

Our set-up is based on a home made NSOM. Polarization control is achieved by sending the Ar^+ laser beam through a chain consisting of a linear polarizer, an electro-optic modulator (EOM) and a quarter-waveplate. The linear polarizer fixes a vertical polarization for the light, selected at 45 degrees with respect to the EOM axis. The EOM behaves like a waveplate providing an electrically variable phase delay between the two components of the incoming beam. We obtain a phase delay varying from 0 to 2π by biasing the EOM crystal with a periodic saw-tooth voltage (typical frequency 3-5 kHz). In these conditions, the laser beam emerging from EOM exhibits time-depending elliptical polarizations. Further passage through the quarter-waveplate produces a linear polarization rotating with the same period of the bias modulation. The laser beam is then coupled into the NSOM optical fiber to illuminate the polymer film in the near-field through the aperture of the metallized tip (nominal diameter 50 nm). An electronic feedback circuit, fed by a photodiode collecting a portion of the laser beam is used to stabilize the laser power within the bandwidth of interest.

The radiation transmitted by the sample, spectrally selected by an interference filter at 488 nm, is collected in the far-field by a lens and sent to a miniaturized photomultiplier (PMT) housed within the NSOM piezo-scanner tube. The photocurrent, after amplification and conversion into a voltage signal, is analyzed by a dual lock-in amplifier, synchronous with the EOM bias modulation. We recorded the demodulated amplitude (*ac*) and phase (ϕ) signals from the lock-in while the NSOM tip scanned the sample surface. We also sent part of the PMT signal to a low-pass filter, in order to acquire a signal (*dc*) representative of the transmitted intensity averaged over all the different polarization states. During each scan we also acquired topographical images of the surface by the shear force method.

In data analysis, we have accounted for the residual optical activity of the NSOM fiber according to the method presented in [3]. Namely, we have produced maps of the local dichroic ratio $\gamma = (I_{\parallel}-I_{\perp})/(I_{\parallel}+I_{\perp})$, $I_{\parallel}$ and $I_{\perp}$ being the intensity of the transmitted field with polarization parallel and orthogonal to a reference axis,

respectively, and maps of the angle θ of the radiation collected by the PMT with respect to a reference axis, by using the following relations:

$$\gamma = \sqrt{\left(\left(\frac{ac}{dc}\right)\cos 2\phi - \left(\frac{ac}{dc}\right)_{fiber}\right)^2 + \left(\left(\frac{ac}{dc}\right)\sin 2\phi\right)^2} \tag{1}$$

$$2\theta = \arctan\left(\frac{\left(\frac{ac}{dc}\right)\sin 2\phi}{\left(\frac{ac}{dc}\right)\cos 2\phi - \left(\frac{ac}{dc}\right)_{fiber}}\right) \tag{2}$$

where the subscript *fiber* refers to measurements carried out on a non-dichroic sample (a glass slide). We note, that the method we have applied is not suitable to truly distinguish between dichroism and birefringence. A more detailed analysis is the subject of further work.

An example of our results is shown in Fig. 1, where a comparison between the θ maps acquired in a pristine film, i.e., non stretched (a), and in a film produced with a drawing ratio of 30 (b) is presented (in both cases, an equal concentration of the two chromophore isomers is used). θ-values are almost randomly spread in the non-stretched sample with sub-wavelength-sized features, whereas in the stretched films regions are clearly discerned characterized by almost constant θ-values. Such regions, which exhibit different topographic features (even if the overall roughness is typically small, in the tens of nm range), are aligned along the drawing direction. Further comparison with the *dc* and the fluorescence maps suggest an inhomogeneous local dispersion and orientation of the chromophore molecules, strongly affected by the drawing parameters. Furthermore, comparative analysis of the results obtained in samples with different isomer concentrations reveals that the macroscopic behavior of the films (larger optical activity for samples with equal concentration) can be interpreted on the mesoscopic scale by considering the specific aggregation processes of the chromophore in the stretched matrix.

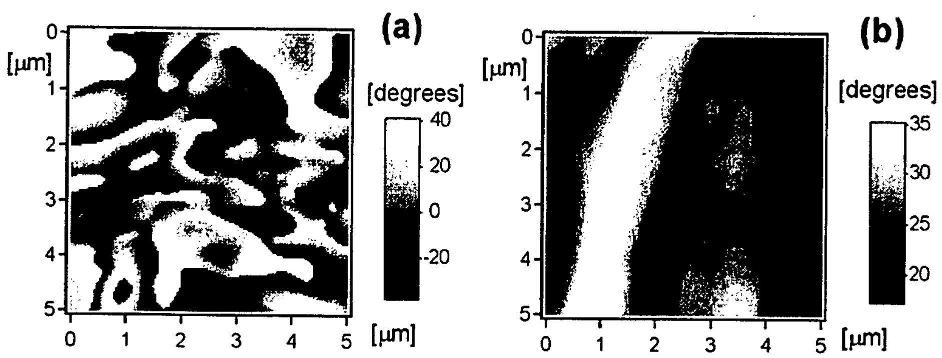

Fig. 1: Maps of θ values obtained during a 5μm x 5μm scan on a non-streched film (a) and in a film stretched with a drawing ratio of 30 (b); islands with randomly spread θ values are observed in (a), whereas a mesoscopic-scale ordering along the drawing direction is evident in (b).

[1] L. Ramoino, M. Labardi, N. Maghelli, L. Pardi, M. Allegrini, and S. Patanè, Rev. Sci. Instrum. **73**, 2051 (2002).

[2] N. Tirelli, S. Amabile, C. Cellai, A. Pucci, L. Regoli, G. Ruggeri, and F. Ciardelli., Macromolecules **34**, 2129 (2001).

[3] P.-K. Wei, Y.-F. Lin, W. Fann, Y.-Z. Lee, and S.-An Chen, Phys. Rev. B **63** 045417 (2001).

EFFECT OF THE ANCHORING GROUP ON SELF-ASSEMBLED MONOLAYERS PROPERTIES

D. Auguste[1], T. Koulminskaia[1], F. Laffineur[1], L. Hevezi[2], J. Delhalle[1], Z. Mekhalif[1]

FUNDP, départ. de Chimie, [1]LISE and [2]CMO, 61 rue de Bruxelles, 5000 Namur, Belgium

Self-assembled monolayers (SAMs) are considered as thin organic films constituted generally of long alkyl chain molecules which posses a particular functional end-group that has specific interaction with the surface. Depending on the surface state and its reactivity of the metal, thiol, silanes, phosphonic and carboxylic acids are the most studied terminal groups. Such molecules have been self-assembled on gold, copper, aluminium, titanium, glass, ... The interest of using such nanostructures is the great variety of properties conferred to the surface. SAMs are in fact used from model of biological membranes or for wettability studies to lubrication or corrosion inhibition applications.

SAMs of alkylsenenolate have been investigated as alternative adsorbates to alkylthiols on gold surfaces [1, 2]. Well organised monolayers have been obtained and a formation mechanism has been proposed [3]. Comparison between monolayer formation of small aromatic disulfide and diselenide molecules has been done on gold [2, 4] and cleavage of S-S and Se-Se bounds allow the formation of stable monolayers with a better organisation observed in the case of disulfide. Selenolates exhibits a greater ability to adsorption than thiolates but are less stable to air oxidation. Selenium derivatives show nevertheless interesting properties for molecular electronics by providing a better metal-molecule electronic coupling than sulfur derivatives [5].

Most papers concern self-assembling of diaromatic diselenide on gold. From our knowledge, very few adsorption of organoselenol on gold were performed [1, 3] and none on other substrates (such as copper or silver). In this work, four types of groups are compared : thiol, disulfide, selenol and diselenide with a partially perfluorinated alkyl chain structure (CF_3-$(CF_2)_3$-$(CH_2)_{11}$-X). The monolayers have been self-assembled on gold and copper. The effect of the metal (nature and oxidation state) on the anchoring group reactivity and the monolayer structure was especially studied . The surface composition, the structure and the organisation as well as the protecting properties of the monolayers have been determined by a multi-technique approach (XPS, PM-IRRAS, EIS, CV, ...).

References

[1] M.G. Samant, C.A. Brown, J.G. Gordon, Langmuir 8 (1992) 1615

[2] F.K. Huang, R.C. Horton, Jr. D.C. Myles, R.L. Garrell, Langmuir 14 (1998) 4802

[3] L.V. Protsailo, W.R. Fawcett, Langmuir 18 (2002) 9342

[4] K. Bandyopadhyay, K. Vijayamohanan, Langmuir 15 (1999) 5314

[5] L. Patrone, S. Palacin, J.P. Bourgoin, Appl. Surf. Sci. (2003) in press

CHEMICAL OPTIMIZATION OF CARBON NANOTUBES TRANSISTORS

S. Auvray, E. Valentin, M. Goffman, S. Palacin, A. Filoramo, V. Derycke and J.P Bourgoin

Laboratoire CEA-MOTOROLA d'Electronique Moléculaire
CEA/DSM/DRECAM/SCM
CEA Saclay 91191 GIF/YVETTE CEDEX
France

Individual semiconducting single-wall carbon nanotubes (SWNTs) can be used as the channel in field effect transistors (FETs). Recent progresses have brought these transistors to a level of performance comparable with state of the art silicon MOSFETs [1,2] . But these advanced devices are not fully optimized. In particular, it was recently recognized that most carbon nanotube transistors work as Schottky barrier transistors. Their performances are limited by the Schottky barriers at the metal-nanotube interfaces. Reducing the barriers by forming ohmic contacts would lead to improved device characteristics in both the on- and the off-states. In parallel to the device optimization issue, the capability to produce large numbers of operational devices is critical for the potential use of nanotube transistors in a future technology.

To address these two issues, we have developed efficient techniques based on chemical modifications of the surface, the nanotube and the metal electrodes. In a first step, we use self-assembly to control the systematic and reproducible placement of SWNTs on selective areas of SiO_2 surfaces [3,4]. Reactive templates of aminopropyltriethoxysilane (APTES) enable the controlled deposition of SWNTs with tunable density and preferential orientation. This chemical modification of the surface is compatible with the production of high quality FETs.

In a second step, we perform a chemical optimisation of the operational p or n-type transistors using either acid or amine vapors.
The acid vapors have a twofold effect: (i) reducing the Schottky barriers at the metal-nanotube interfaces favoring holes injection and (ii) doping the nanotube with holes. That leads to the drastic improvement of all the key device parameters. The maximum hole current in the on-state, the transconductance and the sub-threshold slope can be improved in a continuous fashion by adjusting the acid vapor dose. These effects are mainly due to the highly polar nature of the acid molecule used.
In the case of the amine vapors, we also observed a very significant improvement of the devices performances, this time for what the p-type behavior. Noticeably, the threshold of detection of the effect of the vapors is shown to be in the ppb range.

References:

[1] Javey and al , Nature Material , 1 (2002) 241-246
[2] Wind and al , Applied Physics Letters , 80 (2002) 3817
[3] Choi and al., Surface Science, 462 (2000) 195.
[4] Valentin and al , Microelectronic Engineering , 61-62 (2002) 491-496

THIN FILMS MULTILAYER FOR GIANT MAGNETORESISTIVE SENSOR APPLICATIONS

Marioara Avram
National Institute for Research and Development in Microtechnologies (IMT), P.O.Box 38-160, Bucharest, Romania, fax: 40.21.4908238, tel.: 40.21.4908412/33,
e-mail: marioaraa@imt.ro

The GMR properties are controlled by the materials composition, geometry selected, and the structure of interfaces of the films. A series of experiments involving RF diode sputter deposition of GMR multilayers was presented. The process conditions used to deposit GMR multilayers have been systematically varied and the dependence of magnetotransport properties upon the process environment has been studied. Another systematic series of experiments have been conducted to evaluate the dependence of magnetotransport properties upon composition and morphology of a multilayer structure utilized for magnetic sensing.

Experimental

Three-inch diameter p-type silicon wafers were used for the substrates. A porous silicon film was grown on top of each wafer using an electrolytic method. The porous silicon (PS) film acted as an electrically insulating and diffusion-inhibiting layer between the silicon wafer and the subsequently deposited metal film. The PS layer is a buffer, to give a good surface to grow on. The GMR active region will be only about 100Å thick, with the whole structure being about 300Å, on top of a 0.5 mm thick Si wafer. The test devices were carried out on PS of two porosities (50% and 70%) and two types of contact magnetic metals: Ni and Permalloy. FM / PS interface is influenced by the extraction work and diffusion of the metal in PS. FM / PS / Si-p /Al structure is like a Schottky diode with an I-V redresser characteristics and different values for the resistor R_s. Electrical characteristics of the MIS test structure were performed through I-V measurements (forward and reverse at room temperature) using a Keithley interfaced with a computer. In the case of forward bias the structure is composed by two diodes, one of them forward biased and other one reverse: one diode with heterojunction at the interface PS / Si –p, where the PS band gap is Eg = 1.65 eV and the Si band gap is Eg = 1.1 eV and the other one is a Schottky diode at the FM / PS interface.
The redresser characteristics of the PS/Si-p interface are given by the equation:

$$I = I_0 \exp\frac{q(V - IR_s)}{nkT} \tag{1}$$

where: $$I_0 = SA^* T^2 \exp\frac{qF_b}{kT} \tag{2}$$

V is the diode potential, n is the ideallity factor, A* the Richardson constant that depends on the crystallographic orientation and the type of the semiconductor. The contact resistivity, R_s has a reduce effect compared to the height of the potential barrier F_b, at the FM/PS contact and the carrier concentration. S is the PS surface (~800 m^2/cm^3 for P = 50% and ~300 m^2/cm^3 for P = 70%). At high porosity the dissolution of the thin fibres rises, the pores enlarge and the surface grow. Current density, J_0, ideallity factor, n, and the height of the potential barrier, F_b, are determined from the forward I – V characteristics of the metal / PS contact. The n values are connected to the to (V< 0.1V) existing in the SiO_2 layer to the PS surface. The low values of n low levels of injection are due to a low interface density of states and a good stability of the PS layer. The values of the ideallity factor, n, to high levels of injection are due to: contact resistance of the ferromagnetic metal on porous silicon and the tunnelling of the carrier to the FE/PS interface. In our experiment, all the structures using Fe as a ferromagnet shows a great dispersion of I –V characteristics, while in the case of Ni or Permalloy the I–V characteristics are grouped. The electrical measurements bring in front a high contact resistance because the FM/PS interface is a crowd of contact dots that lead to local injections of carriers and to the focus of the electric field. The table 1 shows the experimental results of the electrical measurements of the MIS test structure in the absence of the magnetic field.

Table 1. The results of electrical measurements

Contact metal	Porosity (%)	I_o (A)	φ_B (eV)	n	Inflection point
Ni	*70*	*1E^-16*	*1,43*	*0,6*	*0,1 V*
	50	*5E^-14*	*1,27*	*0,74*	*0,45 V*
Permalloy	*70*	*1E^-12*	*1,19*	*1,5*	*0,25 V*
	50	*1E^-11*	*1,2*	*1,2*	*0,2 V*
Fe	*70*	*1E^-14*	*1,31*	*0,9*	*0,35 V*
	50	*1E^-11*	*1,1*	*1,6*	*0,45-0,5 V*

The type of the deposition process used and the architecture of the multilayer selected control the GMR properties in the first time [5]. Background pressure is one of the most important parameters to establish in a sputtering system. In a series of experiments, the input power was held constant at 200 W and the background pressure was varied from 10 mTorr (1.33 Pa) (the lowest achievable without losing the discharge) to 50 mTorr (6.65 Pa). For a second series of experiments, the background pressure was held constant at 20 mTorr and the input power was varied from 50 to 350 W.

Figure 1 shows the dependence of the measured GMR ratio upon the background pressure. The maximum GMR ratio was achieved at an intermediate background pressure (20mTorr). The maximum GMR ratio was achieved at an intermediate input power (200W).

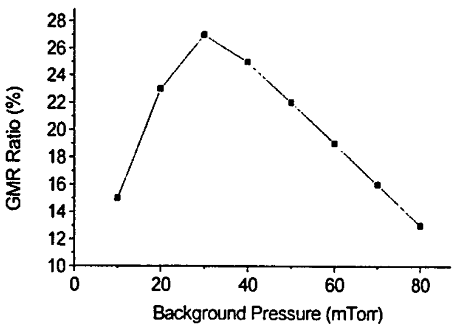

Fig. 1. The dependence of magnetoresistance ratio upon the background pressure for multilayers with a fixed CuAgAu layer thickness of 20Å.

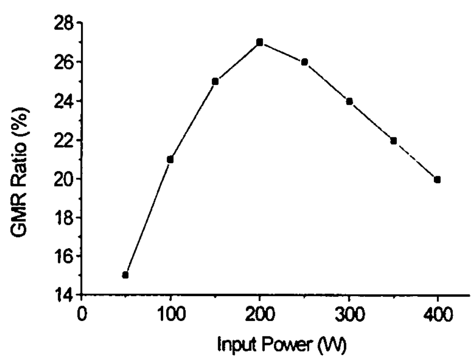

Fig.2.The dependence of magnetoresistance ratio upon the input power for multilayers with a fixed CuAgAu layer thickness of 20Å.

The drop in GMR as the pressure is increased beyond 20mTorr also is linked to a reduction in surface mobility as metal atom energy decreases. Energetic Ar^+ ions transfer their kinetic energy to the metal atoms and induce local heating. Increasing the Ar^+ ions energy will reduce the surface roughness and increase the adatom mobility promoting larger column widths and smooth surfaces, but high energy Ar^+ ions bombardment can also cause interfacial intermixing of the magnetic and nemagnetic atoms. The intermixing fraction decreased with increasing background pressure and/or decreasing input power.

References

[1] LENSSEN, K.-M.H., ADELERHOF, D.J., GASSEN, H.J., KUIPER, A.E.T., SOMERS, G.H.J., VAN ZON, J.B.A.D., *Sensors and Actuators*, **85**, 1, 2000.

[2] GAVRILA, H., CHIRIAC, H., CIUREANU, P., IONITA, V., YELON, A., *Magnetism tehnic si aplicat*, Editura Academiei Romane, ISBN: 973-27-0756-9, 2000.

[3] BAIBICH, M.N., BROTO, J.M., FERT, A., PETROFF, F., ETIENNE, P., CREUZET, G., FRIEDERICH, A., CHAZELAS, J., *Phys. Rev. Lett.*, **61**, 2472, 1988.

[4] DIÉNY, B., SPERIOSU, V.S., GURNEY, B.A., BAUMGART, P., WITHOIT, D.R., *Proceeding of IBM Workshop on Fundamentals of Magnetism in Magnetic Recording*, 21, 1990.

[5] ZOU, W., *Synthesis of Giant Magnetoresistive Multilayers*, University of Virginia, 2001.

DIELECTRIC RESPONSE OF NOVEL NANO-COMPOSITE METAL/SEMICONDUCTOR-POLYMER FILMS

E. Axelrod[1], Yu. Feldman[1] and L.I. Trakhtenberg[2]
[1]Department of Applied Physics, The Hebrew University of Jerusalem, 91904, Israel.
[2]L.Ya. Karpov Institute of Physical Chemistry, 103064, Moscow, Russia.
E-mail: katya@vms.huji.ac.il

The design, structure and dielectric properties of a new generation of metal/semiconductor-containing polymer systems produced by cryochemical solid-state synthesis were investigated. The synthesis consists of low-temperature co-condensation of metal (M)/semiconductor (SC) and monomer vapours followed by low-temperature solid-state polymerisation of the co-condensate [1]. Synthesized materials show specific dielectric responses, which are discussed in relation to material structure and electron transfer between nanoparticles.

The dielectric measurements for investigation of polymer pure matrix PPX, polymer matrix PPX with the addition of Cu (2 vol%) and Zn (8 vol%) and a set of PPX films containing different concentrations of PbS-nanocrystals [2] were taken with a Broad-Band Dielectric Spectrometer BDS 4284 (NOVOCONTROL) in the frequency range 20 Hz ÷ 1 MHz and in the -120 ^{0}C ÷ 100 ^{0}C temperature interval. The typical 3-dimensional spectra of the dielectric losses (ε'') for the studied polymers vs. frequency and temperature are displayed in Fig. 1.

In the M-containing samples, in the temperature interval of –70 ÷ 0 °C and in the low-frequency range, an unexpected dielectric relaxation process for polymers is detected. This process is observed clearly in the sample PPX+Cu. In sample PPX+Zn only traces of this process can be observed, and in the pure PPX matrix the process completely vanishes. This is a typical dielectric response for percolation behaviour [3]. Analysis of dielectric relaxation parameters of this process allowed us to determine fractal properties of the percolation cluster [4]. For the sample, PPX+Cu the calculated fractal dimension D_f is equal to 2.609.

The next relaxation process is typical for amorphous polymers and can be assigned to the α-relaxation that appears in the whole frequency range and in the temperature interval from 50 °C to 100 °C (Fig.1a). The temperature dependencies of the relaxation times of the observed α-relaxation process for pure PPX, PPX+Cu and PPX+Zn samples (Fig. 2) demonstrate an Arrhenius behaviour with the energies of activation 196 kJ/mol, 187 kJ/mol and 201 kJ/mol, respectively, and correlate with the activation energies of the α-process in most known polymer materials [5].

In the SC-containing samples, in the low temperature region –100 °C ÷ –15 °C, a relaxation process is distinctly observed (Fig. 1b). The temperature dependencies of the relaxation times of this low-temperature process demonstrate the Arrhenius behaviour with the energies of activation 4 kJ/mol and 3.3 kJ/mol, respectively (Fig. 3), and can be correlated with two groups of shallow traps in semiconductor nanocrystallites inside the porous polymer matrix.

References:

[1] E. V. Nikolaeva, S. A. Ozerin, A. E. Grigoriev, E. I. Grigoriev, S. N. Chvalun, G. N. Gerasimov, L. I. Trakhtenberg, Mater. Sci. & Eng., C 8-9 (1999) 217.
[2] L. I. Trakhtenberg, E. Axelrod, G. N. Gerasimov, E. V. Nikolaeva, E. I. Smirnova, J. Non-Cryst. Solids, 305 (2002) 190.
[3] A. Gutina, E. Axelrod, A. Puzenko, E. Rysiakiewicz-Pasek, N. Kozlovich, Yu. Feldman, J. of Non-Cryst. Solids, 302 (1998) 235.
[4] A. Puzenko, N. Kozlovich, A. Gutina, Yu. Feldman, Phys. Rev. B 60 (1999) 14348.
[5] Schönhals A 1997, Dielectric Spectroscopy of Polymeric Materials: Fundamentals and Applications, James P. Runt and John J. Fitzgerald (Ed.) 81-106.

Figures:

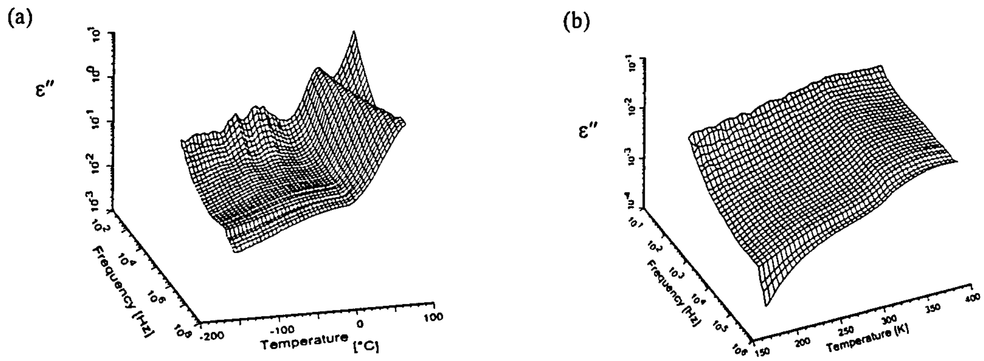

Figure 1. Three dimension plot of the frequency and temperature dependence of the dielectric losses ε" for the samples (a) PPX+Cu, 2vol% and (b) PPX+PbS.

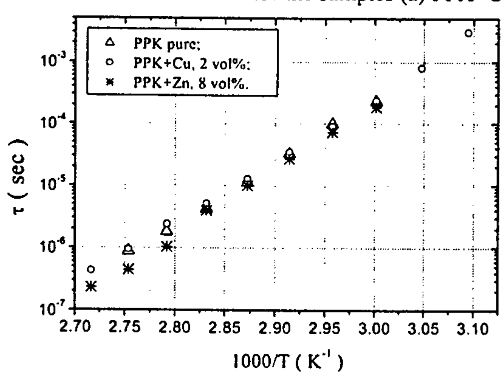

Figure 2. Temperature dependencies of the characteristic relaxation times of the α-process for samples pure PPX (△), PPX+Cu, 2vol% (O), and PPX+Zn, 8vol% (✳).

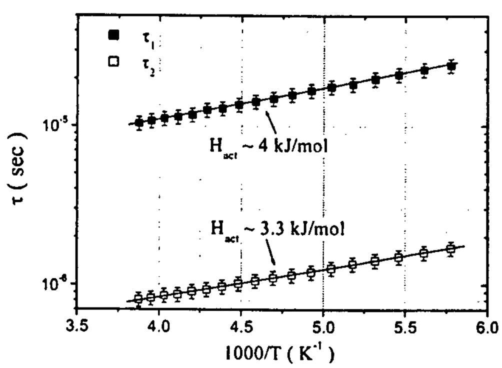

Figure 3. Temperature dependencies of the characteristic relaxation times of the low-temperature process for the PPX+PbS sample.

ZnS :Mn NANOPARTICLES SYNTHESIS AND CHARACTERIZATION

Yvonne Axmann, Alke Petri, H. Hofmann
Powder Technology Laboratory, IMX, EPFL, Lausanne, Switzerland
E-mail: yvonne.axmann@epfl.ch
http://www.epfl.ch/ltp/ltp.en.htm

The optical properties of nanocrystalline semiconductors have been studied extensively in recent years and a wide range of synthetic methods have been developed [1]. Many approaches involve non-aqueous methods and the classical techniques of colloidal chemistry. However, biological and medical applications require water-dispersible nanocrystals that can be covalently coupled to biomolecules for use in e.g. ultra sensitive biological detection.

In our work we characterize L-cysteine coated ZnS:Mn nanoparticles by a variety of methods. The particles are prepared in a colloidal synthesis using L-cysteine as surfactant and show an orange fluorescence at 585 nm characteristic for the $^4T_1 \rightarrow {}^6A_1$ transition of Mn^{2+} ions in a crystalline ZnS-matrix [2]. The absorption spectrum exhibits a shoulder at 285 nm, which is blue-shifted compared with the absorption of bulk ZnS (342 nm) [3] indicating a quantum size effect (Fig. 1). For the determination of the particle size distribution different techniques were applied, for example TEM picture analysis, photon correlation spectroscopy, or analytical ultra centrifugation.

The doping of the particles with Mn^{2+} was investigated by means of atomic absorption spectroscopy. The luminescence intensity shows a maximum at a Mn^{2+} content of 0.2 mol% related to Zinc before the formation of the particles under the chosen experimental conditions. A further increase of the Mn^{2+} content leads to decrease in the fluorescence intensity.
To investigate the adsorption of the surfactant on the particle surface Fourier transformed IR spectroscopy was applied. The absence of the S-H stretching mode for the cysteine adsorbed on the particle surface indicates that the bonding to the particle surface via the sulphur atom.

The most limiting factor for the luminescence intensity of nanoparticles is the radiationless recombination of the electron and the hole at the particle surface. Unsaturated valences at the surface act as recombination centres and so their saturation leads to an increase in luminescence intensity [1]. To saturate these "dangling bonds" the particles are coated with silica. This coating has many advantages, it is chemically inert, optically transparent [4], the shell has a sufficient lattice match with the ZnS and its refractive index is smaller than the one of ZnS so that the excitation light is diffracted into the particle core. The thus coated particles show luminescence intensity, which is 3.5 times higher than the intensity obtained without the silica coating (Fig. 2).

References:

[1] A. P. Alivisatos, J. Phys. Chem., **100** (1996) 13226.
[2] H.-E. Gumlich, J. Lumin., **23** (1981) 73.
[3] N. Murase, J. Phys. Chem. B, **103** (1999) 754.
[4] K. P. Velikov, Langmuir, **17** (2001) 4779.

Figures:

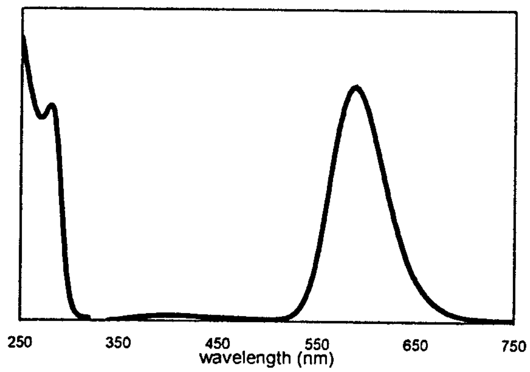

Fig. 1
Absorption (left) and luminescence emission (right) spectrum of $ZnS:Mn^{2+}$ nanoparticles doped with 0.25% Mn^{2+}.

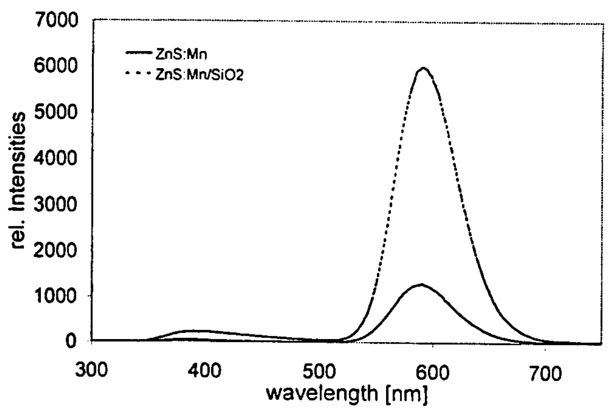

Fig. 2
Comparison of the fluorescence intensities of coated (dotted line) and uncoated $ZnS:Mn^{2+}$ nanoparticles

DISSOCIATION OF H_2 MOLECULES AT NANOCONTACTS

A.Ayuela[1^*], M.J. Puska[1], N. Zabala[2], and R. M. Nieminen[1]

[1] Helsinki UNivresisty of Technology(HUT), Espoo, Finland.
[2] Universidad del Pais Vasco(UPV), Leijona, Vizcaya, Spain.
* Actual address: Donostia International Physics Center (DIPC), Donostia, Spain

The observation of electronic conductance through H_2 molecules between two Pt electrodes has been reported recently in mechanically-controlled break junctions measurements [1]. We have simulated this system by relativistic electronic-structure calculations based in the density-functional theory within the generalized gradient aproximation (GGA) for electron exchange and correlation. According to our results H_2 molecules dissociate irrespective of the shape used for the electrodes. The same is true also for Au electrodes although there are differences between the dissociation mechanisms at Pt and Au nanocontacts. Our results call for improvements for the GGA or alternative interpretation of the experimental result [1-3].

[1] R.H.M. Smit, Y. Noat, C. Untiedt, N.D. Lang, M.C. Van Hemert and J.M. Van Ruitenbeek, Nature 419, 906 (2002).

[2] Sz. Csonka, A. Halbritter, and G. Mih\'aly,E. Jurdik, O.I. Shklyarevskii, S. Speller, and H. van Kempen, Phys. Rev. Lett 90,
116803 (2003).

[3]J. Heurich, F. Pauly, J.C. Cuevas, W. Wenzel, Gerd Schoen. cond-mat/0211635.

Surface Nanopatterning of Metal Thin Films by Physical Vapor Deposition onto Surface-Modified Silicon Nanodots

O. Azzaroni*,#, M. Fonticelli*, P.L. Schilardi*, I. Caretti#, R. Gago#+, L. Vázquez†# and R.C. Salvarezza*

**INIFTA- Universidad Nacional La Plata – CONICET – Argentina*
#Instituto de Ciencia de Materiales de Madrid (ICMM) – CSIC – Spain
+Forschungzsentrum Rossendorf eV – Germany

One of the most active research topics within the nanoscience and nanotechnology fields are those related to large-scale fabrication, in an accurate manner, of nanostructured metal thin films [1]. This interest is due to their potential applications for different technological purposes such as electrocatalysis [2] and optical devices [3]. In order to obtain these nanostructured films different techniques, such as ion sandblasting [4] or nanotransfer printing [5], have been developed. In this work we present results on the large-scale preparation of nanostructured metal thin films from surface-modified silicon nanodots templates [6]. The nanopatterning process is based on the deposition of a copper thin film (approximately 300nm thick) by physical vapor deposition on nanostructured silicon substrates [7] (Fig1.a,b), which were previously surface-modified with an octadecyltrichlorosilane (OTS) self-assembled monolayer in order to promote an easy metal film detachment after deposition. Once the 300 nm thick film has been deposited, a thick (10 μm approximately) film of copper is electrodeposited onto it to improve the mechanical properties of the physically-deposited nanostructured thin film. Thanks to the very low adhesion of OTS layer to the metal film the latter is easily mechanically detached from the template. Thus, the inner face (i.e. that one which was in contact with the nanostructured silicon surface) can be imaged by AFM (Fig1.c,d). These images reveal a nanostructure corresponding to that one of the negative replica of the original nanopatterned silicon template. This metal nanopatterning strategy shows potential applications for accurate large-scale fabrication of nanostructured metal thin films.

† Corresponding author:
Dr. Luis Vázquez
Instituto de Ciencia de Materiales de Madrid (ICMM) – CSIC
Cantoblanco, 28049 Madrid - SPAIN
e-mail: lvb@icmm.csic.es

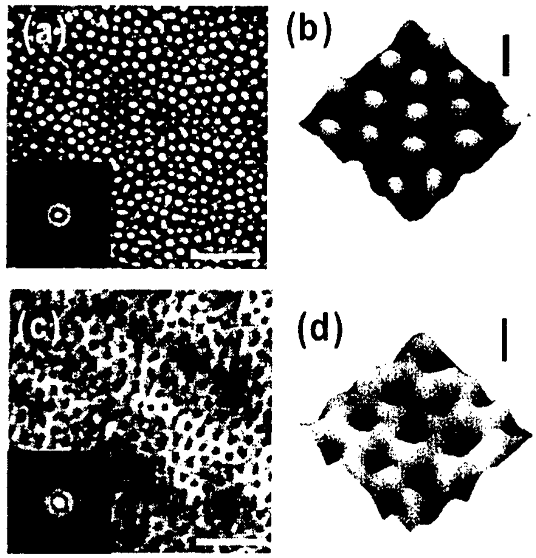

Figure 1. 1 x 1 μm^2 top view AFM images of the silicon nanostructured template [(a), (b)] and the physically-deposited nanostructured copper thin film [(c),(d)]. The horizontal bar in Panel [(a),(c)] corresponds to 200 nm. Insets show the two-dimensional autocorrelation function showing the short-range hexagonal order. Panels [(b),(d)] correspond to 200 x 200 nm^2 three-dimensional AFM images, the vertical bar corresponds to 20 nm.

References:

[1] G.L. Egan, J.-S. Yu, C.H. Kimm, S.J. Lee, R.E. Schaak, T.E. Mallouk, *Adv.Mater.* 12, 1040 (2000)

[2] G.S. Attard, P.N. Bartlett, N.R.B. Coleman, J.M. Elliot, J.R. Owen, J.H. Wang, *Science*, 278, 838 (1997)

[3] M.B. Sobnack, W.C. Tan, N.P. Wanstall, T.W. Preist, J.R. Sambles, *Phys.Rev.Lett.* 80, 5667 (1998)

[4] S. Rusponi, G. Constantini, F. Buatier de Mongeot, C. Borago, U. Valvusa *Appl.Phys.Lett.* 75, 3318 (1999)

[5] Y.-L. Loo, R.L. Willett, K.W. Baldwin, J.A. Rogers, *J.Am.Chem.Soc.* 124, 7654 (2002)

[6] O. Azzaroni, P.L. Schilardi, R.C. Salvarezza, R. Gago, L. Vázquez, *Appl.Phys.Lett.* 82, 457 (2003)

[7] R. Gago, L. Vázquez, R. Cuerno, M. Varela, C. Ballesteros, J.M. Albella, *Appl.Phys.Lett.* 178, 3316 (2001)

NANOMAGNETIC FLUIDS UTILIZATION IN *CHRYSANTEMUM* SP. AND *SOLANUM TUBEROSUM* L. EXPLANTS CAULOGENESIS

Anca Mihaela Baciu
University of agricultural Sciences of Banat County, Timisoara, Romania

In the scientific activity of the Department of Genetics the nanomaterials have been used since from 1985. From the historical point of view the nanomaterials were use in technology, medicine and in the plant kingdom. The most spectacular results were obtained in medicine in the carcigenesis treatment. The nanomaterials were used in biotechnology, especially for improving the regenerative processes.

In biotechnology the nanomaterials were used especially in eukaryote and prokaryote organism.

In our experiments we wanted to understand the magnetic nanoparticles (NMPs) effect upon some species with vegetative reproduction (*Chrysantemum* sp. and *Solanum tuberosum* L.).

The **biological material** consisted in *Chrysantemum* sp. an ornamental plant and sometimes used in homeopathy and *Solanum tuberosum* L. (potatoes) an economic plant.

About Nanomagnetic Fluids

For the biological purposes the Magnetic Fluids have to be biocompatible and bioactive. At the "University Politehnica" the "Complex Fluids" Institute, were prepare different kind of magnetic nanoparticles (Fe_3Co) using biological surfactants (lauric acid, oleic acid, etc.) and suspendants (H_2O-distill, DDW, a plants sap) have been prepared.

In our experiments we use distill water as suspendant (positive control). The experimental variants had different concentrations of magnetic nanoparticles varying from $\theta = 0,037x10^{-3}$ g/cm^3 to $\theta = 0,37x10^{-3}$ g/cm^3 and $\theta = 3,7x10^{-3}$ g/cm^3. They were compared with the positive control and negative control (lauric acid). The growth quantifications, as hight, LAI (Leaf Area Index) were evaluated every seven days until the 28th day. The obtained data were statistical processes.

We found out that the plants i.e. chrysantemum and potato can be maintained for a longer period of time in *in vitro*. For that purpose we tested $\theta = 37x10^{-3}$ g/cm^3 concentration.

The results obtained pointed out also differences in caulogenesis in *Chrysantemum* and *Solanum tuberosum*.

In comparison to controls the nanomagnetic particles repressed the plant growth along all period: from the beginning until the 28th day. The repression effect was more obvious on potato explants than in *Chrysantemum*.

In comparison to lauric acid, representing the negative control, the differences when using magnetic nanoparticles were positive both in *Chrysantemum* and the majority of potatoes.

The lauric acid has represive effect upon the neoplantlets. The strongest effect was in potato where the differences after 28 days were $d=-1,74\pm1,31$ cm.

It is visible the positive influence of nanomagnetic particles in the first life cycle is visible. In *Chrysantemum* a high nanomagnetic particles concentration repressed the plant growth.

The potato revealed a higher sensitivity to nanomagnetic particle presence.

In conclusion it can be stressed the favourable effect of nanomagnetic particle upon *Chrysantemum* caulogenesis can be observed.

The potato *Runica* variety was sensitive to nanomagnetic presence in the growth media.

The nanomagnetic particles can be used to improve the *in vitro* culture technology.

Table 1 The plantlets growth rhythm of Chrsanthemum sp. and Solanum tuberosum L. - Runica variety, cultivated in vitro on a media added with magnetic nanoparticles

Nanoparti-cles conc. θ=g/cm^3	**Chrysanthemum**	**d_1**	**d_2**	**Potatoes**	**d_1**	**d_2**
After 14 days						
H_2Od 0,0	3,82±0,18	-	1,16±0,09	4,93±1,27	-	1,00±0,57
Lauric acid 0,0	2,66±0,29	-1,16±0,09	-	3,93±1,19	-1,00±0,57	-
θ=0,37x10^{-3}	3,08±0,18	-0,74±0,07	0,42±0,09	2,02±0,36	-2,91±0,43	-1,91±0,41
θ=3,7x10^{-3}	2,75±0,29	-1,07±0,09	0,09±0,09	1,94±0,45	-2,99±0,44	-1,99±0,42
After 21 days						
H_2Od 0,0	6,41±0,26	-	1,01±0,10	5,83±1,72	-	1,47±0,84
Lauric acid 0,0	5,40±0,28	-1,01±0,10	-	4,36±1,85	-1,47±0,84	-
θ=0,37x10^{-3}	5,56±0,42	-0,85±0,13	0,16±0,04	2,51±0,61	-3,32±0,60	-1,85±0,64
θ=3,7x10^{-3}	5,65±0,17	-0,76±0,08	-0,76±0,02	4,71±1,06	-1,12±0,67	0,35±0,71
After 28 days						
H_2Od 0,0	8,97±0,23	-	1,15±0,09	7,20±2,83	-	1,74±1,31
Lauric acid 0,0	7,82±0,25	-1,15±0,09	-	5,46±2,75	-1,74±1,31	-
θ=0,37x10^{-3}	8,28±0,42	-0,69±0,13	0,46±0,04	3,34±0,92	-3,86±0,99	-2,12±0,96
θ=3,7x10^{-3}	7,10±0,26	-1,87±0,09	-0,72±0,09	5,98±1,57	-1,22±1,07	0,52±1,05

d_1 - the difference between positive control (H_2Od) and each other variants
d_2 – the difference between negative control (lauric acid) and other variants

Fully Electrically Controlled, Room-Temperature Memory Devices Based on Self-Assembled InAs Quantum Dots

C. Balocco, M. Missous, and A. M. Song
Department of Electrical Engineering and Electronics, UMIST, Manchester M60 1QD, UK

Self-assembled semiconductor quantum dots (QDs), created by epitaxial growth using Stranski–Krastanow mode, have been intensively studied because of their importance in device applications and considerable interests in fundamental physics. While so far most investigations focused on optoelectronic devices such as lasers, LED, and photodetectors, the possibilities to design quantum-dot-based memory devices have recently attracted more and more attention. Because of the single-electron charging/discharging effect in self-assembled QDs, the electric current and therefore power consumption required for memory operations in a QD-based memory device could be substantially lower than in a conventional memory cell. Furthermore, the strong quantum carrier confinement in QDs may lead to much longer charge-retention or memory holding time. The most common and perhaps the simplest design is to embed quantum dots in close vicinity to the two-dimensional electron gas (2DEG) in a high-electron-mobility transistor (HEMT) structure, and the quantum dots are charged and discharged by gate bias. Despite much effort, so far most such devices were demonstrated only at low temperatures[1–4]. Although Koike et al recently presented memory operations at room temperature, the devices required a light excitation to discharge the QDs[5]. From the application point of view, however, both room-temperature and fully electrically controlled memory operations are essential. Furthermore, compared with many measurements on hysteresis in electron density [1, 2], source-drain current [3, 6], and capacitance [6], hardly any time-domain measurement has been carried out to characterise the memory holding time, despite it being one of the most important parameters of memory devices. In this work, we fabricated memory devices using two pseudomorphic different InGaAs/GaAs/AlGaAs HEMT structures, each with five layers of stacked InAs quantum dots. An atomic force microscope (AFM) was used to examine the dot density and room temperature photoluminescence (PL) measurements were carried out to study the carrier confinement energies in the dots, before the fabrications of the memory devices. Our experiments not only demonstrated both room-temperature and fully electrically controlled memory devices, which are, to the best of our knowledge, the first of this type, but also showed a remarkable memory holding time of tens of minutes in real-time characterisation measurements.

Figure 1 shows the schematics of the two wafers grown on rotating substrates in a Thermo VG V90 molecular beam epitaxy growth chamber. Note that wafer #1681 is an inverted, modulation-doped quantum well structure so that the stacked QD layers are much closer to the 2DEG than in wafer #1680. From AFM measurements on an uncapped control wafer, a dot density of about 6×10^9 cm^{-2} was obtained. Figure 2 showed well-defined QD PL peaks at about 1050 nm at room temperature. In wafer #1681, largely because of the inverted structure, PL signals from the InGaAs quantum well were also clearly observed. The fabrication is essentially the same as that of a conventional HEMT, using a standard photolithography combined with a wet etching. A large number of devices were fabricated from both wafers, with the gate length ranging from 2 μm to 5 μm and the gate width from 10 μm to 100 μm. The characteristic of a device fabricated from wafer #1681 is shown in Fig. 3, which is close to that of the devices from wafer #1680. However, in the memory operation measurements, devices from wafer #1681 showed a much stronger memory effect than the devices from wafer #1680, mainly because of the difference in the distance between QDs and 2DEG. Figure 4 presents a pronounced hysteresis in the source-drain current, I_{SD}, versus the gate bias, V_G, curve, measured at a fixed source-drain voltage $V_{SD} = 100$ mV and at room temperature. This is, to the best of our knowledge, the first QD-based HEMT-type memory device that not only is fully electrically controlled but also operates at room temperature. Furthermore, our real-time characterisation experiments have reliably revealed a remarkable typical memory holding time of tens of minutes, which is promising for real applications.

[1] G. Yusa and H. Sakaki, Appl. Phys. Lett. **70**, 345 (1997).
[2] G. Yusa and H. Sakaki, Superlatt. Microstr. **25**, 247 (1999)
[3] H. Kim, T. Noda, T. Kawazu, and H. Sakaki, Jpn. J. Appl. Phys. **39**, 7100 (2000).
[4] A. Schliemann, L. Worschech, S. Reitzenstein, S. Kaiser, and A. Forchel, Appl. Phys. Lett. **81**, 2115 (2002).
[5] K. Koike, K. Saitoh, S. Li, S. Sasa, M. Inoue, and M.Yano, Appl. Phys. Lett. **76**, 1464 (2000).
[6] H. Son, J. Kim, M. Kim, and S. Hong, Jpn. J. Appl. Phys. **40**, 2801 (2001).

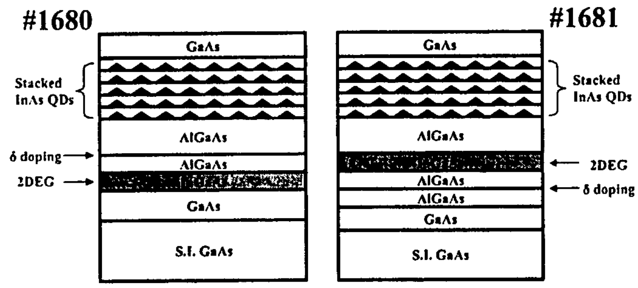

FIG. 1: Schematics of the structures of wafers #1680 and #1681.

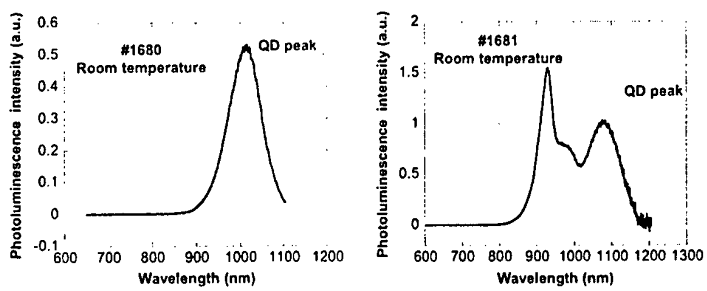

FIG. 2: Photoluminescence spectra from as grown wafers #1680 and #1681. The QD PL peak is around 1020 nm in wafer #1680 and 1080 nm in wafer #1681.

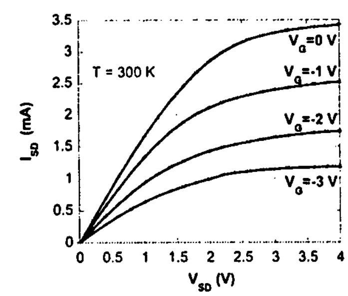

FIG. 3: Typical transistor characteristics of a device fabricated from wafer #1681 with a 5 μm $\times$ 10 μm gate.

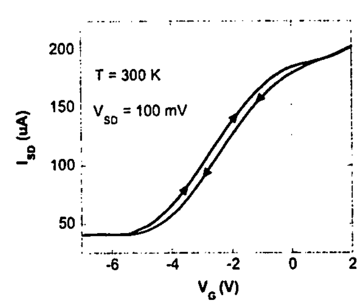

FIG. 4: Memory effect shown by the clear hysteresis in the I_{SD} vs V_G curve, which was obtained at a fixed V_{SD} = 100 mV and measured at room temperature.

Design and characterization of RF ballistic nanodevices

L. Bednarz, Rashmi, L. Gence, B. Hackens, H. Boutry, V. Bayot and I. Huynen

CERMIN, EMIC, PCPM and DICE Labs, Université catholique de Louvain (UCL)
1348 Louvain-la-Neuve, Belgium

Introduction

With conventional semiconductor devices approaching their limits of miniaturization, further advancement of IC technology is possible only through developments in nanotechnology. The industry is facing the challenge of exploring novel nanodevices that can be reproducibly fabricated for mass production and are capable of operating at room temperature, with speeds high enough to enable digital/analog data processing and transmission at ultra-high bit rates (up to sub-millimeter wave frequencies). The growing interest for systems operating at 80 GHz and 160 GHz for direct modulation/demodulation of optical telecommunication carrier essentially requires electronic devices operating up to THz frequencies. In the present work, we exploit the ballistic effects in nano-scaled InAlAs/InGaAs/InP based devices for RF applications up to the THz range. Owing to the large values of electron scattering length (l_e) (higher than 100 nm at room temperature) in InGaAs-based material system, it is possible to fabricate and operate ballistic devices of dimensions comparable to l_e at room temperature [1], with sufficient repeatability and robustness. Those devices are fully compatible with the existing HEMT technology that has already demonstrated cut-off frequencies as high as 562 GHz for 25nm gate pseudomorphic $In_{0.52}Al_{0.48}As/In_{0.7}Ga_{0.3}As$ HEMT [2].

RF characterization of ballistic channels

We first aim to investigate the ballistic and non-linear effects in InGaAs-based nanodevices as a function of frequency, device size, and temperature to provide a physical insight into the ballistic behavior of nanodevices in THz frequency range. Simple ballistic channels have been designed and RF measurements carried out at room and at low temperatures. The preferred geometry for on-wafer characterization at RF frequencies is the coplanar waveguide (CPW) transmission line, because signal and ground pads are located in the same plane, facilitating the contacts (Fig. 1). The 2-DEG resistance presented by ballistic channels was measured as a function of temperature and frequency (Fig. 2). The observed dependence is close to that presented for 2-DEG, over the restricted frequency range 0-2.5 GHz, in the literature [3]. Due to the lack of published experimental results at higher frequencies, modeling is still in progress to validate over a wider frequency range the S-parameters of these simple channels.

Design of RF ballistic nanodevices

Results on ballistic channels show that matching of access impedances to the high impedance presented by the ballistic channel for efficient injection of microwave and millimeter wave signals requires optimization of the topology of 2-DEG channel and RF accesses. To avoid a strong forward reflection of RF signal at the input of ballistic devices and to increase the total conductance, arrays and matrices of devices of various geometries were also fabricated and characterized. From the observed agreement between circuit-oriented modeling and measurement (Fig. 3), it is concluded that crucial parameters for the injection of RF signals are the geometry of the channel, the distance between the CPW metallic pads, and the nature of the contacts between the gas channel and the metallic pads.

Based on these previous RF characterizations, a Y-branch junction has been designed for RF operation. Nonlinear ballistic behavior of three-terminal ballistic junctions (TBJs) has been reported extensively in literature [4]. When finite dc voltages (V_l and V_r) are applied to the left and right-hand side branches of a symmetric TBJ in a push-pull manner ($V_l = -V_r$), the voltage measured at the central branch (V_b) is always negative, thus the TBJ acts as a dc rectifier. This ballistic effect is further enhanced in YBJs, depending on the angle between the two symmetric branches and is expected to offer excellent performance at extremely high frequencies [5-6]. In order to operate the Y-junction in push-pull manner in RF, a 180° phase-shift has to be introduced in one of the input branches. Here it is created around 10 GHz by means of a wideband hybrid coupler (Fig. 4). Such a feeder will enable to demonstrate for the first time the operation of the Y-junction as a frequency-doubler or power detector in the microwave range, in view of extrapolating its design for operation in the THz range. The intrinsic cut-off frequency, sensitivity and linearity of the YBJ frequency-doubler can indeed be improved by

reducing the size and optimizing the device geometry. Experimental results on this ballistic frequency doubler are expected soon.

References

1. A. Song et. al., Jpn. J. Appl. Phys., vol. 40(2), 9A/B, pp. L909-L911, 2001.
2. Y. Yamashita et. al., IEEE Electron Dev. Lett., vol. 23(10), pp. 573-575, 2002.
3. P. Burke et. al., Appl. Phys. Letters, vol. 76(6), pp. 745-747, 2000.
4. H. Q. Xu, Appl. Phys. Letters, vol. 78(14), pp. 2064-2066, 2001.
5. R. Lewen et. al., J. Appl. Phys., vol. 91(4), pp. 2398-2402, 2002.
6. J. Mateos et. al., Communication presented at the IPRM 2003 Conference (Indium Phosphide and Related Materials), Santa Barbara, California, USA, May 12-16, 2003.

Acknowledgements

This work is realised in collaboration with the IEMN and the University of Salamanca, in the frame of the IST-2001-32517 Project "Nanotera" funded by the EC. Acknowledgements are also due to the FRIA and to the National Fund of Scientific Research (FNRS) Belgium, and to the Special Funds of Research, UCL, Belgium.

Figures

(a)

(b)

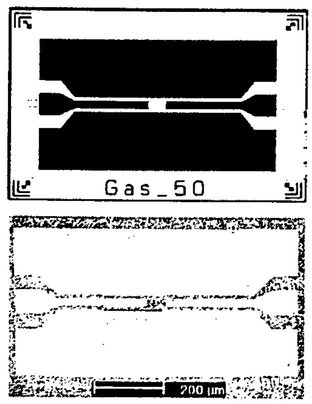

Fig. 1: (a) Lithographic mask and (b) realization of a simple ballistic channel, embedded in CPW accesses.
In Fig. 1(a), dark area is metal and white area is 2DEG channel of length 60 µm and width 26 µm.

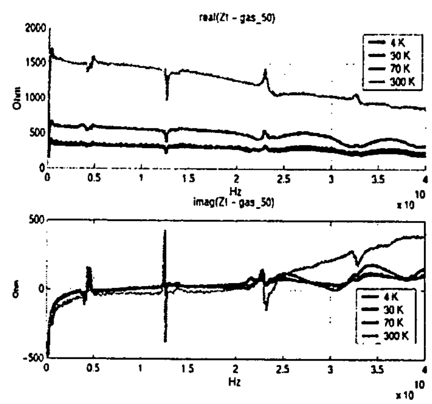

Fig. 2: Impedance of Gas_50 channel extracted from measurements at different temperatures (sharp peaks are due to measurement artifacts).

(a)

(b)

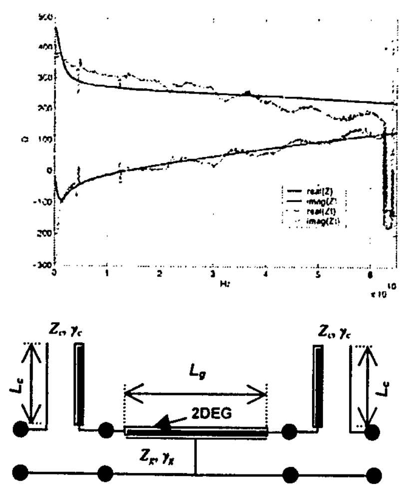

Fig. 3: (a) Measurements and simulation of impedance of Gas_50 at 77 °K, (b) Distributed transmission line circuit used for modeling.

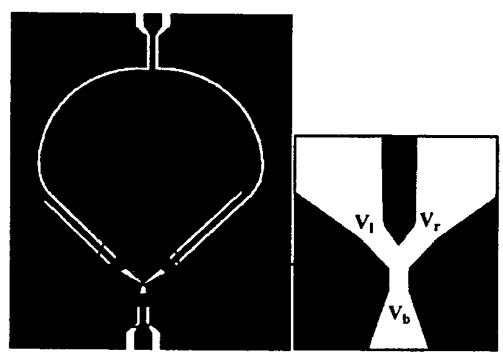

(a) (b)

Fig. 4: (a) RF design for Y-Branch junction device used as frequency doubler, (b) Magnified view of Y-branch junction.

CHARGE TRANSPORT IN SELF-ASSEMBLED COPT$_3$ NANOCRYSTAL ARRAYS

P. Beecher[a], A. Quinn[a], E. Shevchenko[b], H. Weller[b], G. Redmond[a]

[a] Nanotechnology Group, NMRC, Ireland.
[b] Institute of Physical Chemistry, University of Hamburg, Germany.

Monodisperse, chemically-synthesised nanocrystals are promising candidates as building blocks for future 2D and 3D quantum dot architectures due to their monodispersity and self-assembly capabilities. Although such nanocrystals are often referred to as "artificial atoms", there are distinct differences between nanocrystal arrays and crystalline solids, i.e. atomic arrays. Developing an understanding of charge transport in *real* nanocrystal arrays in order to ultimately control the electronic properties is a key milestone en route to future nanocomponent-based architectures.

We report on the fabrication of arrays of 3.8 nm $CoPt_3$ nanocrystals between 70nm gap electrodes by self-assembly. Using variable temperature dc electrical characterisation as a probe of charge transport in the array, we demonstrate that the inter-nanocrystal separation, and hence the electronic properties, can be tuned *in-situ* using mild thermal annealing.

For devices annealed at 80 °C, we observe Coulomb Blockade at temperatures below 35K. Scaling behaviour of the current above the blockade threshold indicates that the current flows through a 2D/3D network *i.e.* there are no significant bottlenecks in the array. Above 35K, the conduction is thermally activated, as expected for an insulating array of monodisperse metallic islands.

Slightly higher anneal temperatures (~100 °C) yield quasi-metallic transport behaviour with a transition from a negative temperature coefficient of resistance (TCR) at low temperatures to a postive TCR above 80K. Devices annealed at 150 °C show fully metallic transport characteristics similar to those of ceramic-metallics. Since the nanocrystals are air-stable to 200 °C, it appears that the nanocrystals do not fuse during annealing, but rather that the anneal-induced inter-nanocrystal coupling is sufficiently strong to delocalise the electron wavefunctions over the array, resulting in tuneable electrical transport behaviour. We believe these results constitute an initial demonstration of *in-situ* thermally induced insulator-metal transitions in self-assembled metal nanocrystal arrays.

PURE MAGNETO-OPTIC DIFFRACTION AND DOMAIN OBSERVATIONS IN PERIODIC DOMAIN STRUCTURES INDUCED IN MAGNETIC THIN FILMS

A. Bengoechea, J. L. Costa-Krämer, P. García-Mochales, R. Alvarez-Sánchez, and F. Briones

Instituto de Microelectrónica de Madrid, IMM (CNM-CSIC)
Isaac Newton 8, PTM, 28760 Tres Cantos, Spain

Magnetic couplings in magnetic heterostructures produce a wide variety of phenomena that have shown in recent years their potential for applications. In addition, conventional magneto-optic techniques, and more recently, Diffraction Magneto-Optic Kerr Effect (DMOKE) in regular arrays of magnetic elements, are very powerful methods that posses the high sensitivity required to monitor magnetization changes in thin films and very small elements. A recent work [1] has reported the appearance of diffraction spots when illuminating a flat Co ferromagnetic surface that is magnetically coupled to an array of magnetic elements. These diffraction spots appeared at angles corresponding to the periodicity of the array only at selected field values, i.e., they could be switched on and off with an applied magnetic field. This work has been extended, studying by Kerr domain observations the domain structures both at the patterned and flat sides of the structures, confirming the appearance of periodic domain structures at the flat ferromagnetic surface. Likewise, we have studied the couplings between the array of magnetic elements and the continuous ferromagnetic film, for different thicknesses and orientations of the array elements with respect to the anisotropy axis of the continuous film.

Our goal is understanding the operative magnetization and coupling processes in these new structures. MOKE and domain observations together with micro-magnetic simulations help to resolve these processes, being domain observations the conventional MOKE hysteresis loops but resolved spatially.

Co stripes –a 1D pattern- and arrays of squares –a 2D pattern- are fabricated by sputtering and lift-off technique on top of a previously sputtered continuous Co layer. MOKE hysteresis loops for Co stripes on continuous Co are measured when light is shined both from the flat side, Fig.1a), and from the patterned side, Fig.1b). The different behaviour displayed in Fig. 1 demonstrates that the Co stripes are exchange decoupled from the continuous Co layer. The negative differential susceptibility observed in Fig.1a) is due to an antiferromagnetic type of coupling between the stripes and the continuous Co.

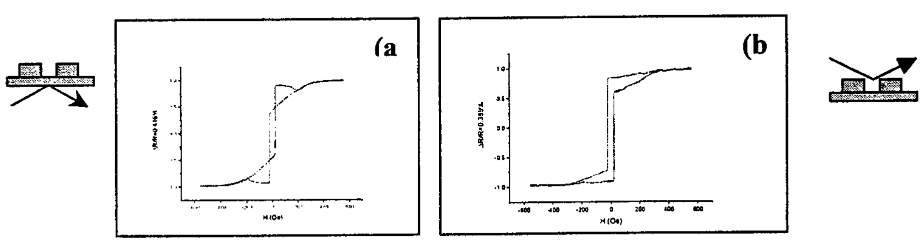

Fig. 1. Transverse MOKE hysteresis loops measured from a) the flat side and b) the patterned side of a structure of Co stripes of 6 μm width (and 9 μm periodicity) deposited on top of a continuous Co layer.

The hysteresis loops from patterned and flat sides are correlated with the domain observations at selected field values for this 1D pattern for arrays of micro-stripes with different widths and periodicities.

Domain images acquired during the magnetization process at the flat side of the Co stripes/Co heterostructures. The domain structure replicates the shape of the periodic array of elements deposited at the opposite side at selected field values (fig. 2). The pure magneto optic contrast explains the appearance of a diffraction spot at selected field values when illuminating this flat side. This replica is due to the magnetostatic coupling between the patterned and the continuous layers. This is possible due to the thickness of the layers, of the order the domain wall width, and a thin nanometric barrier that exchange decouples the pattern and the continuous layers.

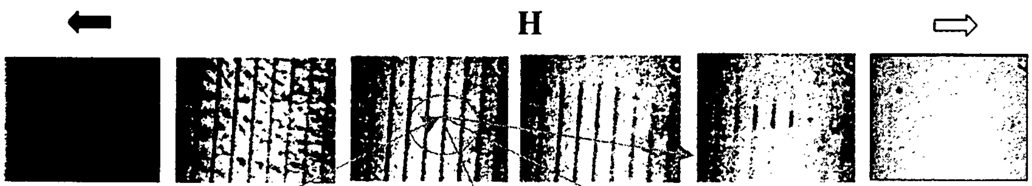

Fig. 2 Pure magneto-optic diffraction: Spots appear at angles corresponding to the periodicity of the array only at selected field values. This replica is due to the magnetostatic coupling between the patterned and the continuous sides.

Both for 1D (fig.3a) and 2D (fig.3b) patterns, and for patterns that are exchange coupled and decoupled from the continuous Co layer, the domain structure observations (fig.3 a&b) and the hysteresis loops measured at flat and patterned sides will be presented. These will be compared with micro-magnetic simulations, studying both reflected and diffracted beams, for different widths and periodicities between elements.

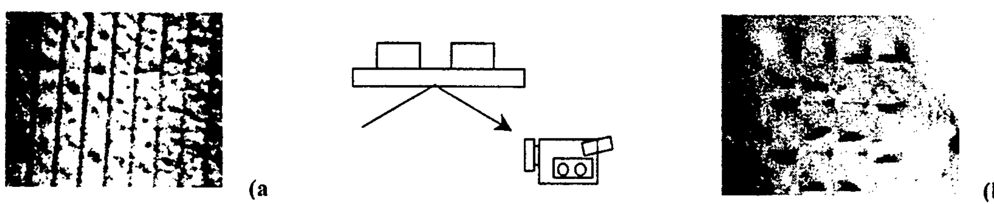

Fig. 3 Domain structure at the flat side of two structures with different patterns at selected field values: a) A continuous Co layer with a 1D pattern of Co stripes deposited at the opposite side and. b) A continuous Fe layer with a 2D square pattern deposited at the opposite side. The images size is around 600x450 μm.

References:

[1] J. L. Costa-Krämer, C. Guerrero, S. Melle, P. García-Mochales and F. Briones, Nanotechnology **14** (2003) 239-244

ELECTRONIC CHARACTERIZATION OF ASYMMETRIC MULTIPLE QUANTUM WELLS

R. Betancourt-Riera, R. Riera, I.E. Marín and J.L. Marín

A complete characterization of double and triple asymmetric quantum wells are studied theoretically. Taking into account the asymmetry due to different widths of the wells with same potential barriers and then with wells of the same widths and different potential barriers. The structures consisting of three levels in two or three coupled quantum wells are optimized for a maximum Raman gain at zero bias.

BAND ALIGNMENTS AND QUANTUM CONFINEMENT IN GAASN/INAS STRAIN-BALANCED NANOSTRUCTURES

L. Bhusal, A. Alemu, A. Freundlich
Texas Center for Superconductivity and Advanced materials, University of Houston, 4800 Calhoun, Houston-77204, Texas, USA.
Email: lbhusal@uh.edu

The unusual large band gap lowering observed in GaInAs with low Nitrogen(N) fraction has sparked a recent interest in development of dilute nitrogen containing III-V semiconductors for long-wavelength optoelectronic devices (IR lasers, detector and solar cells). Most of the work has been concentrated on the development of InGaAsN alloys lattice-matched to the GaAs substrate. The practical limitation in N incorporation in these epilayers has so far prevented the realization of materials with operating wavelengths beyond 1.6 μm (0.8 eV). From a theoretical stand point, longer wavelength materials could be achieved by subjecting the GaAsN alloys to a large biaxial compressive strain e.g by fabricating pseudomorphically strained layers on commonly available InP substrates. While such an approach in principle could allow attaining longer wavelength materials, the large lattice mismatch between GaAsN and InP(4-5% for N<5%) imposes a severe restriction on the total amount of material that can be deposited (few atomic monolayers) prior to lattice relaxation.

We propose to circumvent this limitation by introducing alternating layers of opposite strain in conjunction with GaAsN. We have chosen InAs for this purpose, since tensilely strained on InP InAshas still a relatively low band gap and the lattice mismatch between InP and InAs (3.1% at 300K) has nearly the same order of magnitude, but with opposite sign, as the one between $GaAs_{1-x}N_x$ and InP (4-5% for $x<0.05$). Therefore, by adjusting dot size/epilayer thickness accordingly with respect to the stress magnitude, the composite structure of alternate growth of GaAsN and InAs layers will lead to a lower total strain energy in the system through a strain balance. Consequently, even infinite pseudomorphically strained superlattice thickness can be realized from a sequence of GaAsN and InAs quantum wells if the thickness of GaAsN and InAs in each period is below the critical thickness of their respective single layers. The strain ratio is inversely proportional to the individual layer thickness.

In this work we have undertaken a theoretical investigation of the band structure of this new type of heterostrutures. The numerical modeling for the proposed structure has been done under the envelop function approximation, using a transfer matrix method. The conduction band is treated separately from the valance band by assuming that there is no interaction between them. Strain effects on the band gap of both materials and N-induced reduction of the conduction band of GaAsN were included in the calculations. Based on the theory of Luttinger-Kohn and Bir-Pikus, including the spin-orbit coupling, the valance band of a strained material with zinc-blende summetry is described by a 6x6 Hamiltonian. The study was limited to low practically achievable Nitrogen (N<4%)containing materials.

It is shown that by increasing the composition of N in GaAsN layers the fundamental bandgap of the quantum dot/well superlattice alloys strained on InP substrate could be reduced to well below 0.5 eV (N>2%). In addition the conduction and valence band offsets (band discontinuities) of GaAsN with respect to strained InAs (P) "barriers"

have been evaluated. A critical concentration of N is found, which marks the onset of type-I band alignment, in which holes and electrons are confined in GaAsN, to a type-II band alignment, in which holes and electrons are confined respectively in GaAsN and InAs (P). Hence by controlling the amount of N in the GaAsN, (GaAsN)n/InAs)m quantum dot/well superlattice lattice matched to the InP offers a potential material for long-wavelength device operating beyond 2.2 μm. The modeling data for a bi-dimensional (well) system is also extended to include the evolution of the band structure and electron and hole confinement levels as a function of the dot size and nitrogen content for GaAsN quantum dots imbedded in InAs- InP matrix.

Finally an experimental investigation on these new types of nanostructures has been initiated and in addition to theoretical data preliminary experimental results will be presented at the conference.

References:

[1] S.L. Chuang, C.S. Chang. Phys. Rev. B, **54,** 2491,1996.

[2] S.H. Park, S.L.Chuang, J. Appl. Phys., **87,** 353, 2000

FIELD EMISSION FROM A BUNDLE OF CARBON NANOTUBE PRODUCED BY ARC DISCHARGE METHOD

S. Bini F. Tombolini G. Giannini S. Bellucci
INFN Frascati Via Enrico Fermi 40 00044 Italy
E-mail:simone.bini@lnf.infn.it
http://www.lnf.infn.it

In our laboratory, we have studied electron emission from carbon nanotubes produced by arc-discharge method. Field emission is defined as the emission of electrons from surface of condensed phase into another phase, usually a vacuum , under the action of high (3-6 KV/ μm) electrostatic fields.The stable electron emission at relatively low fields (<10 V/ μm) makes nanotubes very attractive for field emission display application. In the present work, we report the fabrication of a micro machining sample based on arc-produced carbon nanotubes. Carbon nanotubes were synthesized in a dc arc system in helium atmosphere at low pressure, about 0.5 atm. Arc-discharge is a method which was usually used in synthesis of carbon nanotubes in the early stage. Two graphite rods are used as the cathode and anode, between which arcing occurs when DC voltage power is supplied. A large quantity of electrons from the arc-discharge move to the anode and collide into the anodic rod. Carbon clusters from the anodic graphite rod caused by the collision are cooled to low temperature and condensed on the surface of the cathodic graphite rod. The graphite deposits condensed on the cathode contain both carbon nanotubes, nanoparticles, and clusters. The graphite clusters synthesized in these initial experiments contained a small amount of carbon nanotubes. The schematic diagram of arc-discharge apparatus for the synthesis of carbon nanotubes is represented in Fig 1 where the apparatus is connected both to a vacuum line with a diffusion pump, and to a helium supply. The electrodes are two graphite rods, usually of high purity. Typically, the anode is a long rod approximately 6 mm in diameter and the cathode a much shorter rod 13.6 mm in diameter. Efficient cooling of the cathode has been shown to be essential in producing good quality nanotubes. The position of the anode should be adjustable from outside the chamber, so that a constant gap can be maintained during arc-evaporation. A voltage-stabilized DC power supply is normally used, and discharge is typically carried out at a voltage of 20 to 40 V and at a current in the range of 50 to 100 A. When a stable arc is achieved, the gap between the rods should be maintained at approximately 1 mm or less. Carbon nanotubes synthesized by arc-discharge normally have multi-walled structures. We have made with the arc-discharge methode single wall nanotube of a diameter of about 1.5 nm.

The powder containing nanotubes was thoroughly mixed into non conductive epoxy in a volume ratio of approximately 1:1 to produce a conductive matrix of nanotubes.It was deposited on the PVC cylinder, and then mechanically shaped to obtain a well-defined circular emission surface with diameter of order 2mm.Fig 3 depicts the experimental setup for detecting nanotube field emission The sample was placed in a vacuum chamber at 10^{-6} Torr. Using an insulator foil thick 80μm the prepared surface was sandwiched with a cathode brass plate. The sample was then biased at negative voltage V with respect a anode . We can see that the turn on -voltage is near 430 V.The value that we have obtained with error bars are shown in Fig2 The source display a stable and reproducible current-voltage characteristic with activation field of order (6 V/ μm) and emission current of order 1 μA /mm2 after HV conditioning .Further improvement of this technology may lead to easy-to-make and inexpensive flat panel displays

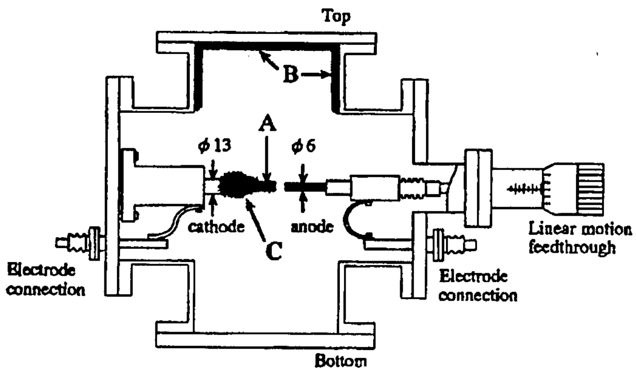

Fig. 1. Schematic diagram of an arc evaporator (horizontal arrangement of electrodes) . (A) Carbonaceous hard deposit grown on the end of the cathode is called "cylindrical hard deposit"; (B) soot grown on surfaces of the cathode is "chamber soot"; (C) soot deposited on the ceiling of the evaporator is "cathode soot"(Saito et al. Carbon 38,169(2000))

Poster

SYNTHESIS, STRUCTURAL, ELECTRICAL AND MAGNETO-OPTICAL CHARACTERIZATION OF PbSe QUANTUM WIRES

M. Brumer, M. Bashouti and Efrat Lifshitz, Dept. of Chemistry and Solid State Institute, Technion, Haifa, 32000, Israel (ssefrat@tx.technion.ac.il)

Semiconductor quantum wires (QWs) are attracting much attention in recent years, due to their rich physical phenomena, differing substantially from the bulk or quantum-dots counterparts. Novel properties are expected in semiconductor QWs, such as enhanced conductivity along the wire, linear polarized optical transitions and long spin-lattice relaxation, all tunable with the width, length (the aspect ratio=length/width) and properties of the surface. This work describes the change in the electronic, electrical, optical and magneto-optical properties of PbSe QWs, upon a change in their width, length and surface properties. The PbSe QWs were selectively chosen for the present study due to their optical activity at the IR spectra regime and the strong size confinement effect on their exciton emission. The research focused on the following issues: (a) Development of colloidal synthesis, which led to a free standing QWs with controlled aspect ratio; (b) Determination of the growth mechanism, governed by initiation of catalyst seed, stabilizing surfactants and thermodynamic and kinetic processes; (c) Capping of the QWs with various organic ligands; (d) Determination of the structural and morphological properties of the aforementioned QWs; (e) Determination of the magneto-optical properties of the materials such as, linear Zeeman splitting of electron and hole energy levels, the spectroscopic g-factor, and angular momentum of electronic states; (f) Electrical transport property of a single QW and its dependence on the physical dimensions and the surface quality.

The colloidal synthesis was carried out at low temperatures (10-117°C), using alkyl-diamines as the surfactants. The crystallographic and morphological properties of the QWs were examined by high-resolution scanning and transmission electron microscopy (HR-SEM and HR-TEM) and electron diffraction (ED). The results showed that a delicate balance between electrostatic and steric interactions, temperature and duration of the reaction, determines the nanocrystallines' shape. Wires with a ~20 nm diameter and a 1-5 μm length are formed at the lowest temperatures (e.g., figure 1), while quantum-rods and cubes are formed at elevated temperatures. Short alkyl-diamine (e.g., ethylene diamine) chains permitted the growth of crystalline wires, while a long organic chain (e.g., hexane diamine) hindered the formation of an ordered structure. The optical (quantum size effect) and magneto-optical (Zeeman splitting, g-factors, angular momentum) properties were investigated by the use of linearly and circularly polarized photoluminescence (LP- and CP-PL) in the presence of an external magnetic field (under resonant/nonresonant excitation). Representative CP-PL measurement is shown in figure 2). The last revealed an angular momentum of J=1/2 for both, the valence and conduction band edges, with similar g-factor (g_e-g_h=0.1). The time-resolved CP-PL showed a relatively long spin relaxation (~70 nsec), showing a potential use in spinstronics devices. The electrical properties of the QWs were studied by measuring the conductivity of a single QW (deposited between metal leads) with a two-probe technique. This electrical measurements showed a typical specific resistance of ρ=0.15 Ωcm (e.g., figure 3).

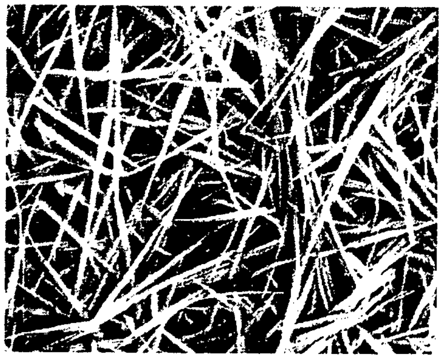

Figur 1: Scanning tunneling micrograph of PbSe nanowires (full scale = 5 μm)

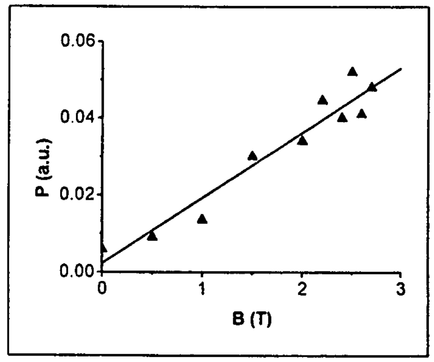

Figure 2: Degree of circular polarization [$P=(\sigma^+ - \sigma^-)/(\sigma^+ + \sigma^-)$] versus strength of an external magnetic field, B (at T=1.4 K), when $P=(g_e-g_h)\mu_B B/4kT$.

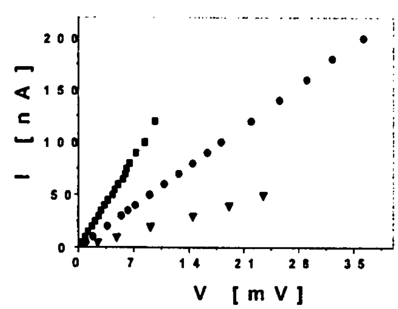

Figure 3: A typical I-V curve of three different single PbSe QWs, measured between two Ag leads (treated with e. beam lithography).

MOVING MOLECULES: DYNAMICAL MODELING AND A NEW STM MANIPULATION TECHNIQUE

S.A. Burke, J.M. LeDue, J.C. Neima, H.J. Kreuzer, M.H. Jericho
email: sarah.burke@mail.mcgill.ca

Since the rise of Scanning Probe Microscopy, the idea of having "hands" as well as "eyes" in this nanoscale world has intrigued those who have entered the field. Experiments involving controlled modification of systems on this scale are becoming increasingly routine, even though the manipulation processes are often not well understood.

To better understand the underlying mechanisms for the contolled manipulation of molecules on surfaces using a Scanning Tunneling Microscope (STM) tip, a classical model of the STM tip–adparticle–substrate system has been developed [1]. The full dynamical equations of motion are solved numerically revealing that net forces of ~1nN on the adparticle during manipulation give rise to kinetic energies of several hundred meV. Results from the simulations agree well with other modelling studies [2] and previously reported experimental results [3].

The model is also used to test a novel new form of manipulation where the tip is circulated around the adparticle, trapping it while the tip is then translated. The model suggests that this technique may be the method of choice on substrates where the adparticle is strongly bound.

Preliminary experimental results for the circulation method applied to C_{60} on Si(111) at room temperature can be interpreted within the framework of the model and will be presented.

References

[1] J.M. LeDue, H.J. Kreuzer, S.A. Burke, M.H. Jericho, and J.C. Neima. Dynamical modeling of STM manipulations of molecules on surfaces. Surface Science Letters, 538(1–2):L465–L470, 2003.

[2] A. K¨uhnle, G. Meyer, S.W. Hla, and K.-H. Rieder. Understanding atom movement during lateral manipulation with the STM tip using a simple simulation method. Surface Science, 499:15, 2002.

[3] L. Bartels, G. Meyer, and K.-H. Rieder. Basic steps of lateral manipulation of single atoms and diatomic clusters with a scanning tunneling microscope tip. Physical Review Letters, 79(4):697, 1997.

CHEMFET ACTIVATION DERIVED FROM A MOLECULAR BINDING EVENT

C.P. Kubiak[1], R.G. Reifenberger[2], E.S. Burns[1]
email: eburns@ucsd.edu

[1]Department of Chemistry, University of California, San Diego, La Jolla, California, USA, 92093-0358

[2]Department of Physics, Purdue University, West Lafayette, Indiana, USA, 47907

The electrostatic potential of thiol derivatized organic molecules bound to the surface of a Au(111) substrate have been previously measured with a modified AFM.[1] Changes to the Self Assembled Monolayer (SAM) were shown to be detectable by monitoring the Surface Potential of the sample. A chemically reactive SAM has been developed that can reversibly bind small gas phase molecules. We have chosen the basic system previously reported in literature consisting of a zinc porphyrin axially ligated to 4-mercaptopyridine[2] and adapted it to a Ruthenium porphyrin. RuTPP(CO) (Ruthenium tetraphenylporphyrin Carbonyl) was self assembled onto a SAM of 4-mercaptopyridine on Au(111) through the pyridine nitrogen to test our ability at detecting a binding event. A binding event at the porphyrin metal center leads to a change in the surface potential of the SAM and activation of a Chemical Field-Effect Transistor (ChemFET) device. Using surface IR methods the axially bound CO mode at ~1978 cm^{-1} for the SAM can be seen. Ligand exchange reactions to substitute the sixth coordination site from CO to other small molecules such as NO are being investigated.

References

1) S. Howell, D. Kuila, B. Kasibhatla, C.P. Kubiak, D. Janes, R. Reifenberger, *Langmuir,* **2002**, *18*, 5120-5125.
2) Z. Zhang, and T. Imae, *Langmuir*, **2001**, *17*, 4564-4568

ChemFET Device

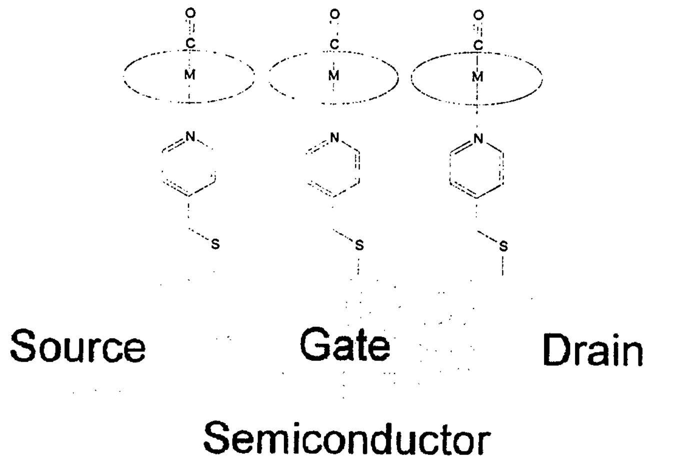

Binding of a molecule to the metal center leads to acitivation of the ChemFET

PARTICLE SIZE EFFECTS ON THE DIELECTRIC PROPERTIES OF $CaMn_7O_{12}$

A. Castro-Couceiro[1], B. Rivas-Murias[2], S. Yáñez Vilar[1], A. Fondado[2], J. Mira[2], J. Rivas[2] and M. A. Señarís-Rodríguez[1]
[1]Dpto. Química Fundamental, Universidade da Coruña, 15071 A Coruña, Spain.
[2]Dpto. Física Aplicada, Univ. de Santiago, 15782 Santiago de Compostela, Spain.

Recently, there is a considerable interest in the high dielectric constants ($\varepsilon' \sim 10^4$ at 300 K) displayed by some perovskite-type materials $ACu_3M_4O_{12}$ (A= Ca, etc; M= Ti, Fe, etc). Although this anomalous behaviour has been extensively investigated in order to know whether the dielectric properties of these systems are intrinsic or extrinsic, the origin of this high permittivity remains unclear [1, 2].

A related compound with similar structure, $CaMn_7O_{12}$, shows also an anomalous high dielectric constant [3]. In this work, we have prepared samples of $CaMn_7O_{12}$ with different particle size to see the effect of this parameter on the dielectric properties of this material. For this purpose we have synthezised the samples by the "Pechini" method, heating the precursor powders at different final temperatures. According to powder X-ray diffraction results, $CaMn_7O_{12}$ (space group $R\bar{3}$) is the major phase for all the samples. Nevertheless, extra peaks on XRD patterns reveal the presence of small amounts of Mn_2O_3 and Mn_3O_4 as secondary phases (<5%, estimated by Rietveld refinement).

SEM micrographs reveal that the grain size of the samples increases from 0.4 μm to 1 μm with the acumulative thermal treatements.

As an example Fig. 1 shows the temperature dependence of the dielectric constant of samples with different particle size and Fig. 2 their frequency dependence at 300 K. Meanwhile, Fig. 3 shows the frequency dependence of the dielectric loss tangent; $\tan \alpha = \varepsilon''/\varepsilon'$.

All the results reveal that, as the particle size increases, the dielectric properties of these materials improve. This is a somehow surprising result, as in traditional dielectric materials the dielectric properties are indeed enhanced as the number of grain boundaries increase.

In any case, these results clearly confirm that the origin of this anomalous high dielectric constant is intrinsic, and is not due to grain boundaries effect.

References:

[1] M. A. Subramanian, Dong Li, N. Duan, B. A. Reisner and A. W. Sleight, Jounal of Solid State Chemistry, 151 (2000) 323.
[2] P. Lunkenheimer, V. Bobnar, A.V. Pronin, A I. Ritus, A.A. Volkov and A. Loidl. Physical Review B, 66 (2002) 052105.
[3] J. Rivas, M. A. Señarís- Rodríguez, J. Mira, A. Fondado and B. Rivas-Murias, Spanish Patent Proposal N. P200300702, March 3, 2003.

Figures:

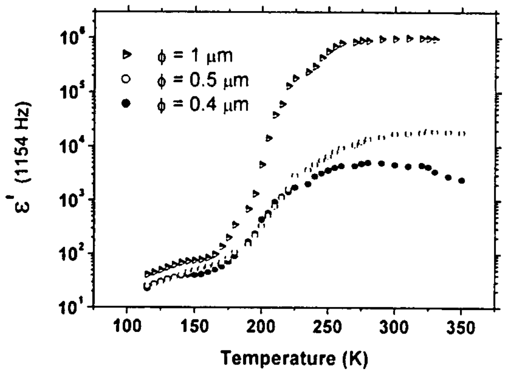

Fig. 1.: Evolution of the dielectric constant with temperature at 1154 Hz.

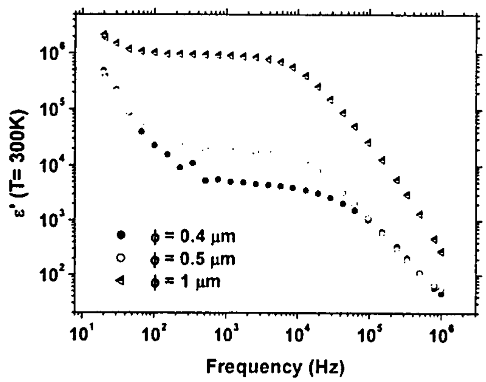

Fig. 2.: Dielectric constant vs frequency at 300 K in materials with different particle size.

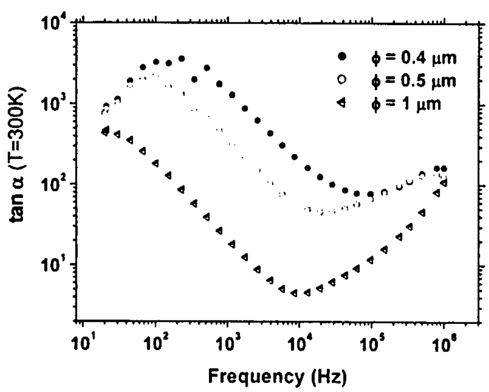

Fig. 3.: Dielectric loss tangent at 300 K.

SCANNING PROBE MICROSCOPY FOR ELECTRICAL CHARACTERISATION OF BIOLOGICAL SAMPLES

I.Casuso[1], G. Gomila[1], A. Errachid[1], O. Ruiz[1], J. Samitier[1], G. Ferrari[2], M. Sampietro[2], C. Pennetta[3], E. Alfinito[3], L. Reggiani[3], J. Bausells[4], N. Jaffrezic-Renault[5], E. Pajot-Augy[6] and R. Salesse[6]

[1]Research Centre for Biolectronics and Nanobioscience and Departament d'Electrónica, Universitat de Barcelona, C/ Martí i Franquès 1, 08028 Barcelona, Spain. E- mail: icasuso@pcb.ub.es http://www.nanobiolab.pcb.ub.es

[2]Dipartimento di Elettronica ed Informazione, Politecnico di Milano, Milano, Italy

[3]INFM-National Nanotechnology Laboratory and Dipartimento di Ingegneria dell'Innovazione, Universita di Lecce, Lecce, Italy.

[4]Instituto de Microelectrónica de Barcelona, Centro Nacional de Microelectrónica, CSIC, Barcelona, Spain.

[5]Laboratoire de Ingénierie et Fonctionalisation des Surfaces, École Centrale de Lyon-CNRS, Lyon, France.

[6]Laboratoire de Biologie Celluler et Moleculer, Institute National de la Recherche Agronomique, Jouy-en-Josas, France

Scanning Probe Microscopy (SPM) is one of the more versatile instruments for the characterization of surfaces with nanometre scale resolution. A part from its use in the realization of topographic images, many other functionalities have been developed in recent years. This has given rise to a bunch of different SPM modes, as for instance capacitance, resistance or magnetic modes [1].

Most of the modes developed so far have been designed for the study of solid state surfaces.

Only recently, these modes have been adapted to the special requirements of biological samples [2,3].

One of the modes whose adaptation to biology may turn out to be more interesting is the electrical mode, allowing the performance of current-voltage or impedance spectroscopy measurements on biological samples. This mode will help, in particular, the development of electronic nanbiosensors [4], with great impact in biomedical and environmental industries. In our Laboratory we have started the adaptation of a commercially available Scanning Probe Microscope to the realization of electrical measurements (current- voltage characteristics and impedance spectroscopy) on biological samples. This adaptation requires, among other things, the design and fabrication of special tips and electrochemical cells or the use of specific electronic instrumentation to adequately pre-amplify the electric signals [4].

In the present communication we will report on the advances performed so far in the adaptation of the SPM for electrical measurements on biological samples, and will present some preliminary results obtained on bacterias and proteins.

[1] "A practical guide to Scanning Probe Microscopy", Thermomicroscopes, 2001

[2] S. Lyndsay, "The scanning probe microscopy in Biology", preprint available at http://green.la.asu.edu/review/content.htm.

[3] V. J. Morris, A. R. Kirby and A. P. Gunning, Atomic Force Microscopy for Biologists, (Imperial College Press, London, 1999).

[4] "Single protein Nanobiosensor Grid Array", (IST-38899), http://nanobiolab.pcb.ub.es/projectes/spotnosed

NANOSCALED INORGANIC COMPOSITES FOR LOCALISED IN-VIVO HEAT GENERATION

Mathieu Chastellain
Powder Technology Laboratory, Swiss Federal Institute of Technology (EPFL), Switzerland
E-mail: mathieu.chastellain@epfl.ch
http://ltp.epfl.ch

Nanoscaled particles showing a superparamagnetic behaviour have been intensively studied these past years for various in vitro as well as in vivo bio-medical applications. Among them, well controlled magnetically induced heat generation inside a body is a promising mean to locally modify specific cells activities [1], [2].

For this purpose nanoparticles are placed in the zone to be treated and heat is generated by external magnetic excitation of the latter. The particles must fulfil several criteria such as biocompatibility and chemical inertness and must be able to interact with the external magnetic field, which is limited in terms of amplitude and frequency for physiological reasons. The particles must then be tailored so that to be sensitive to low energy excitations.

The present work presents the synthesis and characterisation of nanoscaled iron oxide particles embedded or coated with different compounds (Fig. 1 and 2). The particles composition, size distribution and magnetic properties are characterised and compared to the power loss generated when submitting them to low energy alternative magnetic fields (Fig. 3).

References:

[1] J.-C Bacri *et al.*, Scientific and Clinical Applications of Magnetic Carriers, (1997)

[2] A. Jordan, Journal of Magnetism and Magnetic Materials, **201** (1999) 413-419

Figures:

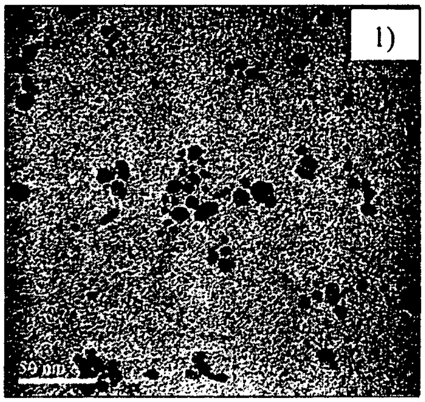

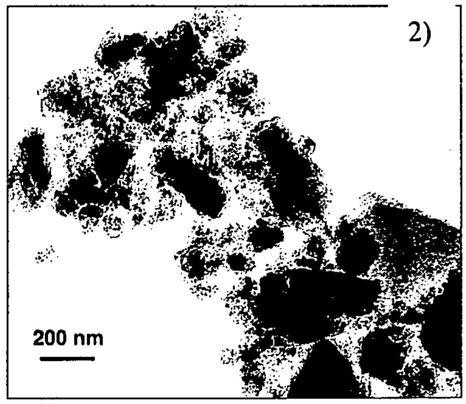

Fig. 1) Bright field TEM picture showing well separated bare iron oxide nanoparticles.

Fig. 2) Bright field TEM picture of iron oxide particles embedded in a silica matrix.

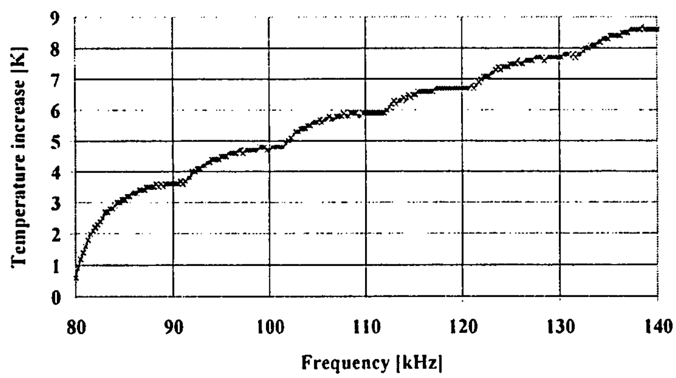

Fig. 3) Heating generated by silica embedded particles when submitted to an external alternative magnetic field of 6 mT and with varying frequencies.

HELICAL ROSETTE NANOTUBES AS MORE EFFECTIVE ORTHOPAEDIC IMPLANTS

A.L. Chun*, H. Fenniri† & T.J. Webster‡
Departments of Biomedical Engineering & Chemistry, Purdue University, 500 Central Drive, West Lafayette, IN 47907
Email: *ailin@purdue.edu, † hf@purdue.edu, ‡ twebster@ecn.purdue.edu

A class of organic nanotubes called helical rosette nanotubes (HRN) have been synthesized. They possess properties suited for various nanotechnology applications such as molecular electronic or photonic devices, drug delivery systems and also implant materials. These HRN are assembled from a single bicyclic block with a Guanine-Cytosine (GC) motif designed to have hydrogen-bond donor-donor-acceptor array on one side and complementary acceptor-donor array on the other side. These building blocks assemble through H-bonds to form the rosette, which then stack to form a nanotube with a hollow core 11 Å across and up to several micrometers long. The tube structure is maintained by electrostatic, hydrophobic and stacking interactions.

A variety of functional groups suited for different applications can be attached to these building blocks. With such flexibility and design, it is thought that these HRN are suited for orthopaedic implants since one can attach growth factors and/or specific bone recognition peptide sequences that will preferentially attract bone cell adhesion. Moreover, HRN possess biologically-inspired nanometer features that resemble naturally-occurring nanostructured constituent components in bone such as collagen fibers and hydroxyapatite ($Ca_{10}(PO_4)_6(OH)_2$) that bone cells are accustomed to interacting with. Previous studies have provided evidence of increased new bone synthesis on nanostructured ceramics, metals and polymers. Yet, currently used orthopaedic materials such as titanium do not possess desirable nanometer surface roughness. This is believed to be one of the reasons why titanium sometimes fails clinically as a bone implant material. In addition, reorganization of tissues adjacent to implants depends largely on protein adsorption, which in turn depends on the initial response of cells to a material. Implant surfaces therefore play an important role in forming the connection and integration between implant and tissue. Much effort has thus been dedicated to developing improved bioactive surfaces.

For the first time, to determine the possibility of utilizing this novel nanomaterial for bone implant applications, *in vitro* cytocompatibility properties of HRN-coated titanium were determined. Compared to uncoated titanium, these studies demonstrated increased osteoblast (bone-forming cell) functions on titanium coated with HRN possessing a lysine side chain (HRN-K1). Preferential osteoblast adherence on HRN-K1 over conventional titanium indicates that HRN-K1 is a non-toxic, cytocompatible and promising nanostructured material for bone tissue engineering applications. In addition, concentrations of HRN-K1 as low as 0.005mg/ml still showed enhanced cell adhesion. This is very encouraging since less material is needed to achieve the same increased cell adhesion properties. It is hoped that through the use of HRN, the optimal material to promote efficient new bone growth will be obtained. Such a criterion is critical for orthopaedic implant success.

DIHEXYLQUATERTHIOPHENE FIELD EFFECT TRANSISTORS FABRICATED BY NANOIMPRINT LITHOGRAPHY AND SOLUTION PROCESS

C.E. Clavijo Cedeño, A.P. Kam, and C.M. Sotomayor Torres

Institute of Materials Science & Dept. of Electrical Engineering, University of Wuppertal, Gauss-Str. 20, 42097 Wuppertal, Germany.

Email: clavijo@uni-wuppertal.de

Organic electronics is leading to interesting applications due to the use of low-cost techniques, as well as to the unique properties of organic-electronic devices. Several methods have been demonstrated which allow low-cost deposition of the organic materials in contrast to the time consuming and expensive high-temperature vacuum evaporation of inorganic semiconductors. Furthermore, the use of nanoimprint lithography (NIL) permits patterning of organic thin films and fabrication of nanometer-size interdigitated electrodes for field-effect transistors (FET) [1]. Figure 1 shows the interdigitated source and drain electrodes for FETs with a channel length (L) of 50 nm.

Previous experiments with organic FETs (OFETs) based on spin-coated dihexylquaterthiophene (DH4T) show low carrier mobilities as a result of non-uniform coverage of the channel using this method [2]. Nevertheless, there is room for improvement of the quality of the organic layer by optimizing the deposition parameters such as solvent, concentration, rotation speed and time. OFETs based on drop-cast deposited DH4T show relatively high mobilities for channel lengths above approximately 10 μm (See Figure 2) [3]. This is a consequence of the tendency of DH4T to form large crystallites with a size of the order of 10 μm when is drop-cast on hexamethyldisilazane (HMDS)-treated SiO_2 substrates. On the other hand, for L below 1 μm the field-effect mobility was drastically reduced. This result can be understood considering that filling of nanometer-size gaps on the substrate between source and drain by large DH4T crystallites is an unlikely process.

Alternative methods for deposition and formation of organic films from solution are Langmuir-Blodget (LB) deposition, dip coating and self-assembly. However, LB deposition requires amphiphilic molecules while DH4T has hexyl groups attached to both ends. In this work, we report on the optimization of the deposition of DH4T films on SiO_2 by spin- and dip coating in order to increase the field-effect mobility of short-channel-length OFETs. Preliminary results show an increase of two orders of magnitude in the field-effect mobility for cast films with respect to spin coated ones. Characterization of the film morphology was done by atomic-force microscopy (AFM) and charge transport was studied by current-voltage measurements on OFETs based on these films.

References:

[1] C.E. Clavijo Cedeño, J. Seekamp, A.P. Kam, T. Hoffmann, S. Zankovych, C.M. Sotomayor Torres, C. Menozzi, M. Cavallini, M. Murgia, G. Ruani, F. Biscarini, M. Behl, R. Zentel, J. Ahopelto. *Nanoimprint lithography for organic electronics*. Microelectron. Eng. **61-62** (2002) 25.

[2] C.E. Clavijo Cedeño, A.P. Kam, and C.M. Sotomayor Torres. Poster TNT2002. Santiago de Compostela. September 2002.

[3] C.E. Clavijo Cedeño and C.M. Sotomayor Torres. In preparation.

Figures:

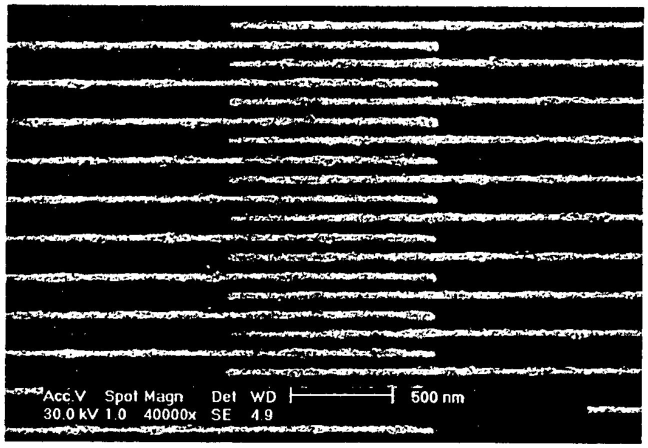

Figure 1. SEM image of interdigitated source and drain nanoelectrodes with a channel length of 50 nm made by EBL.

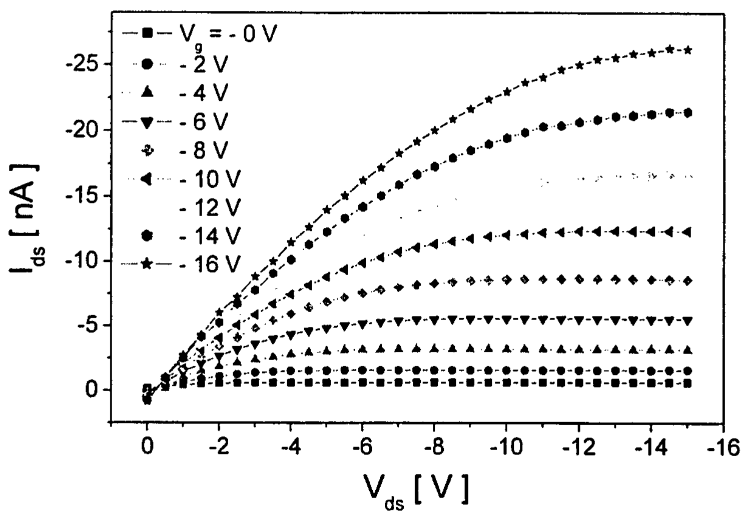

Figure 2. Current-voltage characteristics for a device with L = 200 μm and W = 425 μm. DH4T was drop cast deposited from a chloroform solution. The extracted field-effect mobility was $\mu = 6 \times 10^{-3}\, cm^2\, / Vs$.

ELECTROSTATIC FORCE MEASUREMENTS OF CARBON NANOTUBES, DNA-BASED MOLECULES AND GOLD NANO-RODS

Hezy Cohen,[1] Cristina Gomez-Navarro,[2] Julio Gomez-Herrero,[2] Gil Marcowich[3] and Danny Porath[1]

1.Physical Chemistry Department, The Hebrew University, Jerusalem, Israel
2.Departmento Fisica de la Materia Condensada, Universidad Autonoma de Madrid
3.The School of Chemistry, Tel Aviv University, Ramat Aviv, Israel.

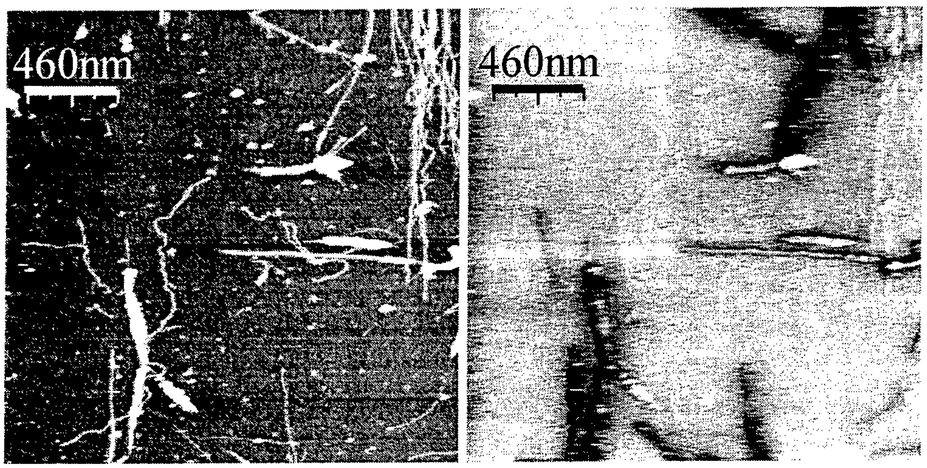

Figure: SFM topography image (2x2 μm^2) of SWCNT and G4-DNA wires having similar dimensions co-adsorbed on a mica substrate (left). A corresponding EFM map showing a frequency shift to lower values (dark signal) for some of the molecules, probably the SWCNT, due to internal polarization exerted by the external electrostatic field (right).

One of the central themes in nanoscience and nanotechnology is the study of the electrical properties of single molecules. This can be done using direct [1,2] or indirect [3,4] methods. Among the leading candidates for nanowires are the single walled carbon nanotubes (SWCNT) and DNA-based molecules.

We will present measurements of the electrostatic force between a metal tip and freestanding objects (gold nano-rods, carbon nanotubes and other DNA-based molecules), deposited on an insulating surface.

EFM enables to investigate electronic properties with no direct contact between the probe and the investigated object, thus eliminating the contacts problem usually encountered in transport measurements. It also reduces the probability of a mechanical deformation of the object by the probing tip. Topographic and corresponding

electrostatic maps will be shown and compared. The measurements were done with a scanning (atomic) force microscope (SFM) in tapping mode for the topographic images and using various advanced methods (plane, retrace and 3-D modes) for the electrostatics. The electrostatic signal was measured as a function of the object's dimensions and the results show the dependence of the electrostatic signal on these dimensions.

References:

[1] D. Porath, A. Bezryadin, S. de Vreis and C. Dekker, Nature (London), **403** (2000) 635.

[2] T. Shigematsu, K. Shimotani, C. Manabe, H. Watanabe and M. Shimitzu, J. Chem. Phys, **118** (2003) 4245.

[3] C. Gómez-Navarro, F. Moreno-Herrero, P.J. de Pablo, J. Colchero, J. Jómez-Herrero, and A.M. Baró PNAS, **99** (2002) 8484.

[4] M. Bockrath, N. Markovic, A. Shepard, M. Thinkham, L. Gurevich, L.p. Kouwenhoven, M.W. Wu and L.L. Sohn, Nano Lett, **2** (2002) 187.

Co GROWTH ON NANOSTRUCTURED Ag/Cu INTERFACES

Javier Cordón[1,2,*] and Enrique Ortega[2,3]
[1]Dpto. de Física de Materiales, Universidad del País Vasco, Manuel Lardizabal 3, 20018-San Sebastian, Spain
[2] Donostia International Physics Center & Centro Mixto CSIC-UPV, Manuel Lardizabal 4, San Sebastian,Spain
[3]Dpto. de Física Aplicada, Universidad del País Vasco, Plaza de Oñate 2, 20018-San Sebastian, Spain
*E-mail: waacovej@scsx03.sc.ehu.es
http://scsx01.sc.ehu.es/waporcoj/nanolab/nanolab.html

The Ag/Cu system can be used to tailor growth, and hence electronic and magnetic properties of Co nanostructures. Ag grows on Cu surfaces with little or negligible intermixing, leading to flat layers with sharp interfaces on Cu(111). On the other hand, periodic, striped Ag/Cu phases are induced by growing submonolayer amounts of Ag on Cu vicinal substrates [1]. Since Co and Ag also display little tendency to form mixed compounds, the idea is using Ag buffer layers and nanostructured templates to modify Co growth on Cu(111).

On flat Cu(111) Ag grows in a perfect layer-by-layer mode with very minor Ag/Cu mixing. Up to 4-5 layers, the Ag(111) surface is characterized by a quasi 10x10 Moiré superstructure, which is explained by a perfect Cu(111) substrate wetting. Ag adlayers display discrete, quantum well states in the perpendicular direction [2], as well as an almost linear decrease in the density of surface electrons [3]. Since both surface potential (Moiré corrugation) and electronic states are Ag-thickness-dependent and differ from Cu(111) or Ag(111) bulk crystals, we expect both Co nucleation and growth to proceed also in a different way. Thus our aim is studying the diffusion and aggregation behavior of two-dimensional Co clusters on Ag layers on Cu(111) by means of in-situ variable temperature STM measurements.

In Fig. 1 we show the STM image for 0.05 ML Co/0.5 Ag ML/Cu(111). Small Co dots nucleate on Ag covered areas, where the Moiré pattern is preserved. As shown in Fig. 2, from 1 ML to 2 ML cluster sizes double (from 28 to 47 Å, and from 3 to 5 Å height) and densities reduce to one half, suggesting faster adatom diffusion for 2 ML. Clusters nucleate at hollow places in the Moiré reconstruction, which are in turn nicely observed in the background. Images suggest very little Ag layer disruption, since there is a minor presence of point defects and superlattice distortions in the 1 ML buffer. Such defects are mostly suppressed at very low Co coverages. We do not observe any special cluster arrangement, discarding long range elastic or electronic interactions at this coverage and temperature [4].

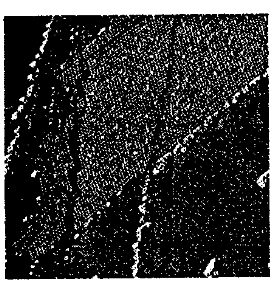

Fig. 1. *0.05 ML Co on 0.5 ML Ag covering Cu(111). Co forms tiny dots on top of the Ag Moiré, by contrast to step edge decoration and large triangular bilayer islands on Cu(111). (Image derivate, 200 nm, 1.5 V)*

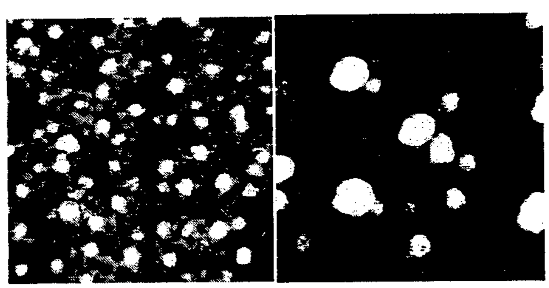

Fig. 2. *0.1 ML Co on 1 ML (left) and 2 ML (right) thick Ag buffer deposited on Cu(111) at 300K. Co cluster size doubles and the density reduces to one half for2 ML, revealing lower adatom diffusion barrier in this case. (Image 50 nm, 1.5 V).*

In contrast to flat Cu(111), Ag evaporation on stepped Cu(111) surfaces induces periodic faceting of the surface, i.e. phase separation of Ag-covered facets and clean Cu stripes [1]. The driving force is the lattice matching of Ag packed layers with different Cu planes, leading to a hierarchy among the different orientation of the Ag-covered facets observed, and hence to a rich morphology that depends on step density, step type and Ag coverage. Fig. 3 shows an example of such Ag/Cu periodic structure obtained in the particular case of Cu(775), with 8.5° miscut towards [11-2], and 0.4 ML of Ag. Current images or topographic derivatives along the horizontal show strong contrast between [773]-oriented Ag-covered facets (105 Å wide) and Cu(111) terraces (130 Å wide). The inset shows the details of the Ag covered facet, with its characteristic Moiré.

Varying substrate miscut and Ag coverage we have examined the stability of such nanostructure upon Co adsorption. The aim is keeping the striped morphology, thereby inducing one-dimensional magnetic behavior. Co adsorption follows the general rule found in infinite systems, i.e., bilayer islands decorating Cu steps and stripe edges while small Co dots nucleate across Ag facets. The topography still shows periodic facets, but the Moiré quickly vanishes and the derivate images loose their contrast. The Moiré and the derivative contrast is generally preserved at low coverage, as shown in Fig. 4 (a) for 0.3 ML. In this case, Co nucleates preferently at Cu stripe edges, and only minor amounts incorporate to Ag stripes. The homogeneity of the array is even improved with respect to Fig. 3, such that stripes are as long as 1 micron. Fig. 4 (b) shows the surface after additional adsorption of 0.4 ML Ag and 1.9 ML Co. We observe the same overall morphology and contrast, strongly suggesting that the Co content periodically changes across the striped structure. The magnetic properties of this Co stripe array are unknown.

Fig. 3. *Ag/Cu striped nanostructure grown on Cu(775). Cu(111) terraces alternate with Ag covered [773] facets (inset) (200nm, 1.5 V, image derivate along the horizontal direction).*

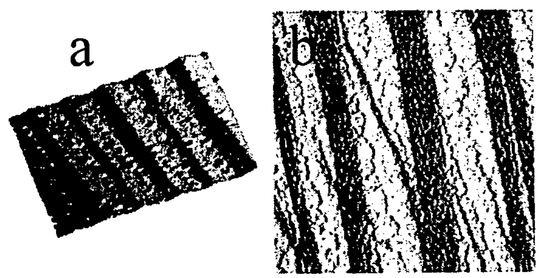

Fig. 4. (a) 0.3 ML *Co evaporation on the striped structure of Fig. 1. Co sticks preferently to steps and Ag stripe edges in Cu terraces (100nm). (b) The same surface after 0.8 ML of Ag and 2.2 ML of Co. The faceted structure and the contrast of Fig.1 is maintained, suggesting the presence of alternating stripes with different Co content (200nm, image derivate along the horizontal direction).*

References:

[1] A. Bachmann et al., Phys. Rev. B **64**, 153409 (2001); A Bachmann et al., Surf. Sci. **526,** L143 (2003).
[2] M. A. Mueller, T. Miller, and T.-C. Chiang, Phys. Rev. B **41**, 5214 (1990).
[3] A. P. Shapiro et al., Solid State Commun., **58**, 121 (1986).
[4] N. Knorr et al., Phys. Rev. B **65**, 115420 (2002).

PROTEIN-BASED BIOELECTRONIC HETEROSTRUCTURES

S. Crittenden*§, J. Hillebrecht†, S. Howell*, R. Reifenberger*, and R. R. Birge†
*Department of Physics, Purdue University, West Lafayette, IN, USA
†Department of Chemistry and Molecular and Cell Biology, University of Connecticut, Storrs, CT, USA
§scott@physics.purdue.edu

Abstract

Bioelectronics offers a potential alternative to Si-based technology because natural evolution and selection have optimized many biological molecules to perform tasks that can only be mimicked by complicated electronic circuits.

Purple membrane (PM) patches containing bacteriorhodopsin (BR) proteins could be harvested from the bacterium and used as the key light-absorbing unit in nanometer-size photodetectors that rely on many of the light sensitive properties inherent in the protein.

We used non-contact scanning probe microscopy to characterize BR films on multiple substrates. Wild type and a variety of mutants were studied. Conductive AFM was used to probe the I(V) characteristics of individual PM patches. A novel micron-scale patterning method was developed. Electrostatic force microscopy techniques were developed to study the photovoltage of PM multilayers on indium tin oxide substrates.

We find a humidity dependant photovoltage response under illumination by a 635 nm photodiode with peak photovoltage in excess of 2V at ~140W/m^2 for ~15% humidity[1]. I(V) data from individual PM patches show evidence for threshold conduction dependant on the relative humidity. Morphological studies show reduced structural stability of membrane patches for all mutants investigated. Taken together, these results reveal many new characteristics of BR that may be of significance for the design of future nanoscale devices.

References

1. S Crittenden, S Howell, R Reifenberger, J Hillebrecht, R Birge, *Nanotechnology* **14** No. 5 (May 2003) 562-565

STUDIES OF NANOSTRUCTURE FILM AND NANOSECOND LIFETIME OF LUMINESCENT POLYTHIOPHENE

Hai Ning Cui , Haiwon Lee, Vasco Teixeira

University of Minho, Physics Department, GRF-Functional Coatings Group, Campus de Azurém, PT-4800-058 Guimarães, PORTUGAL

The thin blend polymer film with nano structure is more important[1-2], when polymers are used as functional materials. It is also a novel method to prepare the micrometer- and nanometer- sized polymeric light emitting diode (LED) [2-3]. Until now one of the interesting candidate polymer is polythiophene [4]. The interest in organic electroluminescence (EL) was revived mainly by Tang and Van Slyke in 1987. Their multilayer device was fabricated by vacuum evaporation method. In recent years, the techniques to form thin films of polymers from solution (or call wet deposition method) were given much attention [5]. Here two wet deposition methods, spin coating and Langmuir-Blodgette (LB), have been used to fabricate the nano-morphology and nano-layer structure films.

In previous work the studies of Langmuir-Blodgette (LB) films of poly 3-(2-(5-chlorobenzotriazole) ethyl) thiophene (PCBET) [6] and energy transfer systems of LB Films of Porphyrins [7] were reported. Here the LB films and ultrasonic spin coating films of PCBET blended with amphibious arachidic acid (AA), Poly- (p- (methyl)-phenylmethacrylate (PMPMA) and polyvinylcarzole (PVK) were prepared and characterized respectively. AFM and LMF indicated that the domain of blend polymer film is of micro size. The energy transfer mechanisms in the blend films have been investigated by nanosecond time-resolved photoluminescence (PL) spectroscopy. The films have been investigated by UV-Vis, PL, fluorescence lifetime, ellipsometry and conductivity measurement. The dynamics of energy transfer in donor-acceptor blends of two combinations and concentration effect of luminescent polymer are crux. The PL and excited state lifetime results suggest that the energy transfer from PVK (and PMPMA) to PCBET leads to the enhancement of PL emission of PCBET. The blended AA molecules can improve the environment of luminescent polymer.

We show here that size controlled nanometer phase structure and nanometer thickness film of blend polymers can be obtained by a physical method under ultra thin phase separation (UTPS) concept. The tip of a modified AFM (atomic force microscopy) investigates the electrical characterization of UTPS in which there are the mono micro/nano phases of semiconductor polymer and insulating matrix. It can directly provide both morphology and electrical properties of micro domain of a blend film of conducting and insulating materials. The lateral force microscopy (LFM) confirmed the results of AFM. The results suggest that the blend leads to the forming of two different separated phase (PCBET and relative blend material).

Figure 1 shows the one of AFM images of the blend films in 4:6 (PCBET:PVK) mixing ratio. It is clear that special interpenetrated network (or nano-domains) is formed at this blend ratio. The domain size is in the range of 90-150 nanometer and the domains are formed mainly from the phase separation of polymers. The surface pressure-area (π–A) isotherms of PCBET /AA on subphase with different evaporating time are shown in Figure 2. This result let us deduce that the better LB condensed monolayer on subphase can be formed at least 28 minutes evaporating time. Much longer evaporating time is not needed. The thickness of 18 layers of PCBET/AA blend film is ~80 nm (one mono-molecular layer is) by result analysis of TEM and Ellipsometer.

After analysis UV absorption and PL spectra of all these films, the large spectral overlap between donor emission and acceptor absorption in the PCBET/PVK, PCBET/PMPMA blend means that energy transfer will be very efficient, and that the fluorescence decay dynamics of the donor polymer depend strongly on the energy transfer process and concentration effect. According as above data the PL spectra were measured after exciting at 235 and 422 nm respectively.

From PL spectra of Figure 3 the peak of PCBET at 600 nm is attributed to the result of energy transfer from PVK. The emission at 600 nm occurs at an excitation of 235 nm, because

the PL emission band (390-460 nm) of PVK overlaps the absorption band (350-440 nm) of PCBET. Under a 235 nm excitation the emission of pure PCBET film was not observed at 600 nm, because PCBET does not directly absorbs the 235 nm light. Interestingly, when the blend polymers were excited at 235 nm, the strong emission of PCBET was observed at 600nm, whereas the intensity of PVK emission in the region of 390-460 nm becomes very weak.

The dynamics of energy transfer in blend system was detailedly investigated by theory model and experiment. Some fluorescence lifetime values of PCBET, PVK, PCBET/PVK and PCBET/AA film are shown in Table 1. The lifetime difference of PCBET (LB) and PCBET (spin) is because oriented order of chains and thiophene rings can improve the environment of luminescence and decrease the non-radiative process after forming of the LB film. That is, the short lifetime 1.31 ns (nanosecond) of PCBET are probably due to aggregated species in the spin coating film of pure luminescent polymer.

The fluorescence lifetime of PCBET/PVK film (4:6) is 21.33 ns, which is between that of PCBET (spin) film (1.31 ns) and PVK film (44.01 ns). These results indicate that energy transfer exists from PVK to PCBET. The data from the concentration effect sample PCBET/AA could be fitted with single exponential component. It can be seen that with increasing concentration of AA, the lifetime of PCBET fluorescence decreases in LB film. This indicates that the non-radiative process of blend PCBET (LB) film becomes more efficient after mixing with AA molecules.

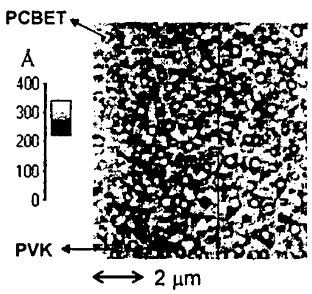

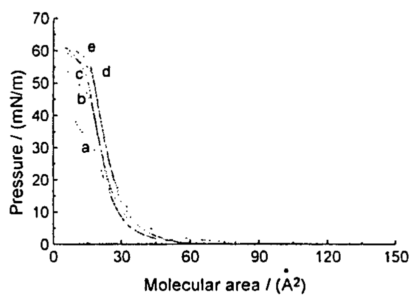

Fig.1. AFM images of PCBET/PVK films at 4:6 mixing ratio. **Fig.2.** π–A isotherms of PCBET/AA on subphase with different evaporating times (a) 10 min (b) 18 min (c) 28 min (d) 38 min (e) 88 min.

Table 1. The fluorescence lifetime values of the films

film	lifetime τ (ns)	χ^2	D.W.
PCBET(spin)	1.31	2.7	1.02
PCBET(LB)	3.33	1.9	1.03
PVK(spin)	44.01	1.8	0.98
PCBET/PVK(4:6)	21.33	1.4	2.10
PCBET/AA(1:2.5)	3.05	1.8	1.95
PCBET/AA(1:10)	1.04	1.4	1.40
PCBET/AA(1:14)	0.81	1.4	1.20

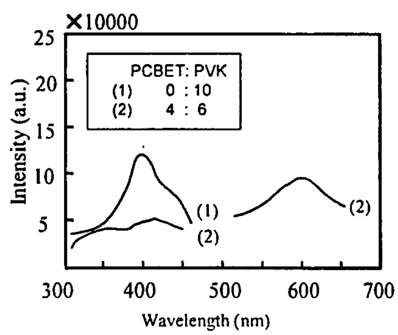

Fig.3. PL spectra of blend films excited at 235 nm.

References

1. Zhu, S.; Liu, Y.; Rafailovich, M. H.; Sokolov, J.; Gersappe, D.; Winesett, D. A.; Ade, H. Nature 1999, 400, 49.
2. Granstrom, M.; Berggren, M.; Inganas, O.; Indersson, M. R.; Huertberg, T.; Wennerstrom, U. Synth. Met. 1997, 85, 1193.
3. Granstrom, M.; Berggre, M.; Inganas, O. Science 1995, 267, 1479.
4. M. Granstrom, M. Berggre, O. Inganas, Science, 267, 1479 (1995).
5. R. Osterbacka, A. J. Pal, H. Stubb, Thin Solid Films, 327-329, 668(1998).
6. Lee,Y. M.; Ahn, J. H.; Kim, E.-R.; Lee, H. Mol. Cryst. Liq. Cryst. 1998, 316, 285.
7. Haining Cui, Wenyun Wang, Enle Zhou and Xiaoguang Zhao, Thin Solid Films 214(1992)238-242.

Nanofabrication by Step and Flash Imprint Lithography

Michael Dickey, Todd Bailey, Steve Johnson, E.K. Kim, Britain Smith,
Nick Stacey, C. G. Willson
Department of Chemical Engineering, University of Texas at Austin,
Austin, TX 78712
E-mail: dickey@che.utexas.edu
willson@che.utexas.edu
http://willson.cm.utexas.edu/

The fabrication of useful devices requires the ability to create arbitrary shapes of different materials accurately and to place them in juxtaposition with high accuracy. There are two approaches to fabricating structures with arbitrary but defined shapes that have dimensions on the length scale of nanometers. The highest resolution methodology is often described as "bottom up" and is exemplified by the stepwise arrangement of individual atoms by, for example, scanning tunneling microscopy techniques. These techniques represent the resolution limit for fabrication; single atom pixel arrangements. The other technique is often termed "top down" and is exemplified by photolithography. The resolution limit of microlithography is now in the range of hundreds of atoms, but it has the advantage of being able to transfer shape images at a data rate of hundreds of gigapixels per second while the single atom placement methodology runs at only about 0.2 pixels per second.[1] Is there hope for achieving controlled but arbitrary image placement at the high data rate derived from parallelism of microlithography and the resolution of the single atom techniques? This is the grand challenge! Step and flash imprint lithography[2] (SFIL) does not offer single atom resolution but it does offer a means to replicate structures with at least an order of magnitude higher resolution than photolithography[3] with no loss in data rate. SFIL has the potential to enable the manufacturing of many kinds of nanoscale structures with useful productivity rates.

The SFIL process, as depicted in Figure 1, utilizes transparent templates and UV curable materials to allow pattern replication at room temperature and low pressures. These process conditions facilitate improved template-substrate alignment as well as minimized magnification and distortion errors. [3] The process achieves high aspect ratio pattern transfer as seen in Figures 3-4, which is ideal for transistor formation, Figure 2. To merit consideration as a potential production methodology, SFIL must provide for high aspect ratio pattern transfer, economically feasible throughput, and controlled defect densities.

The etch barrier material properties are crucial to the effectiveness of SFIL. Vinyl ethers are under consideration as a replacement for acrylates due to the sensitivity of free-radical polymerizations to oxygen.

The status of the SFIL process will be presented together with examples of active structures that have been built by this technique.

References:

[1] P. A. Campbell, *et al.* Nanotechnology, 13(1), 69-74, (2002).
[2] S.V. Sreenivasan,*et al.*, Proc. SPIE 4688: (2002).
[3] S.C. Johnson, *et al.*, Proc. SPIE (in print): (2003).

Figures:

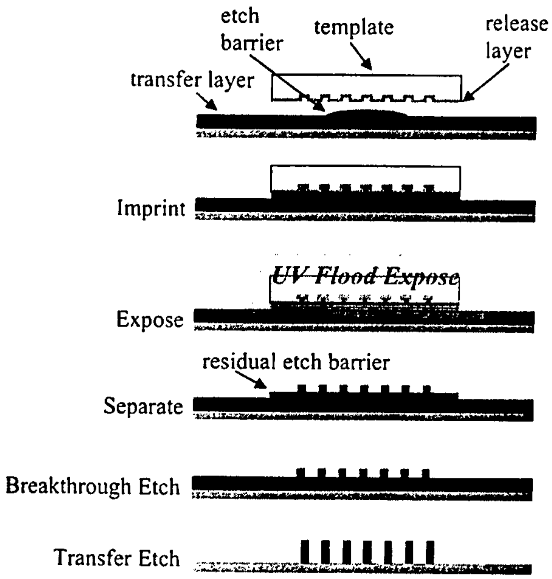

Figure 1. The SFIL process

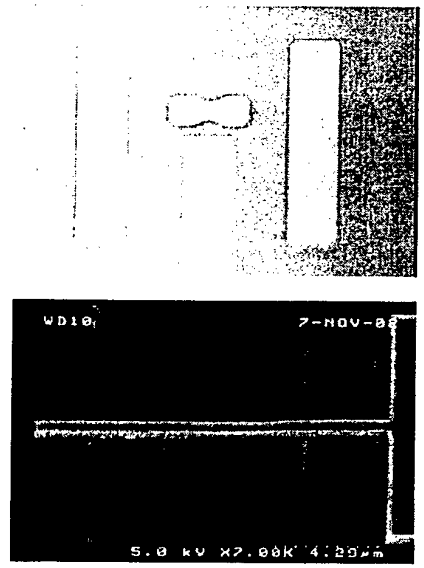

Figure 2. Transistor with 50 nm gate using SFIL (top), Larger transistor (bottom)

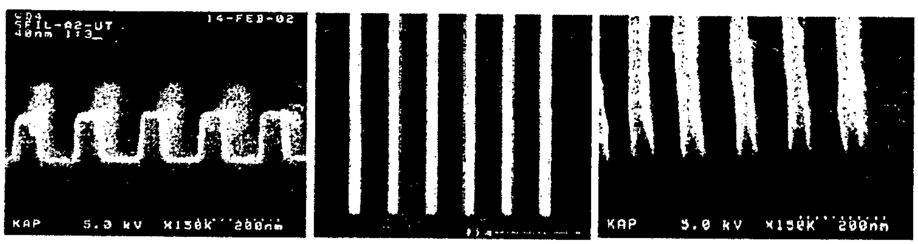

40 nm **30nm** **20nm**

Figure 3. Features fabricated using SFIL

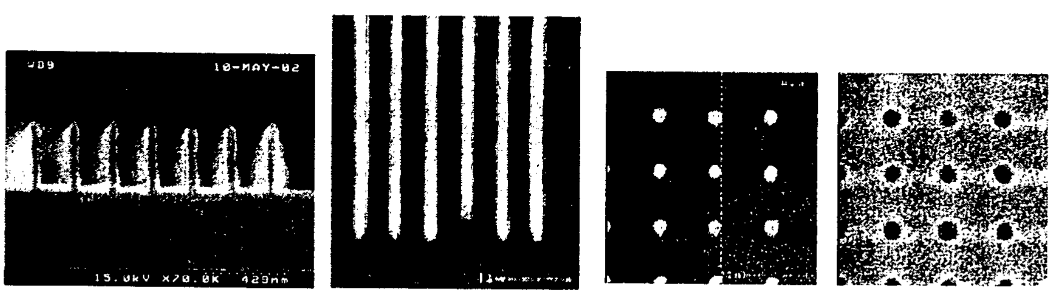

40nm 8:1 aspect ratio 20nm lines 40nm posts 40 nm holes

Figure 4. Various nanoscale features created using SFIL

Electric field assisted assembly of carbon nanotubes between microfabricated electrodes

Maria Dimaki, Kristian Mølhave, Peter Bøggild

Mikroelektronik Centret, Technical University of Denmark, Oersteds Plads, Building 345 east, DK-2800 Kgs. Lyngby, Denmark

Since their discovery in 1991 carbon nanotubes (CNT) have been investigated thoroughly due to their astonishing electrical and mechanical properties. One of the biggest problems with CNT is the difficulty involved with handling them in order to integrate them in novel devices such as field effect transistors. So far various methods have been used in order to manipulate and place the tubes, however the final position of the tube and thus of the device is difficult to know in advance. Several methods have been suggested such as chemical patterning, fluid flow or electric field directed growth and/or assembly [1-3].

In this report we show how an alternating current (AC) electric field can assemble carbon nanotubes between two microfabricated electrodes extending over the edge of a chip. The tubes are dispersed in isopropanol by ultrasonication for periods from 10 minutes to 4 hours. The quality of the solution is evaluated from Scanning Electron Microscope (SEM) images (figure 1). The electrodes used have various shapes and sizes. For our experiments we use electrode spacings (distance between the middle of two neighbouring electrodes) of 2-16 μm. An example is given in figure 2.

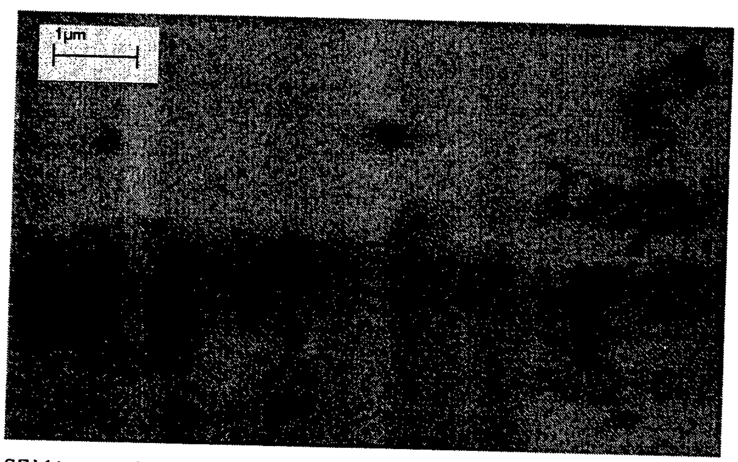

***Figure 1.** SEM image of multiwall carbon nanotubes on a gold substrate. The tubes were dispersed in isopropanol and ultrasonicated for 3 hours*

Theoretical calculations based on the work of Asokan et al. [4] show that a carbon nanotube of 3 μm length in an AC field will experience a force, which for frequencies up to at least 8 MHz will drag it towards regions of high electric field. This is termed positive dielectrophoresis and is in accordance with observations of CNT behaviour under the influence of an AC field. Moreover the AC field will exert a torque on the tubes which will align them along the field lines.

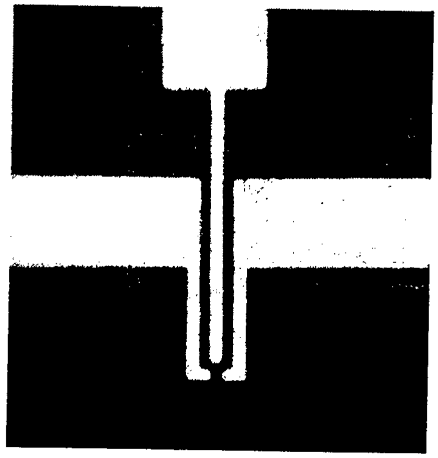

Figure 2. One of the electrode structures used for the experiments. The suspended electrodes are 10 μm long and 2 μm wide.

In our experiments we have used frequencies over 5 KHz and voltages of 1-10 V. We see that the tubes tend to assemble in bundles at regions where there is an electric field. At regions where the field is negligible there are still carbon nanotubes but significantly less and randomly placed (figure 3). We believe this is caused by the evaporation of the isopropanol under which the tubes are left behind at random positions. The bridges created have resistances from a few kΩ to up to a few hundred kΩ.

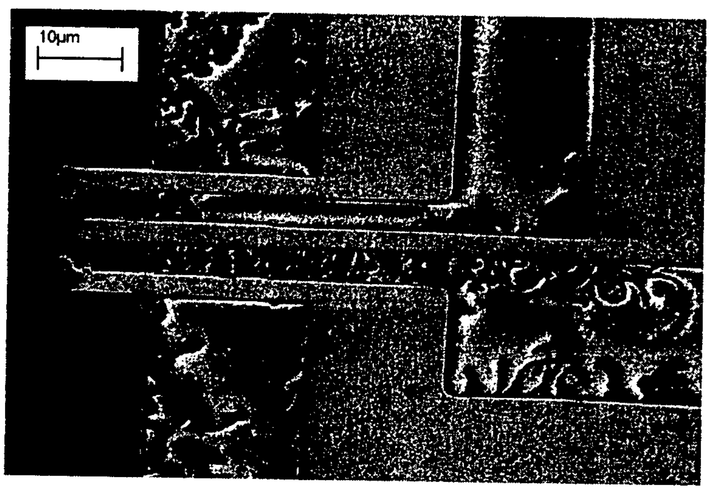

Figure 3. By applying voltage between the lower two electrodes we can preferentially assemble the nanotubes between them. The tubes in the remaining regions can be seen assembling there during the evaporation of the solution.

[1] Chen et al., Applied Physics Letters Vol. 78, No. 23, p. 3714-3716, 2001
[2] Rawlett et al., Nanotechnology 14, p.377-384, 2003
[3] Huang et al., Science Vol. 291 Issue 5504, p.630-633, 2001
[4] Asokan et al., Nanoletters, Vol. 3 No. 4, p. 431-437, 2003

FIELD EMISSION STABILITY OF CARBON NANOTUBES

M.W. Docter, C.W. Hagen, and P. Kruit

Delft University of Technology, Faculty of Applied Sciences, Lorentzweg 1,
2628 CJ Delft, The Netherlands
Corresponding author, E-mail: hagen@cpo.tn.tudelft.nl

There are three main requirements for an electron source in a probe-forming instrument. First a high reduced brightness, which determines the current in the probe. Second a small energy spread, to reduce the effect of chromatic aberration of the probe-forming optics on the probe size. And last but not least, a high current stability and a long lifetime. Carbon nanotubes (CNT) are believed to fulfill at least two of these requirements. The small diameter of CNT's implies a small virtual source size, and therefore a high reduced brightness, and the high chemical and mechanical stability may lead to a high emission current stability and a long lifetime as well.

About four years after the discovery of carbon nanotubes (CNT's) in 1991 [1], research started on CNT's as field emitter [2]. Since then a number of researchers have reported on field emission energy distribution measurements [3,4], brightness estimates [5,6], and emission stability [7-11]. In this work we focus on the stability. Other groups have shown that the field emission images of CNT's on a phosphor screen are different from the images of metal cold field emitters, such as tungsten for instance. The images consist of spots arranged in pentagons and/or hexagons for capped CNT's, and spots arranged in a ring shape for open CNT's. The spots are sensitive to adsorbed gas molecules, which manifests itself in an emission change of the particular site where the gas atom is adsorbed. Depending on the type of gas the emission change after adsorption may be reversible after heat treatment of the CNT. All studies of the influence of gas molecules and gas pressure on the emission stability that we are aware of, give qualitative descriptions and rather speculative explanations of the experimental observations. It is our objective to study this more quantitatively.

The samples we study are obtained from Hata et al. [10], and consist of tiny rods, produced by an arc discharge method, containing multiwalled carbon nanotubes. A rod is glued, using carbon glue, on a tungsten wire loop (wire diameter of 160 μm), and mounted on a xyzr-manipulator in an Ultra-High-Vacuum (UHV) chamber, containing a micro-channel plate and a phosphor screen at about 20 mm distance from the sample. The wire loop allows resistive heating of the sample to desorb any adsorbed gas molecules. Easy sample exchange is facilitated by a load-lock chamber with a linear motion feedthrough to transport the sample to the manipulator. When a voltage is applied between the microchannelplate and the sample the emission current is measured and the emission images on the phosphor screen are captured with a CCD camera.

In fig. 1a a typical emission image of a CNT, preheated to 1100 °C (as determined from pyrometry), is shown. A pentagonal structure is present in the center, surrounded by 5 other patterns which could be either pentagonal or hexagonal. To illustrate this, in fig. 1b some guides to the eye are drawn in the image of fig. 1a. Sometimes the emission from one particular site in this pattern changes. There are different kinds of changes that may occur. First there is the emission increase of one particular site. This could be due to an adsorbed gas molecules coming out of the gas environment or traveling by diffusion over the CNT surface. Then a bright site might jump to another site, probably due to diffusion of the adsorbed molecule. Or a bright site splits into two emitting sites, as is seen in fig. 2a and b, resp. Also two or more adjacent bright sites may show interference fringes, visible as black

lines between sites. Many of these observations have been described by others, but were not always fully explained. We will quantitatively determine the effect that gas pressure has on the number of changes and/or the types of changes in the emission patterns. Then we will study the temperature dependence of the emission patterns, to determine the rate of changes per emission site as a function of temperature. Furthermore we will determine in a similar quantitative way what the effect is of different gas molecules on the emission patterns.
First results will be presented at the conference.

Acknowledgement:
Dr. K. Hata and Prof. dr. Y. Saito from Mie University, Kamihama, Tsu, Japan, are gratefully acknowledged for providing the samples through Dr. N. de Jonge from Philips Research Laboratories, Eindhoven, The Netherlands.

References:
[1] S. Iijima, Nature 354, 56 (1991)
[2] W.A. de Heer, A. Châtelain and D. Ugarte, Science 270, 1179 (1995)
[3] K.A. Dean, O. Groening, O.M. Küttel, and L. Schlapbach, Appl. Phys. Lett. 75, 2773 (1999)
[4] M.J. Fransen, Th.L. van Rooy, P. Kruit, Appl. Surf. Science 146, 312 (1999)
[5] N. de Jonge, N.J. van Druten, Ultramicroscopy 95, 85 (2003)
[6] N. de Jonge, Y. Lamy, K. Schoots, and T.H. Oosterkamp, Nature 420, 393 (2002)
[7] K.A. Dean, B.R. Chalamala, J. Appl. Phys. 85, 3832 (1999)
[8] K.A. Dean, P. von Allmen, B.R. Chalamala, J. Vac. Sci. Technol. B17, 1959 (1999)
[9] K. Hata, A. Takahura, and Y. Saito, Surface Science 490, 296 (2001)
[10] K. Hata, A. Takahura, Y. Saito, Ultramicroscopy 95, 107 (2003)
[11] K.A. Dean, B.R. Chalamala, J. Vac. Sci. Technol. B21, 868 (2003)

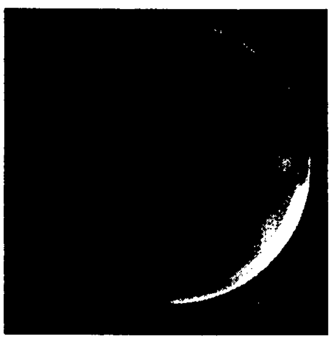

Fig. 1a A typical emission pattern of a multiwalled CNT, at $1.6 \cdot 10^{-6}$ mbar N_2, 2.1 kV extraction voltage, and pre-heated at 1100 °C.

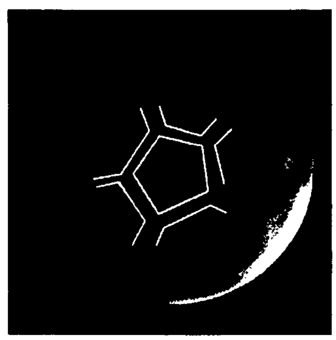

Fig. 1b The lines are guides to the eye to identify the pentagon and/or hexagon patterns in fig. 1a

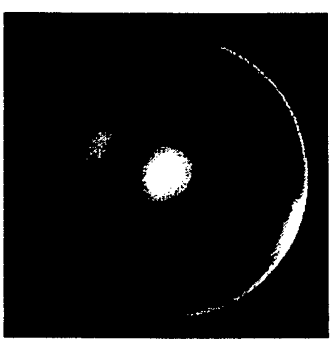

Fig. 2a Enhanced emission in the centre part of the pattern, at $1.8 \cdot 10^{-10}$ mbar, 2.1 kV extraction voltage, pre-heated at 1100 °C.

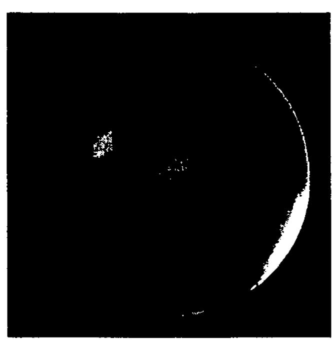

Fig. 2b Same pattern as in fig. 2a, but 2 sec. later. The central spot decreases in intensity and splits in two parts.

NON-RADIATIVE HEAT TRANSFER BETWEEN SILICA NANOPARTICLES: A MOLECULAR DYNAMICS APPROACH

Gilberto Domingues
Laboratoire d'Etudes Thermiques, 86961 Futuroscope Cedex, France

Sebastian Volz, Karl Joulain and Jean-Jacques Greffet
Laboratoire d'Energétique Macroscopique et Moléculaire, Combustion,
Grande Voie des Vignes, Châtenay Malabry 92295, France
volz@em2c.ecp.fr

Due to their thermal insulating properties [1], amorphous silica structures are included in aerogels as nanoparticles (NP). The main contribution to heat transfer in aerogel is supposed to be related to heat conduction between coalesced particles. However it was shown that a heat flux can also be exchange through near field non-radiative contributions which are dramatically increased when the bodies are separated by a few nanometers [2]. This phenomenon is related to the presence of phonon-polaritons in the material such as silica and was predicted based on the fluctuation-dissipation theorem and Maxwell equations including a 'macroscopic' dielectric constant. On a fundamental point of view, the phonon-polariton contribution to the heat transfer between two NPs also represents a basic and general problem, especially when the inter-particles distance is of smaller scale than the macroscopic one.

We propose a Molecular Dynamics (MD) approach to analyze heat transfer between two silica NPs which are close together. Molecular Dynamics technique consists in the computation of all the atomic positions and velocities. The full BKS potential [3] was programmed to calculate the forces between any couple of atoms. There is neither potential cut-off nor limited neighbors list.

The numerical experiment is as follows: the two particles are heated up to two different temperatures in separate simulations by using a conventional gaussian thermostat. The thermostats are removed and an equilibration period leads to a temperature relaxation. This equilibration allows us to remove any thermostat artifacts. Since the time integration is performed through the 5th order Gear predictor-corrector scheme, all the coordinates are saved (positions, velocities, accelerations, first and second time derivative of accelerations) and input in the next simulation step where the particle are put close together (Figure 1). To maintain the inter-NP distance the center of mass of each was fixed. The temperature time evolution of both NPs are then calculated.

We derive the exchange coefficient between both NPs from the temperatures signals. Several conclusions are finally discussed regarding the heat transfer rate and the dynamic properties of the exchange heat flux.

References:

[1] G. Domingues, J.-B. Saulnier, S. Volz, Superlattices and Microstructures, to be published.
[2] J.-P. Mulet, K. Joulain, R. Carminati, J.-J. Greffet, Applied Physics Letters, 78 (2001) 2931.
[3] B.W.H.vanBeest,G.J.Kramer, R.A vanSanten, Physical Review Letters, (1990) .

Figures:

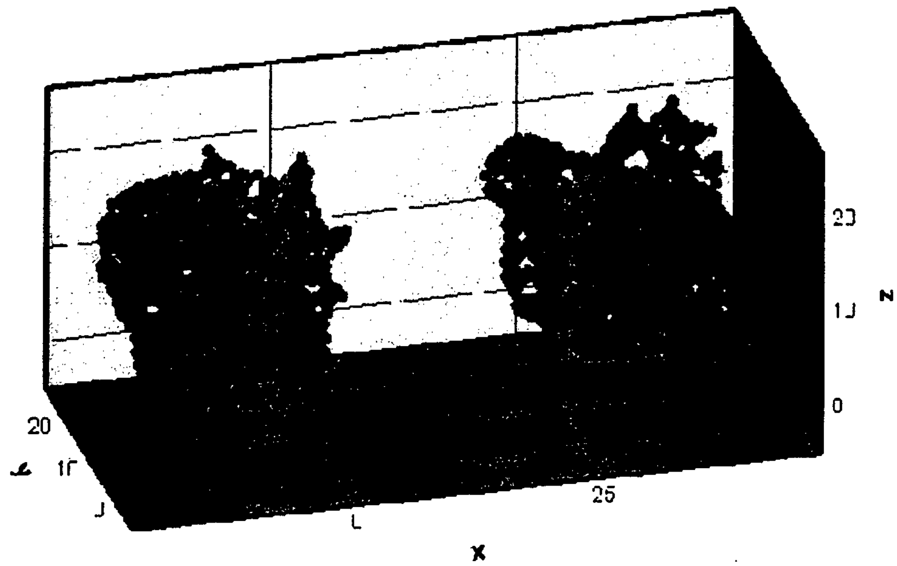

Figure 1: View of the simulated silica particles. The red dots are oxygens atoms and the blue ones represent silicon atoms.

ANALYSIS OF THE BONDING OF H IN THE $Al_{13}H$ CLUSTER

Fernando Duque, Ángel Mañanes,
Departamento de Física Moderna. Universidad de Cantabria. 39005 Santander, Spain.
Francisco Méndez
Departamento de Química. Visión de Ciencias Básicas e Ingeniería.
Universidad Autónoma Metropolitana-Iztapalapa. 09340 México D. F., México
María José López[1], and J. A. Alonso[1,2]
[1]Departamento de Física Teórica. Universidad de Valladolid. 47011 Valladolid, Spain.
[2]DIPC, 20018 San Sebastian, Spain.
E-mail: duquef@unican.es , mananesa@unican.es

Several groups [1] have studied ways of doping Al_{13} in order to form highly stable closed-shell clusters that could act as candidates for novel cluster-assembled materials. The cluster considered in this work, $Al_{13}H$, has a closed shell configuration and is obtained by adding a hydrogen atom to Al_{13}. The experiments [2] have shown that $Al_{13}H$ presents a high stability, and molecular dynamics simulations have predicted that a solid assembled from $Al_{13}H$ clusters may be stable up to 150 K [3].

In the present work, the bonding of hydrogen in the $Al_{13}H$ aggregate is analyzed using the deformation densities and the Fukui functions within the framework of density functional theory, DFT. Although those local concepts have been used before for typical molecular reactions, the present results are an example of the virtuality of the Fukui analysis to study a reaction involving a metallic cluster.

The two panels of the Figure show the charge transfer due to the presence of the H atom over the centre of one of the triangular faces of the oblate icosahedron, which is the equilibrium geometry of the Al_{13} aggregate. Continuous lines indicate an increment of the electronic charge, dash dotted line correspond to the zero, and those regions from which electrons are taken to form the Al_{13} – H bond, are indicated by the dashed lines. There is a net charge transfer from the aggregate to the H site. For the aggregates Al_{13} and $Al_{13}H$ there is a constant density contour, with a value only slightly larger than in bulk aluminum, which encloses the atomic cores. The electron density plots suggest metallic character for Al_{13} and also that the H atom behaves as a proton screened by the electron gas.

The Fukui functions of Al_{13} have maximum values precisely at those sites (Hollow sites) where the H atom is predicted to be located by the total energy calculations, and this fact justifies the preference for those particular locations at the surface of the aggregate. So, the Fukui functions, obtained from ground state calculations for the separate reactants, can be used as meaningful reactivity indexes in studying the interaction of atomic species with metallic clusters. Those reactivity indexes can help to interpret, and moreover to predict, the equilibrium structures found from total energy calculations. Moreover, our study opens up new and relatively simple ways for investigating not only the actual location of the impurity in other metallic aggregates, like those recently synthesized $Al_{12}X^-$ (X=C, Ge, Sn, Pb), but also the formation of cluster--assembled materials based on the study of the local Fukui functions and indexes of the corresponding building clusters.

References:

[1] A. Mañanes, F. Duque, F. Méndez, M. J. López, and J. A. Alonso, J. Chem. Phys., (To be published) (2003).
[2] S. Burkart, N. Blessing, B. Klipp, J. Müller, G. Ganteför, and G. Seifert, Chem. Phys. Lett., **301**, 546 (1999).
[3] J. A. Alonso, M. J. López, L. M. Molina, F. Duque, and A. Mañanes, Nanotechnology, **13** (2002) 253.

Figures:

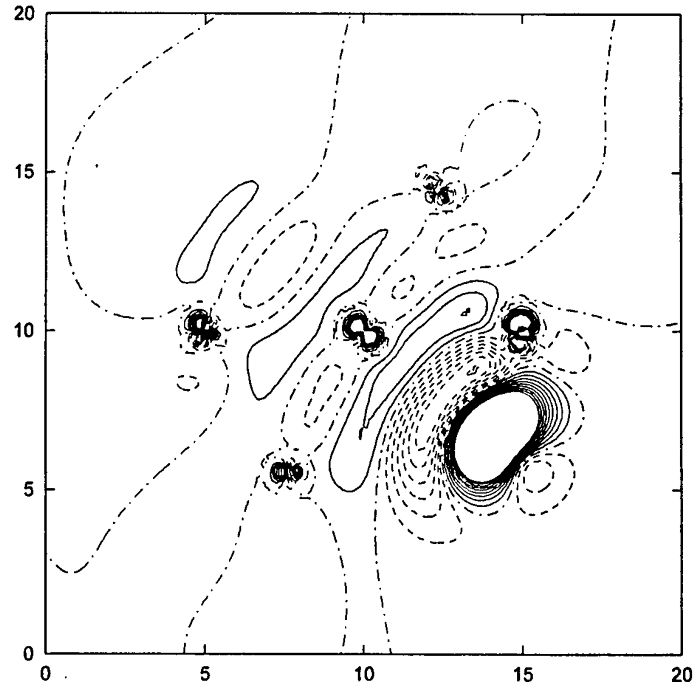

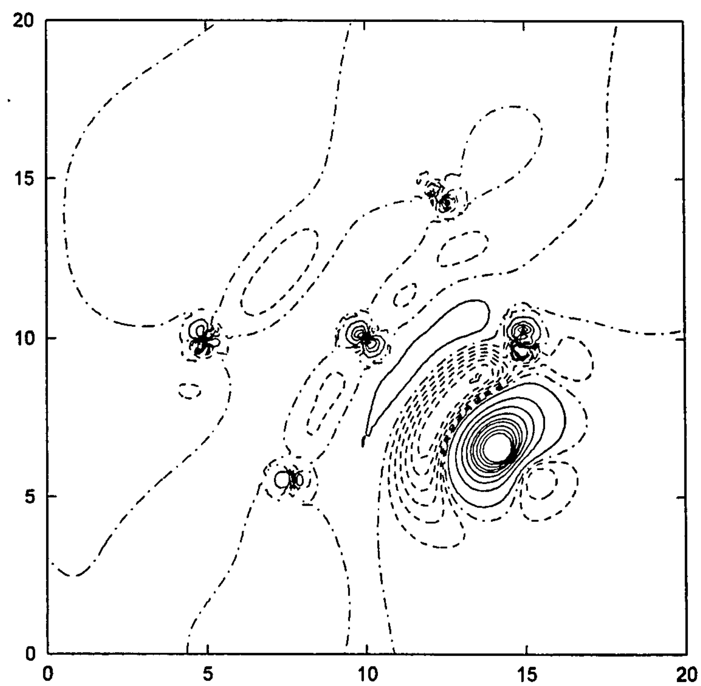

SIZE EFFECTS IN EXCHANGE BIASED NANOSTRUCTURES

Johannes Eisenmenger[1,2], Zhipan Li[1], Oleg Petracic[1], Igor Roschkin[1], Changpen Li[1], Kai Liu[1,3], J. Nogués[4], C. Leighton[5], H. Masuda[6], K. Nishio[6], Ivan K. Schuller[1]

[1]Department of Physics, University of California San Diego, La Jolla, California 92093-0319,
[2]Abteilung Festkörperphysik, Universität Ulm, 89069 Ulm, Germany
[3]Department of Physics, University of California, Davis, California 95616
[4] Institució Catalana de Recerca i Estudis Avancats (ICREA) and Departament de Física, Universitat Autònoma de Barcelona, 08193 Bellaterra, Spain
[5] Department of Chemical Engineering and Materials Science, University of Minnesota, Minneapolis, Minnesota 55455
[6]Applied Chemistry Department, Tokyo Metropolitan University, Hachioji, Tokyo 192-0397, Japan

Nanostructured magnets exhibit interesting physical phenomena and are the subject of intense activity due to their basic research interest and existing and potential applications in a variety of areas. An important issue is the thermal stability of magnetic nanostructures since the anisotropy energy that stabilizes the magnetization scales with the volume. When magnetic materials approach nanometer sizes their magnetic energy becomes comparable to thermal energy at room temperature. Thus thermal fluctuations can destroy the stable magnetization in these small nanostructured magnets. Such instabilities are, already today, one of the biggest problems in the magnetic recording industry [1]. The solution to the superparamagnetic limitation is complex. A possible solution is to bring the ferromagnetic (FM) nanostructure in close contact to an antiferromagnetic (AF) material. The exchange interaction at the interface between both materials adds additional unidirectional anisotropy energy to the systems which can stabilize the magnetization. The unidirectional anisotropy in the AF, initialized by field cooling the sample below the Néel temperature or preparing the AF within an external field, causes a shift of the hysteresis loop of the FM by the so-called exchange bias field. The explanation of this effect is a long-standing problem in condensed matter physics. Progress, theoretical and experimental, has been made in understanding the phenomenology and mechanisms of the exchange bias effect (for reviews see [2]). However detailed mechanisms of the interfacial exchange still remain unclear. In the exchange bias phenomenon one characteristic length scale is the size of the magnetic domains in both ferromagnet and antiferromagnet, which are believed crucial to the mechanism. Patterning films on comparable length scales in the nanometer range changes the magnetic properties and allows to probe various influences on the exchange bias more independently like interface roughness, shape anisotropy, and domain structure in the AFM/FM structures.

In this work we investigate the size effect in patterned FeF_2/Fe bilayers, where the (110) orientation of the twinned, epitaxial, antiferromagnetic FeF_2 layer suggests a completely compensated surface, i.e. the two AF magnetic sublattices point in opposite directions and there is ideally no magnetic net moment. The Fe layer is polycrystalline. Due to extensive experimental and theoretical work on unpatterned biased FeF_2/Fe bilayer this system particularly qualifies to extend those studies towards the investigation of size effects in patterned AFM/FM bilayers. Exchanged biased Fe nanodots on FeF_2 films where fabricated by ion-milling through polymer masks produced by e-beam lithography or a lift-off process of nano-porous alumina masks after evaporation through its pores. The magnetic properties where measured by SQUID magnetometry and magneto-optic Kerr effect (MOKE).

In comparison to the sheet film the magnetization curves of the nanostructured films are significantly changed. Depending on the size of the patterned structures, the change in coercivity, exchange bias and their temperature dependence behaves differently. The differences are discussed in terms of the various influences like i.e. shape anisotropy, interface roughness, domains in FM and AFM layer. For certain structure sizes the patterning process even affects the left-hand and right-hand side of the hysteresis loop differently. This result suggests the significance of different domain structures in the ferromagnetic layer, which are often neglected in present theories of exchange bias. However, considering domains lead to a better understanding of various aspects in exchange biased systems and play certainly an important role in applications.

This work has been supported by the AFOSR, (F49620-01-0393) and in part by the U.C. Davis-New Faculty Research Grant, the Catalan DGR (2001SGR0018), the NEXBIAS European Network (HPRN-CT-2002-0029), and the Alexander von Humboldt Foundation. The authors thank O. Nakamura for establishing the contacts between UCSD and TMU.

References:

[1] Charap, S.H., P.-L. Lu, and Y. He, *IEEE Trans. Magn.* **33**, 978 (1997).

[2] Nogues J. & Schuller I. K. *J. Magn. Magn. Mat.* **192**, (1999) 203; Berkowitz, A.E. and K. Takano, *J. Magn. Magn. Mater.* **200**, 552 (1999); Stamps, R.L., *J. Phys. D: Appl. Phys.* **33**, R247 (2000).

Figure 1: Sketch of ferromagnetic Fe dots on an antiferromagnetic FeF_2 layer.

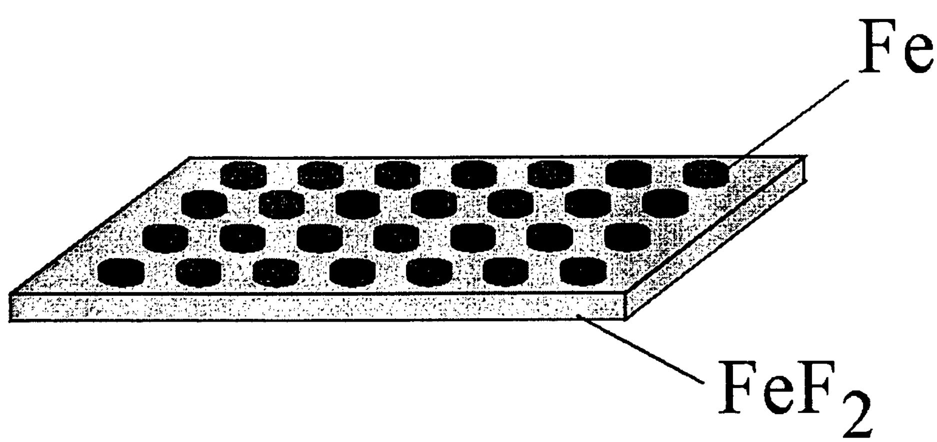

INFLUENCE OF THE CORROSION ON THE SURFACE MAGNETIC DENSITY IN NANOCRYSTALLINE AND AMORPHOUS $Fe_{73.5}Cu_1Nb_3Si_{13.5}B_9$ ALLOY

M. Tejedor, J. A. García, L. Elbaile*, J. D. Santos
Depto. de Física, Universidad de Oviedo. C/ Calvo Sotelo s/n, 33007 Oviedo, Spain.
E-mail: elbaile@pinon.ccu.uniovi.es

A. R. Pierna, G. Vara, F. F. Marzo
Departamento de Ingeniería Química y Medio Ambiente. Universidad del País Vasco.
P.O. Box 1379, 20080 San Sebastian, Spain.

Different articles [1,2] have been devoted to study the corrosion resistance of nanocrystalline materials and metallic glasses because their mechanical and magnetic behaviour is affected by it. Nowadays these materials are used in different technical applications due to their good magnetic properties. In these applications the materials have to work in some cases in aggressive environments that could affect their magnetic properties. In addition, some of these materials are corroded in atmospheric conditions [3]. Then, it is necessary to study how the corrosion affects the magnetic properties of these nanocrystalline and amorphous materials.

Taking into account that corrosion affects mainly the surface characteristics of the material due to the formation of a non-conductive oxide layer in the surface of the samples [4,5], the influence of corrosion on the magnetic properties is a surface phenomena and then, the surface magnetic properties would be the most affected by corrosion.

In this article we present a study of the variation of the surface magnetization with corrosion in $Fe_{73.5}Cu_1Nb_3Si_{13.5}B_9$ in the amorphous and nanocrystalline states.
The amorphous and nanocrystalline samples were oxidized by application of consecutive potential cycles at various sweeps rates in highly alkaline solutions. The surface magnetization was obtained using the transversal magneto-optical Kerr effect.
The results show that after oxidation both surfaces of the ribbons (the air and wheel surface) have the same surface magnetization and then all the study is carried out only in the air surface of the samples.

Other important result is the fact that in the amorphous samples the saturation surface magnetization decreases from 5% to 21% when the oxide surface layer increases from 87 Å to 156 Å.

Finally, after different annealing to produce the nanocrystallization of the samples the results show that the oxidized and not-oxidized samples have the same surface saturation magnetization but it is reached firstly in the not-oxidized samples as is shown in the figure 1 for the samples nanocrystallized after annealing of 60 min. at 520° C.
All these results are explained in the basis of the oxide layer formed in the oxidized samples.

References:

[1] A.Pardo, E. Otero, M. C. Merino, M. D. López, M. Vázquez and P. Agudo, Corros. Sci. 44 (2002) 1993.

[2] M. F. López, M. L. Escudero, E. Vida and A. R. Pierna, Electrochimica Acta 42 (1997) 659.

[3] G. N. Maniar, T. A. Dehold, Adv. Matter. Proc. 1 (1998) 57.

[4] S. Li and J. L. Lou, Corros. Sci. 44 (2002) 1695.

[5] M. F. López, M. L. Escudero, E. Vida, A. R. Pierna, A. Lorenzo, F. F. Mayo, A. Altube and M. Sistiaga, J. Non-Cryst. Solids 235-237 (1998) 796.

Figure:

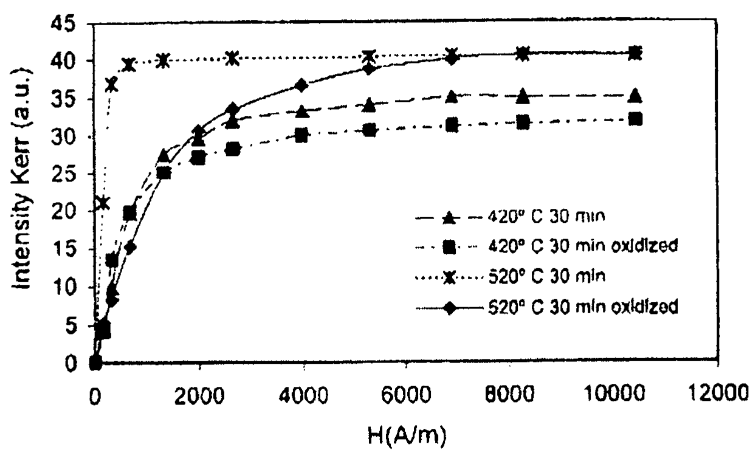

Poster

CONDUCTANCE DISTRIBUTIONS IN QUASI-ONE DIMENSIONAL WIRES: BULK *VERSUS* SURFACE DISORDER

L.S. Froufe-Pérez[1], P. García-Mochales[2], P.A. Serena[3], and J.J. Sáenz[1]

[1]Departamento de Física de la Materia Condensada, and Instituto "Nicolás Cabrera", Universidad Autónoma de Madrid, E-28049 Madrid, Spain.
[2]Instituto de Microelectrónica de Madrid, Centro Nacional de Microelectrónica, Consejo Superior de Investigaciones Científicas, Tres Cantos, E-28049 Madrid, Spain.
[3]Instituto de Ciencia de Materiales de Madrid, Consejo Superior de Investigaciones Científicas, Campus de Cantoblanco, E-28049 Madrid, Spain.

The study of electronic transport through quasi-one-dimensional (Q1D) systems will allow to design future nanoelectronics devices based on metallic nanowires, carbon nanotubes, specific molecules, etc. In such systems, the electronic transport is governed by few conducting channels whose transmission probabilities depend on the system geometry as well as the presence of scattering centers (impurities, vacancies, defects, surface corrugation, etc). Weakly disordered systems (i.e. the electron mean free path l is larger than the system length L; $l/L>1$) are featured by ballistic electronic transport. For increasing disorder (i.e., $L/l >> 1$) diffusive and localized regimes appear [1]. The study of such mesoscopic systems requires a statistical analysis in order to obtain the evolution of the conductance G *versus* the scaling parameter L/l. However, a more valuable information is obtained from the conductance distribution P(G) associated to a given value L/l (i.e. a given average conductance $<G>$). The interpretation of P(G) has been a controversial matter for a long time from a basic point of view. However, notice that P(G) contains essential information to analyze the repeatability of a conductance value for a set of systems fabricated with identical nominal conditions (length, composition, etc). In addition, an accurate knowledge of P(G) is of importance in other fields as in the study waveguides [2].

The electron transport problem in Q1D systems has been afforded in the context of the scaling equation derived by Dorokhov, Mello, Pereyra and Kumar (the so-called the DMPK approach) [3] as well as the Random Matrix Theory (RMT) [4]. Under both approaches, many analytical results have been proposed for the distribution P(G). In particular many studies focused on the crossover region from diffusive to localization regimes[5,6,7]. Very recently [8], we have obtained P(G) distributions using Monte Carlo (MC) approaches showing excellent agreement with numerical Tight-Binding (TB) simulations of bulk disordered (Anderson-like) two-dimensional (2D) systems. However, these results (both, MC and TB) were at variance with calculations on surface disordered wires (SDW) with a free electron model [7,9]. In particular, conductance distributions in the crossover region are rather different when considering surface and bulk disordered systems.

The aim of this work is to analyze the situations where P(G) follows the DMPK predictions and to understand the origin of the deviations of P(G) when some system parameters are varied. Working in the TB framework, we have developed a model to simulate surface (lateral) disorder: Given a nanowire of width N, the disorder is applied on L_W rows (the nearest to one edge of the nanowire). Within these L_W rows, the type of disorder used is Anderson: on-site energies are uniformely distributed between $-W/2$ and $W/2$. The non-disordered zone has zero on-site energy. We have carried out intensive simulations for a huge amount of systems (with time-reversal symmetry) where different parameters have been changed: (disorder strength, width of region where disorder appears (i.e. number of lateral rows L_W affected by the disorder), number of propagating channels, ratio of propagating and evanescent modes, etc). Our results show a non-trivial dependence of P(G) on the system. The results indicate that the presence of strong surface disorder as well as the existence of few propagating modes modify the DMPK P(G) distributions. For example, in Figure 1 we show the variation of P(G) with the disorder stregth (for fixed L_W=3) and how changes from a DMPK like distribution (obtained previously for bulk disorder [5]) to a chaotic cavity like distribution (obtained formerly with surface disorder [7]). In figure 2 it is shown how, changing the propagating/evanescent modes proportion, the distribution varies from a DMPK like to a chaotic cavity like distribution. In the present work we will discuss the reasons leading to the deviation from the DMPK-like behavior of P(G).

References:

[1] B.L. Al'tshuler. P.A. Lee and R.A. Webb, *Mesoscopic Phenomena in Solids* (North Holland, Amsterdam, 1991).
[2] D.S. Wiersma, *et al.*, Nature **390**, 671 (1997); A.A. Chabanov, M. Stoytchev and A.Z. Genack, Nature **404**, 850 (2000).
[3] O.N. Dorokhov, JETP Lett. **36**. 318 (1982); P.A. Mello, P. Pereyra, and N. Kumar, Ann. Phys. (N.Y.) **181**, 290 (1988).
[4] C.W.J. Beenakker, Rev. Mod. Phys. **69**, 731 (1997).
[5] S.A. van Langen, P.W. Brower, and C.W.J. Beenakker, Phys. Rev. E **53**, R1344 (1996).
[6] V.A. Gopar, K.A. Muttalib and P. Wölfle, Phys. Rev. B **66**, 174204 (2002).
[7] A. García-Martín and J.J. Sáenz, Phys. Rev. Lett. **87**, 116603 (2001).
[8] L.S. Froufe-Pérez *et al.*, Phys. Rev. Lett. **89**, 246403 (2002).
[9] M. Leadbeater, V.I. Falko, C.J. Lambert, Phys. Rev. Lett. **81**, 1274 (1998).

Figures:

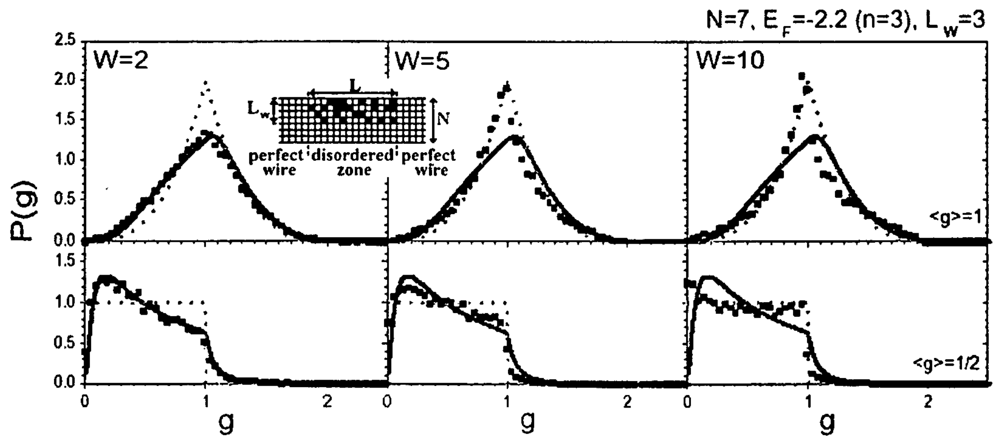

FIGURE 1. Conductance distributions $P(g=G/G_0=G/(2e^2/h))$ (squares) for different disorder strengths (W). In this case the wire has N=7 sites width, with L_W=3 rows affected by disorder; the Fermi energy E_F determines the presence of only n=3 propagating channels. Upper row illustrates the case <g>=1, whereas the lower one corresponds to <g>=0.5. The continuous line denotes the MC solutions to the DMPK scaling equation [5]. Dashed lines represent the RMT solution for a chaotic cavity [7]. Inset: sketch of the model of disorder used.

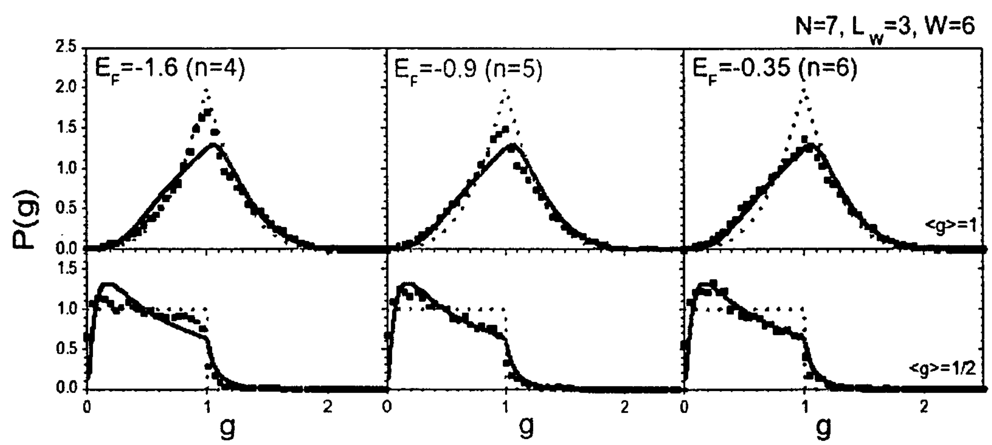

FIGURE 2.. Conductance distributions $P(g=G/G_0)$ (squares) for different number of propagating modes (n=4,5,6). The disorder strength and disorder zone take constant values W=6 and L_W=3 respectively. Upper row illustrates the case <g>=1, whereas the lower one corresponds to <g>=0.5. The continuous line denotes the MC solutions to the DMPK scaling equation [5]. Dashed lines represent the RMT solution for a chaotic cavity [7].

Poster

INTENSITY CORRELATIONS AND FLUCTUATIONS OF TRANSMITTED AND REFLECTED WAVES IN RANDOM MEDIA

L.S. Froufe-Pérez[1], A. García-Martín[2] and J.J. Sáenz[1]

[1]Departamento de Física de la Materia Condensada, and Instituto "Nicolás Cabrera",

Universidad Autónoma de Madrid, E-28049 Madrid, Spain.

[2]Instituto de Microelectrónica de Madrid, Centro Nacional de Microelectrónica,

Consejo Superior de Investigaciones Científicas, Tres Cantos, E-28049 Madrid, Spain.

Todays nanotechnology concepts for new electronic devices are crucially determined by the ``physics of the small scale", in other words, mesoscopic phenomena in condensed matter drives the behavior of nano-devices. Practically any device is designed in such a way that its transport properties are previously chosen to fit certain requirements. Hence, in order to massively produce any device, it is important to control the reproducibility of its transport properties. Since long time ago, it is known that coherent scattering is important in mesoscopic physics, more over, this implies that large sample to sample fluctuations are expected to be found in the transport properties of this systems. Thus, a good knowledge about these fluctuations on the transport coefficients of mesoscopic systems is required if large scale manufacture of the same device is required.

The phenomenology related to mesoscopic solid state systems in connection with electronic transport is much more general. The wave-like behavior of electrons allows us to generalize the basic ideas and results on electron transport through disordered media to the propagation of virtually any wave in a disordered medium. Theoretically and experimentally many facts has been shown to be essentially the same with electrons or with electromagnetic waves.

The propagation of waves through random media produces complex, irregular intensity distributions (*speckle* patterns) [1] which are not nearly as random as intuition suggests. The statistical behavior of such patterns is dominated by the underlying correlations between transport coefficients. In the last decades much attention has been focused on this subject in connection with the discovery of interesting multiple scattering effects [2]. Different phenomena like the enhanced coherent backscattering and intensity correlations in transmitted and reflected electromagnetic and other classical waves are closely connected to weak localization and universal conductance fluctuations (UCF) in electron transport. These interesting phenomena are not restricted to the case of volume scattering. Enhanced backscattering and correlations of the *speckle pattern* intensity arising in the light scattering from randomly rough surfaces have been intensively investigated. Recently much attention has been paid to the reported experimental observation of strong localization and universal conductance fluctuations of light [3].

In this work we add some more insight on the knowledge of correlations and fluctuations of relevant transport coefficients. For this purpose we work on a simplified set of systems known as *quasi-one-dimensional* systems, which can be thought as wires in the context of electronic transport or electromagnetic waveguides when classical waves are addressed. The main feature we will assume for these systems is that scattering is perfectly elastic, i.e. the length of the system is always much smaller than the phase coherence length. In addition, we will have a well defined (and usually small) number of transport channels, since the transversal energy spectrum is discretized.

In order to achieve some understanding about the statistical properties of such systems, one of the most used theoretical tool is the Random Matrix Theory (RMT) [4]. Within this framework, the scattering matrix associated with each sample (for instance a nanowire) belongs to an ensemble of random matrices. Therefore, we can obtain through the statistics of the random scattering matrices, the desired statistical properties for transport coefficients.

Our main focus will be the correlations between reflection coefficients of different channels. If R_{ab} represents the reflection coefficient of a wave incoming from the channel labeled by *a*, and outgoing to the channel labeled by *b*, the correlations are defined as $C^{RR}_{ab\,a'b'} = \langle \delta R_{ab}\, \delta R_{a'b'} \rangle$ where $\delta R_{ab} = R_{ab} - \langle R_{ab} \rangle$. Using standard RMT techniques it can be shown that, under the isotropy assumption, the structure of the RR correlations can be written as:

$$C^{RR}_{ab\,a'b'} = \langle R_{ab} \rangle \langle R_{a'b'} \rangle \left\{ [\delta_{aa'}\, \delta_{bb}' + \delta_{ab'} \delta_{a'b} - \delta_{aba'b'}]\, C_1^{RR}(s) + [\delta_{aa'} + \delta_{bb}' + \delta_{ab'} + \delta_{a'}] C_2^{RR}(s) + C_3^{RR}(s) \right\}$$

Where $C_i^{RR}(s)$ will only depend on the length of the system L normalized to the elastic mean free path l , s=L/l, and on the number of propagating modes.

These functions can be calculated using the results obtained from the solution of the so-called Dorokhov-Mello-Pereyra-Kumar (DMPK) equation, a Fokker-Plank-like equation describing the evolution of the statistics of transport eigenchannels [4,5].

In order to verify the results obtained from RMT we have compared the $C_i^{RR}(s)$ with those obtained using other different methods. First, the coefficients are calculated using standard Monte Carlo techniques on the known solutions of the DMPK equation [6]. Second, we have performed numerical calculations for 'microscopic' scattering models. We have used two different models, bulk disordered waveguides (BDW) in which a lossless waveguide if filled with a collection of scatterers whose strength is randomly chosen, and surface disordered waveguides (SDW), an also lossless waveguide where one of its boundaries is considered to be randomly corrugated.

The scattering in BDW is known to be quite isotropic, thus BDW is very close to fulfill the RMT isotropy requirements. On the other hand, SDW present strong scattering anisotropy [7]. Quite Interestingly, the RMT results can be applied even for of strongly anisotropic systems [8], indicating this fact that the RMT 'macroscopic' approach is applicable in a wide variety of situations. To illustrate this fact, we have plotted in the figure $C_{2,3}^{RR}(s)$ for 5 propagating modes (N) and for the three models. As expected, BDW correlations fit RMT predictions almost perfectly, however, the case of SDW it is not so good but, even in this case, the qualitative behavior is very well captured, although some other statistical properties might differ [8].

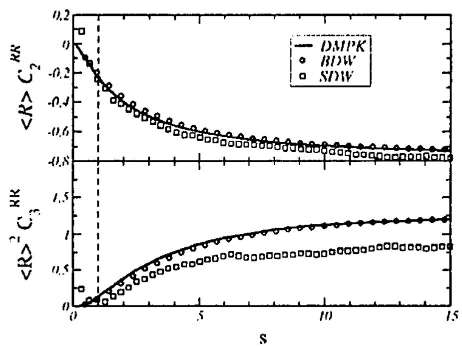

Fig. 1 $C_{2,3}^{RR}(s)$ coefficients for a 5 propagating modes waveguide. Continuous line shows the exact DMPK results while circles and squares correspond respectively to Bulk disordered waveguides and Surface Disordered waveguides, dashed line correspond to a mean free path.

Here we will also show the interplay between correlations and fluctuations, the role of energy and flux conservation and the constrains on the correlations coefficients given by this conservation [9].

References

[1] J.C. Dainty (Ed.), *Laser speckle patterns and related phenomena*, (Springer-Verlag, Berlin, 1984).

[2]P. Sebbah (Ed.), *Waves and Imaging in Complex Media*, (Kluwer, Dordretch, 2001).

[3]D.S. Wiersma *et al.*, Nature **390**, 671 (1997); *ibid.***398**, 207 (1999); F. Scheffold and G. Maret, *ibid.***398**, 206 (1999) ; A. A. Chabanov, M. Stoytchev, and A. Z. Genack, *ibid.* **404**, 850 (2000); J. Gómez-Rivas et al., Phys. Rev. E **63**, 046613 (2001).

[4]C.W.J Beenakker, Rev. Mod. Phys. **69**, 731 (1997)

[5] O.N. Dorokhov, JETP Lett. **36**, 318 (1982); P.A. Mello, P. Pereyra, and N. Kumar, Ann. Phys. (N.Y.) **181**, 290 (1988)

[6] L.S. Froufe-Pérez, P. García-Mochales , P.A. Serena, P.A. Mello and J.J. Sáenz , Phys. Rev. Lett. **89**, 246403 (2002).[7]A. García-Martín, J.A. Torres, J.J. Sáenz and M. Nieto-Vesperinas, Phys. Rev. Lett. **80**, 4165 (1998).

[8]A. García-Martín, F. Scheffold, M. Nieto-Vesperinas and J.J. Sáenz, Phys. Rev. Lett. **88**, 143901 (2002).

[9] J.J. Sáenz, L.S. Froufe-Pérez and A. García-Martín, to appear in NATO Science Series (2003).

DESIGN OF BIOSENSORS: NEW PROTOCOLS TO ACHIEVE "TAILOR MADE" A DIRECT COVALENT IMMOBILIZATION OF BIO-MACROMOLECULES ON SUPER-PARAMAGNETIC PARTICLES

Manuel Fuentes[1], Cesar Mateo[1], Mercedes Casqueiro[2], Roberto Fernández-Lafuente[1], Juan C. Tercero[2] and J.M. Guisán[1].

[1]Laboratorio de Tecnología Enzimática. Departamento de Biocatálisis. Instituto de Catálisis y Petroleoquímica-CSIC. Campus UAM. Cantoblanco. 28049 Madrid (Spain)
[2]Genomica S.A.U., Pol. Industrial Coslada. Coslada. 28820 Madrid. (Spain)

The use of magnetic particles in cell separation, immunoassays, isolation of viruses or organelles, and in molecular genetics has only been recently initiated. Molecular probes bound to paramagnetic particles permit the one step purification and concentration of target molecules, either at the beginning or the end of an analytical protocol.
The correct immobilization of bio-macromolecules on paramagnetic particles is a critical step for many uses of biosensors. Only if this immobilization is properly design, the recognition of the biomacromolecule may be almost fully preserved, unspecific adsorption may be negligible and the results may be fully satisfactory, the biosensor may be used in any kind of medium.
In this presentation, we are going to describe the immobilization of antibodies or aminated DNA probes on paramagnetic particles, trying to fully cover the sensor surface with properly oriented biomacromolecules and designing strategies to avoid the unspecific adsorption of any other molecules that could hinder the real usefulness of this technique.
In this presentation, we describe an universal protocol to bind capture antibody with a correct orientation onto a very inert surface of magnetic particles. The results show that the immunoactivity of immobilized IgG was almost unaltered when the immobilization was carried out through groups present in the region Fc: via Chelate-epoxides or via sugar chain. Better adsorption of the antigen rate was achieved when immobilization was performed via the sugar chains (the IgG sugar chains acts as spacer arms)(Figure 1). Furthermore, in order to avoid the unspecific adsorption, the super-paramagnetic particles covered with IgG immobilized were coated with dextran-aspartic, prevented the ionic adsorption of other bio-molecules.
Moreover, we described a procedure for the immobilization of aminated DNA probes in aminated super-paramagnetic beads based on the use of hetero-polyfunctional polymers, modified dextrans as spacer arms. These molecules are poly-functional and may be modified step by step, to give hetero-functional polymers. They permit to immobilize many DNA probes per dextran molecule, quite far away from the support (avoiding steric hindrances). Its flexibility permits the immobilized molecules almost full freedom of movement. We have used these molecules partially modified with aspartic acid to take advantage of two facts: 1.-The negative charge may partially block the amino groups in the surface preventing ionic adsorption of samples of DNA that could give false positives. 2.-A rapid electrostatic adsorption of the aldehyde dextran on the magnetic particles, followed by a covalent "intramolecular" reaction between the aldehydes of the dextran and the amino groups of the superparamagnetic particles that permit the full coating of the particle surface (very important if the pK of the amino group is not very adequate). The key parameters studied were: unspecific adsorption, the real covalent attachment via the amino group (introduced artificially introduced in the probe) and the stability of the final composite(Figure 2). This super-paramagnetic particles have important advantages in PCR-ELISA assays.

References

1.-Patent PCT/GB02/01059

2.-Patent ES 200202751

Figures

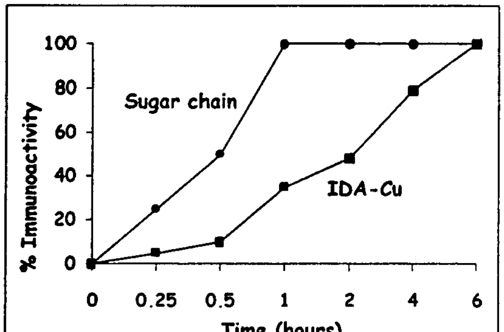

Figure 1

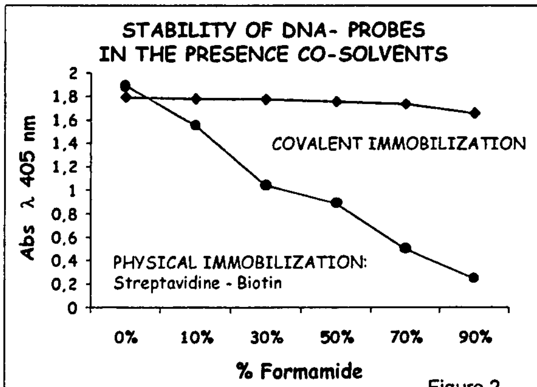

Figure 2

PERFLUOROFUNCTIONALIZATION OF CARBON NANOTUBES

Gemma Gabriel[a], Jaume Casabó[b], Mar Tristany[b], Marcial Moreno[b], Mª Teresa Martínez[c], Carlos Miravitlles[a].

a) Institut de Ciència de Materials de Barcelona, CSIC. (08193) Bellaterra, Spain

b) Universitat Autònoma de Barcelona, Chemistry Dpt. (08193) Bellaterra, Spain

c) Instituto de Carboquímica, CSIC. (50015) Zaragoza, Spain

*gabriel@icmab.es

Carbon nanotubes can be purified by acid, thermal treatment or both. We have carried out an oxidant thermal treatment of the nanotubes produced by an arc discharge, over one hour at 300 °C. The basic goal of this treatment is to increase the amount of oxidized functional groups on the surface. This should allow us to functionalize the nanotubes with a perfluorated molecule.

With this aim, we undertake the synthesis of the amine: 4-perfluorooctylaniline (D. Crich, Tetrahedron). Carbon nanotubes (SWNTs) were functionalized by reaction with thionylchloride and 4- perfluorooctylaniline. Different derivatives also have been synthesized with fluorooctylamine and octadecylamine.

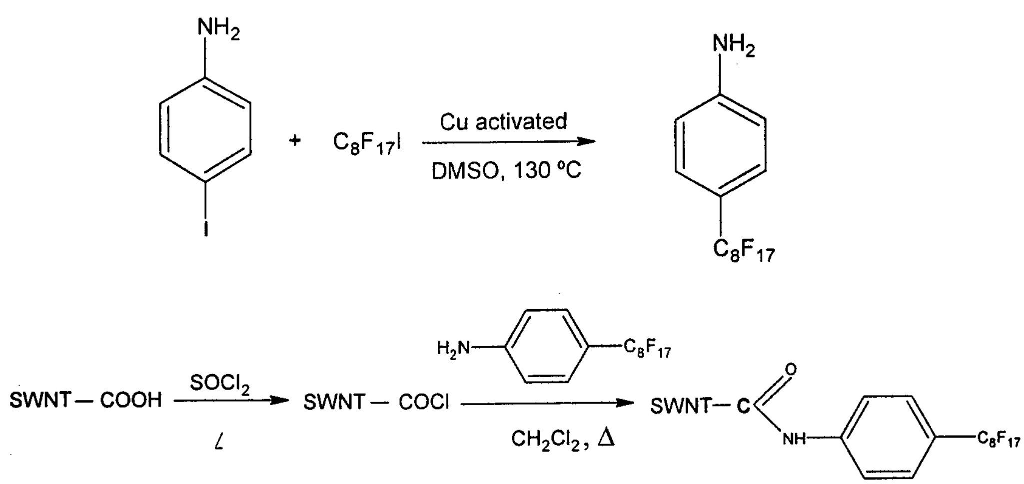

[1]. D. Crich *et al.* Tetrahedron 55 (1999) 14261-14268

MONTE CARLO SIMULATION OF A BALLISTIC Y-BRANCH JUNCTION (YBJ)

J.S. Galloo(1), E. Pichonat(1), Y. Roelens(1), S. Bollaert(1), X. Wallart(1), A. Cappy(1), J.Mateos(2), T. Gonzales(2), H. Boutry(3), B. Hackens(3), V. Bayot(3), L. Berdnarz(3), I. Huynen(3)

(1) IEMN-DHS, CNRS UMR 8520
Avenue Poincaré, BP 69, 59652 Villeneuve d'Ascq, France
E-mail: Jean-Sébastien.Galloo@iemn.univ-lille1.fr
(2) Dpto Fisica Aplicad, Universitad de Salamanca, Salamanca, Spain,
(3) Université Catholique de Louvain, Louvain-La-Neuve, Belgium

Because of the increasing amount of information to be transmitted, the development of digital/analog electronic devices for data processing at ultra-high bit rates and/or on high frequency carriers is a key issue. One way to reach this goal is to study and develop ballistic devices working at room temperature. In such a device, when the active area is smaller than the electronic mean free path, electrons are quite not scattered and are only diffused by walls of the device. The electronic transport becomes ballistic and leads to attractive behaviour. In T-branch junctions, due to ballistic transport of electron, electrical potential V_{out} in the central branch of the YBJ follow a negative parabolic shape, when fixing the two other branches potential, one to +V and the other one to –V (Push-Pull Mode) . These were demonstrated by different ways [1-2], and also by experimental results at room temperature [3-4].

In this paper, we present semi-classical 2D Monte Carlo simulation on Y-branch junctions (figure 1). Influence of the angle θ on DC-characteristics has been studied. Our simulated devices are based on GaInAs/AlInAs heterostructure (figure 2). GaInAs/AlInAs heterostructure presents advantages of technological compatibility with HEMTs and good transport properties of the InGaAs channel at room temperature. We fixed an Indium content of 70% in the GaInAs channel to obtain higher electron mobility. As mean free path in such materials are still larger than 100 nm at room temperature [4], we designed and simulated devices whose active area size is below 100 nm. Length of different branches is 40nm. Width is 20nm. So we assume that electronic transport is ballistic.

In figure 3, potential V_{out} of central branch is represented versus potential V (+V on bottom branch and –V on top branch). First, for angle θ = 180°, which corresponds to T-branch junction, a parabolic shape is obtained. This is in good agreement with previous published works [1], and is related to space charge effect. For lower angle θ, parabolic shape is more pronounced. This behaviour is attributed to a larger injection of carrier in the central branch, which involves a higher potential V_{out}.

This work is supported by the European Commission through the NANOTERA project IST-2001-32517 in collaboration with the IEMN(Lille,France), the University of Salamanca(Spain) and the University of Louvain(Belgium).

References:

[1] Mateos J., Vasallo B.F., Pardo D.,Gonzalez T.,Galloo J.S., Roelens Y.,Bollaert S.,Cappy A., Ballistic nanodevices for terahertz data processing: Monte Carlo simulations., *Nanotechnology*, **14**(2003) 117-122

[2] Xu H.Q., Electrical properties of three-terminal ballistic junctions, *Applied Physics Letters* , **V.78,N°14**(2 april 2001)

[3] Xu H.Q., A novel electrical property of three-terminal ballistic junctions and its applications in nanoelectronics, *Physica E*, **13** (2002) 942-945

[4] Shorubalko I. Xu H.Q., Maximov I., Omling P., Samuelson L., Seifert W.,*Applied Physics Letters*, **79**(2001) 1384

Figures:

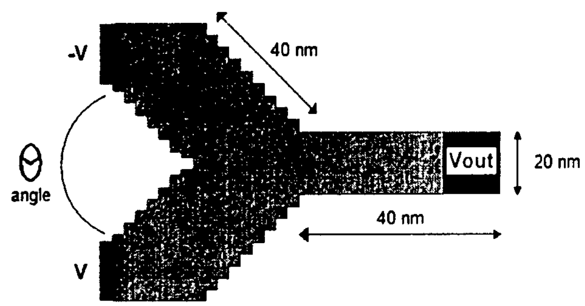

Figure 1: Representation of the simulated Y-Branch Junction(YBJ)

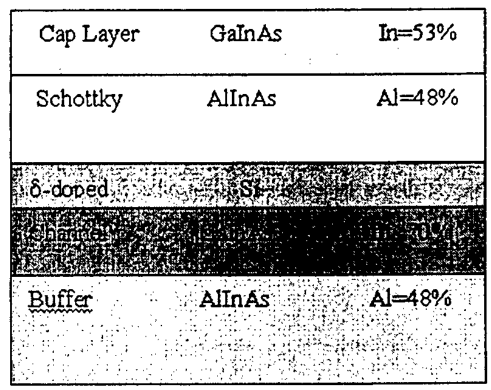

Figure 2: Simulated GaInAs/AlInAs Heterostructure

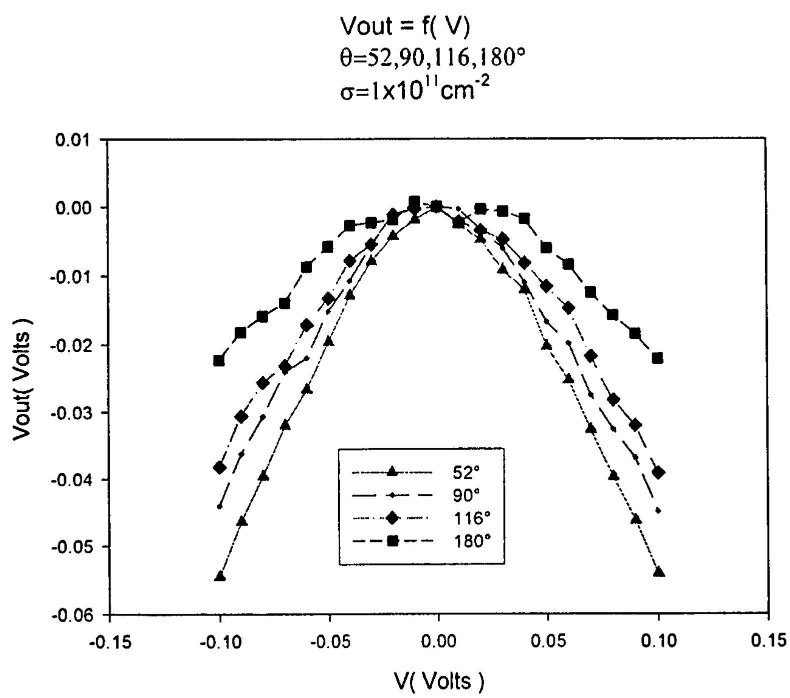

Figure 3: Electric potential at the bottom of the central branch (open circuited) of the YBJ

ELECTRONIC TRANSPORT AND VIBRATIONAL MODES IN THE SMALLEST MOLECULAR BRIDGE: H_2 IN Pt NANOCONTACTS.

Y.García[(1)], J.J.Palacios[(2)], E.San Fabián[(3)], J.A.Vergés[(4)], A.J.Pérez-Jiménez[(5)], and E. Louis[(2)]

[1] Departamento de Física Aplicada, Universidad de Alicante, San Vicente del Raspeig, 03690 Alicante

[2] Departamento de Física Aplicada y Unidad Asociada UA-CSIC, Universidad de Alicante, San Vicente del Raspeig, 03690 Alicante

[3] Departamento de Química-Física y Unidad Asociada UA-CSIC, Universidad de Alicante, San Vicente del Raspeig, 03690 Alicante

[4] Departamento de Teoría de la Materia Condensada, Instituto de Ciencia de Materiales de Madrid ICMM-CSIC, Cantoblanco, 28049 Madrid

[5] Departamento de Química-Física, Universidad de Alicante, San Vicente del Raspeig, 03690 Alicante

We present a state-of-the-art first-principles analysis of electronic transport in a Pt nanocontact in the presence of H_2, which has been recently reported by Smit *et al.* in Nature 419, 906 (2002). Our results indicate that at the last stages of the breaking of the Pt nanocontact two basic forms of bridge involving H can appear. Our claim is, in contrast to Smit *et al'* s, that the main conductance histogram peak is not due to molecular H_2, but to a complex Pt_2H_2 where the H_2 molecule dissociates. A first-principles vibrational analysis that compares favorably with the experimental one also support our claim.

CORRELATION BETWEEN THE GIANT MAGNETORESISTANCE AND THE MICROSTRUCTURE IN CoCu GRANULAR ALLOYS

A. García Prieto, M.L. Fdez-Gubieda
Departamento de Electricidad y Electrónica. Universidad del País Vasco (UPV/EHU).
Apartado 644. 48080 Bilbao, Spain
E-mail: agp@we.lc.ehu.es

The giant magnetoresistance (GMR) effect is a huge decrease of the electrical resistance when a magnetic field is applied. This phenomenon was first discovered in multilayered systems [1] but recently it has been observed that also granular materials composed of magnetic clusters embedded in a non-magnetic metallic matrix present GMR [2,3]. The origin of the GMR is the same in both types of systems: the spin-dependent scattering of the conducting electrons at the interfaces of the magnetic clusters/layers and, to a lesser extent, inside them. This way, the GMR is closely related to the microstructure of the samples.

We have studied Co_xCu_{100-x} (x=5,10,15,20) melt-spun granular alloys in the form of long ribbons in the as-quenched state and annealed between 400 and 650°C. Our aim was to correlate the microstructural changes due to the thermal treatment with the GMR response, which increases from the as-quenched state to the annealed at 450°C and then drops abruptly up to the end of the thermal treatment independently of the composition x. However, a microstructural study of systems composed of such small clusters is complex and we have needed several techniques in order to obtain a complete pattern of the microstructure at each stage of the annealing. It is also noticeable that the microstructural evolution due to the annealing is systematically reproduced for the four compositions (x=5,10,15,20) studied.

First of all, room temperature X-ray diffraction (XRD) experiments performed at the ESRF synchrotron (Grenoble, France) detect a Cu rich fcc phase and, in x=10, 15 and 20 samples, the fraction of the Co atoms which are arranged in a Co-rich fcc phase of 20-40 nm size. When increasing the annealing temperature, the lattice parameters of each phase evolve towards the Cu and the Co bulk values, respectively, evidencing the onset of a segregation process.

Secondly, we have obtained very important microstructural information from the analysis of the room temperature hysteresis loops of all the samples. From this analysis we have identified three different Co arrangements, each one with a different magnetic response: Co superparamagnetic nanoclusters, a Co-rich ferromagnetic phase, which is the one previously detected by XRD, and Co atoms diluted into the Cu matrix with no magnetic contribution. Recent small angle neutron scattering (SANS) experiments have also verified the existence of these Co nanoclusters, responsible of the GMR response.

Finally, by means of the extended x-ray absorption fine structure spectroscopic technique (EXAFS) performed on the Co K edge, we have analyzed the local configuration of the Co atoms, in particular, at the interfaces between the magnetic nanoclusters and the Cu matrix.

Complementing all this information we have deduced the main consequences of the thermal annealing on the microstructure of the CoCu samples and related these structural changes to the GMR evolution. We conclude that the conditions for optimum GMR are highly concentrated small magnetic clusters delimited by well-defined interfaces.

References:

[1] M.N. Baibich, J.M. Broto, A. Fert, F. Nguyen Van Dau, F. Petroff, P. Etienne, G. Creuzet, A. Friederich, J. Chazeles, Phys. Rev. Lett. **61** (1988) 2472.
[2] A.E. Berkowitz, J.R. Mitchell, M.J. Carey, A.P. Young, S. Zhang, F.E. Spada, F.T. Parker, A. Hutten, G. Thomas, Phys. Rev. Lett. **68** (1992) 3745.
[3] J.Q. Xiao, J.S. Jiang, C.L. Chien, Phys. Rev. Lett. **68** (1992) 3749.

NOVEL SIMULATION TECHNIQUE TO ACCELERATE THE THERMAL MAGNETISATION REVERSAL CALCULATIONS IN MAGNETIC SYSTEMS

F.García Sánchez and O.Chubykalo
Instituto de Ciencia de Materiales de Madrid, CSIC, Cantoblanco 28049, Madrid, SPAIN.
E-mail: oksana@icmm.csic.es

R.W.Chantrell
Seagate Research, 2403 Sydney Street, Pittsburgh, PA 15203-2116, USA, .
E-mail: roy.w.chantrell@seagate.com

One of the major limitations of the current magnetic recording media is the superparamagnetic effect[1)]. In the race to increase the magnetic recording density the grain size of the nanostructured materials has become so small (below 10 nm) that the magnetisation state will soon be unstable versus the thermal fluctuations. The use of the numerical techniques is one of the major tools which could be useful to predict the thermal stability of recorded information and, therefore, contribute to the search of novel thermally stable materials and optimise the existed ones. The main difficulty in such calculations is related to the complexity of the magnetic recording media. One of the main problems is that the media properties are normally distributed which leads to the thermal magnetizations decay ranging in time from picoseconds to years. No numerical techniques could possibly calculate such a decay in a full manner. At small time scale (less than ns) the molecular dynamics technique (the integration of the Landau-Lifshitz-Gilbert (LLG) dynamical equation with random term representing thermal fluctuations) is normally plausible. At larger time scale (statistical regime) the kinetic Monte Carlo-based methods are used. This method involves expensive calculations of energy barriers and has many other limitations proper to the Transition State Theory approximation[2].

For intermediate time scale (say, up to seconds) we have been working on the possibility to accelerate the calculations taking into account the dynamical information. Recently [3)], we have reported the so-called Monte Carlo technique with quantified time step. Although, the acceleration of the calculations was significant, we have found that the Metropolis Monte Carlo techniques only correctly describe the information in the so-called thermal regime when the influence of the magnetisation precession is small. Here we report the usage of the Voter[4)] method which was recently proposed in chemical physics and which is also called "Hyperdynamics of the infrequent events". The method consists in modification of the magnetic potential so that the transition state remains unchanged.

$$\Delta V_b = a\theta(\varepsilon_1)(\varepsilon_1)^2, \text{ where } \epsilon_1 \text{ is the lowest eigenvalue of the Hessian H.}$$

The main concern in the application to magnetic systems was the presence of precessional effects. However, we have found that the method correctly describes the mean first

passage time for magnetization reversal of nanoparticles even in the case of small damping (precessional case) (Fig 1).

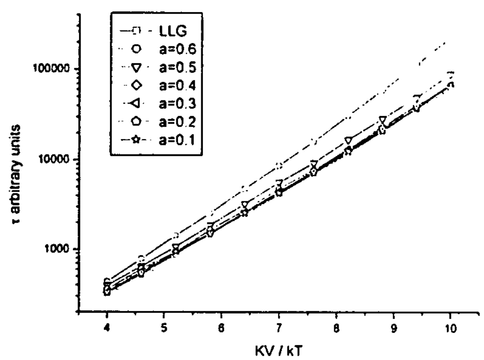

Fig. 1. Switching time (measured in precessional period) of independent magnetic particles as a function of the thermal barrier (KV/kT, where K is the anisotropy constant, V is the volume k is the Boltzman constant and T is the temperature) calculated for different values of the extra potential a, as well as LLG calculation for the same system.

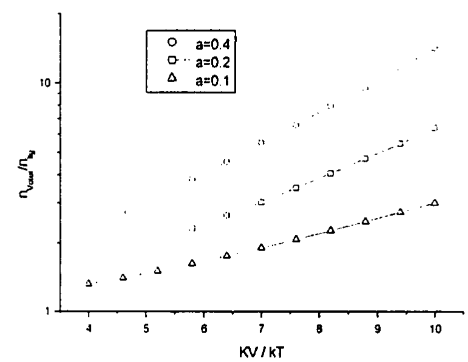

Fig. 2. Ratio of the steps needed by the particle to escape in the new method as compared to the dynamical calculations. It represents a way to quantify the acceleration of the method.

The results of Fig. 1 and Fig. 2 are for the simplest added potential and shows accelerations up to 15 and increasing acceleration with higher barrier energy over thermal energy ratio (KV/kT).

The possible applications of the method are also related to fast thermal switching of small (nanoscale) magnetisation devices, such as magnetic memories, sensors and MEMS in nanosecond to second time scale. It could be also useful in other applications, apart from magnetic systems, where the dynamical information over very large time scale is necessary.

1) D.Weller and A.Moser, IEEE Trans Magn **35** (1999) 4423
2) P-Hoenggi, P.Talkner, M.Borkovec, Rev.Mod.Phys. **62** (1990) 251
3) O.A.Chubykalo, U.Nowak, R.Smirnov-Rueda, M.A.Wongsam, R.W.Chantrell and J.M.Gonzalez Phys Rev B **67** 064422 (2003)
4) A.Voter, J.Chem.Phys. **106** (1997) 4665

OPTIMIZED BASIS SETS FOR THE PARAMAGNETIC, MAGNETIC AND HELICOIDAL PHASES OF IRON

V. M. García Suárez,
Departamento de Física, Universidad de Oviedo,33007 Oviedo, Spain
C. M. Newman, C. J. Lambert,
Department of Physics, Lancaster University, Lancaster, LA1, 4YB, U. K.
J. M. Pruneda
Department of Earth Sciences, University of Cambridge, Cambridge, CB2 3EQ, U. K.
J. Ferrer
Departamento de Física, Universidad de Oviedo,33007 Oviedo, Spain

E-mail: victor@condmat01.geol.uniovi.es
http://conmat10.geol.uniovi.es/victor

We present results of a thorough theoretical study of the different christallographic phases of Iron. We employ an specific implementation of Density Functional Theory based on the use of pseudopotentials and localized wave functions to treat core and valence electrons respectively. We have looked for, and found, an optimal basis set using a variational approach. We have then thoroughly tested its transferability among the different phases of Iron. We have also checked for the accuracy and convergence of the results. Finally, we have implemented the ability to compute helicoidal arrangements of spins and tested it for the g phase of Iron.

Magnetism in Iron has shaped somehow the practical development of Density Functional Theory (DFT). Transition metals and intermetallic compounds are significantly tougher to simulate semiconductors or noble metals. And among metals in the 3d series, those whose ground state is magnetic are more difficult to handle than, say Ruthenium or Tin. The need to correctly reproduce the ground state of Iron prompted in a way the further development of the Generalized Gradient Approximation (GGA) since the Local Density Approximation (LDA) incorrectly predicted a paramagnetic fcc ground state[1]. Likewise, Partial Core Corrections were introduced to improve the accuracy of pseudopotential based DFT calculations for Iron, where core and valence electron densities strongly overlap.

While bcc (a-)Iron is firmly stablished to be a ferromagnet, the scenario for fcc (g-)Iron is more complex, since it stands at a crossing point between high spin ferromagnetic and antiferromagnetic states, and the actual realization depends sensitively on the atomic volume. Thin films of Iron deposited onto a Cu substrate crystalize in the fcc structure up to 11 monolayes with bcc inclusions in the form of stripes and needles. The spins arrange themselves ferromagnetically for thicknesses of up to 4 monolayers, and then display antiferromagnetic ordering up to 11 monolayers. Moreover, Tsunoda discovered a decade ago that g-Iron could be stabilized as pellets of radii up to 100 nm, with a lattice constant of 3.577 A. [2,3] He also found that the magnetic structure of the pellets was helicoidal, with pitch vector $\mathbf{q} = (1, 0, 0.12)$.

A number of authors have looked for the theoretical low energy states appearing in such g-phase. There appear four of them, namely: paramagnetic (P), high spin ferromagnetic (FHS), low spin ferromagnetic (LSF) and antiferromagnetic (A). Within LDA all states are degenerate: they have the same equilibrium lattice constant (3.39 A) and the same binding energy. GGA splits such degeneracy leaving a ground state either antiferromagnetic at a lattice constant ~ 3.50 - 3.55 or high spin ferromagnetic with a ~ 3.63 - 3.70, depending on author [4,5,6].

DFT has been developed to tackle non collinear structures. Since then, a number of articles have appeared in the literature trying to explain the helicoidal structure of g-Iron with partial success. All of them plot the total energy versus pitch vector for given lattice constant, for a range of lattice constants. The first studies, which used both the LDA and the Atomic Sphere Approximations (ASA)[7] found minima at pitch vectors q1 = (0, 0, 0.6) and q2 = (0.5 ,0, 1), with the minimum corresponding to q1 being always lowest in energy for lattice constants a in the range 3.57 - 3.63 A. Korling and Ergon used an adapted collinear GGA approximation together with ASA to study the range of lattice constants 3.60 - 3.65 A[4]. They found minima in the energy for the same pitch vectors, but in their case the state corresponding to q2 was more stable. Kleinman and Bylander used a full potential implementation together with LDA and looked at a lattice constant 3.61, again larger than the experimental one[8,9]. They failed to find an absolute minimum at pitch vector q = (0.1, 0, 1) and concluded that a full and thorough computation of the non-collinear GGA exchange and correlation potential was needed to truly solve the problem. Finally, Knopfle and co-workers, which also used GGA or LDA and a full potential implementation of DFT[6] found an antiferromagnetic ground state at a lattice constant a ~ 3.54 A. They nevertheless noticed that for slightly higher lattice constants -including the experimental value, the energy had a minimum at the experimental pitch vector. They concluded that either the full shape of the potential or the intraatomic non-collinearity of the spins were quintaessential to obtain the right pitch vector.

SIESTA is one of the newest Ab-initio electronic structure and molecular dynamics simulation packages[10]. It uses Norm-Conserving pseudopotentials to treat core-electrons and bases made up of atomic-like wave functions to handle valence electrons. Such approach is very similar in spirit to the venerable phenomenological tight-binding scheme. SIESTA is therefore a promising starting point to tackle materials with medium to strong correlations, such as transition metal magnets and oxides. Bulk Iron then is a good choice to test the current strengths an weakenesses of the package.

The SIESTA package has built into it the possibility to cope with non-collinear commensurate spin structures but only in the LDA approximation. Since LDA fails to provide adequate ground state and lattice constants for magnetic transition metals such as Iron, the implementation of non-collinearity plus GGA is highly desirable, even though very few packages seem to have it. We have undertaken such a task. Moreover, we have also implemented the ability to compute equilibrium properties and the conductance of systems with spiral arrangements of spin. We have used Iron to test both our implementation and the current suitability of SIESTA to handle moderately correlated magnetic systems.

References:

[1] H. J. F. Jansen, K. B. Hathaway and A. J. Freeman, Phys. Rev. B **30**, 6177 (1984).
[2] Y. N. Y. Tsunoda, J. Phys.: Condens. Matter **1**, 10427 (1989).
[3] Y. N. Y. Tsunoda and R. M. Nicklow, J. Magn. Magn. Materials **128**, 133 (1993).
[4] M. Korling and J. Ergon, Phys. Rev. B **54**, R8293 (1996).
[5] E. G. Moroni, G. Kresse, J. Hafner and J. Furthmüller, Phys. Rev. B **56**, 15629 (1997).
[6] K. Knöpfle, L. M. Sandratskii and J. Kübler, Phys. Rev. B **62**, 5564 (2000).
[7] M. Uhl, L. M. Sandratskii, and J. Kübler, Phys. Rev. B **50**, 291 (1994).
[8] D. M. Bylander and L. Kleinman, Phys. Rev. B **58**, 9207 (1998).
[9] D. M. Bylander and L. Kleinman, Phys. Rev. B **60**, R9916 (1999).
[10] E. Artacho, P. Ordejón and J. M. Soler, Phys. Rev. B **53**, R10441 (1996).

TAILORING SURFACE ELECTRONIC STATES VIA STRAIN TO CONTROL ADSORPTION: O/Cu/Ru(0001)

R. Otero*, F. Calleja, V. M. García-Suárez[1], J. J. Hinarejos, J. de la Figuera, J. Ferrer[1], A. L. Vázquez de Parga and R. Miranda

Departamento de Física de la Materia Condensada e Instituto de Ciencias de Materiales "N. Cabrera". Universidad Autónoma de Madrid. Cantoblanco, 28049 Madrid. Spain.

[1]Deparamento de Física. Facultad de Ciencias. Universidad de Oviedo,33007 Oviedo. Spain

*present address: iNANO and CAMP, Institut for Fysik og Astronomi, Århus Universitet, DK 8000 Århus C, Denmark.

Email address corresponding author: rodolfo.miranda@uam.es

The proposed relationship [1] between tensile strain and chemical reactivity is demonstrated for the first few monolayers of Cu deposited on Ru(0001) by tunnelling spectroscopy and microscopy. Strain and reactivity are linked through the population of the surface electronic states. The layer by layer relaxation [2] of the 5.5% in-plane lattice mismatch changes the lateral lattice parameter of the Cu film. Simultaneously, the surface state, which is above the Fermi level for the pseudomorfic monolayer shifts down in energy with increasing thickness until it becomes the occupied surface state of Cu (111).

Ab-initio calculations reveal that this energy shift can be assigned to the decreasing tensile strain of the deposited film. The reactivity of the surface correlates with the population of this state. On a 1 ML Cu film, where the state is depopulated, the sticking coefficient of oxygen is three orders of magnitude larger than on Cu (111). The reactivity is strongly reduced between 2 and 3 layers when the surface state becomes occupied. These results suggest that surface stress (compressive or tensile) in films can be used to tailor chemical reactivity.

References

[1] B. Hammer, Y. Morikawa and J. K. Nørskov, Phys. Rev. Lett. **76**, 2141 (1996).
[2] C. Günther, J. Vrijmoeth, R. Q. Hwang and R. J. Behm, Phys. Rev. Lett. 74, 754 (1995).

MOLECULAR WIRES ON METAL SURFACE

X. Ge[1], J. Kuntze[1], L. Limot[1], R. Berndt[1], P. Jiang[2], A. Gourdon[2] and C. Joachim[2]
[1]Institut für Experimentelle und Angewandte Physik der Universität Kiel, D-24098 Kiel
[2]CEMES-CNRS, F-31055 Toulouse Cedex

We have performed scanning tunneling microscopy and spectroscopy (STM/STS) operating at 5K in UHV on a synthetic molecule ("Lander" molecule, Fig. 1) on Cu(100), Ag(111), $Cu_3Au(100)$ and Cu(111) surfaces to characterize its structural and electronic properties.
Three molecular conformations (parallel-legs, crossed-legs) are identified from the acquired STM image of Lander molecules adsorbed on terraces of Cu(100) (Fig.2). When the molecule adsorbs at the edge of a substrate step, from comparison of calculated STM images via the elastic scattering quantum chemistry (ESQC) technique with experimental data, we conclude that the molecule adsorbs with the wire parallel to the step, two legs remain on the upper terrace and the two other legs adsorb on the lower terrace, which will prevent a good electronic coupling between the wire and the substrate (Fig. 3).
Tunneling spectroscopy of single molecules adsorbed on different metal surfaces reveals a substrate dependent molecular gap. (Fig.4) The spatially resolved spectra over five different parts (A-E in Fig. 5) of Lander molecule show little spatial dependency over the Lander.
Finally we report that the Lander form a straight molecular wires on Cu(111) surface (Fig. 6). The length of the wire is approximately 25-35 nm.

Figures:

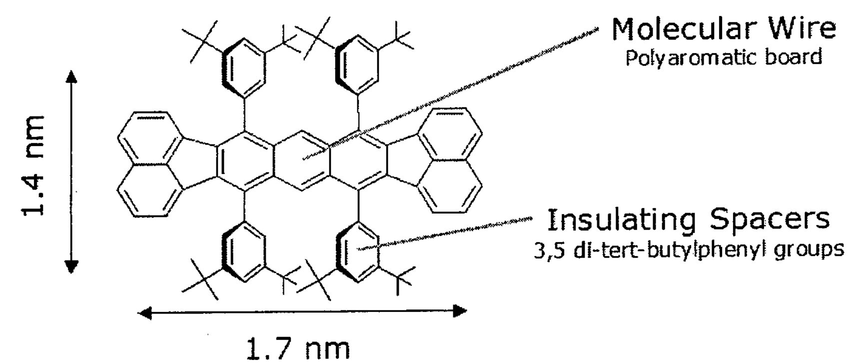

Fig. 1 The structure of Lander molecule

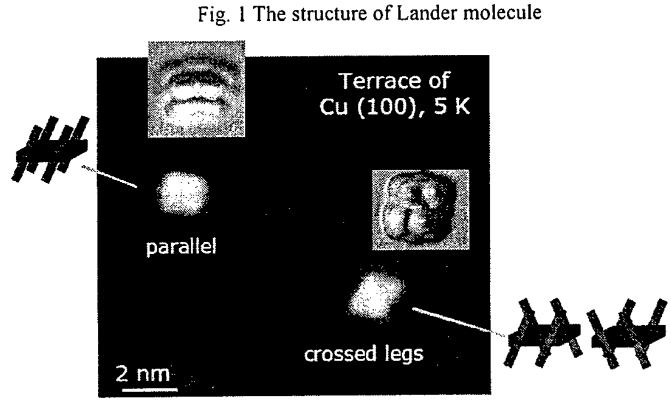

Fig. 2 Three conformations of Lander on terrace

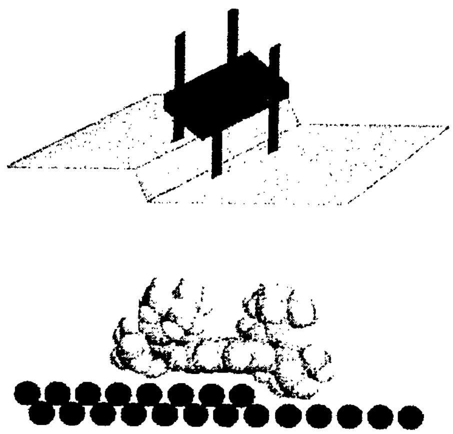

Fig. 3 Lander on edge of substrate step

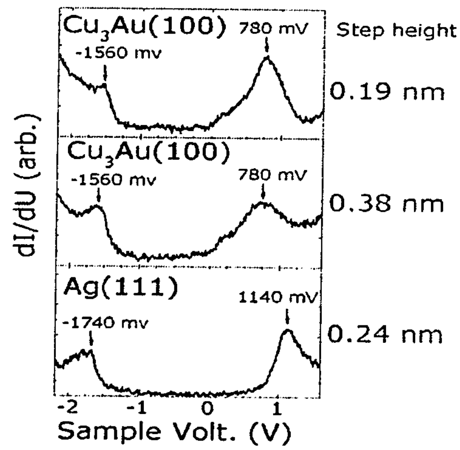

Fig. 4 STS of Lander on different metal surfaces

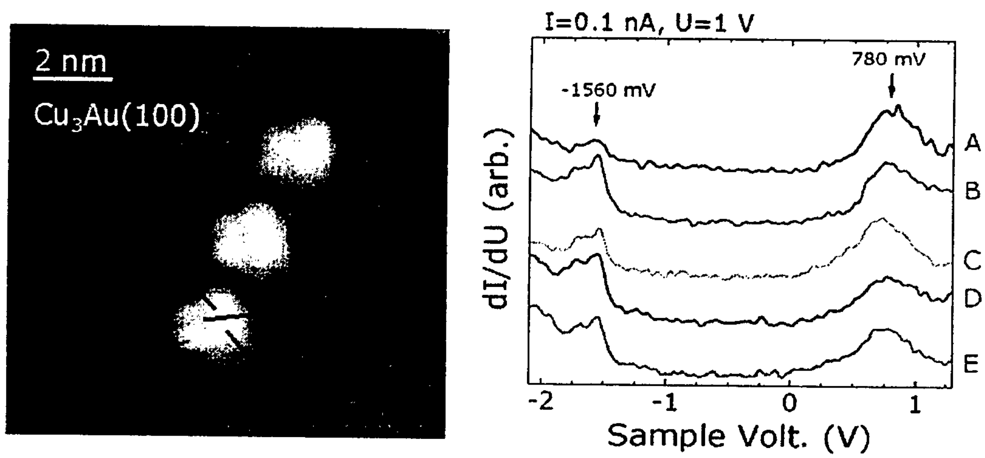

Fig. 5 Spatially resolved spectra over Lander molecule

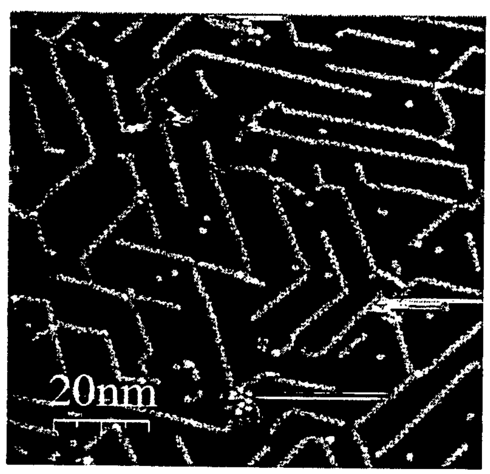

Fig. 6 Lander molecular wire on Cu(111)

MBE GROWN $SrTiO_3$ ON Si AS A BUFFER LAYER FOR FERROELECTRIC FIELD EFFECT TRANSISTORS (FeFETS)

A Gerber [1], H. Kohlstedt [1], V. Vaithyanathan [3], J. Schubert [2;3], O. Trithaveesak [2], R. Waser [1]
[1] Forschungszentrum Juelich, 52425 Juelich, Institut fuer Festkoerperforschung (IFF), Prof. R. Waser
[2] Forschungszentrum Juelich, 52425 Juelich, Institut fuer Schicht und Grenzflaechen ISG, Prof. Ch. Buchal
[3] Pennsylvania State University, Prof. D.G. Schlom
E-mail: a.gerber@fz-juelich.de
www.fz-juelich.de

FeFETs are considered as highly integrable and non-volatile memory devices. In addition, contrary to common FeRAMs, the data read-out scheme is non-destructive. Therefore considerable efforts over the last decades have been performed to transfer FeFETs from a research subject to applications. Although the features of FeFETs are very attractive, serious interface problems between Si and the ferroelectric material (interdiffusion, high trap density etc.) are still considered as an insurmountable barrier. Using a dielectric buffer layer between Si and the ferroelectric material could solve some of these problems. $SrTiO_3$ is suggested to be one of the most promising materials.

Due to the recent advent of high quality interface of MBE grown $SrTiO_3$ on Si with suppressed SiO_2 interface layer and low trap densities, our attempts focus on the development of a FeFET based on this sophisticated deposition technique.

Structural and electrical properties of these MBE grown $SrTiO_3$ films will be presented. We used a (100) oriented silicon substrate and deposited 10 to 30 nm $SrTiO_3$ [1]. The excellent epitaxial STO films are grown in a (001) orientation. Rocking curves with less than 0.9 deg FWHM have been measured (Fig. 1). HRTEM pictures show an atomically abrupt interface with a volume expansion of one or two atomic layers (Fig.2). From RBS measurements we calculated the stoichiometry and found in some samples an oxygen stoichiometry less than O_3.

In addition we studied the electrical properties of these $SrTiO_3$ films using MIS capacitors with platinum top electrodes. We focus on leakage current and capacitance measurements. (Fig. 3). To receive the local current distribution an AFM in contact mode has been used.

We also present first measurements on MFIS Diodes where $PbZr_xTi_{1-x}O_3$ (PZT) is served as a ferroelectric material. The 200nm thin ferroelectric layer was deposited by high pressure oxygen sputter technique at 3mbar oxygen at 645°C. The capacitance of this MFIS structure shows a memory window which is due to the polarisation of the ferroelectric layer. It has a magnitude of the order of 2V (Fig. 4).

References:
[1] J. Lettieri, Ph.D. thesis, Pennsylvania State University, 2002.

Available on-line at: http://etda.libraries.psu.edu/these 202/index.html

Figures:

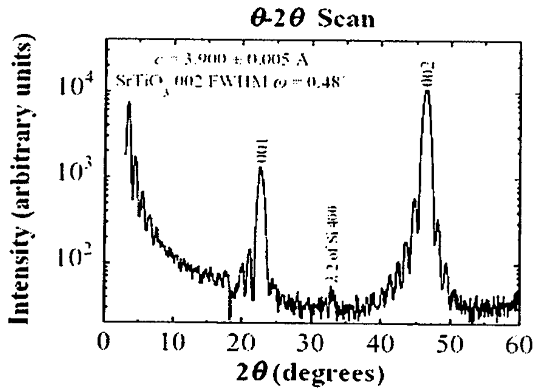

Figure 1: XRD pattern of a $SrTiO_3$ thin film deposited on Si (100)

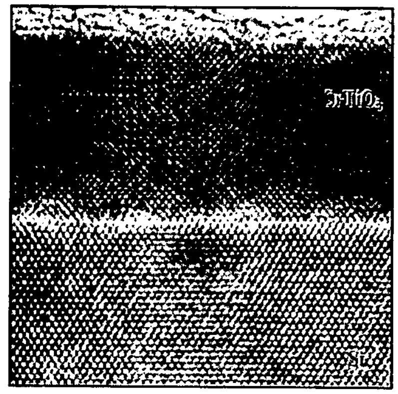

Figure 2: HRTEM picture of a $SrTiO_3$ - silicon interface

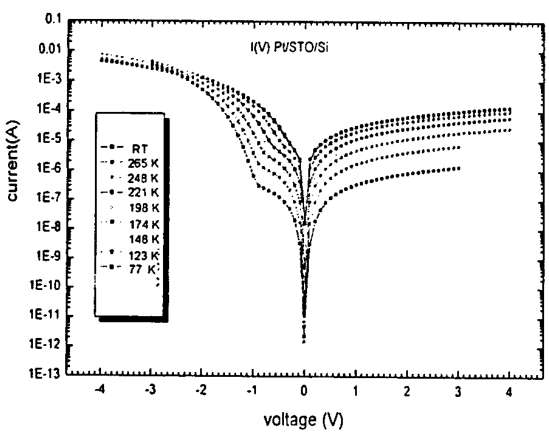

Figure 3: I-V plots of a Pt/STO/Si MIS structure at different temperatures.

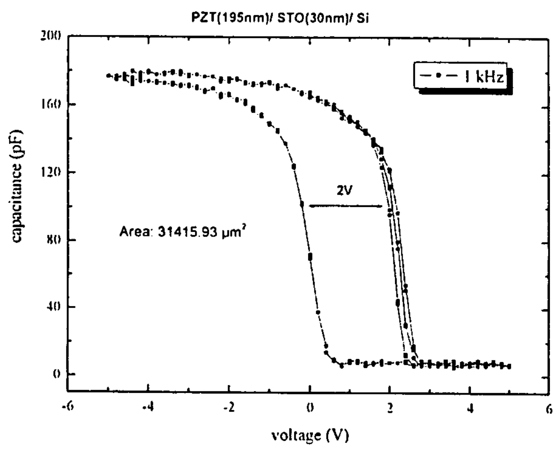

Figure 4: C-V curve of a Pt/PZT/STO/Si MFIS diode at f=1kHz.

Photonic band structure of a Rayleigh Crystal

R. Gómez-Medina[1], A. García-Martín[2], J.J. Sáenz[1], D. Hermann[3], K. Busch[3], and P. Wölfle[3]

(1) Departamento de Física de la Materia Condensada, Universidad Autónoma de Madrid, Cantoblanco, E-28049 Madrid, Spain.

(2) Instituto de Microelectrónica de Madrid, Consejo Superior de Investigaciones Científicas, Isaac Newton 8, Tres Cantos, E-28760 Madrid, Spain.

(3) Institut für Theorie der Kondensierten Materie, Universität Karlsruhe, P.O. Box 6980, 76128 Karlsruhe, Germany.

The optical properties of Photonic Crystals are being studied for application to photonic devices and band-gap materials, with the aim of controlling the flow of light. The periodicity in materials of this type induces an optical band structure quite analogous to the band structure in semiconductors, even more, their band structure, density of states, defects and wave localization properties promise new tools for the design of materials with specified optical properties.

For frequencies far away from any resonance, the light propagation through a photonic crystal can be treated within a very general scattering framework. The method we present here allows to calculate the electromagnetic properties of regular arrays of dielectric cylinders, based only in general quantities to describe the wave scattering. These quantities are the scattering amplitude and the Green function of the system.

We restrict ourselves to the Rayleigh ("small-radius") regime, where the problem allows a semi-analytic treatment. We will demonstrate that, despite the approximations involved, the method we describe here is very powerful and accurate and can be used to describe complex phenomena in photonic crystals.

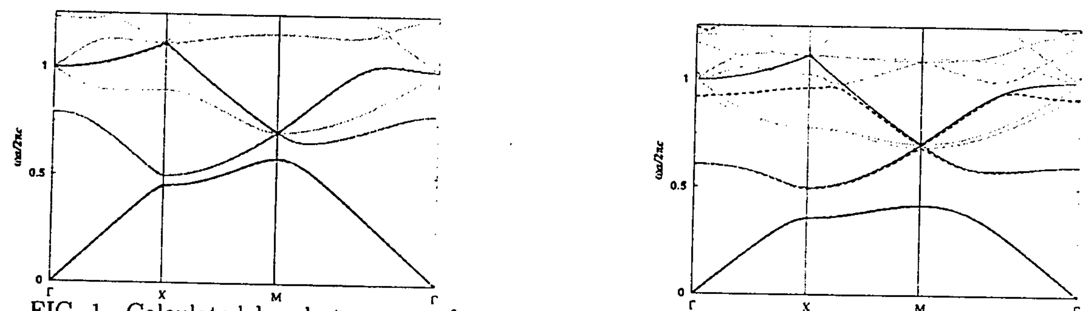

FIG. 1. Calculated band structure of an array of cylinders of Silicon (ϵ = 11.9) in air, with radius (in units of the lattice constant) r/a=0.05 (left) and r/a=0.1 (right). Continuous lines are the results of the method presented here and dashed lines are the result of a multigrid technique depicted for comparison. These plots show that the method is exact for moderate radii and slightly deviates when bands well above the first bandgap are considered.

PROBING THE ELECTROMECHANICAL PROPERTIES OF NANOCONTACTS ON SINGLE WALLED CARBON NANOTUBES

Cristina Gómez-Navarro[1,2], Pedro J. de Pablo[3], and Julio Gómez-Herrero[1]
[1]Departamento de Física de la Materia Condensada. Facultad de Ciencias. Universidad Autónoma de Madrid, 28049, Madrid, Spain
[2]Instituto de Ciencia de Materiales de Madrid, CSIC, Cantoblanco, 28049, Madrid, Spain
[3] Physics of Complex Systems. Division of Physics and Astronomy.Vrije Universiteit. De Boelelaan 1081, 1081 HV, Amsterdam, The Netherlands
e-mail: cristina.gomez@uam.es

The transport properties of carbon nanotubes [1], has been a field of intensive research in the last years. At first sight single walled carbon nanotubes (SWNTs) should exhibit a quantum conductance of $2G_0$ being $G_0=2e^2/h$. However, this theoretical limit is in many cases difficult to reach due to problems with the metal contacts. Theoretical works have been also published in an attempt to understand the influence of the metal contacts in the conductance of the system [2]. However, few experiments have been carried out to determine the properties of the metal-molecule contacts as a function of the mechanical load.

In this work we present an experimental study of the electrical conductance of single walled carbon nanotubes as a function of the loading force and bias voltage applied by an atomic force microscope tip used as one electrode. As the force applied to the nanocontact is increased we observe first, an increment of the conductance due to the contact formation and second, an irreversible drop of the conductance at high loading forces due to the molecule deformation, as expected from previous theoretical works[3]. The differential conductance at high bias, that is blocked along the molecule due to electron-phonon interaction, remains constant during all this process. Using a simple mechanical model we estimate the strain necessary to introduce changes in the electrical transport characteristics of the molecule.We suggest this technique as a possible way to tailor the conductivity of a circuit based on single walled carbon nanotubes.

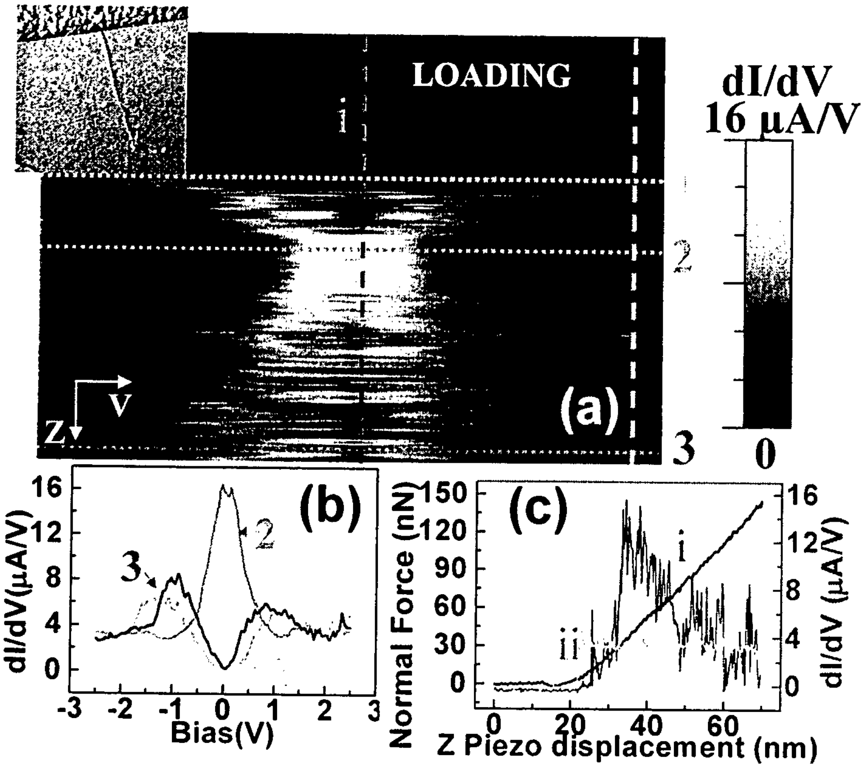

Figure:

a) Differential conductance G(V, Z) (colour scale on the right) plotted as a function of the bias voltage (horizontal axis) and the Z piezoelectric displacement (vertical axis). The bias range was ±2.5 V and the total Z piezoelectric displacement is 70 nm, starting from the feedback position. The inset is a topographic image of the 1.5 nm diameter nanotube where the experiment was performed, connected to a macroscopic gold electrode (image size 1.2x1.2μm^2). b)Differential conductance as a function of the tip-SWNT bias voltage. The curves 1, 2, and 3 are obtained along the horizontal lines drawn in fig. a. c) Conductance as a function of the Z piezoelectric displacement. The curves (i) and (ii) have been obtained along the vertical lines drawn in fig a. In this figure the dependence of the normal force is also plotted (black curve).

References:

[1] S.J. Tans et al. Nature **386**, 474 (1997)
[2] J. J. Palacios, A. J. Pérez-Jiménez, E. Louis, E. SanFabián, J. A. Vergés, Phys. Rev. Lett. **90**, 106801 (2003)
[3] P.L. Lammert, P. Zhang, V.H. Crespi, Phys. Rev. Lett. **84**, 2453 (2000)

COULOMB-BLOCKADE AND SPIN-DEPENDENT TUNNELING IN COBALT NANOPARTICLES

H. Graf, J. Vancea, C. Back and H. Hoffmann

Institut für Experimentelle und Angewandte Physik, Universität Regensburg, 93040 Regensburg, Germany

We report on the observation of the Coulomb blockade at room temperature in cobalt nanoparticles, with sizes ranging between 2 and 5 nm. The Co particle-arrays are contacted via in-plane point contacts. The sharp point contacts have a separation between 10 and 70 nm. Prior to the deposition of the Co particles, we evaporate a thin 1 – 3 nm thick layer of AlO_x on the gap structures. The particles are then grown on the AlO_x layer at temperatures between 300 K and 350 K. The electrical measurements are done inside the UHV apparatus, where all the evaporation steps are done. Magnetoresistance measurement loops with an in-situ elektro-magnet show magnetoresistance values of a few percentages on such samples at 77 K. The Co particles are superparamagnetic at this temperature as Squid measurements indicate.

H. Graf, J. Vancea and H. Hoffmann, Appl. Phys. Lett. **80**, 1264 (2002).

Poster

STACKED LAYERS OF InGaAs QUANTUM RINGS FOR 980nm LASERS

Daniel Granados, Ferran Suárez, María Luisa Dotor and Jorge M. García

Instituto de Microelectrónica de Madrid , CNM (CSIC), C/Isaac Newton 8, PTM
28760 Tres Cantos (Madrid), Spain Email: daniel@imm.cnm.csic.es

Self-assembled semiconductor quantum dots (QDs) formed by lattice-mismatched heteroepitaxy are considered a promising system for various developing optoelectronic technologies and devices. A precise control over QDs height, width and shape is of crucial importance since these morphological characteristics influence the quantum confinement of the charge carriers and therefore determine their optoelectronic properties. Indium segregation effects during QD growth can lead to changes of shape and composition [1], influencing the energy levels of the confined states. A precise understanding of these processes can be used to control the size and the shape of QD [1] for tailoring the emission wavelength of final devices. In particular, a powerful technique to obtain self assembled quantum rings [2,3]] (QR) is based on the morphological changes of QDs grown by molecular beam epitaxy (MBE) which are partially capped with a thin GaAs layer [1].In this way is possible to obtain from each QD a "nanovolcano" or quantum ring.

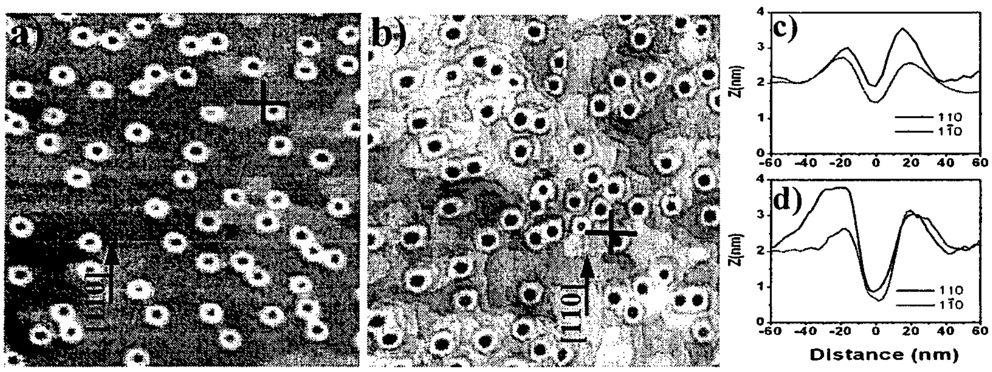

Fig.1. AFM images (1000x1000 nm)of a layer of self assembled InGaAs Quantum Rings **(a)** on GaAs(001), **(b)**top layer of three stacked rings spaced 6nm, and the profile of the marked ring from the single layer **(c)** and the stacked layer **(d)**. The shape and dimensions are preserved.

We present the results on stacked layers of QR for their application on laser structures.

The sample morphology has been characterized by ex situ contact mode Atomic Force Microscopy (AFM). Emission characteristics of the same nanostructes buried in GaAs are measured by Photoluminescence spectroscopy (PL) with a 514.5 nm Ar laser line and a 0.22 m monochromator with a liquid nitrogen cooled Ge diode.

Figure 1, a shows the quantum rings of a single layer sample and b shows that the ring shape and dimensions are preserved when QR are stacked in a 3 period layer with 6 nm spacer. The profiles (figure 1, c and d) depict a slightly bigger hole. Moreover, the optical characterization of capped samples at low temperature demonstrate that the photoluminescence emission does not change significantly from a single layer to a stacked sample pointing that the energy states of the nanostructures are not coupled for 6 nm spacers (figure 2).

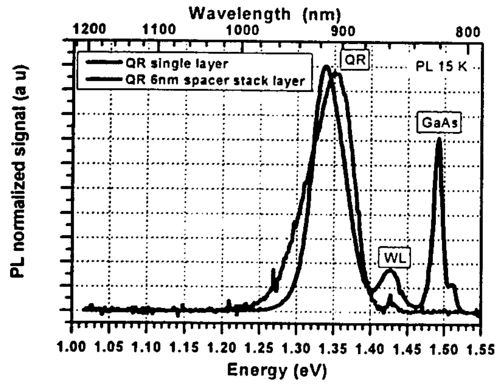

Figure 2. Photoluminescence emission at low T.

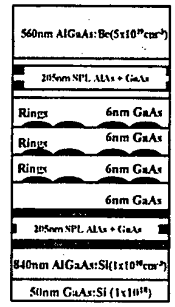

Figure 3.Growth structure of the laser device.

A complete laser structure (figure 3) for operation at RT at ~980 nm with three stacked layers of quantum rings spaced by 6 nm in the active region have been design and grown. The devices have been processed and characterized. Details on the design and on the characterization will be discussed.

This work has been supported by the European Commission Growth program NANOMAT project, contract no. G5RD-CT-2001-00545 and by Spanish MCYT under NANOSELF project TIC2002-04096-C03-03

1. J.M. García, G. Medeiros-Ribeiro, K. Schmidt, T. Ngo and P.M. Petroff, Intermixing and shape changes during the formation of InAs self-assembled quantum dots, Appl. Phys. Lett. 71 (1997) 2014-2016; J.M. García, T. Mankand, T. Holtz, P.J. Wellmann, P.M. Petroff, Electronic states tuning of InAs self-assembled quantum dots, Appl. Phys. Lett. 72 (1998) 3172-3174; R. Songmuang, S. Kiravittaya, O.G.Schmidt, Shape evolution of InAs quantum dots during overgrowth, J. Crystal Growth 249 (2003) 416-417.

2. R. J. Warburton, C. Schaflein, D. Haft, F. Bickel, A. Lorke, K. Karrai, J. M. García, W. Schoenfeld, and P. M. Petroff, Optical emission from single, charge-tunable Quantum Rings , Nature **405** (2000) 926-927.

3. A. Lorke , R. J. Luyken, A. O. Govorov, J. Kotthaus, J. M. García, and P. M. Petroff, Spectroscopy of Nanoscopic Semiconductor Rings , Phys. Rev. Lett. **84** (2000) 2223-2226.

AB INITIO MODELLING FOR MOLECULAR ELECTRONICS

Anton Grigoriev
E-mail: tfsangr@fy.chalmers.se
Göran Wendin
E-mail: wendin@fy.chalmers.se
http://mc2.chalmers.se
Department of Microtechnology and Nanoscience, MC2,
Chalmers University of Technology, SE-412 96 Göteborg, Sweden
Zeljko Crljen
Theoretical Physics Division, Institut Ruder Boskovic, HR-10 002 Zagreb, Croatia
E-mail: crljen@irb.hr
Kurt Stokbro
Mikroelektronik Centret, Technical University of Denmark, DK-2800 Lyngby, Denmark
E-mail: ks@mic.dtu.dk

Using ab initio methods applied to molecular electronics (ME), we investigate structure and electron transport properties of metal-molecule-metal systems where sulphur-containing molecules are connected through "alligator clip" interfaces to two Au(111) surfaces. Computer simulations are conducted with application to molecular junctions, surface adsorption and metal-molecular interfaces.

Precise characterisation of metal-molecule-metal junctions and interfaces is of fundamental importance for the design of ME circuits. Currently studied molecular contacts are based on the properties of aromatic or aliphatic molecules terminated with chemically protected sulphur. The protection group is removed either prior to or upon adsorption and the molecule self assembles between the metal electrode surfaces creating a stable metal-S-molecule. Novel technologies enable creation of metal-molecule-metal sandwiches. In a series of recent experiments, I-V characteristics (IVC) of such devices were measured showing remarkable stability [1-3].

We have chosen sulphur, thiol, methylthiolate, dithiolbenzene (DTB) and oligo(n-phenylene vinylenes) (OPVn), n=3-5 with protected thiol termini, on Au(111) surface as a models. An example is shown in Fig.1. Experimental data is available for DTB [1] and OPV5 [4]. Theoretically calculated IVCs for DTB either use fitting parameters [5] or fail to describe the IVC quantitatively [6]. Contemporary research suggests that the bonding mechanism is responsible for both good stability and enchanced conductivity of the ME devices. Thorough understanding of this mechanism is essential for designing the new ME components with maximum functionality and for interfacing them with conventional circuits. The metal-molecule contact interface is of great importance and determines the order-of-magnitude of the conductivity, but the importance of the binding site and the sensitivity of IVCs are not known. In addition to a flat surface, we also consider such surface defects as vacancies, that can promote molecular adsorption at specific sites, different from the flat surface configuration. In addition, possible isomerisation of the molecules is considered.

In our recent work [7], it was found, that the structure of adsorbed molecules depends on coverage, and that the metal-molecular interface can not always be modelled as a simple atomic contact (e.g., another adsorbate atom could be close to the bridging atom). This implies that determining the structure of molecular contacts in the sandwiched system is a tremendous task. Therefore, we start by testing reasonably simple examples, with special care taken to reproduce the gold surface and the gold bulk substrate. Ab initio density functional methods are used to study the bonding structure of molecular alligator clips. Dependence of the results on coverage is studied. Calculation of the transport properties

is in progress, and it inevitably starts from prepared molecular-on-gold systems relaxed to the ground state configuration. The recently developed TranSIESTA package [9] is used for transport calculations. An important outcome of this research will be to establish reliable models for metal-molecular interfaces, needed for transport calculation. Although the jellium model for contacts is not accepted as sufficiently accurate, the degree of accuracy needed for modelling metal bulk contacts and metal surface is not known. Work is in progress to clarify the structure of the metal-molecular interface and its transport properties in molecular multiterminal devices. We will present results for bias-dependent transmission spectra and IVCs for DTB and OPVn for different adsorption sites and contact groups.

We expect the results of this study to be useful for developing realistic descriptions of transport through the interface, important for preliminary design of new devices.

References:

[1] M.A. Reed, C. Zhou, C.J. Muller, T.P. Burgin, J.M. Tour, Conductance of a Molecular Junction, Science, **278** (1997) 252.

[2] C. Kergueris, J.-P. Bourgoin, S. Palacin, D. Esteve, C. Urbina, M. Magoga, C. Joachim, Electron Transport through a Metal-Molecule-Metal Junction, Physical Review B **59**, (1999)12505.

[3] H.B. Webera, J. Reicherta, F. Weigenda, R. Ochsa, D. Beckmanna, M. Mayora, R. Ahlrichs, H.v. Lohneysen, Electronic transport through single conjugated molecules, Chemical Physics, **281** (2002) 113.

[4] S.E. Kubatkin, A. Danilov, M. Hjort, J. Cornil, J.-L. Brédas, N. Stuhr-Hansen, and T. Bjørnholm, Single electron transport through a single molecule in nine different redox states, submitted to Nanture (2003). (See also TNT02).

[5] Weidong Tian, Supriyo Datta, Seunghun Hong, R. Reifenberger, Jason I. Henderson and Clifford P. Kubiak, Conductance spectra of Molecular Wires, J. Chem. Phys, **109** (1998) 2874.

[6] E. G. Emberly and G. Kirczenow, Comment on "First-Principles Calculation of Transport Properties of a Molecular Device" , Phys. Rev. Lett., **87** (2001) 269701

[7] S. Mankefors, A. Grigoriev and G. Wendin, Molecular alligator clips: a theoretical study of S, Se and S-H adsorption on Au(111), Nanotechnology (2003), in press.

[8] Mads Brandbyge, Jose-Luis Mozos, Pablo Ordejon, Jeremy Taylor, and Kurt Stokbro Density functional method for nonequilibrium electron transport, Phys. Rev., B. **65** (2002) 165401.

Figures:

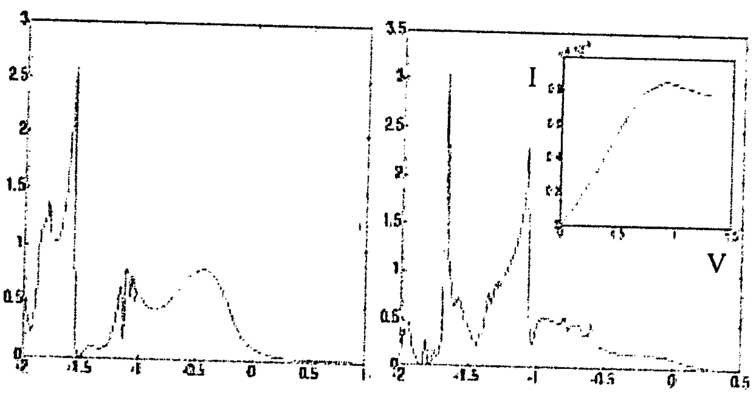

Fig.1 Theoretical transmission curves for Au-OPV3-Au (bulk contacts) at source-drain bias VSD=0V (left) and VSD=1 volt (right). The inset shows the current-voltage characteristic (IVC). QPV3 is adsorbed at the hollow Au site in both electrodes.

COMPARISON BETWEEN TWO MANUFACTURING PROCESSES OF NANOCOMPOSITES COMPOSED OF EPOXY MATRIX REINFORCED WITH CARBON NANOTUBES. MICROSTRUCTURE AND PROPERTIES

R. Guzmán de Villoria, A. Miravete
Departamento de Ingeniería Mecánica, Universidad de Zaragoza, España
W. Masser, T. Martínez, A. de Benito
Instituto de Carboquimica, CSIC, Zaragoza, España

Carbon nanotubes present excellent mechanical properties, and are therefore potentially a perfect reinforcement for a polymer matrix. Because their size is in the order of nanometers, it is however very difficult to get a homogeneus dispersion in the matrix, which is essential for fabrication of nanocomposites. Another difficulty is achieving good adhesion between the nanotubes and the matrix. This paper shows the results of two different methods to fabricate single walled and multiwalled nanocomposites embedded in an epoxy matrix: the mechanical mixing method and the acid treatment method. The manufacturing methods are compared on the basis of dispersion, adhesion and mechanical properties. The comparison shows substantially better results for the acid treatment method.

Figures:

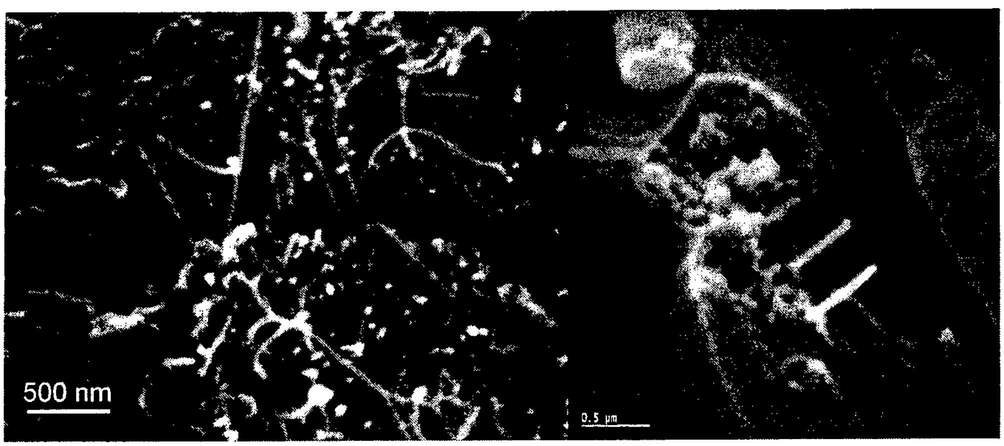

Micrographs of two nanocomposites reinforced with single walled nanotubes (SWNT). The micrograph on the left is manufactured with the mechanical mixture method and the right one with the acid treatment method.

EPOXY MATRIX COMPOSITE MATERIALS REINFORCED WITH CARBON NANOTUBES

R. Guzmán de Villoria, A. Miravete
Departamento de Ingeniería Mecánica, Universidad de Zaragoza, España
W. Masser, T. Martínez, A. de Benito
Instituto de Carboquimica, CSIC, Zaragoza, España

Carbon nanotubes have excellent mechanical properties [1][2], therefore they constitute a potentially perfect reinforcement for a polymer matrix. Due to their nanometric size, it is however very difficult to get a homogeneous dispersion in the matrix, which is essential for fabrication of nanocomposites. Another challenge is to achieve good adhesion between the nanotubes and the matrix. This poster shows a scheme of two different methods to fabricate single walled and multiwalled nanocomposites embedded in an epoxy matrix: the mechanical mixing method and the acid treatment method (fig.1).

These materials are characterized through scanning electron microscopy (SEM) and mechanical testing. The micrographs and the differences between the two methods can be observed in the poster (fig.2). Tensile modulus and tensile strength of the different standard specimens are obtained too. Finally, the manufacturing methods are compared on the basis of dispersion, adhesion and mechanical properties.

Nanocomposites obtained from mechanical mixture method have worse mechanical properties than non-reinforced matrix and have deficient dispersion and adhesion of nanotubes. Microvoids and local stress concentrators may occur.

However, acid treatment method improves properties of non-reinforced matrix. Dispersion and adhesion of nanotubes are improved too. Mechanical properties are better, and the matrix is reinforced by the nanotubes. It could be due to stress transmission between matrix/nanotube

The comparison shows substantially better results for the acid treatment method.

References:

[1] Thostenson E.T., Ren Z. and Chou T. (2001) Advances in the science and technology of carbon nanotubes and their composties: a review. Composites Science and Technology; **61** 1899-1912.

[2] Lau K. and Hui D.(2002) The revolutionary creation of new advanced materials-carbon nanotube composites, Composites: Part B; **33**:263-277.

Figures:

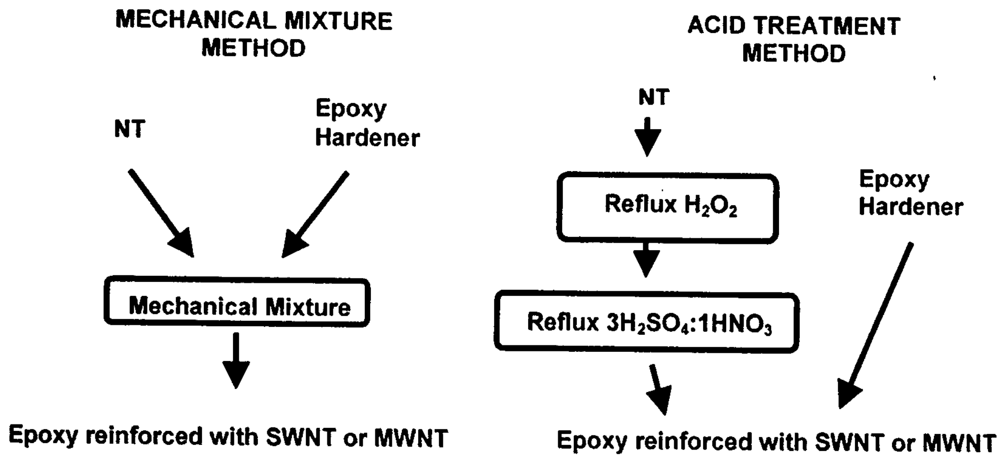

Fig 1. Scheme of the two different methods to fabricate nanocomposites

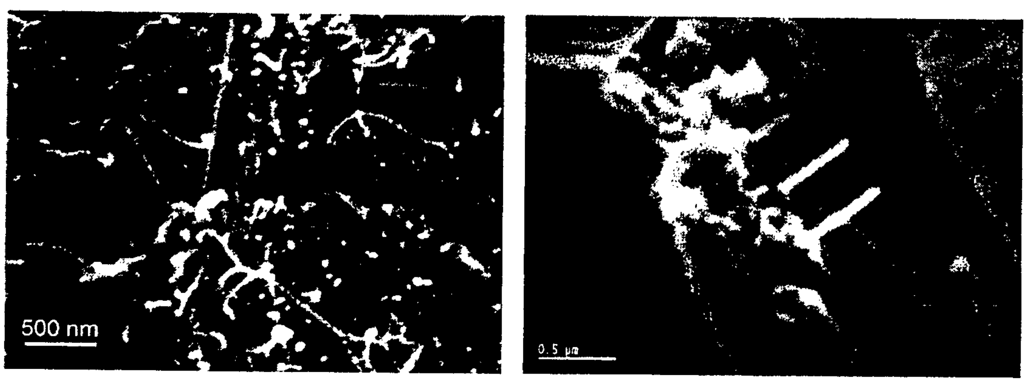

Fig. 2. Epoxy matrix and MWNT ($W_f = 1\%$) (Left) and epoxy matrix and MWNT ($W_f = 0.05\ \%$) (Right)

NONLINEAR ELECTRON TRANSPORT IN InGaAs/InAlAs BALLISTIC DEVICES

B. HACKENS[1], L. GENCE[1], S. FANIEL[1], C. GUSTIN[1], H. BOUTRY[1], L. BEDNARZ[1], I. HUYNEN[1], V. BAYOT[1], X. WALLART[2], S. BOLLAERT[2], A. CAPPY[2], J. MATEOS[3], T. GONZALEZ[3]

[1] *CERMIN, PCPM, DICE and EMIC Labs, Université Catholique de Louvain, Louvain-la-Neuve, Belgium*
[2] *IEMN, Cité scientifique, Villeneuve d'Ascq, France*
[3] *Dpto. Fisicada Aplicada Universidad de Salamanca, Salamanca, Spain*

Recent measurements of the current-voltage characteristics of ballistic devices with broken geometrical symmetry revealed unexpected rectifying effects [1,2]. Theoretical descriptions have been proposed, based either on the hypothesis of coherent transport [3,4] (Landauer-Buttiker formalism) or on semiclassical arguments [5] (Monte-Carlo simulations). One of the purposes of our work is to test experimentally some predictions of these models.

Here, we present measurements performed on two types of mesoscopic devices, fabricated from InGaAs/InAlAs heterostructures using electron beam lithography and wet etching. The electron mean free path in the substrate is larger than 1 μm at low temperature, and the electron density in the two-dimensionnal electron layer is $\sim 2\ 10^{16}\ m^{-2}$.

At first, we discuss the current-voltage characteristics of three asymmetric open quantum dots (QDs). All the QDs are triangular-shaped (Fig. 1) and differ by their area, ranging from $0.086\ \mu m^2$ to $0.273\ \mu m^2$. In a simplified semiclassical picture, electrons entering into the QD from the top or bottom point contact have a slightly different probability to be transmitted through the QD, which should result in an asymmetric V(I) curve resembling that of a classical diod. We measure the differential resistance (dV/dI) of our devices at temperatures between 0.3K and 100 K, as a function of a DC current bias, using a classical four-contacts lock-in technique. Then, we integrate these dV/dI curves in order to obtain V(I). Fig. 1 shows that the differential resistance is indeed asymmetric, and bear signatures of both coherent and ballistic effects. The effect of a small magnetic field is also investigated, in order to separate the different contributions to the nonlinear effect.

Furthermore, we study the temperature dependence of the electron dephasing time inside the QDs, using magnetoconductance measurements (the technique is described in ref. [6]). Our results differ from previous reports in GaAs/AlGaAs [7] and InGaAs/InAlAs QDs [6], which we attribute to a very large energy level spacing inside the QDs (due to a smaller dot area and electron effective mass).

Moreover, we also fabricated a four-terminal cross-shaped device with an artificial symmetry-breaking scatterer located close to one of the leads of the cross (labeled U, Fig. 2). The sample design is based on a recent proposal by Fleischmann and Geisel [3]. The measurement configuration is as follows : current I_{SD} flows between channels S and D, and we measure the voltage V_{LU} between probes L and U. The $V_{LU}(I_{SD})$ characteristic, measured between 4.2K and 130 K exhibits a pronounced nonlinear rectifying behaviour (Fig.2) at least up to 31 K. We compare our experimental results to previous measurements [1] and to existing models. We also discuss the results obtained in other measurement configurations.

Acknowledgements : This work is realized in collaboration with the IEMN and the University of Salamanca, in the frame of the IST-2001-32517 Project Nanotera funded by the EC. Acknowledgements are also due to the FRIA and to the National Fund of Scientific Research (FNRS) Belgium, and to the Special Funds of Research, UCL, Belgium.

References

[1] A.M. Song et al., Phys. Rev. Lett. 80, 3831 (1998);
A. Lofgren et. al., Phys. Rev. B 67, 195309 (2003).
[2] H. Linke et al., Phys. Rev. B 61, 15914 (2000).
[3] R. Fleischmann and T. Geisel, Phys. Rev. Lett. 89, 016804 (2002).
[4] A. M. Song, Phys. Rev. B 59, 9806 (1999).
[5] J. Mateos et al., to appear in the proceedings of the IPRM2003 conference.
[6] B. Hackens et al., Phys. Rev. B 66, 241305 (2002).
[7] A.G. Huibers et al., Phys. Rev. Lett. 81, 200 (1998); Phys. Rev. Lett. 83, 5090 (1999).

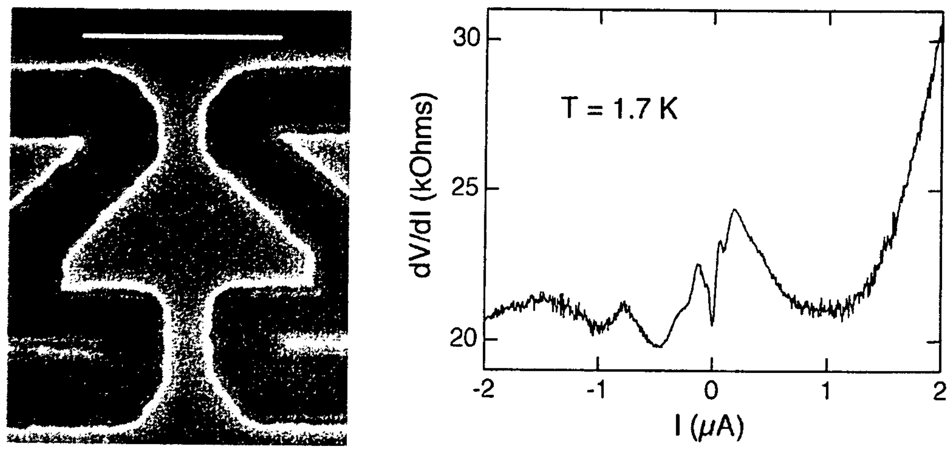

Fig. 1. *Left* : electron micrography of the smallest quantum dot (darkest regions are etched). The white bar on the top represents 500 nm. *Right* : differential resistance of the quantum dot, as a function of the bias current, at 1.7K.

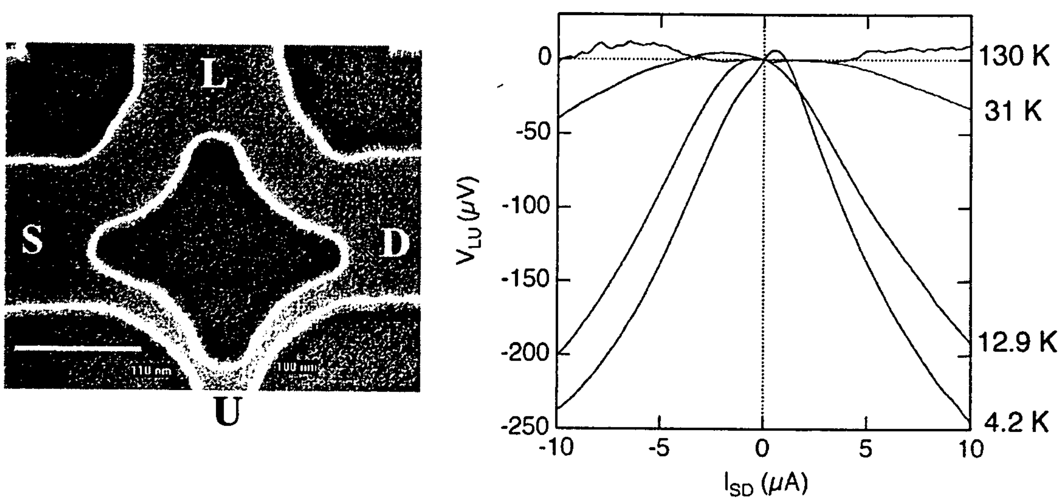

Fig. 2. *Left* : electron micrography of the cross-shaped device (darkest regions are etched). The white bar represents 500 nm. *Right* : V_{LU} (I_{SD}) characteristic at indicated temperatures. A linear fit has been substracted from the raw data (the linear contribution is assumed to originate from the assymetry of the device).

Computing with Locally-Interconnected Josephson Circuits

Jie Han and Pieter Jonker
Faculty of Applied Sciences, Delft University of Technology, 2628 CJ, Delft, The Netherlands
jie@ph.tn.tudelft.nl pieter@ph.tn.tudelft.nl

The continuous miniaturization of electronic components is meeting many technological challenges as the dimensions of devices enter the nanometer realm. CMOS technology is anticipated to reach its physical limit and cease to decrease in size around 2016 [1]. Besides the endeavor devoted to the continuous scaling of CMOS, therefore, novel information processing devices based on new physical phenomena have been investigated as likely alternatives to the electronics beyond CMOS [2]. Due to the characteristics, such as low power consumption, low drive capability and easily local interactions, parallel computing architectures that are highly regular and locally connected, such as the single instruction and multiple data (SIMD) machines [3] and cellular nonlinear networks (CNNs) [4], have been proposed as candidate architectures for large-scale integration of quantum and nanoelectronic devices.

SIMD machines consist of assemblies of identical, simple processor elements (PEs), usually associated with local memories and connected to its nearest neighbors in a linear or square array. A CNN is usually a two or three dimensional regular array of identical cells with analog signals as state variables. The cells are locally interconnected and directly communicate with each other through their nearest neighbors. The SIMD and CNN architectures are both capable of high-speed parallel signal processing and suitable for implementation in VLSI. Because of the use of relatively simple and regular circuit components and their local connectivity, the SIMD and CNN architectures are well suited to the large-scale integration of quantum and nanoelectronic devices.

SIMD machines and CNNs have important applications in image processing and pattern recognition. The CNN architecture, when attached with local memories, can be used to construct a CNN universal machine, which is as universal as a Turing machine [5]. The potential implementations of these architectures using nanoelectronic devices have been investigated, and a quantum CNN has been proposed for the use of quantum dots by exploring their local quantum dynamics and global interactions [6].

Quantum computing has been extensively studied as a computing paradigm employing quantum mechanics [7]. Quantum computers perform massively parallel processing on quantum mechanical superpositions of quantum bits or qubits. Microscopic superconducting circuits of Josephson junctions (Fig. 1) have been proposed to realize qubits [8] [9]. The coherent superposition of two macroscopic persistent-current states on superconducting Josephson circuits has been observed [10] and, more recently, coherent quantum dynamics of this Josephson flux qubit has been demonstrated [11]. The Josephson circuit has thus come up as a promising candidate for quantum computing [12]. Classical binary logic (Fig. 2) can also be obtained from this circuit, establishing a classical parallel computing structure [13]. A quantum CNN architecture (Fig. 3) using the Josephson circuits has recently been proposed [14].

In this paper we report our work on computing structures with locally-interconnected superconducting circuits of Josephson junctions; in particular, the SIMD and CNN architectures, as well as quantum computers, using Josephson circuits are presented. Memory implementations are also studied and, furthermore, the possibility to construct a quantum CNN machine is evaluated. Some issues in actual implementation are discussed. Advantages and disadvantages of these architectures for the use of quantum and nanoelectronic devices are generalized.

This work is supported by Delft University of Technology in its DIRC (Delft Inter-faculty Research Center) program "Novel Computation Structures based on Quantum Devices."

REFERENCES

[1] *International Technology Roadmap for Semiconductors*, 2001 ed. http://public.itrs.net/.
[2] R. Compañó (ed.), *Technology Roadmap for Nanoelectronics*, 2nd ed. European Commission IST programme Future and Emerging Technologies, 2000.
[3] T. J. Fountain, M. J. B. Duff, D. G. Crawley, C. D. Tomlinson, and C. D. Moffat, "The Use of Nanoelectronic Devices in Highly Parallel Computing Systems," *IEEE Tran. VLSI Sys.*, vol. 6, pp. 31-38, 1998.
[4] L. O. Chua and L. Yang, "Cellular Neural Networks: Theory," *IEEE Tran. Circuits Sys.*, vol. 35, pp. 1257-1272; and "Cellular Neural Networks: Applications," *ibid.* pp. 1273-1290, 1988.
[5] K. R. Crounse and L. O. Chua, "The CNN Universal Machine is as Universal as a Turing Machine," *IEEE Tran. Circuit Sys. I*, vol. 43, pp. 353-355, 1996.
[6] G. Toth, C. S. Lent, P. D. Tougaw, Y. Brazhnik, W. Weng, W. Porod, R.-W. Liu and Y.-F. Huang, "Quantum Cellular Neural Networks," *Superlattices and Microstructures*, vol. 20, pp. 473-478, 1996.
[7] M. A. Nielsen and I. L. Chuang, *Quantum Computation and Quantum Information*, Cambridge University Press, 2000.

[8] J. E. Mooij, T. P. Orlando, L. Levitov, L. Tian, Caspar H. van der Wal and Seth Lloyd, "Josephson Persistent-Current Qubit," *Science*, vol. 285, pp. 1036-1039, 1999.

[9] T. P. Orlando, J. E. Mooij, L. Tian, Caspar H. van der Wal, L. S. Levitov, Seth Lloyd and J. J. Mazo, "Superconducting Persistent-Current Qubit," *Phys. Rev. B*, vol. 60, pp. 15398-15413, 1999.

[10] C. H. van der Wal, A. C. J. ter Haar, F. K. Wilhelm, R. N. Schouten, C. J. P. M. Harmans, T. P. Orlando, S. Lloyd and J. E. Mooij, "Quantum Superposition of Macroscopic Persistent-Current States," *Science*, vol. 290, pp. 773-777, 2000.

[11] I. Chiorescu, Y. Nakamura, C. J. P. M. Harmans and J. E. Mooij, "Coherent Quantum Dynamics of a Superconducting Flux Qubit," *Science*, vol. 299, pp. 1869-1871; published online 13 Feb. 2003, 10.1126/science. 1081045

[12] J. Han and P. Jonker, "On Quantum Computing with Macroscopic Josephson Qubits," in *Proc. IEEE-NANO*, pp. 305-308, 2002.

[13] J. Han and P. Jonker, "Novel Computing Architecture on Arrays of Josephson Persistent Current Bits," in *Proc. 5th Int. Conf. MSM*, pp. 636-639, 2002.

[14] J. Han and P. Jonker, "Quantum Cellular Nonlinear Networks using Josephson Circuits," in *Proc. IEEE-NANO*, 2003.

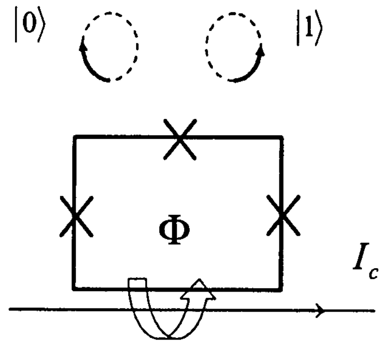

Fig. 1. The Josephson Circuit [8]

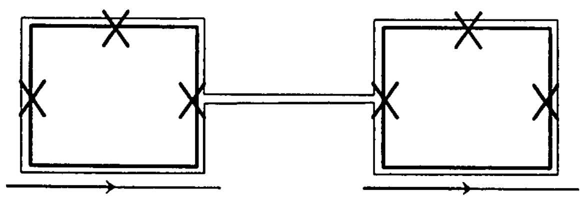

Fig. 2. A Classical Inverter

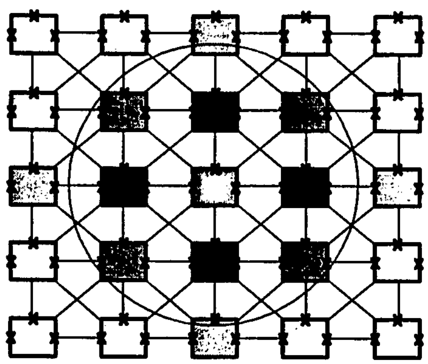

Fig. 3. The Quantum CNNs using Josephson Circuits

QUANTUM INTERFERENCE EFFECTS IN $SrRuO_3$ FERROMAGNETIC OXIDE

G. Herranz, F. Sánchez, B. Martínez and J. Fontcuberta
Institut de Ciència de Materials de Barcelona, CSIC.
Campus U.A.B., Bellaterra 08193. Catalunya. Spain

M.V. García-Cuenca, C. Ferrater and M. Varela
Departament de Física Aplicada i Òptica
Universitat de Barcelona
Diagonal 647, Barcelona 08028, Catalunya. Spain

$SrRuO_3$ is a ferromagnetic oxide that is widely used as electrode in technological nanodevices, due to its good metallicity and chemical stability. It is a 4d itinerant ferromagnet, whith a Curie. temperature of $T_C \approx 160$ K. The ferromagnetism comes from the correlations between electrons that lie in a narrow π^*-band, formed by the hybridization of the 4d-Ru and the 2p-O orbitals. Strong electronic correlations have been proofed experimentally either by specific heat measurements, low-temperature electrical transport or photoemission spectra, among others [1]. Although it has been experimentally verifed that the ground state is a Fermi liquid, it is extremely weak, due to its strong sensitivity to disorder and breaks down at a very low temperature (T ~ 10 K), further confirming the relevance of the correlations between the conduction electrons [2].

Recently we have demonstrated that, under specific conditions of growth, it is possible to introduce a controlled density of defective regions and, thus, offering a way to tune the mean free path of the carriers [3, 4]. This has allowed us to undertake a comprehensive study of the transport properties of epitaxial nanometric $SrRuO_3$ thin films, with thickness down to $t \sim 6$ nm.

At low temperature, for these nanometric thin films, a conspicuous minima in the resistivity – temperature curve appears at a temperature T_{min} (see fig. 1). It is observed that as the microstructural disorder is enhanced, i. e., the residual resistivity ρ_0 increases, the minima appear at a higher T_{min}, i. e., the physical mechanism lying behind these phenomena is enhanced. We have experimentally confirmed the non-magnetic origin of the minima. Thus, the presence of such minima in the ρ – T curves can not been explained by the semiclassical Boltzmann description.

We propose that quantum effects lie behind the existence of the resistivity minima. Indeed, from $\rho_0 \approx 500$ μΩcm, a mean free path of $l \sim 5 - 6$ Å can be estimated, which is comparable to the Fermi electronic wavelength $\lambda_F \sim 5$ Å of the carriers. In view of this, one should expect that quantum effects arising from the interference of the electronic wave functions would be relevant. Indeed, these effects lead to an enhancement of the resistivity at low temperature, since an additional contribution to the scattering of electrons arises from the interference of the electronic wave functions. As the temperature increases, the coherence of the electronic wave functions is suppressed by inelastic scattering events, and the relevance of the quantum interference effects becomes progressively less significant, and a decrease of the resistivity follows. However, at high enough temperature, these quantum effects are totally suppressed, and the common scattering events found in normal metals are recovered. Thus, quantum corrections to the electrical transport could explain the presence of the resistivity minima.

The ρ – T curves at low temperature were fitted according to a model for the conductivity based on the expression [5]

$$\sigma = \sigma_0 + aT^{1/2} \qquad \text{(eq. 1)}$$

where σ_0 is the residual conductivity and the $T^{1/2}$ term is related to the e- - e- interactions corrected by quantum interference effects. We could modify the mean free path of the carriers by specific thin film growth conditions, and a variation of T_{min} was observed in the range 5 K $\leq T_{min} \leq$ 20 K. The ensuing analysis show that as the structural disorder increases the $T^{1/2}$ term is more significant, thus proving that electron – electron interactions are enhanced as the disorder increases.

The results shown here illustrate the extreme sensitivity of the strongly correlated systems to disorder. It must be emphasized that since $l \approx \lambda_F$, we could vary the amount of structural disorder in a clean and homogeneous system, without any modification of its chemical composition. As long as $SrRuO_3$ is a widely used oxide in the fabrication of nanometric technological devices, the findings presented here may have a deep relevance in technological applications.

References:

[1] P. B. Allen et al., Phys. Rev. B **53**, 4393 (1996); M. A. López de la Torre et al., Phys. Rev. B **63**, 052403 (2001); J. Okamoto et al., Phys. Rev. B **60**, 2281 (1999)
[2] L. Capogna et al., Phys. Rev. Lett. **88**, 076602 (2002)
[3] G. Herranz, B. Martínez, J. Fontcuberta, F. Sánchez, C. Ferrater, M. V. García-Cuenca and M. Varela, Appl. Phys. Lett. **82**, 85 (2003)
[4] G. Herranz, B. Martínez, J. Fontcuberta, F. Sánchez, C. Ferrater, M. V. García-Cuenca and M. Varela, Phys. Rev. B 67, 174423 (2003)
[5] *Fundamentals of the theory of metals*, A. Abrikosov, ed. North-Holland (1988)

FIGURE 1

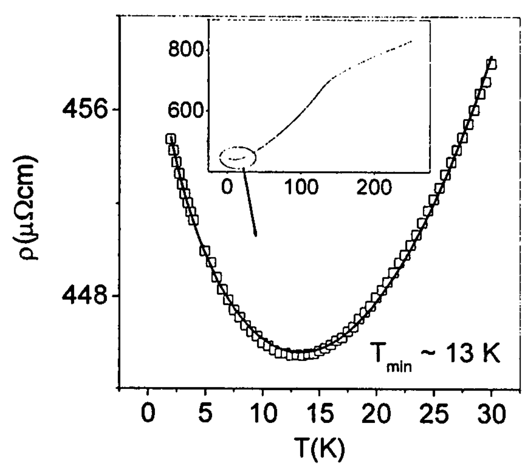

LOW TEMPERATURE GROWTH OF CARBON NANOTUBES BY PLASMA-ENHANCED CVD

S. Hofmann*, C. Ducati, B. Kleinsorge, and J. Robertson
University of Cambridge, UK
E-mail: sh315@cam.ac.uk

Carbon nanotubes and less-crystalline, bamboo-like structured carbon nanofibers are nano-scale building blocks for an increasing number of possible applications. The individual manipulation of these nanostructures is difficult and expensive due to their size. Therefore, thermal chemical vapor deposition (CVD) has gained much attention, as it enables diameter-controlled, position-selective growth of carbon nanotubes on a substrate. We show that plasma-enhanced (PE)CVD not only gives additional vertical alignment of as-grown nanotubes, but also enables growth at significantly lower temperatures.[1] A systematic study of the temperature dependence of the growth rate and the structure of as-grown nanotubes is presented using a direct current plasma-enhanced CVD system with C_2H_2/NH_3 and nickel as the catalyst. Vertically aligned carbon nanotubes were grown on prepatterned substrates at temperatures as low as 120°C. The activation energy for the growth rate was found to be 0.23 eV, much less than for thermal chemical vapor deposition (1.2-1.5 eV)(see figure). The similarity of this value to the activation energy of surface diffusion of carbon on nickel (0.3 eV) suggests PECVD growth at low temperatures occurs by carbon diffusion on the catalyst surface. The result could allow direct growth of nanotubes onto low temperature substrates like plastics, and facilitate the integration in sensitive nanoelectronic devices.

References:

[1] S. Hofmann, C. Ducati, B. Kleinsorge, J. Robertson, Appl. Phys. Lett. , to be published 07/2003.

Figures:

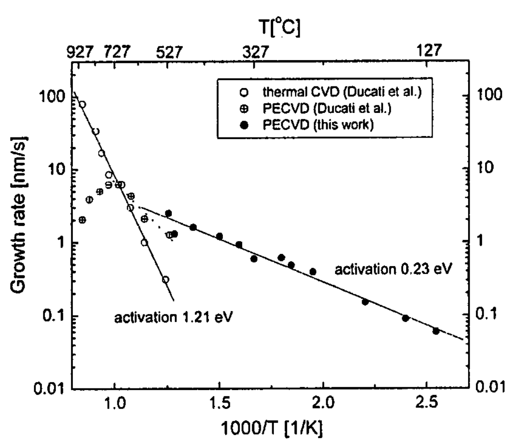

DIELECTRIC CHARACTERIZATION OF MOLECULAR ROTORS AND PADDLE WHEELS

Robert D. Horansky*, Laura I. Clarke*, Mary Beth Mulcahy+, Jose Nunez&, Miguel Garcia-Garibay&, Josef Michl+ and John C. Price*

* Department of Physics, University of Colorado, Boulder, CO 80309-0390
+ Department of Chemistry and Biochemistry, University of Colorado, Boulder, CO 80309-0215
& Department of Chemistry and Biochemistry, University of California, Los Angeles, CA 90095-1569

Molecular rotors, molecules with a rotational degree of freedom about a single bond, are promising elements of nanoscale machinery. Of particular interest are arrays of rotors with permanent electric dipole moments. In these systems the dipole interactions between rotor groups may be controlled or designed to create specific types of behavior, such as ferroelectricity. Through dielectric spectroscopy we measure rotor attributes such as barrier to rotation, polarizability, and homogeneity. Previously, our group presented dielectric results on surface mounted dipolar rotors[1]. These two-dimensional systems showed a broad distribution of rotational barriers owing to interactions with the surface. Presently, we are exploring two second-generation systems that may reduce these surface effects.

First, we consider a three-dimensional crystalline system composed of fluorobenzene rotors surrounded by bulky triphenyl cages (Figure 1). We have observed a narrow distribution of barrier heights consistent with previous NMR data on a non-polar version of this molecule[2]. Because of the high homogeneity of this system we can extract the barrier height, its temperature dependence, and the potential well asymmetries. Neat and clathrate crystals of the same molecule allow us to study this rotor in two distinct local environments.

Secondly, we have studied surface mounted rotors with the rotational axis parallel (rather than perpendicular) to the surface. These rotors consist of two stands supporting a "paddle wheel" rotor between them (Figure 2). This system shows a dielectric response consistent with predicted barrier heights from molecular mechanics. These structures could have applications to enhancing fluid flow at surfaces. In keeping with the surface mounted nature of the molecule, we have observed that rotor response in this system can be suppressed when adsorbates are present on the surface.

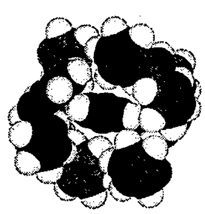

Figure1: Fluorobenzene rotor group (red) group
Surrounded by neighboring triphenyl groups (blue)

Figure2: "Paddle Wheel" rotor with rotating

in green.

References:

1. L.I. Clarke, et. al. *Nanotechnology.*13(4), p. 533 (2002)
2. Z. Dominguez, et. al. *Journal of American Chemical Society.***124**, p. 7719 (2002)

MAGNETIC-FIELD INDUCED CHARGE LOCALIZATION IN VERTICALLY COUPLED QUANTUM DOTS

David Jacob

Depto. Fisica Aplicada, Universidad de Alicante
Cra San Vicente, 03690 San Vicente del Raspeig (Alicante), Spain
E-mail: djacob@physik.uni-hamburg.de

Daniela Pfannkuche

I. Institute of Theoretical Physics, University of Hamburg,
Jungiusstr. 9, D-20355 Hamburg, Germany

We study a pair of vertically coupled identical two-dimensional quantum dots (QDs) subjected to a vertical magnetic field, and containing three interacting electrons . The vertical degree of freedom is described in the so-called "layered electron gas" model [1], where an electron can only be in one of the two layers that define the individual QDs. Thus the electron has an additional spin-like degree of freedom ("isospin"). In this model the electron hopping between the layers is described by the tunnel Hamiltonian. Additionally we incorporate a small electric field in the vertical direction, which breaks the symmetry between the upper and the lower quantum dot. The eigen states and eigen energies are computed by using an exact diagonalization scheme to include electron-electron correlations due to the Coulomb interaction [2,3].

We find that by adjusting the magnetic field to a certain value a vertical electric dipole moment can be induced corresponding to two electron charges localized in the energetically favoured dot and one electron charge in the other. We wish to emphasize that the electric field just serves to break the symmetry. It can in principle be made infinitesimally small (only limited by the floating-point precision) and still one could observe the described localization effect.

The effect can be understood as an anticrossing between the two lowest-lying eigen states to constant total angular momentum (L_Z) and total spin (S,S_Z) mediated by the symmetry-breaking electric field. Looking at the Slater expansions reveals that the nature of the correlation is diffenrent for the two crossing states: One state can be written as a *sum* of an expansion representing a +1/2 isospin configuration (two electrons in the upper QD and one in the lower), and another expansion representing the -1/2 isospin configuration (two electrons in the lower QD and one in the upper) whereas the other state is just given as the *difference* between these expansions. At the crossing point the perfect superposition of the two states thus leads to one state with two electrons in the upper QD and one electron in the lower QD, and the other state with the inverse electron configuration. Depending on the direction of the symmetry-breaking electric field one of these states becomes energetically favourable compared to the other state leading to the described electronic polarization of the system.

We believe that this localization effect is a general property of symmetry-broken double quantum dots containing an odd number of electrons. Therefore double quantum dots containing an odd number of electrons could in principle be used to implement charge qbits as proposed in ref. [4] where the (effective) two-level system representing the qbit is given by the two opposite polarization states. The energy difference between the two states is given by the energy difference between the two QDs caused by the electric field, so that the electric field can be used to switch between the two states.

References:

[1] J.J. Palacios and P. Hawrylak, Phys. Rev. B 51 (3), 1769 (1995)

[2] H. Imamura et al., Phys. Rev. B 53 (19), 12613 (1996)

[3] H. Imamura et al., Phys. Rev. B 59 (8), 5817 (1999)

[4] S.-R. E. Yang et al., Phys. Rev. B 66 (153302) (2002)

Fabrication of Molecular Devices – An Art of Science

Mohammad Shafiqul Kabir
Solid State Electronics Laboratory, Department of Microtechnology and Nanoscience (MC2), Chalmers University of Technology, Gothenburg, Sweden
E-mail: shafiq@ic.chalmers.se

The poster converse the development of different alternative technologies to fabricate different types of nanoscale devices based on non-conventional materials like: molecules, clusters and carbon nanotubes (CNT). We have exploited the quasi one-dimensional nature of these materials in combination with e.g. self assembling techniques, surface treatments and nanolithography for device functionality. Figure 1 (a) depicts our developed work methodology which worked as roadmap to reach our goal.

An important technological aspect of fabrication of molecular devices is to fabricate nano-gaps and nano-electrodes. We have established *two different methods of fabricating sub 5 nm gaps* rather reproducibly (inset of figure 1(b) & (c) respectively). We have successfully introduced a third terminal, which acts as a gate electrode, with an ultra thin oxide (~1-4 nm thick) on aluminum.

An approach to measure conjugated molecules in a system like *metal-molecules-clusters-molecules-metal* was carried out as an early attempt where an unusual time dependent conductance was observed (figure 1(b)). In another attempt to measure single conjugated molecule in a nanogap, we have observed fluctuations at high source-drain bias in the differential conductance plot (figure 1(c)).

We have investigated the electronic properties of gold clusters either capped (bounded by organic legends) or stabilized with some specific organic molecules with the aim of fabricating novel electronic devices. Two different methods of surface treatment prior to clusters alignment were implemented for the experiments performed on the *Tri Octyle Amino Bromine* (TOABr) stabilized gold clusters with a size distribution of 5-7 nm. Clusters aligned on a *–SH terminated SAM* (Self Assembled Monolayer) treated layer exhibited *single electron transistor (SET)* behaviors as expected (figure 2 (a)). In contrast, clusters aligned on a surface functionalized by Markepto Silane showed *field effect* behavior where a transition from nonlinear to linear current voltage characteristics as a function of gate voltage is observed *for the first time* (figure 2 (b)). It is also intriguing to observe the *field effect transistor (FET) behavior for the first time* from the device based on (-SH) terminated gold clusters (figure 2 (c)).

We have developed and optimized a technology to orient individual carbon nanotubes using electric field distribution control in the submicron scale, to facilitate the assembling of nanotubes between predefined electrodes (figure 3 (a)). Fabrication of devices by making the electrodes on top of the nanotubes was also carried out. Many of the fabricated devices showed very interesting results. In one of the investigated IV characteristics of crossed CNTs at various temperatures, the current voltage characteristics changed from linear behavior to non-linear as a function of temperature. At some electrode pairs of the same device, gate dependence of IV characteristics at 1.4 K shows coulomb oscillations (figure 3(b)).

An important observation from all these experiments and analysis is that: "the characteristics of an electronic 'nano-device' not only depends on the intrinsic properties of the materials but is also strongly correlated with the method of device fabrication".

Reference:

[1] **Fabrication and Characterization of Molecular Devices** – Mohammad Shafiqul Kabir, Licentiate thesis, Chalmers University of Technology, ISSN: 0280-2872, 2003

Keywords: Electron Beam Lithography (EBL), Photo lithography, Reactive ion etching (RIE), e-beam evaporation, resistive evaporation, Atomic Force Microscopy (AFM), Scanning Electron Microscopy (SEM), Transmission Electron Microscopy (TEM), Self Assembling.

Figures:

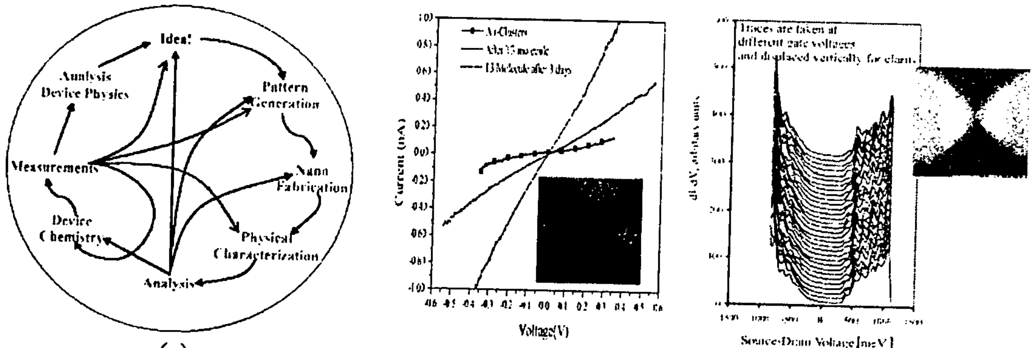

(a) (b) (c)

Figre 1: (a) Closed loop of the work methodology for fabricating molecular devices. (b) IVas a function of time for T3 conjugated molecules. Inset the AFM topography of the ~ 5 nm gap made by angle evaporation technique. Side gates are also visible. (c) Conductance fluctuation at high source-drain bias for T3 molecules. Inset the SEM micrograph of a < 5 nm gap made by shot modulation technique, Al gate is underneath.

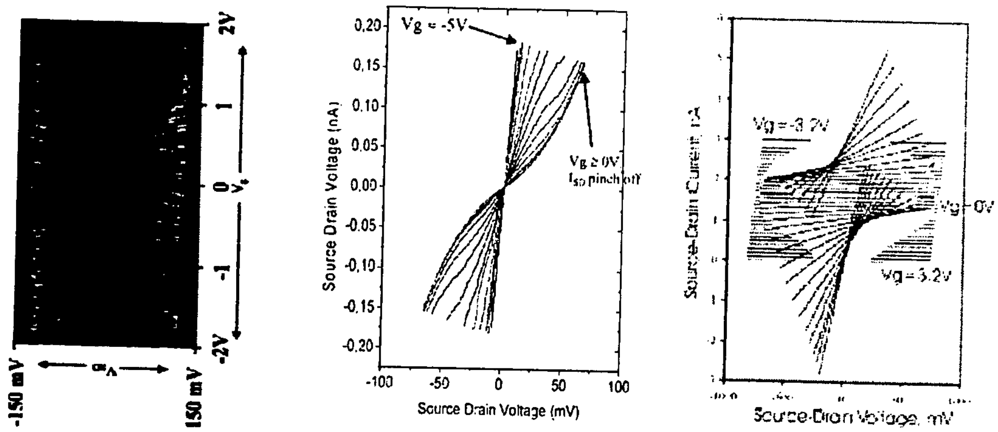

Figre 2: (a) Stability diagram of a SET device based on TOABr stabilized gold clusters. (b) & (c) Field effect behavior of two different gold clusters.

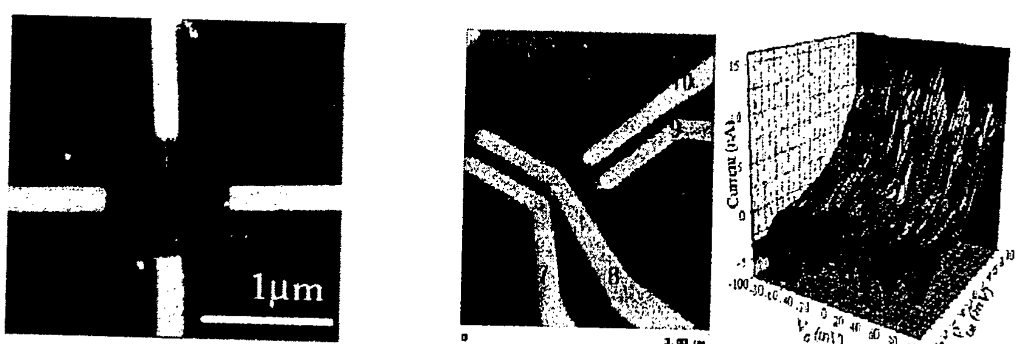

(a) (b)

Figre 3: (a) Nanotubes aligned by electric field induced trapping. (b) Nanotube device made by electrodes on top of the nanotubes and corresponding IV characteristics as a function of gate voltage.

MAGNETIZATION REVERSAL IN ULTRATHIN, NANOSTRUCTURED EPITAXIAL Fe FILMS ON GaAs(001)

W. Kipferl, M. Dumm, R. Pulwey and G. Bayreuther

Institut für Experimentelle und Angewandte Physik, Universität Regensburg,

93040 Regensburg, Germany

Email: wolfgang.kipferl@physik.uni-regensburg.de

Homepage: http://www.physik.uni-regensburg.de/forschung/bayreuther/

High quality epitaxial Fe films were grown on GaAs(001) by molecular beam epitaxy. Dot arrays with several million dots of well defined circular shape (diameter 500 - 100 nm; thickness 2 nm = 14 monolayers) were fabricated by electron beam lithography and lift-off technique. The magnetic properties of the samples were investigated by MFM, MOKE, AGM and SQUID magnetometry between 10 and 350 K.

All films have an in-plane uniaxial magnetic anisotropy with the easy axis along [110] which is conserved during patterning. This intrinsic uniaxial anisotropy always forces the magnetization of the dots in remanence into a single domain state as inferred from the high remanence of 100 %. Magnetization reversal shows a strong increase of the coercive fields, H_C, with decreasing diameter in comparison to the continuous film (see Fig. 1). The very sharp switching behavior of the dot arrays indicates a high uniformity of dot size and shape. The measured coercivity values are in good agreement with micromagnetic simulations (LLG Scheinfein Micromagnetics, see Fig. 2) at 10 K for all samples, whereas at room temperature the experimental H_C values are smaller than those calculated using the magnetization and anisotropy values for 300 K without explicitly considering the role of thermal excitations for the reversal process. This is explained by thermal excitation of additional spin wave modes due to the lateral confinement [1].

Support by the Deutsche Forschungsgemeinschaft is gratefully acknowledged (grant No FOR 370).

Reference

1) W. Kipferl, M. Dumm, M. Rahm, and G. Bayreuther, J. Appl. Phys **93**, 7601 (2003)

Figures

1) magnetization reversal of patterned Fe/GaAs(001) films with different diameter at 10 K

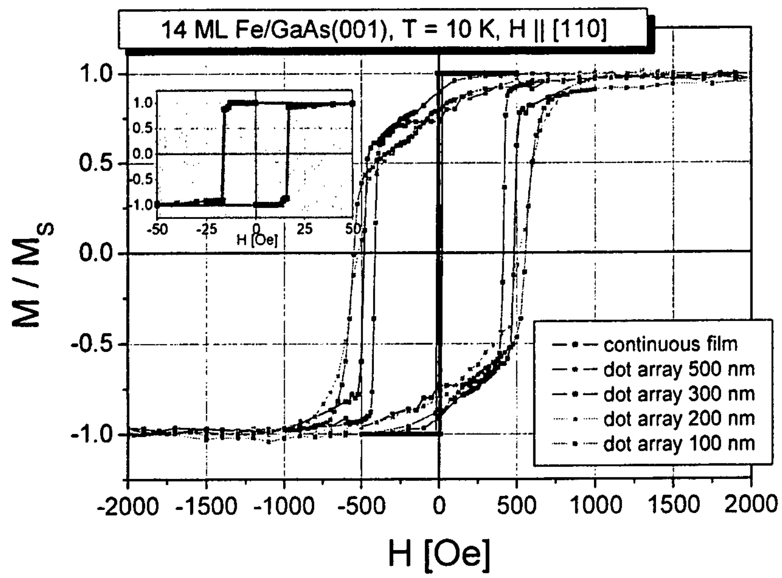

2) simulated magnetization loops of patterned Fe film with diameter 500 nm, T = 10, 300 K

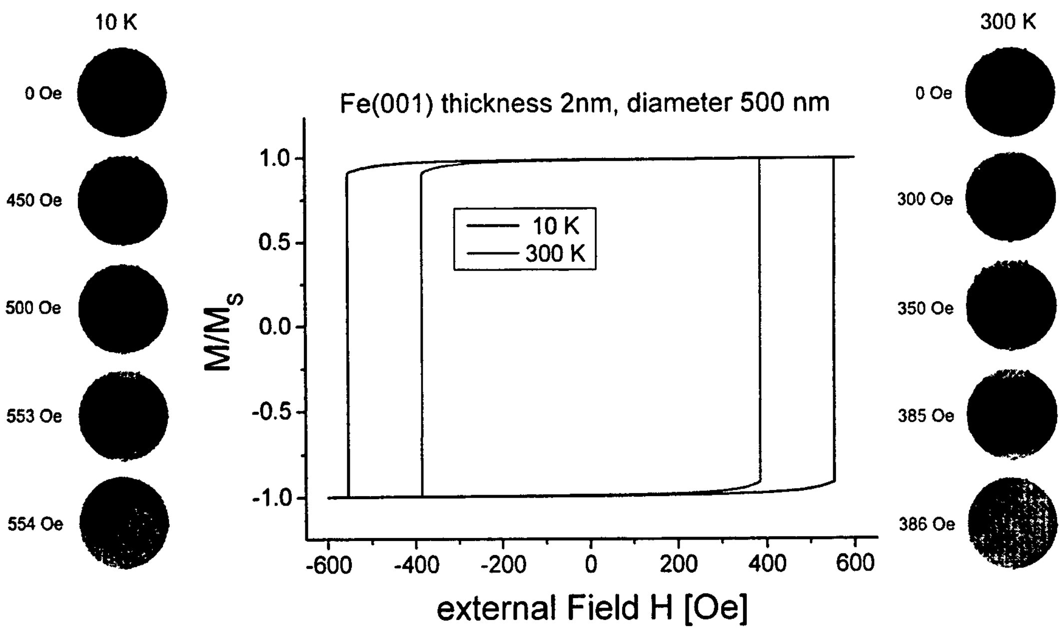

Poster

A QUANTUM RANDOM NUMBER GENERATOR ON MAGNETIC FLUX QUBITS

Viktor O. Ledenyov[1], Dimitri O. Ledenyov[2] and Oleg P. Ledenyov[1]

[1]National Scientific Center Kharkov Institute of Physics and Technology, UKRAINE
[2]Department of Electrical and Computer Engineering, James Cook University, AUSTRALIA
ledenyov@ieee.org

The current trend in industry is to develop a new generation of nanoscale size electronic devices. The fundamental properties of nanoscale electronics may be described by the quantum theory, as it was predicted by Feynman [1] and Deutsch [2]. The quantum computation devices have the advanced properties, including the use of new computation processing algorithms. Shor [3] and Grover [4] proposed the possible realization of the high efficient quantum computation algorithms for both the large number factorization and search in a large database tasks. We propose the quantum random number generator, which operates with the large numbers and produces the final result after the one quantum step. The random number generators have many applications in the communication, cryptography, computation.

Introduction

The usual random number generators may be developed using the two main approaches: the software based realization of algorithmic computations and the hardware based implementation with the special registration systems. The mathematical algorithmic probability theory [5, 6] predicts that the algorithmic procedures must be as long as 2^N computations to find the real independent random number with the N binary digits, and this operation takes long time. As a result, now, most of the algorithmic random generators produce the pseudorandom numbers using the fast algorithms. The physical random number generators use the different classical and quantum phenomena to make the string with the random positions of 0 and 1. All the classical phenomena are deterministic, and may be reversed in time, therefore, after the "long" work, all the properties may be computed and predicted. The quantum random processes such as the atom decay and quantum fluctuations are used in some models as the basic processes for the random number generators, but the random number must be the accumulation of at least N atom decays or other events for the determination of N digits. The time delay in this quantum process is a limiting factor for its use in the fast near-real-time applications.

Substantiation

We propose the use of the massive time parallelism of quantum wave functions, when they transform from the entangled states to the projection basic states in the Hilbert space of quantum system. These properties are used in quantum computation process for the realization of quantum computers [7]. In our approach, we place the M quantum particles in quantum "black" box **B** to produce the random number with N binary digits (M<N). M is the random number. This state may be described by the wave function $\mathbf{\Psi(M, B_M)}$ in the initial Hilbert space. The position of each particle in the box is not known. We "scatter" this state on the S body, which contains the macroscopic number of particles to the final state with N quantum boxes. The 2^N vectors of independent binary states create the system of basis vectors of the final Hilbert space. During the time of scattering process, the wave functions of both the scattering system and the initial state are linked by expression $\mathbf{S\Psi(M, B_M) \Rightarrow \Sigma_i \{\Sigma_k \alpha_i \cdot\Psi_k(0/1, B_{0/1})\}}$, where $\mathbf{\Sigma_i}$ is the infinity sum, $\boldsymbol{\alpha}_i$ – complex coefficients, k – from 1 to 2^N. In the final state, after the measurement procedure, the wave functions are reduced to the N wave functions. In other words, all the spaces may be complementary to the algebra A with the

special operation θ of the vector multiplication of vectors in the states space $\Psi_f = \Psi_i \,\theta\, \Psi_s$. After the moment, when the vectors of the algebra are projected on the N boxed states, the positions of the boxes with the quantum particles (1) and the positions of the empty boxes (0), may be measured reducing all other states to the one. All these 1 and 0 produce the string with the N binary digits, which is the random number obtained in one step quantum scattered process. It is possible to use the non-analytic scattering operator S. In this case, the scattering operation is generated by the phase transition operation, and it destroys the order parameter of the system, and creates the new parameter. This operation occurs in macroscopic quantum system, and the wave functions of all the particles scatter on the macroscopic number of particles of the scattering system. The interesting algorithm is the scattering process in the quantum electromagnetic system in the box with the Leonardo da Vinci (LdV) quantum mirror walls. This box represents the state with M quantums and with all the infinity mirror images, which in quantum state may not be discerned from the real states. Using the mirror, we can initiate the very entangled state with the infinity number of states and the quantum random evolution. There are some specific quantum limitations for the quantum translation, transposition and rotation operations of the quantum images in mirrors.

Modeling

The system, which operates using this algorithm, may be realized as the square lattice of the $N^{1/2}xN^{1/2}=N$ holes in the superconducting film with the diameter of hole $D\sim\lambda$ and film thickness $d > \lambda$, the holes lattice parameter $a > \lambda$, where λ is the magnetic field penetration depth. For example, N is equal 1024. The S operator is represented as the fast laser heating-cooling process, which heats up the lattice to the temperature $T>T_C$ and destroys the superconducting state, but it leaves the superconducting boundary and conserves the full magnetic flux (number of particles). This is the "black" box state. When the laser is switched off, the superconducting film is cooled down in 10^{-8}sec. This stage is the scattering process, when the wave functions of flux quantums and the wave function of lattice are fully entangled. The random positions of the flux quantums in the holes may be monitored by the N SQUID sensors, which are positioned on the inverse surface of ground plate and have the sensitivity $10^{-5}\ \Phi_0 Hz^{1/2}$. The random number has the 1024 binary digits and it is selected from the 2^{1024} numbers. We investigated the switching time from the entangled to pure states; the nature of physical phenomenon, which may destroy an independence of quantum states in the lattice; the role of the LdV superconducting mirror and the time of complete operation.

Conclusions

We developed a new model of the quantum random number generator and its realization on the magnetic flux qubits.

References

[1] R.P. Feynman, Int. J. Theor. Phys., **21**, 467-488 (1982)
[2] D. Deutsch, Proc. R. Soc. London A, **400**, 97 (1985)
[3] P.W. Shor, Proc. 35th Ann. Symp. Found.Comp. Science ed. by Goldwasser (IEEE Comp. Soc. Press, Los Alamitos, CA), p. 124 (1994); SIAM J. Sci. Statist. Comput., **26**,1484 (1997)
[4] L. K. Grover, Phys. Rev. Lett. **79**, 325 (1997); Phys. Rev. Lett. **79**, 4709 (1997)
[5] A.N. Kolmogorov, "Sankhya", ser. A, v. 25, 369 (1963)
[6] P. Martin-Lof, IEEE Transactions, IT, v.14, 662 (1968)
[7] H.-K. Lo, S. Popescu and T. Spiller, Introduction to Quantum Information and Computation, World Scientific, Singapore (1998)

Triple-Gate MOSFETs fabricated with Interference Lithography

M. Lemme, C. Moormann, H. Lerch, M. Möller, B. Vratzov, H. Kurz
Advanced Microelectronic Center Aachen (AMICA), AMO GmbH, Huyskensweg 25,
52074 Aachen, Germany, E-Mail: Lemme@amo.de, http://www.amo.de

The commercial success of the semiconductor industry for the past decades has been largely driven by continuous reduction of device dimensions. At the turn of the 21st century, a transition from micro- to nanoelectronics has taken place, as transistor dimensions have reached the sub-100nm level. The main benefit of this scaling, besides reduction of cost, has been increased transistor current drive and hence increased switching speeds. The international technology roadmap for semiconductors (ITRS) predicts, that this trend will continue at least until the year 2015 [1]. By then, novel, non-planar device architectures such as Triple-Gate-MOSFETs in Figure 1 or FinFETs on SOI material may be necessary to achieve functional devices [2], as they yield excellent control of the gate over the channel and thereby strongly reduce off-state leakage currents [3][4]. In addition, Triple-Gate MOSFETs can enhance the transistor drive current, if the line to space ratio is chosen accordingly [5].

Interference lithography (IL) or holographic lithography is the preferred method for fabricating periodic, quasi-periodic and spatially coherent patterns. Its relatively simple and maskless operation principle, utilizing the interference of two or more coherent planar wave fronts, is ideal for low cost full wafer exposures of sub 100 nm features.

In this work, a fabrication process for Triple-Gate-MOSFETs is presented, where interference lithography has been integrated into an SOI-CMOS process. After channel doping, IL has been mixed with optical lithography to define source and drain of the transistor as shown in Figure 2. The elevated source and drain regions (Mesa) have been etched using an SF_6 / O_2 plasma process. After thermal gate oxidation and poly-silicon deposition, the gate has been etched using HBr-chemistry. Doping has been achieved by ion implantation and rapid thermal activation. A scanning electron microscope image of a Triple-Gate-Transistor is shown in Figure 3.

The Triple-Gate-MOSFETs have been electrically characterized to demonstrate the feasibility of the process. An example of transistor output characteristics are shown in Figure 4.

References:

[1] International Technology Roadmap for Semiconductors: 2002 Update, International Sematech, http://public.itrs.net/Files/2002Update/2002Update.pdf, 2002.

[2] H. P. Wong, D. J. Frank, P. M. Solomon, C. H. Wann and J. J. Welser, "Nanoscale CMOS", Proceedings of the IEEE, **87**, No. 4, pp. 537-569, April, 1999.

[3] Y.-K. Choi, T.-J. King and C. Hu, "Nanoscale CMOS Spacer FinFET for the Terabit Era", IEEE Electron Device Letters, **23**, pp. 25-27, No. 1, January, 2002.

[4] M. Lemme, T. Mollenhauer, W. Henschel, T. Wahlbrink, M. Baus, B. Spangenberg and H. Kurz, "Nanoscale SOI-MOSFETs with non-planar Multiple Gates", Proceedings of the 4th European Workshop on Ultimate Integration of Silicon, ULIS 2003, Udine / Italy, pp. 15-18, March 20-21, 2003.

[5] M. Lemme, T. Mollenhauer, W. Henschel, T. Wahlbrink, M. Heuser, M. Baus, O. Winkler, B. Spangenberg, R. Granzner, F. Schwierz, H. Kurz, „Influence of Channel Width on n- and p-type Nano-Wire-MOSFETs on Silicon on Insulator Substrate", in press: Microelectronic Engineering 67-68C, 810-817, 2003.

Figures:

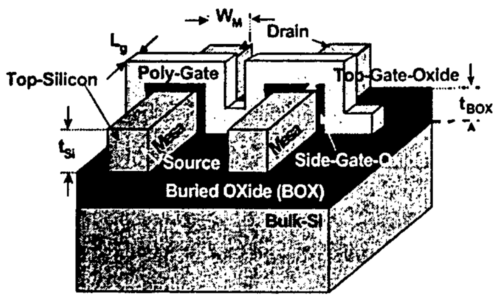

Figure 1: Schematic of a Triple-Gate-MOSFET

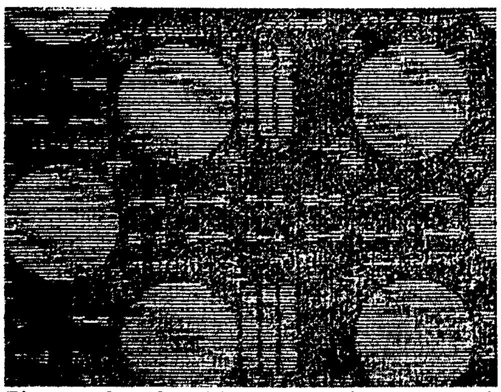

Figure 2: Combined interference and optical lithography

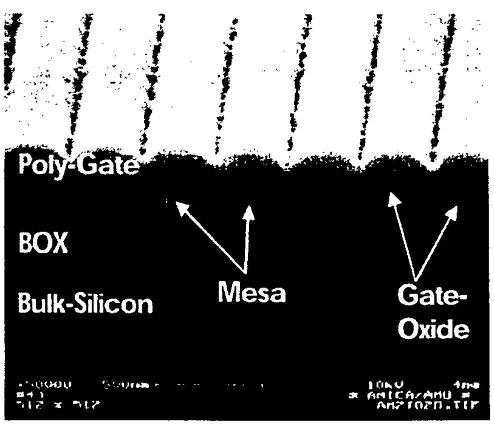

Figure 3: Scanning electron microscope image of a Triple-Gate-MOSFET with seven parallel channels.

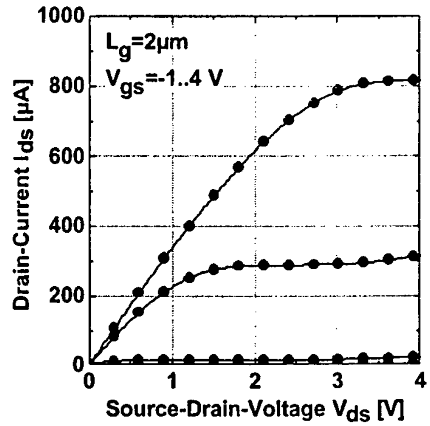

Figure 4: Measured output characteristics of a Triple-Gate-MOSFET.

HYBRID-BASIS MODELING OF TRANSPORT THROUGH MOLECULE-SEMICONDUCTOR INTERFACES

Gengchiau Liang, Avik Ghosh, Titash Rakshit, and Supriyo Datta
School of Electrical and Computer Engineering, Purdue University, West Lafayette, IN 47906, USA
E-mail: liangg@purdue.edu

Molecular electronics promises to be the basis for the next generation of electrical devices, following considerable progress in experimental techniques and theoretical studies in the area. There have been many theoretical simulations of conducting properties of molecular devices using both first-principles and semi-empirical methods. Most of the first-principles calculations give accurate results for isolated molecules; however, transport properties of molecules require an accurate description of the molecule and its interface with the contact under non-equilibrium conditions. Usually the localized basis-sets that describe molecules very well are not efficient in characterizing bulk properties of the contact, although the latter are quite important for determining the functionality of a device. Semi-empirical calculations like Extended Huckel Theory (EHT) or effective mass method are typically better equipped to modeling both the bulk and the surface physics of contacts.

In this work, we develop formalism to couple two different basis functions in order to accurately model the molecules and the contacts. As an example, we use EHT with optimized tight-binding parameters to describe bulk silicon, and couple it with an ab-initio basis, 6-31g(d), to simulate the contact surface atoms and the molecules grown on silicon. Such a coupling is achieved by matching the surface green's function in real space in both basis sets. We will use this hybrid-basis formalism to describe STM measurements on molecules like styrene grown on silicon. Our simulations predict a prominent negative-differential resistance (NDR) in such molecular I-Vs due to the interaction between the molecular levels and the silicon band-edge. Our results are corroborated by preliminary experiments by Mark Hersam's group at Northwestern University.

CLASSIFICATION OF THREE-TERMINAL JUNCTIONS CARBON NANOTUBES

L. Chernozatonskii, S. Lisenkov

Institute of Biochemical Physics, RAS, Moscow,119991, Russian Federation

The carbon nanotube junctions have recently emerged as excellent candidates for use as building blocks in the formation of nanoscale electronic devices. The discovery of localized bends in multiwalled pure carbon nanotubes has inspired theoretical investigations of simple two-point tube junctions in single-walled tubes [1,2]. If such a heterojunction is formed by two nanotubes, one semiconducting and the other metallic, the junction will function like a rectifying diode.

Connecting different single-wall carbon nanotubes to form three-terminal heterojunctions have been proposed recently [3,4]. In particular, we suggested the use of carbon nanotube "T" and "Y junctions" as three-terminal nanoscale molecular electronic devices.

Earlier experiments observations of carbon nanotube Y junctions did not attract much attention for electronic applications due mainly to the difficulties associated with their synthesis and the complexities of their structures. In order for the Y-junctions to be useful from device perspective, controlled and high-yield production of these junctions is required. Recently, Y-junction nanotubes have been produced by using Y-shaped nanochannel alumina as templates [5], and by pyrolysis of methane over cobalt supported on magnesium oxide [6].

It is very important to know which construction the real junction corresponds. So we must know all possible constructions of their three-terminal nanotube junctions.

We present the general classification of quasi two-dimensional single-wall carbon nanotube 3-terminal junction - planar Y ("fork"-, "slingshot"-, "bough"- types (fig.1*a,b,c*)), T-junctions (fig. 1*d*). Although pristine nanotubes contain only hexagonal arrangement of carbon atoms, formation of a multiterminal junction requires the presence of topological defects in the form of pentagons, heptagons and octagons. This is essential for maintaining sp^2 configuration for all carbon atoms in order to maximize stability. It is interesting to note that topological defects in multiterminal junctions including the Y-junctions obey a generalization of the well-known Euler's formula modernized for three-terminal junctions carbon nanotube with open ends:

$$n(7)+2n(8)-n(5)=6\ , \qquad (1)$$

where $n(5)$, $n(7)$ and $n(8)$ are the number of pentagons, heptagons and octagons, respectively.

Our classification is based on introducing topological heptagon (H) and octagon (O) defects in the hexagonal graphitic net. The set of tables allows to get a set of various topological defects for given indices (n,0) – "armchair" or (n,n) "zigzag" SWNT's as stems and branches and symmetries that are necessary for generation of three-terminal nanotube junction. Thus, (aaa)-, (aza)-, (azz)-,(zzz)-,(zza)-,(zaa) – combination with different angles between branches are considered, and corresponding structures with defect types (H6, H4O1, H2O2, O3) are modeled by molecular dynamic methods too.

Using the equation (1) we perform the computer simulation of different types of three-terminal junctions according our classification. We sow that one Y- or T-junction can be transform in another with neither Stone-Wales transformation or including or excluding C_2 cluster connecting two heptagons.

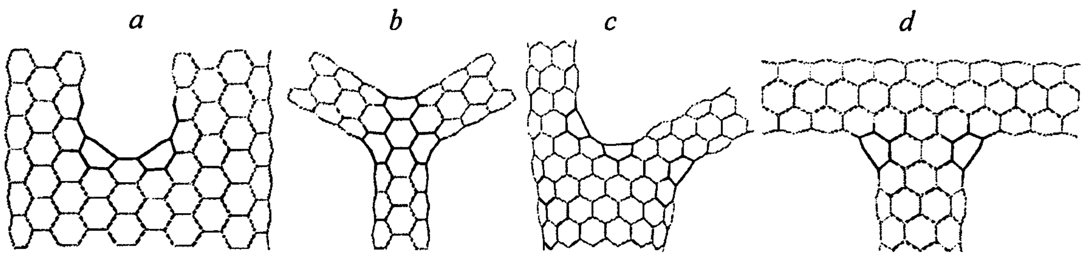

Fig.1 The types of three-terminal junctions carbon nanotubes : *a-c* - Y –junctions, *d* – T-junction.

[1] L. Chico, V.H. Crespi, L.X. Benedict, S.G. Louie, and M.L. Cohen, Phys. Rev. Lett. **76**, 971 (1996).

[2] J.C. Charlier, T.W. Ebbesen and Ph. Lambin, Phys. Rev. B **53**, 11108 (1996).

[3] L.A. Chernozatonskii, Phy. Lett. A **172**, 173 (1992)

[4] M.Menon and D. Srivastava, Phys. Rev. Lett. **79** 4453 (1997).

[5] J.Li, C. Papadopoulos, J. Xu. Nature, **402**, 253 (1999) .

[6] W.Z. Li, J.G. Wen and Z.F. Ren. Appl. Phys. Lett., **19**, 1879 (2001).

CURRENT DISTRIBUTION IN B/N DOPED CARBON NANOTUBES

Yi Liu

Physics Department, McGill University

Using density functional theory and Keldysh nonequilibrium Green's functions, we investigate electron current density distribution in molecular electronic devices. In particular, we present the current distribution in pristine (5,5) armchair carbon nanotube as well as in nanotubes with substitutional doping of boron and nitrogen impurity atoms. The presence of impurity breaks the uniformity of current distribution around the carbon rings. For the more electronegative impurity of nitrogen, the current density is attracted toward the side of the tube where the N atom is located; but for the less electronegative impurity of boron, the opposite happens. We measure the current redistribution due to the impurity doping.

EXCHANGE ANISOTROPY OF AGREGATED Co/CoO FINE NANOPARTICLES IN SPHERICAL SUPERSTRUCTURES

Carlos Luna, Mª del Puerto Morales, Carlos J. Serna and Manuel Vázquez
Instituto de Ciencia de Materiales de Madrid (CSIC), 28049 Madrid, Spain
E-mail: cluna@icmm.csic.es

The relevance of magnetic nanocrystals in advanced research technology has been growing in the last years due to their great scientific interest and their spectacular potential applications in nanotechnology [1]. Particularly, astonishing chararacteristics of highly ordered ultra-fine nanosized magnetic particles arranged in superlattices can be achieved by self-assembling preparation processes. That is considered to be of real interest for the development of future magnetic storage systems [2,3].

Considering the possibility of data storing of 1 bit per particle, one of the exigencies of the upsurge of the recording density is to reduce the grain size. A clear limitation for this reduction is the non-stability of the ferromagnetic behavior of ultrafine particles due to thermal fluctuations of magnetisation that makes particles with size smaller than the critical one to behave as superparamagnetic [3]. So, a larger magnetic anisotropy is required to keep stable magnetisation at room temperature of particles a few nanometers in size. In a very recent work, it has been shown that the Ferromagnetic/Antiferromagnetic (FM / AFM) magnetic coupling is a powerful source to achieve an extra-large anisotropy [4]. For example, the blocking temperature of 4 nm size nanoparticles can be increased from 10 K to about 290 K by embedding such particles in an antiferromagnetic matrix (CoO). Thus, additional studies about the magnetic exchange coupling are required to gain a more complete knowledge about this phenomenon.

In the present work, Co nanocrystalline particles 8 nm in diameter with a core-shell structure (Co/CoO), have been prepared by the so-called *polyol process* [5] in the presence of surfactants. When these nanoparticles are deposited onto a substrate from a colloidal dispersion and slowly evaporation of the solvent, they spontaneously form self arrangements consisting in spherical superstructures with diameters around 300-400 nm (Fig. 1a). The thermal evolution of coercivity of these particles has been analysed after field cooling, FC, and zero field cooling, ZFC, processes. The coercivity measured after FC process takes larger values than after ZFC process. Moreover, the hysteresis loops obtained by field cooling from 300 to 5 K in a field of 70 kOe are shifted along the applied field orientation (Fig. 1b). It can be observed that below 150 K, hysteresis loops begins to shift and the coercivity increases. The loop displacement is more important as the temperature decreases suggesting that when the oxide layer starts the blocking process, an additional anisotropy arises.
These experimental results are interpreted considering the unidirectional anisotropy induced by exchange coupling between the ferromagnetic particle core and the antiferromagnetic oxide shell.

References:

[1] J. L. Dormann, D. Fiorani (Eds). Magnetic Properties of Fine Particles. North-Holland, Amsterdam, 1992.
[2] S. Sun, C. B. Murray, D. Weller, L. Folks, A. Moser. Science 287 (2000) 1989.
[3] S. Anders, S. Sun, C. B. Murray, C. T. Rettner, M. E. Best, T. Thomson, M. Albrecht, J.-U. Thiele, E.E. Fueelerton, B.D. Terris. Microelectronic Engineering 61-62 (2002) 569
[4] V. Skumryev, S. Stoyanov, Y. Zhang, G. Hadjipanayis, D. Givord, J. Nogués. Nature 423 (2003) 850.
[5] F. Fiévet, J. P. Lagier, M. Figlarz, MRS Bull. 14 (1989) 29.
P. Toneguzzo, G. Viau, O. Acher, F. Fiévet-Vincent and F. Fiévet, Adv. Mater. 10 (1998) 1032.
[6] C. Luna, M. P. Morales, C. J. Serna, M. Vázquez. Nanotechnology 14 (2003) 268.

Figures:

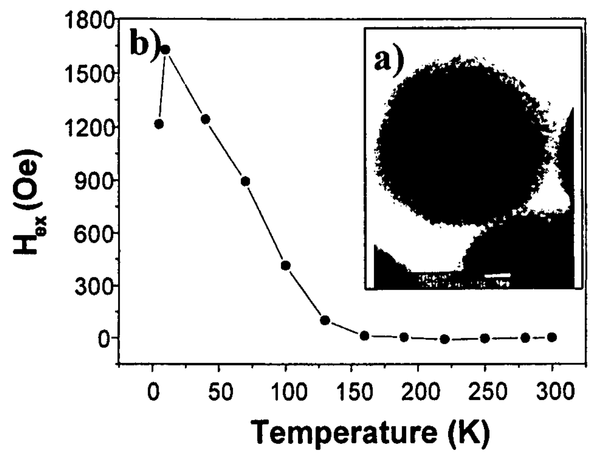

Fig. 1. a) TEM image of the superstructure organisation of Co nanoparticles synthesised in the presence of oleic acid. b) Thermal dependence of Exchange Field defined by $H_{ex} = \frac{-\left(H_C^{Right} + H_C^{Left}\right)}{2}$ where H_C^{Right} and H_C^{Left} represent the field at which the magnetization is vanished on the right and on the left respectively.

STRUCTURAL AND ELECTRONIC PROPERTIES OF BUCKLED CARBON NANOTUBES

E. Machado and P. Ordejon

Institut de Ci`encia de Materials de Barcelona (CSIC), Campus de la U.A.B. E-08193
Bellaterra, Barcelona, Spain
E-mail: 1. machado@icmab.es . 2. ordejon@icmab.es
http://www.icmab.es/dmmis/leem/

At present there is a considerable interest towards the exploitation of the exceptional electronic and mechanical properties of carbon nanotubes (NT's). Based on the possibility of making nanotube-based microelectronics, research groups have fabricated various individual single wall nanotube electronic devices [1, 3].
However, now it is necessary to get a good understanding of how the geometrical and electronic properties of NT's would change when defects are present. This is especially important when it is necessary to manipulate the shape of NT's in order to obtain these designed devices.
Applying mechanical force on a NT can originate a bent within that NT.
If the strain is sufficient, the bent nananotube deforms into a buckle, i.e, a severe distortion of the atomic structure where all the strain is concentrated locally.
Scanning tunneling microscopy and spectroscopy measures done by Jansenn *et al* [2] on a semiconducting nanotube have shown how the local electronic structure changes. They report localized states below the conduction band.
Here we present *ab-initio* Density Functional Theory calculations to study the effect of a strong structural distortion, a buckle, on the structural and electronic properties of a metallic (8,8) and a semiconducting (13-0) nanotube. Our results on the semiconducting NT show localized states above the valence band. We compare these to the experimental and discuss the nature of this states. At the same time we simulate STM images in the the region of these states. In the case of the metallic NT we compare our result with similar calculation present in the literature [4, 5]

References

[1] S.J. Tans, A.R.M. Verschueren, and C. Dekker, Nature (London) **391**, 49 (1998)
[2] J.W. Janssen, S.G. Lemay, M. van den Hout, M. Mooij, L.P. Kouwenhoven, and C. Dekker, *Kirchberg 2001 Conference Proceedings*, edited by H. Kuzmany, J. Fink, M. Mehring, and S. Roth, AIP Conf. Proc. No. 591 (AIP, Melville, NY, 2001), pp. 293-297
[3] H.W.Ch. Postma, T. Teepen, Z. Yao, M. Grifoni, and C. Dekker, Science **293**, 76 (2001)
[4] A. Rochefort, P. Avouris, F. Lesage, D.R. Salahub, Phys. Rev. B **60**, 13824 (1999)
[5] M.S.C. Mazzoni, H. Chacham, Phys. Rev. B **61**, 7312 (2000)

Poster

REAL-TIME SIMULATION OF AFM TIP-SURFACE COHESIVE INTERACTIONS

Sylvain Marlière[1,2], Daniela Urma[1,2], Jean-Loup Florens [1], Florence Marchi[2]
1 ICA-ACROE, 46 Av. Félix Viallet, 38031, Grenoble Cedex, France
2 LEPES, CNRS, 25 Avenue des Martyrs, BP166, 38042 Grenoble Cedex9, France
E-mail : marliere@imag.fr

The manipulation of nano-objects requires specific instruments as Atomic Force Microscopes (AFM). Despite qualities and performances of these devices, many physicists complained about the lacks of adequate man-AFM interfaces, since the experimentalist can not control the AFM tip during the sample scan [1] or feel in real-time the results of his actions on the sample surface [2]. Since the information we can extract from a nano-scene is complex and above all, a-priori foreign to our common sense and daily experience, an efficient communication of human perception/action processes and the physical actions and behaviours in the nano-world is a non-trivial task. Several works as those of [3,4,5] deal with the implementation of a multi-sensory AFM-human operator interface allowing the experimentalist to see, to hear and to touch the nano-objects in real-time during the manipulation. The first stage of these works was to enrich the conventional instrument by adding a force-feedback device allowing the user to feel the forces applied to and returned by the AFM tip. Thus, the architecture of the developed instruments was a conventional teleoperator architecture composed of a force feedback manipulator, signal transmitters and AFM.

The work presented here aims to a similar objective: allowing the experimentalist to act on and feel the nanoworld phenomena during the manipulation by the use of multisensory representations including the force feeling. Nevertheless, keeping in mind the differences between the human world and the nanoword, we assume that simulation is an imperative layer to adapt in real time the specificities and the information between human and nano worlds. Thus, a crucial challenge is to have at our disposal minimal models of the nanoscene, able to be simulated in real-time, which could be inserted between the user's multisensory interfaces and the real nanoscene.

In this context, our paper presents a minimal model able to simulate in real-time the complex phenomenon of approach-withdraw interaction that appears between an AFM tip and a sample surface in contact mode. This interaction is a cohesive interaction presenting a hysteretic behaviour as shown in approach-withdraw curve (fig.1). Figure 2 illustrates our minimal model equivalent to the physical elements: the piezo-actuator controlled in Oz position, the cantilever, the tip, the sample surface and the tip-surface interaction.

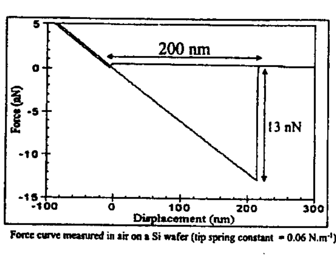

Fig.1 The observed approach-withdraw interaction curve

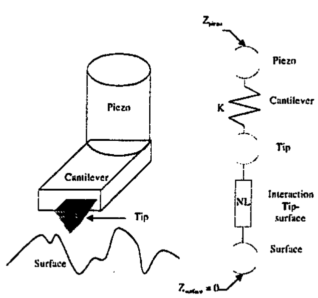

Fig.2 Minimal model of the AFM piezo-tip-surface

Fig. 3 Feeling the approach-withdraw interaction

The real-time simulation of this model produces the correct approach-withdraw curve, with hysteresis phenomenon, and thus without any element in the model which exhibits explicitly memory function. The force applied on the tip during the approach-withdraw procedure is transmitted to the experimentalist in real time through the virtual model and a Force Feedback Gestural Device, making thus possible a human haptic perception of the approach-withdraw interaction (Fig.3).

In order to validate the results of this minimal real-time model, we developed a Simulink model presented in fig.4, respecting the functional principle of each component of a real AFM. This simulation uses as input data the physical parameters that characterise a silica sample surface and returns two results that correspond to the observation of the real AFM functionality: a tip-surface interaction curve corresponding to Lennard-Jones potential, and an approach-withdraw force curve. The results of this study match with the practical results already obtained by physicists [6] and prove the validity of our approach in modelling the tip-surface cohesive interaction.

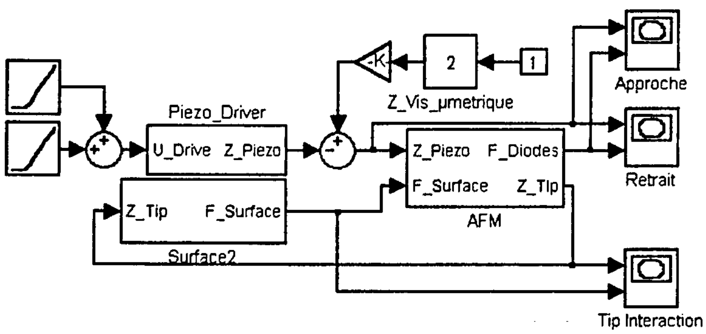

Fig. 4 Simulink model of AFM

The minimal model presented has been easily designed and implemented in real time by means of the Cordis-Anima modelling and simulation system [7]. The work presented here plays the role of a test bed for a generic use of this simulation, necessary to design minimal real-time models and to insert them in the new nanomanipulation instruments. That is a first step in the designing of the instrumental complete chain composed of force feedback nano-feeler, simulation, multi-sensory nano-manipulator, real nanoscene, which allow scientists to manipulate nano-objects in real time and to avoid the classical trials et errors methods.

References

[1] M. Guthold, M.R. Falvo, W.G. Matthews, "Controlled Manipulation of Molecular Samples with the nanoManipulator", IEEE/ASME Transactions on Mechatronics, 2000

[2] M.R. Falvo, R.M. Taylor II, A. Helsert, V. Chi, F.P.Brooks Jr., "Nanometer-scale rolling and sliding of carbon nanotubes", Rev. Nature, vol. 397, January 1999, pp. 236-238

[3] R.M. Taylor, W. Robinett, V.L. Chi, F.P.Jr. Brooks, W.V. Wright, R.S. Williams and E.J. Snyder, "The Nanomanipulator: A Virtual-Reality Interface for a Scanning Tunneling Microscope", Computer Graphics: Proceedings of SIGGRAPH'93, August 1993

[4] Fong T., Conti F., Grange S., Baur C., "Novel interfaces for remote driving: gesture, haptic and PDA", SPIE Telemanipulator and Telepresence Technologies VII, Boston, MA, November, 2000

[5] 3rdTECH, "NanoManipulator DP-100", Overview v1.0, 9 novembre, 2000

[6] S. Decossas, G. Cappello, G. Poignant, L. Patrone, A.M.Bonnot, F. Comin, and J. Chevrier, Europhys. Lett., 53 (6), pp.742-748, 2001

[7] C. Cadoz,A. Luciani, J.L. Florens,"CORDIS-ANIMA:a Modeling and Simulation System for Sound and Image Synthesis: The General Formalism", CMJ vol.17/1-MIT Press, 1993

APPROACHING NANO-SPACES: 1-DOF NANOMANIPULATOR

Annie Luciani[1], Sylvain Marlière[1,2], Florence Marchi[2], Joel Chevrier[2], Daniela Urma[1]
1 ICA-ACROE, 46 Av. Félix Viallet, 38031, Grenoble Cedex, France
2 LEPES, CNRS, 25 Avenue des Martyrs, BP166, 38042 Grenoble Cedex9, France
E-mail : urma@imag.fr

The actual tendencies in nanotechnology domain are pointed for creating more and more advanced nano-manipulators that are requested in many applications [1,2]. Fields like: *biology* [3] where a convivial tool to manipulate directly the alive materials at a nano-scale does not exist, *educational sciences* [4] where an efficient nano-manipulator could enrich the theoretical descriptions of the phenomenon by a direct and sensorial approach of the nano-sciences, *physics* [5] where no means to control a carbon nanotubes manipulation exist today, are only few examples from the widespread area of nano-manipulator applications.

Building a nano-manipulator as an independent workstation, which will integrate a force sensor at the nanometric scale (the AFM tip) and an interface for experimentalist that will allow him to act in real time and to use all his cognitive capabilities (senses, knowledge, learning) in the nano-world is our project that will offer a new and complete multi-sensory representation of the nano-world phenomena in our macroscopic universe.

In the aim of realizing a successful multi-sensory interface allowing, thus, human presence in the nano-world, we present in this paper the first results from the 1-DOF nano-manipulator development that connects an Atomic Force Microscope (AFM) with our 20 N (permanent regime) Force Feedback Gestural Device (FFGD). The application of the AFM-FFGD coupling contains a redefining of the real-time remote-control handling, bringing in the concept of mixed reality. The designed models described in this paper represent the basics of the virtual reconstructions of a nano-scene.

We connect the AFM with the FFGD by intercalating a real-time processor between these two devices (fig.1). The real-time processor Telluris, developed in our laboratory, allows any physical modelling with 3kHz bandwidth for the force feedback sensitivity. In order to obtain system functionality independent of the software builder signal processing and commands, the coupling imposes the design of the electronic and computer considerations described below. In order to validate our results with regard to the original prints, we preserve the electronic system of the builder and the PC acquisition card. The analogical signals of the AFM head are intercepted, treated and transmitted to the real-time processor architecture by a home-developed acquisition card illustrated in fig.2. This treatment allows obtaining a signal shape according to the functional and regulation modes of the AFM.

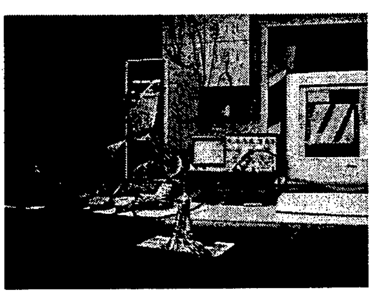

Fig.1 AFM, real time processor, and FFGD chain

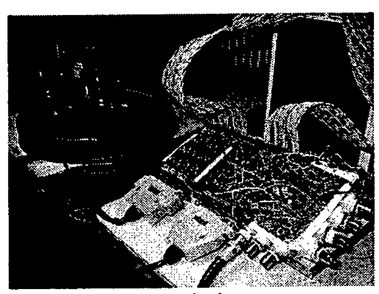

Fig. 2 AFM-real-time processor acquisition card

In parallel with technical developments we have studied the constituents of the nano-manipulator from a *modelling and virtual reality* point of view. We have defined different models that reconstruct at the human scale the interactions between sample surfaces and AFM tips at the nanometre scale.

To analyze the critical behaviour of nano-objects deposed on a sample surface, we have realized a first model that simulates the Van-Der-Waals interactions by creating a virtual tip, which is connected to a piezo element by a spring and which interacts with the surface (hysteresis effect). A more elaborate model illustrated in fig.3 implements the *two-wheeler* metaphor, which allows moving, lifting and bringing an object on the surface. This model provides to the user information about the characteristics of the AFM tip, in particular if its cohesion with the object to be moved is strong enough for realizing such operations. We can thus put in evidence some delicate situations that appear in real actions, and obviously at different scale rates.

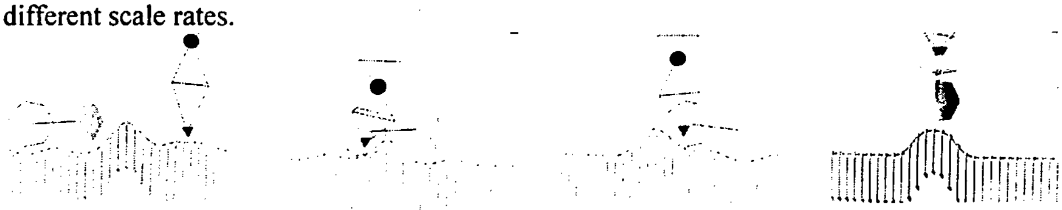

Fig. 3 Model for moving and grasping a nano-object on a surface

The first results we have obtained are determinant for the next developments concerning the multi-sensory nano-manipulator. The user commands the AFM tip thanks to the FFGD control lever and he can feel the cohesive nano-forces amplified at the Newton order (by a 10^9 factor). The virtual manipulations allow calibrating the real manipulations in a non-destructive way, and offer a contact between the user and the nano-world, with a force feedback, visual and auditory representation. The designed architecture deals not only with a scale-changing command, but also with a simulation platform, which allows reconstructing the nanometre world in a virtual system, and includes an estimation of the operator possibilities, his capacities face to this environment. Feeling the *sticking and takeoff* phenomenon as a measure of the approach-withdraw interaction of the AFM tip with the surface shows the extent of the capabilities, which can be henceforth exploited for the future developments.

References

[1] M.C. Cavusoglu, D.Feygin and F. Tendik - "A critical Study of the Mechanical and Electrical Properties of the PHANToM Haptic Interface and Improvements for High Performance Control", PRESENCE Rev., vol. 11, Issue 6, pp. 555-568, Decembre 2002,

[2] P.T. Szemes, N.Ando, P.Korondi and H. Hashimoto - "Telemanipulation in the Virtual Nano Reality", Transaction on Automatic Control and Computer Science, vol. 45 (49), no.1, pg. 117-122, 2000

[3] T. R. Ramachandran, C. Baur, A. Bugacov, A. Madhukar, B. Koel, A. Requicha, and C. Gazen, "Direct and Controlled Manipulation of Nanometer-Sized Particles Using Novel Non-Contact AFM Based Techniques", Fifth Foresight Conference on Molecular Nanotechnology, November 5-8, 1997, Palo Alto, California

[4] Fong T., Conti F., Grange S., Baur C., "Novel interfaces for remote driving: gesture, haptic and PDA", SPIE Telemanipulator and Telepresence Technolgies VII, Boston, MA, November, 2000

[5] F. Marchi, V. Bouchiat, H. Dallaporta, V. Safarov, and D. Tonneau, "Growth of silicon oxide on hydrogenated silicon during lithography with an atomic force microscope", J. Vac. Sci. Technol. B16 (6), Nov/Dec 1998, pp. 2952-2955

SELF-ASSOCIATION AND SEPARATION STEREOSELECTIVE IN A CHIRAL LIQUID–CRYSTAL COLESTERIC POLYMER UNDER ACHIRAL CONDITIONS

Roser Marsal Berenguel[1], Leoncio Garrido[1], Mercedes Pérez-Méndez[1] and Manuel Martín-Pastor[2]

[1] Instituto de Ciencia y Tecnología de Polímeros, CSIC. C/ Juan de la Cierva, 3. 28006 Madrid.

[2] Laboratorio Integral de Estructura de Biomoléculas Jose. R. Carracido, Unidade de Resonancia Magnética, RIAIDT, Universidad de Santiago de Compostela. 15782 Santiago de Compostela, (SPAIN) .

Cholesteric chiral liquid-crystal polyester PTOBEE $[C_{26}H_{20}O_8]_n$ **(1)**, synthesized from the racemic mixture of their starting materials, showed an unexpected stereoselective separation of polymer units which incorporate a higher excess of one enantiomer at the expenses of the other when the polycondensation reaction products are decanted into a large excess of toluene.

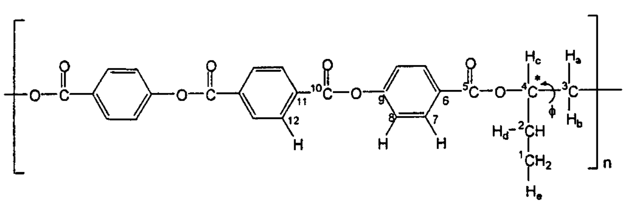

An NMR diffusion study of PTOBEE obtained for a sample with ~70% enantiomeric excess revealed the formation of a complex by self-association of several polymer units with an unexpectedly higher tendency of the complex to be formed when the sample is further diluted. Cross saturation transferred NMR experiments showed the high stability of this complex which is in slow exchange equilibrium with the single polymer unit.

The results suggest that both effects, the enantiomeric excess obtained during the recrystalization and the high tendency to the formation of the complex in diluted samples of this polymer could be related. Polymer units incorporating a certain excess of one of the enantiomers could result in a privileged spatial geometry of the substituents which favors its self-aggregation, resulting in its faster precipitation during the recrystalization process.

SUB-MICRON PATTERNS CREATED BY A COMBINATION OF TOP-DOWN AND BOTTOM-UP TECHNIQUES

Pascale.Maury, David.N.Reinhoudt, Jurriaan Huskens.

Laboratory of Supramolecular Chemistry and Technology, MESA + research institute, University of Twente, P.O.Box 217, 7500 AE Enschede, The Netherlands.

Email:p.a.maury@ct.utwente.nl

Recently, a number of new soft-lithography techniques, such as microcontact printing (MCP), micromolding in capillaries (MIMIC), and nanoimprint lithography (NIL) have appeared. These techniques allow getting patterns with small feature sizes at low cost and high throughput compared to conventional lithography techniques. Simultaneously, methods based on the self-assembly of molecules have been developed and these approaches are known as bottom-up approaches. An example is the formation of self-assembled monolayers (SAMs). An important property of SAMs is that the molecules assemble by themselves into highly ordered layers, with a thickness of one molecule. Top-down and bottom-up approaches can be combined as shown in microcontact printing and dip-pen nanolithography. Here NIL[1] was chosen to pattern a substrate and then self-assembly was used to form a SAM on the bare areas after removal of the residual layers, see figure . One of the advantages of NIL is that it allows producing patterns with nanometer-size features on different kinds of substrates. SAMs can be formed on the exposed part of the substrate from solution or gas-phase.

The NIL stamp with nanometer features was prepared using shadow-mask evaporation through a nanostencil[2]as on figure 1. The nanostencil membrane contained 500 nm holes and was used to produce metal pillars on a Si substrate, figure 2. Clogging of the apertures of the membrane led to stamps with conical features. Here, this was used as an advantage since separation of stamp and substrate after imprinting becomes easier among the conical shape of the stamp features. Imprints were made on polymethylmethacrylate (PMMA) 350 K, see figure 3 and 4 and characterized by scanning electron microscopy (SEM) and atomic force microscopy (AFM).

Different kinds of SAMs were characterized on bare substrates to evaluate possible NIL-induced damage on the monolayer using ellipsometry, contact angle measurements and electrochemistry. SAMs were formed both from solution (e.g. thiols on gold in ethanol) and from gas-phase (silanes on silicone) on the patterned substrate. After removal of the polymer, characterization of patterned SAMs was performed indirectly after further processing steps. After patterning a gold-coated substrate with thiols we proceeded to transfer the pattern on the gold layer by wet etching. The patterned gold layer (typically 20 nm thick) can be easily investigated with SEM. Furthermore, attachment of fluorescent molecules to NH_2-terminated SAMs permits observation of the pattern using confocal microscopy.

Figures

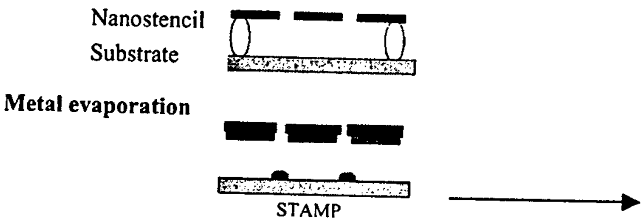

Figure 1: Shadow mask evaporation using nanostencil for stamp fabrication

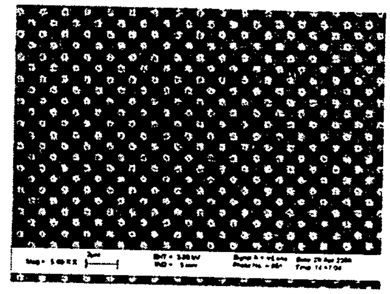

Figure 2: SEM image of 500 nm Cr. dots on Si

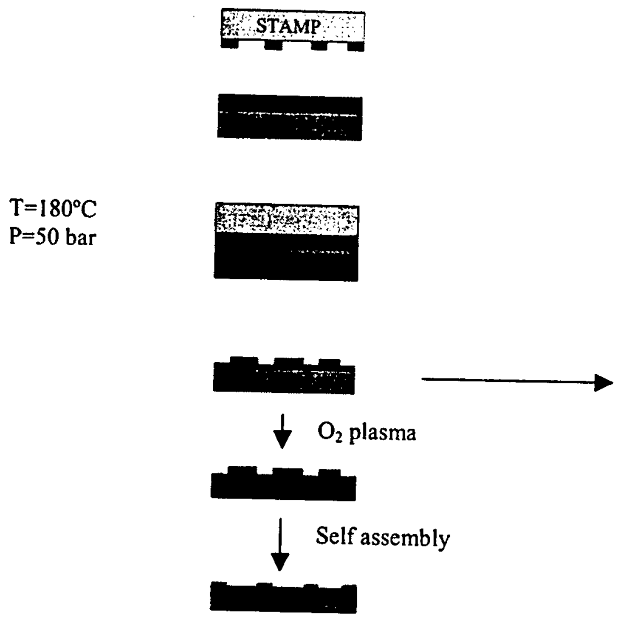

Figure 3:NIL followed by self-assembly process

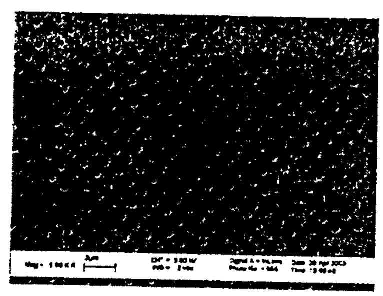

Figure 4: SEM image of imprinted holes using the stamp seen above

References

1. Chou SY, Krauss PR, Renstrom PJ. Imprint of sub-25 nm vias and trenches in polymers. APL 1995;67:3114.

2. Kolbel M, Tjerkstra WR, Brugger J, Van Rijn CJM, Nijdam W, Huskens J, et al. Shadow-mask evaporation trough monolayer-modified nanostencils. Nanoletters 2002;4-2.

MICROSTRUCTURAL CHARACTERISATION OF THE FORMATION OF ELLIPSOIDAL IRON METAL NANOPARTICLES

R. Mendoza-R[1], O. Bomati-Miguel[1], M.P. Morales[1], P. Bonville[2] and C.J. Serna[1]
[1] Instituto de Ciencia de Materiales de Madrid, CSIC, 28049-Cantoblanco, Madrid, Spain
[2] CEA, CE Saclay, Service of Physique de l'État Condensé, 91191 Gif-sur-Yvette, France
E-mail: rmendoza@icmm.csic.es

The characterisation of nanoparticles is not an easy task due to their small dimensions and very often the overlapping of information due to secondary effects such as a wide particle size distribution that distorts the measurements. In this sense the use of monodispersed solids with very narrow particle size distribution, assures a good correlation between crystallochemical and in this case, magnetic properties [1, 2].

In the last years several methods have been developed to produce iron oxide particles by forced hydrolysis of iron salts in solution [3]. The morphology of the particles can be controlled by adjusting the amount of phosphate in the initial solution and the production rate can be significantly increased by adding urea in the reaction media. By controlling the experimental conditions, uniform solids consisting of hematite particles of around 50 nm in width and axial ratios of 5 and 7 have been obtained and they constitute the precursors of this work.

The metallic iron particles have been prepared by a reduction of uniform hematite particles and this transformation has been observed by Transmission Electron Microscopy (TEM). Fig. 1 shows the electron diffraction pattern, morphology, as well as the corresponding high-resolution electron micrograph. Its monocrystal character is preserved during the reduction. Every iron particle seems to be composed of several sub-particles of around 30 nm in diameter. Therefore, it is reasonable to speculate that these sub-particles must be aligned along the same crystal direction, giving rise to a monocrystal diffraction pattern. In addition, an oxide layer of around 2 nm is surrounding the metal particle, which is responsible for the stabilisation against further oxidation of the metal core and it was produced in the passivation process. It should be emphasised that this material has been stable for at least 3 years without any additive.

The final metal particles have also been characterised by Mössbauer spectroscopy and the percentage of oxide against metal has been calculated from the spectra at 4.2 K. Magnetic hysteresis loops at room temperature of the samples with different axial ratio have been measured in a vibrating sample magnetometer (VSM) and shown that the main effect on the coercivity is due to the particle morphology. On the other hand, time dependence measurements of the magnetisation lead to an activation volume that corresponds to the crystal size observed by TEM.

References

[1] E. Matijevic, Chem. Mater. **5**, 412 (1993)
[2] T. Sugimoto Ed. "*Fine particles: synthesis, characterisation and mechanism of growth*" (New York: Marcel Dekker, 2000)
[3] M.Ocaña, M.P.Morales, and C.J.Serna. J.Colloid Interface Sci. 212, 317 (1999)

Figures

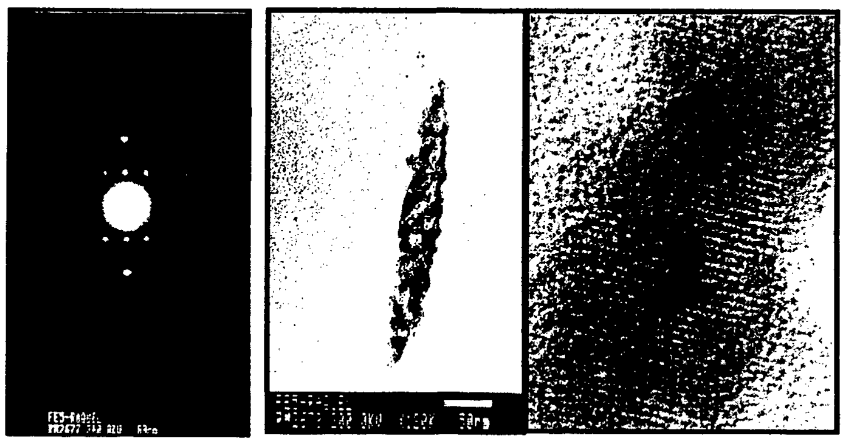

Fig. 1. Electron diffraction pattern, TEM image and high resolution image of an iron metal particle obtained by reduction of hematite.

MULTIWALL CARBON NANOTUBES FOR MICROWAVE VACUUM DEVICES AND PARALLEL E-BEAM LITHOGRAPHY

E. Minoux, L. Gangloff, P. Vincent, J-P. Schnell and P. Legagneux,
Thales Research & Technology, France
K.B.K. Teo, R. Lacerda, M. Chhowalla, D.G. Hasko, H. Ahmed, G.A.J. Amaratunga and W. I. Milne,
Department of Engineering, University of Cambridge, UK
V. Semet and Vu Thien Binh
University Claude Bernard Lyon, France
O. Gröening
University of Fribourg, Switzerland
Email : eric.minoux@thalesgroup.com

The integration of multiwall carbon nanotubes (MWCNTs) as cold field emitters in electronic devices is being investigated for several applications such as microwave amplifiers and parallel e-beam lithography. The interest in MWCNTs is motivated by their large aspect ratio which generates high electric field enhancements for obtaining electron emission at low voltage. Using catalytic plasma enhanced chemical vapour deposition (PECVD) [1,2,3], vertically aligned carbon nanotubes can be grown with a high degree of control over their location, alignment, height and diameter. Fig. 1 shows an array of 5 μm height and 50 nm diameter vertically aligned MWCNTs.

Future 10-50 W microwave amplifiers could be based on arrays of MWCNTs delivering $1 A.cm^{-2}$ and modulated at 30 GHz. In order to study the feasability of this goal, we have measured the field emission properties from individual MWCNTs. After a conditioning process [4], the electron emission was found to be stabe and followed the Fowler-Nordheim emission mechanism with a maximun current of ~10 μA per nanotube before degradation. A theoritical approach based on these results and simulation shows that such performance could be obtained with an array of 5 μm height nanotubes with a 10 μm pitch. We measured an emitted current of $0.7 A.cm^{-2}$ from a $0.36 mm^2$ CNT array (Fig. 2), field emission properties will be presented and discussed.

For parallel e-beam lithography, we have recently proposed a revisited concept based on an array of electron microguns independently driven by an active CMOS pixel array [5,6]. The microgun consists of a MWCNT as electron emitter, an extracting and a focusing lens. We have recently shown that MWCNT based microcathodes with an integrated and self aligned gate electrode exhibit excellent field emission characteristics [7]. Fig 3 shows a microgun based on individual 0.5 μm height MWCNT. Arrays of 22.500 microgun exhibit a threshold voltage of around 25 V and a maximum peak current density of $1.4 mA/cm^2$ at 40V (fig. 4).

This work was funded by the European commission through the IST-FET projects *Canvad* and *Nanolith.*

References:

[1] Z. F. Ren, Z. P. Huang, J. W. Xu, J. H. Wang, P. Bush, M. P. Siegal, and P. N. Provencio, Science **282**, 1105 (1998); Z. F. Ren, Z. P. Huang, D. Z. Wang, J. G. Wen, J. W. Xu, J. H. Wang, L. E. Calvet, J. Chen, J. F. Klemic, and M. A. Reed, Appl. Phys. Lett. **75**, 1086 (1999).
[2] V. I. Merkulov, D. H. Lowndes, Y. Y. Wei, G. Eres, and E. Voelkl, Appl. Phys. Lett. **76**, 3555 (2000).
[3] K. B. K. Teo, S-B Lee, M. Chhowalla, V. Semet, Vu Thien Binh, O. Groening, M. Castignolles, A. Loiseau, G. Pirio, P. Legagneux, D; Pribat, D. G. Hasko, H. Ahmed, G. A. J. Amaratunga and W. I. Milne, Nanotechnology **14** (2003) 204-211.

[4] V. Semet, V. T. Binh, P. Vincent, D. Guillot, K. B. K. Teo, M. Chhowalla, G. A. J. Amaratunga, W. I. Milne, P. Legagneux, and D. Pribat, Appl. Phys. Lett. **81**, 343 (2002).
[5] P. Legagneux, G.Pirio, E. Balossier, J-P Schnell, D. Pribat, K.B.K. Teo, M. Chhowalla, D.G. Hasko, G.A.J. Amaratunga, W. I. Milne, V. Semet, Vu Thien Binh, W.H. Bruenger, H. Hanssen and D. Friedrich, Phantoms Newsletter **5**, 8 (2002).
[6] K.B.K. Teo, M. Chhowalla, G.A.J. Amaratunga, W. I. Milne, P. Legagneux, G.Pirio, L. Gangloff, D. Pribat V. Semet, Vu Thien Binh, W.H. Bruenger, J. Eichholz, H. Hanssen, D. Friedrich, S.B. Lee, D.G. Hasko and H. Ahmed, J. Vac. Sci. Technol. B **21**, 693 (2003).
[7] G. Pirio, P. Legagneux, D. Pribat, K. B. K. Teo, M. Chhowalla, G. A. J. Amaratunga, and W. I. Milne, Nanotechnology **13**, 1-4 (2002).

Figures:

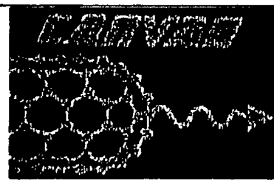

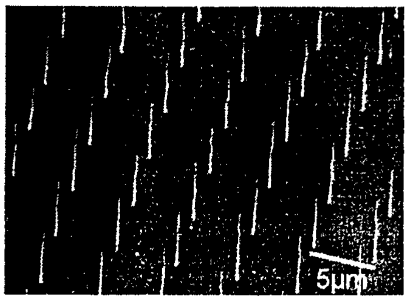

Fig. 1 : Array of 5 µm height and 50 nm diameter MWCNTs with a pitch of 5 µm

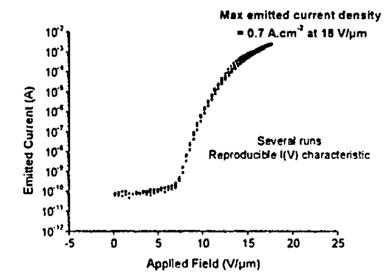

Fig. 2 : Field emission from a 0.36 mm² CNT array

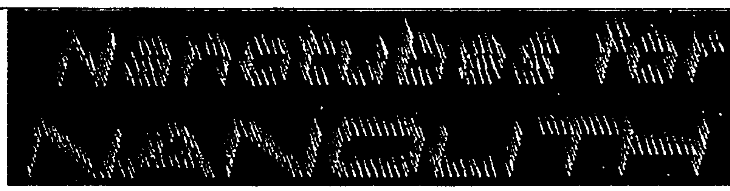

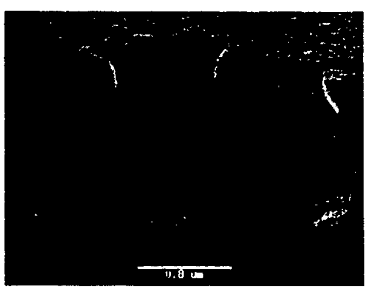

Fig. 3 : Tilted SEM view of a microcathode after growth of a 1 µm height nanotube

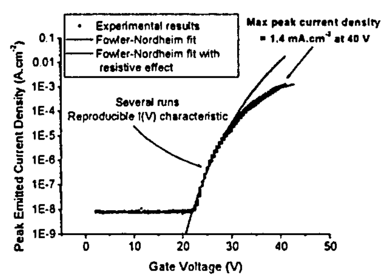

*Fig. 4 : Peak current density of an array of 150*150 microcathodes as a function of the applied voltage*

Electron Beam Deposition of Solid Gold Nanostructures and Soldering of Carbon Nanotubes

*Kristian Mølhave[1], Dorte Nørgaard Madsen[1], Anne Marie Rasmussen[2], Anna Carlsson[2], Charlotte Clausen Appel[2], Michael Brorson[2], Claus H. J. Jacobsen[2], Peter Bøggild[1]

[1] Mikroelektronik Centret, Technical University of Denmark, 2800 Lyngby, Denmark
[2] Haldor Topsøe A/S, Nymøllevej 55, 2800 Lyngby, Denmark
*E-mail: krm@mic.dtu.dk

Electron beam deposition (EBD) is an attractive method for rapid fabrication of three-dimensional nanostructures and soldering of nanocomponents [1,2,3]. We have developed a setup for EBD in an environmental scanning electron microscope (ESEM) and present here successful deposition of solid gold nanostructures and soldering of carbon nanotubes to micro structures. As precursor gas we used dimethyl-gold-acetylacetonate (vapor pressure 0.01 Torr).

A TEM investigation of the electron beam deposited tips revealed a unique shell structure for tips deposited in a water vapor atmosphere. Fig. 1 shows typical tips deposited in an 80%Ar/20%O2 mixture (A) and water (B). From the TEM images and energy dispersive energy X-ray analysis, we found that tips deposited in the presence of the gasses N_2, 80%Ar/20%O_2, and 60%He/40%H_2, consisted of about 3 nm gold particles embedded in a carbonaceous matrix, as shown on Fig. 1A. However, for depositions at a water vapor pressure above 0.5 Torr, the tips contain a gold core with high density (Fig 1B), surrounded by a shell of carbon/gold material. The structure of the shell is similar to the material in the tips deposited in the other gasses. The gold content of the core increases with the beam current used during deposition.

When scanning the electron beam to acquire images in the presence of the source, thin contamination layers almost void of gold are deposited on the imaged surfaces (Fig 1C). Furthermore, tip fabrication in the presence of the source was found to lead to deposition on the sidewalls of other tips up to a few microns away. We observed that tips with such asymmetric contamination layers generally were deformed by exposure to subsequent electron radiation in SEM or TEM as seen in Fig 1D. Preliminary experiments indicated that the contamination layers can be greatly reduced by using shutters to turn off the supply of precursor gas between depositions.

There are strong indications that the gold cores are solid, crystalline gold. We found long-range order in the core lattice planes over distances comparable to the diameter of the cores (Fig 2), i.e. much larger than the nanocrystallites in the crust. Quantitative measurements of the mass-thickness of the tips by scanning transmission electron microscopy (STEM) also indicated a solid gold core.

By slowly scanning the beam during deposition, three-dimensional gold structures can be made. Free-standing gold wires with a core diameter of just 20 nm were deposited from a multiwalled carbon nanotube. The TEM image in figure 3 shows a gold wire firmly connected to the nanotube, where the deposition process has clearly pinched the carbon nanotube at the intersectingon. We have previously reported gold deposition in ESEM used for highly conductive and mechanically strong soldering of carbon nanotubes on microelectrode surfaces [3]. The results presented here further indicate that electron beam deposition in an environmental SEM can be used to wire-bond nanostructures and to fabricate free-standing

metallic nanostructures that may conveniently be integrated in NEMS structures, simply by pointing and moving the electron beam.

References:

[1] H.W. Koops et al., SPIE 2780 (1996) 388.
[2] K. Edinger, J. Vac. Sci. Tech. B, **19** (2001) 2856.
[3] D.N. Madsen et al., Nanoletters, **3** (2003) 47.
[4] A. Folch et al. APL 66 (1995) 2081; A. Folch et al. J. Vac. Sci. Tech. B 14 (1996) 2609

Figures:

Figure 1: The shell structure of the deposited tips. (A) This structure consisting of gold particles embedded in amorphous carbon was observed for depositions in N_2, 80%Ar/20%O_2, and 60%He/40%H_2. (B) In tips deposited in water vapor pressures above 0.5 Torr, a gold core was found. The core is surrounded by a crust of material similar to the material in A. (C) Contamination layers can be seen surrounding the crust. (D) SEM image showing the extreme bending of originally straight tips with contamination layers, after subsequent exposure to electron radiation.

Figure 2: TEM image of a gold core. The lattice pattern extends for tens of nanometers (the white line).

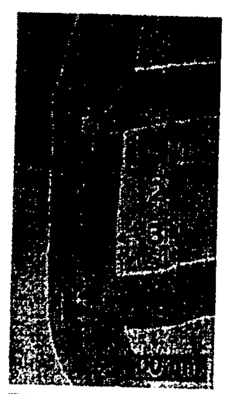

Figure 3: Wires (1) deposited by scanning the electron beam. The deposition started on the freely hanging carbon nanotube (2). Contamination layers cover the nanotubes and depositions (3)

GMR EFFECT IN CuCo ANNEALED MELT-SPUN RIBBONS

N. Murillo[a], H. Grande[a], I. Etxeberria[b], J. J. Del Val[b], J. González[b], S. Arana[c] *and* F. J. Gracia[c].

[a]New Materials Department, CIDETEC Foundation, Pº Miramón 196, 20.009-San Sebastián. Spain

[b]Departamento de Física de Materiales, Facultad de Químicas, Universidad del País Vasco (EHU/UPV) P.O. Box 1072 20080-San Sebastián. Spain

[c]Departamento de Microelectrónica y Microsistemas, Centro de Estudios e Investigaciones Técnicas de Gipuzkoa (CEIT) P.O. Box: 1.555, 20.018-San Sebastián. Spain

Dr. Nieves Murillo. Tel.: +34-943-309022; fax: +34-943-309136; e-mail: nmurillo@cidetec.es

Granular magnetic materials exhibiting giant and negative magnetoresistence (GMR) - discovered in 1992 [1,2]- have attracted much attention in recent years. These materials consist of ferromagnetic nanoparticles, usually of Co or Fe embedded in a nonmagnetic metallic matrix (typically Cu, Ag or Au). In zero magnetic field, when magnetic moments of the particles are not aligned (e.g. oriented randomly) the resistivity of the material is high. When the external magnetic field aligns these moments, the resistivity decreases like in the early discovered multilayered GMR materials [3]. The effect is large and almost independent of the magnetic filed direction.

In this work, the magnetoresistence and the structure of conventionally annealed melt-spun $Cu_{100-X}Co_X$ (X= 10 *and* 15) alloys are studied. The samples were isothermally annealed in vacuum at the temperature of 475 ºC and 525 ºC for 1 hour in order to achieve the optimum GMR effect. Transmission Electron Microscopy (TEM) observation in the annealed samples revealed the presence of particles with the mean size of a few nanometers. For the majority of the particles, the size distribution is not very wide but a number of much large particles are also seen in TEM micrographs. It has been found essential differentiation of the particles are also present) in the as-quenched samples, whereas the annealing results in the formation of small fcc-Co crystallites. The magnetoresistence ratio $\Delta R/R$ was measured by means of a DC-conventional four-wire method under magnetic field up to 15 KOe applied in the ribbon plane, perpendicular to the direction of electric current flowing along the sample. Changes in $\Delta R/R$ up to 4,5% has been obtained. Promising results for future applications were obtaining.

References.

[1] A. E. Berkowitz, J. R. Mitchell, M. J. Carey, A. P. Young, S. Zhang, F. E. Spada, F. T. Parker, a. Hutten, G. Thomas; Phys. Rev. Lett., 68 (1992) 3745.

[2] J. Q. Xiao, J. S. Jiang, C. L. Chien; Phys. Rev. Lett.; 68 (1992) 3749.

[3] M. N. Baibich, J. M. Broto, A. Fert, F. Nguyen van Dan, F. Petroff, G. Grenzer, A. Friederich, J. Chuzelas; Phys. Rev. Lett., 61 (1988) 2472.

CoFe2O4-POLYPYRROLE(PPy) NANOCOMPOSITES: NEW MULTIFUNCTIONAL MATERIALS

N. Murillo[a], E. Ochoteco[a], Y. Alesanco[a], J. A. Pomposo[a], J. Rodriguez[a], J. González[b], J. J. del Val[b] and J. M. González[c],

[a]New Materials Department, CIDETEC Foundation, Pº Miramón 196, 20.009-San Sebastián. Spain

[b]Departamento de Física de Materiales, Facultad de Químicas, Universidad del País Vasco (EHU/UPV) P.O. Box 1072 20080-San Sebastián. Spain

[c]Departamento de Propiedades Ópticas, Magnéticas y de Transporte, Instituto de Ciencia de Materiales de Madrid, CSIC Cantoblanco, 28049 Madrid, Spain

Corresponding author: Dr. Nieves Murillo. Tel.: +34-943-309022; fax: +34-943-309136; e-mail: nmurillo@cidetec.es

The discovering of intrinsic conductivity in organic polymeric materials, intrinsically conducting polymers (ICPs), open new possibilities for the development of molecular electronics. This increasing interest leads to coordinate scientific research community efforts in order to develop new and multifunctional materials. ICPs have been applied in different fields, such as electrostatic charge dissipation (ESD), electromagnetic interference shielding (EMI), metallisation of printed circuits board, conductive fabrics, sensors, etc. In this work, we have focused our research in chemically synthesized polypyrrole (PPy). The advantage of chemically synthesized ICPs is the possibility of obtaining bulk quantities for industrial applications. By combining in a single material the electrical conductivity of ICPs and the magnetic properties of micro/nanopowder ferrites, new multifunctional materials could be developed.

A wide range of conductivity in ICPs can be obtained from different reaction conditions [1]. Here, we have selected appropriate chemical synthesis conditions to obtain PPy with electrical conductivity of 160±4 S/cm, as measured by the four point probe method. This material was physically processed with micro/nanopowder ferrites ($Co_1Fe_2O_4$ composition) obtained by the microemulsion method [2]. These physically mixed materials were compared with a $Co_1Fe_2O_4$-PPy composite (electrical conductivity 111±7 S/cm). The composite material was prepared in two steps:

a) microemulsion synthesis of micro/nano-$Co_1Fe_2O_4$ particles and,

b) chemical polymerization of PPy over these particles.

The microstructural behavior of the PPy-covered $Co_1Fe_2O_4$ particles has been studied by X-ray diffraction (DRX) and transmission electron microscopy (TEM) to understand the magnetic nanoparticle-conducting polymer interphase region. The microstructure of the sample has been correlated with the magnetization measurements performed at 1 Tesla from nearly 0 K to ambient temperature in a vibrating sample magnetometer (VSM).

References.

[1] P. A. Calvo, J. Rodríguez, H. Grande, D. Mecerreyes and J. A. Pomposo, Synthetic Metals, 126 (2002) 111.

[2] N. Moumen, M. P. Piloni, Chem. Mater., 8 (1996) 1128.

ELECTROCHEMICAL CHARACTERIZATION OF SINGLE WALLED CARBON NANOTUBES AND POLYPYRROLE COMPOSITES AS ELECTRODES IN SUPERCAPACITORS

I. Cendoya[1], N. Murillo[1], L. Ganborena[1], O. Miguel[1], E. Ochoteco[1], J. A. Pomposo[1], H. Grande[1]

A. Ansón[2], M. A. Callejas[2], W. Maser[2], A .M. Benito[2], M. T. Martinez[2]

[1] Fundación CIDETEC, Paseo Mikeletegi 61, 20009, San Sebastián, Spain

[2] Instituto de Carboquímica (CSIC), Miguel Luesma Castan 4, 50018 -Zaragoza, Spain

Carbon nanotubes are attractive materials to be used as electrodes of electrochemical energy storage devices, such as Li-ion secondary batteries, hydrogen storage for fuel cell and supercapacitors due basically to their superb characteristics of chemical stability, low mass density and large surface area. In this work, the use of Carbon Nanotubes and Polypyrrole composites as electrodes for supercapacitors is investigated. An improvement of capacitance is expected by the preparation of these composites. Such a modification will supplies apart from electrostatically charges accumulation also faradaic pseudocapacitance effects.

With this aim, Single Walled Carbon Nanotubes (SWNTs) were obtained by means of electric arc-discharge[1]. Several electrodes of SWNT/PPy composite are fabricated to improve the specific capacitance of pure SWNT. In our experimental procedure, SWNT are coated with high conductivity Ppy (200 S/cm) by in situ chemical polymerisation of Pyrrole[2]. Morphological characterisation of as grown SWNT and composites has been done with high-resolution transmission electron microscopy (TEM) and Raman spectroscopy.

Electrodes for supercapacitors were formed by pressing a mixture of composite material and a binding agent (polyvinylidene fluoride, PVDF). Two identical electrodes were separated by a porous thin polymer (Celgard 3401, Hoechst) soaked in 7.5N KOH. To evaluate the specific capacitance values of the SWNT/PPy nanocomposites electrodes, galvanostatic charge-discharge cycling test, cyclic voltammetry and an ac impedance test were performed.

The SWNT-PPy composite electrodes show higher specific capacitances than as grown SWNT electrodes (See Fig. 1). Long durability (over 2000 cycles) was obtained for such electrodic materials. Coating by PPy increases the specific capacitance demonstrating a synergy between the two components of composite.

References:

[1] C. Journet, W.K. Maser, P. Bernier, A. Loiseau, M. Lamy de la Chapelle, S. Lefrant. Nature **388**, (1997) 756.
[2] P. A. Calvo, J. Rodríguez, H. Grande, D. Mecerreyes, J. A Pomposo. Synthetic Metals **126**, (2002) 111-116.

Figures:

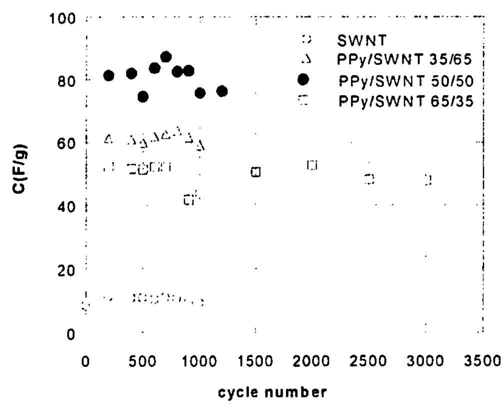

Fig.1.- Supercapacitors Capacitances as function of cycle number

ACCURACY LIMIT OF OPTICAL INTERFEROMETRY FOR NANOMETROLOGY

Victor Nascov
National Institute for Laser, Plasma and Radiation Physics, PO Box MG-36, R-76900 Bucharest, Romania
e-mail: nv@ifin.nipne.ro

Optical interferometry has been a classical method in metrology, commonly used for measurement and testing with micrometer accuracy. Even in nanometrology, optical interferometry is nowadays a main tool for measurement and testing, but in order to increase the sensitivity and accuracy, one use phase-shift interferometry or multiple wavelength interferometry and of course, advanced means for detection and information processing [1]. In any case the accuracy on measuring lengths or wavelengths depends on the accuracy one can determine the fringe spacing and the fringe position. Many authors report in their paper statements like this: "We get the fringe spacing with a relative accuracy of 1/1000" without any justification.

Our paper states out the highest degree of accuracy that one can actually get by measuring interference fringes that are digitally recorded and affected by statistical noise.

For example in case of a digitized 1D sequence of straight, equispaced fringes with N samples:

$$I_m = I_0 + I_1 \cdot \cos\left(\frac{2\pi}{N} \cdot N_f \cdot m + \varphi\right), \quad m = 0, 1, \ldots, N-1 \tag{1}$$

we have found by analytical calculus [2, 3] that the number of fringes N_f and the phase parameter φ can be determined with the following statistical uncertainties:

$$\sigma_{N_f}^2 = \sigma_I^2 \cdot 6/\pi^2 I_1^2 N, \quad \sigma_\varphi^2 = \sigma_I^2 \cdot 2/I_1^2 N \tag{2}$$

assuming that there are additive gaussian noise with 0 mean and σ_I^2 variance in the image of the fringe pattern. The relative statistical error of the adimensional parameter N_f is the same as that of the fringe spacing. We created computer programs for fringe processing based on least squares fitting or discrete Fourier analysis [2, 3]. We proved the theoretical results (2) by statistically processing the results of a lot of simulated fringe patterns (100000) and we concluded that these formulas estimate well the actual uncertainties in fringe processing if the fringe pattern contains at least 3 sine fringes (1) or 15-20 not harmonic fringes (Fabry Perot), which may have as well not uniform contrast. The statistical errors (2) do not depend on the number of fringes if the sampling doesn't go fewer than 8 samples for fringe spacing. Another conclusion is that just the sine, straight and equispaced fringe pattern are the most suitable for measuring wavelength / displacement with maximum accuracy.

As an application we design an interferometer for measuring wavelength / displacement with relative accuracy of 10^{-11}, that being the accuracy of specifying the international etalon of meter nowadays. We choose a Murty interferometer in a setup that provides straight equispaced fringe pattern: a few minutes optical wedge whose faces make up an optical path δ. Determining the number of fringes N_f we can get the wavelength λ relative to a reference wavelength λ_0 of an etalon source which makes a fringe pattern with N_{f0} fringes. The accuracy get by now is not so good, but it can be improved using as well the phase parameter φ and designing the interferometer to work at high interference order. Firstly we get a coarse value λ^* of the wavelength based on the proportionality between fringe spacing and wavelength. Then we compute the interference order k and at last we get the wavelength λ with increased accuracy:

$$\lambda^* = N_{f0} \cdot \lambda_0 / N_f, \quad k = [\delta/\lambda^*], \quad \lambda = \frac{2\pi\delta}{2k\pi + \varphi}, \quad \frac{\sigma_\lambda}{\lambda} = \frac{\sigma_\varphi}{2k\pi} \tag{3}$$

Hence, the larger the interference order k is, the better the accuracy of wavelength will be. The interference order k cannot be increased indefinitely, but as long as can be determined with an accuracy of one unit, using the fringe number N_f:

$$\sigma_k = k \cdot \frac{\sigma_{N_f}}{N_f} < 1 \quad \Rightarrow \quad \frac{\sigma_\lambda}{\lambda} > \frac{\sigma_\varphi}{2\pi} \cdot \frac{\sigma_{N_f}}{N_f} = \frac{\sqrt{3}}{\pi^2 N \cdot N_f} \cdot \frac{\sigma_I}{I_1} \tag{4}$$

Thus we have found the accuracy limit on measuring the wavelength using the whole information contained in the straight equispaced fringe pattern with N samples.

Assuming a sampling rate of 20 samples on a fringe spacing (N_f=N/20) and a relative noise of 5% ($\sigma_I / I_1 = 0.05$), the wavelength can be measured with a relative accuracy of 10^{-11} only if the input data has at least N=30000 samples. Instead of a 1D sampled sequence, we can equivalently process a 2D image having the same number of samples. When building the interferometer, to ensure this accuracy we should use a 10 time better sampling, for example a CCD with 0.3 Mpixels (640 ×480).

The same interferometer can measure as well displacements with the same relative accuracy, but only using the parameter φ because the number of fringes N_f gives not any information about displacement (it depends only on the wedge angle). By automatic fringe counting one can measure large displacements.

For measuring fixed lengths we should design another type of interferometer, one witch gives rings of Jamin or Newton's type, because these fringe patterns contain information for precise length measuring [4], without need of displacements and fringe counting. As light source we should use the best stabilized He-Ne laser (λ=632.99139822 nm), which is one of the radiation source recommended by the "Bureau International des Poids et Measures" (Paris) to be used as maximum precision etalon.

We shall provide analytical expressions for the statistical errors on processing these fringe patterns that would be useful to design the corresponding interferometers as we have already showed in case of straight equispaced fringe pattern.

References

1. R. Schödel, G. Bönsch, "Interferometric measurements of thermal expansion, length, stability and compressibility of glass ceramics", Proc. of the 3rd Euspen International Conference, Eindhoven, The Netherlands, May 26th –30th, 2002
2. V. Nascov, A. Dobroiu, D. Apostol, V. Damian, "Statistical processing of elementary fringe patterns", Proceeding ATOM Conference, Volume SPIE **5227**, in press
3. V. Nascov, A. Dobroiu, D. Apostol, V. Damian, "Statistical processing of straight equispaced fringe patterns using the discrete Fourier analysis", Proceeding of Optical metrology Symposium, Munchen, June, 2003, to be published in SPIE volume
4. V. Nascov, A. Dobroiu, D. Apostol, V. Damian, "Automatic digital processing of Newton's rings fringe pattern", Volume SPIE **4430**, pp 835-841, 2001

LOCAL ELECTRONIC CHARACTERIATION OF CONJUGATED POLYMER FILMS USING CONDUCTING-PROBE ATOMIC FORCE MICROSCOPY

Garret O'Brien, Aidan Quinn, Gareth Redmond.

Nanotechnology Group, NMRC, Cork, Ireland.

Conjugated polymers have recently emerged as promising new materials with respect to their potential for application in photonic devices such as, light emitting diodes (LEDs), photodiodes, photovoltaics and displays. Correlation of local electronic properties with film morphology is a key challenge to be addressed in order to understand (and therefore control) charge injection, transport and recombination since it is becoming increasingly clear that device performance is strongly affected by film morphology and preparation conditions. To date, investigation of charge transport in these materials has mostly been limited to bulk devices, in the simplest case consisting of a polymer layer ~100 nm thick sandwiched between two metallic electrodes.

Recently, Alvarado et al.[1] reported a Scanning Tunneling Spectroscopy-based method which can be used to determine the threshold voltages (above and below the Fermi energy) for charge injection into polymer films ~ 3 nm thick, corresponding to the electron- and hole-polaron energy levels. The single-particle energy gap between these levels, E_{gsp}, can be used (in conjunction with optical absorption data) to determine the exciton binding energy, E_b, for the material, a key parameter for electroluminesence. However, this method does not allow reliable characteristion of the polymer film morphology.

We present a more flexible method, Conducting-Probe Atomic Force Microscopy (CP-AFM), which is used as a local probe of *both* the morphology and charge injection characteristics of spin-cast polymer films (Scheme 1). We apply this technique to films with thicknesses comparable to those used in bulk devices. Silicon wafers with a 100 nm thick evaporated gold electrode were used as substrates. MEH-PPV films were spun onto the substrates in a nitrogen glovebox with sub-ppm levels of oxygen and water, followed by a mild anneal (50 °C) under vacuum. AFM measurements were made under high vacuum (10^{-6} mbar) using commercial metal-coated tapping mode AFM probes.

CP-AFM studies of 60 nm MEH-PPV films show smooth morphologies (rms roughness 3.6 nm for a 1 μm^2 area). Tip-height *vs* bias voltage (z-V) sweeps taken at constant tunnel current show clear charge injection thresholds at both positive and negative bias (Figure 1). Statistical analysis of measured single-particle gap energies, E_{gsp}, shows a distribution across the surface with peaks corresponding to exciton binding energies of 100 meV and 400 meV respectively (Figure 2). Analysis of measured E_{gsp} values for MEH-PPV films prepared under ambient conditions show a large density of mid-gap states confirming that the preparation route is critical for these devices.

In conclusion, we have characterised the local morphology and electronic characteristics of device-like MEH-PPV films using a unique combination of nanoscale imaging and spectroscopy. Future work will focus on correlation of the electro-optic properties of conjugated polymer films with film morphology and preparation conditions.

---

[1] S.F. Alvarado *et al.*, Phys. Rev. Lett. **81**, 1082, (1998).

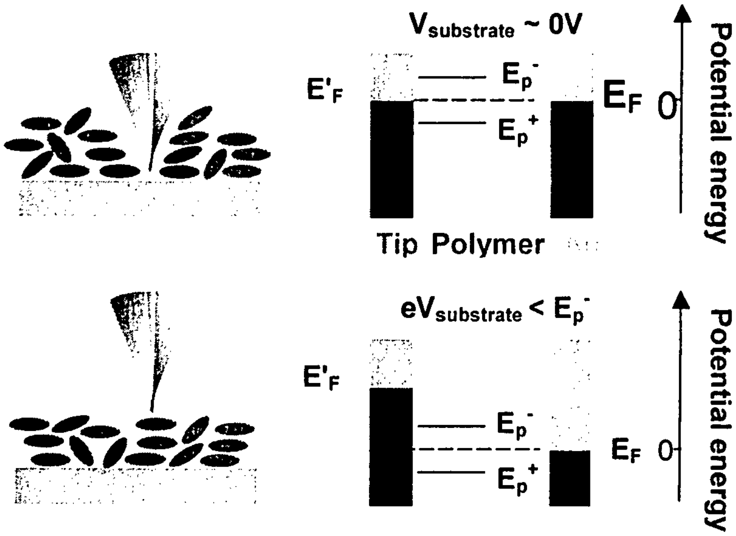

Scheme 1. zV measurement using CP-AFM to probe carrier injection thresholds in a conjugated polymer film.

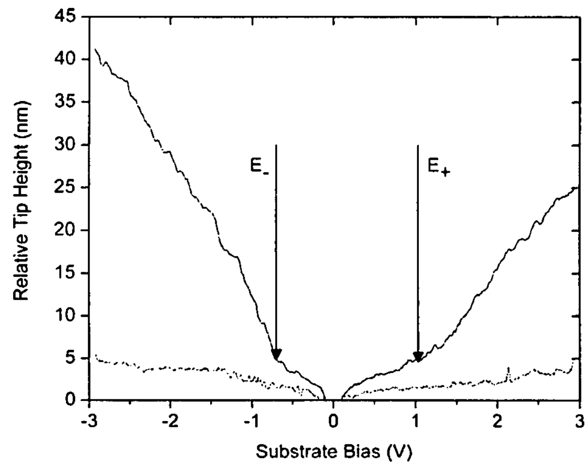

Figure 1. zV data measured for a 60 nm thick MEH-PPV film (zV data measured for a bare Au substrate shown in red).

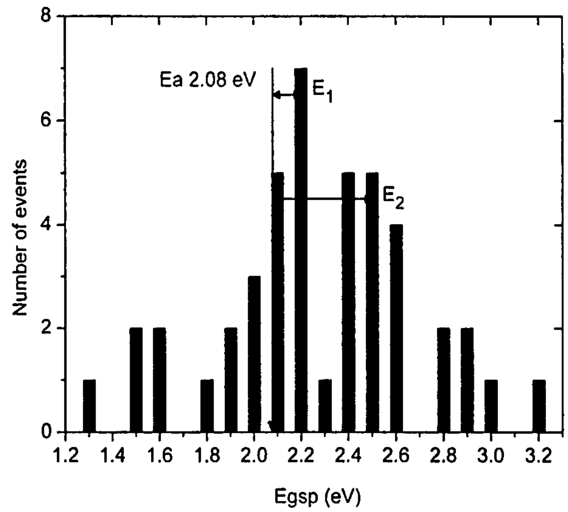

Figure 2. Statistical analysis of measured single-particle gap energies, Egsp, for a 60 nm thick MEH-PPV film. Optical absorption threshold, Ea, acquired from UV-Vis spectra. E_1 and E_2 denote exciton binding energies values, E_b, of 100 meV and 400 meV respectively.

QUANTUM SIZE EFFECTS IN Pb NANOISLANDS GROWN ON Cu(111)

E. Ogando[1], N. Zabala[1,2], E. V. Chulkov[2,3], M.J. Puska[4]
[1]Elektrika eta Elektronika Saila, UPV-EHU 644 P.K., 48080 Bilbao, Spain
[2]Donostia International Physics Center (DIPC) and Centro Mixto CSIC-UPV/EHU 1072 P.K., 20080 Donostia, Spain
[3]Departamento de Física de Materiales, Facultad de Ciencias Químicas, UPV-EHU 20018 Donostia, Spain
[4]Laboratory of Physics, Helsinki University of Technology, P.O.Box 1100, FIN-02015 HUT, Finland
E-mail: eoa@we.lc.ehu.es

Metallic slabs grown on different kind of surfaces exhibit quantum well states (QWS) [1]. In particular, Pb layers deposited on Cu(111) show these QWS's trapped between the Cu-Pb interface (due to the energy band gap of Cu in the (111) direction) and vacuum. The discrete electronic structure of these slabs plays an important role in the energy of the system, being responsible for the higher stability of some islands heights. This effect has been observed in STM experiments, as the frequent appearance of islands of magic heights [2].

Quantitative analytical models and self-consistent electronic calculations of free-standing slabs have been used to enlighten the origin of this height selection: when the energy of a Pb discrete state lies at the Fermi level its high density of states destabilizes the slab, favoring the evolution into another configuration. In this study, we perform electronic structure calculations within the Density Functional Theory and using a simple one-dimensional model that reproduces the physical features of the real system. One of the main advantages of this model is that we take into account the effect of the Cu substrate, neglected in previous electronic structure calculations. We focus on the properties related to the Pb-Cu interface and the stability of the nanoislands through the total energy calculations.

The lateral size of the Pb islands is so big that they can be modeled as infinitely extended slabs of desired monolayers height. Then, we have solved self-consistently the Kohn-Sham equations (using the real space MIKA code [3]) for the direction perpendicular to the slab, z. We have modeled the Pb slab with stabilized jellium, the free electron character of Pb at Fermi level justifies this election. For Cu potential we have used a z-dependent pseudopotential, by unscreening the potential of ref. [4], which reproduces correctly the Fermi level and the energy band gap of Cu in the (111) direction.

In fig. 1 we show the energy oscillations, multiplied by the Pb thickness in order to amplify the oscillation amplitude and make them more clear. Note that, when selecting the energy corresponding to an integer number of monolayers, we obtain a shell and supershell structure, similar to the one found in clusters and nanowires [5,6]. For slabs the mechanism for the appearance of the supershell structure is the mismatch between the

electrons Fermi wavelength and the atomic layers width. An energy minima can be related to more stable islands, and in the figure they show a very good correspondence with the most probable measured island heights [2]. The behavior of the electrons at the Cu-Pb interface and the reliability of other simple models, as the soft-well potentials, have been studied.

In conclusion, we have shown that our calculation leads to good agreement with recent experiments [1,2]. Although the physical mechanism for the appearance of magic heights in nanoislands can be explained using free-standing slabs, the interactions between the Cu substrate and the Pb layers have to be taken into account: our calculations for the unsupported Pb layers gives significantly worse results.

References

[1] R. Otero, A. L. Vázquez de Parga and R. Miranda, Surf. Sci. **447**, 143 (2000).
[2] R. Otero, A.L. Vázquez de Parga and R. Miranda, Phys. Rev. B **66**, 115401 (2002).
[2] T. Torsti, M. Heiskanen, M.J. Puska and R.M. Nieminen, Int. J. Quantum Chem. **91**, 171 (2003).
[4] E. V. Chulkov, V. M. Silkin and P. M. Echenique, Surf. Sci. **437**, 330 (1999).
[5] W. A. de Heer, Rev. Mod. Phys. **65**, 611 (1993).
[6] A.I. Yanson, I.K. Yanson and J.M. van Ruitenbeek, Nature **400**, 144 (1999).

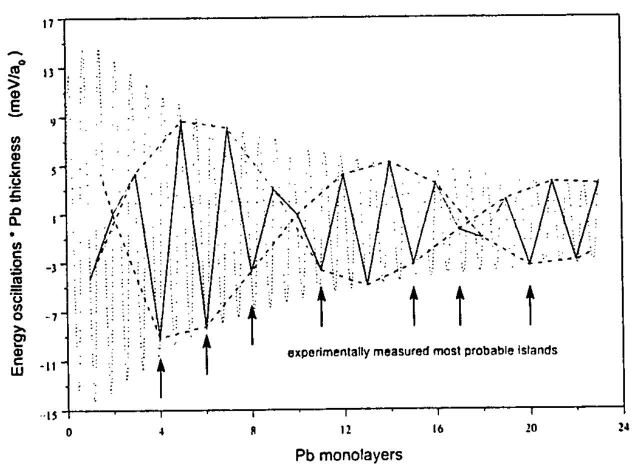

Figure 1: *Energy oscillations times the Pb thickness as a function of the Pb thickness (dotted line). The energy for the discrete monolayers has been selected (continuous line). The arrows point out the measured most probable island heights [2]. The dashed line is plotted as a guide to the eye to show the shell and supershell structure.*

ENHANCED PHOTOTHROMBIC ACTIVITY OF PHOTOSENSITIZERS BY NANOENCAPSULATION STRATEGIES

B. Pegaz, Y.N. Konan, E. Debefve, J-P Ballini and H. van den Bergh
Institute of Environmental Engineering, Swiss Federal Institute of Technology (EPFL), CH-1015 Lausanne, Switzerland. E-mail: bernadette.pegaz@epfl.ch

Introduction

Photodynamic therapy (PDT) is a new treatment of choroidal neovacularization associated to age-related macular degeneration (AMD) based on the combined use of light and photosensitizing agents [1]. Owing to the lack of selectivity of the commonly used photosensitizers for the treatment of AMD, it is of utmost importance to find innovative pharmaceutical formulations such as nanoparticles for improving the targeting ability of the photosensitizers and enhancing their photothrombic activity. In the present work, using chick's chorioallantoic membrane (CAM) vasculature as in vivo model, organic nanoparticles loaded with photosensitizer such as chlorin e_6 were investigated in terms of pharmacokinetics and photothrombic activity in comparison with free dye.

Materials and methods

Photosensitizer

Chlorin e_6 was obtained from Porphyrin Products (Frontier Scientific, Logan, USA). The solution of chlorin e_6 (1 mg/ml) was freshly prepared by dissolving in dimethylsulfoxide (Sigma-Aldrich, Steinheim, Germany).

Nanoparticle preparation and characterization

Poly(D,L-lactid acid) provided by Boehringer Ingelheim (Ingelheim, Germany) was used as biodegradable polymer. The nanoparticles were prepared using the emulsification-diffusion technique as previously described [2]. Briefly, an organic phase consisting of polymer and chlorin e_6 dissolved in benzyl alcohol were emulsified with an aqueous solution of poly(vinyl alcohol) (17 % (m/m)). Then, distilled water were added to the resulting emulsion in order to allow complete diffusion of the benzyl alcohol into the aqueous external phase, leading to the formation of nanoparticles. The particle suspensions were purified by cross-flow filtration using a Sartocon® Slice device fitted with an ultrafiltration membrane (Sartorius, Goettingen, Germany). After the addition of trehalose to the particle suspensions (trehalose:nanoparticles mass ratio of 2:1) were frozen and freeze-dried at 0.001 mbar in a Lyolab CII (Secfroid, Switzerland). The particle mean size and the polydispersity index were assessed by photon correlation spectroscopy using a Zetasizer® 5 000 (Malvern, Worcesterhire, England). The chlorin e_6 content and entrapment efficiency were determined spectrophotometrically at 653 nm (Spectrophotometer HP8452, Hewlett-Packard GmbH, Waldbronn, Germany).

CAM preparation

For pharmacokinetics and PDT studies, fertilized chicken eggs were disinfected,and transferred into a hatching incubator set at 37°C and 60 % humidity and equipped with an automatic rotator (SARL SAVIMAT, Chauffry, France). On the third day of embryo development (EDD), an approximately 3 mm diameter hole was bored into the eggshell at the narrow apex and covered with self-adhesive tape. Egg incubation was then continued in a static position. On EDD13, the holes were extended to a diameter of about 3 cm and the embryos were placed under an epi-fluorescence microscope (Olympus).

Fluorescence pharmacokinetics

The fluorescence pharmacokinetics was performed as previously described [3]. Briefly, a volume of 10 µl containing an adequate amount of the PS was injected intravenously under a microscope. Fluorescence imaging was performed using the excitation filtered light of a Hg-arc lamp at 420 ± 20 nm and emission filter 700 nm long-pass during approximately 30 minutes at regular time intervals. Quantitative fluorescence images of the CAM surface were recorded as a function of time. The evolution of fluorescence intensity in the blood circulation was followed up after injection. The time-dependent evolution of the fluorescence intensity inside the blood vessels (I_{in}) with respect to the surrounding tissue (I_{out}) was expressed by means of normalized photographic contrast C_{phot},

$$C_{phot} = (I_{in}-I_{out})/[(I_{in}+I_{out}) \times C_{phot,max}]$$

Wherein $C_{phot,max}$ represents the highest photographic contrast following administration.

Phototoxicity assays

On EDD 13, eggs were placed under the microscope and the treatment area was defined by placing a small Teflon ring on the CAM. Prior to injection, an autofluorescence of CAM surface was recorded. The injection of the dye was performed directly under the microscope and its distribution was controlled by fluorescence microscope. After homogenous distribution of the photosensitizer within the

blood circulation, PDT was performed using a filtered Hg-arc lamp at 420 ± 20 nm at a fluence rate of 141 mW/cm^2. For each drug dose, light doses ranging from 5 to 20 J/cm^2 were applied to the CAM. Then, the eggs were covered with a cling foil and returned to the incubator for 24 hours. Twenty-four hours post-irradiation, vascular occlusion was controlled by means of fluorescence angiography, performed by injection of 10 µl of sulforhodamine 101 (5 mg/ml.) Fluorescence angiographies pre- and post- PDT were compared and scored according the arbitrary score (Table 1).

Table 1: Damage criteria for photosensitizer with irradiation.

Damage scale	Criterion
0	No damage.
1	Partial closure of capillaries (Ø < 10 µm).
2	Closure of capillaries, partial closure of blood vessels (Ø < 30 µm) and size reduction of bigger blood vessels.
3	Closure of vessels (Ø < 30 µm) and partial closure of bigger vessels.
4	Total closure of vessels (Ø < 70 µm) and partial closure of bigger vessels.
5	Total occlusion of the irradiated area

Results and discussions

Fluorescence pharmacokinetics

The nanoparticulate formulation was tested in the CAM model with respect to its extravasation in comparison with free chlorin e_6 solution. It can be seen from Fig. 1 that over a period of more than 20 minutes the chlorin e_6 -loaded nanoparticles stay intravascular after a short dilution period, while free chlorin e_6 fluorescence decreases over the entire time period. Thus, the risk to damage neighboring structures in the case of PDT of AMD is strongly decreased. Leakage of chlorin e_6 from vessels can be avoided by using biodegradable nanoparticulate carriers; therefore increased selectivity of photodynamic therapy can be achieved.

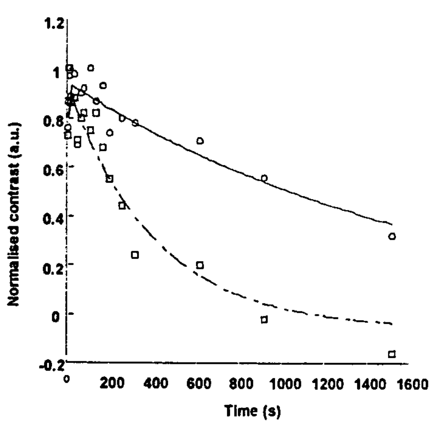

Figure 1: Leakage of chlorin e_6-loaded nanoparticles (-O-) as compared to free dye -□-) as measured by means of fluorescence contrast in the CAM model.

PDT assays

The photothrombic activity of both chlorin e_6-loaded nanoparticles and free dye was evaluated by varying drug concentration and light dose. As shown in Fig.2, the desired vascular stasis and occlusion were observed when nanoparticles were used at drug concentration and light dose up to 1 mg/kg and 10 J/cm^2, respectively. In contrast, at these experimental conditions, free chlorin e_6 solution exhibited no significant vascular effect. The relatively low drug concentrations required to induce satisfactory vascular effects indicate that nanoparticulate formulation offer superior photothrombic efficacy. Furthermore, similar results were obtained in preliminary studies performed with pheophorbide a encapsulated into organic nanoparticles (data not shown). These results encourage the production of more complex nanostructures with capabilities such as specific drug delivery.

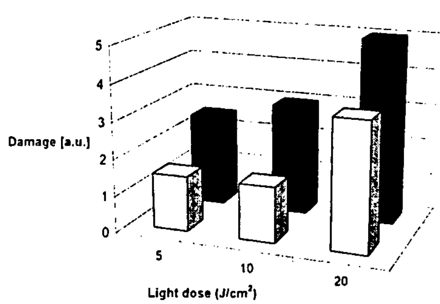

Figure 2: Photodynamic activity of nanoparticles loaded with chlorin e_6 (black bars) compared to free dye (white bars)

Conclusions

In this study, we demonstrated that the encapsulation of PS into organic nanoparticles should be considered as an effective strategy for improving the photothrombic activity of these dyes on CAM model. The relatively low drug concentration and light dose required to induce satisfactory vascular damage indicate that these formulations offer superior photoactivity. Thus, an enhancement of phototherapeutic index of photosensitizing agents can be obtained. Furthermore, the risk to damage neighboring structures in the case of PDT of AMD is strongly decreased since leakage of chlorin e_6 from vessels can be avoided by using biodegradable nanoparticulate carriers.

References

1. van den Bergh et al., *Arch ophthalmol.*, 117 (1999) 1161-1173.
2. Konan et al., *Eur. J. Pharm. Biopharm.*, 55 (2003) 115-124.
3. Lange et al., *Invest. Ophthalmol. Vis. Sci.* 42(2001) 38-46.

Poster

DRIFT-DIFFUSION MODEL FOR MINIBAND TRANSPORT IN SEMICONDUCTOR SUPERLATTICES

Álvaro Perales
Dpto. Automática, Escuela Politécnica, Universidad de Alcalá.
N-II, Km. 31,600, 28871 Alcalá de Henares (Madrid), Spain.
E-mail: alvaro.perales@uah.es

Ramón Escobedo and Luis L. Bonilla
Dpto. Matemáticas, Escuela Politécnica Superior, Universidad Carlos III de Madrid.
Av. de la Universidad 30, 28911 Leganés, Spain.
E-mail : escobedo@math.uc3m.es bonilla@ing.uc3m.es

Since the work by L. Esaki and R. Tsu [1], important quantum effects such as Bloch oscillations, Wannier-Stark localization and formation of electric field domains have been observed in semiconductor superlattices [2].
Electronic transport in superlattices is well described by rate equations in two different limits, miniband transport (which is appropriate for strongly coupled SL), and sequential tunneling (for weakly coupled SL) [3, 4]. In general, these models should be justified by a derivation from the semiclassical Boltzmann equation or from quantum kinetics (using Density-Matrix, Green Functions, or Wigner Function formalisms) [3]. Rate equation models can be analyzed and simulated in detail, and they describe very rich dynamical behavior, including self-sustained oscillations, diferent kind of bifurcations, and driven and undriven chaos [4].

A drift-diffusion model of miniband transport in strongly coupled superlattices is derived from the single-miniband Boltzmann-Poisson transport equation in the relaxation time aproximation. We use a consistent Chapman-Enskog method to analyze the hyperbolic limit at which collision and electric field terms dominate the others terms in the Boltzmann equation. The reduced equation is of the drift-diffusion type, but diffusion and drift do not obey the Einstein relation except in the limit of large temperatures compared to miniband width. Analytical derivation is supported with numerical calculations to justify approximations.

References:

[1] L. Esaki and R. Tsu
IMB Research Note **RC-2418** (1969)
[2] H. T. Grahn (Ed.)
Semiconductor Superlattices. Growth and electronic properties
World Scientific 1995
[3] A. Wacker
Semiconductor Superlattices: a model system for nonlinear transport
Physics Reports **357** (2002) 1-11
[4] L.L. Bonilla
Theory of nonlinear charge transport, wave propagation, and self-oscillations in semiconductor superlattices
J. Phys.: Condensed Matter **14** (2002) R341-R281

RADIATION EMITTED FROM A DRIVEN QUANTUM DOT IN A MICROCAVITY

José Ignacio Perea[(1)] , Diego Porras and Carlos Tejedor

Departamento de Física Teórica de la Materia Condensada (C-V), Facultad de Ciencias, Universidad Autónoma de Madrid, E-28049 Madrid, Spain.
(1) E-mail: nacho.perea@uam.es

The quantum properties of the radiation emited by a quantum dot (QD) in a microcavity is investigated. The QD is described by a two level system in strong coupling with one cavity mode. We include dissipation and incoherent pumping contributions by coupling to photons and phonons reservoirs respectively.Both, espontaneus emission through leaky modes and transmision of cavity modes to the external photons reservoir have been considered.

We obtain the master equations of this system and solve them with a Runge-Kutta adaptative step size method. We analyze the ocupations of states, coherences (off diagonal terms), the average number of photons inside the cavity. Moreover, the second order correlated function at zero delay, as a indication of the coherence of states inside, is obtained, finding sub-poissonian (maybe squeezed states), poissonian (coherences states) and super-poissonian (clasical states) distributions depending of the selected range of parameters.

In order to compare with experiments, we use the quantum regression theorem to get the first order correlated function as a function of the delay. Its fourier transform gives the intensity of emission, I(w), for which one obtains linewidths and can observe detuninng effects.

MAGNETIZATION OF AMORPHOUS $(Co_{0.3}Fe_{0.7})_{73.5}Nb_3Cu_1Si_{13.5}B_9$ RIBBON AND THEIR EVOLUTION AFTER HEAT TREATMENTS

A. Fernández[1], M.J. Pérez[1], M. Tejedor[1] and V. Madurga[2]
Dpto. de Física. Universidad de Oviedo, Calvo Sotelo S/N, 33007 Oviedo, Spain
Dpto. de Física, Universidad Pública de Navarra, 31006 Pamplona, Spain
E-mail: mjp@pinon.ccu.uniovi.es

Magnetization measurements by magnetic gravimetry and by the induction method were made on a $(Co_{0.3}Fe_{0.7})_{73.5}Nb_3Cu_1Si_{13.5}B_9$ ribbon as quenched and after annealings during one hour at 300°C and 400°C, below the crystallization temperature. Analysis by X-ray diffraction on those samples were performed as well.

The main change observed in the magnetization curves after the annealing process was the increasing of the magnetization saturation. A magnetic softening of the material was also observed by the induction method.

The thermomagnetic analysis of the annealed sample did not show changes in the crystallization process but only in the magnetization saturation.

Nevertheless the X-ray diffraction analysis of the samples showed a low intensity peak in the case of the annealing samples not appearing in the as-quenched samples. We interpreted this increasing in the magnetization saturation as due to a nanocrystallization process after annealing.

COERCIVE FIELDS AND MAGNETIC ANISOTROPY OF AMORPHOUS CO-SI FILMS WITH DILUTED ARRAYS OF ANTIDOTS

A. Pérez-Junquera,[a*] J. I. Martín,[a] M. Vélez,[a] J. M. Alameda,[a] J. V. Anguita,[b] F. Briones,[b] E. M. González[c] and J. L. Vicent[c]

[a]Dpto. Física, Universidad de Oviedo, c/ Calvo Sotelo s/n, 33007 Oviedo, SPAIN

[b]Instituto de Microelectrónica de Madrid, CNM-CSIC, Isaac Newton 8, PTM, Tres Cantos, 28760 Madrid, SPAIN

[c]Dpto. Física de Materiales, Fac. de Física, Universidad Complutense, 28040 Madrid, SPAIN

[*] Corresponding aut. Tel.: 00-34-985103325; fax: 34-985103324; e-mail: junquera@string1.ciencias.uniovi.es

Patterned magnetic nanostructures have received much interest in recent years as they provide the ability to control and design the magnetic behavior for specific applications, as well as to study fundamental magnetic properties [1]. Much attention has been devoted to the analysis of small magnetic particles surrounded by non magnetic material. However, the reverse structures, i.e. antidot arrays defined over continuous magnetic films, present potential advantages for magnetic data storage [2] and offer the possibility of tailoring the properties of the continuous film such as coercivity or magnetic anisotropy [3]. In this work, 40 nm thick amorphous Co_xSi_{1-x} films, that present well-defined in-plane uniaxial anisotropy [4], have been patterned with arrays of antidots by electron beam lithography and plasma etching [5]. The interplay between the original films anisotropy and that induced by the demagnetizing fields present in the lithographically defined holes has been studied as a function of array symmetry (square or rectangular) and antidot shape (circular or elongated).

In particular, arrays of circular and elliptical antidots of 0.5 μm - 5 μm dimensions have been prepared (see Fig. 1), with center-to-center interhole distances much larger than hole dimensions, so that it is a diluted regime where each antidot can be considered as an isolated inclusion in the homogeneous film. The array area is 500 μm × 500 μm. The antidot depth can be controlled and varied with etching time, being characterized with atomic force microscopy measurements (Fig. 1).

The magnetic behaviour of the arrays has been analyzed by magnetooptical transverse kerr effect (MOTKE) with a focused laser of 300 μm in diameter in an experimental setup that allows the rotation of the sample respect to the magnetic field as well as the determination of the sample magnetization vector. Some of the changes observed in the patterned structures respect to the continuous amorphous film are: moderate increases in coercivity (Fig. 2), and magnetic anisotropy dominated by that of the original film but with significant additional contributions due to the shape anisotropy of the artificial array. It can result in higher anisotropy fields (Fig. 2) or strong modifications in the angular dependence of the coercive field (Fig. 3), that can be interpreted in terms of the presence of lithographically induced anisotropy directions.

Work supported by Spanish CICYT.

References:

[1] For a review, see J. I. Martín, J. Nogués, K. Liu, J. L. Vicent and I. K. Schuller, J. Magn. Magn. Mater. 256 (2003) 449.

[2] R. P. Cowburn, A. O. Adeyeye, and J. A. C. Bland, Appl. Phys. Lett. 70 (1997) 2309.

[3] P. Vavassori *et al.*, J. Appl. Phys. 91 (2002) 7992.

[4] M. Vélez *et al.* , IEEE Trans. Magn. 38 (2002) 3078.

[5] J.I. Martín *et al.*, IEEE Trans. Magn. 36 (2000) 3002.

Figures:

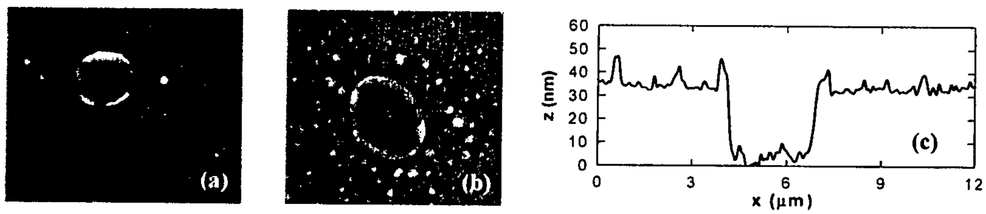

Fig. 1: Atomic force microscopy (15 μm × 11 μm) images of (a) a circular antidot from a rectangular array and (b) an elliptical antidot from a square array. (c) Depth profile across the hole in panel (a). We observed that the holes are only about 35 nm depth.

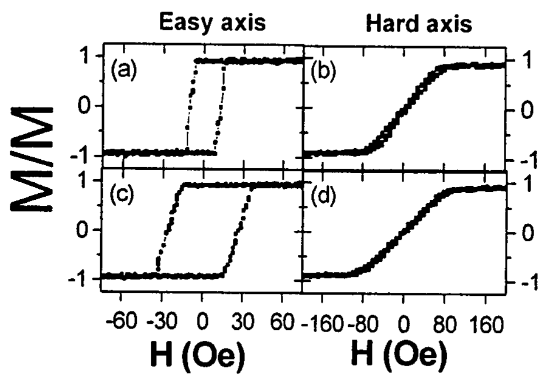

Fig. 2: MOKE loops for: (a)-(b) unpatterned film; (c)-(d) square lattice (20 μm × 20 μm) of elliptical holes (5 μm long and 3.5 μm wide) in a array of 500 μm × 500 μm.

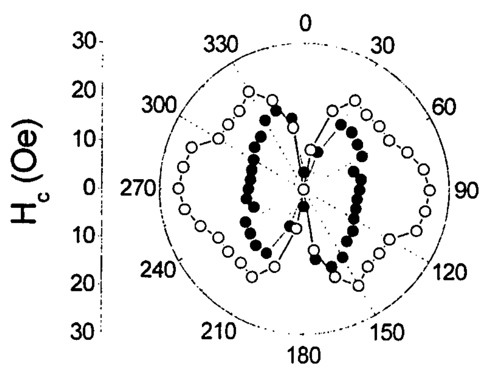

Fig. 3: Angular dependence of the coercivity for magnetooptical transverse Kerr effect hysteresis loops. Closed circles, unpatterned film; hollow circles, square lattice (20 μm × 20 μm) of elliptical holes (5 μm long and 3.5 μm wide) in a array of 500 μm × 500 μm.

PLANAR ORGANIC PHOTONIC CRYSTALS FABRICATED BY SOFT LITHOGRAPHY

D. Pisignano, L. Persano, G. Gigli, P. Visconti, M. De Vittorio and R. Cingolani
NNL, National Nanotechnology Laboratory of Istituto Nazionale di Fisica della Materia (INFM), c/o Dipartimento di Ingegneria dell'Innovazione, Università di Lecce, via Arnesano, I-73100 Lecce, Italy
E-mail: dario.pisignano@unile.it
http://www.nnl.it

Besides the conventional waveguiding effect, due to contrast of refractive indexes between the propagating core and its surrounding media, a novel technique of controlling light propagation relies on photonic crystal structures [1]. Actually, by means of such devices it is possible to induce distributed feedback (DFB) in propagating radiation, thus realizing microcavities and solid state lasers. Moreover, by introducing linear defects in the periodic structure of the photonic crystal, it is possible to realize optical waveguides, splitters, bends, to address the electromagnetic wave towards specific spatial regions [2]. This approach offers several advantages with respect to the traditional one, as it allows a perfect integration of devices into planar optical circuits. However the realization of photonic crystals for near infrared or optical wavelengths needs very long exposures by electron beam lithography so that novel, faster and low-cost lithographic techniques are desirable.

We employ mechanical patterning methods, including soft hot embossing [3] and nanoimprinting lithography [4], to fabricate planar photonic crystal structures by organic materials. Our devices, presenting periodicities comprised between 400 and 600 nm, include solid state DFB lasers (Fig. 1 and Fig. 2) and two-dimensional photonic crystals (Fig. 3), and use both optically inert polymer matrices and light-emitting compounds exhibiting optical gain. In particular, we report about organic DFB cavities, whose peak wavelength, λ_m, is related to the cavity geometry by: $m\lambda_m = 2n_{eff}\Lambda$, where n_{eff} indicates the effective refractive index of the propagating mode, m is the diffraction order, and Λ is the periodicity of the DFB grating. We demonstrate a directly printed DFB laser, exhibiting single-mode emission at 630 nm, with a full width half maximum (FWHM) of about 1 nm and a pump threshold of 650 μJ/cm^2 at room temperature. The mechanical lithography processes allow a high-fidelity pattern transfer without reducing the emission yield, thus opening the way to the one-step realization of organic-based optoelectronic devices. With respect to conventional parallel-mirror cavities [5], this approach turns out to be strategic for the realization of organic electrically pumped lasers, as the electron-photon coupling is directly affected by the optical mode density.

References:

[1] J. D. Joannopoulos et al., Photonic Crystals - Molding the Flow of Light, Princeton University Press (1995).
[2] S. G. Johnson et al., Phys. Rev. B, **60** (1999) 5751; Phys. Rev. B **62** (2000) 8212.
[3] Y. Xia and G. M. Whitesides, Angew. Chem. Int. Ed., **37** (1998) 550.
[4] S. Y. Chou, P. R. Krauss, and P. J. Renstrom, Appl. Phys. Lett., **67** (1995) 3114; Science, **272** (1996) 85.
[5] D. Pisignano, M. Anni, G. Gigli, R. Cingolani, M. Zavelani-Rossi, G. Lanzani, G. Barbarella, and L. Favaretto, Appl. Phys. Lett., **81** (2002) 3534.

Figures:

FIG. 1

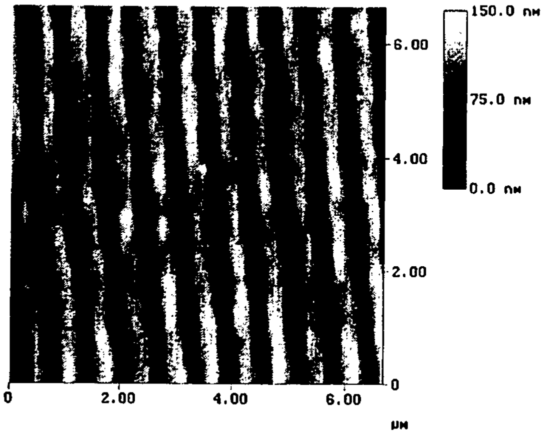

FIG. 2

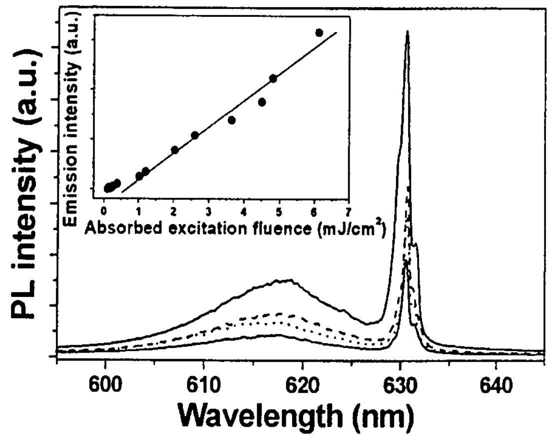

FIG. 3

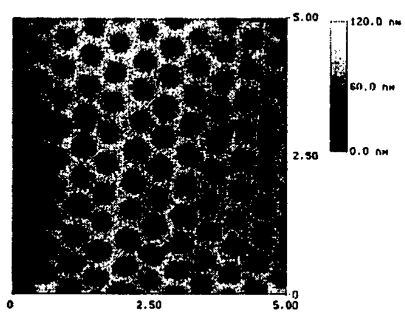

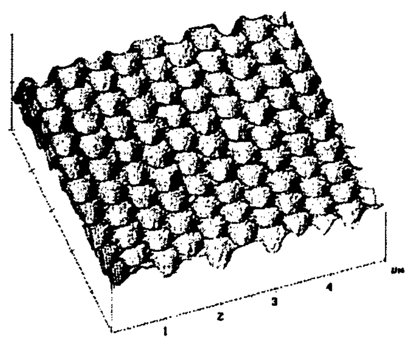

Fig. 1. Two-dimensional view of a patterned oligothiophene grating, imaged by Atomic Force Microscopy.

Fig. 2. DFB emission spectra collected at different absorbed excitation fluences. Inset: DFB peak emission intensity vs. fluence of the absorbed excitation beam. The solid line is a linear fit to the experimental data.

Fig. 3. Two (top) and three (bottom)-dimensional view of nanoimprinted Poly(methylmethacrilate) photonic crystal.

Poster

LUMINESCENCE QUANTUM YIELD OF ORGANIC ONE-DIMENSIONAL PERIODIC NANOSTRUCTURES

D. Pisignano, M. F. Raganato, L. Persano, G. Gigli, R. Cingolani
NNL, National Nanotechnology Laboratory of Istituto Nazionale di Fisica della Materia (INFM), c/o Dipartimento di Ingegneria dell'Innovazione, Università di Lecce, via Arnesano, I-73100 Lecce, Italy
E-mail: dario.pisignano@unile.it
http://www.nnl.it

Modern soft lithography techniques [1], including capillary force microscopy [2], micromolding in capillaries [3], and nanoimprinting [4], allow to transfer patterns with high resolution (up to sub-10 nm) and excellent fidelity onto a very large number of organic compounds. We employed these techniques to print one-dimensional nanostructures with sub-micron periodicity, Λ, onto organic films of several different light-emitting materials (Fig. 1). We studied and compared the emission and absorption properties of the chromophores before and after the lithography processes, demonstrating that soft techniques actually preserve the optical properties of light-emitting molecules.

In particular, we investigated the photoluminescence efficiency of different compounds, η_{PL}, by placing the samples into an integrating sphere. We found that all our patterned light-emitting materials show enhanced luminescence emission (up to a factor of more than 50%) with respect to the untextured film, as a consequence of the printed nanostructure (Λ=600 nm).

The improvement of the luminescence performance is attributed to the variation of the angular distribution of the light emission, induced by the sub μm-scale features of the pattern [5]. In fact, the high refractive index of light-emitting organic film with respect to the surrounding layers (i.e. glass and air), often determines an enhanced waveguiding effect inside the slab, and the consequent reduction of the luminescence efficiency because of self-absorption. Conversely, a patterned surface (with $\Lambda\cong$ the emission wavelength) may enhance the light emitted towards certain forward directions (Fig. 2), and consequently decrease the effective length covered by the photons and the self-absorption inside the organic slab. The increase of η_{PL} in organic one-dimensional organic nanostructures can be a fundamental advantage for the realization of efficient organic-based active photonics.

References:

[1] Y. Xia and G. M. Whitesides, Angew. Chem. Int. Ed., **37** (1998) 550.
[2] D.-Y. Khang, H. Yoon, and Hong. H. Lee, Adv. Mat., **13** (2001) 749.
[3] D. Pisignano, G. Gigli, P. Visconti, A. Zocco, A. Perrone, and R. Cingolani, Journ. Vac. Sci. Techn. B, **20** (2002) 2248.
[4] S. Y. Chou, P. R. Krauss, and P. J. Renstrom, Appl. Phys. Lett., **67** (1995) 3114; Science, **272** (1996) 85.
[5] B. J. Matterson, J. M. Lupton, A. F. Safonov, M. G. Salt, W. L. Barnes, and I. D.W. Samuel, Adv. Mat., **13** (2001) 123.

Figures:

FIG. 1

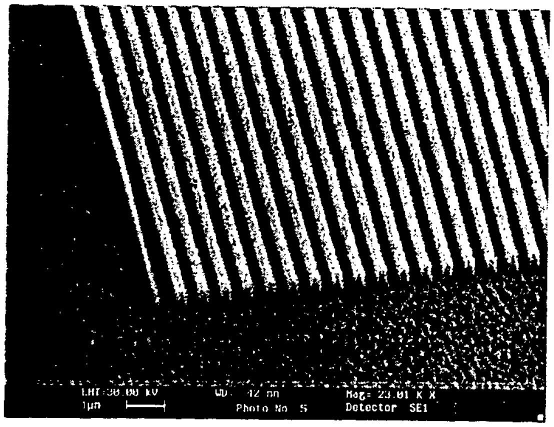

FIG. 2

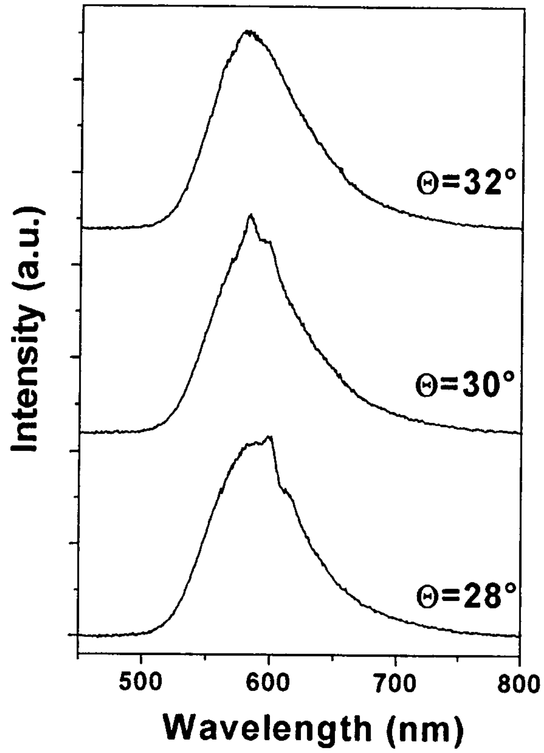

Fig. 1. A Silicon one-dimensional master grating (periodicity 600 nm), imaged by Scanning Electron Microscopy.

Fig. 2. Normalized angle-resolved luminescence spectra and diffraction PL peaks of a printed light-emitting organic grating around a polar emission angle of 30°.

ORIENTED IMMOBILISATION OF BIOMOLECULES ONTO GOLD NANOPARTICLES

Marcos Pita, José María Abad, Antonio L. De Lacey, Carlos Gómez-Moreno & Víctor M. Fernández.
Instituto de Catálisis-CSIC, c/ Marie Curie, s-n, Campus de Cantoblanco, 28049 Madrid. Spain
E-mail: alopez@icp.csic.es

There is a continuous interest in the development of biosensors as simple bio-diagnostic tools. Their potential applications could be expanded to novel horizons by using the concepts administered in natural nanometer-scale systems. On the basis of tailoring organized protein architectures in ordered and defined nanostructures, self assembled monolayers (SAMs) technology in conjunction with nanoparticles are suitable candidates. The simplicity and adaptability of SAM technique coupled with the control of molecular orientation and packing density at a surface allows the creation of numerous artificial biomolecular recognition structures at nanoscale level.

In this work, we shall present different strategies for nanostructured surfaces preparation with different functionalities for biomolecule immobilization on nanoparticles. The metallic nanoparticles synthesis in small and homogeneus particle size provides a platform for nanostructure building by SAMs nanochemistry. This allows the complementary ligands incorporation to specific binding sites present in the biomolecule (antibody, enzyme) or introduced by genetic engineering gives a specific and oriented immobilization.

A judicious use of these strategies should help to optimize the interactions between immobilized biomolecules and their corresponding targets. In addition, nanoparticles properties facilitate the development of bio-diagnostic easy techniques.

RNA POLYMERASE AS AN INFORMATION-DEPENDENT MOLECULAR MOTOR

Richard T. Pomerantz, Michael Anikin, Jordanka Zlatanova and William T. McAllister
Email: rtpomerantz@yahoo.com

RNA Polymerase (RNAP) is a powerful biomolecular machine whose motion along DNA can be controlled in an information-dependent manner with nanometer scale precision. As RNAP copies the information in the DNA template to RNA it translocates along the DNA, exerting a linear force of 15-20 pN[1]. This forward motion is dependent on the presence of the next incoming ribonucleotide triphosphate (NTP), which is encoded by the DNA template strand sequence. Withholding the required NTP results in the formation of a stable halted elongation complex in which the enzyme remains statically bound to the DNA template until transcription is resumed by addition of substrate[2]. Immobilizing RNAP to a solid surface, such as Ni^{2+}-agarose beads, confers the ability to limit the mixture of substrates for each polymerization step, which can be as small as 1 base-pair or 0.34nm[3]. In this manner, RNAP can be incrementally 'walked' or positioned along DNA with nanometer scale precision. Here we utilize modified versions of bacteriophage T7 RNAP, which contain ligand-binding motifs fused to the amino-terminus of the enzyme, in order to facilitate controlled movement and positioning of biomolecules and nanodevices[3-6]. Self-assembly of novel DNA nanodevices driven by modified T7 RNAP are demonstrated by atomic force microscopy (AFM)[7].

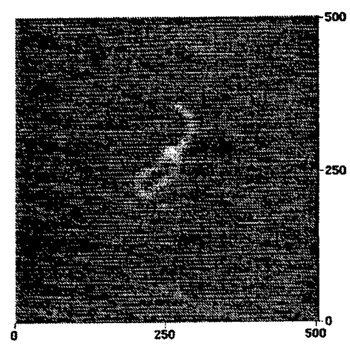

Intramolecular DNA nanodevice

1. Yin et al., Science. 270, 1653-1657 (1995).
2. Mentesana et al., J Mol Biol. 302, 1049-1062 (2000).
3. Kashlev et al., Gene. 130, 9-14 (1993).
4. Ostrander et al., Science. 249, 1261-1265 (1990).
5. Keefe et al., Protein Expr Purif. 23, 440-446 (2001).
6. Pavletich et al., Science. 252, 809-817 (1991).
7. Hansma et al., J Struct Biol. 127, 240-247 (1999).

CARBON NANOTUBE T-JUNCTION: STRUCTURAL PROPERTIES AND DEVICE APPLICATIONS

I. Ponomareva L. A. Chernozatonskii
Institute of Biochemical Physics of RAS,Kosygina st., 4, Moscow, 119991 Russia
A. N. Andriotis
Inst. of Electronic Structure and Laser Foundation for Research and Technology-Hellas 71110 Heraklio, Greece
M. Menon
Department of Physics and Astronomy, University of Kentucky,Lexington, KY 40506-0055

The discovery of carbon nanotubes by Iijima [1] was followed by observation of complex nanotube junctions in experiments. Single wall carbon nanotube (SWCN) junctions offer the possibility of use in nanoscale electronic devices. A two-terminal heterojunction formed by two nanotubes, one semiconducting and the other metallic, can function like a rectifying diode. The three-terminal junctions, however, are more versatile since the third terminal could be used for controlling the switching mechanism, power gain, or other transisting applications that are needed in any extended molecular electronic circuit. Among the three-terminal junctions formed by carbon nanotubes, the most interesting (from a device perspective) are the ``T-" and ``Y-junctions". Very recently, experimentalists have succeeded in developing template-based chemical vapor deposition (CVD) [2] and pyrolysis of organometallic precursor with nickelocene and thiophene techniques [3] that allows for the reproducible and high-yield fabrication of carbon nanotube Y-junctions [2,3]. More recently, experimentalists have succeeded in creating X-shaped molecular connections by welding achieved by electron beam irradiation of crossing SWCNs [4].

We present energetically efficient topological sequences involving two SWCNs leading to the formation of T-junctions using tight-binding molecular dynamics simulations. The initial configuration in our simulations involve a capped SWCN approaching the wall of another SWCN. In the final configuration the two nanotubes coalesce to form T-junctions with appropriate arrangement of topological defects. No structural defects (vacancies or interstitials) are present at any step of the process and the transformation is achieved only through topological defects. The total number of carbon atoms remain the same at each step.

We explore the lowest energy pathway for the process. Since the initial and final geometries involve only sp^2 bonding for all carbon atoms, it is reasonable to assume that having only sp^2 bonding during each of the intermediate steps of coalescence would provide the lowest energy pathways. The intermediate steps involve formation of many topological defects in the form of pentagons, heptagons, octagons, etc. Furthermore, the defects must obey a generalization of the well known Euler's formula specifying the local bond surplus at the junction [5].

We propose a sequence of intermediate steps leading to the formation of two distinct T-junctions in which all carbon atoms remain sp^2 coordinated throughout. The structures are relaxed at each step using generalized tight-binding molecular dynamics (GTBMD) scheme of Menon and Subbaswamy [6].

We illustrate the formation of a (5,5)-(10,0)-(5,5) (and (9,0)-(10,0)-(9,0)) T-junction by bringing a capped zig-zag (10,0) nanotube near an arm-chair (5,5) (zig-zag (9,0)) nanotube wall containing defects. These defects could arise due to localized e-beam or ion-beam irradiation induced localized heating/welding at the location of the junction point[4]. These defects can very well be initiated by the formation of a Stone-Wales defect [7] followed the separation of pentagon-heptagon pairs.

More insights can be gained from a study of energies at various steps leading to the formation of the two T-junctions. The structures are fully relaxed at each step and the total energy is calculated using the GTBMD scheme. The relative energies at each step in the formation of the two T-junctions are plotted in Fig.1 (large circles and squares). We have also calculated intermediate energy points (small circles and squares) that rule out the presence of

large barriers between the steps. As seen in the figure, an increase in energy (indicating a barrier to the process in steps **1-3** is followed by a drop in energy (in steps **3-8** without any significant barrier. The activation barrier to the process, thus, is the overall increase in energy in steps **1-3**. Once the initial barrier is overcome, the formation of the junction in steps **3-8** can be driven by the lowering of energy as shown in Fig.1.

We next investigate the transport properties of T-junctions obtained in our simulations. The quantum conductance of the SWCN T-junction is calculated using a Green's function embedding scheme [8] The Green's function is constructed using the same Hamiltonian as used for obtaining structural relaxation. The current voltage characteristics were calculated by applying a voltage V_s on the stem branch, and a gate V_g voltage on the left (right) branch and keeping the right (left) branch grounded. For $V_g = 0.0$ eV (i.e., only voltage applied through the stem terminal) a rectification of the current for positive V_s voltages is observed.

We have presented an atomistic picture of energetically efficient pathways for the formation of SWCN T-junctions through a sequence of steps starting with one in which a capped SWCN is brought near the wall of another SWCN. During the entire process no structural defects are generated and the transformation is achieved through creation/annihilation of topological defects, while all carbon atoms retain their sp^2 coordination. Recent experimental advances in electron beam welding techniques have greatly increased the plausibility of synthesizing T-junctions as proposed in the simulations. We have also calculated the transport properties of the thus formed T-junctions. The I-V characteristics indicate rectification. Application of gate voltage resulted in current modulation in the primary channel.

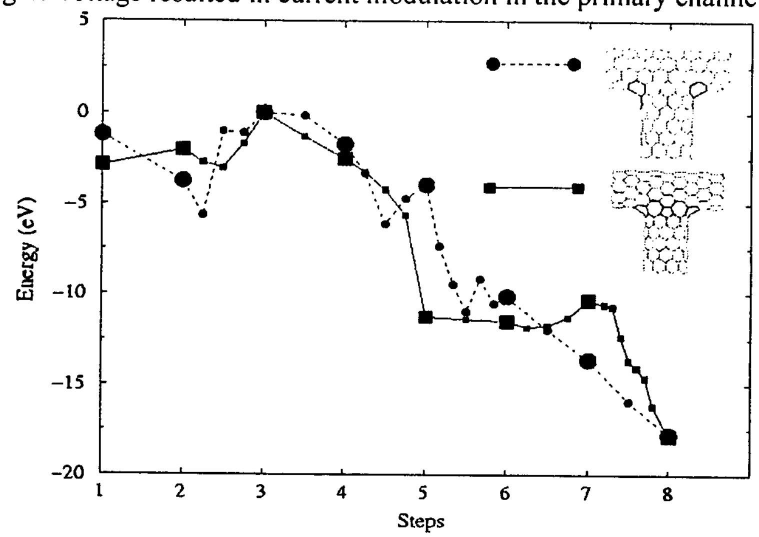

Fig1. Relative energies calculated using GTBMD schemes at each steps for (9,0)-(10,0)-(9,0) and (5,5)-(10,0)-(5,5) T-junctions (large circles and squares). Intermediate energy points are shown in small circles and squares.

References

[1] S. Iijima, Nature 354, 2148 (1991).
[2] J. Li, C. Papadopoulos, and J. Xu, Nature 402, 253 (1999).
[3] B. C. Satishkumar, P. J. Thomas, A. Govindraj, and C. N. R. Rao, Appl. Phys. Lett. 77, 2530 (2000).
[4] M. Terrones, F. Banhart, N. Grobert, J.-C. Charlier, H. Terrones, and P. M. Ajayan, Phys. Rev. Lett. 89, 075505 (2002).
[5] V. H. Crespi, Phys. Rev. B 58, 12671 (1998).
[6] M. Menon, E. Richter, and K. R. Subbaswamy, J. Chem. Phys. 104, 5875 (1996).
[7] A. J. Stone and D. J. Wales, Chem. Phys. Lett. 128, 501 (1986).
[8] A. N. Andriotis and M. Menon, J. Chem. Phys. 115, 2737 (2001).

PREPARATION AND CHARACTERIZATION OF ZIRCONIA COATINGS DOPED WITH Gd_2O_3 AND CO-DOPED WITH Y_2O_3 AND Gd_2O_3

A. Portinha[a], V.Teixeira[a]*, J. Carneiro[a], M.F. Costa[b]

[a] University of Minho – Physics Department, GRF-Functional Coatings Group, Campus de Azurém, 4800 Guimarães, Portugal

[b] University of Minho - Physics Department, Campus de Gualtar, 4700 Braga, Portugal

*Corresponding author: fax: +351-253510401, tel.: +351-253510465/400, email: vasco@fisica.uminho.pt

$ZrO_2Gd_2O_3$ and $ZrO_2Y_2O_3Gd_2O_3$ nanocomposite coatings were deposited by reactive DC magnetron sputtering with different atomic percentage of dopants. The influence of the percentage dopants in the high temperature phases stability of zirconia at room temperature has been studied by X-Ray Diffraction (XRD) as well its influence in the microstructural parameters and residual stresses. XRD measurements were used to characterize the coatings structures and to study the influence of Gd addition in the high temperature stabilized phases. Energy Dispersive X-ray Spectroscopy (EDX) was also used to assess the thin film composition. Scanning Electron Microscopy (SEM) was used to measure the film thickness, to observe microstructure of the film cross-section and to analyze the surface morphology. The surface microtopography was analyzed by atomic force microscopy (AFM) and non destructive laser microtopography. The roughness of the produced coatings was evaluated and related with the optical parameters obtained by Optical spectroscopy.

SYNTHESIS OF Fe-Co NANOPARTICLES AND THE EFFECT OF AL(III)-DOPING ON THEIR MAGNETIC PROPERTIES

Raul Pozas[1], M. Puerto Morales[2], Manuel Ocaña[1] and Carlos J. Serna[2]

[1]Instituto de Ciencia de Materiales de Sevilla (CSIC-UNSE), Americo Vespucio s/n, Isla de la Cartuja, 41092 Sevilla, Spain

[2]Instituto de Ciencia de Materiales de Madrid (CSIC), Cantoblanco, 28049 Madrid, Spain.

The most advanced magnetic recording flexible media essentially consist of acicular particles compossed by a Fe-Co alloy core coated with a layer enriched in several elements [1-3]. The synthesis of such metal particles is usually carried out from oxyhydroxyde precursors (goethite) through two consecutive processes, the dehydration of goethite and the further reduction of the resulting hematite to obtain α-Fe [3, 4]. The high temperatures involved in this method can promote interparticle sintering and, therefore, the lost of the acicular shape. This effect can be minimised by doping or coating the precursors with antisintering agents, such as Al, Y, Si, B, Sn cations [1, 5] which also favour the chemical stability of the the metal particles against oxidation.

In this work, we have obtained Fe, Fe-Co and Al(III)-doped Fe-Co metal particles (<100 nm) from undoped, Co(II)-doped and Al(III)-Co(II)-doped acicular goethite precursors. Our objective is to analyse the effect of the doping with Co and Al cations on the crystallochemical and magnetic properties of the final metal particles. Such precursors (goethite and doped-goethite) were prepared by oxidation with air of $FeSO_4$ solutions containing $Al(NO_3)_3$ and/or $Co(NO_3)_3$ solutions when required, precipitated with Na_2CO_3 [6]. TEM observation revealed that the obtained Co-doped and Al-Co-doped goethite particles were slightly smaller than the undoped ones, keeping the same axial ratio. EDX analyses confirmed the presence of the doping cations in each particle. whereas, XPS measumerents showed that aluminum was mainly concentrated in the particle outer layers. Such an Al(III) enrichment was enhanced during the reduction to iron, while cobalt diffuse toward the inner part of iron particles forming a Fe-Co alloy. While the Fe-Co alloy increases the saturation magnetization of Fe [3, 5], the presence of Al(III) on the particle outer layers of the precursors inhibited the growth of iron crystals, better preserving the acicular shape of iron particles, which had a very favourable effect on the coercivity of the metallic samples. Therefore, the presence of both Co metallic and Al(III) cations is essential to obtain iron particles with good magnetic properties.

References

[1] M.P. Sharrock, IEEE Trans. Magn. **36** (2000) 2420.
[2] M.P. Morales, S.A. Walton. L.S. Prichard, C.J. Serna, D.P.E. Dickson and K. O'Grady, J. Magn. Magn. Mater. 190 (1998) 357.
[3] S. Hisano and K. Saito, J. Magn. Magn. Mater. 190 (1998) 371.
[4] N. Sugita, M. Maekawa, Y. Ohta, K. Okinawa and N. Nagai, IEEE Trans. Magn. **31** (1995) 2854.
[5] K. Okamoto, Y. Okazaki, N. Nagai and S. Uedaira, J. Magn. Magn. Mater. 155 (1996) 60.
[6] R. Pozas, M. Ocaña, M.P. Morales and C.J. Serna, J. Colloid Interf. Sci., 254 (2002), 87-94.

MOLECULAR ELECTRONIC DEVICE MODELING: FET and RTD

Titash Rakshit
School of Electrical and Computer engineering, Purdue University

Device miniaturization is progressively heading towards dimensions that are comparable to the dimensions of molecules. Molecules are promising candidates as future electronic devices because of their small size, chemical tunability and self-assembly features.

FET: We address the question of whether a molecule used in a device configuration can offer any performance advantages relative to standard silicon devices. The first device we look at is standard three-terminal device with a short molecule(~1nm) as the channel. A self-consistent solution of coupled quantum transport and Poisson's equations shows that even for extremely short channel lengths a "well-tempered" molecular FET demands much the same electrostatic considerations as a "well-tempered" conventional MOSFET. We show that just as in a silicon-channel MOSFET, the gate oxide needs to be much smaller than the channel length (length of the molecule) for the gate control to be effective. It is therefore natural to investigate alternate principles of molecular transistor action, such as using conformational degrees of freedom. For instance, a gate field coupled with a molecular dipole moment could cut off the current by tilting it away from the contact (drain). We derive a general result that can be used to evaluate and compare transconductance of different field-effect mechanisms in molecular transistors, both electrostatic and conformational. We show that the conformational component helps the electrostatics of gate control but can lead to significant advantages only if the dipole moment of the molecule is comparable to the charge times the thickness of the gate oxide. Detailed numerical results for specific examples are presented in support of the analytical results.

RTD: Traditionally molecular electronic efforts, both theoretical and experimental have focused on molecules bonded to gold substrates. However, recent advances in growing molecules on silicon have demonstrated the feasibility of molecular electronics on silicon. Silicon-based molecular electronics will enable the development of integrated devices that can take advantage of the infrastructure provided by the powerful silicon-based IC industry. Silicon has a bandgap that can give rise to novel effects like NDR (negative differential resistance) that may have possible circuit applications. We demonstrate through first-principles transport calculations that the presence of silicon band-edge does lead to NDR in molecules docked on heavily-doped silicon substrates. Our results agree well with experimental observations by Hersam *et. al*.

ELECTRICAL CHARACTERISATION OF Py/Gd/Py TRILAYERS IN THE CIP CONFIGURATION

*R. Ranchal[a], E. López[a], M.C. Sánchez[a], C. Aroca[b], P. Sánchez[b].
[a] Dpto. Física de Materiales, Fac. CC. Físicas, U.C.M., Madrid, Spain.
[b] Inst. Sist. Opt. y Microt. (ISOM), E.T.S.I. Telecomunicación. U.P.M., Madrid, Spain.
*rociran@fis.ucm.es

Multilayers comprise of thin layers of Transition Magnetic Metals and Gadolinium (Gd) show an antiferromagnetic coupling at the interfaces. This coupling can be used to create a domain wall (DW) in the Gd and/or in the Transition Metal layer depending on the temperature and the thickness of the Gd and the Transition Metal [1]. Furthermore, the electrical properties appear to be very important in the study of the characteristics of nanostructures [2]. In this work an electrical characterisation of Py/Gd/Py trilayers is performed in the current in plane (CIP) configuration.

Samples were grown in a dc-magnetron sputtering system on corning glass-substrates. In all the samples the thickness of Py layers was of 200 nm. The Gd thickness was of 50, 100, 150 and 200 nm. The magnetic properties of the trilayers were determined by the longitudinal Kerr effect and VSM magnetometry at different temperatures. The electrical measurements were carried out using a dc method and a conventional four point configuration. In all the cases, the electric current flows in the magnetic easy axis. A ^{4}He closed cycle refrigerator was employed in order to measure in a temperature range of 10 to 300 K. The magnetoresistance (MR) was measured with the magnetic field in both parallel and perpendicular directions to the current. At room temperature it is observed a decrease on the magnetoresistance for the higher magnetic fields. At low temperature this behaviour disappears (Figure 1). Figure 2 shows the resistivity as a function of the temperature measured for a magnetic field of 200 Oe applied in the same directions as those used for the magnetoresistance. The $(R_{par} - R_{per})/R_{per}$ coefficient as a function of the temperature presents a maximum as it is shown in figure 3.

Taking into account the exchange interaction at the Py/Gd interface and the polycrystalline structure of the Gd layers the main results observed in these samples can be explained.

References:

[1] J. L. Prieto, M. G. Blamire, J. E. Evetts, Phys. Rev. Lett. **90,** 027201 (2003).

[2] J. A. González, J. P. Andrés, M. Arranz, M. A. López de la Torre, J. M. Riveiro, J. Appl.

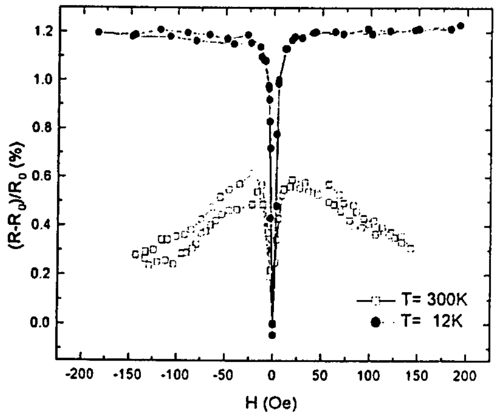

Figure 1. Experimental MR for the sample with a Gd thickness of 100 nm. The magnetic field is parallel to the current at (□) 300 K and (●) 12 K.

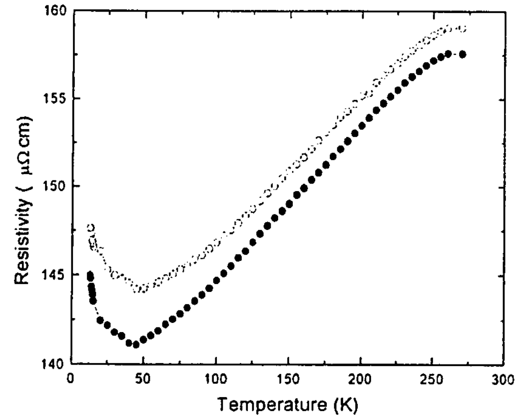

Figure 2. Electrical resistivity as a function of the temperature for a magnetic field of 200 Oe in the case of (○) magnetic field parallel and (●) perpendicular to the current. The Gd thickness was of 100 nm.

Phys. **92,** 914 (2002).

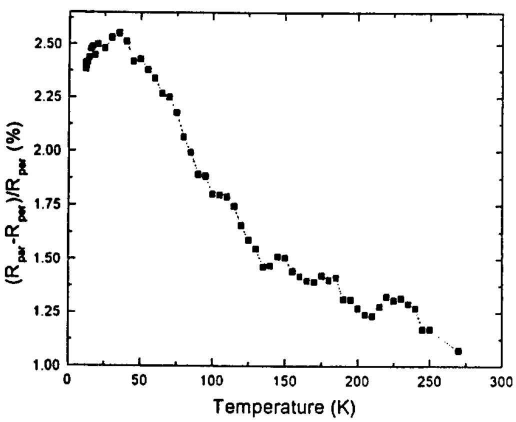

Figure 3. $(R_{par} - R_{per})/R_{per}$ as a function of the temperature for the sample with a Gd thickness of 100 nm. Both R_{par} and R_{per} are measured for a magnetic field of 200 Oe.

FABRICATION AND STUDY OF THE ELECTRONIC TRANSPORT PHENOMENA OF METAL-MOLECULE-METAL JUCTIONS BY CONDUCTING PROBE ATOMIC FORCE MICROSCOPY

Imma Ratera, Jinyu Chen, Frank Ogletree and Miquel Salmeron.
Lawrence Berkeley National Laboratory, 1 Cyclotron Road, 94720 Berkeley, USA
E-mail: salmeron@lbl.gov

In the field of molecular electronics, using molecular wires as components in electronic circuits is an appealing idea: such systems can be synthesized with feature lengths of just a few nanometers, so if we could assemble them onto a chip we would gain orders of magnitude in integration levels. In order to advance such a technology, however, several physical issues that have been a major concern for conventional microelectronics need to be addressed at the nanoscale.

The study of the electron transport phenomena in organic molecular films produced by either self-assembly (SAM) or Langmuir-Blodgett method are of most interest for applications as possible microelectronics components (diodes and switches) can be achieved by using these techniques. In this poster we will present an overview of recent work of electronic transport in nanoscale molecules for which experimental results are available.

To probe metal-molecule-metal junctions, one could use several techniques as STM, KFM or mechanical control break junction (MCB). However these techniques experiments have demonstrated that unambiguous contact to a nanoscale object is difficult to achieve. The utility of conductive probe atomic force microscopy (CP-AFM) provides excellent control over mechanical contacts, especially for single-molecule and SAMs studies. So we will use the CP-AFM technique to study the conductivity of metal-molecule-metal junctions fabricated by contacting metal supported self-assembled mono or multilayers with the metallic coated conductive atomic force microscope (AFM) tip.

One of the main goals in measuring conductivity at the nanoscale is to obtain current-voltage characteristics of nanoscale devices. In particular we will establish CP-AFM to study the electron transport as function of different parameters as the orientation and the molecular dimensions of the molecules on the film. The role of having multilayer, which we can expose to different mechanical excitations it has also been studied. The ability to vary the load on the microcontact is a unique characteristic of these junctions and also opens opportunities for exploring electron transfer as a function of molecular deformation. We will also study the role of the junctions, the contact of the terminal functional groups with the electrodes and the chemistry to modulate current-voltage characteristics.

ELECTRON ENTANGLEMENT VIA INTERACTIONS IN A QUANTUM DOT

Gladys León[1], Otto Rendon[2], Horacio Pastawski[3], Ernesto Medina[1]
[1] Centro de Física, Instituto Venezolano de Investigaciones Científicas, Caracas, Venezuela
[2] Departamento de Física-FACYT, Universidad de Carabobo, Valencia, Venezuela
[3] Facultad de Matemáticas, Astronomía y Física, Universidad Nacional de Córdoba, 5000 Cordoba, Argentina

We study a spin-entangler device for electrons, with a Coulomb interaction U, via a quantum dot proposed by Oliver et al[1]. The main advantage of this model, compared to others in the literature, is that single particle processes are forbidden. Within this model we calculate two electron transmission in terms of the T-matrix formalism to all orders in the tunneling amplitudes V and in the presence of i) external orbitals and ii) semi-infinite leads to show the appropriate physical limits. New qualitative results are found when external leads are considered non-perturbatively. In particular we recovered Oliver's fourth order results in the `external orbital' case, in the limit of small coupling of the dot to the external states, and a small imaginary part is added to the eigenergies. When leads are attached, the system effectively filters the singlet portion to all orders of perturbation theory. We discuss the role of the coulomb site interaction in the generation of the entangled state.

[1] W. D. Oliver, F. Yamaguchi, and Y. Yamamoto, Phys. Rev. Lett. **88**, 037901 (2002).

ULTRASENSITIVE, REAGENTLESS AFFINITY SENSORS EEXPLOITING TARGET-SENSITIVE LIPOSOMES

Alexandre Restrepo[1#], Kristin Horton[2], Ioanis Katakis[2] & Ciara O'Sullivan[1*]

1 Nanobiotechnology & Bioanalysis Group - Department of Chemical Engineering - Universitat Rovira i Virgili - Av. Països Catalans No. 26
Tel: (+34) 977558560
* e-mail: ckosulli@etseq.urv.es
# e-mail: arestrep@etse.urv.es
Tarragona – Spain.

2 Bioengineering and Bioelectrochemistry Group - Department of Chemical Engineering - Universitat Rovira i Virgili - Av. Països Catalans No. 26
Tarragona – Spain.

Abstract:

Knowledge gleaned from the human genome project together with a growing awareness of the importance of early detection of biomarkers or environmental contaminants has resulted in an increased necessity to achieve lower and lower assay detection limits. Signal amplification is thus an important tool in the development of biosensors for such targets, where the desired limit of detection may be as low as a few molecules of DNA or antigen. Amperometric detection strategies for redox molecules can be inherently limited by the fact that each analyte molecule can accept or donate only a relatively small number of electrons. Coupling this limitation with the background noise inherent in measuring very small currents, the limits of detection attained with electrochemical amperometric detection do not achieve levels that they should. Additionally, most currently available biosensor configurations require addition of reagents thus not lending themselves to facile use and disposability. The objective of this work is the development of ultrasensitive, reagentless affinity sensors based on the exploitation of target sensitive liposomes and substrate recycling schemes using the enzyme alkaline phosphatase as the reporter molecule for the following of affinity interactions. The work to be carried out can be divided into (a) transduction (b) immobilisation (c) signal amplification.

Acknowledgements:

This study has been carried out with financial support from the Commission of the European Communities, specific RTD programmes Quality of Life and Management of Resources Programme contracts CD-CHEF QLRT-2001-02077, and Competitive and Sustainable Growth Program, MICROPROTEIN G5RD-CT-2002-00744. It does not necessarily reflect their views and in no way anticipates the Commission's future policy in this area.

FIRST PRINCIPLES STUDY OF THE Si(111)5x2(Au) SURFACE

Sampsa Riikonen
Donostia International Physics Center (DIPC), Paseo Manuel de Lardizabal 4,
20018 Donostia-San Sebastian, Spain
E-mail: swbriris@sc.ehu.es

Daniel Sanchez-Portal
Centro Mixto CSIC-UPV/EHU and Donostia International Physics Center (DIPC),
Paseo Manuel de Lardizabal 4, 20018 Donostia, Spain
E-mail: sqbsapod@sc.ehu.es

In surface physics, the monolayers and submonolayers on substrates are of fundamental interest from both theoretical and technological point of view. The atoms deposited on substrates can be used to form arbitrary surface structures with desired electronical and chemical properties. One can try to control processes such as catalysis and corrosion or create structures that exploit quantum phenomena.

The deposition of metallic atoms, especially of gold, on silicon substrates results in a great variety of structures, depending on the amount of monolayers and the annealing process used [1]. The system obtained after the deposition of 0.4-0.5 monolayers of gold on Si(111) surface has been studied over decades. Different studies of the structure of this surface produced somewhat contradictory results. However, the advance of the experimental techniques has allowed an increase of the amount and quality of the information available. In particular, only quite recently, a simple model where the gold atoms form monatomic wires has been proposed [2] that seems to explain the earlier data quite well.

Gold nanowires have been demonstrated, but mainly using stepped surfaces. The spontaneous arrangement of the flat Si(111)5x2(Au) structure into nanowires calls for a thorough analysis. Also the structures with low dimensionality in general, yield a great variety of interesting quantum phenomena.

We took the proposed structure [2] as a starting point and performed *ab-initio* molecular dynamic simulations. We are thus able to test the stability of the structure and analyze its electronical and structural properties. The calculations were done using the SIESTA code [3] that uses localized atomic orbitals as a basis. The calculation is done using a finite slab and the 5x2 unit cell. Our methodology includes the saturation of the bottom silicon layer with hydrogen. Dielectric effects on the slab are eliminated by letting the bottom hydrogen layer to relax during the simulations. We tested the reliability of our computational method by simulating a few well-known surface reconstructions of silicon and comparing with an earlier calculation [4]. Spin-orbit interaction was not included in our calculations but it will be introduced later on.

Preliminary results show that the proposed structure is a stable one. We also give the height position of the atoms, because in the proposed model [2], the height of the atoms was missing due to the limitations of the experimental method. Bandstructures are obtained and the character of the different bands are analyzed and compared to the photoemission data [5].

References:

[1] R. Plass and L. D. Marks, Surf. Sci. **380** (1997) 497-506
[2] L. D. Marks, R. Plass, Phys. Rev. Lett. **75**, 2172 (1995)
[3] J. M. Soler, E. Artacho, *et. al.*, J. of Physics: Condensed Matter **14**, 2745 (2002)
[4] R. D. Meade, D. Vanderbilt, Phys. Rev. B **40**, 3905 (1989)
[5] K. N. Altmann, J. N. Crain, Phys. Rev. B **64**, 035406 (2001)

ELECTRICAL PROPERTIES OF NANOTUBES WITH SELF-ALIGNED SIDE GATES

L. A. W. Robinson[1]*, S. B. Lee[1], K. B. K. Teo[2], M. Chhowalla[2], G. Amaratunga[2], W. I. Milne[2], D. G. Hasko[1], and H. Ahmed[1]
[1]Microelectronics Research Centre, Cavendish Laboratory, University of Cambridge, Madingley Road Cambridge, CB3 0HE, United Kingdom
[2]Engineering Department, University of Cambridge, Trumpington Street, Cambridge, CB2 1PZ, United Kingdom
*E-mail: lawr2@cam.ac.uk

A method for the precise positioning of electrodes to carbon nanotubes is needed. Self-aligned, side-gate structures to suspended multi-walled carbon nanotubes (MWCNT), where the nanotube acts as an evaporation mask have been previously fabricated [1]. In such fabrications a line of metal is evaporated over a suspended nanotube, resulting in an island of metal which forms on the nanotube, the width of this island increases as the metal is deposited, forming a wedge shape, and thus allowing thick evaporations with the island remaining separated from the bulk metal. The island is removed during lift-off leaving a set of self-aligned electrodes with nanotube to electrode spacing of less then 20 nm. We now present the electrical behavior of nanotube transistors with self-aligned side gates and highlight the advantages that self-aligned side gates have over alternative gating techniques such as back-gates, side-gates and top-gates.

References

[1] L A W Robinson, S-B Lee, et al., Nanotechnology. 14, 290-293 (2003)

SIZE EFFECTS AND FERROELECTRIC TUNNEL JUNCTIONS

Julio Rodríguez Contreras, Hermann Kohlstedt, Rainer Waser

Institut für Festkörperforschung, Forschungszentrum Jülich, 52425 Jülich, Germany

In the last few years, remarkable progress has been made in the investigation of the ferroelectric thickness limit. This is partly due to the accelerating interest in ferroelectric materials for technological applications, and it is partly due to the natural scientific interest in understanding and studying the limits of physical phenomena.

Within this talk, size effects in ferroelectrics will be discussed and the concept of a ferroelectric tunnel junction will be presented.

The primarily studied heterostructures have been $Pt/PbZr_{0.52}Ti_{0.48}O_3/SrRuO_3$ and $SrRuO_3/BaTiO_3/SrRuO_3$, both grown on $SrTiO_3$ (100) substrates. The ferroelectric film thickness varied from 2 nm to 250 nm. Three different deposition techniques have been used, namely high-pressure sputtering, molecular beam epitaxy, and pulsed laser deposition. The outstanding thin film quality has been demonstrated by various analytical methods, among them XRD, RBS, AFM, HRTEM, and RHEED (for MBE-grown thin films). In order to measure ferroelectric properties, the heterostructures have been patterned into capacitors using either a lift-off process, an ion-beam etch technique, or a shadow mask. Subsequently, ferroelectric hysteresis loops have been obtained with the FE module of the aixACCT TF Analyzer 2000. Compared to the fabrication of capacitors, a more complex process has been applied to pattern tunnel junctions. In total, three photo mask steps defined tunnel junctions by conventional photolithography and ion beam etching.

The first part of my talk is about the thickness dependence of the remanent polarization and the coercive field, which have been studied in the range of 6 nm to 250 nm. Various origins of size effects have been identified. In some cases, extrinsic effects, e.g. film composition, surface roughness, and defects, are likely to be the reason for this phenomenon. However, given that ferroelectricity is a cooperative phenomenon like superconductivity and magnetism, the size effect is expected to be prominent even in the absence of extrinsic factors. Mechanical and electrical boundary conditions will be shown to alter the ferroelectric film thickness at which the size effect starts playing a role.

The second part of my talk deals with ferroelectric tunnel junctions, where the term *ferroelectric* refers to a property of the barrier material. The device consists of a ferroelectric layer sandwiched between metal electrodes. The thickness of the ferroelectric layer is thin enough to allow for electron tunneling. For the first time, the influence of macroscopic parameters, such as the spontaneous polarization and strain on quantum-mechanical electron tunneling through a ferroelectric tunnel barrier is studied experimentally. In addition, the experimental work is accompanied by theoretical ideas and predictions concerning the manifestation of piezo- and ferroelectricity in direct electron tunneling.

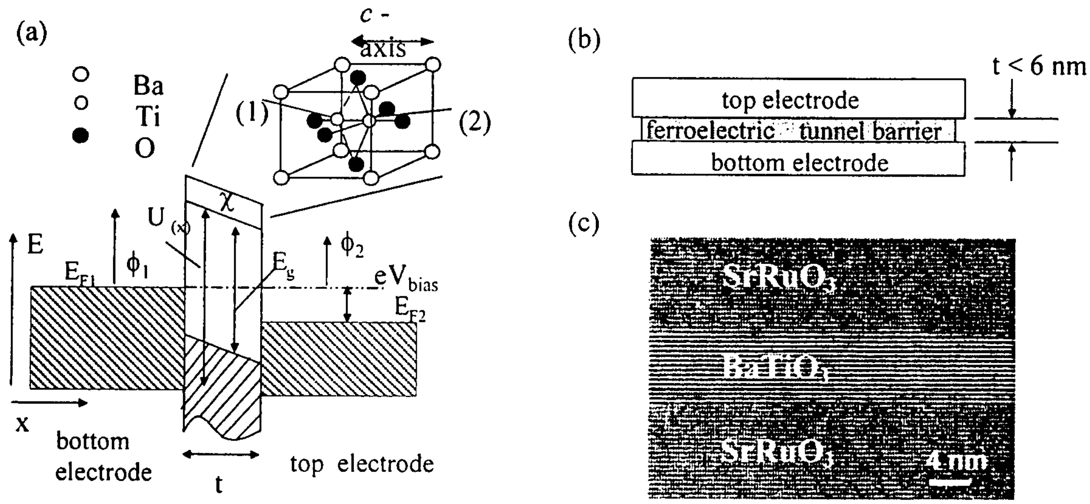

Figure 1. Concept of a ferroelectric tunnel junction: (a) simplified band diagram; E_F is the Fermi energy, χ is the electron affinity of the insulator, ϕ_1, ϕ_2 are the barrier heights at the electrodes, V_{bias} is the bias voltage across the junction, and (1)-(2) are possible positions of the Ti atoms; (b) schematic cross-sectional view of the FTJ; (c) HRTEM image of a MBE-grown $SrRuO_3$/5-nm-$BaTiO_3$/$SrRuO_3$ heterostructure.

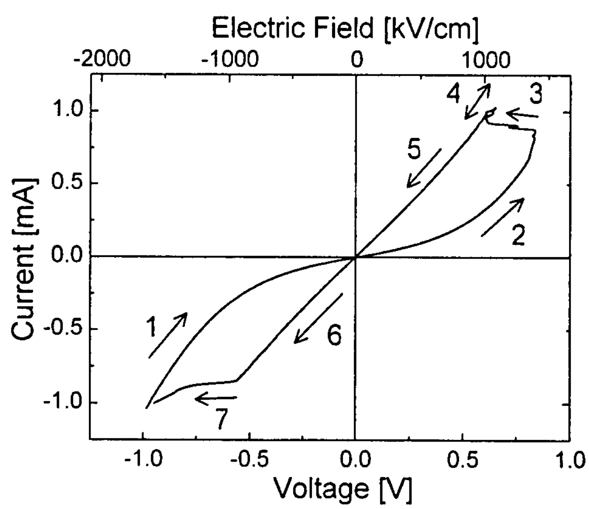

Figure 2. Typical *I-V* curve of a SRO/6 nm BTO/SRO tunnel junction. Please note clear switching events at –550 mV and 600 mV. Numbers from 1 to 7 and arrows show the direction of scan.

SPM AND LASER ABLATION: A POTENTIAL ANOTOMOGRAPH?

Ilmar Kink, Kristjan Saal, Rünno Lõhmus, Madis Lobjakas, Ants Lõhmus
Institute of Physics, University of Tartu, Riia 142, EE-51014 Tartu, Estonia
E-mail: ilmar.kink@fi.tartu.ee
http://www.fi.tartu.ee

Scanning probe microscopy (SPM) is now well-established tool for surface analysis, however, it can reveal only limited information about subsurface properties of a sample. Its sensitivity along a surface normal is severely constrained to a few topmost atomic or molecular layers only. However, the subsurface region is of great interest for many applications because the surface of a sample can be easily contaminated misrepresenting the true nature of the sample. Therefore, there are active developments of new methods for below surface nano-scale imaging going on in several research laboratories. Currently there are only very few techniques available that are capable of spatial 3D imaging at this length-scale and typically these are applicable only in special cases.

There have been attempts to employ an idea of creating a nanotomograph by stepwise removal of surface layers of a sample, taking SPM images after each removal procedure, and subsequently creating 3D images from the images by computerized processing [e.g. 1]. However, this simple idea has turned out to be technically very challenging. The main obstacle is how to spot the same location on the sample with the SPM probe if the sample is removed for the surface removal procedure, or how to protect the probe if the sample is kept in place during the removal procedure. Alternately, one can make surface processing in the SPM removing neither the sample nor the probe. Such *in situ* SPM-tomograph has been successfully applied in cases of selective electrochemical reactions [2] or selective chemical etching [3]. However, the general disadvantage of the latter approach is that the SPM tip is located in vicinity of processing area and can be modified as well if not destroyed.

In our previous work [4] we demonstrated an efficient *in situ* scanning probe analysis and subsurface imaging with a single device, which performs pulsed laser ablation of surface layers and precise resetting of far-removed AFM probe after ablation. The laser ablation technique offers several advantages for controllable removal of surface layers. The laser beam is easily guided and focused to a desired region of the sample by simple optics. The ablation depth depends on the deposited energy that can be controlled by selecting appropriate frequency of the laser pulses. In some cases the laser ablation does not require any additional expensive apparatus (e.g. vacuum chambers etc.) and can be performed in SPM vicinity in air atmosphere. Application of excimer lasers is quite common in pulsed laser deposition techniques [5] because these lasers offer sufficient energy density (>1 J/cm2) and their lasing transitions typically occur in the suitable wavelength range of 150-400 nm where most materials have strong absorption bands and correspondingly short penetration depths.

In our presentation we will demonstrate our latest achievements and results in development and application of newly designed experimental set-up that consists of a modified AFM, UV excimer laser, vacuum chamber etc. We will present AFM data showing influence of eximer laser radiation on mica surface at low fluencies and discuss possibilities of creating a nanotomograph using combination of SPM and laser ablation.

References:

[1] R. Magerle. Phys. Rev. Lett. **85** (2000) 2749.
[2] E.M. Siebel, U. Memmert, R. Vogel, U. Hartmann. Appl. Phys. A **66** (1998) S83.
[3] A.A. Bukhareav, *et al*, Russian J. Appl. Chem. **73** (2000) 1332.
[4] I. Kink, *et al*, in AOMD-3 Proceedings (SPIE, 2003).
[5] S.M. Green, *et al*, in *Pulsed Laser Deposition of Thin Films*, ed. D.B. Chrisey and G.K. Hubler (Wiley-Interscience Pub., New York, 1994).

SOLUTIONS FOR GINZBURG-LANDAU FUNCTIONALS WITH CONSTRAINTS

Pedro Nel Sánchez
Departamento de Física Aplicada, Universidad de Alicante, San Vicente del Raspeig, Alicante, 03690, España.
Juan José Palacios
Departamento de Física Aplicada y Unidad Asociada UA-CSIC, Universidad de Alicante, San Vicente del Raspeig, Alicante, 03690, España.
E-mail: pnsl@alu.ua.es
jjpalacios@ua.es

In type-II superconductors appears a mixed state where the magnetic field penetrates inside the superconductor in flux lines (vortices) carrying a quantum of flux [1]. These vortices form a triangular lattice that minimize the repulsion energy between two vortices. For finite superconductors the surface effects introduce new phenomena for the lattice like surface superconductivity and the interaction between vortices and the surface current. Palacios [2] using lower Landau levels in superconducting strips showed that their magnetic behavior includes the appearing of rows of vortices and surface superconductivity when the magnetic field is greater than H_{C2}.

These strips are used in the study of pinning of vortices in the presence of a net current inside the strip. So we need to change the Ginzburg-Landau functional to include a constraint which takes into account the existence of this current.

In this work we show how to calculate semi-analytically the vortex state in strong type-II superconducting strips with a net current. Our order parameter is a linear combination of lower Landau levels and we minimize the Ginzburg-Landau functional applying Lagrange multipliers as it was proposed by Kosov [3] and Johnson [4]. With this method we found that for 2 components it is necessary that the symmetry (-k, k) does not exist.

Additionally we use this method for a Bose-Einstein condensate in an elonged harmonic potential where the constraint is the conservation of the particle number and the Lagrange multiplier is the chemical potential..

References:

[1] A. A. Abrikosov, Zh. Eksperim. I Teor. Fiz, **32**, 1442 (1957)
[2] J. J. Palacios, Phys. Rev. B, **57**, 10873 (1998)
[3] D. S. Kosov, cond-mat/0209347 (2002)
[4] M. D. Johnson and O. Heinonen, Phys. Rev. B, **51**, 14421 (1995)

SUBSTRATE ORIENTATION EFFECTS ON THE STRANSKI-KRASTANOV GROWTH MODE

S.N. Santalla*, C. Kanyinda-Malu and R.M. de la Cruz

Departamento de Física, Universidad Carlos III de Madrid, Av. de la Universidad 30, 28911 Leganés (Madrid), Spain.

*e-mail: ssantall@fis.uc3m.es
http://bacterio.uc3m.es/investigacion/solido/gente/rosa

As it is well established, one of the parameters which influences greatly the Stranski-Krastanov (S-K) growth mode in low-dimensional strained heterostructures is the substrate orientation. A change in the Miller indexes of the substrate allows to control the strain relaxation in the heteroepitaxial systems inducing consequently modifications in the onset of the S-K growth mode, or even, in some cases, the inhibition of this mode. For instance, RHEED and STM measurements of InAs grown on GaAs (110) and GaAs (111) surfaces revealed that the growth is always two-dimensional layer by layer and strain is relieved by the formation of misfit dislocation [1]. However, when InAs epitaxial layers are grown on high index substrates such as (311) and (511) GaAs, the PL spectra indicated a delay in the three-dimensional growth mode onset [2]. On the other hand, appropriate changes of substrate orientation induce different morphologies of the islands for the same epitaxial film. This phenomenon is observed by STM in Ge/Si (001) and Ge/Si (111) quantum dots [3]. Although there are extensive experimental results on the substrate orientation effects, to our knowledge, they have not been theoretically studied. Therefore, the aim of this work is to investigate the islanding mechanism dependence with the substrate orientation for Ge/Si and InAs/GaAs heterostructures. The importance of these low-dimensional strained systems for fabrication of optoelectronic devices is reported elsewhere [4, 5].

Within the framework of the continuum elasticity theory, we have characterized the S-K growth mode in terms of the transition thickness and the accumulated stress for increasing Miller indexes of the substrate. Assuming a coherent behavior at the substrate/film interface, we propose a sigmoidal law which defines the lattice dependence with the thickness to describe the relaxation mechanism. This dependence was successfully applied in Ge/Si (001) and InAs/GaAs (001) quantum dots [6, 7]. Also, the non rigid substrate approximation is taken into account, where film as well as substrate are strained. The validity of this approach was previously shown in the investigated heterostructures [6, 7]. To evaluate the transition thickness, we analyze the stability regions of the free energy density in terms of the slope, the order parameter. For higher Miller indexes, a metastability region is obtained which induces changes in the S-K onset. The delay of this onset as the substrate orientation departs from (001) is discussed in terms of the degree of strain relaxation in the dots. Finally, the transition thickness and compressive stress values obtained in our model are in good agreement with the experimental ones. Figure 1 shows the diamond structure of Ge in (001) and (111) orientations, respectively.

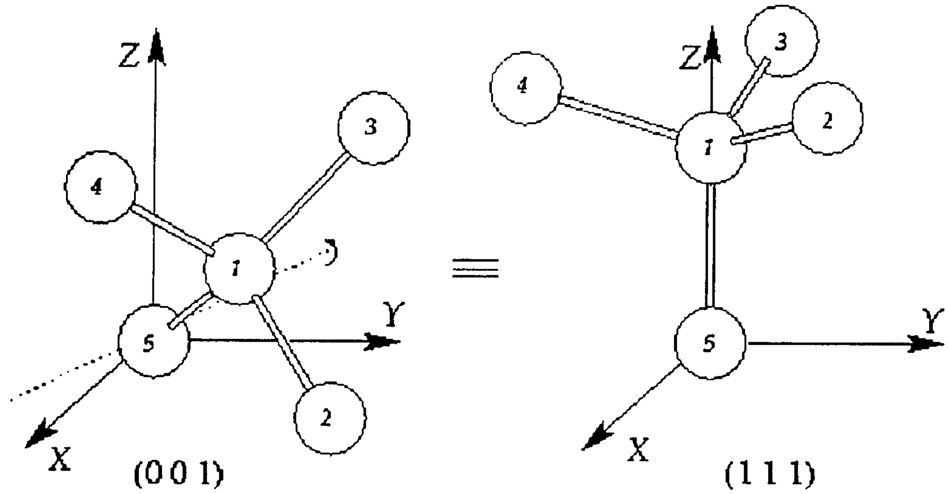

Figure 1. Rotation from (001) to (111) around the axis [1 –1 0] in the diamond structure.

References

[1]. B.A. Joyce, T.S. Jones amd J.G. Belk, J. Vac. Sci. Technol. B **16**, 2373 (1998).
[2]. S. Sanguinetti, G. Chiantoni, E. Grilli, M. Guzzi, M. Henini, A. Polimeni, A. Patané, L. Eaves and P.C. Main, Mat. Sci. Engineering B **74**, 239 (2000).
[3]. B. Voigtländer, Surf. Sci. Reports **43**,127 (2001).
[4]. G. Wedler, J. Waltz, T. Hesjedal, E. Chilla and R. Koch, Phys. Rev. Lett. **80**, 2382 (1998).
[5]. A. Fiore, J.X. Chen and M. Llegems, Appl. Phys. Lett. **81**, 1756 (2002).
[6]. S.N. Santalla, C. Kanyinda-Malu and R.M. de la Cruz, Physica E **17**, 480 (2003).
[7]. S.N. Santalla, C. Kanyinda-Malu and R.M. de la Cruz, J. Crys. Growth **23**, 190 (2003).

A STUDY OF STRANSKI-KRASTANOV GROWTH MODE USING A FRENKEL-KONTOROVA MODIFIED MODEL

S. N. Santalla[1]*, J. Rodríguez-Laguna[2], C. Kanyinda-Malu[1] and R.M. de la Cruz[1]

[1]Departamento de Física, Universidad Carlos III de Madrid, Av. de la Universidad 30, 28911 Leganés (Madrid), Spain.
[2]Instituto de Física Teórica, UAM-CSIC, 28049 Cantoblanco (Madrid), Spain

*e-mail: ssantall@fis.uc3m.es
http://bacterio.uc3m.es/investigacion/solido/gente/rosa

In typical heteroepitaxial semiconductor systems such as Ge/Si and InAs/GaAs, the length scales of the mechanism growth physics is of the order of a few monolayers (e.g. size of the transition thickness and critical thickness, width of non-interacting misfit dislocations, etc.) These lengths, measured on atomic scales, entail many physical phenomena, basically in the prediction of macroscopic behavior like the surface morphology or surface reconstruction, phase transition and other features associated with the deposition of the atomic layers.
One of the models more extensively used is the valence force field (VFF), where the macroscopic elastic constants of a crystal are directly proportional to the second derivatives of the total interatomic potential energy [1-3]. In fact, this model was sucessfully applied to analyze the strain relaxation and interfacial stability and to evaluate the stress distributions in III-V semiconductor heteroepitaxial systems [4-5]. However, the application of VFF model entails large time of computing work because all the terms which represent the contributions to the potential energy arise from different spring constants corresponding to the several interactions between nearest neighbors [2].
To overcome this difficulty, many authors use atomistic-like scheme of Frenkel-Kontorova (F-K) pattern. Within this model, the equilibrium positions of atoms in the growing layer result from the competition between the preferred interatomic separation of these atoms, which interact through harmonic springs, and the periodicity imposed by the rigid potential of the substrate [6]. Due to its universality, the F-K model was widely applied with success in many areas of condensed-matter physics to study complex static and dynamical phenomena arising from purely local interactions [7]. Following the F-K model applied by Ratsch and Zangwill [8] to characterize the phase diagram of III-V heteroepitaxial structures as a function of the total number of atoms, we extend this treatment to investigate macroscopic parameters envolved in the Stranski-Krastanov (S-K) growth mechanism. In our study, the one-dimensional classical F-K is turned to 1+1 dimensions by addition of an extra potential in the growth direction. The tentative potential, whose shape is similar to that of Markov and Trayanov [9], accounts on the interaction of the atoms of the growth film with the substrate material. To illustrate the effectiveness of this new approach, analytical and numerical calculations are done to predict the transition thickness and the phase diagram in the coherently grown Ge/Si islands. Figures 1 and 2 show the atomic F-K configuration and the tentative potential shape, respectively.

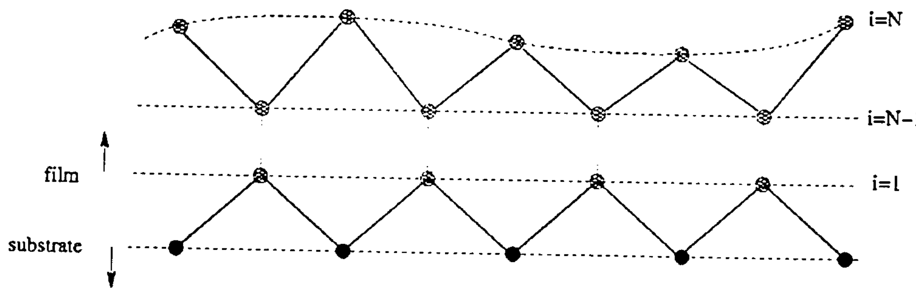

Figure 1. Frenkel-Kontorova modified configuration scheme.

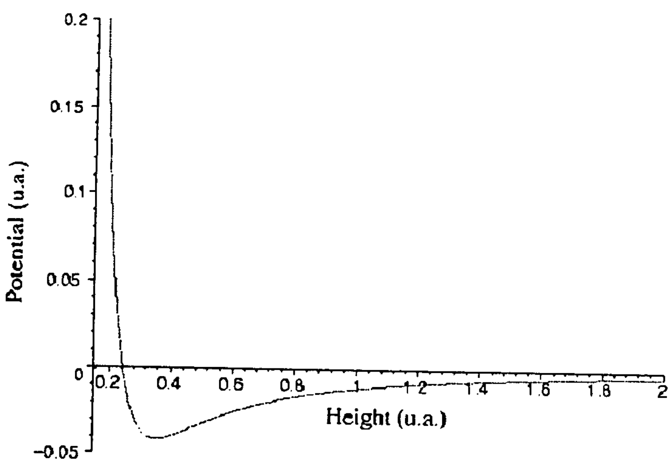

Figure 2. Tentative potential along the growth direction.

References

[1]. Dynamical theory of crystal lattices, M. Born and K. Huang, ed. Oxford University Press 1954.

[2]. M.J.P. Musgrave and J.A. Pople, Proc. Roy. Soc. (London) **A268**, 474 (1962).

[3]. P.N. Keating, Phys. Rev. **145**, 637 (1966).

[4]. D. Maroudas, L.A. Zepeda-Ruiz, R.I. Pelzel, B.Z. Nosho and W.H. Weinberg, Computational Mat. Sci. **23**, 250 (2002).

[5]. P. Raiteri, F. Valentinotti and L. Miglio, Appl. Surf. Sci. **188**, 4 (2002).

[6]. Low-dimensional semiconductor structures-Fundamental and devices applications, ed. K. Barnham and D. Vvedensky, Cambridge University Press 2001.

[7]. Chuang-I Chou, Choon-Lin Ho and Bambi Hu, Phys. Rev. E **55**, 5092 (1997).

[8]. C. Ratsch and A. Zangwill, Surf. Sci. **293**, 123 (1993).

[9]. I. Markov and A. Trayanov, J. Phys.: Condens. Matter **2**, 6985 (1990).

IMPROVEMENT OF LATERAL RESOLUTION OF MICROCONTACT PRINTING

Fuminobu Sato, Masamichi Fujihira
Department of Biomolecular Engineering, Tokyo Institute of Technology
4259 Nagatsuta, Midori-ku, Yokohama 226-8501, Japan
Email: mfujihir@bio.titech.ac.jp
http://www.fujihira.bio.titech.ac.jp/

A chemically sensitive imaging mode based on adhesive force detection by pulsed-force-mode atomic force microscopy (PFM-AFM) [1,2] and its application to characterization of microcontact printing (μCP) [3-5] will be presented. PFM-AFM enables imaging of adhesive forces between tip and sample surfaces, simultaneously with topographic imaging. Since the adhesive forces are related to interaction between chemical functional groups on the tip and sample surfaces [6-10], we combined the adhesive force mapping with chemically modified tips [11-14] to accomplish imaging of a sample surface with chemical sensitivity. Namely, PFM-AFM has been used as a chemical force microscopy [15-17]. The force mapping both in air and pure water with CH_3- and COOH-modified tips clearly discriminated between the chemical functional groups on the patterned alkanethiol self-assembled monolayers (SAMs) on gold consisting of COOH- and CH_3-terminated regions prepared by μCP [18,19].

Generally, non-annealed gold substrates, such as sputtered and vapor-deposited gold films, were widely used for μCP. Sizes of grains of such films become the smaller, the better pattering of etched films in nanometer scales can be performed by alkanethiol-gold μCP. However, granular roughness of non-annealed gold substrates prevents SPM observation of topography of mixed SAMs of μCP, because the height difference between two types of thiol derivatives is smaller than the granular roughness [20]. Thus, it is necessary to characterize SAMs on Au(111) terraces to improve both packing of SAMs and lateral resolution of SPM imaging of μCP.

Finally, preparation procedures for chemically modified tip and sample surfaces will be presented in detail. In particular, how to improve packing of SAMs and lateral resolution of μCP into nanometer scales, will be discussed.

References

[1] A. Rosa-Zeiser, E. Weilandt, O. Marti, Meas. Sci. Technol. **8** (1997) 1.

[2] T. Miyatani, M. Horii, A. Rosa, M. Fujihira, O. Marti, Appl. Phys. Lett. **71** (1997) 2632.

[3] A. Kumar, G.M. Whitesides, Appl. Phys. Lett. **63** (1993) 2002.

[4] Y. Xia, G.M. Whitesides, Angew. Chem. Int. End. **37** (1998) 550.

[5] B. Michel, A. Bernard, A. Bietsch, E. Delamarche, M. Geissler, D. Juncker, H. Kind, J.-P. Renault, H. Rothuizen, H. Schmid, P. Schmidt-Winkel, R. Stutz, H. Wolf, IBM J. Res. Develop. **45** (2001) 697.

[6] G. Bar, S. Rubin, A.N. Parikh, B.I. Swanson, T.A. Zawodzinski, M.-H. Whangbo, Langmuir 13 (1997) 373.

[7] R.C. Thomas, J.E. Houston, R.M. Crooks, T. Kim, T.A. Michalske, J. Am. Chem. Soc. 117 (1995) 3830.

[8] T. Han, J.M. Williams, T.P. Beebe, Jr., Anal. Chim. Acta 307 (1995) 365.

[9] A. Noy, C. Daniel Frisbie, L.F. Rozsnyai, M.S. Wrighton, C.M. Lieber, J. Am. Chem. Soc. 117 (1995) 7943.

[10] J.M. Williams, T. Han, T.P. Beebe, Jr., Langmuir 12 (1996) 1291.

[11] T. Nakagawa, K. Ogawa, T. Kurumizawa, S. Ozaki, Jpn. J. Appl. Phys. **32** (1993) L294.

[12] T. Nakagawa, K. Ogawa, T. Kurumizawa, J. Vac. Sci. Technol. B **12** (1994) 2215.

[13] Y. Okabe, M. Furugori, Y. Tani, U. Akiba, M. Fujihira, Ultramicroscopy **82** (2000) 203.

[14] M. Fujihira, Y. Tani, M. Furugori, U. Akiba, Y. Okabe, Ultramicroscopy **86** (2001) 63.

[15] C.D. Frisbie, L.F. Rozsnyai, A. Noy, M.S. Wrighton, C.M. Lieber, Science **265** (1994) 2071.

[16] A. Noy, D.V. Vezenov, C.M. Lieber, Annu. Rev. Mater. Sci. **27**(1997) 381.

[17] H. Takano, J.R. Kenseth, S.-S. Wong, J.C. O'Brien, M.D. Porter, Chem. Rev. **99** (1999) 2845.

[18] Y. Okabe, M. Furugori, Y. Tani, U. Akiba, M. Fujihira, Ultramicroscopy **82** (2000) 203.

[19] M. Fujihira, M. Furugori, U. Akiba, Y. Tani, Ultramicroscopy **86** (2001) 75.

[20] F. Sato, H. Okui, U. Akiba, K. Suga, M. Fujihira, Ultramicroscopy, in press.

Metamorphic modulation-doped InGaAs/InAlAs heterostructures with high electron mobility grown on GaAs substrates.

E. S. Semenova, A. P. Vasilev, A. E. Zhukov, S. S. Mikhrin, A. R. Kovsh, V. M. Ustinov, Yu. G. Musikhin, A. G. Gladyshev, S. A. Blokhin, N. N. Ledentsov

A. F. Ioffe Physico-Technical Institute, Russian Academy of Sciences,
26 Politekhnicheskaya, 194021, St. Petersburg, Russia
E-mail:esemenova@mail.ioffe.ru

Abstract: Modulation-doped heterostructures were grown by molecular beam epitaxy in the InGaAs/InAlAs metamorphic material system. Optimization of the low-temperature compositionally-graded buffer layer allowed us to improve the structural perfection of active layers. Electron mobility in 2D channel of metamorphic structure grown under optimum conditions (8100 cm^2/Vs at 300K) noticeably exceeds typical values achieved in GaAs-based strained InGaAs/AlGaAs heterostructures.

Modulation doped (MD) InGaAs/InAlAs heterostructures epitaxially grown on InP substrates are currently widely used for the fabrication of low-noise high-speed transistors [1]. The main advantage of that system in comparison with the InGaAs/AlGaAs structures on GaAs substrates is a possibility to exploit higher indium content in channel layers (usually 50% against 20% in case of strained InGaAs/GaAs QW). This leads to higher conduction band discontinuity and lower electron mass. As a result, higher electron concentration ($>2\times10^{12}$ cm^{-2} against $\sim1\times10^{12}$ cm^{-2}) and higher mobility (>10000 cm^2/Vs against ~6000 cm^2/Vs) are achieved in 2D electron gas of InGaAs/InAlAs/InP heterostructures. However, GaAs substrates have several significant advantages over InP, namely larger size of commercially available wafers, lower fragility and lower cost. This motivates an interest to so-called metamorphic structures grown on GaAs substrates, in which specific epiaxial regimes and design of In(Ga)AlAs buffer layer are used to change gradually the lattice constant of epilayer from GaAs to InP while burying most of dislocations inside the buffer layer [2-6]. At the same time, a possibility to fabricate metamorphic GaAs-based structures, whose transport and structural characteristics will be comparable to those based on InP, is still challenging due to incomplete suppression of propagation of treading dislocations and surface roughness [5].

In the present work we report on the optimization of MBE growth conditions for metamorphic InAlAs/InGaAs/GaAs MD heterostructures that allowed us to improve significantly material quality and achieve room-temperature electron mobility as high as 8100 cm^2/Vs.

The structures studied were grown in a Riber 32P MBE machine on semi-insulating GaAs(100) substrates. Reflection high-energy electron diffraction (RHEED) pattern was *in situ* monitored to control surface morphology of epilayers. Composition and structural quality were evaluated by high-resolution x-ray diffraction (HRXRD). Carrier concentration and mobility were measured by the Van der Pauw method using a BioRad setup at 77 and 300 K temperature. Surface morphology and degree of strain relaxation were studied by scanning (SEM) and transmission (TEM) electron microscopy.

High lattice mismatch between InP and GaAs (~3.5%) leads to impossibility of direct epitaxial growth of thick and structurally perfect layers having a lattice constant matched to InP on GaAs substrates. In such a case, strain relaxation proceeds by the formation of threading dislocations that propagate through whole thickness of the epitaxial layer. As an example Fig. 1 shows cross-section TEM image of 0.6-μm-thick $In_{0.3}Ga_{0.7}As$ layer grown on GaAs. MD heterostructures under investigation are based on $In_xAl_{1-x}As$ buffer layer with linearly-graded In content (from 10% to 58%). The following layer sequence was used starting from the substrate: 0.9-μm-thick InAlAs gradient layer and 0.4-μm-thick

$In_{0.52}Al_{0.48}As$ layer, 40-nm-thick $In_{0.53}Ga_{0.47}As$ channel layer, 5-nm-thick $In_{0.52}Al_{0.48}As$ spacer layer, 10-nm-thick n-type doped $In_{0.52}Al_{0.48}As$ barrier layer, 15-nm-thick $In_{0.52}Al_{0.48}As$ Schotky-layer, and, finally, 7-nm-thick $In_{0.53}Ga_{0.47}As$ contact layer. Gradient layer is deposited at low temperature (see below) while all the rest layers are grown at 500^0C.

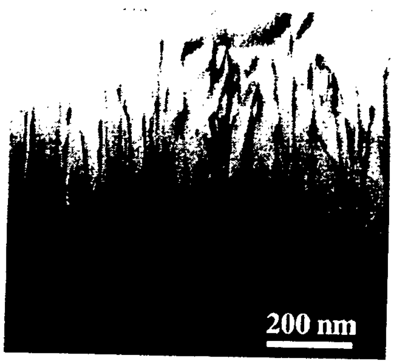

Fig. 1 TEM micrographs of InGaAs (x~30%)structure on GaAs substrates

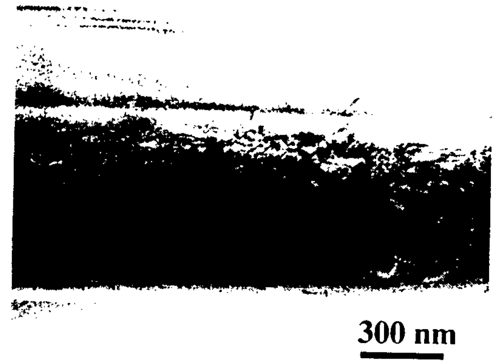

Fig. 2 TEM micrographs of InGaAs/InAlAs/GaAs MDHS with metamorphic gradient buffer on GaAs substrates

We have found that the deposition of the buffer layer at sufficiently low temperatures ($\leq 400^0$C) is a key point to prevent propagation of threading dislocations into the upper (active) layers. It is clearly seen in cross-section TEM image in Fig. 2. At the same time, the surface morphology of the MD heterostructure also strongly depends on the growth regimes for the buffer layer. We have found however that very low temperatures (around 350^0C) lead to a 3D growth mode as it follows from the spotty RHEED pattern observed. In opposite, at higher growth temperature ($\sim 400^0$C) 2D growth mode persists.

Thus, optimized growth condition (400^0C) allows us to prevent dislocation propagation and still have smooth interfaces. In its turn, this suppresses electron scattering due to interface roughness and thus improves electron mobility in 2D gas. In optimized structure the electron mobility reaches 8100 and 33100 cm^2/Vs at room temperature and 77K, respectively, with the electron concentration of 1.2×10^{12} cm^{-2}. Similar structure grown on InP substrate (without gradient buffer layer) demonstrated the electron mobility of 11050 and 51670 cm^2/V s.

In conclusion, the optimization of metamorphic gradient buffer of modulation doped heterostructures based on GaAs allowed us to prevent dislocation propagation into the active layers and improve surface morphology. We achieved room-temperature mobility of 8100 cm^2/V s which is well comparable to that of InP-based structures and noticeably superior to pseudomorphic GaAs-based structures.

Acknowledgments

This work was supported by “Physics of Solid State Nanostructures ” program and joint research program between *A. F. Ioffe Physico-Technical Institute* and Nanosemiconductors Gmbh, Germany.

References

[1] L. D. Nguyen, L. E. Larson, and U. K. Mishra, Proc. IEEE **80**, 494 (1992)
[2] W.E.Hoke,P.J.Lemonias,J.J.Mosca,J.Vac.Sci. Technol.B 17 (3)(1999)1131.
[3] M.Zaknoune,B.Bonte,C.Gaquiere,IEEE Electron Device Lett.19 (9)(1998)345.
[4] Guanwu Wang,Youngkai Chen,William J.Scha.,IEEE Trans.Electron Devices 35(7)(1988)818.
[5] M.Behet,K.Van der Zanden,G.Borghs.Appl.Phys. Lett.73 (1998)2760.
[6] T.Mishima,K.Higuchi,M.Mori,J.Crystal Growth,150 (1995)1230.

Theoretical study of molecular-scale conductors

Nikolai Sergueev and Hong Guo

Center for the Physics of Materials and Department

of Physics, McGill University, Montreal, PQ, Canada H3A 2T8

Using molecules as functional units for modeling nanoelectronic systems has been the topic of ever increasing activity over the last two decades. Although experimentally there is a rapid progress in measuring transport characteristics of molecular-scale devices including the true I-V curves [1,2], from theoretical point of view the accurate prediction still remains to be a challenge.

Recent theoretical research has been focussed on gaining qualitative understanding as well as on the development of *ab initio* methods of computing transport properties. The Density Functional Theory (DFT) has served as a basis for the most of these studies. The majority of condensed matter simulations based on the conventional DFT [3,4] solve only finite systems, such as isolated molecules or periodic systems consisting of supercells. The molecular-scale conductor though is neither finite nor periodic. It usually consists of a molecule connected to the infinite electrodes where the external bias potentials are applied which makes the device to be out of equilibrium. To overcome these difficulties new formalism is required to model the quantum transport in molecular electronics.

In this work we briefly describe a method based on DFT within the Keldysh nonequilibrium Green's function formalism so that nonlinear charge transport properties of nanoelectronic device can be predicted without any phenomenological parameters [5,6]. We then review a recently developed formalism of electron-phonon interactions and show that vibrational modes of molecule has to be taken into account to perform the current calculations. Finally we apply these theories to investigate a C_{60} molecular junction connected to the metal electrodes.

REFERENCES

[1] C. Joachim, J. K. Gimzewski, R. R. Chlitter, and C. Chavy, *Phys. Rev. Lett.* **74** (1995) 2102.

[2] H. Park, J. Park, A. K. L. Lim, E. H. Anderson, A. P. Alivisatos, and P. L. McEuen, *Nature* **407** (2000) 57.

[3] M. C. Payne, M. P. Teter, D. C. Allan, T. A. Arias and J. D. Joannopoulos, *Rev. Mod. Phys.* **64** (1992) 1045.

[4] P. Ordejón, E. Artacho, and J. M. Soler, *Phys. Rev. B* **53** (1996) R104441.

[5] J. Taylor, H. Guo and J. Wang, *Phys. Rev. B* **63** (2001) 245407.

[6] M. Brandbyge, J.-L. Mozos, P. Ordejón, J. Taylor, and K. Stokbro, *Phys. Rev. B* **65** (2002) 165401.

FORMATION OF BI-DIMENSIONAL ORGANIC MOLECULAR ASSEMBLIES ON COPPER AND ZINC SUBSTRATES

F. Sinapi[a,b], J. Delhalle[a], Z. Mekhalif[a]

[a] *Facultés Universitaires Notre-Dame de la Paix*
Chemistry Department, LISE
Rue de Bruxelles 61, B-5000 Namur, Belgium
[b] *Fonds pour la Formation à la Recherche dans l'Industrie et dans l'Agriculture*
Rue d'Egmont 5, B-1000 Bruxelles, Belgium

Copper and zinc are two metals commonly used in the manufacture of various types of products which applications are ranging from pipelines in water distribution systems to construction, decoration or protection of steel in the car industry. To protect those metals from corrosion (in atmospheric and other environments) and to promote adhesion of organic coating or adhesives, we had recourse to the chemistry of self-assembly. In this context, the grafting of an alkanethiol molecule has been firstly considered. Prior modification, it is of major importance to activate the bare substrates in order to obtain reduced surfaces predisposed to form strong thiolate bonds.

The (3-mercaptopropyl)trimethoxysilane (MPST), $(MeO)_3Si\text{-}(CH_2)_3\text{-}SH$, is the organothiol molecule which has been chosen. The different behavior of this bifunctionnal molecule on copper and on zinc will be especially commented. Once the MPTS molecule chemisorbs onto the substrates by the thiol function forming a self-assembled monolayer, it presents a trimethoxysilane terminal group ($-Si(OMe)_3$) pointing out at the surfaces.

The next challenge has been the determination of hydrolysis conditions able to bring those groups trough a siloxane framework (Si-O-Si) containing silanol functions (-SiOH) as shown at Figure 1. This has to be done without any alteration of the modified substrates. Two pH-different solutions have been selected for those experiments: an acidic medium for the copper substrates and an alkaline solution for the zinc surfaces.

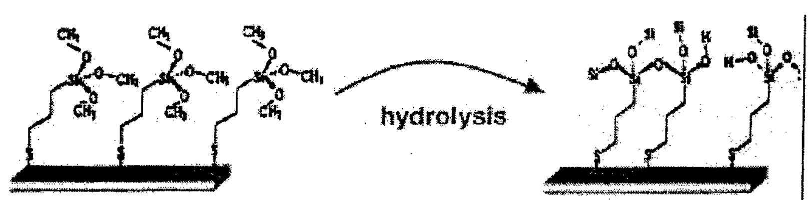

***Figure 1**: schematic view of hydrolysis process of the MPTS film on metallic surfaces*

To increase the organization of the molecular assembly and to further prevent oxidation of the substrates modified by the hydrolyzed monolayer, the grafting of a second organic molecule has been optimized. The (3-heptafluoroisopropoxy)propyltrichlorosilane (HIPS), $SiCl_3\text{-}(CH_2)_3\text{-}O\text{-}CF(CF_3)_2$, has been chosen for that purpose. This molecule reacts by condensation of its terminal trichlorosilane group ($-SiCl_3$) on the silanol functions still present in the network.

The main techniques used throughout this work in order to characterize each stage of the bi-dimensional films formed on copper and zinc substrates are X-ray Photoelectron Spectroscopy (XPS) and contact angle measurements. An intense fluorine signal confirmed

the grafting of the second layer on the XPS spectra while analyses of the doubly modified surfaces have evidenced hydrophobic properties by contact angle measurements. By way of example, the Figure 2 presents XPS C1s spectra of the MPTS/HIPS bilayer formed on a Cu surface at each stage. The C1s signal visible after the MPTS grafting (Figure 2a) is made of two components standing for the two distinct types of carbon environment of the MPTS molecule: carbon from the alkyl chains (C_1 – 285.0 eV, HS-($\underline{C}H_2)_3$-Si(OMe)$_3$) and carbon from the methoxy groups (C_2 - 287.0 eV, HS-$(CH_2)_3$-Si(O$\underline{Me})_3$). After measurement of the relative areas of those two peaks, it appears than the experimental ratio C_1/C_2 corresponds to the theoretical value of 1.0 suggesting than only few carbon pollutants are physisorbed at the surface of the modified copper sample. Subsequently to hydrolysis, the component attributed to the methoxy functions has almost disappeared of the C1s spectrum leaving only the C1s signal corresponding to aliphatic carbon (Figure 2b). This evidences the successfulness of the acidic treatment to form the expected siloxane network by hydrolysis. Finally, after grafting of HIPS, four components are required to achieve a proper fit of the signal which appears in the C1s binding energy window (Figure 2c): the aliphatic component at 285.0 eV and three additional peaks describing the HIPS molecule itself (287.0 eV, 290.5 eV and 293.3 eV for –C-O-, -CF and –CF_3, respectively. The relative areas of the four components correspond to the structure of the HIPS molecule (two –$\underline{C}F_3$ groups for one –$\underline{C}$F and one –$\underline{C}$-O- function).

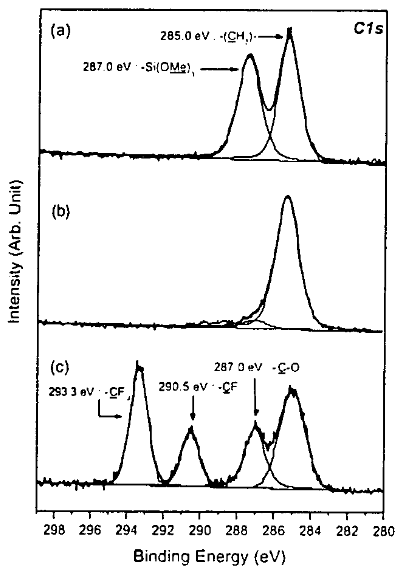

***Figure 2** : XPS C1s spectra for a copper substrate modified by MPTS (a), by MPTS and hydrolysed (b) and covered by a bilayer (MPTS + HIPS)*

The electrochemical cyclic voltammetry technique has been performed in proper conditions to evaluate the blocking of the substrates at each step of their modification while the polarization curves have furnished essential information useful to compare the dissolution rate of copper and zinc along with the chemical modifications. The electrochemical measurements have proven than the second organic layer increase considerably the protective efficiency of the organic coverage. As an example, a blocking factor of 50 % for a modified polycrystalline copper substrate was increased to 85 % with the formation of the bimolecular organic structure.

Acknowledgements

One of the authors (F.S.) is grateful to the "Fonds pour la Recherche dans l'Industrie et l'Agriculture - FRIA" for a doctoral fellowship. We acknowledge support from the "Région Wallonne" for the financial support, "Synatec Project" (RW N° 0014526) and the "Belgian National Interuniversity Research Program on quantum size effects in nanostructure materials" (IUAP P5/01).

COATING OF MOLECULAR FILMS PREPARED FROM ORGANOSILANES ON STAINLESS STEEL SURFACES

F. Sinapi[a,b], A. Naji[a], J. Delhalle[a], Z. Mekhalif[a]

[a] *Facultés Universitaires Notre-Dame de la Paix*
Chemistry Department, LISE
Rue de Bruxelles 61, B-5000 Namur, Belgium
[b] *Fonds pour la Formation à la Recherche dans l'Industrie et dans l'Agriculture*
Rue d'Egmont 5, B-1000 Bruxelles, Belgium

Due to a favorable combination of advantageous properties, like their low cost, high strength, ease of machining and shaping, corrosion resistance, etc., stainless steels are considered to be good candidates for construction and automotive industries supplies, for bipolar plate materials for the polymer electrolyte membrane fuel cells, but also for numerous biomedical applications, etc. This alloy is used in many areas of technology, some of which require the development of coatings and/or primers for efficient use [1,2].

In this context, the chemistry of the self-assembly is a field which present a great technological interest. Through the deposition of molecules with specific symmetry or functionalities, surfaces can be tailored for particular applications.

Organosilane molecules with a general structure of Y-spacer-SiX_3 have taken on special significance in recent years in the field of surface modification. Silane-based self-assembled methods can be applied on such surfaces as silica, glass, and metal oxides, where surface hydroxyls can react with proper chemically active groups, typically methoxy- or chlorosilanes [3]. On one hand, the process responsible for the monolayer formation is relatively simple and leads to strongly linked molecules to the substrates and, on the other hand, the large variety of chemical Y functionalities brings a suitable coupling effect allowing for numerous applications. It is believed that, in many cases, the self-assembled monolayers of trifunctional silanes form closely packed and well-aligned molecular films [4,5].

In practical applications, alkoxysilanes are the most often used among organosilane coupling agents because they are relatively easy to prepare and they can be grafted from aqueous organic solutions [6]. However, to yield dense monolayers, they usually require relatively concentrated solutions (10^{-2} to 1 M) as well as a control of their oligomerisation in solution. Grafting with trichlorosilyl groups is an attractive alternative because a low concentration (10^{-3} M) in apolar hydrocarbon solvent (like toluene) and a short reaction time are sufficient to form tightly packed self-assembled monolayers. Unfortunately, due to the reactivity of halosilane moieties, the number of chemically compatible Y groups is much more restricted than the case of alkoxysilanes which limits the possibilities in further surface modifications.

In this contribution, we will focus our attention on the ability of the silane groups to chemisorb on mechanically polished stainless steel surfaces. Accordingly, the tridecafluoro-1,1,2,2-tetrahydrooctyltrichlorosilane (F_3C-$(CF_2)_5$-$(CH_2)_2$-$SiCl_3$) and the tridecafluoro-1,1,2,2-tetrahydrooctyltriethoxysilane (F_3C-$(CF_2)_5$-$(CH_2)_2$-$Si(EtO)_3$), two organosilanes of similar chain length terminated with essentially non reactive Y functions, have been chosen as

probe molecules. A schematic view representing this type of organic assembly is displayed at Figure 1.

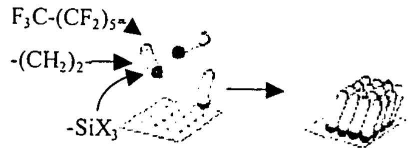

***Figure 1** : schematic view representing the grafting of organosilane molecules on a stainless steel surface*

The differences in reactivity properties of the trichlorosilane ($-SiCl_3$) and the triethoxysilane ($-Si(EtO)_3$) terminal functions on stainless steel surfaces will be especially commented. We will show that silanization by triethoxysilanes in dry conditions cannot produce monolayer films with high density due to steric hindrance. The influence of various parameters involved in the modification procedure of the surfaces will be evidenced upon the organosilane self-assembled monolayers formation. We will particularly insist on the effect of pH of the modification solution and immersion time of the samples upon chemisorption of the two organosilanes.

XPS characterization, optical microscopy imaging as well as contact angle measurements have been performed in order to characterize the stainless steel surfaces modified by the two molecules.

References

[1] M.F. Lopez, A. Gutierrez, F.J. Perez Trujillo, M.P. Hierro and F. Pedraza, J. Electron Spectroscopy and Related Phenomena **114** (2001) 825-829.

[2] M.L. Apicella, G. Cicala, A. Neri and G. Traversari, J. of Nuclear Materials **212** (1994) 1541-1545.

[3] A.V. Krasnoslobodtsev and S.N. Smirnov, Langmuir **18** (2002) 3181-3184 and references cited therein.

[4] D. Cossement, C. Pierard, J. Delhalle, J.-J. Pireaux, L. Hevesi and Z. Mekhalif, Surface and Interface Analysis **31** (2001) 18-22.

[5] D.G. Kurth and T. Bein, Langmuir **11** (1995) 3061-3067 and references cited therein.

[6] R.R. Rye, G.C. Nelson and M.T. Dugger, Langmuir **13** (1997) 2965-2972 and references cited therein.

Acknowledgements

One of the authors (F.S.) is grateful to the "Fonds pour la Recherche dans l'Industrie et l'Agriculture - FRIA" for a doctoral fellowship. We acknowledge support from the "Belgian National Interuniversity Research Program on quantum size effects in nanostructure materials" (IUAP P5/01).

CONSEQUENCES OF CLUSTER BASED MODELS FOR THE ELECTRODES IN SINGLE MOLECULE CONDUCTION CALCULATIONS

Gemma C. Solomon, Jeffrey R. Reimers, Noel S. Hush

School of Chemistry, The University of Sydney

NSW Australia 2006

E-mail: solomon@chem.usyd.edu.au

Despite considerable progress in the methods used to calculate the currents through single molecules there remains a lack of quantitative agreement between calculated and experimental results. In fact, the calculated current is typically several orders of magnitude higher than that obtained experimentally. There are a number of factors in the system that can contribute to this disparity but one of the most significant is the method by which the electrodes are modelled.

For computational ease semi-infinite electrodes are represented by a cluster of atoms, some of which may be treated as part of the molecule. For quantitative agreement it is necessary to expand these clusters so as to improve the approximation to a semi-infinite electrode. Unfortunately, with the expansion of the electrode come resonant states that provide highly conducting pathways with no physical origin. These states can be removed, as they are in real systems, by the breaking of symmetry or phonon interactions.

We show that the fictitiously high currents produced by many calculations are due to unphysical constraints placed on the relative geometries of the electrodes and present some improved computational schemes.

NUMERICAL ANALYSIS OF QWL CHARACTERISTICS

Andreea Rodica Sterian

Academic Center in Optical Engineering and Photonics,
Bucharest Polytechnical University, Bucharest, Romania, sterian@physics.pub.ro

The rate equations model of the QWL with the Channin or Agrawall gain saturation factor as well as the model using a third equation for the carriers in the heterostructure with separate confinement (SCH) are used for numerical analysis of the QWL characteristics.

The simulations are based on adaptive step 5th order Runge-Kutta algorithm and on LU decomposition and forward / backward substitution algorithm to study transient and dynamic behaviour of the device respectively frequency response of the device using Mathcad programming medium.

The model with linear gain saturation was integrated for a constant injection signal, while the model with nonlinear gain saturation was studied for injected signals constant, sinusoidal and a dreptunghiular one, which for some few periods was defined correspondingly.

Another program was elaborated for the third considered QWL model „with carriers transport", for similar (constant, sinusoidal and dreptunghiular) injection signals.

The obtained waveforms of the I_i and the output optical power P are graphically represented for each situation separately (Fig. 1).

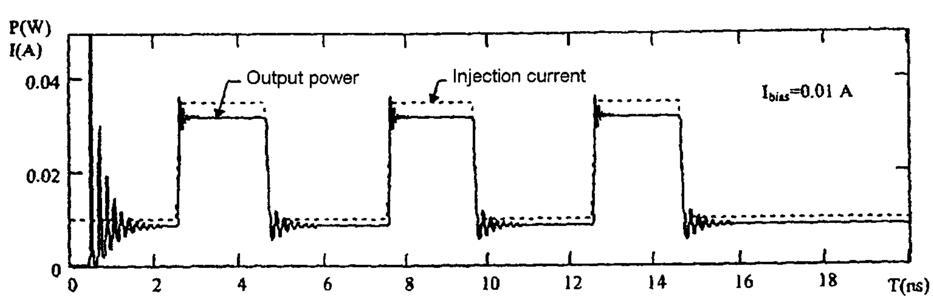

Fig. 1. Output power and injection current versus time when the QW laser is excitet with a train of pulses

The frequency response was studied using the small signal equations, written in the matriceal form, being easy implementable in Mathcad (Fig. 2).

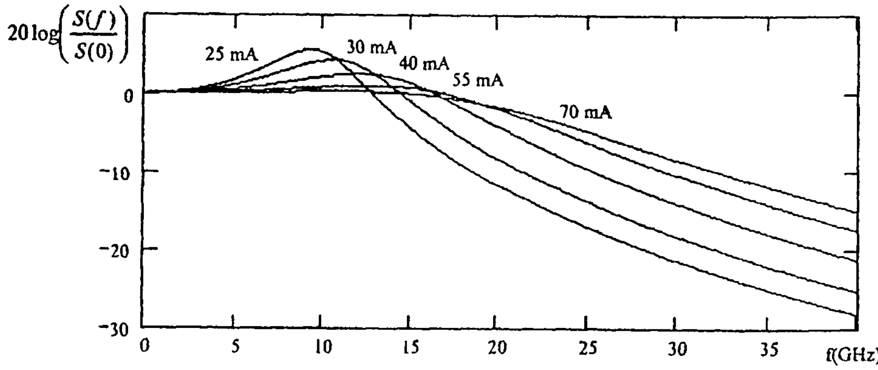

Fig. 2. Frequence respons of the QW laser for different biasing current ($S(f)$ is the foton density)

The bandwidth of the QWL is dependent of the injection current and the gain coefficient, fact illustrated graphically.

The values of the models parameters for numerical simulation are disponible in literature or are imposed by the particular studied device.

At low injection signals the results are in full agreement with theoretical predictions but at high injection level specific limits are observed.

The technological parameters of some practical structures, determinated using the obtained results were verified using the properties of these structures established by equivalent circuit method.

CONDUCTING MOLECULAR NANOSTRUCTURES ASSEMBLED FROM CHARGE-TRANSFER COMPLEXES GRAFTED ONTO SILICON SURFACES

John C. Stires, Dustin S. Siegel, Jinny C. Kwong, Jonathan B. Caballero, Clifford P. Kubiak*

University of California, San Diego, Dept. of Chemistry and Biochemistry, 9500 Gillman Drive, La Jolla, CA 92093, Phone: (858)822-2477, Fax: (858)534-5383

* To whom correspondence should be addressed: Telephone: (858) 822-2665. Fax: (858) 534-5383. E-mail: ckubiak@ucsd.edu

Heterodimeric electon-donor/electron-acceptor charge-transfer complexes chemisorbed onto Au(111) by attachment of the electron-donor to the surface have been shown through scanning tunneling microscopy and Kelvin probe experiments to exhibit nearly Ohmic anisotropic conductivity at low bias through the extended pi-orbital system. The electrical properties of the charge-transfer complex are vastly different than those of the electron-donor alone which exhibits insulating behavior at low bias. In an extension of this work, analogous charge-transfer complexes are attached to semiconducting or insulating surfaces with the intent of designing molecular electronic devices. Fabrication of nanoscale molecular electronic devices is achieved by attaching one component of a charge-transfer complex to a silicon surface by chemically directed self-assembly. The single component-functionalized surface is then used as a substrate on which the second component of the charge-transfer complex is deposited by the atomic force microscopy method, dip-pen nanolithography. Derivatives of hexamethylbenze (electron-donor) with terminal olefins attached to crystalline silicon surfaces via hydrosilylation form monolayer-functionalized silicon surfaces that are expected to have insulating properties. Well-defined features can be "drawn" onto the donor-functionalized surfaces by dip-pen nanolithography using tetracyanoethylene (electron-acceptor) as the "ink." The resulting charge-transfer complex nanostructures have conducting properties suitable for device function and are flanked by an insulating monolayer, thus creating "wires" made from charge-transfer complexes.

Keywords: Molecular electronics, charge-transfer complex, dip-pen nanolithography

Charge-transfer complex on Si surface

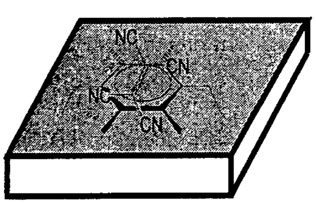

Multi-pen DPN charge-

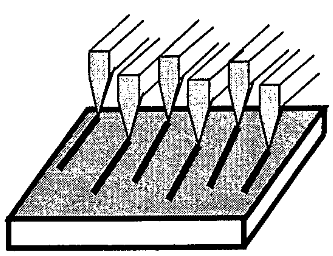

A FETmade of

transfer complexes

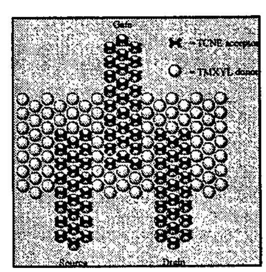

SUB 10-nm ELECTRON BEAM LITHOGRAPHY USING SOL-GEL-BASED OXIDE RESISTS

K.R.V.Subramanian, M.S.M. Saifullah and M.E.Welland

The Nanoscience Centre, IRC in Nanotechnology, University of Cambridge, 11 J. J. Thompson Avenue, Cambridge CB3 OFF, United Kingdom

We present direct writing of sub-10 nm structures by an electron beam using spin-coatable inorganic resists of Al_2O_3, TiO_2 and ZrO_2 prepared by chemically reacting their respective metal alkoxides with β-diketones or β-ketoesters. Aluminium tri-sec butoxide was stabilized with acetylacetone and various β-ketoesters while titanium and zirconium butoxides have been stabilized with benzoylacetone. This resulted in the formation of a chelated complex. This complex was found to be stable in air.

Electron beam exposed spin-coated inorganic resists were found to be amenable for development in common organic solvents such as acetone and gave negative patterns. These resists are more than a million times sensitive to an electron beam than the sputtered films thus bringing their sensitivity very close to conventional organic resists such as calixarene.

FTIR data from regions exposed to varying electron doses show the breakdown of the chelate ring under the electron beam and this make them insoluble in organic solvents such as acetone. This was exploited to produce sub-10 nm lines. This approach offers a new way of patterning inorganic nanostructures without using the lift-off technique and offers greater freedom to write complex structures.

HYBRID ORGANIC/INORGANIC COMPOSITES BASED ON SEMICONDUCTOR NANOCLUSTERS IN POLYMERS

M. Tamborra [a], M. Striccoli [b], R. Comparelli [a], M. L. Curri [b], A. Petrella [a], D. Cozzoli [a], A. Agostiano [a,b]

a Dipartimento di Chimica, Università di Bari, via Orabona 4, I-70126 Bari, Italy

b CNR IPCF Sez. Bari c/o Dip. Chimica, Università di Bari, Via Orabona 4, I-70126 Bari, Italy

E-mail: agostiano@area.ba.cnr.it

II-VI nanocrystals (NCs) are receiving considerable attention for applications in optoelectronics and photonics as optical switches, sensors, electroluminescent devices and lasers [1]. The ability to synthesize nanoparticles of specific dimensions allows obtaining systems with tunable emission, given the strong dependence of the first optical transition on size. For most applications the biggest challenge to successfully using NCs is improving their optical properties. Colloidal methods provide effective routes to prepare semiconductor NCs that are soluble in organic solvents and with a narrow size distribution, while surface chemistry is an efficient tool not only to organize and immobilize the NCs, but also to effectively modify the emission properties. The possibility to perform manipulation of prepared nanocrystals by properly engineering the surface by means of capping exchange procedures enables the nanocrystals to be placed in almost any chemical environment, being soluble in organic solvent.

Much recent effort has been directed toward the fabrication of polymer nanocomposites containing nanometer-sized nanocrystals of inorganic semiconductors. Highly monodisperse quantum dots, coupled with polymers, offer an unprecedented level of control over the molecular architecture of the composite materials. Processed nanocrystals can be converted into functional nanostructured materials by exploiting their incorporation in to polymer matrix and selective positioning onto suitably patterned substrate by using self-assembling techniques.

Hybrid organic-inorganic heterostructures can provide new venues to a more extensive comprehension of NC physical behavior, to modulate and exploit their properties on a mesoscopical scale, and, even more important, to create completely new and original materials having designed characteristics and high degree of flexibility for different applications. These composite can be fabricate in 3D structures with customized properties, depending on the nanocrystals and on the polymeric moieties but also on their peculiar and specific interactions.

Several polymers, with different structural, optical and mechanical properties are potential candidates. In this work both transparent, insulating, such as PMMA, polystyrene and semiconducting polymer, MEH -PPV have been used to test the possibility of create these new composite materials and check their optical properties.

Conjugated polymers are another interesting class of material for combination with NCs, being ideal candidates for realizing large-area devices. They possess favourable optoelectronic properties and easy processability as thin solid films, behaving like a bulk, amorphous, semiconductor in solid state form. In many cases, their energy gap and the ionization potential can readily be tuned by chemical modification of the polymer chains. The wider band gap materials can be effectively used to passivate the non-radiative recombination sites existing on the surface of the nanocrystals due to unsaturated bonds, enhancing the optical performances and improving, the photochemical stability.

In this work, hybrid nanocomposites based on high luminescent CdS NCs [2] and PMMA and polystyrene polymers have been prepared and their optical properties investigated in function of nanocrystals concentration in the matrix. PL measurements indicate a narrowing of NCs spectral features and an enhancing of the emission intensity.

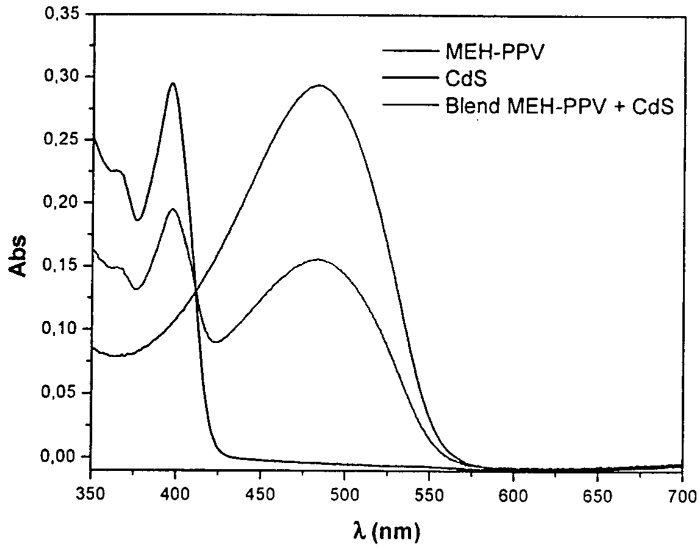

Figure 1: Absorption spectrum of a blend formed by MEHPPV polymer and CdS in $CHCl_3$

Spectroscopic measurements have performed on MEH-PPV/CdS nanocrystal blend, showing that remarkable wavelength shifts are not observed for both of the two components spectral features, thus suggesting a negligible ground-state charge-transfer between the polymer and the nanocrystals. Moreover, there is no evidence for any absorption corresponding to an indirect charge-transfer transition between the two mixture components [3].
New results on electrical measurements for oxide TiO_2 dot and nanorod [4] composites with low molecular weight MEH-PPV polymer report for the effective role of blend in increasing the electrical transport. In fact in this respect, the use of dispersed hetero-junctions can be advantageous due to the availability of numerous interfaces for enhanced charge transfer between the mixture components.

References

[1] Alivisatos A. P., Science, **271** (1996) 933.
[2] Zezza F., Comparelli R., Striccoli M., Curri M.L., Tommasi R., Agostiano A., Della Monica M., Synthetic Metals, (2003) in press.
[3] Greenham N.C., Peng X., Alivisatos A.P., Physical Review B, **54** (1996) 17628.
[4] Cozzoli P. D, Kornowski A., Weller H. submitted for publication

STUDY OF SURFACE CONDUCTIVITY OF (100) DIAMOND: STM AND FFM (FRICTION FORCE MICROSCOPY) MEASUREMENTS

Gheorghe Tanasa

Molecular Materials and Nanosystems (M2N), Department of Applied Physics, Eindhoven University of Technology, Den Dolech 2, 5600 MB Eindhoven, The Netherlands

E-mail: g.tanasa@tue.nl
http://www.phys.tue.nl/FOG
http://www.phys.tue.nl/MMN

Co-authors:

O. Kurnosikov and C.F.J. Flipse, Department of Applied Physics, Eindhoven University of Technology, The Netherlands

W. Deferme and M. Nesladek, Institute for Materials Research (IMO), Diepenbeek, Belgium

The unique properties of diamond make it an exceptional material for a large variety of applications, such as in optical components, electronic devices and wear-resistant coatings.
Recent progress in the field of chemical vapor deposition (CVD) synthesis provides a very important tool for obtaining smooth high-purity homoepitaxial diamond films. During the last years a lot of experimental work has been focusing on the hydrogenated and clean diamond surfaces, since the electrical and frictional properties of diamond are strongly influenced by the presence of hydrogen (Ref.1-4).
Although pure diamond is known to be an insulator, conduction measurements are possible even on " undoped " diamond films. The conductivity mechanism involved remains elusive but is mostly related to impurities, defects, amorphous structures, grain boundaries or adsorbed water and the presence of hydrogen termination seems to be a necessary but not sufficient factor. In this respect nanofriction experiments could also provide a good indication upon the presence of the surface hydrogenation.
In the present work tunneling and friction force measurements have been carried out using a Variable Temperature (VT) UHV-AFM/STM on a homoepitaxially grown (100) diamond surface. The atomically resolved structures corresponding to carbon dimers (Fig.1) and the friction force maps are discussed in relation to the sample preparation and subsequent surface structure and properties.

References:

[1] F. Maier, M. Riedel, B. Mantel, J. Ristein, and L. Ley, Phys.Rev.Lett. **85** (2000) 3472
[2] K. Bobrov, A.J. Mayne, A. Hoffman, G. Dujardin, Surf. Sci **528** (2003) 138-143
[3] R.J.A. van den Oetelaar, C.F.J. Flipse, Surf. Sci. **384** (1997) L828-L835
[4] G.J. Germann, S.R. Cohen, G. Nuebauer, G.M. McClelland, H. Seki, D. Coulman, J.Appl.Phys. **73** (1993) 163

Figures:

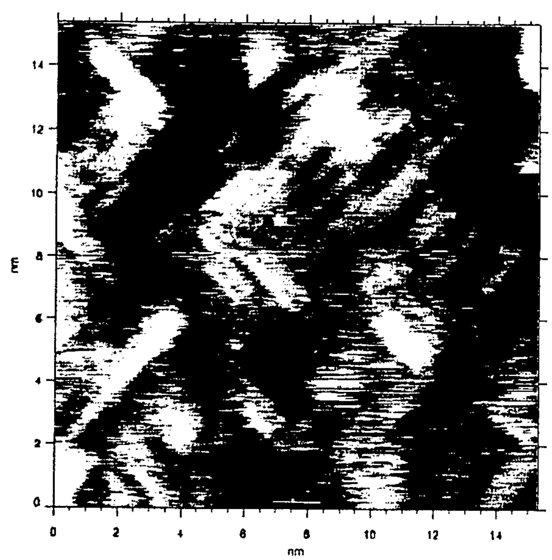

Fig.1 STM topographic image of the hydrogenated (100) diamond surface. Dimer rows are visible (0.5 nm separation).

ATOMIC NANOFABRICATION WITH A LASER COOLED CESIUM BEAM

F. Tantussi*, A. Camposeo, F. Cervelli, F. Fuso, M. Allegrini and E. Arimondo

Istituto Nazionale per la Fisica della Materia, Dipartimento di Fisica Enrico Fermi,
Università di Pisa,
Via F. Buonarroti 2, I-56127, Pisa, Italy
Phone: +39 050 2214 293; FAX +39 050 2214 333
http://www.df.unipi.it/~fuso/nanolito/; http://nanocold.df.unipi.it
* Corresponding Author: tantussi@df.unipi.it

Nanofabrication is one of the building blocks of nanothecnology research and large efforts are devoted to develop new approaches. In fact, optical lithography is reaching its physical limits, mainly due to diffraction phenomena, and novel configurations must be designed to overcome this technological limitation and enable feature size well below 100 nm.

Atom lithography [1] has attracted recently a large interest, as it represents a new fabrication approach with the advantages of standard optical lithography, but not limited by diffraction effects and potentially able to produce structures with typical features in the range of few tens of nm. Atom lithography is conceptually similar to optical lithography, the main difference being the replacement of the light beam with a neutral particle beam. The atomic beam can be space segregated using both physical or light masks, the latter being one of the most interesting features of atom lithography. In fact an atom in a quasi resonant non uniform e.m. field feels a force, known as dipole force, described by the relation:

$$F_{dip} = -\frac{h\gamma^2}{8\delta I_{sat}} \nabla I(x) \tag{1}$$

where I_{sat} is the saturation intensity of the atomic transition, γ the natural linewidth, δ the detuning of the e.m. field with respect to the atomic transition and $I(x)$ its intensity. In the simple case of a one-dimensional standing wave with wavelength $\lambda=2\pi/k$, $I(x) = I_0 \sin^2(kx)$, and atoms will be pushed toward the minima or maxima of the standing wave, depending on the sign of the detuning, generating an array of nanolines spaced $\lambda/2$. The so focussed atom beam can be directly deposited on a proper substrate or used to impress a particle sensitive resist that allows to transfer the generated pattern to the substrate after an etching step. The advantage of using a neutral particle beam and a light mask is that diffraction does not represent a limiting factor as in optical lithography, since the de Broglie wavelength of a particle beam is, generally, well below 1 nm. Furthermore, limitations related to the periodicity of the light mask can be overcome by using holographic masks or a proper movement of the substrate during the deposition. The main limiting factors in the space resolution of thetechnique are related to the divergence of the atomic beam, and to effects of chromatic and spherical aberrations, due to its non perfect monocromaticity.
We are currently developing an atom lithography experiment where a laser-cooled cesium beam, that is a beam with a reduced longitudinal velocity, is used. The main aim of our implementation is to fully understand the limits of the technique, as the exploitation of cold atoms is expected to reduce the contribution of the above mentioned broadening phenomena.

We have built an apparatus where a pyramidal funnel of atoms is used, i.e., a simplified configuration of magneto-optical trap (MOT) able to produce a beam of slow cesium atoms. The atomic beam leaving the funnel is then collimated by using resonant laser light, as in standard laser cooling techniques. The main advantage of our configuration with respect to effusive atom sources is the lower longitudinal velocity of the beam (10 m/s vs hundreds of m/s typical for thermal beams). This leads to a larger interaction time during the collimating

and focusing stages, which is expected to give rise to sharper deposited structures. Laser radiation for the experiment operation is provided by a set of diode lasers, working around 851 nm.

We have characterized the atomic beam leaving the funnel [2] by measuring its density, size, divergence, longitudinal velocity and temperature. Induced fluorescence images, acquired using a CCD camera, and absorption measurements show a beam divergence of 25 mrad, a longitudinal velocity in the range 7-12 m/s (depending on the trapping parameters) and a flux up to 4×10^9 atoms/s. The atomic beam diameter (FWHM) is 1 cm measured 30 cm downward the funnel apex, at the position of the substrate.
The collimation is based on a 2D optical molasses. The collimating laser beam is elliptical in shape (13 mm x 6 mm), with the longer axis along the longitudinal direction, leading to an interaction time ~1 ms. We were able to reach less than 2 mrad (corresponding to the measurement uncertainty) in beam divergence, leading to a beam intensity above 7×10^{10} atoms/cm^2 s over an area of a few mm^2 at the deposition region [3].

Atom focussing is accomplished by a 1D stationary wave, leading to beam segregation into an array of parallel planes, spaced exactly one half the wavelength (~ 426 nm). The segregated atomic beam is used to impress a thiole-based SAM resist, and standard wet-etching procedures are applied to transfer the pattern onto the underlying gold substrate. Sample analyses, carried out by measuring the diffraction of light with different wavelengths by the grating of lines and trenches transferred to gold, demonstrates the attainment of equi-spaced parallel lines. Preliminary AFM observations (Fig. 1) reveal a lateral definition of the lines well below 100 nm, mainly limited by the grain size of the resist and by local defects of the used substrates.

The work is supported by EC through RTD-IST "NANOCOLD" and by CNR through Progetto Applicativo "Nanotecnologie".

References:

[1] D. Meschede and H. Metcalf, J. of Phys D:appl. Phys. 36 R17 (2003).
[2] A. Camposeo, A. Piombini, F. Cervelli, F. Tantussi, F. Fuso, and E. Arimondo, *Optics Comm.* 200 231 (2001).
[3] A. Camposeo, F. Cervelli, A. Piombini, F. Tantussi, F. Fuso, M. Allegrini, and E. Arimondo, *Mat. Sci. Eng. C* 23 217 (2003).

Figures:

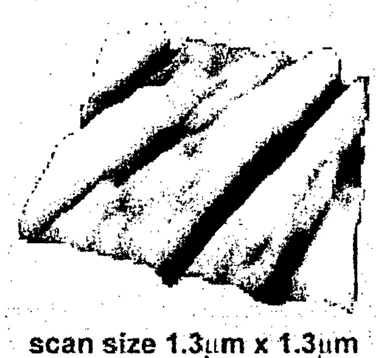

Fig. 1: 3D perspective view of an AFM image acquired on one of our samples fabricated with a one dimensional standing wave.

MAGNETIC PROPERTIES OF FE@CU@FE "ONION-LIKE" NANOPARTICLES PREPARED BY THE MICROEMULSION TECHNIQUE

T. Tarrazo, J. Rivas, and M.A.López-Quintela
Laboratory of Magnetism and Nanotechnology
Instituto Tecnológico de Santiago, Campus Universitario Sur
Universidad de Santiago de Compostela, E-15782 Santiago de Compostela, Spain

The study of the properties of nanomaterials is nowadays a very important topic from both, scientific and technological point of view. In particular, multilayers of ferromagnetic-non magnetic materials are one of the keys for the achievement of new developments in Spin Electronics [1]. Until now a lot of very exciting results have been obtained in 2D multilayers using physical preparation techniques, like sputtering, beam epitaxy, etc [2]. In this work we will show that by means of a chemical preparation technique, namely, the microemulsion method [3], one can obtain multilayer nanoparticles (0-dimensional "onion-like" particles) showing a very reach behaviour, similar to that observed in the bidimensional world.

Fe@Cu@Fe "onion-like" nanoparticles were prepared using AOT-based microemulsions by the successive reaction technique [4]. In brief, the technique consists: 1) preparation of Fe cores of 4nm size. 2) After the formation of these kind of particles, new reactants were introduced into the microemulsions to prepare a Cu shell around the Fe cores. The Cu thickness, which can be varied by changing the reactant concentrations, was in the range 0.5 – 1.0 nm. 3) Finally, a third layer of Fe was deposited onto the previous particles with a thickness of around 0.7 nm.

The magnetic properties of the samples were studied using a Vibrating Sample Magnetometer at room temperature after precipitation and washing. All this procedure was performed under an inert atmosphere in order to avoid the oxidation, as much as possible. The as-obtained particles are passivated by a surfactant layer which can be eliminated by heating the samples at T_e = 300°C, as it can be seen in the thermogavimetric analysis performed (figure 1). It has been observed that all the surfactant can be removed after a 3h annealing treatment.

In order to see the influence of the surfactant protecting layer on the magnetic properties of our assembly of particles, we have prepared different samples treated under reduction conditions (H_2 atmosphere) at various temperatures and annealing times. In order to see the evolution of the magnetic properties with the reduction treatment below T_e, in figure 2 it is shown the magnetic behaviour of particles with a Cu layer of 0.7nm. In figure 2a one can see a magnetization curve of the as-obtained particles corresponding to a superparamagnetic behaviour of the samples. After a heat treatment of 200 °C during 3 h, it is observed (figure 2b) a clear evolution towards a antiferromagnetic behaviour of isolating particles. When the heat treatment is enough to eliminate the surfactant passivating layer, the samples begin to behave as a granular alloy, as it can be observed in figure 3, corresponding to the behaviour observed after an annealing of 3h at 300°C. The magnetic behaviour can be now identified with an aintiferromagnetic interlayer exchange coupling between the unprotected particles. This behaviour is similar to that obtained by Parkin et al [5] for $[Fe\text{-}Cr(1.15nm)]_N$ multilayers with N =2, obtained by magnetron dc sputter deposition in a high vacuum system.

References:

[1] M. Ziese and M. J. Thornton (Eds.), " Spin Electronics", Lectures Notes in Physics, Springer, 2001.
[2] S.A. Wolf and D.M. Treger (Eds.), "Special Issue on: Spintronics Technology", Proceedings of the IEEE, **Vol. 91**, No.5, May 2003.
[3] M.A. López-Quintela, Current Opinion in Colloid and Interface Science, 2003, -en prensa-.
[4] M.A. López-Quintela, J. Rivas, M.C. Blanco, C. Tojo, "Synthesis of nanoparticles in microemulsions", in "Nanoscale Materials", Ed. by L.M. Liz Marzán and P.V. Kamat. Kluwer Academic Plenum Publ., 2003, Chapter 6, pp.135-155.
[5] S.S.P.Parkin, A.Mansour and G.P.Felcher, Appl. Phys. Lett. , 1991, **58**, 1473.

Figures:

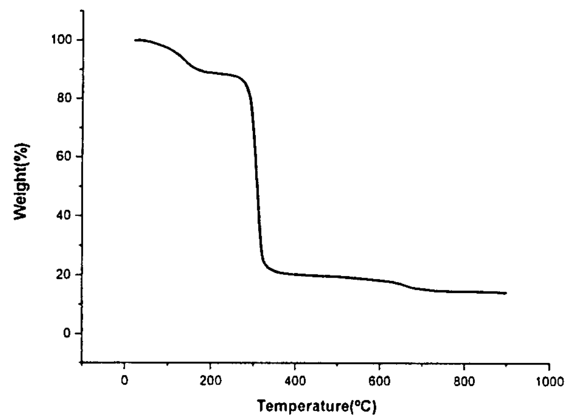

Figure 1. Thermogavimetric analysis of the surfactant-passivated onion-like nanoparticles showing the surfactant decomposition at $T_e = 300°C$.

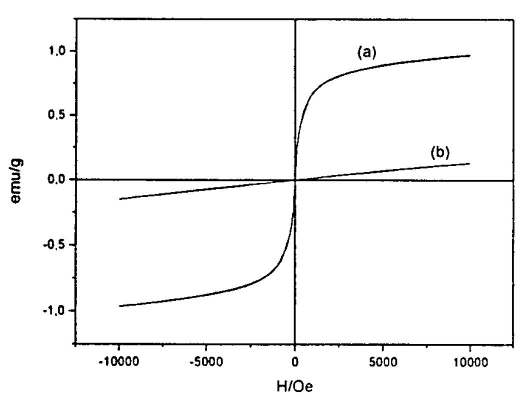

Figure 2. Hysteresis loops of the surfactant protected Fe@Cu@Fe nanoparticles: a) as-obtained; b) after a heat treatment with H_2 at 200°C during 3h.

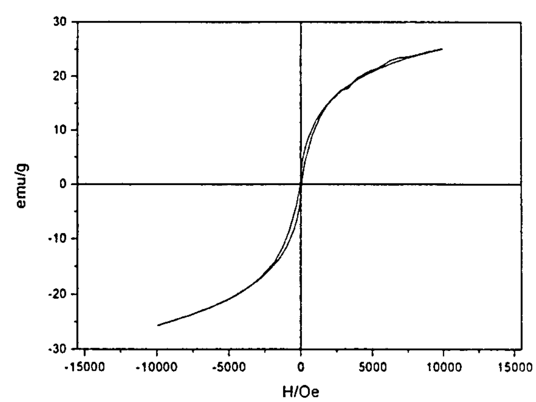

Figure 3. Hysteresis loop of the same sample as figure 2a after a heat treatment with H_2 at 300 °C during 3h. Under these conditions the surfactant is removed.

NOVEL Sb:SnO_2 TIPS FOR REALISING OF STM/SNOM HYBRID MICROSCOPY

Tanel Tätte[1,2], Valter Reedo[1,2], Tea Avarmaa[1], Rynno Lõhmus[1], Uno Mäeorg[2], Mats-Erik Pistol[3], Ants Lõhmus[1]
[1]Institute of Physics, University of Tartu, 142 Riia St., 51014, Tartu, Estonia;
[2]Institute of Organic and Bioorganic Chemistry, University of Tartu, 2 Jakobi St., 51014,Tartu, Estonia;
[3]Division of Solid State Physics, Lund University, Box 118, S221, Lund, Sweden
E-mail: tanelt@ut.ee

Abstract

Conductive and transparent aperture tips are the substantial presumption for creation of STM/SNOM hybrid microscopy. For this purpose only a few techniques have been proposed, which are either expensive or having poor reproducibility [1-3]. We have proposed a simple and cheap sol-gel technique to prepare of fibres with a suitably sharp apex, so that they can be used as SPM tips [4]. In present investigation we have extended the scope of materials in addition to SnO_2 also TiO_2 and SiO_2. The fibres were spun off from a high viscosity solution of polymerised alkoxide and dopants, hydrolysed in humid air and baked at 520 °C for several hours. The radii of the resulting tips were estimated by transmission electron microscopy to be less than 50nm for TiO_2 and SnO_2 tips.

The resistivity of the transparent SnO_2 fibres was measured using different Sb-doping (0.5-1 w%) of the tin oxide. The temperature dependence of the conductivity and the light absorption were investigated down to liquid He temperatures.

Introduction

STM/SNOM is a hybrid device affording to gather the information about the surface morphology and topology working in STM microscopy mode simultaneously using local optical near-field excitation. The creation of such kind instrument is described in some publications [1-3]. In spite of those investigations STM/SNOM hybrid has not found wide use.

The serious drawback restricting the development of STM/SNOM is the complicated production process of suitable sensors. The suitable tip should have the properties enabling focusing the optical near-field radiation to the same point with the location of arising the tunnel current on the surface. In case of STM/SNOM subatomic resolution can be achieved simultaneously with maximum resolution (about 50-100 nm) of near-field optical microscopy and spectroscopy. For this purpose aperture and apertureless tips have been used [1-3]. The drawback of applied technologies is the high cost laborious preparation methods and the low resolution in STM mode at the case of apertureless kind of tips.

Process

The result of our investigation is creation of STM/SNOM hybrid microscopy and the cheap technology for preparing sensors for that. In our resent work we have described first time the sol-gel synthesis of the Sb doped tin oxide tips with properties suitable for application as STM/SNOM sensors [4]. Obtained tips had apex radius about ~50nm. We also demonstrated that material maintain its electrical conductivity and optical transparency down do liquid He-temperature. We have demonstrated that generality of the sol-gel technology enables to obtain TiO_2 and some other oxide based tips.

The sol-gel technique carried out in this work can be divided to four steps: the precursor synthesis, tips spinning, their post-producing treatment and characterisation of tips.

Suitable precursors have been obtained by adding water to alkoxide followed by heating in opened vessel. Those methods are similar to the techniques used for making precursors of oxide fibres [5,6]. It was noticed that high viscosity and high rate of gelation of the precursor material are the most significant factors at producing tips sol-gel method. The MALDI-TOF analysis for oxide precursor materials indicated that the precursors for TiO_2, SnO_2 and SiO_2 tips are polymers with the molecular masses up to some thousands. Long linear chains of polymeric components are the essential for obtaining high viscosity precursor materials.

For the spinning of fibres by classical glass rod method was used in which a jet was spun off from the viscous sol precursor into the humid air for gelation process. Tips were obtained if the sol jet was broken off in the air. The two step post-producing treatment of tips was carried out with the aim to obtain tips with higher hardness, optical transparency and electroconductivity. The hydrolysis of tips in humid air was followed by the heat treatment up to 520 ^{0}C in air.

Conclusions

By this work we have demonstrated that the tips obtained by sol-gel method are able to work in SPM mode with resolution of few nanometres. The advantage of tips obtained by sol-gel method is their high mechanical and chemical stability, appropriate geometry and low cost.

Acknowledgements

This work has been supported by Estonian Science Foundation (grant No 5015) and Estonian Technological Agency (grant No. 21/it).

References

[1] D.W. Pohl, W.Denk and M.Lanz, Appl. Phys. Lett. 44 (1984) 651
[2] K.Nakajima, V.Jakobsen, J.Noh, T.Isoshima, M.Hara, RIKEN Review 38 (2001), 52-56
[3] M.Ohtsu (Ed.), Near-field Nano/Atom Optics and Technology. Springer, Tokyo, 1998
[4] T.Tätte, T.Avarmaa, R.Lõhmus, U.Mäeorg, M.-E.Pistol, R.Raid, I.Sildos, A.Lõhmus, Mat. Sci.& Eng. C 19 (2002) 101-104
[5] S.Sakka, T.Yoko, J. Non-cryst. Solids 147&148 (1992) 394-403
[6] L.Klein (Ed.), Sol-Gel Optics Processing and Application, Kluwer, 1994, p.109-139

MAGNETOCHEMISTRY AND SPECTROSCOPIC STUDIES INVOLVING SINGLE WALLED NANOTUBES

Laura Taylor, Jerry Purcell, Jennifer Jones, Jessana Smith, Katie Olsen, Kim Harris, Thomas Manning

Department of Chemistry, Valdosta State University, Valdosta, Georgia 31698, USA

We have completed a preliminary series of experiments that compare the silicate shells of marine organism diatoms to Single-Wall NanoTubes (SWNT), Multi-Wall Nano Tubes (MWNT), Exfoliated Graphite (EG), and silica beads as templates for producing nanostructures of the manganese acetate cluster (Mn12). Mn12 ($Mn_{12}[CH_3COO)_{16}(H_2O)_4O_{12}]\bullet 2CH_3COOH\bullet 4H_2O$) exhibits magnetic properties because of the molecular arrangement within the cluster and exhibits no exchange couplings between the individual clusters. Data from a Scanning Electron Microscope (SEM), High Resolution Transmission Electron Microscopy (HRTEM), Laser Diffraction, and Superconducting Quantum Interference Device (SQUID) are discussed in terms of research that can be directed towards the use of diatoms as well as other materials for templates for nanostructures. Mn12 grown in EG and SWNT exhibits shifts in its blocking temperature and a quenching of Quantum Tunneling of Magnetization (QTM) observed in the hystersis loop. We attribute these shifts to a shift of the Mn-O vibrational energy levels caused by forces exerted when the graphic sheets encapsulate the cluster.

Photothermal emission (PTE) from black substances is a well-known interference in FT-Raman spectroscopy when incorporating a relatively high power near infrared laser as the radiation source. PTE appears as a large, broad spectral feature in the 2800-3300 cm^{-1} region. We demonstrate that when KBr(s) is used as a matrix for measuring the FT-Raman spectra of Single Wall Nanotubes (SWNT) the PTE is quenched. We attribute this reduction to thermal transfer of energy from the SWNT to the KBr matrix. Expanding the research to related alkali-halide salts, we found a reduction of PTE in KCl and NaBr but minimal reduction of PTE in the NaCl matrix. We measured PTE in a KBr matrix containing Multiwall Nanotubes (MWNT), Graphite Dust, and Buckmisterfullerene (C_{60}) and found that PTE either remained constant or increased.

MODELLING THE ADSORPTION OF ALKANES ON Au(111) SURFACE

Gilberto Teobaldi

Dipartimento di Chimica "G. Ciamician", Università di Bologna, V. F. Selmi 2, 40126, Bologna, Italy

E-mail: nemo@ciam.unibo.it

Adsorption of alkanes on a Gold substrate is simulated by a simple computational scheme that combines the "glue model" for Gold [1], a standard force field for alkanes [2] and a combination of the charge equilibration model [3] and the Born-Mayer potential for their interaction. The adsorption energies of 10 short chains on the Au(111) surface are reproduced with an average error of less than 1 kcal mol^{-1}. The results allow extension of the use of the model to investigate the appeareance/disappeareance of ordered deposition on gold of longer alkanes [4]. The unexpected transition to disorder occurs for chains between 18 and 26 carbon atoms and has been ascribed to the mismatch between the Au(111) lattice and the CH_2-group periodicity, a feature that is here is shown to hinder the formation of short, *i.e.* docking, C-Au distances.

References:

[1] Ercolessi, F.; Parrinello, M.; Tosatti, E. *Philos. Mag. A*, **1988**, *58*, 213

[2] Allinger, N. L.; Yuh, Y. H.; Lii, J.-H. *J. Am. Chem. Soc.* **1989**, *111*, 8551-8566

[3] Rappe, A.K.; Goddard III, W.A. *J. Phys. Chem.*, **1991**, *95*, 3358

[4] Marchenko, O.; Cousty, J. *Phys. Rev. Letters,* **2000**, *84*, 5363-5366

Electromechanical model of an AFM-characterized resonating nano-scale cantilever

Jordi Teva[1], Gabriel Abadal[1], Zachary Davis[2], Jaume Verd[1], Xavier Borrisé[3], Anja Boisen[2], Francesc Pérez-Murano[3], Núria Barniol[1]

[1] Dept. Enginyeria Electrònica. Universitat Autònoma Barcelona. E- 08193 Bellaterra. Spain
[2] Mikroelektronik Centret. Denmark Technical University. Lyngby. DK-2800 Denmark
[3] Institut de Microelectrònica Barcelona (IMB-CNM) Campus UAB. 08193 Bellaterra Spain
E-mail: Jorge.teva@uab.es

A resonating nano-cantilever excited electrostatically through a parallel driver electrode, is the basis of a mass sensor developed for having high mass and spatial resolution [1]. A cantilever mass increment, due to molecule absorption, implies a shift on the resonant frequency. In order to detect and amplify the capacitive current which is used as a readout signal, a CMOS circuitry is monolithically integrated along with the cantilever based transducer.

The cantilever driver transducer is modelled by a precise electromechanical model in order to have a good prediction of the current signal levels [2], as well as the need for the optimisation of excitation voltages and of the transducer geometrical dimensions.

Previous models have been developed in order to predict the cantilever driver static and dynamic behaviours [3]. However, the new model here presented takes into account the bended static deflection shape of the cantilever and the fringing field effect on the electrical cantilever-driver interaction due to the cantilever finite dimensions. In this model, the static deflection shape obtained from solving the Euler-Bernouilli equation by a 2D finite element simulator [4] is taken as the initial operating point for the dynamic simulations.

The static deflection versus driver-cantilever voltage characteristic, as well as the dynamic oscillation amplitude versus frequency of the excitation voltage, have been optically measured in order to validate the model (figs 2 & 3). The Young modulus of the cantilever has been determined by applying a known force at its end and measuring its deflection using an atomic force microscope[5]. Mass density and quality factor are derived by fitting the model predicted static and dynamic curves to the experimental points.

References:

[1] http://www.uab.es/nanomass/

[2] Z.J.Davis, G.Abadal, B.Helbo, O.Hansen, F.Campabadal, F.Pérez-Murano, J.Esteve, E.Figueras, R.Ruiz, N.Barniol, A.Boisen. High mass and spatial resolution mass sensor based on Nano-cantilevers Integrated with CMOS. Transducers'01 Conference Technical Digest, pp 72-75 (2001)

[3] G. Abadal, Z.J. Davis, B. Helbo, X. Borrisé, R. Ruiz, A. Boisen, F. Campabadal, J. Esteve, E. Figueras, F. Pérez-Murano, N. Barniol. *Electromechanical model of a resonating nano-cantilever-based sensor for high-resolution and high-sensitivity mass detedction.* Nanotechnology. 12, 100-104 (2001).

[4] http://bsac.berkeley.edu/cadtools/sugar/sugar/

[5] Sriram Sundararajan, Bharat Bhushan, Takahiro Namazu, Yoshitada Isono, *Mechanical property measurements of nanoscale structures using an atomic force microscope.* Ultramicroscopy 91, 111-118, (2002).

Acknowledgments:

This work is partially funded by the projects NANOBIOTEC (CICYT-DPI2000-0703-C03) and NANOMASS II (EU-IST-2001-33068).

Figures:

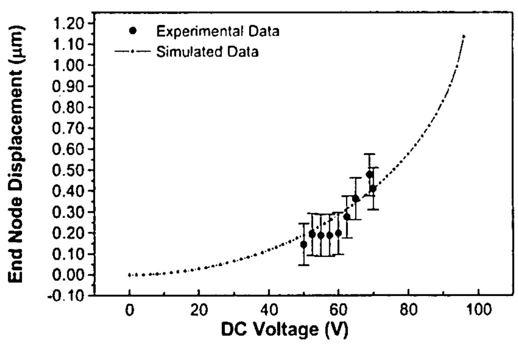

Figure 1: Static behaviour: experimental and simulated end cantilever displacement versus static voltage applied.

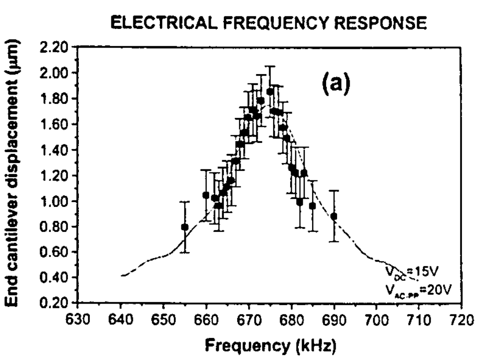

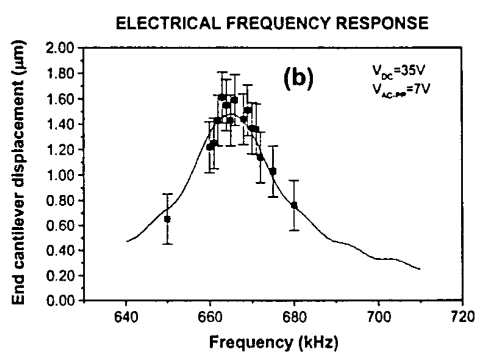

Figure 2: Dynamic behaviour: experimental and simulated dynamic oscillation amplitude versus excitation signal frequency for: a) V_{DC}=15; $V_{AC\text{-}PP}$=20V; b) V_{DC}=35; $V_{AC\text{-}PP}$=7V;

RESONANT RADIATIVE AND NON-RADIATIVE COUPLING BETWEEN A MOLECULE AND A METALLIC TIP

M. Thomas, R. Carminati and J.-J. Greffet
Laboratoire d'Energétique, Moléculaire et Macroscopique, Combustion.
Centre National de la Recherche Scientifique, Ecole Centrale Paris, 92295 Châtenay-Malabry Cedex, France
Tel : + 33 1 41 13 10 66, Fax : + 33 1 47 02 80 35, E-mail : remi@em2c.ecp.fr

J.R. Arias-Gonzalez and M. Nieto-Vesperinas
Instituto de Ciencia de Materiales de Madrid
Consejo Superior de Investigaciones Cientificas, Cantoblanco, 28049 Madrid, Spain

Abstract: We study numerically the radiative and non-radiative decay rates of a molecule close to the apex of a metallic tip. We show that both rates present a resonance at different frequencies which, in general, do not coincide. This behavior is explained by a general model describing the resonant behavior of the electromagnetic response of the tip. We also investigate the influence of a small defect located close to the tip apex. We show that it may substantially modify the ratio between the radiative and non-radiative contributions, and induces a frequency shift of the resonances. This may explain why experiments on single-molecule fluorescence dramatically depend on the tip quality.

OCIS codes: (290.5840) Scattering, molecules; (260.2510) Fluorescence; (260.5740) Resonance

Sharp metallic tips producing highly localized and bright sources can be used to enhance the fluorescence of single molecules [1]. A recent numerical study of the field scattered at the apex of gold tips of various shapes has shown that local-field enhancement factors of several thousands can be expected [2]. While the tip induces a strong enhancement of the local field, it also creates new channels for the desexcitation of the molecule. The competition between radiative and non-radiative decay is a key point for the optimization of the techniques and a fundamental issue in nano-optics [3]. It has been studied numerically in various geometry [4,5] or using a simplified tip model and an electrostatic approximation [6]. The results demonstrated the importance of non-radiative coupling at short distance and the influence of the transition-dipole orientation with respect to the structure. Strong tip-molecule coupling can be obtained when the emission frequency corresponds to a resonance of the tip. Such a situation is expected to induce both a local-field enhancement and a higher decay rate of the molecule, but does not ensure an enhanced *radiative* emission rate. From a practical point of view, a key issue is to find a situation in which, at the emission frequency of the molecule, a resonance enhances the radiative decay only.

The purpose of this work is to present a quantitative study of this problem, using a numerical simulation able to account for optical resonances in small particles or tips with great accuracy [7]. We directly compute the radiative and non-radiative decay rates, as well as the local field enhancement factor for different distances to the tip and different orientations of the transition dipole (see Fig.1). We focus on the importance of the position of the excitation and emission frequencies with respect to the resonant frequencies of the tip. In particular, we study the influence of a small defect located close to the tip apex Two main results are put forward: (1) For a given tip, the resonant frequencies of the radiative and non-radiative decay rates do not coincide. It is shown that, in order to enhance the local field (excitation) and the radiative decay rate (emission), one should *not* use a tip whose resonance coincide with the transition frequency. (2) The presence of a defect may substantially modify the ratio between the radiative and non-radiative contributions, and induces a frequency shift of the resonances. This may explain why experiments on single-molecule fluorescence dramatically depend on the tip quality. In view of these results, we think that this study should have broad experimental applications.

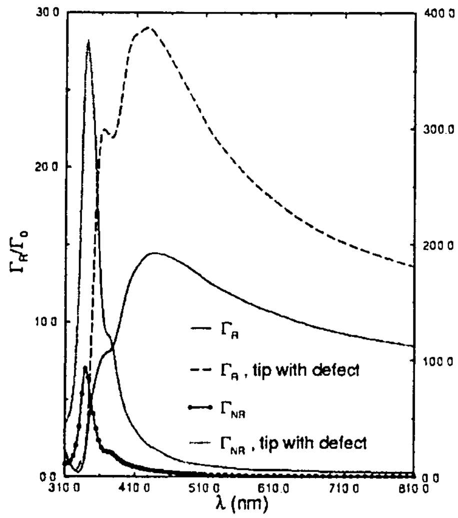

Fig. 1. Radiative (Γ_R) and non-radiative (Γ_{NR}) emission rates close to a silver tip, with or without defect.

[1] E.J. Sanchez, L. Novotny and X.S. Xie, Phys. Rev. Lett. 82, 4014 (1999).
[2] J.T. Krug, E.J. Sanchez and X.S. Xie, "Design of near-field optical probes with optimal field enhancement by FDTD electromagnetic simulation", J. Chem. Phys. 116, 10895-10901 (2002).
[3] V.V. Klimov, M. Ducloy and V.S. Letokhov, "Spontaneous emission of an atom in the presence of nanobodies", Quant. Electronics **31**, 569-586 (2001).
[4] R.X. Bian, R.C. Dunn, X.S. Xie and P.T. Leung, "Single molecule emission characteristics in near-field microscopy", Phys. Rev. Let. **75**, 4772-4775 (1995).
[5] L. Novotny, "Single molecule fluorescence in inhomogeneous environments", Appl. Phys. Let. **69**, 3806-3808 (1996).
[6] J. Azoulay, A. Debarre, A. Richard and P. Tchenio, "Quenching and enhancement of single-molecule fluorescence under metallic and dielectric tips", Europhys. Lett. **51**, 374-380 (2000).
[7] J.R. Arias-Gonzales and M. Nieto-Vesperinas, "Near-field distributions of resonant modes in small dielectric objects on flat surfaces", Opt. Lett. 25, 782-784 (2000).

THREE ELECTRODE TITRATION FOR DIRECT pK_a MEASUREMENT OF TiO_2 NANOPARTICLES

S. Tirosh, O. Melamed, A. Zaban
Department of Chemistry, Bar-Ilan University Ramat-Gan, 52900, Israel

The high surface to volume ratio inherent in nanosize materials necessitates the exploration of their surface properties. These properties are important for both basic research and applications such as photocatalysis[1], dye sensitized solar cells[2], batteries[3] and full cells[4]. The acidity of the surface is one of the surface parameters that are important by themselves but at the same time they provide insight into other surface properties of the investigated material.

Thus the ability to measure the surface acidity of nanoparticles at high resolution will significantly enhance the characterization quality of these materials. Previous studies of the surface properties of metal oxides reported the pKa of several metal oxides in aqueous solutions[5]. However, in these studies the pKa value is determined indirectly using extensive modeling resulting in both low resolution and model dependent accuracy.

In a preliminary system where we used simple potentiometric titration we showed that we can measure directly the pKa of nanosize TiO_2 (p25). However the amount of powder needed is very large ca. 10g per titration. This amount needed to overcome ions surface complexations that are part of the titration procedure (titration executed in HNO_3 and the titrant is NaOH), and side titrations of impurities that may "screen" inflection points (for example titration of H_2CO_3 and Na_2CO_3).

Thus, it is important to develop a titration method for nanosize metal oxides that allowed the monitoring of its inflection points with relatively low amount of powder(the lowest is the better). This work expose our recent develop of such method - The "three electrode titration". It contains internal reference electrodes that cancel out all side titrations and stream effects. The titrations here were executed with different TiO_2 powders (commercial and home synthesized). Modifications of this titration system are examine here in order to reduce noises.

1. F. Cavani, E. F., F. Parrinello, F. Trifiro *App. Catalys.* **1988**, *38*, 311-325.

2. Ferrere, S.; Zaban, A.; Gregg, B. A. *J. Phys. Chem. B* **1997**, *101.*

3. F. Zhang, S. P., B. B. Owens *Electrochem. Solid St.* **2001**, *4*, 131-136.

4. J. R. Smith, F. C. W., R. L. Clarke *J Applied Electrochem.* **1998**, *28*, 1021-1033.

5. Koopal, L. K. In *Studies in Surface Science and Catalysis*; A. Dabrowski, V. A. T., Ed.; Elsevier Science B. V.: Amsterdam, Lausanne, New York, Oxford, Shannon, Tokyo, 1996; Vol. 99.

DEPOSITION, PURIFICATION TREATMENT AND X-RAY TESTS OF CARBON SWNT FOR CHANNELING APPLICATIONS

F.Tombolini, S. Bellucci, V. Biryukov, S. Bini, G. Giannini

LNF-INFN Laboratori Nazionali di Frascati ,Via Enrico Fermi 40, 00044 Frascati (Roma),Italy
E-mail: francesca.tombolini@lnf.infn.it

In recent years, with creation of nanotubes, there has been a substantial interest in channeling in nanostructures**[1-3]**. Since 1991 **[4]**, there has been a lot of study on carbon nanotubes to understand their formation and properties. Carbon nanotubes stick out in the field of nanostructures, owing to their exceptional mechanical, capillarity, electronic transport and superconducting properties **[5-7]**. They are cylindrical molecules with a diameter of order 1 nm and a length of many microns **[8]**. They are made of carbon atoms and can be thought of as a graphene sheet rolled around a cylinder **[9]**. Nanotubes can be made of different diameter, length, and even material other than carbon [20]. Creation of suitable channeling structures, from single crystals to nanotubes, of sufficient quality would make a strong impact onto accelerator world. A particle beam channeled in nanotube could be efficiently steered (deflected, focused,undulated, extracted from accelerator, etc.) in the way quite similar to crystal channeling.

Compared to bent crystal technique, however, nanotubes offer unique characteristics like bigger angular acceptance and potentially bigger dechanneling lengths **[1-3]**. It was shown **[3]** that a bent carbon nanotube of 1.4 nm diameter has a significant effective potential well *Ueff* even for bendings equivalent to @ 300 Tesla or pv/R^3 1 GeV/cm (the beam momentum ratio to curvature radius), so there exists an opportunity to steer particle beams by nanotubes, similarly to bent crystal channeling technique.

As shown in computer simulations **(10)**, nanotubes can efficiently channel particle beams thus making a basis for a new technique of beam steering at accelerators. The most critical factor in implementation of this technique is the alignment of nanotubes within the sample .To this purpose in our laboratory we produce well-aligned bundles of nanotubes. With the arc discharge method we make linear e non distorted single-wall carbon nanotubes as shown in a preliminary STM image(fig.1). The detailed procedure of arc discharge method is presented in the poster of Bini et al. We also produce, in the inner cylindrical cathode deposite, bundle of multi-wall carbon nanotubes that could be used for channeling. By field emission measurements we estimate a density of carbon nanotubes of about 0.025 tubes for square micrometer. But carbon nanotubes raw material contain numerous by-products, like amorphous carbon, fullerene and carbon polyhedra.so they must have purified without damaging their cilindrical structure.

To this purpose we have sonicated our samples in IPA for about 30 minutes and then we have put them in a furnace at temperature of about 700 celsius degree to oxidate all amorphous carbon. In this way we purify our sample to obtain a better density of nanotubes.

To test the structure of carbon nanotubes we use X-ray test to determine deformations to the honey comb cylindrical structure.

Finally next step in this direction will be to use CVD method to satisfy the request of channeling: the best alignment of carbon nanotubes within the sample.

1. V.V. Klimov and V.S. Letokhov, *Phys. Lett. A* **222**, 424 (1996)
2. L.G. Gevorgian, K.A. Ispirian, K.A. Ispirian. *JETP Lett.* **66**, 322 (1997)
3. N.K. Zhevago and V.I. Glebov, *Phys. Lett. A* **250**, 360 (1998)
4. S. Iijima, *Nature* **354**, 56 (1991) Appl. Phys. Lett. 80, 2973 (2002)
5. M. Bockrath, et al., *Nature* **397**, 598 (1999); Z. Yao, et al., *Nature* **402**, 273 (1999)
6. S. Bellucci and J. Gonzalez, *Eur. Phys. J. B* **18**, 3 (2000); ibid. *Phys. Rev. B* **64**, 201106 (2001) (Rapid Comm.)
7. A. Yu. Kasumov, et al., *Science* **284**.1508 (1999); M. Kociak, et al., *Phys. Rev. Lett.* **86**, 2416 (2001)
8. R. Saito. G. Dresselhaus, M. S. Dresselhaus, *"Physical Properties of Carbon Nanotubes"* (Imperial College Press,
London, 1998)
9. T.W. Ebbesen, *Phys. Today*, **49**, 26 (1996)
10 S. Bellucci, V. M. Biryukov, Yu. A. Chesnokov, V. Guidi, W. Scandale *"Channeling of high energy beams in nanotubes" Presented at* ***COSIRES*** *2002 (Dresden, 24-27 June 2002)*

20-2 NANOMETER LITHOGRAPHY WITH ELECTRON BEAMS

M.J. van Bruggen, N. Silvis Cividjian, C.W. Hagen*, and P. Kruit

Delft University of Technology, Faculty of Applied Sciences, Lorentzweg 1, 2628CJ Delft, The Netherlands
* Corresponding author, E-mail: hagen@cpo.tn.tudelft.nl

With Electron Beam Induced Deposition (EBID) in Scanning Electron Microscopes (SEM) it is possible to create patterns without using resist. The EBID mechanism is based on the dissociation of complex, so-called precursor molecules adsorbed onto a substrate surface. It is a direct deposition method and a large variety of materials can be deposited on any surface. However, these structures rarely have sizes below 20 nm, although the probe sizes of the instruments are substantially smaller. We have recently modelled this process in a Monte Carlo method [1] and were the first to explain in detail why the minimum structure size was 20 nm. Through that insight we could also propose a method to fabricate structures as small as 2 nm and were able to write some simple carbon structures almost that small [2](see figs.1-3).

Fig.1. A 3D intensity plot of a TEM image of a Carbon line deposited directly on a carbon film using EBID in a state of the art STEM. The FWHM of the line is 6.5 nm

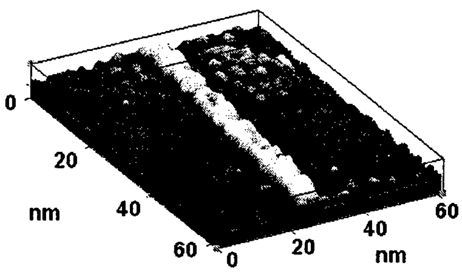

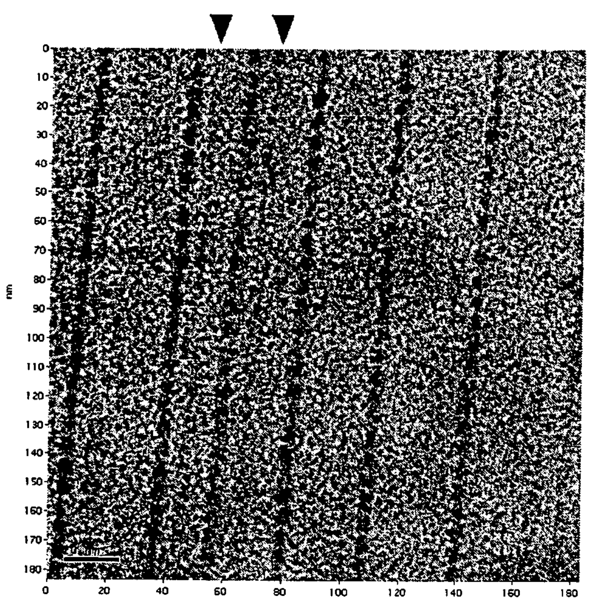

Fig. 2. TEM image of five arrays of C dots deposited on a C film. The arrows point to the smallest arrays of dots, with an estimated average dot diameter below 2 nm.

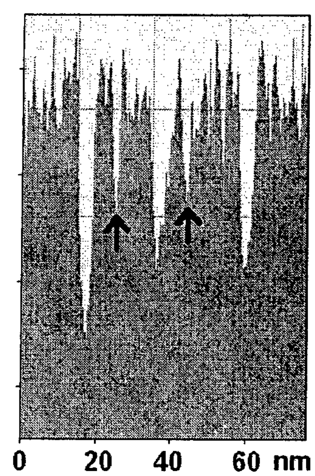

Fig. 3. Integrated cross-sectional plot across the parallel dot arrays of fig. 2. The arrows point to the arrays with sub-2 nm dots.

These structures were written in a state-of-the-art Scanning Transmission Electron Microscope (STEM) using a 1 nm probe and 200 keV electrons. The substrate used

was an uncleaned 10 nm thin carbon foil that provided by itself sufficient hydrocarbons as a precursor. The secondary electrons generated in the substrate, as well as in the deposit, cause the dissociation of the precursor into a carbon deposit and some volatile components. The exposure dose, defined as the charge needed to fill a unit area with 6.5 nm wide lines (as in fig. 1) is 6010 C/m^2. This is only three times larger than the statistical shot-noise limited dose needed to write 1 nm wide lines in resist-based electron beam lithography (10^4 electrons in a 1-nm pixel). Therefore, the EBID-STEM method has potential to become a viable lithography technique for the fabrication of 20-2 nm structures. The roadmap as presented by the international semiconductor community (ITRS International Technology Roadmap for Semiconductors) forms the basis for future developments in the semiconductor industry. The present "node" is 90 nm, with isolated structures already at 65 nm. There is a view as to how one can go down to 22 nm isolated structures, expected to be in production in 2013. However, it might stop there: there hardly are any ideas about how to continue. The EBID-STEM method may become very useful in this area. Apart from the necessity to create a new technology for future generations of micro electronics, the availability of such technology will immediately be applicable in the rapidly growing field of nanoscience and technology. This includes such diverse disciplines as nanophysics, micro-, nano-, and molecular electronics, spintronics, data storage, molecular biology and –biophysics, nanochemistry and nanofluidics.

We presently develop the instrumentation for the EBID-STEM technique, which is based on a dedicated STEM and includes extensive gas handling facilities, variable temperature substrate holder, pattern generator, etc. To develop the technique further into a fast-lithography technique we develop a multibeam source, such that many parallel beams write nanostructures simultaneously. The necessity for multiple beams becomes clear when the throughput is calculated for typical currents in sub-nm probes in combination with electron doses as mentioned above. We propose a set up in which the flood illumination of a Schottky thermal field emitter is divided into multiple beams by an aperture array. These beams are then focused by a lens array to obtain plural images of the original source, which are projected onto the wafer by the optics of the STEM in which the multibeam source will be mounted. Using a Schottky source implies a high brightness, needed for EBID, combined with both uniformity and current stability. The resulting sub-nm beams are scanned over the wafer simultaneously, while the desired pattern can be written by switching them on and off individually by means of beam blankers, which are incorporated in the multibeam source module. The whole unit could be fabricated using micro-electro-mechanical systems (MEMS) manufacturing technology.

Acknowledgement: the support of H.B. Groen, FEI Company, The Netherlands, is gratefully acknowledged.

References

[1] N. Silvis-Cividjian, C.W. Hagen, L.H.A. Leunissen, P. Kruit, Microelectron. Eng. **61-62**, 693 (2002)

[2] N. Silvis-Cividjian, C.W. Hagen, P. Kruit, M.A.J. v.d. Stam, H.B. Groen, Applied Physics Letters **82**, 3514 (2003).

MONTE CARLO ANALYSIS OF FOUR-TERMINAL BALLISTIC RECTIFIERS

B. G. Vasallo, T. González, D. Pardo and J. Mateos
Departamento de Física Aplicada, Universidad de Salamanca
Plaza de la Merced s/n, 37008, Salamanca, Spain
E-mail: a50343@usal.es

The use of devices exploiting ballistic transport of electrons is one of the possible approaches for overcoming the limits of traditional scaling when reaching the nanometer range. Indeed, recent works have achieved an important improvement of this type of devices using InGaAs channels with high In content [1,2], for which room temperature operation is possible, since the mean-free-path of electrons in this material is still larger than 100 nm at 300 K. In particular, novel semiconductor rectifiers based on ballistic electron transport have been fabricated by inserting a triangular scatterer (antidot) into the center of a ballistic cross junction [3].

The design cycle of ballistic structures can be significantly accelerated by using simulation tools for the determination of the optimal geometry of the devices, thus becoming a valuable alternative to the expensive and time-consuming test-and-error procedure. In this work we present a microscopic analysis, performed by means of Monte Carlo (MC) simulations, of the transport properties of ballistic rectifiers with geometries similar to that studied in [3], based on AlInAs/InGaAs channels. For the correct modeling of these devices, a 3D simulation would be necessary to take into account the effect of the lateral surface charges and the real geometry of the structures. However, a 2D MC model can be enough to describe these devices if some simplifications and assumptions are made. For instance, the real layer structure is not considered; instead, a background doping is assumed [4]. To ensure the accuracy of this approximation the values of two important parameters must be carefully chosen: the background doping in the channel and the lateral surface charge density. MC simulations, based on a semiclassical transport description, provide an insight of the processes taking place inside the devices, thus allowing us to relate the macroscopic results of the experiments with the microscopic behavior of electrons. Our model is able to qualitatively reproduce the main features of the ballistic effects measured in real rectifiers [3], thus indicating that coherent transport plays no significant role on the main characteristics of these devices. Moreover, due to the versatility of the MC method, our approach allows us to analyze and optimize different possible geometries for the ballistic rectifier (dimensions, shape of the scatterer, opening angle of the lateral branches, etc.) and to study its behavior at different temperatures.

As an example of the results we obtain, Fig. 1 shows the values of the potential between the bottom and top branches (V_{BT}) at several temperatures when biasing left and right branches in push-pull fashion, $V=V_L=-V_R$, obtained from the MC simulation of the device sketched in the inset. When biasing right and left branches in this fashion, a negative potential appears in both central branches (bottom and top), but with different values due to the unequal width of the opening space between the horizontal and the top/bottom branches, leading to an asymmetric injection of carriers into them. The behavior of V_{BT} for low V remains parabolic up to a given biasing, for which the unbalanced injection of charge into the top and bottom branches reaches a saturation regime. This behavior is due to the ballistic transport of electrons, and thus disappears when increasing the temperature and transport becomes diffusive. More detailed results of this study will be presented at the conference.

References:

[1] K. Hieke and M. Ulfward, *Phys. Rev. B*, **62** (2000) 16727.
[2] I. Shorubalko, H. Q. Xu, I. Maximov, P. Omling, L. Samuelson and W. Seifert, Appl. *Phys. Lett.*, **79** (2001) 1384.
[3] A. M. Song, P. Omling, L. Samuelson, W. Seifert, I. Shorubalko and H. Zirath, *Jpn. J. Appl. Phys.*, **40** (2001) L909.
[4] J. Mateos, B. G. Vasallo, D. Pardo, T. González, J. S. Galloo, S. Bollaert, and A. Cappy, *Nanotechnology*, **14** (2003) 117.

Figures:

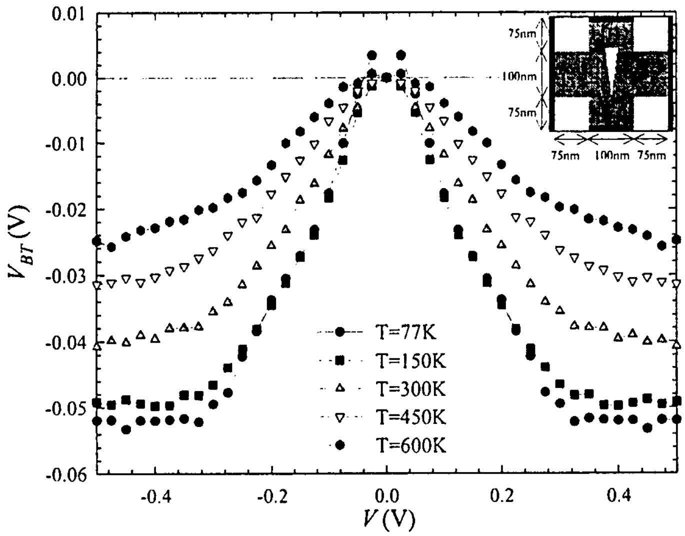

Fig. 1. V_{BT} as a function of V when biasing with $V=V_L=-V_R$ the ballistic rectifier with the geometry shown in the inset at different temperatures.

LONG WAVELENGTH LASERS GROWN ON METAMORPHIC GaAs SUBSTRATES

A.P. Vasilyev, A.E. Zhukov, S.S. Mikhrin, , A.R. Kovsh, N.A. Maleev, E.S. Semenova,
N.V. Kryzhanovskaya, A.G. Gladyshev, M.V. Maximov, V.M. Ustinov, N.N. Ledentsov

A.F.Ioffe Physico-Technical institute, RAS
194021, St. Petersburg, Russia

We report on novel approach for achieving efficient photoluminescence in the 1.3-1.5 μm range from heterostructures grown on GaAs substrates. We demonstrate that a high-quality InGaAs layer can be grown on top of metamorphic buffer on GaAs substrate. This InGaAs layer is used to accommodate strained InGaAs quantum well of higher indium content or InAs QDs. The quantum-well luminescence reaches 1.26 μm at room temperature while the intensity is only 30% lower than that of conventional InGaAs strained quantum well placed in a GaAs matrix. For 1.5 μm range stacked InAs/InGaAs quantum dots are used as an active media of metamorphic InGaAs-InGaAlAs lasers grown on GaAs substrates. QD lasers with high quantum efficiency (η_i>60%) and low internal losses (α < 3-4 cm -1) are realized. The transparency current density per single QD layer is estimated as ~70 A/cm^2 and the characteristic temperature is 60 K (20 – 85^0 C). The emission wavelength exceeds 1.51 μm at temperatures above 60^0 C.

Self-organized In(Ga)As quantum dots and nitrogen-containing quantum wells [1] have been proposed for creating active region of long-wavelength GaAs-based lasers. At the same time their laser characteristics are still inferior in comparison with conventional InGaAs/GaAs quantum-well lasers of the 0.95-1.1 μm range. In case of InGaAsN quantum-well structures low-temperature growth of the active region (~420^{0}C), which is required to prevent phase separation, usually results in formation of non-radiative recombination centers.

A possibility to exploit metamorphic growth mode for the wavelength lasers has not been studied in detail yet in spite of the fact that such an approach is currently widely used for HEMT structures [2]. A virtual substrate, which has larger lattice parameters and lower bandgap as compared to the GaAs, can be created by the deposition of sufficiently thick metamorphic InGa(Al)As buffer layer directly on initial GaAs substrate. Such an approach allows one to avoid growing the active region at very low temperatures and, simultaneously, to exploit wavelength extension in QW or QD lasers.

Heterostructures under investigation were grown by molecular beam epitaxy on GaAs(100) substrates with a 0.5-μm-thick metamorphic buffer deposited at 400^{0}C. The rest epitaxial layers were grown at 500^{0}C. In the first sample (referred to as MMQW) a 8-nm-thick $In_{0.4}Ga_{0.6}As$ quantum well was inserted into a 0.5-μm-thick $In_{0.21}Ga_{0.79}As$ matrix layer confined by short-period $In_{0.21}Ga_{0.79}As$/ $In_{0.21}Al_{0.79}As$ superlattices. The second structure has active region comprised of multiple QD sheets deposited on top of a metamorphic $In_{0.2}Ga_{0.8}As$ layer and formed using 2.7 ML InAs deposition and a 4-nm-thick $In_{0.4}Ga_{0.6}As$ layer overgrowth. 45 nm-thick $In_{0.2}Ga_{0.8}As$ spacers were used to separate 10 planes with QDs.

Diode lasers based on InGaAs QW with 100-μm-wide stripes demonstrate room-temperature lasing at 1.29 μm (as show on Fig.1.) with the minimum threshold current density of 3.3 kA/cm^2 (0.4 kA/cm^2 at 85K).

In Fig. 2. we show the dependence of the threshold current density on the inverse cavity length for MMQD laser. 2 mm-long cavities demonstrate threshold current densities ~1.4 kA/cm^2 . The transparency current, estimated as extrapolation of the threshold current density to the infinite cavity length is ~700 A/cm^2 (~70 A/cm^2 per single QD sheet).

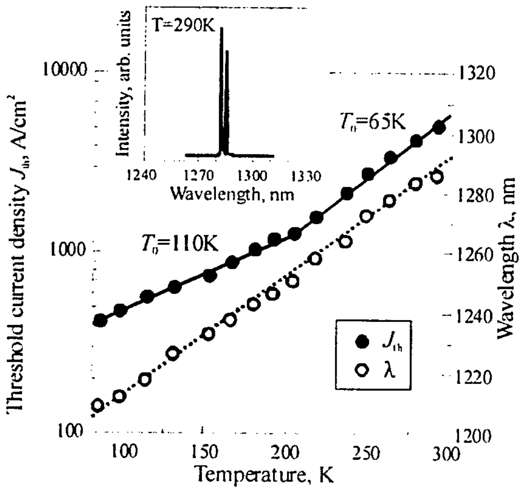

Fig. 1. Dependences of the threshold current density and lasing wavelength on the temperature. Stripe width is 100 μm.
Inset : lasing spectrum at the room temperature (290 K).

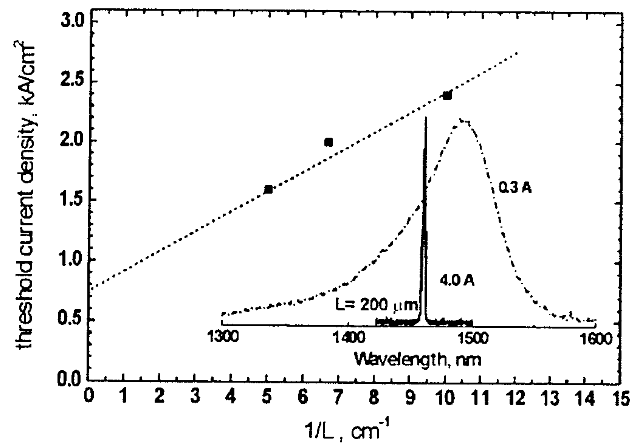

Fig. 2. Dependences of the threshold current density on the inverse cavity length measured at room temperature. Stripe width is 100 μm.
Inset : electroluminescence and lasing spectra for the sample with a 2 mm cavity length.

In conclusion, we fabricated broad-area metamorphic InGaAs QW and InAs/InGaAs QD lasers. For QW laser lasing at 1.29 μm was demonstrated. For QD laser High quantum efficiency, low losses and high temperature operation was demonstrated. The results obtained show the potential of these structures for metropolitan area networks edge- and surface- emitting lasers.

This work was supported by Russian Foundation for Basic Research and Program of the Ministry of Science of Russia "Physics of Solid State Nanostructures".

References

[1] V.M.Ustinov and A.E.Zhukov, Semicond. Sci. Technol. 15(8), R41-R54 (2000).
[2] Sh.-I. Gozu, T. Kita, Y. Sato, et al., J. Cryst. Growth 227 –228, 155-160 (2001).

Fonctionalization of multi-walled carbon nanotubes with silanes

L. Vast[1], A. Destrée[2], N. Moreau[2], Z. Mekhalif[1], A. Fonseca[2], J.B. Nagy[2], J. Delhalle[1]

Département de Chimie, Facultés Universitaires Notre-Dame de la Paix, Namur, Belgium
[1] LISE, [2] RMN

There is intense interest in carbon nanotubes (CNT) since their discovery by Ijima in 1991 [1]. CNT posses unique structural and electronic properties [2] which promise a wide range of potentiel use in many applications such as microelectronics, hydrogen storage [3] and composite polymer [4].
However the poor solubility of these CNTs is a considerable disadvantage for their use. To increase their solubility and enhance the strength of adhesion of them with polymer matrix [5], researchers have chemically fonctionalized the nanotubes wall for the manufacture of the next generation of composite material. Chemical modification as coupling of amine with carboxyl moities already present on the nanotube wall [6] or fluorination under F_2 gas [7] were studied previously.

The objective of this study is to link covalently three functionalized trichlorosilanes : CF_3-$(CF_2)_5$-$(CH_2)_2$-$SiCl_3$ (*FTCS*), CN-$(CH_2)_3$-$SiCl_3$ (*CPTCS*) and CH_2=CH-$(CH_2)_6$-$SiCl_3$ (*7OTCS*) onto multi-walled carbon nanotubes (MWNTs).

The MWNTs used in this work are produced by the catalytic process (CVD) by passing mixture of some gases (ethylene and nitrogen) over a catalyst bed of $Al(OH)_3$, Fe and Co (Figure 1). The chemical treatment of raw MWNTs consists first of an oxidation step with a H_2SO_4/HNO_3 solution. After this treatment, amorphous carbon is removed, mostly MWNTs are isolated and their surface is modified by a higher density of various surface functional group (hydroxyl, carbonyl and carboxyl). To reach a maximum density of hydroxyl moieties on the nanotubes sidewall, which can react favourably with silane, the oxidised MWNTs are reduced with DIBAL-H and finally reacted with toluene solution of trichlorosilane(Figure 2).

Indeed, we obtained three differents functionalized carbon nanotubes (Figure 3).
At each step of their modification, nanotubes were characterised with X-ray Photoelectron Spectroscopy, Thermogravimetry, Transmission Electron Microscopy and Fourier Transform InfraRed Spectroscopy.

References :

[1] S. Ijima, Nature 354 (1991) 56
[2] S. Ijima, C. Brabec, A. Maiti, J. Bernholc, J. Chem. Phys. 104 (1996) 2089
[3] H. Dai, Surface Science 500 (2002) 218
[4] C. Pirlot, I. Willems, A. Fonseca, J. B. Nagy and J. Delhalle, Advanced Engineering Materials, 4(3) (2002) 109
[5] D. R. Askeland, The Science and Engineering of Materials, 3rd edn., PWS Publishing, Boston, MA, 1994
[6] U. Dettlaff-Weglikowska, J.M. Benoit, P-W Chiu, R. Graupner, S. Lebedkin, S. Roth, Current Applied Physics 2 (2002) 497-501
[7] H. Touhara, F. Okino, Carbon 38 (2000) 241

Financial Support : La Région Wallonne, Binanoco Project (RW n°115008)

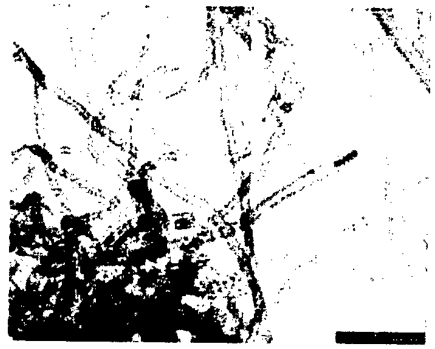

Figure 1 : TEM image of raw multi walled carbon nanotubes.

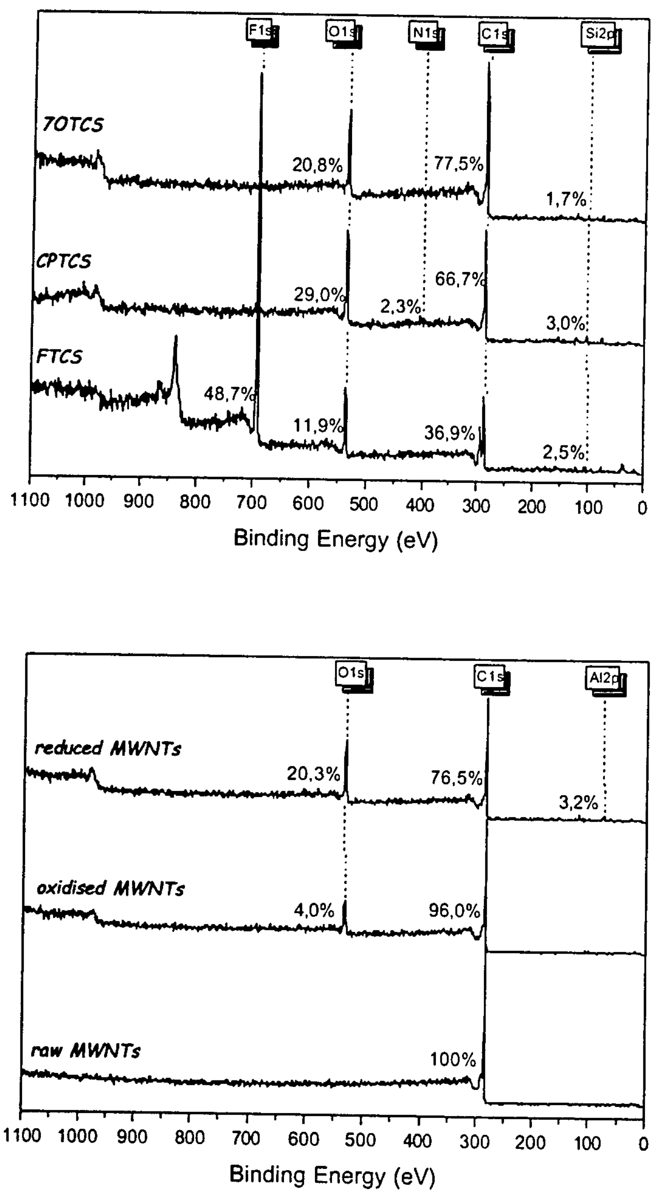

Figure 2 : XPS survey spectra of MWNTs after each modification.

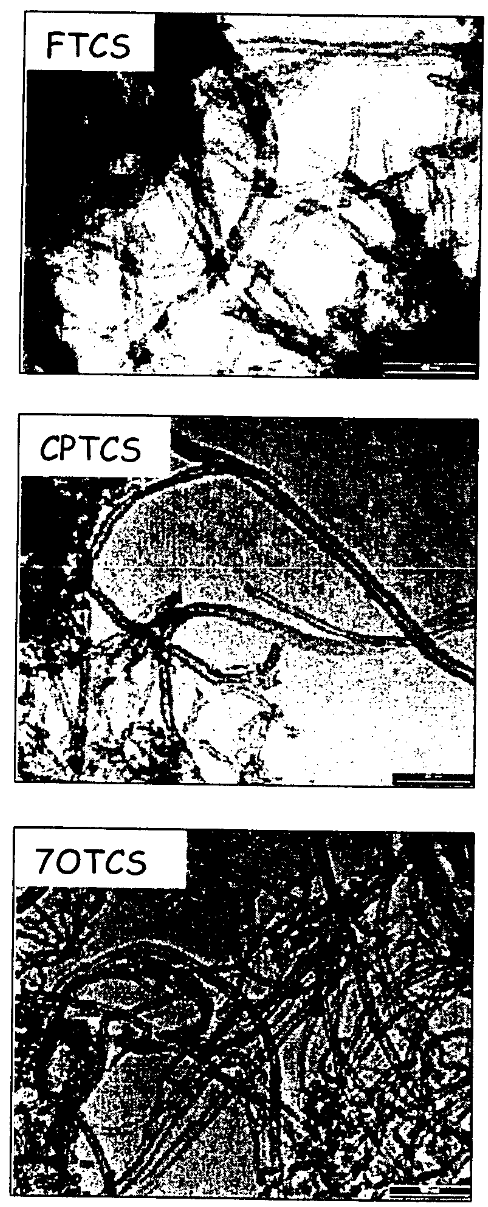

Figure 3 : TEM images of functionalised MWNTs.

TIMESCALES OF NANOSTRUCTURING TECHNIQUES: IONIC CONDUCTION IN SILVER SULPHIDE FILMS AND LOCAL OXIDATION OF TITANIUM FILMS

J.A. Vicary, L. Picco, A.D.L. Humphris, M.J. Miles

H.H. Wills Physics Laboratory, University of Bristol, Tyndall Avenue,
Bristol, BS8 1TL, UK
Email: james.vicary@bristol.ac.uk

The ability to pattern surfaces on the nanometre scale in short timescales is of great importance in the fabrication of nanostructures and nanoscale devices. Recent work has focused on two nanostructuring techniques, and the application of these on millisecond timescales and beyond. In addition, this work assesses the potential of these processes to be used on a high-speed Resonant Scanning Microscope (RSM), a new member of the SPM family of microscopes. Short write timescales would open up the possibility of their use for data storage.

The patterning of a silver sulphide substrate with silver nanostructures has been achieved. Silver sulphide is a solid electrolyte, the chemical properties of which allow the conduction of both electrons and ions through the material, under the influence of an electric field. Silver sulphide films were prepared from silver substrates by immersing in a sodium sulphide solution. The chemical composition of these samples was confirmed with x-ray photoelectron spectroscopy (XPS) analysis.

By using an AFM in contact mode, a bias was applied between a platinum coated tip and the sample, inducing a flow of silver ions through the silver sulphide layer and onto the surface. The resulting structures were then imaged with an AFM in intermittent contact. To date, nanostructures with sizes < 200nm have been patterned on timescales of < 0.5s.

Further nanostructuring has been achieved using the local oxidation technique. Investigations have been concerned with determining the critical reaction time for the formation of titanium oxide on a titanium substrate. Work has focused on the fabrication of arrays of local oxidations. Optimisation of the write speed has been investigated by varying the tip-sample separation and voltage pulse strength and duration.

Results to date have confirmed oxidation speeds on the millisecond timescale with structures ~ 50 nm wide and 10 nm high being created with −12 V pulses of 10 ms duration. On-going work focuses on the microsecond timescale.

CANTILEVER-BASED-SENSOR WITH ELECTROCHEMICAL CURRENT DETECTION

María Villarroya[1], Francesc Pérez-Murano[2], Cristina Martín[2], Zachary Davis[3], Anja Boisen[3], Jaume Esteve[2], Eduard Figueras[2], Josep Montserrat[2], Núria Barniol[1].
1 Dept. Enginyeria Electrònica. Univ. Autònoma de Barcelona. 08193 Bellaterra. SPAIN
2 Institut de Microelectrònica de Barcelona(CNM). CSIC. Campus UAB. 08193 Bellaterra. SPAIN
3 Mikroelektronik Centret. Danmarks Tekniske Universitet.Lyngby.DENMARK
e-mail: Maria.Villarroya@uab.es
http://einstein.uab.es/ecas

The aim of this work is to develop cantilever-based sensors operating in liquid for biochemical applications. The sensing principle of this device consists on detecting the change on the electrochemical current level when a voltage difference is applied between a deflecting functionalised cantilever, acting as one of the electrodes and a reference fixed electrode placed at the free extreme of the cantilever (see Fig.1). To be able to detect the change on the electrochemical current, the distance between both electrodes has to be smaller than 100 nm [1]. To achieve these dimensions microfabricated structures connect the two electrodes and using nanolithography techniques the electrodes separation is defined. The sensing principle is that due to reactions on the functionalised surface, the cantilever deflects, producing a change on the distance between the electrodes (Fig 2). This change provokes a variation of the electrochemical current detected, because the electrochemical current is extremely sensitive to the distance between electrodes.

The design and fabrication of the sensor has been done combining standard microfabrication processes with AFM lithography [2] using SOI substrates. Using normal bulk micromachining techniques a window is open from the backside to allow the liquid to contact the sensor (fig. 3). The separation between the two electrodes has been defined with the AFM probe on an Al mask. The Al_2O_3 is removed and by accurate dry etching the two electrodes are separated. In the first prototype, separation between the 1 μm thick Si electrodes, of 50 nm has been achieved (Fig. 4). These results will allow to detect variations on the electrochemical current level due to the cantilever deflection.

References

[1] A. J. Bard, P.R. Unwin, D.O. Wipf and F. Zhou. *Scanning Electrochemical Microscopy.* Scanned Probe Microscopy. AIP Conference Proceedings 241. (1992). Pag.235-247.

[2] Z.J.Davis, G.Abadal, O.Hansen, X.Borrisé, N.Barniol, F.Pérez-Murano, A.Boisen *AFM lithography of aluminium for fabrication of nanomechanical systems* Ultramicroscopy, to be published june 2003.

Acknowledgments

This work has been partially funded by the projects NANOBIOTEC (CICYT-DPI2000-0703-C03) and NANOMASS II (EU-IST-2001-33068).

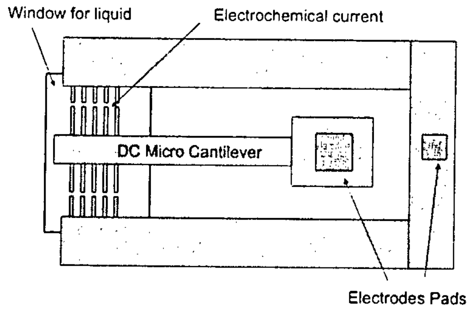

Fig 1. Top view of the sensor structure. The small fingers at the end of the cantilever will constitute the two electrodes for the electrochemical current detection (separation between them less than 100 nm)

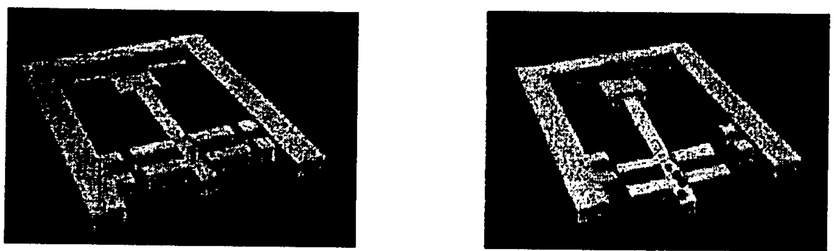

A) Cantilever in rest B) Cantilever deflected

Fig 2. Schematic illustration of the sensor (cantilever with two fingers).

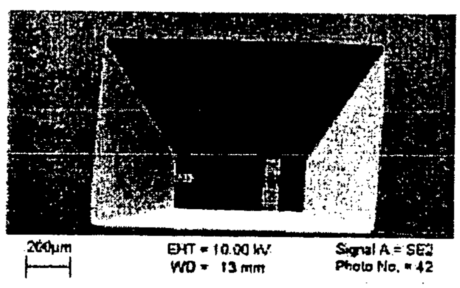

Fig 3. Back side view of the sensor window to allow liquid operation.

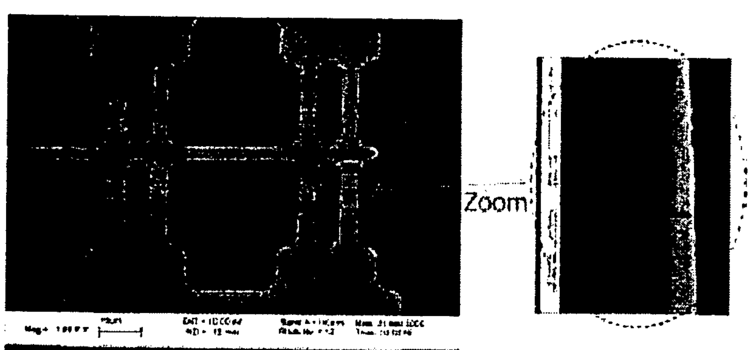

Fig 4. A) SEM image of the end of the cantilever structure shown in figure 3; in circles the separation lines for defining the electrodes. B) One of the separation lines in detail. The separation has been defined by AFM lithography. The width is less than 50 nm.

DYNAMIC BEHAVIOR OF A SINGLE MOLECULE INSERTED IN A SELF-ASSEMBLED MONOLAYER MATRIX AT LOW TEMPERATURE

S. Wakamatsu, S. Fujii, U. Akiba, and M. Fujihira*
Department of Biomolecular Engineering, Tokyo Institute of Technology,
4259 Nagatsuta Midori-ku, Yokohama, 226-8501, Japan.
E-mail: mfujihir@bio.titech.ac.jp

The electrical properties of single phenylene oligomers, $HSCH_2(C_6H_4)_{m-1}C_6H_5$ (m = 1, 2, 3), were studied in terms of the dependence of the tunneling current on the length of the oligomers using self-assembling techniques and scanning tunneling microscopy (STM) [1]. It is important to isolate single molecules in an insulating matrix for the measurement of the conductivity of the single molecule. Bicyclo[2.2.2]octane derivative (BCO) was used for a SAM matrix [2], in which the single molecules were inserted at molecular lattice defects. The isolated single molecules of phenylene oligomers inserted in the SAM matrix were observed as protrusions in STM topography using a constant current mode with a W tip. We estimated the dependence of the tunneling current on the molecular length of phenylene oligomers, i.e. the decay constant β. This was accomplished by measuring the heights of protrusions of individual phenylene oligomers in STM images and by analyzing the heights using the bilayer tunnel junction model. The reasonable value of $\beta = 5.3\ nm^{-1}$ for the single phenylene oligomers at the sample bias voltage of +1.0 V was obtained from the STM measurement of the molecular protrusion (Fig. 1).

In this STM measurement, we observed motion of the single molecules inserted in the BCO SAM matrix at room temperature [3]. It was revealed that the isolated single molecules exhibited two types of motions. One was the change in tilt of the molecular axis at a fixed position (Fig. 2), and the other was lateral motion in the SAM matrix (Fig.3). These motions of the single molecules at room temperature were most likely caused by large and mobile vacancies of single molecular defects in the SAM matrix. However, it is difficult to mention what is a crucial factor for these motions of the inserted single molecules and the BCO matrix molecules. Thermal energy, electric field between the tip and the substrate, and the van der Waals interaction between the tip apex and the molecule can be candidates as the crucial factor.

In this study, we tried to observe the dynamic behavior of the single molecule in the BCO SAM matrix at low temperature. We investigate the effect of the thermal energy on the motions of the single molecules in the BCO SAM matrix.

References:

[1] S. Wakamatsu, S. Fujii, U. Akiba, and M. Fujihira, *Ultramicroscopy* in press.
[2] S. Fujii, U. Akiba and M. Fujihira, *Chem.Commun.* (2001) 1688.
[3] S. Wakamatsu, S. Fujii, U. Akiba, and M. Fujihira, *Nanotechnology* **14** (2003) 258.

Figures:

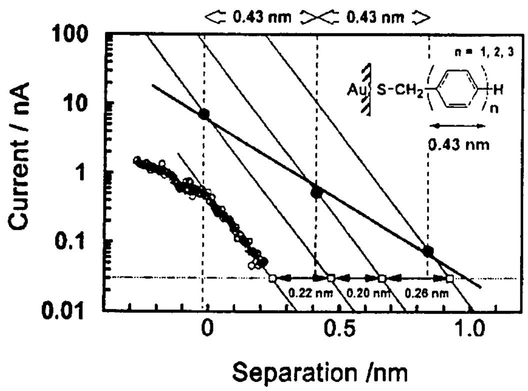

Fig. 1. The dependence of the tunneling current on the length of the oligomers at the same constant sample bias voltage of +1.0 V through W tip/vacuum/oligophenylene SAM-Au(111) junction.

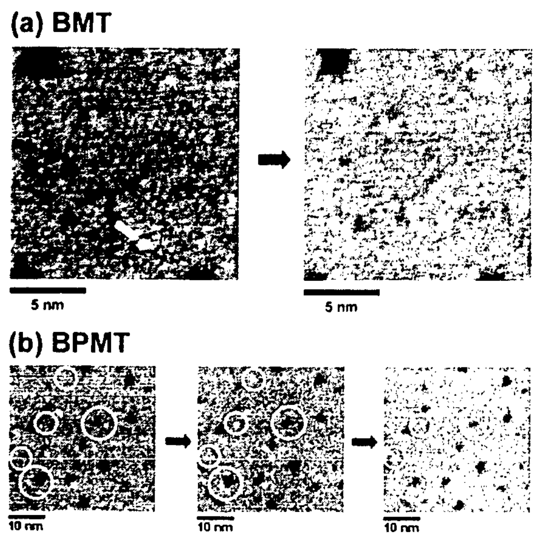

Fig. 2. Time-lapse STM images of (a) benzenemethanethiol (BMT) and (b) 4-biphenylmethanethiol (BPMT) inserted in the BCO SAM matrix. Each image was recorded under a constant condition with a sample bias of +1.0 V and a tunneling current of 30 pA at room temperature. (a) 15 × 15 nm^2 STM successive images of the SAM containing an isolated BMT molecule. The isolated BMT molecule indicated by an arrow suddenly disappeared. (b) A series of 40 × 40 nm^2 STM images of the SAM containing isolated BPMT molecules. Some isolated BPMT molecules switched on and off at the positions highlighted by circles. This type of motion is due to the tilt of the inserted molecule.

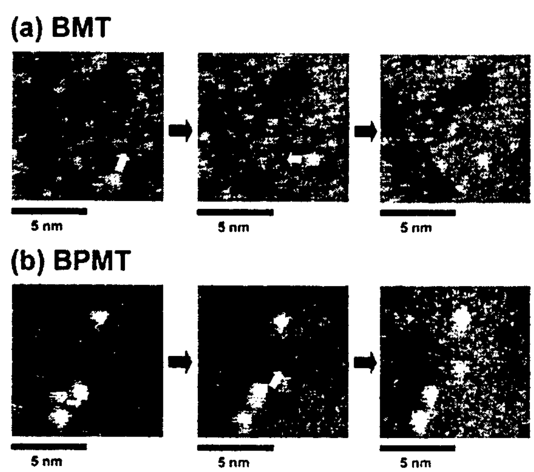

Fig. 3. Series of time-lapse STM images (10 × 10 nm^2) of (a) BMT and (b) BPMT. Each image was recorded under a constant condition with a sample bias of +1.0 V and a tunneling current of 30 pA at room temperature. Some isolated molecules move in the directions indicated by arrows in the BCO SAM matrix.

Poster

BIMETALLIC RUTHENIUM COMPLEXES AS ACTIVE ELECTROCHEMILUMINESCENT SALT IN LED's

S.Welter[1], K. Brunner[2], J.W. Hofstraat[2], and L. De Cola[1]

1 Molecular Photonics Group, University of Amsterdam, Nieuwe Achtergracht 166, 1018 WV Amsterdam, The Netherlands

2 Philips Natuurkundig Laboratorium, Prof. Holstlaan 4, 5656 AA Eindhoven, The Netherland

We have used di-nuclear ruthenium (II) complexes in polymer light emitting diodes to generate light emission from triplet state emitting compounds to improve the quantum yields and lifetimes of the devices. Upon doping the polymer we obtained red emission from the ruthenium complex at forward bias and green emission from the polymer at reverse bias. This represents the first elecroluminescent device with fully-reversible, voltage-dependent, switching between two emissive colours[1].

The polyphenylene bridging ligand connecting both ruthenium metal centres is crucial for the mechanism of the device, as it helps to redistribute the charge of the reduced complex by formation of a stable bipolaron and consequently acts as an electron transfer mediator. Spectro-electrochemistry and transient absorption spectroscopy indicate the delocalisation of the negative charge on the bridging ligand. The mechanism for light generation at both biases will be shown.

The morphology of the emissive layer was investigated by Secondary Ion Mass Spectroscopy and Atomic Force Microscopy. SIMS and AFM measurements show that the distribution of the ruthenium complex in the polymer layer is homogenous and no phase separation is observed (Fig.1).

1. Welter, S., et al., *Electroluminescent Device with Reversible Switching between Red and Green Emission. Nature* (**2003**) 421, 54 - 57.

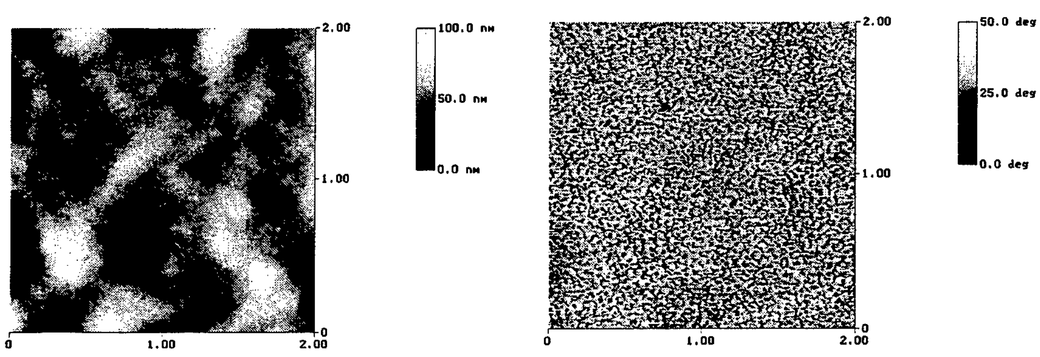

Figure 1. AFM measurements of polymer LED doped with bi-metallic ruthenium complex. Measurements were done with a non-covered silicon tip in tapping mode. a: height image, b: phase image.

CONSTRUCTIVE NANOLITHOGRAPHY AND NANOCHEMISTRY: LOCAL PROBE OXIDATION AND CHEMICAL MODIFICATION

D. Wouters[1], U. S. Schubert[1]
[1]Laboratory of Macromolecular Chemistry and Nanoscience, Center for Nanomaterials (cNM),
Eindhoven University of Technology and Dutch Polymer Institute (DPI), P.O. Box 5600 MB, Eindhoven, The Netherlands
email address corresponding author: u.s.schubert@tue.nl

In the current field of available techniques that are used in the production of sub-micrometer sized devices, UV and UV mask lithography are the most widely used and studied techniques. However these techniques are limited by the minimal obtainable size of the structures that can be reached. Research into new techniques is concentrated around electron beam lithography and scanning probe-based techniques as dip-pen lithography and scanning probe oxidation. The latter one has two main advantages. First it is capable of producing well-defined nanopatterned substrates with relative ease on a number of different substrates. Secondly it also introduces local groups with chemical reactivity that allow for local substrate reactions and modifications. Because a broad variety of modification reactions and compounds are available, structures created in this fashion can be employed not only in semi-conductor applications but also in sensor and smart coating devices. In this contribution the technique of local probe oxidation and subsequent chemical modification and fabrication of nanometer-sized structures on octadecyltrichlorosilane (OTS) passivated silicon wafers is presented. By applying a bias voltage on a conductive AFM-tip the OTS layer on the surface can be oxidized very locally [1, 2]. The oxidation changes the local properties of the surface, thus opening routes to controlled surface modification via both absorption as well as chemical modification routes.

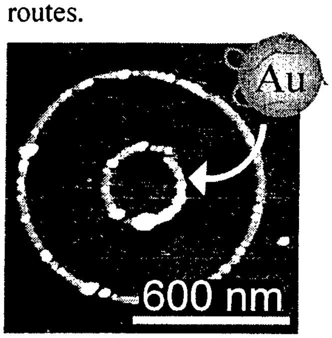

Fig. 1 TM-Height image (1.1 × 1.1 µm, z-range 18 nm) of cationic gold nanoparticles adsorbed to an oxidized structure.

Presented here are results of the (sequential) functionalization of surfaces with (cationic) gold nanoparticles, quaternary ammonium salts and the covalent attachment of functional silanes with for example polymerizable side groups. Subsequently these "functional" structures were exposed to polymerization reactions or thiol bearing proteins creating complex function nano-structured 'devices'.

References

[1] S. Höppener, R. Maoz, S. Cohen, L. Chi, H. Fuchs, J. Sagiv, Adv. Mat. 14, 1036 (2002).
[2] D. Wouters, U. S. Schubert, (2003) submitted.

Sub-nm resolution scanning tunneling spectroscopy magnetic imaging of Fe/Mn/Fe(001) multilayer film

T.K. Yamada[1], A.L. Vazquez de Parga[2], M.M.J. Bischoff[1], G.M.M. Heijnen[1], T. Mizoguchi[3], H. van Kempen[1]

1. NSRIM, Univ. of Nijmegen, NL-6525 ED Nijmegen, The Netherlands

2. Univ. Autonoma de Madrid, Dep. Fisica de la Materia Condensada, 28049 Madrid, Spain

3. Faculty of Science, Gakushuin Univ., 171-8588 Mejiro, Tokyo, Japan

The development of ultra-thin magnetic multilayer films has lead to considerable practical applications such as spin electronic devices. Although the intermixing (or interface roughness) were suggested to occur at the interface in the multilayer films, the magnetic structure at the interface layers and how the magnetic structure relates to the geometric and intermixing is not clear. In the present study we demonstrate the direct observation of the magnetic structure at the first layers of the magnetic multilayer film by spin-polarized scanning tunneling spectroscopy (SP-STS), which can be used to image magnetic domain structures down to the sub-nm scale. Using Fe-coated W tips, we found antiferromagnetic coupling of ferromagnetic body-centred tetragonal (bct) (001) Mn layers on Fe(001) [1]. Since we can control the Mn layers very well, this is a good sample to study the magnetism. We studied Fe/Mn/Fe(001) multilayer film. By studying the growth, intermixing, electronic structure, and magnetic structure of the Fe films on Mn(001), we found that the Fe film thicker than fourth layers have the same properties as body-centred cubic Fe(001). However, for first-fourth Fe layers intermixing with Mn takes place and the film presents different magnetic properties, i.e., the in-plane magnetization of each Fe layer couples non-collinearly [Fig. 1].

[1] T.K. Yamada *et al.*, Phys. Rev. Lett. **90** (2003) 056803.

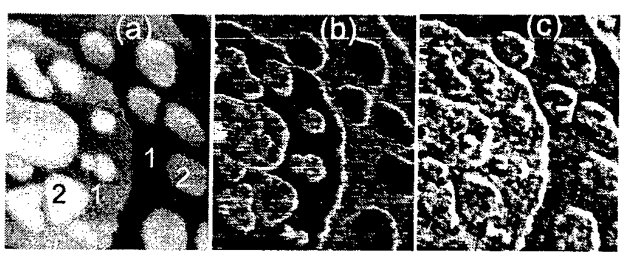

Fig.1 Magnetic structures obtained on the surface of 1.5 ML of Fe. (a) and (b) were obtained by an Fe-coated W tip. A topographic image (a) and dI/dV maps at +0.2 V (b),(c) were obtained with the lock-in amplifier technique. The set point was $V_S = +0.2$ V, $I = 0.2$ nA. The size is 100×85 nm^2. Numbers in (a) denote the stacking number of the Fe layers. After measuring (b), the tip was changed by applying a voltage pulse at different place and (c) was obtained [T.K. Yamada *et al.*, Appl. Phys. Lett. **82** (2003) 1437]. These observation can be explaned by non-colinear coupling between magnetizations of the Fe layers.

LUMINESCENT PROPERTIES OF ZnS-PASSIVATED CdS:Mn CORE/SHELL QUANTUM DOTS: PHOTO- AND ELECTRO-LUMINESCENCE

Heesun Yang* and Paul H. Holloway
Department of Materials Science and Engineering, University of Florida, Gainesville, FL 32611-6400 USA
E-mail: hyang@ufl.edu, Tel.: 352-846-3325, Fax: 352-392-4911

Semiconductor quantum dots (nanocrystals) doped with impurity as a luminescent material are the subject of intensive investigation. The engineering of the band gap by control of the crystal size can result in tunable band-edge emission. By doping the nanocrystals with luminescent activators, the excitation can be tuned by quantum size effects while the emission energy is largely unchanged. In either case, nanocrystals have a high surface-to-volume ratio and surface states act as centers for luminescent quenching and photobleaching.[1,2] To reduce these detrimental effects of surface states on luminescent properties, more effective surface passivation is imperatively desired which will lead to efficient and photostable luminescence.

Yellow-emitting CdS:Mn/ZnS core/shell quantum dots (ZnS-passivated CdS doped with Mn luminescent centers) were developed via reverse micelle chemistry. Synthesized CdS:Mn/ZnS core/shell quantum dots were measured to have a core diameter of 2.3 nm and a shell thickness of 0.4 nm (which corresponds to 1.5 monolayers of ZnS). Photoluminescence (PL) emission spectra of organically (*n*-dodecanethiol) and inorganically (ZnS) passivated CdS:Mn quantum dots are compared in Fig. 1 (a) and (b), respectively. While *n*-dodecanethiol-passivated CdS:Mn nanocrystals show a distinct surface defect-related peak at ~ 450 nm, as well as a broad Mn^{2+}-related ${}^4T_1$-${}^6A_1$ transition peak at ~ 600 nm, ZnS-passivated CdS:Mn core/shell nanocrystals exhibit much sharper Mn^{2+} emission which is not related to surface defects. This is presumably the result of effective passivation of CdS surface states by the ZnS shell and consequent suppression of nonradiative/radiative recombination transitions at the surface. We also have measured a high PL quantum yield of 18 - 28 % from CdS:Mn/ZnS quantum dots. The dependence of PL emission intensity upon the amount of UV irradiation has been observed for both organically and inorganically passivated CdS:Mn nanocrystals, and is shown in Fig. 2. In contrast to a significant reduction of emission intensity with increasing time (increasing fluence) for *n*-dodecanethiol passivated CdS:Mn nanocrystals, CdS:Mn/ZnS core/shell nanocrystals exhibit a slightly increased intensity and subsequent stable intensity (good photostability) with increasing UV irradiation time. The initial increase in emission intensity is attributed to an irreversible UV-stimulated photooxidation by oxygen in the air of the ZnS shell surface.[3]

Direct current (dc) electroluminescent (EL) devices were fabricated using a hybrid organic/inorganic multilayer structure of ITO//PEDOT-PSS//(poly(N-vinylcarbazole) (PVK)//CdS:Mn/ZnS nanocrystal//Al. The poly(3,4-ethylenedioxythiophene)/poly (styrenesulfonate) (PEDOT-PSS) layer was used for enhanced hole injection from the indium tin oxide (ITO) transparent conducting electrode. EL spectra as a function of applied voltages are shown in Fig. 3. Only yellow emission from the CdS:Mn/ZnS nanocrystal layer was observed, with no emission from the PVK conjugated polymer. EL emission exclusively from the nanocrystal layer of this multilayer structure was concluded to result from radiative electron-hole recombination occurring predominantly

in that layer. This selective confinement of charge carriers into the nanocrystal layer was explained by the lower energy barrier for hole injection from the PVK into the nanocrystals, versus a relatively large barrier for electron injection from the quantum-shifted CdS:Mn/ZnS nanocrystals into the PVK.

References:

[1] X. Peng, M. C. Schlamp, A. V. Kadavanich, and A. P. Alivisatos, J. Am. Chem. Soc.,
119 (1997) 7019.

[2] M. A. Hines, P. Guyot-Sionnest, J. Phys. Chem., 100 (1996) 468.

[3] L. Manna, E. C. Scher, L. Li, and A. P. Alivisatos, J. Am. Chem. Soc., 124 (2002) 7136.

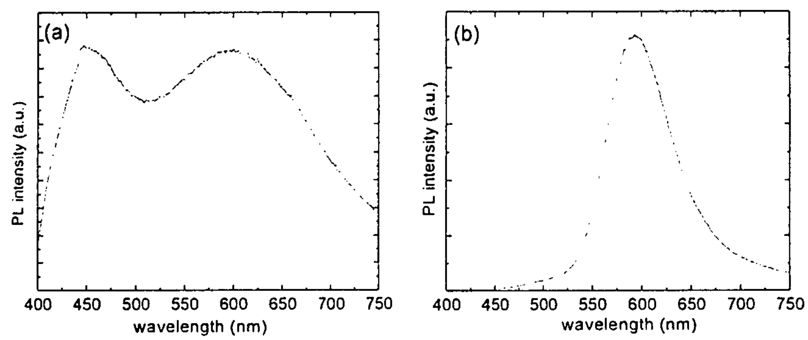

Fig. 1. PL emission spectra of (a) *n*-dodecanethiol- and (b) ZnS-passivated CdS:Mn nanocrystals. The 325 nm HeCd laser source was used for the excitation.

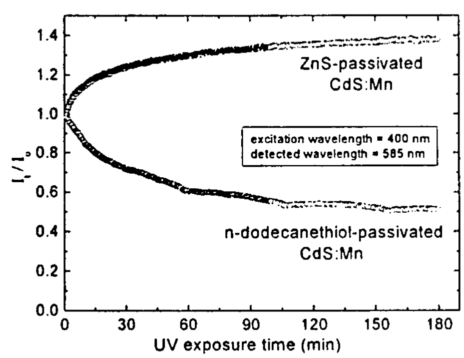

Fig. 2. Dependence of PL emission intensity of *n*-dodecanethiol- and ZnS-passivated CdS:Mn nanocrystals on UV irradiation time

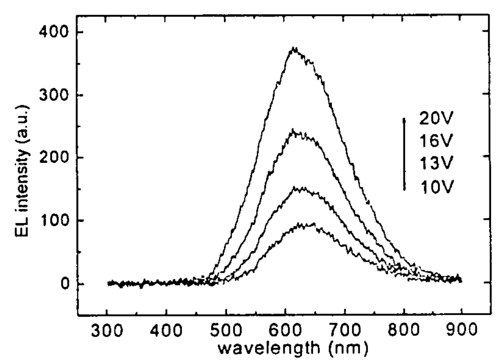

Fig. 3. EL spectra from an ITO//PEDOT-PSS//PVK//CdS:Mn/ZnS//Al hybrid device as a function of applied voltages.

SINGLE-WALL NANOTUBES GROWN BY CHEMICAL VAPOUR DEPOSITION USING ACETYLENE

M. H. Yang+, A. S. Teh, R. G. Lacerda, K. B. K. Teo, N. L. Rupesinghe, M. Chhowalla*, K. Koziol**, D. Roy, D. G. Hasko***, G. A. J. Amaratunga and W. I. Milne

Engineering Department, University of Cambridge, Trumpington Street, Cambridge, CB2 1PZ, UK

*Rutgers University, Ceramic and Materials Engineering, Piscataway, New Jersey 8854

**Department of Material Science and Metallurgy, University of Cambridge, Pembroke Street, Cambridge, CB2 3QZ, UK

***Microelectronics Research Centre, Cavendish Laboratory, University of Cambridge, Madingley Road, Cambridge CB3 0HE, UK

+ email: mhy23@cam.ac.uk

Chemical vapour deposition (CVD) has been considered one of the most promising techniques for the production of both single-wall (SWCNT) and multi-wall (MWCNT) carbon nanotubes. For the full exploitation of the unique properties of SWCNTs, much work is still needed to reliably integrate them with electronic devices. Most of the SWCNT growth in the literature are based on using methane as the source of carbon, and a gaseous or liquid phase metal solution as the catalyst. In this present work, we report the preparation of SWCNTs by CVD using acetylene and a triple layer of solid catalyst [Al (10 nm), Fe (0.5-1.5 nm) and Mo (0-1.5 nm)] similar to that used by Delzeit *et al.* [1].

The Fe catalyst acts as the main precursor for the nanotube growth. However, the nucleation of the tubes would not be possible without an Al layer. The role of Mo (0.3-1 nm) is to enhance the yield of SWCNTs. In our growth technique, MWNTs were found to grow at temperatures of 750-900 ^{0}C. By increasing the temperature to 1000^{0}C we were able to produce SWCNTs. The SWCNTs were grown using only acetylene with flow rates between 50-500 sccm upon the solid catalyst. The presence of SWCNTs was verified by TEM. The TEM images shows that most of the SWCNTs were found to be isolated and not in bundles, which is commonly encountered (Fig.1). The evidence for this was further strengthened by the appearance of radial breathing modes (~180 cm^{-1}) using Raman spectroscopy (not shown). Using the peak position, we estimated the average nanotube diameter to be around 1.3nm.

By using a solid catalyst, the controlled and precise patterning of the catalyst is possible via electron beam lithography. This technique was used to achieve the growth of SWCNTs between contacts or patterns (Fig. 2). Interestingly, the SWCNTs appear to self-assemble between metal contacts. This characteristic could prove vital for the integration of SWCNT into electronic devices. Electronic measurements show that the resistivity of the tubes are between 0.03-0.6 Mega-Ohms. This interesting method of controlling the nanotube growth and position enables the fabrication of complicated structures for SWNT nano-electronic applications in the future.

[1] Delzeit *et al.*, Chemical Physics Letters 348, 368 (2001).

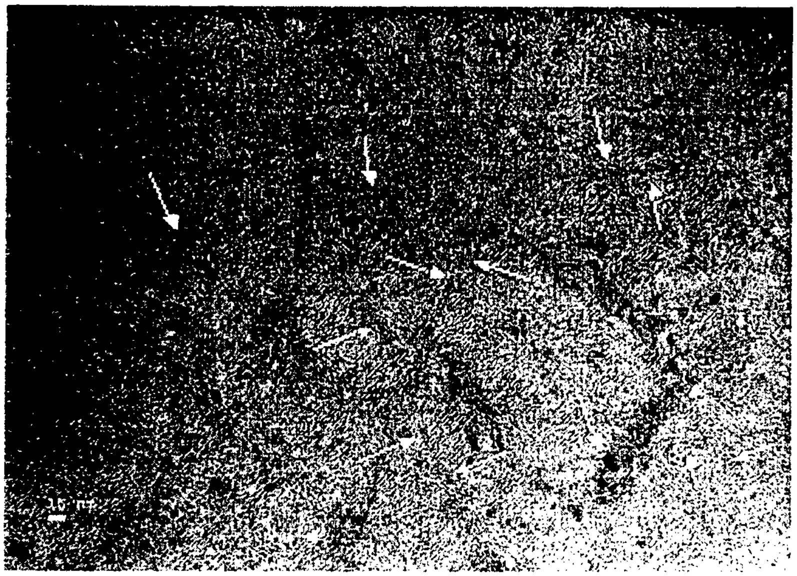

Figure 1 - Transmission Electron microscopy of single-wall carbon nanotubes grown by CVD using C_2H_2 at 1000 °C.

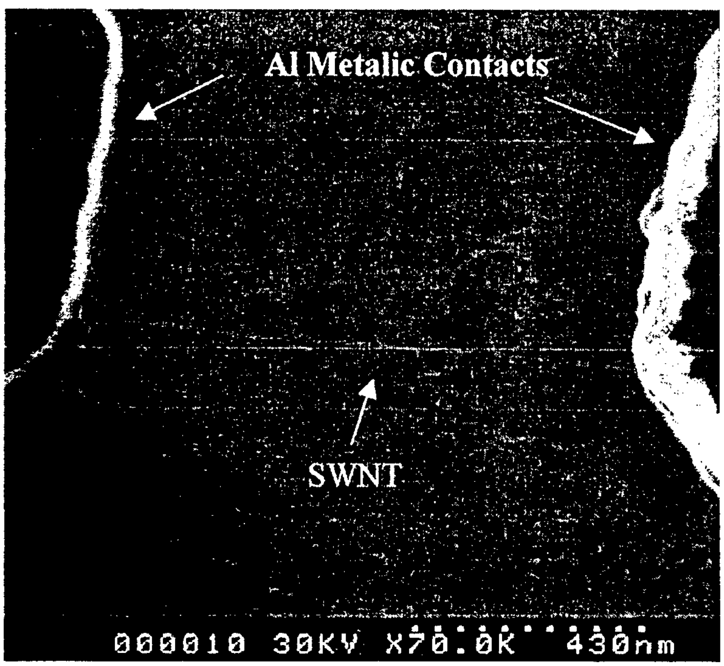

Figure 2 – SWCNT between two metallic contacs.

Posters - Session B

SUBMOLECULAR INVESTIGATION OF THE TWO-DIMENSIONAL ORGANIZATION AND PHOTOCHEMICAL REACTIVITY OF β-SUBSTITUTED AND α-FUNCTIONALIZED OLIGOTHIOPHENES AT THE LIQUID-SOLID INTERFACE

Mohamed M. S. Abdel-Mottaleb, Elena Mena-Osteritz, Peter Bäuerle.*
Abteilung Organische Chemie II der Universität Ulm. Albert-Einstein-Allee 11, 89081 Ulm, Germany. Fax: +49-731-50-22840, E-mail: mohamed.abdel-mottaleb@chemie.uni-ulm.de

Oligothiophenes[1] have been intensively studied as promising materials for electronic devices. The combination of excellent electronic properties, stability under ambient conditions, and good transport properties have allowed their application , for example, in organic light emitting diodes and thin-film transistors.[2] We have previously reported on the organization of 3,3'''-dialkylated quaterthiophene derivatives at the liquid-solid interface.[3] The molecules were found to organize in a densely well ordered monolayer, in which the packing pattern of the molecules was dependent on the length of the alkyl chains.

In this contribution we investigate the effect of functionalization of the oligothiophene backbone. In this context, the packing pattern of a non-iodinated didodecyl quaterthiophene **1** at the liquid-solid interface is compared to those of the mono-, and diiodo analogous molecules **2** and **3**, respectively (Fig.1). The presence of the iodine atoms was found to significantly alter the packing pattern of the molecules (Fig.2). Furthermore, preliminary results indicate the occurrence of photochemical dimerization of **2** at the liquid-solid interface upon irradiation with UV light.

References:

[1] P. Bäuerle, in Electronic Materials: The Oligomer Approach (Eds.: K. Müllen, G. Wegner), Wiley-VCH, Weinheim, **1998**, Chapter 2.

[2] M. G. Harrison, R. H. Friend, in Electronic Materials: The Oligomer Approach (Eds.: K. Müllen, G. Wegner), Wiley-VCH, Weinheim, **1998**, Chapter 11.

[3] R. Azumi, G. Götz, T. Debaerdemaeker, P. Bäuerle Chem. Eur. J., **6** (2000) 735.

Figures:

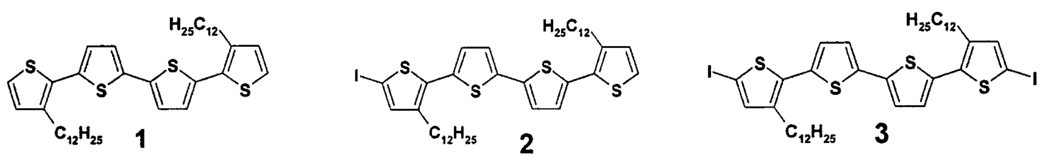

Figure 1 Chemical Structures of oligothiophene derivatives investigated

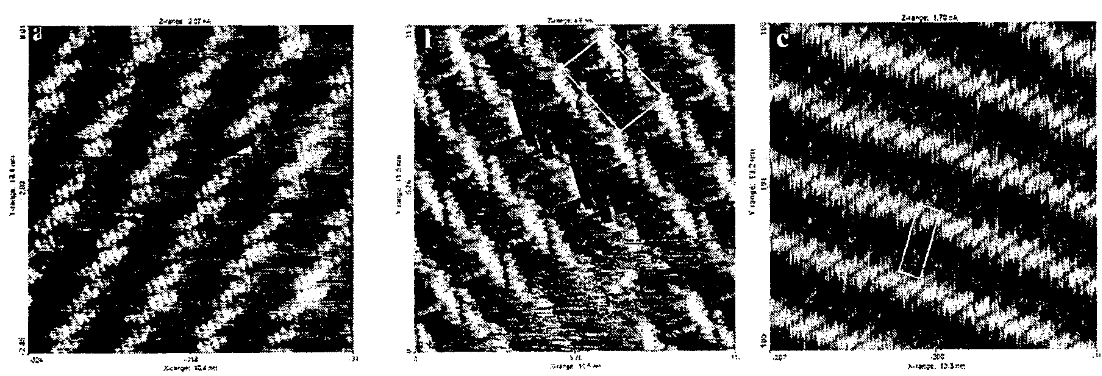

Figure 2 a, b, and c STM images of the monolayers of **1**, **2**, and **3** derivatives, respectively.

LANGMUIR AND LANGMUIR BLODGETT FILMS OF STRONGLY NON-LINEAR-OPTICALLY (NLO) ACTIVE AMPHIPHILIC MOLECULES

S. Acharya[†], P. Krief[†], R. Ginzburg[†], V. Khodorkovsky[†], J. T. Klug[‡] and S. Efrima*[†,#]
[†] Department of Chemistry, [‡]The Institutes of Applied Sciences, [#]The Ilse Katz Center for Meso and Nanoscale Science and Technology, Ben-Gurion University, Beer-Sheva, 84105, Israel
E-mail: acharya@bgumail.bgu.ac.il

The Langmuir Blodgett (LB) technique is an important method for the fabrication of films with nanometric thickness. It is suitable for photonic applications based on second harmonic generation which require the assembly of chromophores in a non-centrosymmetric arrangement in miniaturized nanoscale systems. We present a study of the Langmuir and LB films of 2-(4-[Hexadecyl (methyl) amino] phenylmethylene)-1,3-dioxo-5,6-indanedicarboxylic acid [**1**] and related molecules. These molecules are designed by us and tested to have specially intense NLO activity.

Our work involves the measurement of π/A isotherms of the corresponding Langmuir films at various temperatures, and the spectroscopic, atomic force microscopy and contact angle characterization of the LB films.

Figure 1 shows the π-A isotherms of **1** at different temperatures. The isotherms at higher temperatures (32 and 28°C) show a low pressure 2D liquid-expanded phase followed by a liquid-condensed or solid region, which collapses slightly below 50 mN/m. At lower temperatures the liquid-expanded region gradually disappears and only the liquid-condensed or solid phases are evident before collapse above 50 mN/m. The increase of the collapse pressure might be due to a more ordered arrangement of the hydrocarbon chains at lower temperatures.

We deposited Z-type LB films of **1** (deposition only in the up-stroke) at two extreme temperatures (32 and 11°C) from water at pH 5.5. The films are hydrophobic (contact angle 67°). The UV-vis absorption spectra of these films shown in figure 2 indicate a uniform transfer of the molecules with a transfer ratio close to unity, which depends somewhat on the deposition conditions. The linear dependence of the optical density of the absorption maximum versus the number of layers is observed for all cases (inset of figure 2) and suggests a regular transfer of the films. The absorption spectra deposited at 11°C (maximum at ~ 482 nm) are slightly blue shifted compared to that deposited at 32°C (maximum at ~ 491 nm, figure not shown) suggesting a tighter association of the molecules at low temperature, as seen in the isotherms themselves.

The analysis of polarized absorption spectra of the LB films at different incident angles of the light with respect to the film (α = 30°, 45°, and 60°) reveals that the average orientation of the major axis of the chromophore with respect to the glass substrate is 52-56°, irrespective of the surface pressure.

The AFM image of a 3-layer LB film of **1** deposited at a surface pressure 40 mN/m at 11°C is shown in Figure 3. The molecules are closely packed, forming aggregates. The depth profile of the image (Figure 4), indicates an average thickness of each monolayer to be ~ 3-4

nm, in corresopndence to the tilt found for the chromophore and an upright alkyl chain orientation. It also shows that the amphiphile aggregates are two-dimensional, molecularly thick perpendicular to the surface.

Interestingly, a similar study of a closely related molecule, which differs from **1** by only one additional double bond in the bridge between the two conjugated sub-systems, deposits as LB films in both the down- and up-strokes (with a hydrophilic slide). Recall that **1** deposited only in the up-strokes. Yet the films are invariably hydrophobic (contact angle of 67°). Thus also here Z-type films probably form, but via rearrangments of the films during or immediately after deposition. We also report results for the SHG measured from these films.

References:

[1] H. Schwartz, R. Mazor, V. Khodorkovsky, L. Shapiro, J. T. Klug, E. Kovalev, G. Meshulam, G. Berkovic, Z. Kotler and S. Efrima, J. Phys. Chem. B, **105** (2001) 5914.

Figures:

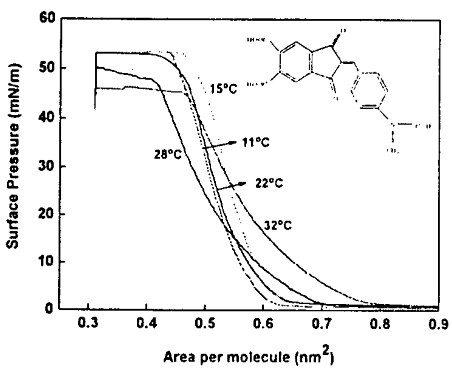

Figure 1 - Pressure area isotherm at different temperature. The inset shows the molecular structure of **1**.

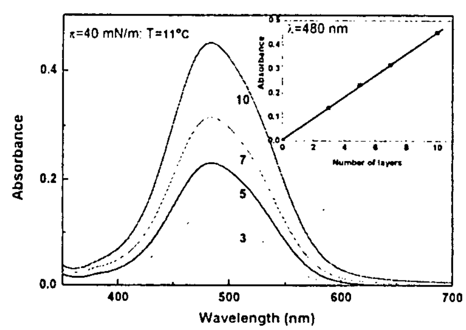

Figure 2 - UV-vis absorption spectra of LB films of **1** for different number of deposited layers. The inset shows absorbance versus number of LB layers.

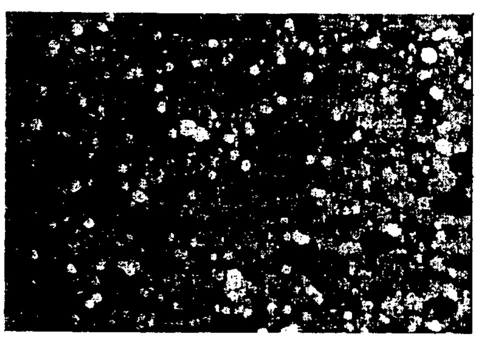

Figure 3 - AFM image of 3 layers of **1** transferred onto a glass plate at a surface pressure 40 mN/m. Scan length 10 μm.

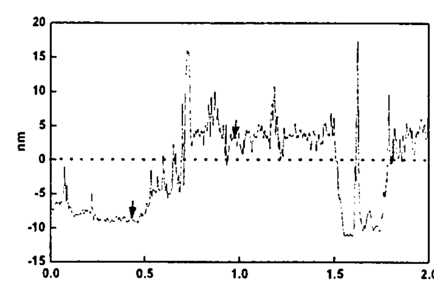

Figure 4 - AFM section analysis of 3 layers of LB films of 1 at pressure 40 mN/m, and temperature 11°C.

SELF-ASSEMBLY OF THIOLATES WITH ALICYCLIC MOIETIES ON AU(111)

M. Suzuki, S. Fujii, S. Wakamatsu, U. Akiba, and M. Fujihira*
Department of Biomolecular Engineering, Tokyo Institute of Technology
4259 Nagatsuta Midori-ku, Yokohama, 226-8501, Japan.
E-mail: mfujihir@bio.titech.ac.jp

Self-assembled monolayers (SAMs) of thiolates with bulky cage hydrocarbons have been formed on Au(111) and characterized using scanning tunnelling microscopy (STM) [1,2]. Among SAMs with thiolates on Au(111), the most popular ones are SAMs with linear hydrocarbon (n-alkane) thiolates. Their structure, energetics, and growth kinetics have been extensively studied [3].

In this study, SAMs of thiolates with a cyclo- or a bicylo-alkane moiety (c and d in Fig. 1) were formed on Au(111). Their SAM structures were characterised using STM and compared with those of linear alkane thiolates (a and b in Fig. 1). In addition, we tried to investigate their electrical properties in terms of dependence of tunnelling currents on the number of the alkane chains in the alicyclic moieties. For this purpose, we prepared mixed SAMs, in which two of three kinds of thiolates were molecularly mixed. By comparing STM height differences between the two thiolates in the mixed SAMs under a constant-current mode, we attempted to distinguish their electrical properties.

References:

[1] S. Fujii, U. Akiba, and M. Fujihira, Chem. Commun., (2001) 1688.
[2] S. Fujii, U. Akiba, and M. Fujihira, J. Am, Chem. Soc., **124** (2002) 13629.
[3] F. Schreiber, Prog. Surf. Sci., **65** (2000) 152.

Figures:

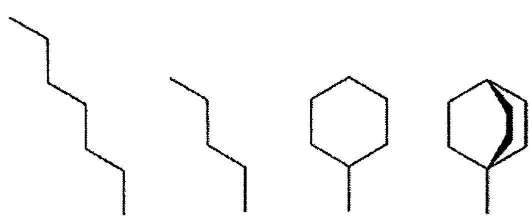

a b c d

Figure 1.

INTERACTION OF MOLECULAR AND ATOMIC HYDROGEN WITH CARBON NANOTUBES

J. A. Alonso * [1,2], J. S. Arellano [3], L. M. Molina [4], A. Rubio [1] and M. J. López [2]

* Email: jaalonso@fta.uva.es

1. Donostia International Physics Center, 20018 San Sebastián, Spain.
2. Departamento de Física Teórica, Universidad de Valladolid, 47011 Valladolid, Spain.
3. Area de Física Atómica Molecular Aplicada, Universidad Autónoma Metropolitana Azcapotzalco, 02200 México D.F., México.
4. Institute of Physics and Astronomy, Aarhus University, DK-800 Aarhus C, Denmark.

Density Functional calculations have been performed to study the interaction of molecular and atomic hydrogen with (5,5) and (6,6) single wall carbon nanotubes and graphene. Static calculations allowing for different degrees of structural relaxation have been performed, in addition to dynamical simulations. Molecular physisorption inside and outside the nanotube walls is predicted to be the most stable state of those systems when the local density approximation (LDA) is used to describe the exchange and correlation effects between the electrons. The predicted binding energies for physisorption of the H_2 molecule outside the nanutobes are in the range 0.04-0.07 eV. This means that uptake and release of molecular hydrogen from nanotubes is a relatively easy process, as many experiments have proved. A chemisorption state, with the hydrogen molecule dissociated and the two hydrogen atoms bonded to neighbor carbon atoms, has also been found. However, reaching this dissociative chemisorption state for an incoming hydrogen molecule, or starting from the physisorbed molecule, is difficult because of the existence of a substantial activation barrier. The dissociative chemisorption deforms the nanotube and weakens the C-C bond. This effect can catalyze the shattering and scission of the tube by incoming hydrogen molecules with sufficient kinetic energy.

SHAPE STABILITY ON SELF-ASSEMBLED InAs NANOSTRUCTURES: KINETIC AND THERMODYNAMIC ANALYSIS

H.R. Gutiérrez[1], R. Magalhães-Paniago[2,3], J.R.R.Bortoleto[1] and M.A.Cotta[1].
[1] UNICAMP, IFGW, DFA/LPD - CP 6165, 13081-790 Campinas, SP, Brazil.
[2] LNLS, 13084-971, Campinas,. SP, Brazil
[3] Univ.Fed.Minas Gerais., ICEx, DF, 30123-970, Belo Horizonte, MG, Brazil
E-mail: monica@ifi.unicamp.br

InAs nanostructures in an InP matrix have received much attention in the last years. Recently, we have reported the conditions that determine the InAs shape transition - from wires to dots – for films grown on (100) InP substrates by Chemical Beam Epitaxy. We have obtained intermediary states containing both wires and dots in the same sample. However, the grown of such self-assembled nanostructures requires a complete understanding and control of the formation mechanisms. In this sense we have obtained a complete picture of the InAs nanostructures formation. InAs growth evolution was monitored by Reflection High Energy Electron Diffraction (RHEED). The samples were analyzed by Atomic Force Microscopy (AFM) and High Resolution Transmission Electron Microscopy (HRTEM). The influence of the temperature, growth rate and the InAs thickness on the wires formation was studied. Our results suggest that the wires are a metastable shape originated by the anisotropic diffusion on the InP buffer layer during the formation of the first InAs monolayer. This kinetically controlled process occurs in a well-defined range of growth conditions, which determine the distribution, homogeneity and shape of the resulting nanostructures. However, another significant factor to determine the shape, size and facet formation in these nanocrystals is strain distribution. The characterization of this parameter can be performed using grazing incidence x-ray scattering, an accurate method sensitive to both local lattice parameter variations and nanostructure lateral size. All measurements were done as a function of the scattering angle (radial) and the sample rotation (angular). Angular scans (which are size sensitive) at different radial positions (strain sensitive) were correlated with AFM and TEM measurements. A remarkable anisotropy was observed for strain distributions parallel and perpendicular to the wires. The higher strain relaxation was measured along the [110] direction, perpendicular to the wires. This large strain anisotropy was not observed for samples with dots as the dominant surface shape.

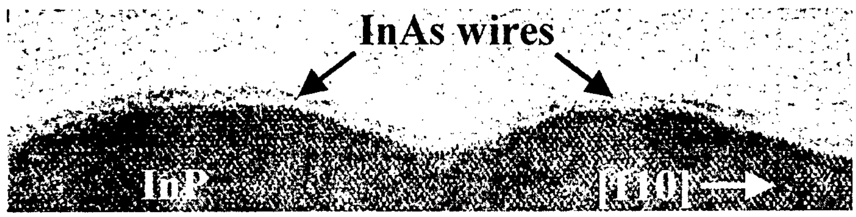

Fig.1 - Cross section TEM of the InAs nanowires grown on InP.

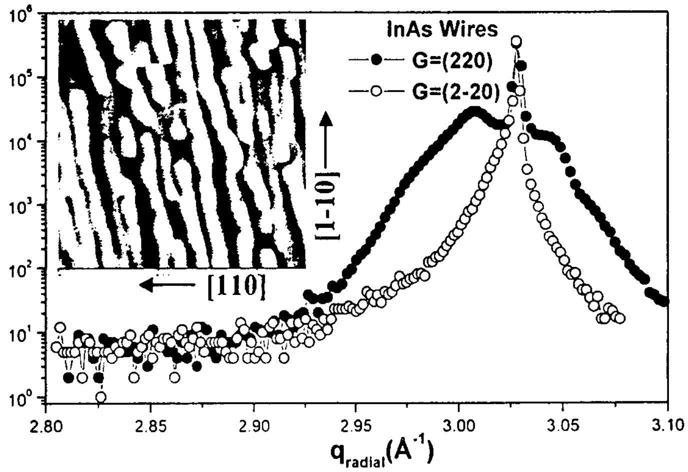

Fig.2 - Grazing incidence x-ray scattering profiles for the InAs wires grown on InP. A large anisotropy in strain relaxation can be observed for measurements on the two crystallographic directions.

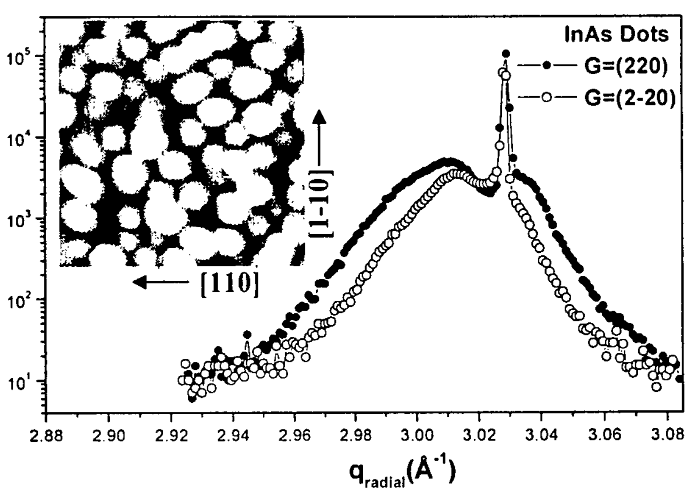

Fig.3 - Grazing incidence x-ray scattering profiles for the InAs dots grown on InP. The large anisotropy observed for the wires is no longer observed. Small differences between the two scans are associated to small InAs wires on the surface, in very low density.

Poster

ELECTRICAL PROPERTIES AND CARRIER TRANSPORT IN InAs/InP NANOSTRUCTURES

K.O.Vicaro[1], H.R.Gutiérrez[1], J.R.R.Bortoleto[1], F.Plentz[2], P.A.Schulz[1] and M.A.Cotta[1]
[1] UNICAMP, IFGW, CP 6165, 13081-790 Campinas, SP, Brazil.
[2] Univ.Fed.Minas Gerais., ICEx, DF, 30123-970, Belo Horizonte, MG, Brazil
E-mail: monica@ifi.unicamp.br

In this work we explore spatially-resolved electrical properties of InAs/InP semiconductor nanostructures, mainly wires and dots. For that we have used Kelvin-Probe microscopy (KP), conductive atomic force microscopy (C-AFM) as well as electron-beam litographically-processed devices in order to access the parallel conductance of the grown nanostructures. C-AFM provided current imaging measurements as well as I-V spectroscopy. The InAs/InP nanostructures were grown by Chemical Beam Epitaxy in the Stranski-Krastanov mode. All samples were n-type, non-intentionally doped. KP measurements on InAs films - few monolayers thick - grown on InP have shown that the position of the Fermi level is affected by the presence of the InAs film either on the top surface or under a thin InP layer. The evaluated Fermi level position is also influenced by the type of grown nanostructure (dots or wires). This result suggests a suppression of the depletion region, probably due to accumulation of carriers in the InAs structures. With C-AFM this assumption could be verified. We observed that InAs/InP dots and wires on the top surface of the sample present much larger electrical currents than the wetting layer. Spatial changes in this current are related to the electrical contact between the conductive tip and the nanostructure. I-V spectroscopy measurements show that the general electrical characteristic is that of a Schottky contact, due to oxidation by exposition to air. However, I-V curves show different threshold bias values when wetting layer, wires or dots are measured. Such values correlate well with the expected band gap energy for these nanostructures. On the other hand, e-beam lithography was used to fabricate a 400nm wide gap in between two metallic contacts on top of a 2-□m wide mesa with the InAs nanostructures. I-V curves from this ensemble of nanostructures present a large peak in conductance at ~0.15V, observable even at room temperature. These results are interpreted in terms of the carrier transport processes in the wire-dot-wire assembly in the sample.

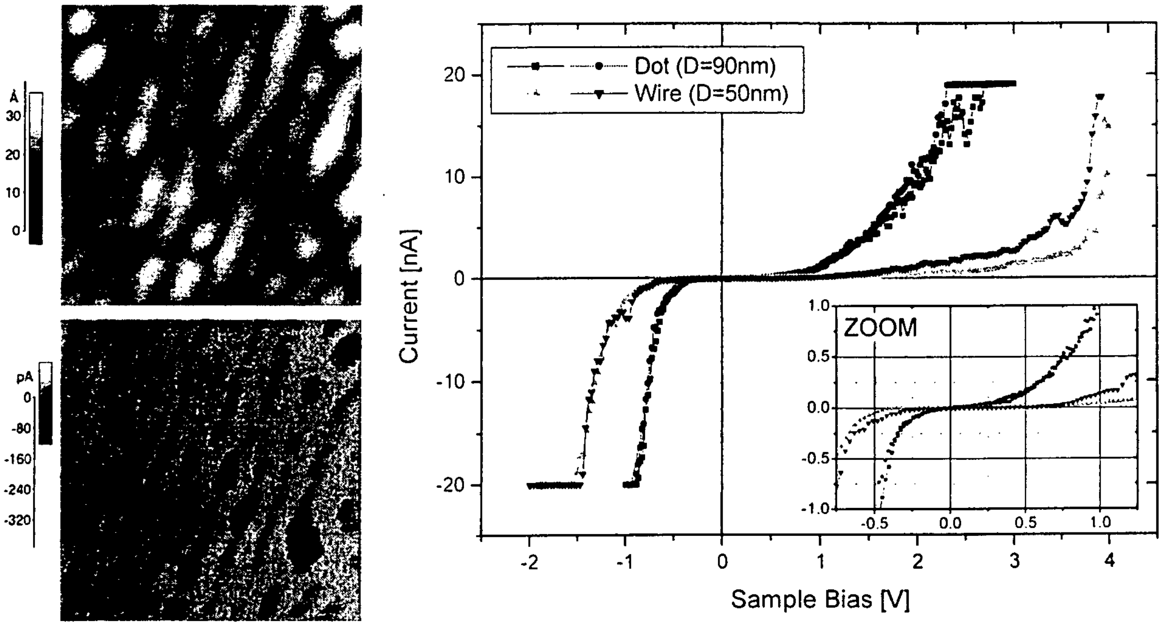

Fig.1 - (a) Topography and electrical (V_{sample} = -0.3V) AFM images of the InAs/InP sample showing wires and a few dots (scan size = 0.3μm); (b) C-AFM local IxV curves acquired on a wire and a dot with different lateral dimensions.

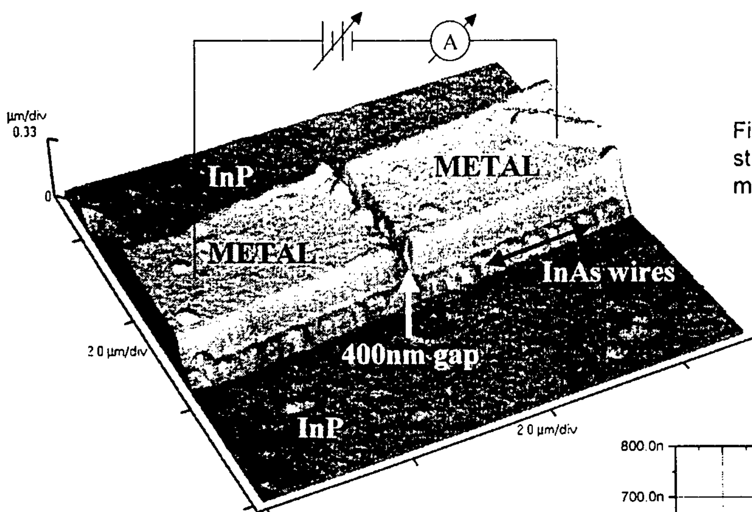

Fig.2 – Processed mesa structure for conductance measurements

Fig.3 – Voltage dependence of the conductance between the metal contacts for the sample with InAs wires and dots.

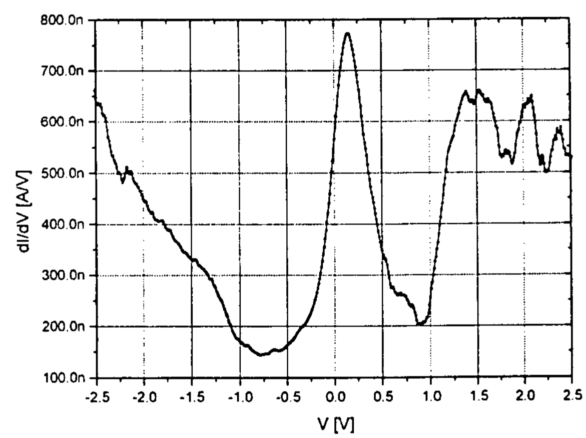

A TEM STUDY OF THE FORMATION OF NOBLE METAL NANOWIRES BY USING NANOSTRUCTURED MESOPOROUS SILICA TEMPLATES

Jordi Arbiol [♣,♠], Emma Rossinyol [♠], Andreu Cabot [♠], Francesca Peiró [♠], Albert Cornet, Joan Ramon Morante [♠], Fanglin Chen [♦] and Meilin Liu [♦]

[♣] SCT, Universitat de Barcelona, Lluís Solé i Sabarís, 1-3, E-08028 Barcelona,
E-mail: arbiol@giga.sct.ub.es
http://nun97.el.ub.es/~arbiol/

[♠] EME Enginyeria i Materials Electrònics, Departament d'Electrònica, Universitat de Barcelona, Martí i Franquès 1, E-08028 Barcelona.

[♦] School of Material Science and Engineering, Georgia Institute of Technology, Atlanta, GA 30332-0245, USA.

In this communication, we report our findings in mesoporous silica as nanostructured template for noble metal nanowire production. The development of catalytic systems by using nanostructured mesoporous materials is nowadays attracting much attention [1, 2]. The addition of noble metals in order to modify the base mesoporous materials characteristics has been shown to improve their physical and chemical properties [3, 4]. There are mainly three different kinds of mesoporous molecular sieves (MMS). The first one is the so-called M41S family of silica and aluminosilicates. The second one is the hexagonal mesoporous silica HMS and MSU families. The hexagonal SBA-15 materials exemplify the third family. Here we have selected the SBA-15 mesoporous silicas because they have long range order, large monodispersed mesopores and thicker walls, which make them more thermally and hydrothermally stable than previous materials. Moreover, by selecting the growth conditions we can determine the pore size of the mesoporous aggregates and therefore the final width of the obtained metal nanowires (from 3 to 10 nm).

SBA-15 mesoporous silica was synthesized following procedure reported by Zhao et al. [5] using Pluronic P123 triblock copolymer ($EO_{20}PO_{70}EO_{20}$). Metal additives were introduced into mesoporous silica by impregnation of the SBA-15 silica with 0.01M aqueous solution of palladium chloride, ammonium tetrachloroplatinate, potassium pentachlororuthenate and gold chloride hydrate, followed by slow evaporation of water. TEM was carried out using a Phillips CM30 SuperTwin electron microscope operated at 300 keV with 0.19 nm point resolution. For TEM observations, silica mesoporous powders were ultrasonically dispersed in n-Hexane and deposited on amorphous holey carbon membranes.

In the present work, we characterize and model SBA-15 mesoporic silicas loaded with Pt, Pd, Au and Ru. Depending on the impregnation conditions, these metals can be found deposited as nanoclusters on the surface of the mesoporous structure or included within the silica hexagonal pores (from nanoclusters to nanowires). In order to demonstrate that the nanowire formation occurs inside the pores of the mesoporous aggregates, we have performed a tomographic TEM study of the nanostructures, obtaining 3D reconstruction models. The proposed TEM analysis allows following the nanowire formation inside the tube. Once we have obtained the nanowires inside the pores, we are able to extract them by chemically attacking the SiO_2 mesopore walls and release the noble metal nanowires. The proposed methodology offers the possibility to obtain a wide range of metal nanowires (with lengths up to 1 micron) and moreover, select their widths (from 3 to 10 nm).

References:

[1] S. H. Joo, S. J. Choi, I. Oh, J. Kwak, Z. Liu, O. Terasaki and R. Ryoo, Nature, **412** (2001) 169.
[2] D. Trong, D. Desplantier-Giscard, C. Danumah and S. Kaliaguine, Appl. Catal. A, **222** (2001) 299.
[3] J. V. Ryan, A. D. Berry, M. L. Anderson, J. W. Long, R. M. Stroud, V. M. Cepak, V. M. Browning, D. R. Rolison and C. I. Merzbacher, Nature, **406** (2000) 169.
[4] J. Arbiol, A. Cabot, J. R. Morante, F. Chen, M. Liu, Appl. Phys. Lett., **81** (2002) 3449.
[5] D. Zhao, Q. Huo, J. Feng, B. F. Chmelka and G. D. Stucky, Science, **279** (1998) 548.

Figures:

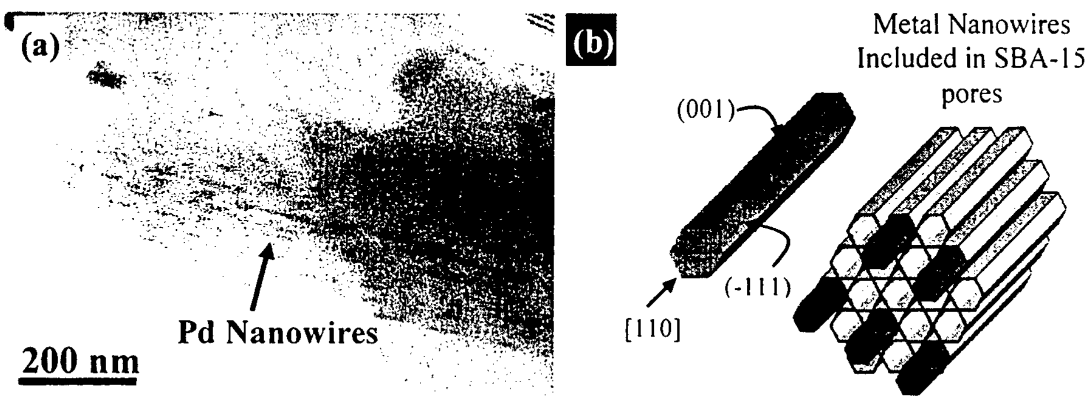

Fig. 1. (a) Bright field TEM view of a Pd modified mesoporous silica composite. Notice that there is Pd on the composite surface, and Pd that has been included inside the pores. **(b)** Pd modified mesoporous silica model with the palladium adopting non-regular hexagonal prism morphology.

MEASUREMENT OF ELASTICITY AND FRICTION USING ATOMIC-FORCE MICROSCOPE CANTILEVER TORSIONAL RESONANCE

M. Reinstädtler, A. Caron, U. Rabe, and W. Arnold

Shear stiffness and friction phenomena can be investigated by evaluating the torsional resonances of AFM cantilevers. The torsional resonances of the cantilevers are excited by a piezoelectric transducer placed below the sample which generates in-plane sample surface vibrations while the sensor tip is in contact with the sample. At low lateral surface vibration amplitudes the sensor tip remains in elastic contact with the sample surface, and the cantilever behaves like a linear oscillator with viscous damping and a certain set of resonances frequencies. If the surface vibration is increased above a critical amplitude, typically 0.2 nm, the maximum of the resonance curves does not increase any more and the curves develop a plateau at their highest amplitude. Numerical simulations of a corresponding nonlinear oscillator driven by a dry friction element produced curve shapes as in the experiment. This led us to the conclusion that the plateaus in the resonance curves indicate the onset of stick-slip in the relative tip-sample oscillation. This is confirmed by the fact that the critical surface amplitude increases with increasing static cantilever load. Furthermore, for a bare silicon sample it is higher than for lubricated silicon.

ON SUPERPARAMAGNETIC AND MAGNETIC CONTRIBUTIONS IN NANOCOMPOSITES

M. Chipara, D. Hui[1], S. M. Vilarino[1], S. Balascuta,
R. Skomski[2], D. Leslie Pelecky[2], A. Lau[3], M. Bubacz[1], J. Zhou[2], R. Artiaga[4], D. J. Sellmyer[2]

Indiana University Cyclotron Facility, Bloomington, IN 47408-1398, USA
[1]University of New Orleans, Department of Mechanical Engineering, LA, USA
e-mail: smartin1@uno.edu
[2]University of Nebraska, Department of Physics and Astronomy, Lincoln, NE 68503, USA.
[3]The Hong Kong Polytechnic University, Department of Mechanical Engineering, Hong Kong.
[4]University of La Coruna, EPS Ferrol Avda. Mendizábal, SPAIN.

Much research has been focused on nanocomposites obtained by dispersing magnetic nanoparticles within polymeric matrices. As most magnetic nanoparticles were obtained by energetic milling, a relatively broad distribution of particles size is expected. Most magnetic nanoparticles exhibit magnetic single domains. Nevertheless, when the size of magnetic particles is further decreased, the competition between thermal fluctuations and magnetic properties is modified up to a point where thermal fluctuations are sufficiently large to destroy the magnetic order and to impose superparamagnetic features. The deconvolution of superparamagnetic and magnetic contributions is extremely important for near future applications such as ultra high-density magnetic media.

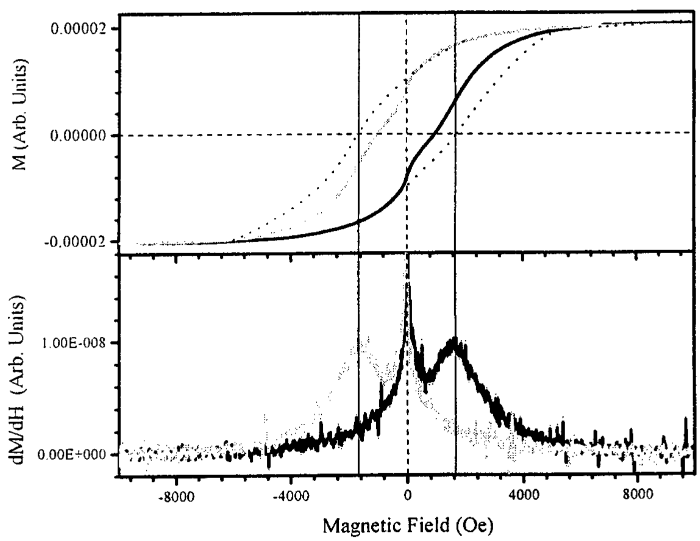

FIGURE 1.
TOP PANEL: The hysteresis loop of BaFe-SBS for the sample spun at 2500 rotations per minute (magnetic measurement in the parallel configuration).
BOTTOM PANEL: The first derivative of the hysteresis loop versus the applied magnetic field, for the sample spun at 2500 rotations per minute (magnetic measurement in the perpendicular configuration).

A method to deconvolute the superparamagnetic and magnetic contributions to the hysteresis loops is presented.

Composites have been obtained by dispersing barium ferrite (BaFe) nanometer sized magnetic nanoparticles into a dilute chloroform solution of poly(styrene-b-butadiene -b-styrene) (SBS) triblock copolymer. BaFe nanopar-ticles were introduced in a so-lution of 1% styrene-buta-diene-styrene copolymer in chloroform and sonicated in air at 50^0C for about 10 hours. Magnetic nanocomposite films were deposited on Si wafers by spin coating at various frequencies. After deposition, the samples were dried in vacuum at 50^0C for several days. Further details are given in [1]. The magnetic properties of BaFe-SBS films were measured

the Alternating Gradient Force Magnetometer (AGFM) in both parallel and perpendicular configurations. The inspection of hysteresis loops reveals slight distortions, at very small magnetic fields (see Figure 1). The first derivative of the hysteresis loop with respect to the magnetic field has been used to analyze more accurately these distortions. As shown in Figure 1, the dependence of the first derivative of the hysteresis loop on the external magnetic field presents two peaks, one located close to H=0 and the other at higher magnetic field. The location of the high field peak is close to the coercive field. The discrepancy between the position of this peak and the coercive field estimated from the hysteresis loop will be analyzed. From Figure 2 it is observed that by increasing the spinning frequency, the weight of the super paramagnetic peak is increased. This reflects the removal of the bulkier BaFe nanoparticles during the spinning process.

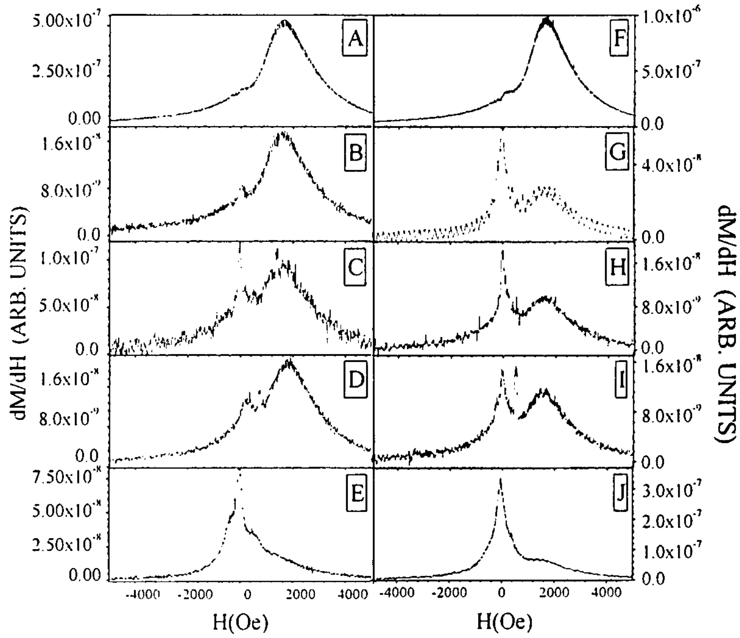

FIGURE 2.

LEFT PANEL
The first derivative of the hysteresis loop of BaFe-SBS for samples spun at various frequencies (magnetic measurement in the perpendicular configuration). A = 500 rotations/min, B = 750 rotations /min, C = 1000 rotations /min, D = 4000 rotations /min, and E=5000 rotations /min.

RIGHT PANEL
The first derivative of the hysteresis loop of BaFe-SBS for samples spun at various frequencies (magnetic measurement in the parallel configuration). F = 1000 rotations/min, G = 2500 rotations/min, H = 4000 rotations/min, I = 5000 rotations /min, and J = 7500 rotations /min

References

1. M. Chipara, D. Hui, J. Sankar, D. Leslie-Pelecky, A. Bender, L. Yue, R. Skomski, D. J. Sellmyer. On styrene-butadiene-styrene-barium ferrite nanocomposites, Composites B, to appear.

STUDY OF MAGNETIC NANOSTRUCTURES INDUCED BY ION BOMBARDMENT

A .Asenjo, E. Carrasco, O. Rodríguez de la Fuente, J.M. Rojo
Dpto. Física de Materiales, Universidad Complutense de Madrid, 28040 Madrid Spain
Email: aasenjo@icmm.csic.es

Recently, a great effort in the optimization of the nanofabrication methods is observed. The most extended technique is the lithography by UV light as well as by ion or electron beam. However, the techniques based on self-organized effects reveal as the most efficient method to obtain nanostructures in a large scale. In this sense, some good results have been obtained by using the growth of island in UHV [1] and ion irradiation in semiconductors [2,3] or metals [4,5]. In this work, we present a method for the production of magnetic nanostructures by ion bombardment of thin films. The change on topography and magnetic behavior [6,7] due to the irradiation with low energy ions at high dose [8] has been studied.

Amorphous CoCr thin films have been grown by sputtering onto glass. The roughness of the samples before ion erosion (Fig 1) is about 0.5nm (rms value measured from the Scanning Force Microscopy images). After exposing the thin films to low energy (1keV) Ar^+ ions, an increase in the roughness is observed. Figure 2 shows the height distribution plots obtained from the SFM data. The broadest distribution corresponds to the samples irradiated with highest flux and dose. Under certain irradiation conditions, the thin film evolves to a nanostructured surface (Fig 3). In this range of bombardment parameters, the size of the structures increases with the dose as shown in the PSD graphic (Power Spectra Density calculated from the Fast Fourier Transform) in Figure 4.

References:

[1] Z. Sefrioui, J.L. Menendez, E. Navarro, A. Cebollada, F. Briones, P. Crespo and A. Hernando, Phys. Rev. B **64** (2001) 224431

[2] S. Facsko, T. Dekorsy, C. Koerdt, C.Trappe, H. Kurz, A. Vogt, H.L. Hartnagel, Science, **285** (1999) 1551-1553

[3] R. Gago, L. Vázquez, R. Cuerno, M. Varela, C. Ballesteros, J. M. Albella, Appl. Phys. Lett., **78** (21) (2001) 3316-3318

[4] S. Rusponi, G. Costantini, C. Boragno, and U. Valbusa, Phys. Rev. Lett. **81**, (1998) 2735–2738

[5] O. Malis, J.M. Pomeroy, R.L. Headrick and J.D. Brock, Mat. Res. Soc. Symp, Vol 647, Materials Research Society, O9.5.1- O9.5.6 (2001).

[6] W.M. Kaminsky, G. A.C. Jones, N.K. Patel, W.E. Booij, M.G. Blamire, S.M. Gardiner, Y.B. Xu and J.A.C. Bland, Appl. Phys. Lett. **78** (11) (2001) 1589-1591

[7] T. Devolder, J. Ferré, C. Chappert, H. Bernas, J.P. Jamet and V. Mathet, Phys. Rev. B, **64**, (2001) 064415

[8]O. Rodríguez de la Fuente, M.A. González and J.M. Rojo, Phys. Rev. B, **63**, (2001) 085420

Figure 1

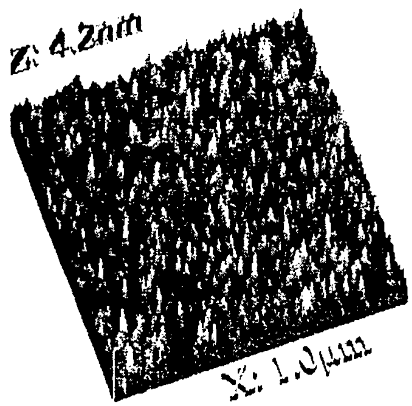

Figure 2

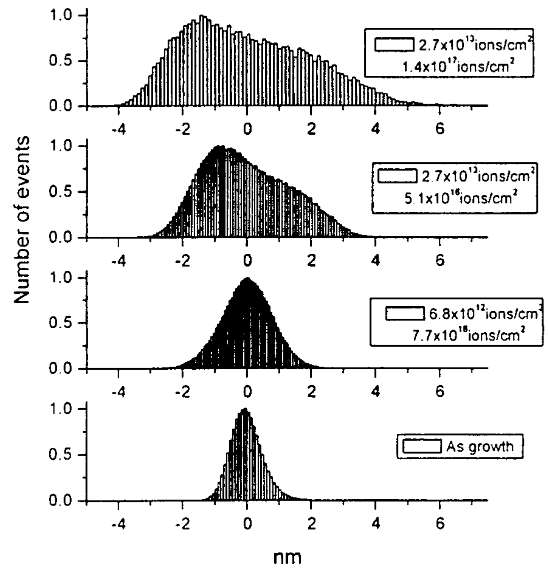

Figure 3

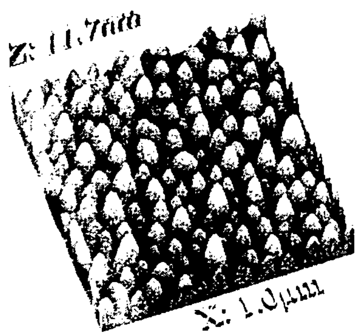

Figure 4

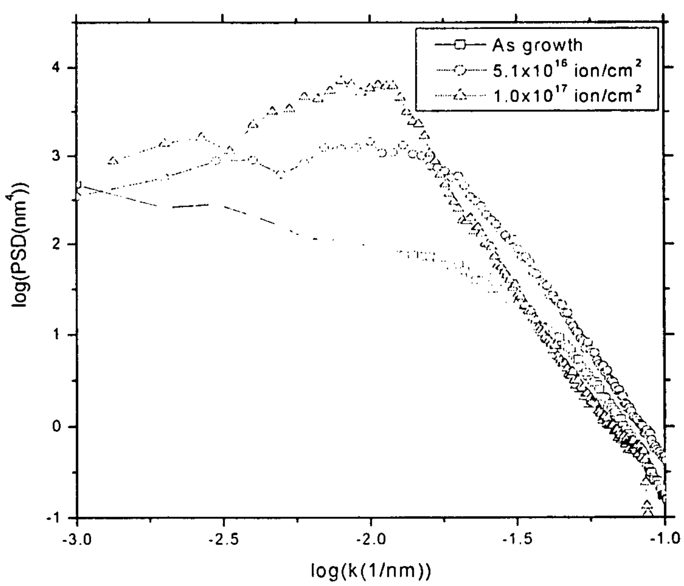

MOS NANOTRASISTOR MOBILITY MODELLING

Florin Babarada, Marcel D. Profirescu, Adrian Rusu
University "Politehnica" of Bucharest, Romania,
tel. : +4021 4113193, email: fbabarada@edil.pub.ro

The new challenge of Nanotechnology needs most precise models for active devices. From this point of view the design of linear analog circuits lacks models for state-of-the-art MOS transistors to accurately describe distortion effects. This is mainly due to inaccurate modelling of the mobility degradation effect i.e. the dependence of carrier mobility in the inversion layer on the normal electric field. A new mobility relation in agreement with experiment was obtained using quantum mechanical transport analysis.

Since the scaling down of MOS transistor dimensions is accompanied by a decrease in gate oxide thickness and an increase in substrate doping, the effective electric field may reach very high values in nanodevices and as a result the expression of carrier mobility $\mu = \frac{\mu_0}{1+\theta_\mu E_{eff}}$ (1) becomes inaccurate. μ_0 is the bulk mobility, θ_μ is an empirical parameter and the effective normal electric field $E_{eff} = -\frac{(Q_{dep}+\eta Q_{inv})}{\varepsilon_{Si}}$ (2); η is an empirical parameter which is taken to be 1/2 for electrons and 1/3 for holes. In strong inversion, neglecting the influence of drain voltage, $Q_{inv} = -C_{ox}(V_{GS}-V_T)$ and $Q_{dep} = -\gamma C_{ox}\sqrt{V_{SB}+\Phi_B}$ (3). The semi-empirical formulation (1) is still used to describe the mobility degradation effect in most state-of-the-art MOSFET models. Since mobility degradation is dependent on the normal electric field, it will particularly affect the higher-order derivatives of drain current to gate voltage $\frac{\partial I_D}{\partial V_{GS}}$ (g_m), $\frac{\partial^2 I_D}{\partial V_{GS}^2}$ (g_{m2}) and $\frac{\partial^3 I_D}{\partial V_{GS}^3}$ (g_{m3}). For a long-channel n-type transistor where the effect of mobility reduction is dominant this model cannot predict the zero-crossing in the third-order derivative and a better description of surface mobility is necessary.

The channel mobility must be treated quantum-mechanically because the thickness of the inversion layer is in the order of a few Å, smaller than the wavelength of carriers. Quantum-mechanical calculations show that energy subbands of electrons and holes are formed in different energy valleys. The spacing of these subbands increases with increasing normal electric field i. e. in the weak inversion region, where many subbands are occupied, quantum effects get washed out, but in the strong inversion region, where very few subbands are occupied, quantum effects become important. The high order derivatives (g_m), (g_{m2}) and (g_{m3}), shown in figure 1 has been calculated from the measured harmonics using the circuit from figure 2. Including Coulomb scattering, phonon scattering and surface roughness scattering mechanisms we obtained the following expression for mobility $\mu = \frac{\mu_0}{\theta_c + \theta_{ps}\sqrt{\theta_{ph} E_{eff}^{2/3} + \theta_{sr} E_{eff}^4}}$ (4). Using this mobility in the expression for the current we obtained a very good fit between experiment and modelling, (see figure 1).

In strong-inversion both hole and electron mobility is mainly limited by two scattering mechanisms: phonon scattering and surface roughness scattering, but they still exhibit a different dependence on the effective normal field E_{eff}. The results can be extended to short channel transistors, when the gate voltage dependency of series resistance can be also incorporated in the models. In order to minimize distortion in circuits, it is often important to make the third-order derivative zero. This is possible for long channel n-type MOS transistors, where mobility degradation is more dominant

than the effect of series resistance. The DC-biasing point for which g_{m3} becomes zero, is essentially determined by the presence of the E_{eff}^2 term and can be accurately predicted using equation (4).

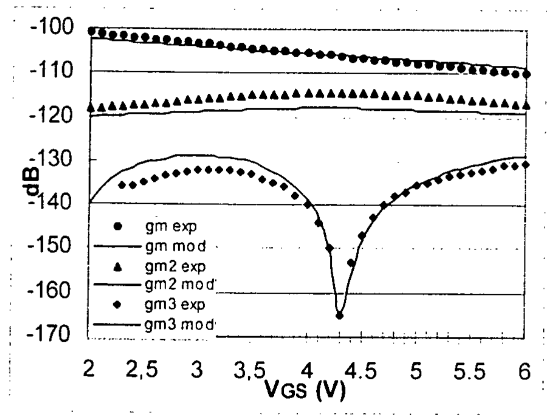

Figure 1. Measured (exp) and modelled (mod) values of (g_m), (g_{m2}) and (g_{m3}), versus V_{GS} for n-type transistor at V_{SB} = 0V using equation (4).

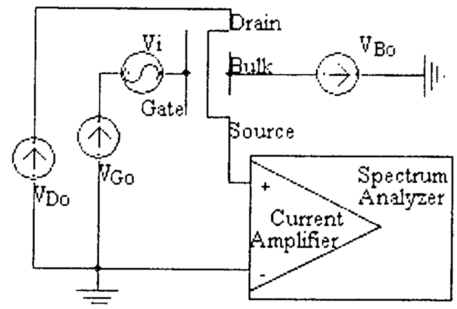

Figure 2. Circuit used for harmonics measurement

References:

[1] B.K. Ridley, "The Electron-Phonon Interaction in Quasi-Two-Dimensional Semiconductor Quantum-Well Structure", *Journal of Physics Part C: Solid State Physics*, Vol. 15, pp. 5899-5917, 1982.

[2] A.G. Sabinis and J. T. Clements, "Characterisation of the Electron Mobility in the Inverted <100> Si Surface", *IEDM Tech. Dig.*, pp. 18-21, 1979.

[3] J.R. Baker, *Fundamental Aspects of Quantum Transport*, In Handbook on Semiconductors (T.S. Moss Ed), Vol. 1. North-Holland, 1982.

[4] A. Rusu, "Toward a Demonstration of the Non-Linear Electrical Conduction Law", *International Semiconductor Conference*, pp. 421-424, Sinaia, 2001.

[5] W. Magnus, W. Schoenmaker, *Quantum Transport in Sub-Micron Devices,* Springer-Werlag, 2002.

[6] K. Ridley, *Quantum Processes in Semiconductors*, 3rd Ed, Calendon Press-Oxford, 1993.

[7] J.J. Liou, A. Ortez-Conde, F. Garcia-Sanchez, *Analysis and Design of MOSFETs, Modeling Simulation and Parameter Extraction,* Kluwer, 1998.

[8] M. Lundstrom, *Fundamentals of Carrier Transport*, Addison-Wesley, 1990.

[9] G Dima, G. Antonoiu, M. D. Profirescu – *Transport Parameters Extraction in Semiconductors Using Monte Carlo Method,* Printech, Bucharest, 1999.

[10] Y. Fu, M. Willander, *Physical Models of Semiconductor Quantum Devices*, Kluwer, 1999.

[11] D. Schroeder, *Modeling of Interface Carrier Transport for Device Simulation,* Springer-Verlag, 1994.

[12] P.J. Price, "Two-Dimensional Electron Transport in Semiconductor Layers", *Annals of Physics*, Vol. 133, pp. 217-239, 1981.

[13] F. Stern, and W.E. Howard, *Properties of Semiconductor Surface Inversion Layers in Electrical Quantum Limit*, Physical Review, Vol. 163, 1967.

[14] D.A. Neamen, *Electronic Circuit Analysis and Design*, Irwin, 1996

DESIGN AND DEVELOPMENT OF NANOSCALE SENSORS FOR ENHANCED MAGNETORESISTIVE RESPONSE

Ll. balcells[1,2], J.V. Anguita[1], Ll. Abad[2], V. Laukhin[2,3], J. Fontcuberta[2] and B. Martinez[2]

[1]Instituto de Microelectrónica de Madrid (CNM-CSIC),Isaac Newton 8-PTM, 28760 Tres Cantos, Spain.

[2]Institut de Ciència de Materials de Barcelona (ICMAB CSIC), Campus UAB, 08193 Bellaterra, Spain.

[3]Institució Catalana de Recerca i Estudis avançats (ICREA). Pg. Lluís Companys 23, 08010 Barcelona, Spain.

Magnetic and magnetoresistive sensor are widely used in different branches of today's technology covering from automotive to microelectronic applications. The fast development of these applications requires a continuous improvement of the performances of these devices. In this sense patterned magnetic nanostructures (PMN) represent a very interesting approach since their magnetoresistive response can be very different from that in thin film or bulk material. Magnetic domains in PMN can be precisely controlled by pattern's size and shape and, therefore the magnetoresistive response can be substantially improved with an appropriate design.

Different devices based on these PMN have already been tested in metals [(1)] but up to now no data have been reported in magnetic oxides. In this work we present the development of magnetic sensors based on PMN fabricated in fully spin polarized manganese oxide thin films ($La_{1-x}L_xMnO_3$, L=Ca, Sr). The design and sizes of the PMN sensors are have been selected to control the nucleation and number of magnetic domains in order to take advantages of the magnetoresistance generated by domain walls.

The fabrication of the PMN with different shapes (full squares, square frames) and sizes have been performed by using high-resolution e-beam lithography. The magnetotrasport properties of the different PMN are analyzed as a function of the size and aspect ratio.

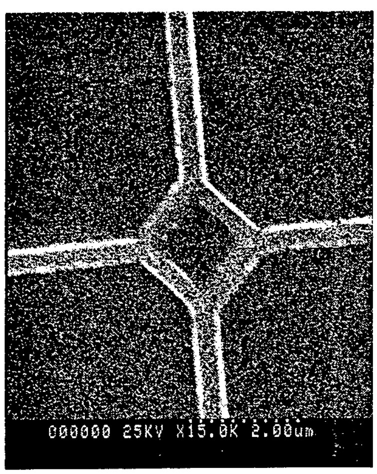

SEM image of a square frame sensor

(1) S.Y. Chou, proceedings of the IEEE, Vol. 85, 652 (1997)

INCOMPRESSIBLE STATES IN DOUBLE QUANTUM DOTS

N. Barberán and J. Soto

Dpto. ECM Facultadde Fisica, Universidad de Barcelona, Diagonal 647, 08028 Barcelona.

We study the incompresible states of vertically coupled quantum dots within the lowest Landau level regime by means of an exact diagonalization calculation. We identify the magic values of the total angular momentum M of incompressible states by the origin of the plateaux obtained in the Coulomb contribution to the total enery versus M. The full phase diagram driven by the inter-dot tuneling strength and the inter-dot distance shows hat the interplay of these two parameters determines transitions between incompressible and compressible states and between double quantum dots and two decoupled single quantum dots. We study different collective excitations over the filling factor equal to two ground states. The dipolar excitation allows us to consider the applicability of the Khon theorem to the case of a double quantum dot. The behaviour of the excitations that increse the angular momentum and simultaneously changes spin and parity shows that the canted state has short range order signaled by the magnetoroton type minimum in the dispersion relations of these modes.

COMPARATIVE STUDY OF FERROFLUIDS BASED ON DEXTRAN-COATED IRON OXIDE AND METAL NANOPARTICLES FOR CONTRAST AGENTS IN MAGNETIC RESONANT IMAGING

M.C. Bautista[1]*, O. Bomati-Miguel[1], X. Zhao[1], M.P. Morales[1], R. Pérez de Alejo[2], J. Ruiz-Cabello[2] and S. Veintemillas-Verdaguer[1]

[1]Instituto de Ciencia de Materiales de Madrid, CSIC, Cantoblanco, 28049-Madrid (Spain)

*E-mail: cbs@icmm.csic.es

[2]Universidad Complutense de Madrid, Unidad de RMN, Pº Juan XXIII 1, 28040-Madrid (Spain)

Colloidal suspensions of magnetic nanoparticles have found application in biomedicine as new contrast agents for Magnetic Resonant Imaging (MRI) [1]. The advantage of using this material showing superparamagnetic behaviour, is its higher registered signal at much lower doses than paramagnetic contrast agents such as gadolinium salts, avoiding secondary effects for the human body.

Commercial products are based on iron oxide nanoparticles obtained via precipitation in solution of iron salts and subsequent size selection process that leads to a uniform solid with particle sizes around 5 nm. Recently, a new synthesis process has been developed in our laboratory to produce magnetic nanoparticles by pyrolysis of iron pentacarbonyl solutions induced by laser [2]. This method allows the preparation of iron oxide and metal iron nanoparticles with sizes around 5 nm and a very narrow particle size distribution in a single step [2, 3].

In this work, colloidal suspensions of iron oxide and metal iron nanoparticles prepared by laser pyrolysis have been obtained by coating the particles with dextran in an aqueous media giving rise to biocompatible ferrofluids. The structural characteristics of the powders and the size of the aggregates in the colloidal suspensions have been analysed and correlated with the magnetic properties of both solids and fluids. For the first time up to our knowledge, a stable ferrofluid based on metal particles has been obtained with an aggregate size smaller than 100 nm and therefore with application in biomedicine (Fig. 1). The magnetic behaviour of this material in comparison to the iron oxide fluid and the commercial products shows a much higher saturation magnetisation (73 emu/g) and susceptibilities of the order of 4000 emu/gT (Fig. 2).

In addition, the MR response of the ferrofluids has been measured in order to gain information about the influence of the crystallochemical and magnetic properties on their relaxation behaviour. The main parameter affected by the presence of the magnetic nanoparticles is the transversal relaxation times T2 and the corresponding relaxivity R2 values are of the order of 50 $(\mathrm{mmol/l})^{-1}\mathrm{s}^{-1}$. From this study an evaluation of the possibilities of these materials as contrast agents for MR imaging has been estimated.

References

[1] A.E. Merbach and E. Tóth, *The chemistry of contrast agents in medical magnetic resonance imaging*. John Wiley & Sons, LTD, 2001, p 417.

[2] S. Veintemillas-Verdaguer, M.P. Morales and C.J. Serna, "Continuous production of γ-Fe_2O_3 ultrafine powders by laser pyrolysis", *Mater. Letters.*, vol. 35, pp. 227-231, 1998.

[3] S. Veintemillas-Verdaguer, O. Bomati-Miguel, M.P. Morales, P.E. Di. Nunzio and S. Martelli. "Iron ultrafine nanoparticles prepared by aerosol laser pyrolysis", *Mater. letter.*, vol. 57, pp. 1184-1189, 2003.

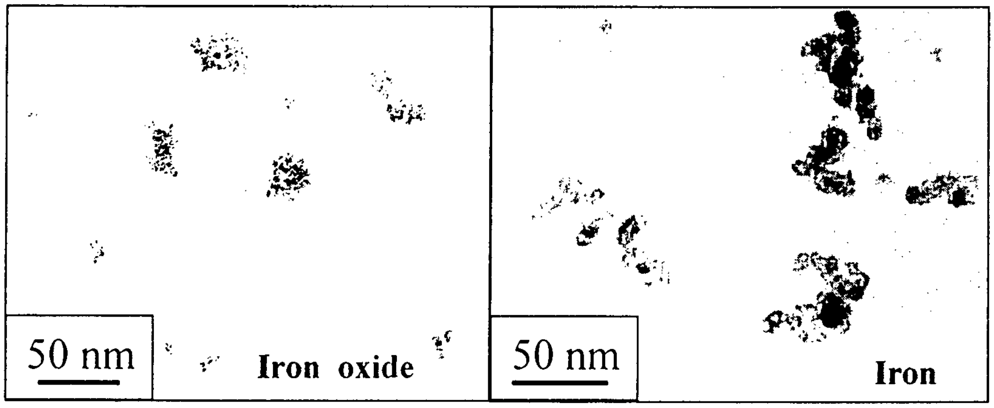

Fig. 1. TEM images of the dispersions of dextran-coated magnetic nanoparticles prepared by laser pyrolysis.

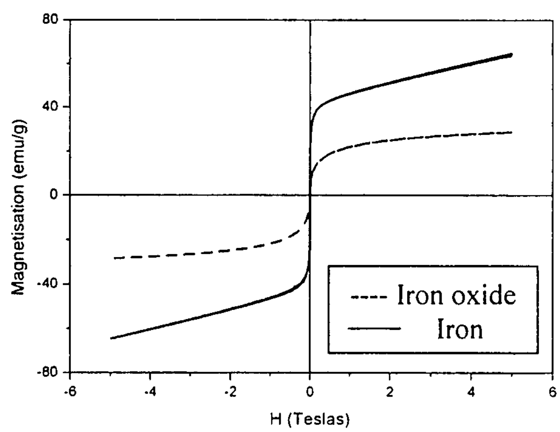

Fig. 2. Magnetic behaviour at room temperature of the colloidal dispersions.

NUCLEOBASE DERIVED MONOLAYERS OF CONJUGATED POLYMERS FOR NUCLEOTIDE RECOGNITION

Amir Berman and Chen Jie

Dept. of Biotechnology Engineering, and the Ilse Katz Center for Nano Scale Science and Technology, Ben-Gurion University, Beer-Sheva, Israel

E-mail: aberman@bgumail.bgu.ac.iul

Conjugated polydiacetylene Langmuir films with cytosine (PDC) headgroups at various surface dilutions are formed on aqueous solution in the presence or absence of the complementary nucleobase, Guanosine (G). A detailed study of the film organization in response to the PDC surface dilution is presented. At 2:1 dilution ratio the PDC/PDOH mixed film exhibit regular long-range linear arrangement.

Hybridization of the film with complementary short oligonucleotides yielded a supramolecular PDC/DNA assembly that is organized in long-range parallel order.

The polymer consist of combination of low band-gap conjugated polymer organic semiconductor with specific recognition sites at its surface. Binding of complementary DNA strand, induce conformational changes that are manifested in changes of the charge carrier properties as measured by conducting probe AFM on a local scale.

FORMATION AND CHARACTERIZATION OF GLUTAMATE DEHYDROGENASE MONOLAYERS ON SILICON SUPPORTS

L. Blasi*, L. Longo, P. Pompa, G. Ciccarella, G.Vasapollo, R. Cingolani and R.Rinaldi.

National Nanotechnology Laboratory of INFM c/o Department of Innovation Engineering, University of Lecce, Italy * E-mail address: laura.blasi@unile.it

Protein films on solid substrates are key components of molecular devices such as micro- and nano-biosensors and biocompatible materials. The development of enzyme-based biosensor requires, therefore, a detailed understanding of the protein immobilization process and of their possible conformational and functional changes.

Among several different fields in which biosensors can be usefully employed, monitoring the Glutamate concentration in solutions can have great importance, as Glutamate favors the transfer of amino groups among different amino acids [1], moreover, as Glutamate acts as excitatory neurotransmitter within the central nervous system, disruptions of its metabolism are related to other clinical disorders, including Alzheimer's disease and schizophrenia[2]. For these reasons, Glutamate Dehydrogenase (GDH) could have great importance, as GDH reversibly catalyzes the oxidative deamination of Glutamate to α-ketoglutarate and ammonia, GDH-based devices would allow to accurately monitorize the Glutamate concentration in solutions [3]. The enzyme monolayers were deposited on silicon supports by two different immobilization processes involving 3-aminopropyltriethoxysilane: the "three-step" (Fig. 1) and the "four-step" procedures (Fig. 2) based on the covalent binding of biomolecules . Detailed analyses were carried out to study conformational changes induced by the immobilization procedure on silicon supports using Atomic Force Microscopy (AFM), enzymatic assay, Fourier-transform infrared spectroscopy (FT-IR) and fluorescence spectroscopy.

Atomic Force Microscopy images of the "three-step" immobilization procedure revealed a protein film with a thickness of ~5 nm, which is consistent with the theoretical thickness of a structure involving one monolayer of Glutamate Dehydrogenase on top of the two preparatory layers (Fig.3), whereas in images of the surface derivatizated by the "four-step" procedure, only some significant structures (4.2 nm high and 80 nm wide) are visible, which can be assigned to monomolecular islands of protein (Fig.4).

The capability of the immobilized enzyme to retain its activity after repeated analyte exposure is very important for the exploitation of the devices; to this aim, we have measured the activity of immobilized GDH in our solid films. The immobilized enzyme with both procedures was assayed spectrophotometrically following the decrease in absorbance(A)of NADH at 340nm using the reversible reaction α-ketoglutarate $+NH_4^+$ +NADH $\leftrightarrow$ Glutamate + $NAD^+ + H_2O$. The reaction rate for the three-step immobilized enzyme is remarkably faster ($dA/dt = -1.67 \times 10^{-3} \pm 3 \times 10^{-5}$) than that characteristic of the spontaneous oxidation of NADH ($dA/dT = -4.04 \times 10^{-4} \pm 2.1 \times 10^{-5}$) [4], which is similar to the one of the four-step procedure ($dA/dt = -2.97 \times 10^{-4} \pm 1.5 \times 10^{-5}$ (Fig. 5).

In Fig. 6a the FT-IR spectrum of the immobilized GDH enzyme is compared to that of native GDH. Some of the absorption bands are peculiar of the Glutamate Dehydrogenase enzyme(the band around 3400/cm, 2960/cm, the two bands at 1700-1600/cm). We have applied FT-IR to the analysis of derivatized silicon surfaces before exposure to enzyme solution. Figure 6b compares the IR spectra of silicon surfaces derivatized by the three-step procedure before and after enzyme immobilization. Figure 6c shows the surface derivatized by the four-step procedure before and after enzyme immobilization. The typical bands of the GDH enzyme appear in the IR spectrum after the incubation in the enzyme solution of silicon surfaces derivatized by the three or four-step procedure. These data confirm the covalent linkage of the enzyme on the functionalised silicon surfaces for both immobilization procedures.

The emission spectrum is an important indicator of the integrity of the protein globular fold [5], hence, *Trp* photoluminescence represents an ideal tool for monitoring protein conformational changes and interactions with other molecules [6]. The photoluminescence of the enzyme immobilized by the three step-procedure exhibits a fluorescence spectrum identical to that of native GDH in buffer (λ_{max} = 340.5 nm), revealing that this kind of immobilization does not affect the fold pattern of the native enzyme (Fig.7). The same analyses were performed on the protein film obtained with the four-step procedure, without any detectable fluorescence .
Our results demonstrate that the binding through the "three step" procedure does not affect the fold pattern of the native enzyme, suggesting that this immobilization method could be suitable for the development of stable enzyme-based planar- biosensors.

References:

[1] Tatcher, B.J., Storey, K.B., Biochem. Cell Biol., **79** (2001) 11.
[2] Kelly, A., Stanley, C.A, Ment. Retard. Dev. Disabil. Res. Rev., **7** (2001) 287.
[3] Fisher, H.F., Methods Enzymol., **113** (1985) 16.
[4] Alivisatos, S.G.A., Ungar, F., Abraham, G.J. Biochemistry **12** 2616.
[5] Eftink, M.R., Methods Biochem. Anal. **35** (1991) 127.
[6]Chen, Y., Barkley, M.D., Biochemistry **37**(1998) 9976.

Fig. 1

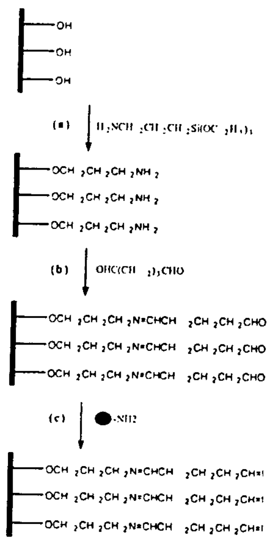

Fig. 2

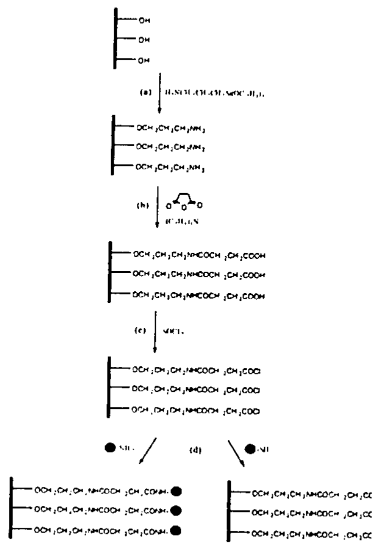

Fig. 3

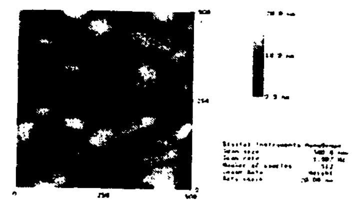

Fig. 4

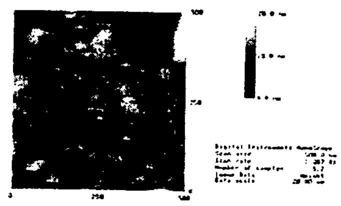

Fig. 7

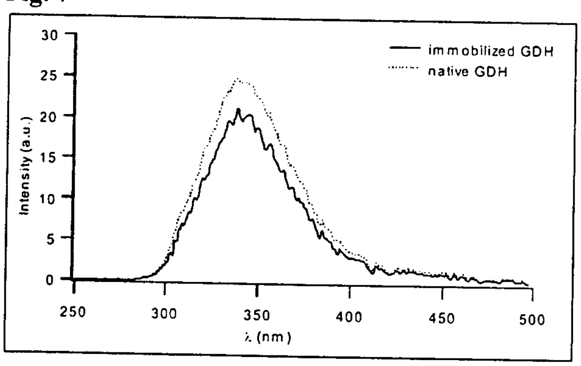

Fig. 6

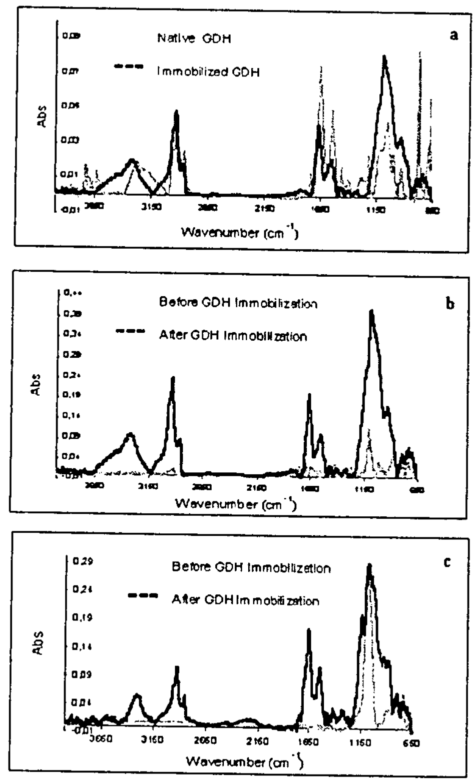

Fig. 5

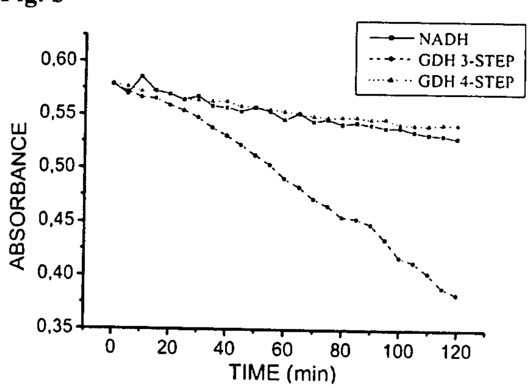

CHAOTIC BILLIARDS AS MODEL IN NANOTECHNOLOGY

Florentino Borondo, Rosa M. Benito and Diego Wisniacki
Dep. Química, C-IX; Universidad Autónoma de Madrid; Cantoblanco 28049, (Madrid), Spain
Dep. Física y Mecánica; ETSI Agrónomos, Universidad Politécnica de Madrid; 28040 (Madrid) Spain
E-mail: f.borondo@uam.es

There has been an increasing interest in the study of chaotic phenomena in recent years, both in dissipative and Hamiltonian systems. This phenomena are very important, among other areas, in the field of Nanotechnology. The transport of ballistic electrons in semiconductor heterostructures, experimentally analyzed recently [1], can be studied properly by means of quantum billiard models, using the methods of nonlinear dynamics [2].

Even though at classical level, there is a precise characterization of the relevant structures (for instance: atractors, stable and unstable manifold, periodic orbits, homoclinic points, entropies, Lyapunov exponents, etc.) at quantum level there is no equivalent knowledge. For this reason, some of the most active fields of research in quantum chaos are: quantum mechanical evolutions for long times, semiclassical evaluation of eigenenergies and eigenfunctions in terms of classical invariants, statistical study of fluctuations and parametric correlations of different properties of the system, or resummation techniques using symbolic dynamics, in order to treat divergent semiclassical trace formulae to eigenenergies, eigenfunction, and probability transitions.

These theoretical problems find an inmediate application in mesoscopic systems. As a matter of fact, it has been possible to make semiconductor submicron-sized structures such that the electron transport occurs in the ballistic regime [3]. Recent experiments have uncovered a variety of interesting transport anomalies all of which demonstrate the importance of the geometrical characteristics. These anomalies can be succesfully analyzed in terms of classical billiards ball models. However, at very low temperatures quantum interference effects become important, giving rise to large fluctuations in transport conductance, which can be analyzed within the semiclassical framework of chaotic scattering in quantum billiards [4].

In this contribution we will consider the phenomenon of probability localization through scarring of the wave functions in chaotic billiards. Scarring was brought to the attention of the scientific community by Heller [5], who provided the first explanation for their existence using wave packet dynamics. Since then, a lot of analytical work, numerical evidence, and experimental tests in a variety of systems have confirmed the existence and relevance od scarring.

Recently, we have taken a major step in this directions with the development of numerical techniques which allow the investigations of short time dynamics influeced by classical periodic orbits, and the phenomenology derived from it in chaotic billiards [6].

References:

[1] P.B. Fromhold et al., Nature **380**, 608 (1996); Y. Takagaki and K. H. Ploog, Phys. Rev. E **62**, 4804 (2000).
[2] A. J. Lichtenberg and M. A. Lieberman, *Regular and Chaotic Dynamics* (Springer-Verlag, Berlin 1992).
[3] C.M. Marcus et al, Phys. Rev. Lett. **69**, 506 (1992).
[4] B.D. Simons and B.L. Altshuler, Phys. Rev. Lett, **70**, 4063 (1993); A.D. Stone and H. Brus, Physica B 189, **43** (1993); H. Baranger, R. Jalabert and D. Stone, Chaos **3**, 665 (1993).
[5] E. Heller, Phys. Rev. Lett. **53** 1515 (1984).
[6] G.G. de Polavieja, F. Borondo and R.M. Benito, Phys. Rev. Lett. **73**, 1613 (1994); D. A. Wisniacki, F. Borondo, E.G. Vergini and .R.M. Benito, Phys. Rev. E **62**, R7583 (2000); *ibid* 63, 66220 (2001); *ibid* 67, xxxx (2003).

HYDROGEN ADSORPTION ON SINGLE WALL CARBON NANOTUBES

A.Ansón, M.A.Callejas, A.M.Benito, W.K.Maser, M.T.Martínez.
Instituto de Carboquímica, CSIC, C/ Miguel Luesma Castán, 4, 50018 Zaragoza, Spain.

None of the existing technologies for hydrogen storage fulfil the requirements for mobile applications and nanostructured carbons are being investigated as potential hydrogen adsorbents. Hydrogen adsorption in Carbon Nanotubes (CNTs) has been object of huge interest since they are light, hollow and porous systems that seem ideal candidates for hydrogen storage. Nevertheless there is a big controversy due to the dispersion of both theoretical and experimental studies

The determination of the hydrogen adsorption capacity for one well-characterized sample by using several measurement devices seems a good method to determine the real storage capacity on a given sample. It is very often difficult to find good correlation between adsorption data obtained by different measurement techniques for the same material. This fact probably contributes to the discrepancies around the real sorption capacity of a given carbon material.

Hydrogen adsorption data on as-grown and modified SWNTs in a volumetric equipment (Quantachrome Autosorb-1), in a gravimetric equipment (IGA-001) and by an electrochemical method are reported (see Table 1). SWNTs were produced by the arc-discharge method [1] with Ni 2 at.% and Y 0.5 at.% as catalysts. A range of hydrogen pressure up to 20 bar is covered, the adsorption data being far from the DOE target. It is interesting to note that the results here are compatible with other previous studies [2-5].

References

[1] Journet C., Maser W.K., Bernier P., Loiseau A., Lamy de la Chapelle M., Lefrant S., Deniard P., Lee R., Fischer J.E. Large-scale production of single-walled carbon nanotubes by the electric-arc technique. Nature 388 (1997) 756.

[2] R.Ströbel, L.Jörissen, T.Schliermann, V.Trapp, W.Schütz, K.Bohmhammel, G.Wolf, J.Garche. Hydrogen adsorption on carbon materials. Journal of Power Sources 84 (1999) 221-224.

[3] X.Chen, U.Dettlaff-Weglikowska, M.Haluska, M.Hulman, S.Roth, M.Hirscher and M.Becher. Pressure Isotherms of Hydrogen Adsorption in Carbon Nanostructures. Mat.Res.Soc.Symp.Proc. Vol. 796 (2002) Z9.11.1-6.

[4] A.Züttel, P.Sudan, PhMauron, T.Kiyobayashi, Ch.Emmenegger, L.Schlapbach. Hydrogen storage in carbon nanostructures. International Journal of Hydrogen Energy 27 (2002) 203-212.

[5] G.Gundiah, A.Govindaraj, N.Rajalakshmi, K.S.Dhathatheyan, C.N.R.Rao. Hydrogen storage in carbon nanotubes and related materials. J.Mat.Chem., 2003, 13, 209-213.

Table 1. Comparative data of hydrogen adsorption for as-grown (S205) and modified (S205+350) SWNTs obtained by the three measurement techniques presented in the text.

Measurement technique	Temperature	S205		S205+350	
		p [mbar]	Hydrogen wt%	p [mbar]	Hydrogen wt%
Autosorb-1	77 K	1023	0.317	1023	0.924
	298 K	931	0.008	1034	0.012
IGA	77 K	992	0.175	1001	0.811
		19993	0.670	19996	1.390
	298 K	993	0.025	1000	0.013
		19996	0.073	20001	0.100
Electrochemical	Room	Room	0.08	Room	0.28

OPTICAL RESPONSE OF nc-Si:Er THIN FILMS PRODUCED BY rf SPUTTERING AS A FUNCTION OF MICROSTRUCTURE

M.F. Cerqueira[1], M.V. Stepikhova[2], M. Losurdo[3], Teresa C. Monteiro[4], Isabel Gomes[1]
[1]Departamento de Física, Universidade do Minho, Campus de Gualtar 4710-057 Braga, Portugal.
[2]Institute for Physics of Microstructures RAS, 603600 Nizhnij Novgorod, GSP-105, Russia
[3]Plasma Chemistry Research Center, CNR, Via Orbona, 4, 70126 Bari, Italy
[4]Departamento de Física, Universidade de Aveiro, Campus de Santiago 3700 Aveiro, Portugal
Contact and presenting author: E-mail: fcerqueira@fisica.uminho.pt

Semiconductor nano-structures of typical size < 10*nm*, are of considerable current interest because of the new physics involved and the potentialities for device applications.
Erbium doped silicon (Si:Er) is a recognised candidate to become the material for emitters and detectors to be used in optical telecommunication systems. However, the efficiency of energy transfer from Si matrix to Er centres at operating temperatures and the problem related with the strong PL temperature quenching makes questionable the effectiveness of this system. As predicted, more perspective in this case would be the use of low dimensional Si structures, where the Si nano-crystallites can act as an active species for the excitation of rare earth ions. Studies of the photoluminescence of Er-doped nanocrystalline silicon films constitute an important probe for these applications.
In this contribution we show the ability to produce by the reactive magnetron sputtering method Er-doped nc-Si:H thin films emitting at room temperature.
Erbium doped nanocrystalline silicon thin films were produced by the reactive magnetron sputtering technique at fixed RF power, substrate temperature and gas mixture composition but varying bias conditions (grounded, and different negative bias). The samples have been studied by several techniques. For the structural characterisation we used X-ray in the grazing incidence geometry and Raman spectroscopy. The chemical studies were done using RBS technique. Spectroscopic ellipsometry (SE) has been combined with the previous techniques to resolve the film microstructure and composition. In particular, while XRD, Raman and RBS give averaged information on the crystallinity and films composition, successful supplementation by SE helps to resolve the films "anatomy". Thus, the distribution along the film thickness of the volume fractions of nanocrystalline/amorphous silicon and SiOx phases has been obtained. The effect of electric field applied during the growth on the crystal strain in films will be discussed based on the Raman scattering spectroscopy data.
Efficient photoluminescence has been observed in grown structures in both visible and 1.54μm wavelength regions, but the presence simultaneously of these two PL components, as determined and confirmed by TEM analysis, strongly depends on Si nanocrystals distribution in films. In this contribution we will discuss the Er-related photoluminescence as a function of the samples microstructure and strain effects. The luminescence analysis will be accomplished by the time resolved spectroscopy data obtained for the first time in these structures.

CONTROL OF NANOSIZE APERTURE USING PHYSICAL VAPOR DEPOSITION FOR NSOM APPLICATION

S.S. Choi[1*], J.T. Ok[1], C.K. Chun[1], D.W. Kim[1], J.W. Kim[2], J.H. Boo[2], J.S. Yang[3]

(1) Research Center for Nanoscience and Technology, Sun Moon University
Ahsan, ChungNam, 336-708, Korea.

(2) Department of Nanoscience, Sungkyunkwan University,
Suwon, Kyung Gi Do, Korea.

(3) Department of mechanical Engineering, Myoung Gi University
Yongin, Kyung Gi do, Korea

*E-mail address: sscphy@email.sunmoon.ac.kr, sscphy@empal.com

The subwavelength size silicon oxide aperture array as nearfield optical probe was successfully fabricated using semiconductor microfabrication techniques including anisotropic TMAH wet etching followed by stress-dependent oxidation and isotropic water-diluted HF solution. [1,2] Initially, the (5 x 5) □m^2 size patterns were fabricated on the silicon wafer followed by V-groove formation using alkaline solution Si bulk micromachining. The nanosize silicon oxide aperture array was revealed after the water diluted HF acid etching. The nano-size opening was carefully controlled with various water-diluted HF acid solution. The opening rate was varied from 22 nm/min to 28 nm/min. The oxide thickness at the apex of the oxide pyramid was estimated to 97 nm. This proves to be quite agreeable to the previous measurements by scanning electron microscopy. Finally, the Al thin metal film was coated on the nanosize oxide pyramid aperture. The diameters of the metal apertures less than 100 nm were formed using thermal evaporator deposition techniques. In order to better control the diameter of the oxide aperture, the deposition of Al/Ti thin films followed by reflow process will also be performed.

[1] S.S. Choi, M. Y. Jung, D. W. Kim, J.W. Kim, J.H. Boo, J. Vac. Sci. Technol. B21, 118(2003).

[2] Y. Mitsuhashi, Jpn. J. Appl. Phys. 37, 2079(1998).

MODELING OF THERMAL MAGNETISATION DECAY IN NANOSTRUCTURED MATERIALS FOR MAGNETIC RECORDING APPLICATIONS

O.Chubykalo and F.García Sánchez
Instituto de Ciencia de Materiales de Madrid, CSIC, Cantoblanco 28049, Madrid, SPAIN.
E-mail: oksana@icmm.csic.es

R.W.Chantrell
Seagate Research, 2403 Sydney Street, Pittsburgh, PA 15203-2116, USA, .
E-mail: roy.w.chantrell@seagate.com

One of the major limitations of the current magnetic recording media is the superparamagnetic effect[1)]. The constant increase of the recording density has lead to the situation when the grain size of the nanostructured conventional Co-based media is so small that its magnetization is unstable versus the thermal fluctuations. This has stimulated many researchers to search for alternative media among which one could mention perpendicular recording media, ac-coupled media or patterned media. Some hope is also related to recently discovered self-organized FePt particle arrays[2)]. One of the major techniques which could help to predict the thermal stability is the use of numerical techniques. Recently[3)], we have developed a numerical method capable to calculate long-time thermal magnetisation decay in a fully interacting system. Unlike many previously used method, it relies on the calculation of energy barriers separating different magnetisation states in a multidimensional space. Therefore, both magnetostatic and exchange magnetic interactions could be taken into account in a full manner and their influence on thermal magnetisation stability could be predicted. Metropolis Monte Carlo algorithm is used to define magnetisation pathes in a multidimensional space along which the energy barriers are determined. Consequent kinetic Monte Carlo algorithm samples the possible choise of the magnetisation trajectories.

We report the calculations of thermal stability in several model nanostructured systems simulating a) conventional longitudinal recording media.b) perpendicular media c) FePt particles arrays, with regular and post-annealed structures. Our main goal is to predict the influence of the interactions, mainly exchange on the thermal magnetisation decay. Traditionally, the exchange interactions are thought to deteriorate initially the signal-to-noise ratio, so that the conventional longitudinal media consists of columnar isolated Co grains with segregation of Cr which produces their isolation. The exchange interactions could possibly enforce the thermal stability, coupling the small grains together to produce a larger barrier for magnetisation reversal. Our results show that the untextured conventional longitudinal recording media is initially more stable in the presence of exchange interactions. At the same time, once started, the magnetisation decay is faster. In the perpendicular recording media, which is highly textured, some stability may be achieved in the presence of exchange.

1) D.Weller and A.Moser, IEEE Trans Magn **35** (1999) 4423
2) S.Sun, C.B.Murray, D.Weller, L.Folks and A.Moser, Science **287** (2000) 1989
3) O.Chubykalo and R.W.Chantrell, to be published

PROPERTIES OF ZnO THIN FILMS GROWN BY USING A CHEMICAL SOLUTION DEPOSITION PROCESS

Gabriela Ciobanu, Gabriela Cârjă
The "Gh. Asachi" Technical University, Faculty of Industrial Chemistry,
Bd. D. Mangeron 71, 6600, Iaşi, Romania
E-mail: gciobanu03@yahoo.co.uk

Transparent conductive oxide films that are both transparent in the visible region and electrically conducting have been studied widely in the last years as a results of their extensive applications in optoelectronic devices. This includes energy efficient windows, burglar alarms and windows heaters, as well as electrodes for solar cells and especially for flat panel display such as liquid crystal displays, plasma display panels, field emission, etc [1].

Zinc oxide has been receiving much attention in recent years due to its many technological applications. The optical transmittance of ZnO thin films in the UV, VIS and NIR ranges and electrical conductivity are both shown to be high [2]. Consequently, these films have a wide variety of applications, such as surface acoustic wave, bandpass filters, optical waveguides, and laser deflectors using piezoelectric or piezooptic [3,4]. Also, they are used as transparent conducting oxide coatings, gas sensors and varistors [5].

Thin granular ZnO films can be produced through various physical and chemical methods, as it follows: the chemical precipitation in streams at air pressure, the chemical precipitation from stream at low pressure of the organo-mettallic compounds, the reactive precipitation with ionic beam, the reactive thermal evaporation, cathodic spraying of magnetron type in continuos or alternative current, cathodic microwave spraying, deposition through shock waves in conic configuration, cyclotronic resonance of electrons in oxygen plasma etc [6-9].

There is growing interest in developing techniques for preparing ultrathin semiconductor nanoparticle films. This work is motivated by the size-dependent electronic and optical properties of semiconductors, which lead to a range of potential applications in electronic and optoelectronic devices, solar cells, photoelectrodes, photocatalysts, and sensors. The wet chemical syntheses of ultrathin semiconductor films represent a simple and inexpensive alternative to more technologically demanding chemical vapor deposition and physical techniques. The precise control of film thickness, crystallinity, and morphology are significant problems to be overcome in wet chemical synthesis.

This paper presents a chemical method for production of thin granular ZnO films through chemical precipitation technique. The method consists in obtaining thin granular ZnO film (about 300-500 nm in thickness) by thermal decomposition of zinc hydroxide, $Zn(OH)_2$, the ε-orthorhombic form, formed as a consequence of precipitating from alkaline solution of zinc acetate, in presence of ethylenediamine on a solid support (glass, i.e.). Utilization of this method implies investment economies, simplicity as work technique and the final production of some good quality thin ZnO films with many practical applications.

The ZnO films were characterized for surface morphology and crystallinity by scanning electron microscopy (SEM) and x-ray diffractometry (XRD), respectively. Optical transmission through the films was measured in the wavelength range 300-1000 nm by means of a spectrophotometer. The optical energy gap was estimated by extrapolating the square of the absorption coefficient versus the wavelength energy. The electrical conductivity was measured by the van der Pauw method.

The SEM micrographs (Fig.1) of the ZnO samples reveal existence of regular-shaped crystals (i.e., "coral" shaped crystals with rotation elements that develop themselves from a central spherical nucleus) about 0.28–0.83 μm.

The XRD patterns for the pure ZnO samples points out only the reflection maximum characteristic to ZnO. X-ray diffraction analysis indicates that the crystallites of ZnO films are preferentially oriented along the c-axis, [002] direction of the hexagonal crystal structure.

The ZnO thin films are transparent (90 % optical transmittance) in the near UV, VIS and near IR ranges. These films have a band gap of 3.20-3.25 eV; these values are smaller than E_g of 3.35 eV found for bulk crystalline ZnO, but are close to another values in literature for ZnO films. The electrical conductivity of ZnO films increases with film thickness. Measurements of the activation energy show that ZnO films have one donor level around 50 meV under the conduction band and another at 150 meV below the conduction band.

References:

[1] M. Chen, Z.L. Pei, X. Wang, Y.H. Yu, X.H. Liu, C. Sun, L.S. Wen, J. Phys. D: Appl. Phys., **33** (2000) 253.
[2] K.L. Chopra, S. Major, D.K. Pandya, Thin Solid Films, **102** (1983) 1.
[3] A. Maldonado, M dela L. Olvera, R. Asomuza, S. Tirado-Guerra, J. Vac. Sci. Technol. A, **18 (5)** (2000) 2098.
[4] M. Kadota, Jpn. J. Appl. Phys., **36** (1997) 3076.
[5] D.R. Clarke, J. Am. Ceram. Soc., **82** (1999) 485.
[6] A.E. Jienenz-Gonzales, J.A.S. Urueta, R. Suarez-Parra, J. Cryst. Growth, **192** (1998) 430.
[7] D. Shimoto, S. Tanaka, T. Torikai, T. Watari, M. Murano, J. Ceram. Process. Res., **2 (4)** (2001) 184.
[8] N.I. Kovtyukhova, E.V. Buzaneva, C.C. Waraksa, B.R. Martin, T.E. Mallouk, Chem. Mater., **12** (2000) 383.
[9] S. Roy, S. Basu, Bull. Mater. Sci., **25 (6)** (2002) 513.

Figures:

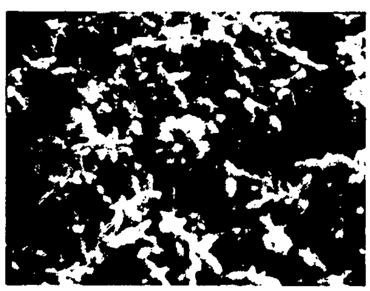

Fig.1. SEM micrograph taken on the surface of ZnO film prepared by chemical precipitation technique

TEMPLATED GROWTH OF CARBON NANOTUBES IN COBALT SUBSTITUTED MCM-41

Dragos Ciuparu, Sangyun Lim, Yuan Chen, David Harding, Gary Haller, Lisa Pfefferle
Yale University, Department of Chemical Engineering, New Haven, CT 06520.
E-mail: dragos.ciuparu@yale.edu

Current nanotube synthesis methods produce nanotubes of a wide range of sozes and structures. Separation of the desired tubes from a complex mixture, followed by alignment is required for their use in electronic applications. An important development is the use of zeolite channels as templates to synthesize uniform SWNT [1-3]. An intriguing finding from this zeolite work is that interactions with the channel walls during nanotube formation were observed to lead to selection of a particular nanotube form [3]. This is extremely important if control could be achieved for a range of diameters. Zeolites, however, are not an ideal choice for a SWNT template because of their lack of pore size flexibility. The ideal template material should allow control of both composition and channel size because, if they can be varied independently, selective growth of specific forms of metallic or semiconducting SWNT could possibly be achieved.

Our strategy is to synthesize carbon nanotubes inside the pores of MCM-41 mesoporous molecular sieves (MPMS) having a parallel system of pores uniform in size and structure. Transition metal catalysts are incorporated into the pore walls of the MPMS template stabilizing dispersed catalytic sites. MPMS templates with metals incorporated in the framework exhibit good structural stability. Thus, a critical feature of our work is the ability to control the pore size and topology of the MPMS template independent of its chemical composition. This is important because the proximity/nature of nucleation sites in a pore may affect carbon nanotube structure. The catalytic site for carbon nanotube synthesis is provided by framework substitution with cobalt. In the work reported here carbon nanotubes were grown using CO disproportionation. The results reported here demonstrate that aligned, uniform carbon nanotube synthesis can be engineered using MPMS templates with pore diameters of 2 to 4 nm. The optimal reaction temperature was found to be 1025K.

We have used a MCM-41 template substituted with Co (0.66 wt%). Physisorption data was collected on a freshly calcined sample, on the carbon loaded template and after the carbon was removed. Pore spacing was determined by XRD. The pore size of the catalytic template was about 2.8 +/- 0.1 nm (FWHM) with a wall thickness of 0.9 nm. The template structure was stable under the reaction conditions used and the pore size distribution was insignificantly affected by carbon deposition and removal.

Pretreatment involving partial reduction was important to good selectivity. The catalyst was exposed to pure hydrogen during heating from room temperature to 775K at 20K/min and held at 775K for 5 minutes. Subsequently the reactor was purged with Ar for 30 minutes, heated to 1025K in Ar and then exposed to pure CO flow for 4 hours. After carbon deposition the catalyst was purged for 15 minutes with Ar to flush the remaining CO from the reactor and then cooled in flowing Ar to room temperature.

Carbon on the samples was characterized by a variety of techniques including nitrogen physisorption, transmission electron microscopy (TEM), UV-vis, near-IR and Raman spectroscopy.

After the reaction protocol for CO disproportionation described above the TEM images (Fig.1), NIR and Raman (Fig.2) spectra indicate the presence of SWNT showing a narrow diameter distribution. An interesting observation is that SWNT prepared and left in the template can be directly analyzed using NIR spectroscopy in a variety of configurations (diffuse-reflectance or transmission), whereas standard purified samples obtained from other sources could not be identified likely due to the high density of defects and oxygen adsorption. Raman spectra recorded at different excitation wavelengths with samples before any cleaning or purification showed almost no signal in the D-band region characteristic for disordered carbon, confirming the high quality of the SWNT produced.

The results presented here suggest that MPMS templates with metals incorporated in the framework exhibit good structural stability and can be used for growth of ordered SWNT of uniform size and structure at yields and selectivity promising for large scale applications. Synthesis selectivity is enhanced by the partial reduction of the template catalyst. We will also present our most recent results on the synthesis of pure boron nanotubes.

References:

[1] Z.K. Tang, H.D. Sun, J. Wang, et al., *Bulletin of Materials Science*, **22**(3): 329 (1999).
[2] K. Mukhopadhyay, A. Koshio, N. Tanaka, et al., *Japanese Journal of Applied Physics, Part 2: Letters*, **37**(10B): L1257 (1998).
[3] H.D. Sun, Z.K. Tang, J. Chen, et al., *Applied Physics A: Materials Science & Processing*, **69**(4): 381 (1999).

Figures:

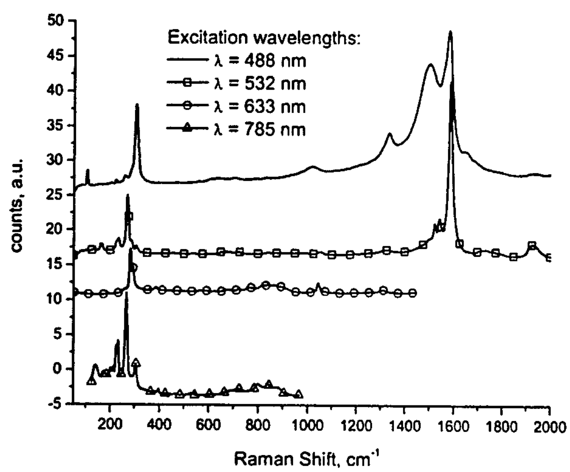

Figure 1. Raman spectra recorded for unpurified SWNT samples in template

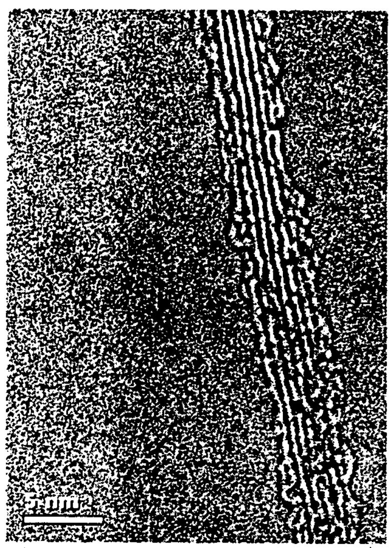

Figure 2. High resolution TEM image of a templated synthesized and purified SWNT

PATTERNING OF SOLID SURFACES BY UV AND PLASMA ETCHING OF ALKYL AND THIOALKYL SILANE MONOLAYERS – AFM, CONTACT ANGLE AND SPECTROSCOPIC STUDIES

J. Cohen, S. Botbol, R. Golan, J. Jopp, Y. Golan, S. Efrima
The Ilse Katz Center for Meso and Nano Scale Science and Technology, Ben-Gurion University, Beer-Sheva, Israel
E-mail: jcohen@bgumail.bgu.ac.il

Patterning of semiconductor, metal and insulator surfaces is of recent prime interest in nano-science and technology. We present a comparative study of the micro-scale patterning of GaAs, glass and mica substrates by alkyl- and thioalkyl- silane monolayers, using either UV or plasma etching. In the first step the silanes adsorb onto the initially oxidized and hydrophilic surfaces via the silane group, probably with a concomitant lateral polymerization. Then, under a mask, regions of the monolayer are stripped off by ozone etching, and different monolayers are deposited in the exposed areas. Alternatively, UV radiation is used to convert the "dangling", moderately hydrophobic thiol groups (of the adsorbed thioalkylsilanes) into hydrophilic sulfonate functionalities (usually going through an intermediate methyl thioester).[1] Decoration of the thiolated regions with silver colloids enables a clear imaging of the surface patterns with AFM. Static and dynamic measurements of contact angles prior and succeeding the various stages of treatment, AFM force mapping, and XPS are utilized to characterize the films and the patterns.

Figure 1 shows a force mapping (Force Volume mode of a Dimension 3100 Digital Instruments Scanning Probe Microscope) of a clean glass substrate (contact angle ~10-20^o) initially treated with octylsilane (contact angle ~78±2^o) and then one half was exposed to ozone (UVOCS ozone cleaning system) for 15 min. The treated and non-treated areas clearly show vastly different forces, demonstrating the effectiveness of the stripping by the plasma, and the narrow transition region (~10μm).

Treating glass with a thioalkyl silane changes the contact angle from 10-12^o to 58±5^o. Next we form the respective methyl ester by reaction with acetylchloride, resulting in a contact angle of 67±5^o. Finally, UV (254nm) light photofragments the adsorbed molecules, forming probably sulfonates (contact angle 30±8^o). The contact angles confirm the changes in the chemical identity of the exterior of the adsorbed monolayer.

Figure 2 shows the AFM image of a mica substrate treated with thiopropylsilane onto which silver colloids were deposited. Even after washing and treatment in an ultrasonic cleaner, the ~10nm silver particles adhere to the surface, suggesting a strong bond to the thiol groups. This demonstrates that the thioalkylsilane adsorbs to the mica via the silane group, leaving the thiol free to react. Notice the better resolution observed in the phase contrast.

Figure 3 shows the same thiolpropylsilane treatment followed by silver colloid deposition on a GaAs substrate. Once again the silver particles seem to adsorb to the surface, indicating that also for GaAs the adsorption of the thiolpropylsilane is most probably via the silane group (attaching to the native oxide on the solid). Treating GaAs with a thioalkyl silane changes the contact angle from 10-12^o to 53^o. The latter angle is the same as that obtained on glass, strongly suggesting a similar structure of the monolayer. Similarly, adsorbing octylsilane to GaAs gives a contact angle of 82^o, again in good correspondence to the observation on glass.

In summary, we study here various aspects of monolayer formation on GaAs as compared to glass and mica, with the intention of developing new patterning methodologies.

References:

[1] R. J.Collins and C. N. Sukenik, *Langmuir* **1995**, 11, 2322-2324.

Figures:

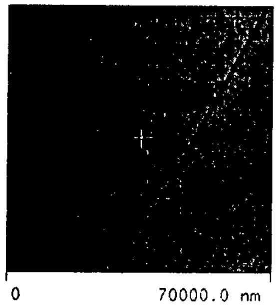

Fig. 1. Force mapping of an alkylsilanized glass after ozone treatment of the right lower side. The black line is a free-hand mark of the transition region between the plasma-treated and non-treated sides.

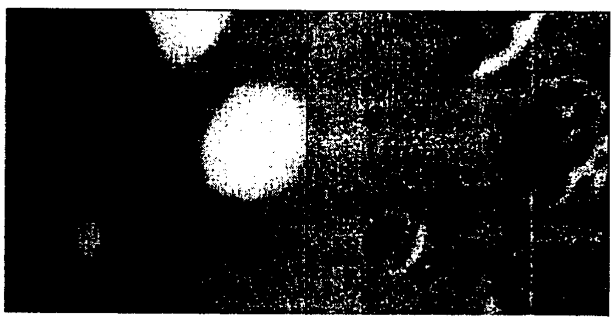

Fig. 2. AFM tapping mode image of a thiopropylsilanized mica substrate with silver colloids deposited onto it (Height contrast – left, Phase contrast – right). 122nmx122nm area. Maximum height scale is 5nm.

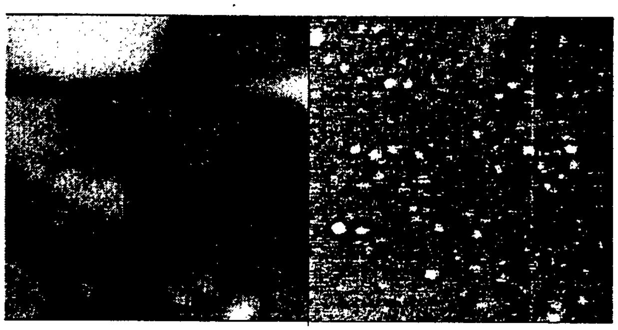

Fig. 3. AFM tapping mode image of a thiopropylsilanized GaAs substrate with silver colloids deposited onto it (Height contrast – left, Phase contrast – right). 250nmx250nm area. Maximum height scale is 10nm.

LANGMUIR-SCHÄFER FILMS OF BIS Zn-ETHANE-BRIDGED PORPHYRINS DIMER: SPECTROSCOPICAL, PHOTOCHEMICAL AND MORPHOLOGICAL PROPERTIES

S. Conoci[a], S.Coffa[a], B.Pignataro[b], S. Sortino[b], R.Tafuro[c], L. Valli[c], V.V. Borovkov[d] and Y.Inoue[d]

[a] Softcomputing Si-optics & Post Silicon Technologies Corporate R&D, ST Microelectronics, Stradale Primosole 50, I-95125 Catania, Italy. E-mail: sabrina.conoci@st.com

[b] Dipartimento di Scienze Chimiche,Università di Catania, Viale A. Doria 95125 Catania, Italy

[c]Dipartimento Ingegneria dell'Innovazione,Università di Lecce, Via Monteroni 73100 Lecce, Italy

[d]Inoue Photochirogenesis Project, ERATO, JST, 4-6-3, Kamishinden, Toyonaka-shi, Osaka 560-0085, Japan

The last years have witnessed increasing interest on porphyrins thin films. These systems are indeed extremely versatile for a large variety of applications in many fields of technological interest encompassing photoconductors, optical actuators, switches and chemical-sensors [1].

Bis-zinc ethane-bridged porphyrin dimer (**1**) has showed unique temperature and solvent dependent *syn-anti* conformational switching proprieties in solution [2,3]making these compounds promising candidates for optical switches and sensors applications. In this work, we report the results of our recent investigation focused on the spectroscopic, photochemical and morphological features of Langmuir-Shaefer (LS) films of **1**.

Thin films (1-24 layers) of **1** have been then transferred on solid surfaces, by LS method (horizontal lifting). The combination of UV-Vis spectra of these films with the limiting area extrapolated by the isotherm curve, provided significant indication concerning the conformation adopted by **1** in the films. Laser flash photolysis measurements addressed to point out the excited triplet state of **1** did not show significant transient signals. This might be due to rapid triplet-triplet annihilation processes that govern the fate of the excited porphyrins in the closed packed LS structure. In order to circumvent this problem, we moved to a second strategy namely the study of LS films obtained by transferring of mixed porphyrin/arachidic acid monolayers. In this case, we were able to record a transient spectrum with an absorption maximum centered at ca. 500 nm and safely attributable to the triplet state of **1**. The decay of this species was mono-exponential with a rate constant $k_1 = 1.6x10^5\ s^{-1}$ and no new transient was generated concurrently. Finally, the overall spectroscopical and photochemical proprieties have been tentatively correlated with the films morphology inspected by Scanning Force Microscopy.

References:

[1] F.Kampas, K.Yamashita, J.Fajer, Nature, 1980, 284, 40; R.Jones, R.H.Tredgold, A.Hoorfar, Thin Solid Films, 1985, 123, 307; R.B.Beswick, C.W. Pitt, Chem.Phys. Lett., 1988, 143, 589; M.Vandevyver , Thin Solid Films, 1992, 210, 240; N.A.Rakow, K.S.Suslick, Nature 2000, 406, 710.
[2] V.V.Borovkov, J.M.Lintuluoto and Y. Inoue, J.Phys.Chem.B, 1999, 103, 5151-5156.
[3] V.V.Borovkov, J.M.Lintuluoto, M. Fujiki and Y. Inoue, J.Am.Chem.Soc., 2000, 122, 4403-4407.

Figures:

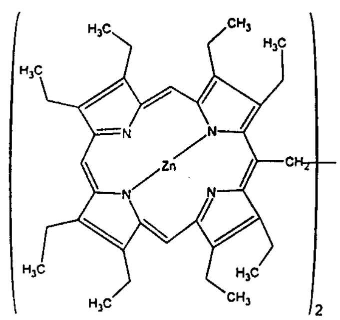

Figure 1. Bis-zinc ethane-bridged porphyrin dimer (**1**) molecular structure

ZEOLITE MICROMEMBRANES

Ester Mateo[a], Ruth Lahoz[b], Xermán de la Fuente[b], Andrés Paniagua[c], Joaquín Coronas[a,*] and Jesús Santamaría[a]
[a]Department of Chemical and Environmental Engineering, University of Zaragoza, 50009 Zaragoza, Spain, coronas@unizar.es
[b]Institute of Material Science of Aragón, CSIC-University of Zaragoza, 50018 Zaragoza, Spain
[c]Department of Earth Sciences, University of Zaragoza, 50009 Zaragoza, Spain

Zeolites are silicate or aluminosilicate crystalline materials with a very regular and microporous structure (pore size from 0.3 to almost 1.2 nm). During the last 50 years, zeolite have found massive industrial applications as adsorbents, ion exchangers and catalysts. New applications of zeolites and related microporous and mesoporosus materials are leading to new generations of catalysts [1], membranes [2] and membrane reactors [3] and now, very recently, to sensors [4] and reaction and separation microdevices [5]. On the other hand, "lab-on-a-chip" is becoming an increasingly familiar concept to express the miniaturization of chemical, biological and biomechanical analyses [6]. A lab-on-a-chip system can be viewed as a scaled-down analog of a chemical processing plant, because many process functions are similar, in which a drastic reduction of reactants consumption is achieved. The base of the success of such as microdevices is the selectivity of the reaction and separation steps (and even their integration in only one step) involved in a given process. Eventually, this means the preparation of thin films or membranes with the desired active material, a zeolite, for instance.

Most of the zeolite membranes reported in the literature are of the MFI type, which include silicalite and ZSM-5 [2,7]. A wide variety of synthesis methods of zeolite layers have been reported: mainly, the liquid phase hydrothermal synthesis, the dry gel method and the secondary (seeded) growth. Even talking about the same zeolitic phase, the synthesis method and the corresponding conditions influence considerably on the permeation characteristics of the zeolite membranes obtained. Also, it is important the kind of substrate on which the synthesis takes place and the pretreatments performed on them. For instance, concerning the support it is important its chemical composition (alumina, steel, clay, glass, etc.) and pore size (related to its roughness surface): large pores means an easier penetration of the synthesis solution into the support porosity, while small pores difficult this phenomenon and the membrane is usually prepared as a continuous zeolite layer on the support. Besides, several pretreatments can be found described in the literature to improve the result of the zeolite membrane preparation: seeding the support to control the nucleation and growth processes, seeding by laser ablation, masking the support with wax to protect it from the synthesis mixture and reduce its invasion, etc.

In this work, silicalite micromembranes were prepared on individual cylindrical straight holes of less than 100 μm of internal diameter (see Figure 1, top-left) produced by a niodimium YAG laser treatment of stainless steel sheets with thickness ranging from 20 to 70 μm. The zeolite silicalite, with the MFI-type structure, was synthesized in the hole by liquid phase hydrothermal synthesis. The molar composition of the precursor gel for the silicalite synthesis was: $KOH/TPABr/TEOS/H_2O$= 1/1/4.5/1000 [8], where TPABr is tetrapropylammonium bromide. In all the cases the hydrothermal synthesis took place in a Teflon-lined stainless steel autoclave at 100-175 °C for 20-72 h.

All the obtained samples were characterized by XRD showing that silicalite was the only crystalline phase present in the micromembranes after the preparation. Figure 1 shows some microscopy images of the silicalite micromembranes. Figure 1 top-right is a general top view of several holes covered by zeolite material. Bottom-left optical microscopy image corresponds to a

70 μm deep hole completely filled with silicalite crystals, while the SEM image from the bottom right shows the characteristic morphology of intergrowth silicalite crystals. These crystals, using a 20 μm deep hole and at optimised synthesis conditions, have giving rise to a thinner polycrystalline membrane. At this moment, these micromembranes are being tested for the separation of mixtures of butane isomers.

Financial support from MCYT and DGA, both in SPAIN, is gratefully acknowledged.

References

[1] A. Corma, M.J. Díaz-Cabañas, J. Martínez-Triguero, F. Rey, J. Rius, Nature, 418 (2002) 514.
[2] J. Coronas, J. Santamaría, Separ. Purif. Method., 28 (1999) 127.
[3] J. Coronas, J. Santamaría, Catal Today., 51 (1999) 377.
[4] S. Mintova, T. Bein, Micropor. Mesopor. Mater., 50 (2001) 159.
[5] Y.S.S. Wan, J.L.H. Chau, A. Gavriilidis, K.L. Yeung, Chem. Commun. (2002) 878.
[6] A.W. Chow, AIChE J., 48 (2002) 1590.
[7] A.S.T. Chiang, K. Chao, J. Phys. Chem. Solids, 62 (2001) 1899.
[8] P. Bernal, G. Xomeritakis, M.Tsapatsis, Catal. Today, 67 (2001) 101.

Figure 1. Scanning electronic and optical microscopy images of different zeolite micromembrane samples. Top left: fresh support. Top right: top view of the support after the hydrothermal synthesis. Bottom left and right: cross sections.

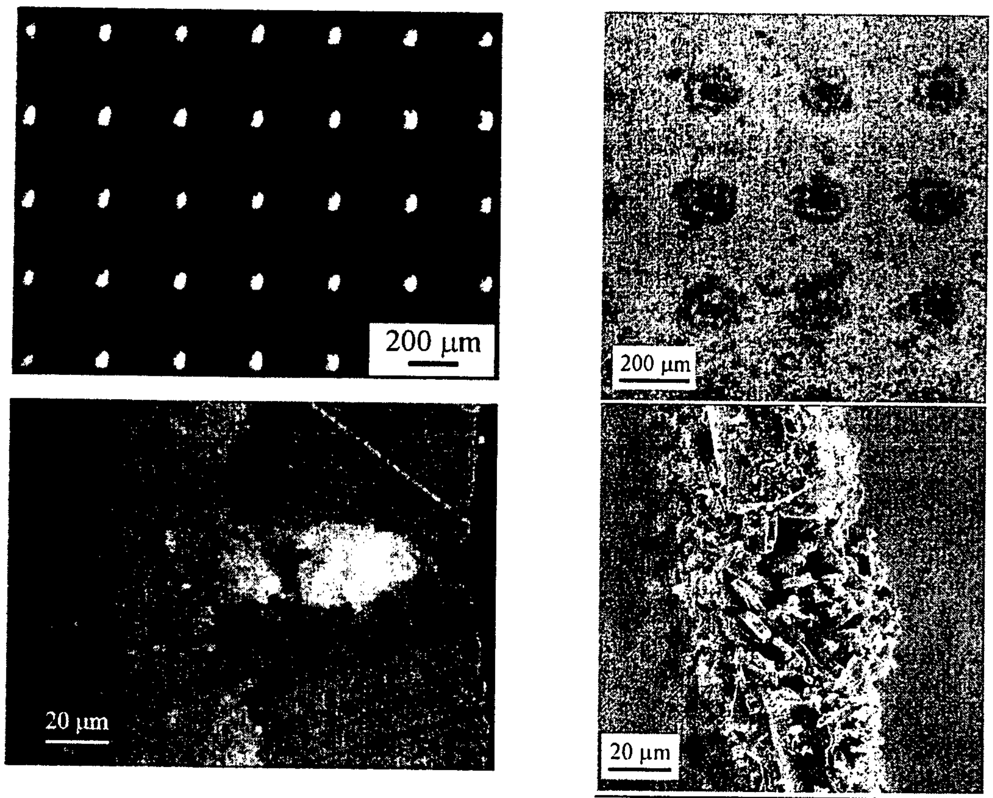

MOLECULAR FILTERING WITH NANOSTRUCTURED INTERPHASES

Víctor Sebastián, Montse Vilaseca, Óscar de la Iglesia, Ester Mateo, Alberto Navajas, Inés Tiscornia, Miguel Urbitzondo, Marisa Pedernera, Andrés Paniagua, Reyes Mallada, María Pilar Pina, Carlos Téllez, Joaquín Coronas*, Miguel Menéndez and Jesús Santamaría
Department of Chemical and Environmental Engineering, University of Zaragoza, 50009 Zaragoza, Spain, coronas@unizar.es

Micromecanical systems such as microreactors or membrane microseparators need to be constituted by smart nanostructured materials able to interact very specifically with molecules or even ions and atoms. Porous solids, i.e., zeolites and related materials, are just this kind of materials. Active materials not only at their surfaces but also through the bulk. The pores of solids are classified according to size: micropores (under 2 nm), mesopores (in the range of 2 to 50 nm) and macropores (larger than 50 nm). Some authors also distinguish between ultramicropores, very close in size to molecules (c. 0.7-1 nm), and supermicropores from approximately 1 to 2 nm. Zeolites are silicate or aluminosilicate crystalline materials with a very regular and microporous structure (pore size from 0.3 to almost 1.2 nm). Molecules adsorbed in the intracrystalline void space of a zeolite are in strong van der Waals interaction with their surroundings, as if they were solvated by the microporous framework. This is what Derouane denominates the confinement effect [1], that also may occur at the external surface of the zeolite and that responses from their dramatic impact as solid solvents in organic and fine chemicals synthesis, among other important adsorption properties.

Traditionally, zeolites have found industrial applications of paramount importance as adsorbents, ion exchangers and catalysts. New applications of zeolites and related materials are leading to new generations of catalysts [2], membranes [3] and membrane reactors [4], and now, very recently, to sensors [5] and reaction and separation micromecanical systems [6]. Microsystems provide opportunities to design more efficient chemical process, reducing reagents and energy consumption.

In this work we present something like a toll-box useful to produce new microsystems or to modify existing ones incorporating zeolite and related materials in their formulation:

1. Preparation as continuous films (membranes) of several classical zeolites such as silicalite, ZSM-5, zeolite A, mordenite, etc.
2. Preparation as continuous films of other microporous materials such as titanosilicates (ETS-10 and some of its isomorphes) and AlPOs or mesoporous materials such as MCM-41 and MCM-48.
3. Synthesis of nanocrystals (60-120 nm) of the zeolites (mostly silicalite, see Figure 1, top-left, and zeolite A) mentioned above. These nanocrystals are useful as seeds for producing zeolite membranes or preparing coatings with them.
4. Use of supports with different chemical composition (alumina, steel, clay, glass, etc.), pore size and geometry (tubes; grids, see Figure 1, top-right; plates; sheets; monoliths, see Figure 1, bottom-left; hollow fibers; etc.).
5. Modification of the supports by several techniques such as impregnation with different materials, acid attack, polishing with diamond powder, laser treatments, etc.
6. Modification of the different zeolitic phases prepared by ion-exchange, impregnation, hydrothermal postreatments, chemical vapor deposition, etc. The end of these modifications is to increase the crystallinity and to adjust the pore size

of the membranes, and thus their performance, and also to modify their catalytic activities.

These techniques have been used to produce membranes that separate in gas phase or by pervaporation complicated mixtures (of permanents gases, isomers, azeotropic ones, etc.), and membrane reactors in which reaction and separation are integrated to increase the yield of a given process. Also, gas sensors based on semiconductor oxides (SnO_2, see Figure 1, bottom-right) have been modified with zeolites giving rise to an increase of their selectivity.

Financial support from MCYT and DGA, both in SPAIN, and from the European Community is gratefully acknowledged.

References

[1] E.G. Derouane, J. Molec. Catal.A: Chem., 134 (1998) 29.
[2] J. Weitkamp, Solid State Ionics, 131 (2000) 175.
[3] J. Coronas, J. Santamaría, Separ. Purif. Method., 28 (1999) 127.
[4] M.P. Bernal, J. Coronas, M. Menéndez, J. Santamaría, Chem. Eng. Sci., 57 (2002) 1557.
[5] S. Mintova, T. Bein, Micropor. Mesopor. Mater., 50 (2001) 159.
[6] Y.S.S. Wan, J.L.H. Chau, A. Gavriilidis, K.L. Yeung, Micropor. Mesopor. Mater., 42 (2001) 157.

Figure 1. SEM images of different zeolite membrane samples. Top left: silicalite nanocrystals. Top right: detail of silicalite crystals prepared on a stainless steel the grid. Bottom left: a film of ZMS-5 on the channel of a cordierite monolith. Bottom right: cross section of a continuous layer of silicalite grown on a SnO_2 film.

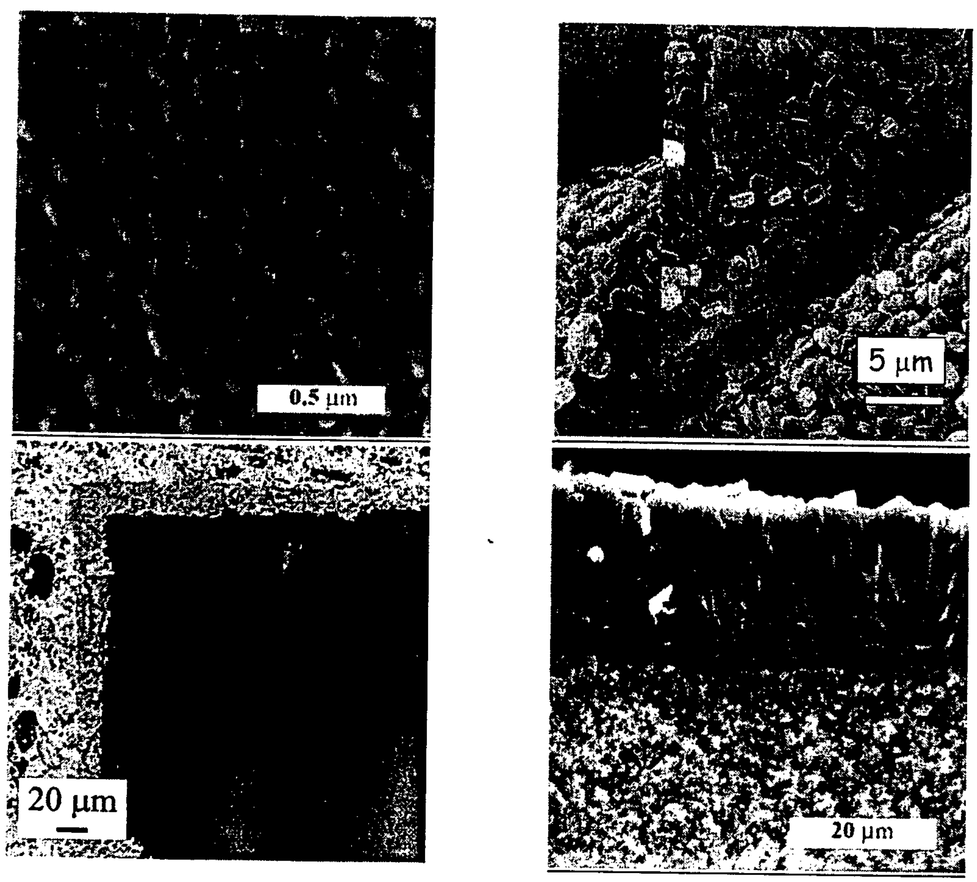

CHARACTERIZATION OF SPECTRALLY SELECTIVE COATINGS FOR GLASS WINDOWS FOR THE AUTOMOTIVE INDUSTRY

Manuel F. M. Costa; V. Teixeira; C. M. Nunes; A. Monteiro

Universidade do Minho, Departamento de Física
4710-057 Braga, Portugal
mfcosta@fisica.uminho.pt

The increasing depletion of the ozone layer imposes the need for tighter control of the solar light transmission on car's glass windows. An efficient blocking of the undesired wavelengths specially in the near ultra violet and infrared, is needed. Physically Vapour Deposited (PVD) coatings like sputter deposited metal oxide and nitride thin multilayered and graded ones are being used for spectrally selective and energy-efficient windows.

In this communication we shall report on the results of our research on the development of chromium oxide thin multilayered coatings for car' windows glass. The adherence defects and stress often derives from irregularities flaws defects and stress on the glass where the coating is deposited upon. Furthermore the homogeneity of the coatings thickness is also important. Thus the thickness and topographic evaluation of the coating on the glass and the previous defects' location on the glass surface should be performed. Furthermore a large array of characterization techniques of surface and interfaces using advanced surface analysis systems, such as XPS, AES, XRD, SEM; TEM, AFM, STM, UPS were employed and its results summarily presented. We will focus on the roughness and microtopographic inspection of tungsten oxide films

1. Method

The microtopographers we used in this work are based on optical active triangulation with oblique incidence and normal (and or specular) observation, and mechanical sample's scanning[1]. The surface to be inspected is scanned by an oblique laser beam. The incident light is collimated and focused. A small, diffraction limited, bright spot is thus projected onto the sample. The bright spot is perpendicularly imaged onto an electronic photosensitive detection system in order to assess its lateral position. The area of the surface to be inspected is scanned point by point by the "sensor's tip" (the light beam focused onto the surface). The depth resolution depends of the system used and on its particular configuration. The MICROTOP.03.MFC[1-2] is a robust and versatile system specially designed to accurately perform the microtopographic inspection of the rough surface of small samples It allows the inspection of a large variety of surfaces with resolutions that can be driven down to the submicron level with dynamic ranges up to 1:5000 (or 1:25000 with vertical scanning). The MICROTOP.06.MFC[3] maintain the main characteristic of its predecessor gaining an increased versatility with the incorporation of a second specular reflection arm. Now height measures on mirror like surfaces or optically non-rough surfaces, can be performed with accuracy in the nanometer range and resolution in the sub-nanometer range with dynamic ranges up to 1:10000 with proper vibration isolation. The inspection of a number of thin films and coatings is then possible with good resolution and reliability.
Figure 1.

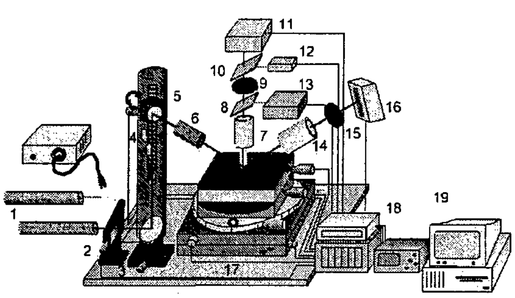

Figure 1. The MICROTOP.06.MFC: 1. light sources; 2: Vibration isolation; 3. Neutral filter; 4. Beam steering; 5. Incidence angle control; 6. Incidence optics; 7. Normal observation optics; 8. and 9. Beam splitters; 10. Interference filter; 11. Detection system; 12. Photodetector; 13. Video camera and illuminator; 14. Specular observation optics; 15. Interference filter; 16. Specular detection system 17. Positioning system; 18. Data acquisition and control system; 19. Microcomputer.

2. Results and discussion

A series of tungsten oxide coatings for intelligent glass windows were produced in our magnetron sputtering chamber with different stechiometry and deposition conditions(5). Several other types of electrochromic films were also produced(6). As an example we will present a few results of the evaluation

of a 529nm thick WO3+ W20O58 film with an optical band gap of 3.05. Its was produced at a pressure of 1.3x10-2 mbar, with a substrate temperature of 200°C during 22 minutes. The film was chosen because it presents a significant roughness as well as a pronounced curvature due to residual stress. Spite having a typical transmission spectrum those were the horse results obtained. Elsewhere details about the characteristics and efficient of our coatings are presented(5). The residual stress of the as-deposited PVD coating causes bending of the coating/substrate system. If residual stresses are present, but the overall deflection is small compared with the substrate thickness, then by symmetry the coated substrate will take up a spherical curvature in the region away from the edges[6]. Near the edges a complex stress state will be present but away from the edges this reverts to a simple stress state where stresses normal to the substrate and shear stresses are zero[7].

Below on figure 2. we present the results of the stress evaluation of a 123 nm thick β tungsten thin film deposited on .15 mm thick glass blade at 4×10^{-2} mbar during 6 minutes. The substrate-target distance was 60mm and the sputtering current of 0.23 A. The calculated transversal compressive stress ranges between -461 and -447 MPa (454.38 +/- 6.84 MPa) across the central region of the film.
Figure 4.

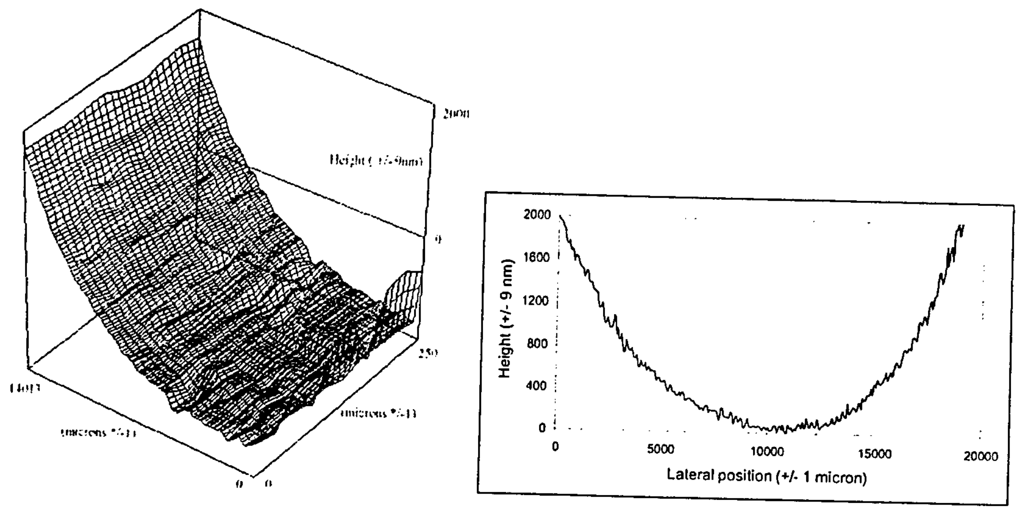

Figure 2. On the left the microtopography of a 250 μm slice of a 20 mm large WO film. On the right a profile of another zone of the tungsten film. A calculated stress of about 454 MPa was obtained.

The performance of our system allows a reliable and efficient inspection of the PVD coatings produced in our thin films' laboratory in order to detect flaws and defects, to evaluate the films roughness but also to determine stress distribution on our films.

References

[1] Manuel F. M. Costa; "Surface inspection by an optical triangulation method", Optical Engineering, 35(9) 2743-2747 (1996).

[2] Manuel F.M. Costa; J.B. Almeida; System of Optical Non Contact Microtopgraphy, Applied Optics 32, 4860-4863 (1993).

[3] Manuel F. M. Costa; "Triangulation Based Sensor for Non-Contact Micro and Nano Topographic Surface' Inspection", "ICAPT'2000, Quebec City, Canada, July 2000", SPIE Vol. 4087, 1214-1221 (2000).

[4] A. Monteiro, M. F. Costa, B. Almeida, V. Teixeira, J. Gago, E. Roman; "Influence of deposition conditions on the microstructure structural and optical characerization WO3 sputtered coatings on ITO coated glass substract", Proceedings of the "3th International Conference on Coatings on Glass, Maastrich, Neederlands, 29/10- 2/11/2000", pp 779-785 (2000).

[5] Manuel F.M. Costa, V. Teixeira, C. M. Nunes, "Microtopographic Inspection of Cr-Cr_2O_3 Cermet Solar Absorbers" "SPIE conference on Solar Optical Materials XVI, Denver, Colorado, July 1999", SPIE Vol. 3789, 140-148 (1999).

[6] P. A. Flinn, D. S. Gardner, W. D. Nix, IEEE Trans. Electron Devices, ED-34 (13), p. 689, 1987.

[7] V. Teixeira, "Mechanical integrity in PVD Coatings due to the presence of residual stresses", Thin Solid Films, 2001 (in print).

Poster

SPATIAL FIELD AND INTENSITY CORRELATIONS IN QUASI-ONE-DIMENSIONAL WIRES

Gabriel Cwilich[(1)] – Luis S. Froufe-Perez[(2)] - Juan José Saenz[(2)]
Department of Physics - Yeshiva University,
2495 Amsterdam Ave. New York, NY, 10033 USA[(1)]
Departamento de Fisica de la Materia Condensada,
Universidad Autonoma de Madrid, 28049 Madrid, Spain[(2)]
E-mail: cwilich@ymail.yu.edu , juanjo.saenz@uam.es

When studying the speckle pattern of a wave propagating coherently through a disordered medium, the correlations between the transport coefficients leads to long-range effects that appear in the intensity-intensity correlations. The different contributions to these effects have been studied both diagrammatically(1) and in a macroscopic approach(2) and are generally referred as the C_1, C_2 and C_3 contributions.

Recently the intensity correlations in a random system have been studied experimentally very carefully in the spatial domain, in the microwave regime, in a quasi one-dimensional geometry in the diffusive regime(3). They show interesting symmetries between the roles of sources and detectors, and they find that all contributions can be expressed in terms of a single function, the field-field correlation.

In this work we show that their results for the correlations can be obtained within the general macroscopic framework of Random Matrix Theory (RMT) applied to coherent transport in quasi one-dimensional cavities. We will show that the structure of the correlations follows from the isotropy hypothesis of the statistical distribution of the transmission eigenvalues, which in RMT is shown to be independent of the specific transport regime of the sample. That extends the range of validity of the results obtained(3) beyond the diffusive regime. Furthermore we can show that the source-detector symmetries arise as a natural consequence of general properties of the eigenfunctions corresponding to the geometry of any propagating cavity. All their experimental results can be recovered in the large-N (number of propagating channels) limit.

Recent calculations obtained in this framework of the correlations between the channels for systems of small length(4) allow us to make predictions on the behavior of the spatial intensity correlations as a function of the size of the system.

References:

(1) S. Feng, C. Kane, P.A.Lee and A.D. Stone, Phys. Rev. Lett. **61**, 834 (1988).
(2) P.A. Mello, E. Akkermans and B. Shapiro, Phys. Rev. Lett. **61**, 459 (1988).
(3) P. Sebbah, B. Hu, A.Z. Genack, R. Pnini and B. Shapiro, Phys. Rev. Lett. **88**, 123901, (2002).
(4) A. Garcia-Martin, F. Scheffold, M. Nieto-Vesperinas and J.J. Saenz, Phys. Rev. Lett. **88**, 143901, (2002).

STRONG MAGNETOELASTIC CONTRIBUTION TO THE MAGNETOCRYSTALLINE ANISOTROPY IN A (110) TERFENOL-D THIN FILM

L. Benito*, J. I. Arnaudas*, C. de la Fuente*, M. Ciria*, C. Dufour+, K. Dumesnil+ and A. del Moral*

*Depto. de Física de la Materia Condensada - Instituto de Nanociencia de Aragón & Instituto de Ciencia de Materiales de Aragón, Universidad de Zaragoza & CSIC, E-50071 Zaragoza, Spain; + Laboratoire de Physique des Matériaux (UMR CNRS 7556), University H. Poincaré - Nancy I, BP 239, F-54506 Vandoeuvre cedex, France

E-mail: cesar@unizar.es

The bulk alloy $(Tb_{0.27}Dy_{0.73})Fe_2$ (Terfenol-D) has been widely studied due to its remarkable magneto-mechanical properties at room temperature (RT). On decreasing the temperature, Terfenol-D undergoes a spin reorientation transition, the easy axis changing from <111>, above 250 K, to <100> at low temperatures [1 U. Atzmony et al. Phys. Rev. B 7 (1973) 4220]. The molecular-beam epitaxy technique has allowed the growth of epitaxial Terfenol-D thin films [2], opening the possibility of studying the influence of factors like stress, thickness, growing conditions, etc., in the magnetic behaviour of these systems [3 PRB Mougin].

In this work we present magnetic anisotropy measurements performed in a (110) Terfenol-D film, 600 Å thick, epitaxially grown on a sapphire substrate. The magnetic torque curves have been determined by using a vibrating sample magnetometer, which allows us to measure the angular dependence of both, the parallel, $M_{\parallel}$, and perpendicular to the applied field, $M_{\perp}$, components of the total magnetization, **M**, up to 2 Tesla (notice that the torque exerted on the sample by the magnetic field is $\tau = |\mathbf{M}\times\mathbf{B}| = MB\sin\alpha = M_{\perp}B$, where $M_{\perp} = M\sin\alpha$, with α the angle between **M** and **B**). In Fig. 1 we show the magnetic torque at B = 2 T, at RT, as a function of the angle, θ, between **M** and a reference direction in the crystal. The fourfold symmetry, associated with the cubic structure within the (110) plane, is clearly observed. To investigate the spin reorientation we have also performed a torque measurement at 140 K, where a reorientation of $\approx 15°$ of the easy axis direction is apparent.

The analysis of the experimental torque curves has been carried out considering magnetocrystalline anisotropy up to eight order and the magnetoelastic energy up to second order. We have used the experimental magnetoelastic coupling parameters earlier obtained for this sample [4] and the epitaxial strains measured at zero field [3 ???]

It is now accepted that Nanotechnology is one of the key enabling technologies for sustainable and competitive growth in Europe. Nanoelectronics is certainly now the branch with the most significant commercial impact and covers a huge range of interdisciplinary areas of research and development such as Molecular electronics, Bioelectronics, Spintronics, Nanoimprint, Nanoscale Optics, Lithography, Architecture, Nanoprobes, etc...It is also accepted that a significant investment will be required to ensure Europe's competitiveness in nanotechnology.

At this stage, it is impossible to predict the exact course the nanoelectronics revolution will take and, therefore, its effect on our daily lives. We can, however, be reasonably sure that Nanotechnology will have a profound impact on the future development of many commercial sectors. The impact will likely be greatest in the electronics sector, where the demand for technologies permitting faster processing of data at lower costs will remain undiminished.

STRUCTURAL ANOMALY AND GIANT MAGNETORESISTANCE IN Co/Ag DISCONTINUOUS MULTILAYERS

J. A. de Toro, J. P. Andrés, A. J. Barbero and J. M. Riveiro

Departamento de Física Aplicada, Universidad de Castilla-La Mancha,
13071 Ciudad Real, Spain
E-mail: joseangel.toro@uclm.es

A convenient procedure to obtain magnetic nanogranular materials is the synthesis of the so-called *discontinuous multilayers*, where the nominal thickness of the deposited magnetic layer is not high enough to yield a true continous layer. The size of the nanoparticles is usually controlled through the variation of the nominal thickness of the magnetic element [1]. In this work, however, the giant magnetoresistance effect has been optimized through the variation of the non-magnetic layer thickness, which has been used before as a mean to tune the interaction between layers of nanoparticles of a certain size [2].

Silver and cobalt are a common choice in the fabrication of granular structures due to their marked inmiscibility [3]. The multilayer series $[Ag_x/Co_3]_{200}$, for x ranging from 3 to 100 Å, has been grown using a magnetron RF sputtering and high purity targets. The nominal thickness of the Co layers was fixed to $t_{Co} = 3$ in order to ensure their granular character even for relatively thin Ag layers. The variation of t_{Ag} was seen to affect significantly the size of the Co nanoparticles (estimated from fits of the magnetisation to the Langevin function) all along the studied x interval.

Figure 1 shows the magnetoresistance loops at room temperature of a few selected samples. A maximum GMR as high as 13.8 %, at 15 kOe, was measured in a sample with $x = 12$ Å. The fit to the Langevin function of its magnetisation yielded a mean magnetic moment of 4700 μ_B. Larger particles, obtained for thinner Ag layers, resulted in a decreased GMR due to interparticle interactions.

The intergranular interactions were studied by two methods: the usual plot of magnetoresistence as a function of reduced magnetisation, and the measurement of the temperature dependence of the field cooled (FC) and zero-field cooled (ZFC) magnetisation. Both analysis yielded consistent results. The samples with the highest interactions exhibited typical spin-glass features, like a plateau-like FC curve below the maximum of the ZFC branch, as expected from some recent reports on superspin glasses in discontinous multilayers [4].

The silver layers were highly textured in the [111] direction. Figure 2 shows their lattice parameter as a function of the layer thickness. The existence of two regimes in the evolution of the lattice parameter towards the bulk value can be easily noticed. The change of slope between these two regimes is accompanied by a strong anomaly detected in various samples of the batch $[Ag_{12}/Co_3]_{200}$ (Fig. 2 shows two of them). The interest of this anomaly is twofold, for the samples where it occurs are precisely those exhibiting the highest GMR in all the series.

References:

[1] S.E. Paje, M.A. Arranz, J.P. Andrés and J.M. Riverio, J. Phys. Condens. Matter, **15** (2003) 1071.

[2] F. Luis, F. Petroff, J. M. Torres, L. M. García, J. Bartolomé, J. Carrey, and A. Vaurès, Phys. Rev. Lett. **88**, 217205 (2002).

[3] John Q. Xiao, J. Samuel Jiang, and C. L. Chien, Phys. Rev. B, **46** (1992) 9266.

[4] S. Sahoo, O. Petracic, C. Binek, W. Kleemann, J. B. Sousa, S. Cardoso. and P. P. Freitas, Phys. Rev. B **65**, 134406 (2002).

Figures:

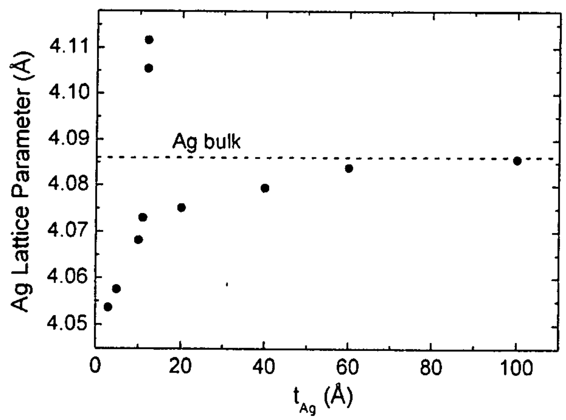

Fig.1.- Lattice parameter obtained from the (111) reflexion of f.c.c. Ag as a function of the layer thickness. The dashed line marks the bulk value.

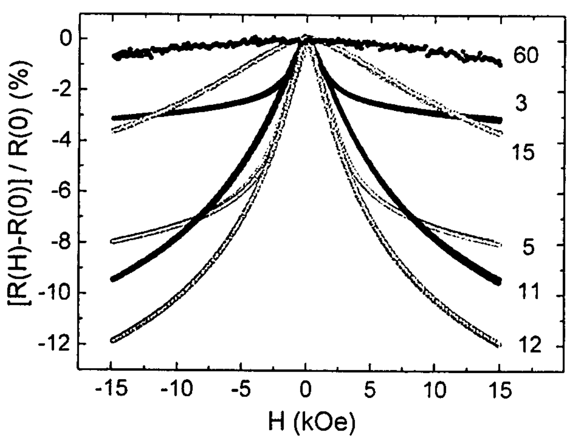

Fig. 2.- Magnetoresistance loops at room temperature for selected Ag layer thicknesses.

INFLUENCE OF DIFFERENT METALS ADDITION ON NANOCRYSTALLINE MGH_2 SYNTHESIZED BY REACTIVE MECHANICAL MILLING UNDER H_2 ATMOSPHERE

S. Doppiu, P. Solsona, T. Spassov*, S. Suriñach and M.D. Baró
Departament de Física, Universitat Autònoma de Barcelona, 08193 Bellaterra, Spain.
* Department of Chemistry, University of Sofia "St.Kl.Ohridski", 1 J. Bourchier Str., 1126 Sofia, Bulgaria

Hydrogen conversion technologies have been developed during the last years, in order to use hydrogen as alternative energy to the conventional fuels. Hydrogen as an energy currency is environmentally compatible, since its production from electricity (or directly from solar energy), its storage and transportation, and its end use do not produce any pollutants (except some NOx if hydrogen is burned in air). However, hydrogen storage remains an open problem for its possible use like fuel especially in the automotive industries. In the last years, the possibility to store hydrogen in various materials was extensively studied (1-3). Among them, MgH_2 is considered as one of the most promising candidates, because of its light weight, the high amount of H_2 that can be stored (7.6wt.%), its low cost and abundance on the earth. Nevertheless, the high decomposition temperature and the slow hydrogen absorption-desorption kinetics, are limiting factor for industrial applications. In order to improve the hydriding-dehydriding kinetics, a large number of investigation were focused towards the preparation of nanocomposites based on MgH_2 with an absorption capacity close to that of pure magnesium (4).

In this study, the synthesis of nanocrystalline MgH_2 was performed by reactive ball milling under H_2 atmosphere. The effect of different metals addition (Ni, Al) was as well investigated. Milling was carried out with a planetary mill (Frtch P5) using stainless steels balls and vials, under 6 bars of H_2. The sample thermostability was studied by means of differential scanning calorimetry (DSC) and thermo-gravimetry (TG) analysis. The samples obtained were also characterized by X-ray diffraction analysis (XRD), using Cu-Kα radiation. From the diffraction patterns, microstructural parameters, as crystallite sizes and microstrain, and phase percentages were evaluated by means of Rietveld full profile-fitting procedure (5). Three different compositions were studied, Mg, $Mg_{87.7}Ni_{11.3}$ and $Mg_{87}Ni_{10}Al_3$. Milling under H_2 induces gradual conversion of Mg in nanocrystalline MgH_2 with crystallite sizes around 6nm. In Figure 1 are reported the diffraction patterns together with the calculated profiles for the three compositions.

Interestingly, no formation of mixed hydrides was detected during milling. It is worth to note that no formation of mixed hydrides was detected during milling, only when almost complete transformation of Mg in MgH_2 is obtained, Ni starts to react forming Mg_2NiH_4.

In Figure 2 the DSC traces of the three samples are presented. It can be observed that addition of Ni and Al strongly influences the desorption kinetic. Indeed, the decomposition temperature considerably decreases when in the mixture are added Al and/or Ni.

In conclusion, the addition of Ni and Al into MgH_2 nanoparticles plays a key role in the hydrogen desorption. This study provides promising results for the hydrogen storage industry since the inclusion of these two elements was found to lower the temperature at which occurs the desorption.

Aknowledgment

This work has been carried out in the framework of the EU-HPRN-CT-2002-00208, 2001SGR00189 and CERMAE 2003 research projects.

References

1) Zaluski, L.; Zaluska, A.;Strom-Olsen, J.O. Journal of Alloys and Compounds, **288**. (1999) 217.

2) Zaluski, L.; Zaluska, A.;Strom-Olsen, J.O. Journal of Alloys and Compounds, **253-254**, (1997) 70-79.

3) 4 Bobet, J.-L.; Desmoulins-Krawiec, S.; Grigorova, E.; Cansell, F.; Chevalier, B., Journal of Alloys and Compounds, **351**, (2002) 217-221

4) G. Barkhordarian, T. Klassen and R. Bormann, Scripta Materialia, **49,** (2003) 213-217.

5) Lutterotti, L.; Ceccato, R.; Dal Maschio, R.; Pagani, E., Mater. Sci. Forum, **278-281**, (1998) 87-92.

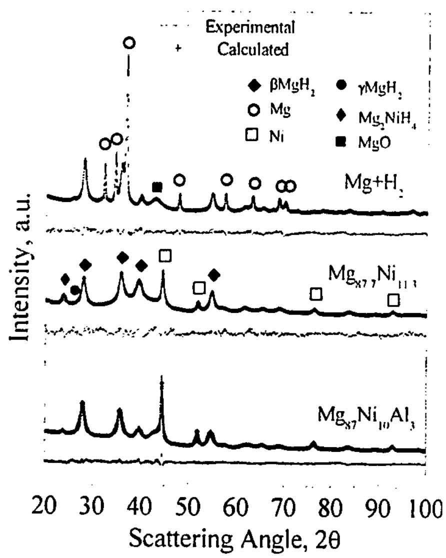

Figure 1. X-ray patterns (line) and calculated profiles (∇), of the samples Mg, $Mg_{87.7}Ni_{11.3}$, $Mg_{87}Ni_{10}Al_3$ milled under H_2 atmosphere. Differences between experimental and reconstructed patterns were also included.

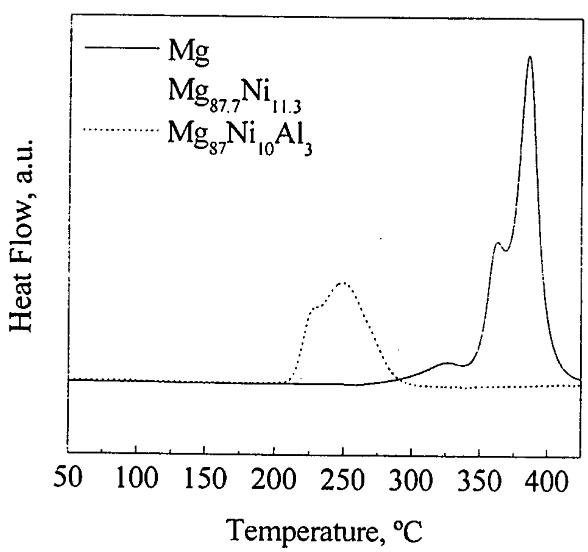

Figure 2. DSC traces of the samples Mg (line), $Mg_{87.7}Ni_{11.3}$(dotted line) and $Mg_{87}Ni_{10}Al_3$ (dashed line).

FABRICATION OF SIZE-TUNABLE AND SHAPE-CONTROLLED HIGH QUALITY FLUORESCING METAL SULFIDE QUANTUM-DOT NANOPARTICLES

Narayan Pradhan, Beni Katz, and Shlomo Efrima
Department of Chemistry and the Ilse Katz Center for Meswo and Nano-Scale Science and Technology, Ben Gurion University of the Negev, Beer Sheva, Israel 84105
Email: efrima@bgumail.bgu.ac.il

We synthesize shape and size controlled high quality semiconductor metal sulfide quantum dots in a single-pot and single-source approach using various metal alkyl salts of xanthates, thiocarbamates, and thiocarbonates. The method is a simple and convenient approach for the synthesis of crystalline, nearly mono-dispersed particles (Fig. 1) using low temperatures (70°C to 150°C), in a way that is insensitive to air (oxygen and humidity). We also extended our method to the synthesis of core/shell CdS/ZnS and ZnS/CdS particles under simple and mild conditions. The CdS and CdS/ZnS particles exhibit a narrow (30-40nm) excitonic photoluminescence (Fig. 2). All the emission and absorption peaks are tunable (by varying the size of the particles) with a change of reaction temperature, the concentration and/or the reaction time. A unique special extremely narrow (FWHM = 10nm) intense emission peak was observed for a stepwise synthesis of ZnS/CdS particles (Fig. 3). We also produce CdS particles of different shapes (spherical, elliptical and rods) using the same precursor but changing the reaction parameters and precursor concentration. Highly ordered ZnS nanowires with and without coating of CdS were fabricated using the same synthesis procedure but with increasing annealing time and at a high reaction temperature (~200°C). All these semiconductor nano materials were prepared using alkyl amine as the solvent as well as the capping agent. The high-luminescence particles are tested for imaging applications by comparing to green fluorescent protein in embryo cells.

Reference:

N. Pradhan, S. Efrima, "Single-Precursor, One-Pot Versatile Synthesis under Near Ambient Conditions of Tunable, Single and Dual Band Fluorescing Metal Sulfide Nanoparticles", J. Am. Chem. Soc., 125 (8), 2050-2051 (2003)

Fig. 1 - TEM micrograph of CdS particles.

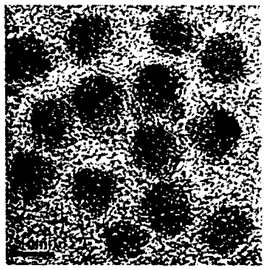

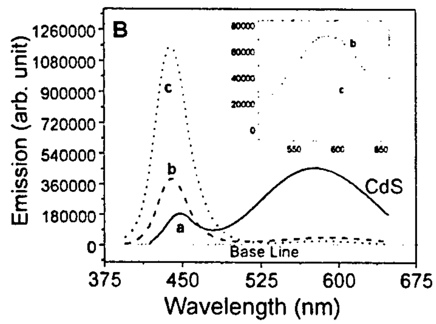

Fig. 2 – Photoluminescence of core-shellCdS-ZnS particles. Curve 'a' is the PL spectrum for bare CdS and curve 'c' is that for ZnS shelled particles. Curve 'b' is for a partially shelled sample. Inset – Amplified broad band emission.

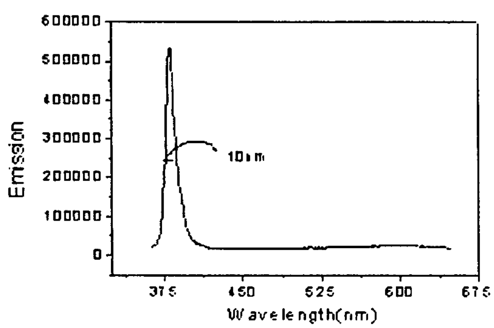

Fig. 3 - PL spectra of the extremely narrow band emission at 380nm for ZnS-CdS particles.

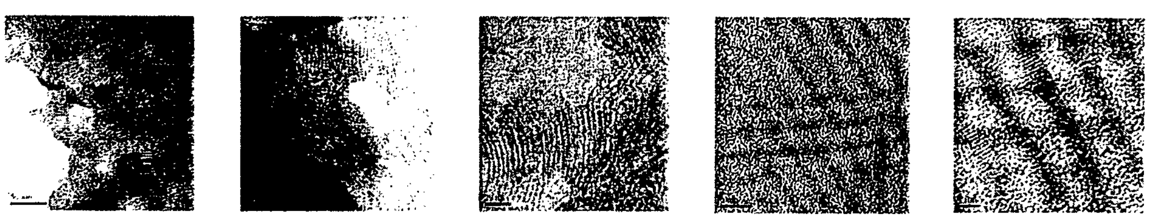

Fig. 4 - TEM micrographs of ZnS (and CdS) nanowires (1.2nm width).

TRIBOLOGICAL PROPERTIES OF CN/TiCN/TiN/Si MULTILAYER DETERMINED BY AFM

C.Morant[a], D. Mendiola[a], A.Verdaguer[b], F.Sanz[b], E.Elizalde[a], J.M Sanz.[a]

[a] Departamento de Fisica Aplicada.Universidad Autonoma de Madrid

28049 Madrid Spain

[b] Departament de Química-Física, Universitat de Barcelona, Martí i Franqués 1, 08028 Barcelona Spain

The mechanical properties of new hard coatings based on a multilayer structure have been investigated at the nanometer scale. Multilayer coatings have been intensively studied in the last years to enhance tribological performance of the coatings. Materials most frequently investigated are compounds of Ti (CN/TiN, TiCN/TiN, TiC/TiN, TiN/Ti) [1-3]. In this work we have studied the hardness enhancement by depositing an elastic and hard film (CN) on hard and brittle layers (TiCN, TiN).

The multilayer structures of CN/TiCN/TiN on silicon substrate have been deposited by dual ion beam sputtering using a combination of TiN, TiC and C targets and an $Ar\text{-}N_2$ mixture discharge gas. Nanomechanical properties of each layer have been determined measuring nanoindentation, nanofriction and nano-scratching by means atomic force microscopy. Nanoindentation and nanoscratching experiments were performed with AFM using a stainless steel cantilever (k_c =265Nm^{-1}) with a diamond tip, whereas the friction behaviour of each layer was evaluated taking AFM friction images of the surface while the normal force was increasing during the scanning. In this last experiments levers of smaller spring constant were used (k_c =14Nm^{-1} and k_c =0.25Nm^{-1}).

We have found that the hardness increases for each successive layer, while the friction decreases in the same way. Moreover, the nanoscracth measurements (see figure) shows a drastic increase of wear resistance for each layer.

All these results indicate that the multilayer combines ultrahard behaviour with good tribological and wear properties.

References

[1] E. Bemporad, C. Pecchio, S. De Rossi, F. Carassiti, Surf. Coat. Technol 146 (2001) 363-370.

[2] X.A. Zhao, C.W. Ong, Y.C. Tsang, C.L. Choy, P.W. Chan, J.Vac. Sci. Technol. A 15(1) (1997) 99-106.

[3] K.J. Ma, C.L. Chao, D.S. Liu, Y.T. Chen, M.B. Shieh, Journal of Materials Preccesing Technology 127 (2002) 182-186

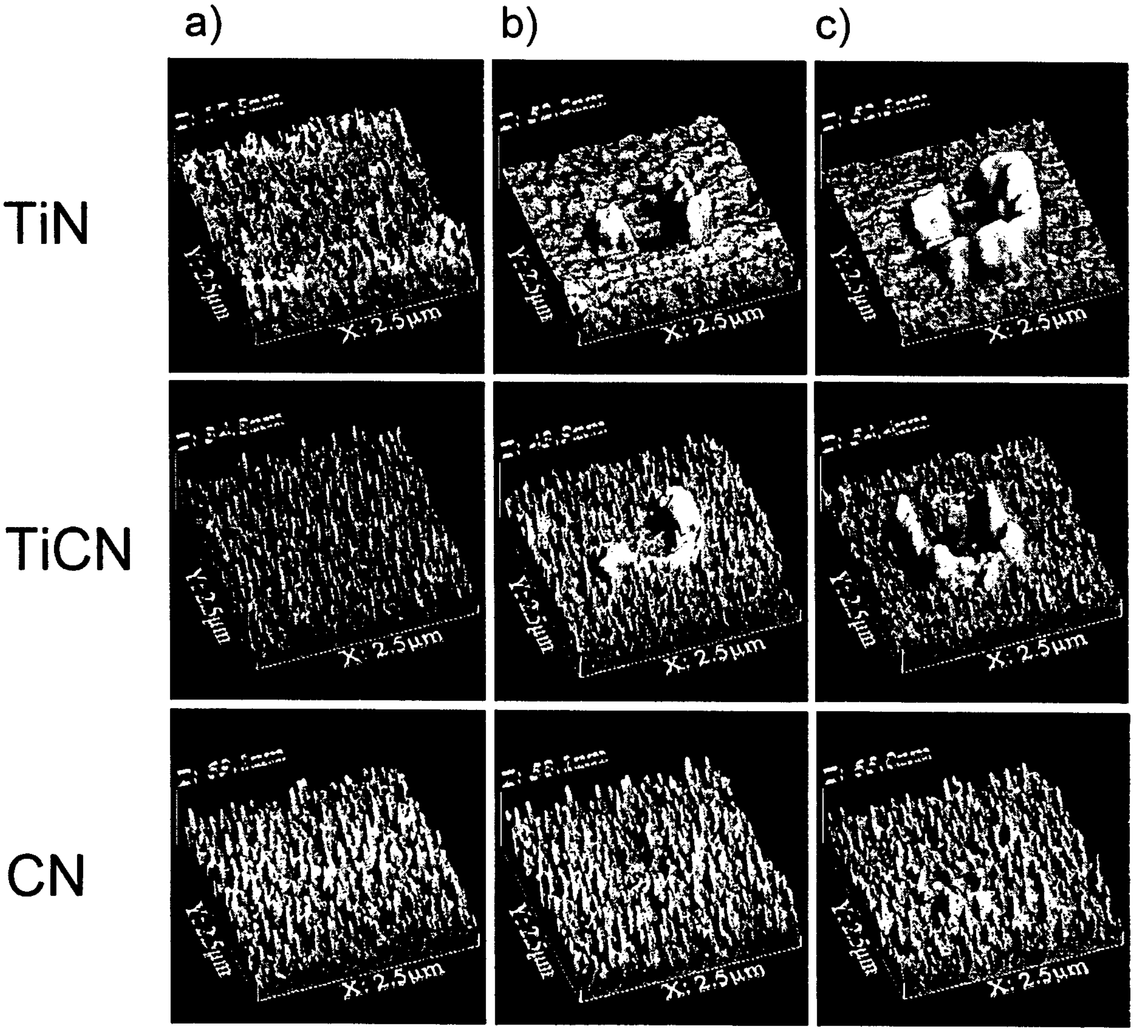

AFM images (tapping mode) of the CN/TiCN/TiN multilayer. It is shown each layer, as labeled, before (a) and after (b,c) nano-scratch tests. The tests were realized scanning in contact mode an area of 1µmx1µm with the diamond tip. a) surface as deposited, b) after scanning in contact mode (Load=270µN), c) after scanning in contact mode double time and double load (Load=540µN).

SELECTED THERMAL EMISSION OF ELECTRONS FROM DIFFERENT CONFIGURATIONS IN InAs/GaAs QUANTUM DOTS

O. Engström, M.Malmkvist, Y.Fu*, H.Ö.Olafsson and E.Ö.Sveinbjörnsson
Department of Microtechnology and Nanoscience (MC2) and *Department of Physics
Chalmers University of Technology, S-412 96 Göteborg, Sweden
E-mail:olof.engstrom@mc2.chalmers.se
www.mc2.chalmers.se

Thermal emission of electrons from different configurations in InAs/GaAs quantum dots (QDs) have been investigated by Deep Level Transient Spectroscopy (DLTS). The different charging states of the QDs can be used to fill and empty the QDs selectively, thus making it possible to obtain separate peaks in the DLTS spectra for different electron configurations and the corresponding activation energies. We find that the two *s* configurations have different activation energies for electron emission and assign this to the spread in QD size and not to charging effects.

Understanding the mechanisms for thermal emission of charge carriers from QDs is important for their applications in lasers, optical detectors or future dynamic memories and cellular automata devices. For InAs/GaAs QDs with base and height dimensions of about 20 nm and 5 nm, respectively, the electron configurations mainly includes an *s* shell capturing two electrons and a *p* shell occupied by four electrons with an energy scheme as shown in Fig. 1. Investigating this system by DLTS requires that the QDs are positioned in a depletion region of a p-n junction or a Schottky diode. For such a situation a number of escape paths exist as shown in the diagram of Fig.1. Besides the direct emission from *s* to the GaAs conduction band (CB) and a two-step excitation process from *s* to *p* and further to the CB, also tunneling from *s* and *p*, respectively, to the CB occurs due to the high electric field in the depletion region.

Self assembled InAs QDs were prepared by MBE growth from a 3.1 ML thick InAs layer on top of a 1.5 μm thick GaAs buffer layer on a GaAs substrate and with a 0.5 μm thick cap layer of GaAs. The structure was finished by evaporating a gold contact as a Schottky barrier on the cap surface and an ohmic contact on the substrate surface, respectively.

As the filling and emptying of electrons in the QDs depend on the position of the bulk Fermi level in relation to the electron energy levels of the QDs, these processes can be controlled by changing the reverse bias of the depletion region. Relative to the bulk Fermi level, the QDs with two *s* electrons captured (*s2*) will have an energy higher than those with one *s* electron captured (*s1*) as a result of different charging of the QDs. This makes it possible to study the two *s* electrons separately in DLTS without interference between close lying DLTS peaks. From capacitance vs voltage data, we find that the QDs of the present devices are completely emptied by electrons for reverse biases exceeding 2 V. Fig. 2 shows DLTS spectra for a constant filling voltage of 0.5 V and a varying emission voltage between 1.5 and 2.0 V. At the lowest emission voltage, only *s2* leaves the QDs as *s1* stays below the bulk Fermi level. In Fig. 3, the emission voltage is kept constant while the filling voltage is varied in the region 0.5 – 1.9 V. At the higher filling voltages only *s1* is captured and emitted because the QD energy is raised by the charge of *s1* so that the energy level of *s2* stays above the bulk Fermi level thus thwarting the capture of *s2*. Determining the activation energies by standard method for electron emission from the separated *s1* and *s2* spectra in Figs. 2 and 3, respectively, we find the values 157 meV for the *s1* emission and 120 meV for *s2* from the activation curves, shown in Fig. 4.

It is readily shown by simple statistical arguments that the free energy for emission of the *s* electrons is independent of the charging of the QDs. The most probable cause of the difference in activation energies for the *s1* and *s2* emissions in Fig. 4, therefore, is that the two curves represent different parts of the QD size distribution. When selecting the *s1* emission by keeping the filling voltage at a high value (Fig.3), QDs with larger size and lower electron eigen energies are favored, while correspondingly, smaller QDs with higher eigen energies dominate for lower emission voltages when *s2* is selected (Fig. 2). Under this condition, the selection method utilized in our experiments gives an estimate of the spread in activation energy within the QD ensemble. Other possibilities for the difference are different temperature dependences of the electron capture cross sections or different entropy properties for electron exchange of the two electron configurations.

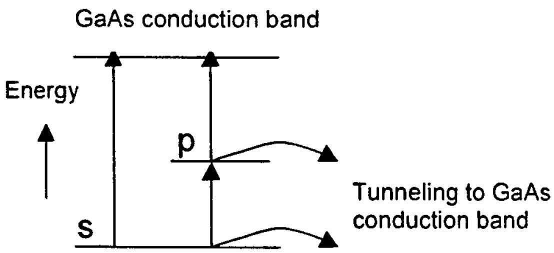

Fig. 1 Energy level scheme.

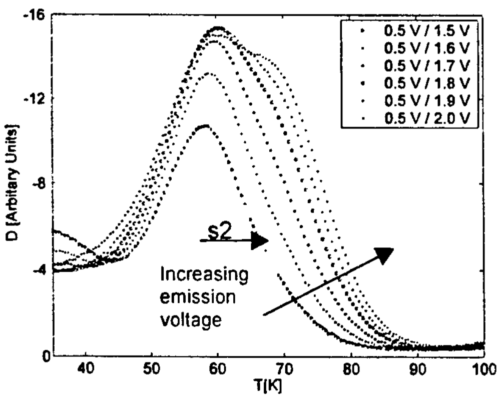

Fig. 2 DLTS spectra for a constant filling voltage of 0.5V and emission voltage varied 1.5 – 2.0 V. The curve marked *s2* is for 1.5 V emission voltage and corresponds to the emission of only the second captured electron. With increasing emission voltage also the *s1* peak grows at 70K. Below 40K the *p* level has a peak that disappears for higher voltages due to tunneling.

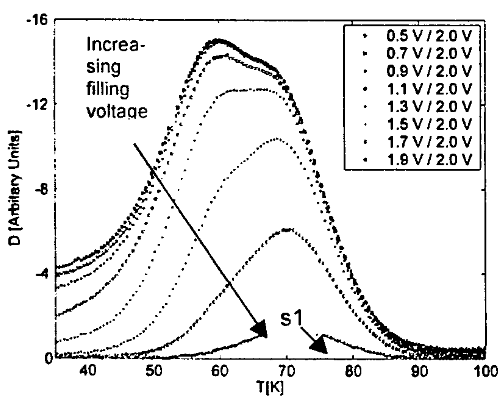

Fig. 3 DLTS spectra for a constant emission voltage of 2.0 V and filling voltage varied 0.5 – 1.9 V. The curve marked *s1* is for 1.9 V filling voltage and corresponds to the emission of only the first captured electron. With increasing filling voltage the *s2* peak at 58K decreases. Pronounced tunneling can be seen at temperatures below about 50K.

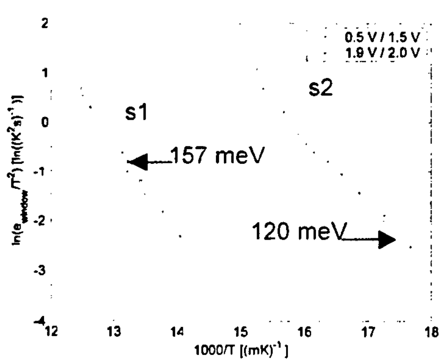

Fig. 4 Arrhenius plot for the s1 and s2 thermal emission rates obtained by standard method from DLTS spectra. Energy values given are the activation energies obtained from the plots.

InP NANOWIRES ANS NANOTUBES

Louis F. Feiner[1], Erik P.A.M. Bakkers[1], Marcel A. Verheijen[1],
Jorden A. van Dam[2], Silvano De Franceschi[2], and Leo Kouwenhoven[2]
[1]Philips Research Laboratories, Prof. Holstlaan 4, 5656 AA Eindhoven, The Netherlands
[2]Department of Nanoscience, Delft University of Technology, P.O.Box 5046, 2000 GA Delft, The Netherlands

It is well established that the electronic structure of semiconducting nanowires is determined by both the chemical composition and the radial quantum confinement, the latter being governed by the diameter. We demonstrate that the confinement effect in such one-dimensional structures can be enhanced substantially in nanotubes as compared to nanowires.

We report the synthesis of optically active Indium Phosphide (InP) nanotubes [1] via the same vapor-liquid-solid (VLS) growth mechanism by which crystalline nanowires, showing excellent electrical properties, are fabricated. The nanotubes are formed at higher temperatures than at which nanowires grow, and a simple model explaining their formation is presented. The nanotubes are crystalline and have the (bulk) zinc blende structure and therefore represent a new class of tube materials. The wall thickness can be controlled by the synthesis temperature and is in the range of 2-20 nm. The tubes show photoluminescence, which is considerably (by up to 0.7 eV) blue-shifted with respect to bulk emission, indicating that the optical properties are not dominated by defect states. Using a simple effective mass model, we show that the blue-shift is controlled by the wall-thickness, explaining why the shift is substantially larger than achievable in nanowires.

[1] Erik. P.A.M. Bakkers and Marcel A. Verheijen, J. Am. Chem. Soc. **125**, 3440 (2003).

REVERSIBLE LOGIC BASED ON ELECTRON WAVEGUIDE Y-BRANCH SWITCHES

Erik Forsberg

Dept. of Microelectronics and Information Technology,
Royal Institute of Technology, Electrum 229, SE-164 40 Kista, Sweden
E-mail: erikf@imit.kth.se

For more than a decade a large amount of research aimed at demonstrating nanoelectronic components has been performed (for reviews see e.g. [1, 2]). Besides being interesting physics in its own right, a major driving force behind such research is the predicted end-of-the-road of the scaling of MOSFETs. Electron waveguides is one class of devices studied in this field, and of these, the Y-branch switch (YBS) [3] is especially interesting. This is due to two reasons; the response to applied bias is monotonic, and the applied bias necessary to achieve switching when the YBS is operated in the coherent regime is not thermally limited [4]. Combined, these two factors promise a device suitable for high-density packing through an expected tolerance to fabrication defects and very low power dissipation.

MOSFETs have however historically proved themselves very competitive and it has even been suggested that as long as we are considering computation in a von Neumann architecture, CMOS will always be competitive from an energy viewpoint no matter what switching technique is used [5]. The conclusion for the near future is then that for any new nanoelectronic device technology to be viable it should be possible to integrate within a Si-CMOS environment. Further ahead completely new types of architectures need to be considered.

Within this context, the lack of a thermal limit for switching in the YBS makes it very interesting to study this device as a base for reversible computing. As is well-known, Landauer's Principle states that it is the act of discarding information that incurs energy loss [6] and by constructing a reversible computer in which the input data is not discarded, calculations can be performed with arbitrarily small energy loss [7]. Such a computer requires reversible logic gates, i.e. gates from which the input can be reconstructed from the output. So far, the YBS has only been considered for conventional Boolean logic [8] but in this paper implementations of reversible gates, such as a controlled-NOT (reversible XOR) gate and a Fredkin exchange gate, based on the YBS are proposed and discussed. As e.g. the Fredkin exchange gate can serve as a basic building block for any kind of logic operation [9], these proposed gates promise very compact circuits with extreme low power dissipation. Furthermore, as such reversible gates form a necessary (however not sufficient [10]) requirement for the realization of quantum computing, the possibility of utilizing the proposed structures for quantum logic will also be addressed.

References

[1] D. Goldhaber-Gordon, M. S. Montemerlo, J. Christopher Love, G. J. Opitek, and J. C. Ellebogen, Proc. IEEE, vol. 85, no. 4, 51 (1997).

[2] R. Compañó, ed., *Technology Roadmap for Nanoelectronics* (Office for the Official Publications of the European Communities, Luxembourg, 2000).

[3] T. Palm and L. Thýlen, Appl. Phys. Lett. **60**, 237 (1992).

[4] T. Palm, L. Thyén, O. Nilsson, and C. Svensson, J. Appl. Phys. **74**, 687 (1993).

[5] J. A. Hutchby and V. V. Zhrinov, keynote at the SRC/TNT Nanoelectronics Workshop, Santiago de Compostela, Spain, Sept. 2002.

[6] R. Landauer, IBM J. Res. Develop. **3**, 183 (1961).

[7] C. H. Bennet, IBM J. Res. Develop. **17**, 525 (1973).

[8] T. Palm, J. Appl. Phys., **79**, 8076 (1996).

[9] E. Fredkin and T. Toffoli, Int. J. Theor. Phys. **21**, 219 (1982).

[10] D. P. DiVincenzo, Fortschr. Phys. **48**(9-11), 771 (2000).

Figure

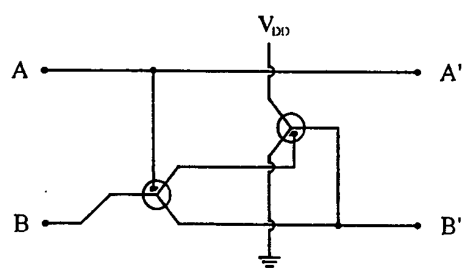

A	B	A'	B'
0	0	0	0
0	1	0	1
1	0	1	1
1	1	1	0

Figure 1: Proposal of a controlled-NOT gate based on two YBSs with the corresponding truthtable.

NEW FAMILIES OF CARBON NANOTUBES BASED ON GRAPHYNE MOTIFS

V. R. Coluci[1,2], S. F. Braga[1], S. B. Legoas[1], D. S. Galvão[1] and R. H. Baughman[2]
[1]Instituto de Física Gleb Wataghin, Universidade Estadual de Campinas
CP 6165, 13083-970 Campinas, SP, Brazil
[2]NanoTech Institute and Department of Chemistry, University of Texas
Richardson, Texas 830688, U.S.A.
E-mail: galvao@ifi.unicamp.br

Since the early report of graphite-based carbon nanotubes (CNT) by Iijima [1], as a by-product of fullerene synthesis, the carbon science has experienced an intense growth with the discovery of new and exciting phenomena.

Although much of the recent works on nanotubes have been focused on graphitic structures, alternative structures containing heteroatoms (N, B, etc.), as well as various carbon-free nanofibers, have been recently synthesized [2]. We believe that other types of pure carbon nanotubes are feasible using different accessible hybridization states of carbon. One possibility is to use graphyne sheets as structural motifs. Graphyne is an allotropic form of carbon proposed by Baughman, Eckhardt, and Kertesz in 1987 [3].

Graphyne is the name for the lowest energy member of a family of carbon phases consisting of planar molecular sheets containing only sp and sp^2 carbon atoms. The presence of acetylenic groups in these structures introduces a rich variety of optical and electronic properties that are quite different from those of ordinary carbon nanotubes. Just as a sheet of graphite (graphene) can be rolled to form different types of CNTs (armchair, zigzag, or chiral), various graphyne-based nanotubes (GNTs) are similarly possible (Figure 1).

We report here structural and electronic properties for the families of graphynes shown in Figure 1 (as both infinite planar sheets and nanotubes) using tight-binding (TB) and ab initio density functional methods. TB calculations for idealized geometries were carried out using the methodology of Saito et al. [4]. We have also performed ab initio density functional (DFT) calculations for the graphyne sheets using the SIESTA [5] code in the generalized gradient approximation. Although the TB approach is quite simple, comparisons of predictions of the TB and DFT methods show that the main electronic features of graphyne and related structures are in good agreement [6]. Using the TB approach the geometrical transformation of a flat sheet into nanotubes can be easily simulated using a slicing process [2], which is not feasible using DFT methods.

Of the three graphyne nanotube families analyzed here, two provide metallic behavior for armchair tubes and either metallic or semiconducting regime for zigzag nanotubes. A diameter and chirality independent badgap is predicted for the γ-graphynes (Figure 2). Besides unusual electronic properties the holes in GNTs (Figure 1) can enable unprecedented shell doping, as well as rapid materials transport through the nanotube sidewalls. Studies to synthesize these remarkable structures are in progress.

References:

[1] S. Iijima, Nature (London), **354** (1991) 56.
[2] S. B. Sinnott and R. Andrews, Crit. Rev. Solid State Mater. Sci., **26** (2001) 145, and references therein.
[3] R. H. Baughman, H. Eckhardt and M Kertesz, J. Chem. Phys., **87** (1987) 6687.
[4] R. Saito et al., Phys. Rev. B, **46** (1992) 1804.
[5] P. Ordejón, E. Artacho, and J. M. Soler, Phys. Rev. B, **53** (1996) R10441.
[6] V.R. Coluci, S.F. Braga, S.B. Legoas, D.S. Galvão, and R.H. Baughman, Mat. Res. Soc. Symp. Proc., **739** (2003) H.5.6.1.

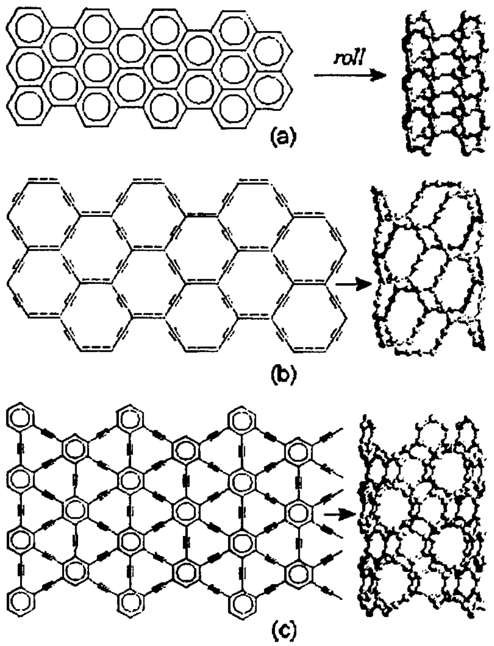

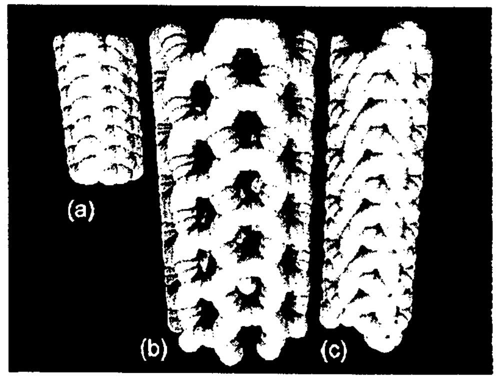

Figure 1. Structural (left) and 3D-representation (above) of conventional carbon nanotubes (a) and α- and γ-graphyne nanotubes (b and c, respectively).

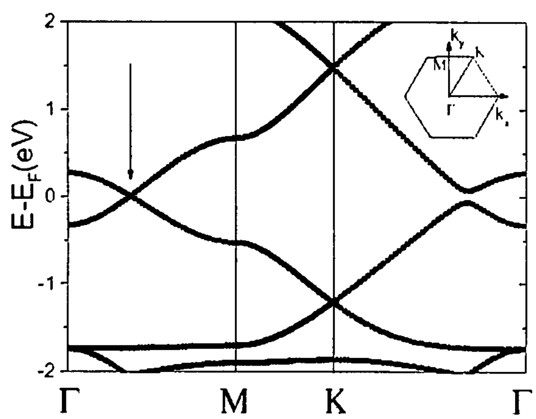

Figure 2. Band structure of the γ-graphyne sheet obtained from DFT calculations.

Work supported in part by the Brazilian Agencies FAPESP, CNPq, IMMP/MCT, CAPES, and the Robert A. Welch Foundation.

GIGAHERTZ NANOMECHANICAL OSCILLATORS BASED ON CARBON NANOTUBES

S. B. Legoas[1], V. R. Coluci[1], S. F. Braga[1], P. Z. Coura[2], S. O. Dantas[2], and D. S. Galvão[1]
[1]Instituto de Física Gleb Wataghin, Universidade Estadual de Campinas, UNICAMP
CP 6165, 13083-970 Campinas, SP, Brazil
[2]Departmento de Física, UFJF, 36036-330, Juiz de Fora, MG, Brazil
E-mail: galvao@ifi.unicamp.br

The technological advances have led to the need for creating functional devices at nanometer scale [1]. There have been continuing efforts in fabricating nanomechanical systems operating in high frequencies, but gigahertz range is beyond our present micromachining capabilities [2,3].

A breakthrough in this area has been obtained by Cumings and Zettl [4]. They demonstrated the controlled and reversible telescopic extension of multiwalled carbon nanotubes (MWNTs), thus realizing ultralow-friction nanoscale linear bearings (Figure 1a). These results indicate that the fabrication of nanomechanical systems operating in high frequencies is now a possible realization. This achievement was possible due to the discovery of a method whereby the ends of a MWNT can be carefully opened in a way that the core nanotubes are left fully intact and protruding.

Similarly to graphite, the intershell interactions in MWNTs are predominantly van der Waals [1], and since the interlayer corrugation is small it is expected that individual cylinders of MWNTs might easily slide or rotate with respect to one another. Depending on the distance separation between two adjacent nanotubes, it is possible to have an almost perfect sliding surface [5]. The van der Waals interactions between the nanotubes create a restoring force that cause the inner tube to retract (Figure 1) [2,4,6] and can be the physical basis (and whithin our present technological capabilities) to build nanodevices.

Using static models on a slightly modified Cumings and Zettl set up, Zheng et Jiang [2] (Figure 1b) have showed that multishelled nanotubes could lead to gigahertz nanooscillators. We have carried out molecular dynamics studies for these systems in the framework of classical mechanics with standard molecular force fields [6], in order to analyze the reliability of such nanodevices and to determine the importance of temperature and time fluctuations, The calculations were carried out considering structures containing up to 6,000 carbon atoms. Different nanotubes types (single and multiwalled armchair, zigzag, chiral, and combinations) were analyzed. Our results show that sustained oscillatory behavior (Figure 2) is possible (for all kind of tube combinations) only when a perfect coupling (when the radii differences between inner and outer tubes are of ~ 3.4 Å) occurs. For other couplings, although the telescopic and retractile movements are possible, dissipative forces and momentum exchange among the nanotubes compromise the sustained oscillatory regime. Our results showed that multishell nanotubes can be used to make functional nano-oscillators in gigahertz range.

References:

[1] L. Forró, Science, **289** (2000) 560.
[2] Q. Zheng and Q. Jiang, Phys. Rev. Lett., **88** (2002) 045503.
[3] K. E. Drexler, Nanosystems: Molecular Machinery, Manufacturing and Computation (Wiley, New York, 1992).
[4] J. Cuming and A. Zettl, Science, **289** (2000) 602.
[5] R. Saito et al., Chem. Phys. Lett., **348** (2001) 187.
[6] S.B. Legoas, V.R. Coluci, S.F. Braga, P.Z. Coura, S.O. Dantas, and D.S. Galvão, Phys. Rev. Lett., **90** (2003) 055504.

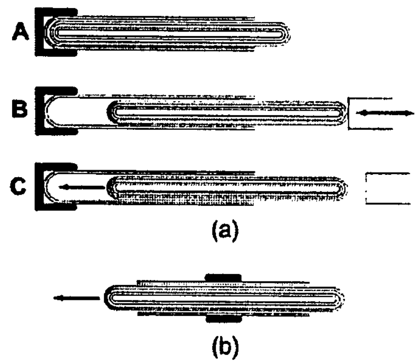

Figure 1. (a) Shematic representation of Cumings and Zettl experimental set up [4]. The A, B, and C sequences represent the experimentally observed controlled core nanotube reversible telescoping. (b) Schematic setup of carbon nanotubes oscillators proposed by Zheng et Jiang [2].

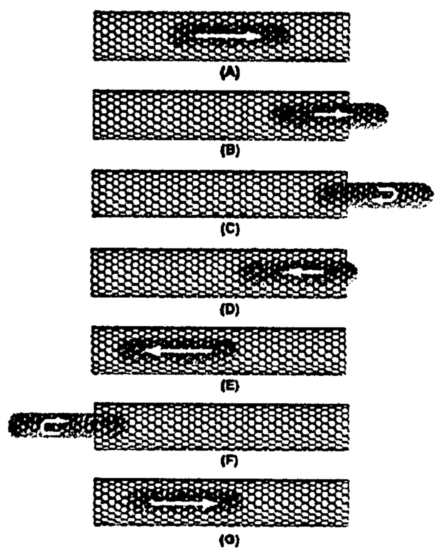

Figure 2. Snapshots from the molecular dynamics simulations showing the sustained oscillatory behavior of a (9,0) nanotube inside a (18,0) one with its double length.

Work supported in part by the Brazilian Agencies FAPESP, FAPEMIG, CNPq, IMMP/MCT, and CAPES.

SILVER NANOPARTICLES PREPARED VIA SOL-GEL

M. A. García[1,*], M. García-Heras[2], E. Montero[3], E. Cano[2], C. Sada[4], S. E. Paje[5], G. De Marchi[4], M. A. Villegas[2], J. M. Bastidas[2], P. Mazzoldi[4], J. Llopis[3]

[1]Instituto de Magnetismo Aplicado. P.O. Box 155. 28230 Las Rozas (Madrid). Spain
[2]Centro Nacional de Investigaciones Metalúrgicas, CSIC. Avda. Gregorio del Amo, 8, 28040 Madrid, Spain.
[3]Departamento de Física de Materiales, Facultad de Ciencias Físicas, Universidad Complutense de Madrid. Avda. Complutense s/n, 28040 Madrid, Spain.
[4]INFM, Dipartimento di Fisica, Universita' di Padova, via Marzolo 8, 35131 Padova, Italy
[5]Dpto. Física Aplicada, E.T.S.I. Caminos, Universidad de Castilla-La Mancha 13071 Ciudad Real, Spain

* Corresponding author: E-mail: miguelag@renfe.es

In the last years, growing attention has been paid to the incorporation of metallic nanoparticles into dielectric matrices, because new optical properties arises from the presence of those particles into the network. This is the case of silver nanoparticles incorporated into silica based glasses, which exhibit interesting features as high non-linear susceptibility, optical absorption ascribed to plasmon resonances and others. These optical properties are strictly related to the glass-particles ensemble microstructure, so it is essential to develop preparation methods that allow to control the incorporation and reduction of metallic ions in the matrix, and the subsequent nucleation and growing process of the particles.
Most efforts has been focussed on the achievement of glassy films doped with metals in order to achieve an easy integration in optoelectronic devices. There are several techniques to fabricate those films, these including sol-gel route, ion exchange, sputtering or ion implantation. Among these techniques, sol-gel route results specially attractive for the preparation of coatings, as this is a low -temperature-process that provides good homogeneity of coatings, and easy control of silver concentration and thickness.
We present here an structural and optical characterization of silver doped glasses, prepared via sol-gel, describing the formation process and stating the relationship between preparation parameters (mainly substrates and annealing temperature and atmosphere) and the structural and optical features of the system.

Wave propagation in Photonic Crystal waveguiding structures

D. Hermann[1], A. García-Martín[2], J.J. Sáenz[3], R. Gómez-Medina[3], K. Busch[1], and P. Wölfle[1]

(1) Institut für Theorie der Kondensierten Materie, Universität Karlsruhe, P.O. Box 6980. 76128 Karlsruhe, Germany

(2) Instituto de Microelectrónica de Madrid, Consejo Superior de Investigaciones Científicas, Isaac Newton 8, Tres Cantos, E-28760 Madrid, Spain.

(3) Departamento de Física de la Materia Condensada, Universidad Autónoma de Madrid, Cantoblanco, E-28049 Madrid, Spain

Waveguiding structures built into Photonic Crystals form the basic elements of the upcoming integrated optics technology and thus their transmission and reflection properties are of great interest. To date, the theoretical description of such structures is practically limited to general computational methods such as FDTD or FEM simulations that make little or no use of the information available through the fact that these defect structures are embedded in the highly ordered lattice of a Photonic Crystal.

We present a novel approach for the computation of electromagnetic wave propagation in Photonic Crystal (PC) waveguides. The approach uses a generalized scattering matrix method together with a basis of localized photonic Wannier functions that are best suited to describe the localized fields occuring in PC defect structures and waveguides. By construction, Wannier functions correctly incorporate the symmetry properties of the underlying Photonic Crystal and, as a consequence, represent a set of localized basis functions that is well-suited to the description of defect structures in them.

The method shown here allows efficient investigation of finite-sized PC samples, various defect and waveguiding structures.

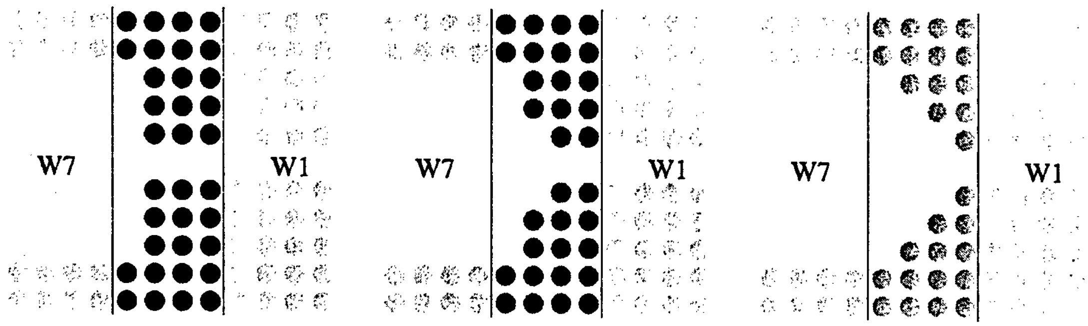

FIG. 1. Example of three different waveguiding structures.

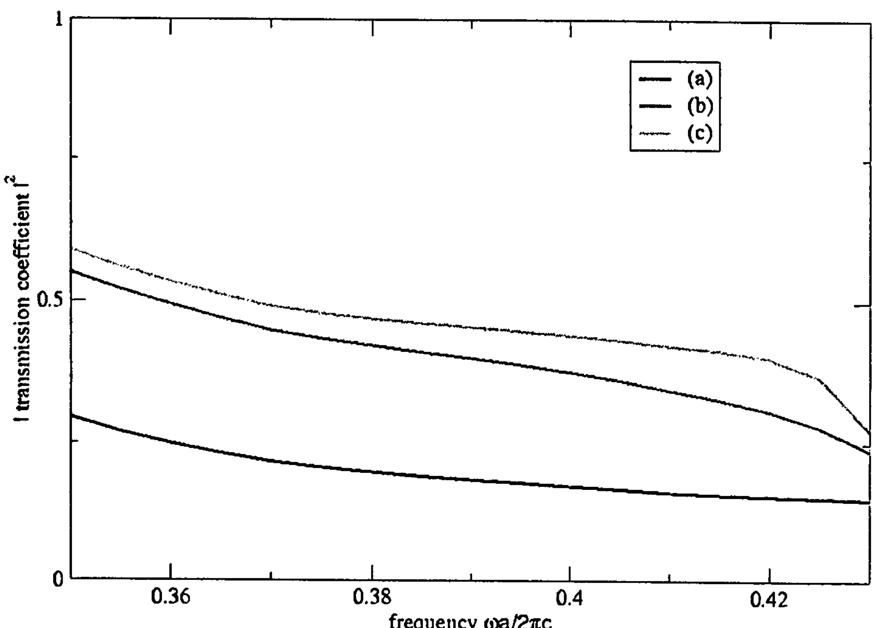

FIG. 2. Transmission coefficient corresponing to the structures shown in Fig.1 when only the guided mode with the largest $|\bar{k}|$ in propagation direction is excited in the incoming field from the left ($I_m^L = \delta_{m1}$) and there is no incoming wave from the right ($I^R \equiv 0$)

DEPOSITION AND CHARACTERIZATION OF SEMICONDUCTOR NANOCRYSTALS ON ULTRATHIN POLYCONJUGATED SUBSTRATES AT THE AIR-WATER INTERFACE

Yuval Golan, Nataly Belman, Yevgeniy Lifshitz and Amir Berman*
Department of Materials Engineering, Ben-Gurion University, Beer-Sheva 84105, Israel
*Department of Biotechnology Engineering, Ben-Gurion University,
Beer-Sheva 84105, Israel
E-mail: ygolan@bgumail.bgu.ac.il

Ultrathin films of polydiacetylene (PDA) are unique templates for growth of oriented semiconductors due to their electrical conductivity and long range crystalline order with a distinct linear alignment of the conjugated chains. This work focuses on the formation of PDA films at the air-water interface and their use as substrates for several nanocrystalline semiconductors such as PbS, CdS and Ag_2S in an attempt to achieve controlled crystal size and size distribution, morphology and orientation in these new hybrid organic-inorganic materials. The nanocrystal deposition is carried out by reacting aqueous salt solutions of the required cations with controlled amounts of H_2S gas in a sealed chamber. After deposition of the nanocrystals, the sample is either transferred onto solid support using the Langmuir-Schäffer technique and characterized *ex-situ* by AFM, TEM and electron diffraction, or characterized *in-situ* using synchrotron grazing incidence X-ray diffraction (GIXD).
The CdS and PbS (both composed of divalent metal cations) nanocrystals were found to be linearly arranged along the polymer chains, and their orientation controlled by the linear axis of the polymer film (Fig. 1a and Fig. 2). On the other hand, the monovalent Ag_2S apparently has a much weaker affinity for the polymer template (note that the nanocrystals are seen mostly *in voids* in the template in Fig. 1b), suggesting favorable packing of divalent cations with the polymer headgroups versus unfavorable association of the template with the monovalent silver ions. The mutual relationship of the strongly interacting nanocrystals and template will be emphasized: The metal cations in the aqueous subphase affect the polymer packing and structure, while in turn, the polymer template controls the nanocrystals spatial arrangement and orientation.

Figures:

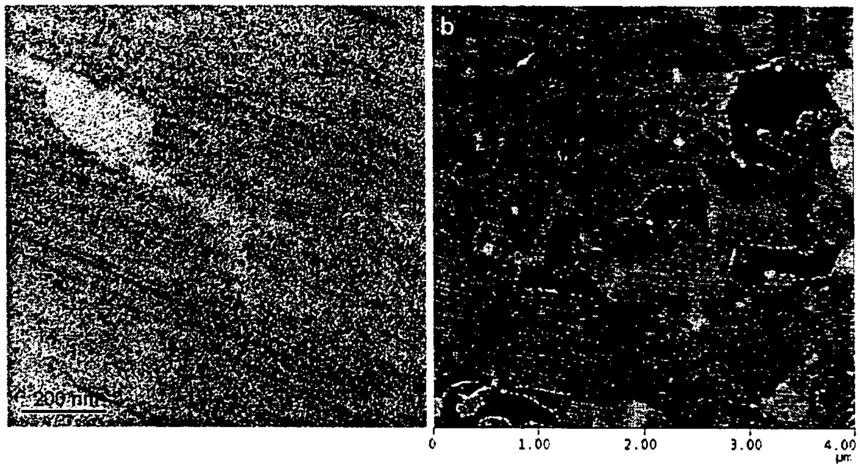

Figure 1: (a) Bright field TEM image of CdS (divalent Cd) nanocrystals on PDA. (b) Topography AFM image of Ag_2S (monovalent Ag) nanocrystals on PDA.

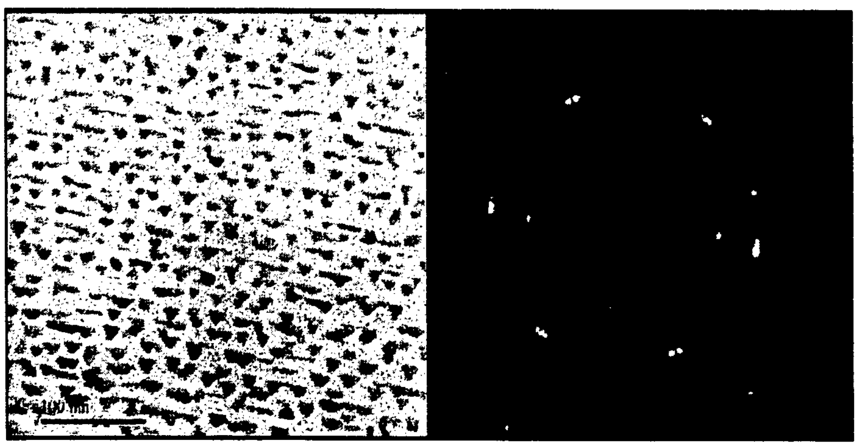

Figure 2: TEM image and electron diffraction pattern obtained from oriented PbS (divalent Pb) nanocrystals on PDA

FANO-LIKE RESONANCES IN THREE-QUANTUM DOT AHARANOV-BOHM RINGS

I. Gómez[1], F. Domínguez-Adame[1], P. Orellana[2]
[1]GISC, Departamento de Física de Materiales , Universidad Complutense, E-28040 Madrid, Spain
[2]Departamento de Física, Universidad Católica del Norte, Casilla 1280, Antofagasta, Chile

Since U. Fano propossed in 1961 a theoretical framework to explain the shape of some He resonances observed in electron inelastic scattering experiments [1], a large variety of systems [2, 3, 4] have shown what seems to be an ubiquitous phenomena that fits into this framework: the Fano effect. Recent advances in nanotechnology have made it possible to study interference phenomena like the Fano effect on Aharanov Bohm rings made of quantum dots. Thus, both experimental [5, 6] and theoretical works [7, 8] have been devoted to this effect, which turns out to be a consequence of the quantum mechanical interference between the quantum dot resonant state and the continuum [1]. In this work we study electron transport through a quantum wire coupled to a three-quantum dot Aharanov-Bohm ring by using a noninteracting Anderson tunneling Hamiltonian. In this system we have observed the appearance of Fano-like resonances on the conductance. We have investigated the asymmetry and the position of the conductance resonances finding closed expressions for them. Phase jumps related to the Fanolike resonances are also studied. In adition, Aharanov-Bohm oscillations as well as conductance dependence on the magnetic field have been investigated.

References

[1] U. Fano, Phys. Rev. 124, 1866 (1961).
[2] R. K. Adair, C. K. Bockelman, and R. E. Peterson, Phys. Rev. 76, 308 (1949).
[3] F. Cerdeira, T. A. Fjeldly, and M. Cardona, Phys. Rev. B 8, 4734 (1973).
[4] J. Faist, F. Capasso, C. Sirtori, K. W. West, and L. N. Pfeiffer, Nature 390, 589 (1997).
[5] A. Yacoby, M. Heiblum, D. Mahalu, and H. Shtrikman, Phys. Rev. Lett. 74, 4047 (1995).
[6] K. Kobayashi, H. Aikawa, S. Katsumoto, and Y. Iye, Phys. Rev. Lett. 88, 256806-1 (2002).
[7] K. Kang, Phys. Rev. B 59, 4608 (1999).
[8] Z. Y. Zeng, F. Claro, and A. Pérez, Phys. Rev. B 65, 085308-1 (2002).

ELECTROSTATIC FORCE MICROSCOPY ON CARBON NANOTUBES

S. Gómez-Moñivas, C. Gómez-Navarro, J. Gómez-Herrero and J. J. Sáenz.
Departamento de Física de la Materia Condensada e Instituto Nicolás Cabrera. Universidad Autónoma de Madrid, 28049 Madrid, Spain.
E-mail: sacha.gomez@uam.es

By applying a voltage between a force microscope tip and a sample, electrostatic force microscopy (EFM) has been used to study different properties of both metallic and insulating surfaces. Recent EFM experiments on carbon nanotubes adsorbed on a dielectric sample [1] have pointed out the ability of EFM to study the dielectric response of single molecules. However, the exact nature of the contrast mechanisms is not well understood. Since EFM is a non-local technique due to the long-range nature of the electrostatic interaction, the detailed shape and dimensions of the tip must be taken into account for a precise calculation of electrostatic force. The lateral resolution [2] and other important magnitudes [3] can be strongly affected by the dimension and shape of the tip.

In this work we present a detailed theoretical analysis together with EFM experiments of the electrostatic interaction between the EFM tip and multi-walled carbon nanotubes (MTNT) of different lengths and radii. The electric field distribution (and the associated electrostatic force) between the EFM tip and a nanotube adsorbed on a dielectric sample is analyzed in detail. The contrast mechanisms and performance of different EFM operation modes will also be discussed. As we will show, the calculated force gradients as well as the simulated images are in striking agreement with the experimental results.
[*This work has been supported by the EU IST project "DNA-based molecular nanowires" - IST-2001-38951-*]

References:

[1] C. Gómez-Navarro et al., PNAS **99**, 8484 (2002); Nanotechnology **13**, 314 (2002).

[2] S. Gómez-Moñivas, J.J. Sáenz, R. Carminati and J.J. Greffet. Appl. Phys. Lett **76** 2955 (2000), S. Gómez-Moñivas, L.S. Froufe, A.J.Caamaño and J.J. Sáenz. Appl. Phys. Lett **79**, 4048 (2001), S. Gómez-Moñivas, L.S. Froufe, R. Carminati, J. J. Greffet and J.J. Sáenz. Nanotechnology **12**, 496 (2001).

[3] S. Gómez-Moñivas, J.J. Sáenz, M. Calleja and R. García, *Field induced formation of nanometer-sized water bridges,* Phys. Rev. Lett., *in press* (2003).

Figures:

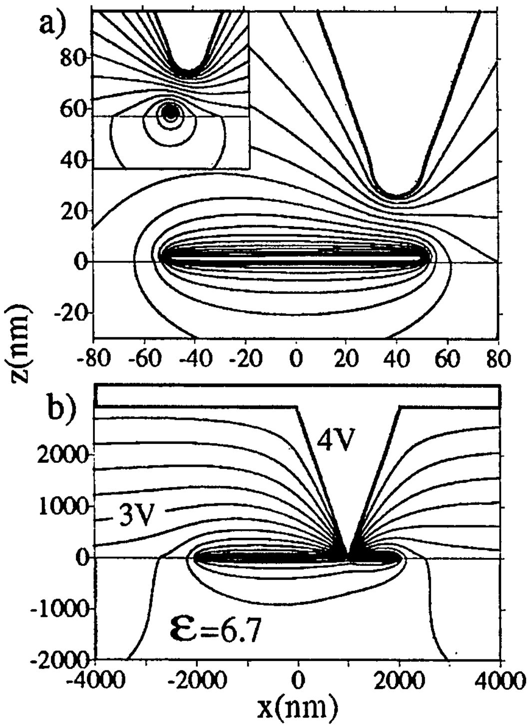

Electrostatic potential distribution inside an Electrostatic Force Microscopy. a) tip-sample region. b) Simulation including the cantilever. The sample is a metallic nanowire on a dielectric sample.

TOWARDS SINGLE PROTEIN NANOBIOSENSORS

G. Gomila[1], A. Errachid[1], O. Ruiz[1], J. Samitier[1], G. Ferrari[2], M. Sampietro[2], C. Pennetta[3], E. Alfinito[3], L. Reggiani[3], J. Bausells[4], N. Jaffrezic-Renault[5], E. Pajot-Augy[6] and R. Salesse[6].

[1]Research Centre for Biolectronics and Nanobioscience and Departament d'Electrónica, Universitat de Barcelona, C/ Martí i Franquès 1, 08028 Barcelona, Spain. E-mail: E-mail: ggomila@pcb.ub.es http://www.nanobiolab.pcb.ub.es

[2]Dipartimento di Elettronica ed Informazione, Politecnico di Milano, Milano, Italy

[3]INFM-National Nanotechnology Laboratory and Dipartimento di Ingegneria dell'Innovazione, Universita di Lecce, Lecce, Italy.

[4]Instituto de Microelectrónica de Barcelona, Centro Nacional de Microelectrónica, CSIC, Barcelona, Spain.

[5]Laboratoire de Ingénierie et Fonctionalisation des Surfaces, École Centrale de Lyon-CNRS, Lyon, France.

[6]Laboratoire de Biologie Celluler et Moleculer, Institute National de la Recherche Agronomique, Jouy-en-Josas, France

Molecular bioelectronics is currently a research field in fast development and expansion. By coupling biomolecules to non-biological electronic transducers, molecular bioelectronic systems could one day be used in a wide variety of apparatus, including biosensors, devices for driving bitransformations, biofuel cells and maybe even biocomputers. A major thrust in molecular bioelectronics is the development of chemical biosensors, with uses ranging from clinical diagnostics to environmental applications.

The ultimate limit in the miniaturization, sensitivity and specificity of such a chemical biosensors will be reached when their active part consists of a single biomolecule. In order to reach such a limit many difficulties have to be overcome. Among others we cite the fabrication of low resolution nanoelectrodes, the production and purification of a sufficient amount of the corresponding biomolecule, the elaboration and transfer of monolayers of the biomolecules on the nanoelectrodes, the characterisation and modelling of the electrical properties of single biomolecules and the design of a very sensitive read out electronic interface.

In the present communication we present the first steps covered towards the development of a single protein olfactory nanobiosensor inside the european project Single Protein Nanobiosensor Grid Array.

References

"Single Protein Nanobiosensor Grid Array" (SPOT-NOSED, IST2001-38899), www.nanobiolab.pcb.ub.es/projectes/spotnosed.

INFORMATIONAL DESCRIPTION OF AVOIDED CROSSINGS IN NANOTECNOLOGICAL SYSTEMS

R. Gonzalez-Ferez[1] and J. S. Dehesa[2]

[1]University of Heidelberg, Germany
[2]Universidad de Granada, Spain

In this poster/comunication we provide an information-theoretic description of some highly-non-linear phenomena of nanotecnological systems (atoms, molecules) called as avoided crossings. Our main contribution is the suggestion of two new parameters (Shannon's entropy, Fisher's information measure), in addition to the conventional ionization energy, to characterize this most distintive characteristic spectral phenomena. Applications to some specific dynamical states of hydrogenic atoms will be supplied [1,2].

References:

[1] R. Gonzalez-Ferez and J. S. Dehesa, Chem. Phy. Lett. 373, 615 (2003)

[2] R. Gonzalez-Ferez and J. S. Dehesa, Phy. Rev. Lett.(under revision)

FREE-STANDING III-V SEMICONDUCTOR NANOWIRES

J. C. González[1], H. R. Gutiérrez[2], J. Bettini[1], D. Zanchet[1], F. M. Matinaga[3] M.A. Cotta[2] and D. Ugarte[1]
[1]Laboratório Nacional de Luz Síncrotron, Caixa Postal 6192, 13084-971 Campinas SP, Brazil.
[2]Instituto de Física Gleb Wataghin, DFA/LPD, UNICAMP, CP 6165, 13081-970 Campinas-SP, Brazil.
[3]Departamento de Física, UFMG, CP 702, 30123-970, Belo Horizonte, MG, Brazil
e-mail: gonper@lnls.br

The concept of using nanostructures as building blocks for electronic and optoelectronic devices has attracted great interest in recent years [1, 2]. In this work, we describe our recent results on the growth of free-standing III-V (NW's) by Chemical Beam Epitaxy (CBE). III-V NW's were grown using Au nanoparticles (NP's) acting as seeds within a vapor-liquid-solid growth process.

Atomic Force Microscopy (AFM) was used to measure the diameter and spatial distribution of the Au NP's spin coated on different substrates. The size distribution of the original Au NP's solution was also characterized by Transmission Electron Microscopy (TEM). The morphology, crystal structure and chemical composition of the wires were characterized by Field Emission Scanning Electron Microscopy (FE-SEM), TEM and Energy Dispersive X-ray Spectroscopy (EDS). Photoluminescence (PL) was used to investigate the optical properties of the NW's.

Using this method free-standing nanowires of approximately 50 nm in diameter and longer than 5000 nm can be easily obtained. The grown NW's were crystalline, as verified by electron diffraction and TEM, and mainly oriented along the [100] and [110] crystallographic directions. The NW's were also found to be stoichiometric. InP/InAs/InP one-dimensional heterostructures were also grown, as is shown in Fig. 1. However, the nanowires morphology strongly depends of the gown conditions, in particular the flux of group III precursors and substrate temperature.

Low temperature PL experiments in undoped and doped InP NW's revealed a small quantum confinement in the wires and confirmed the good crystalline quality of the wires, observed by TEM.

References:

[1] X. Duan, Y. Huang, R. Agarwal and C. M. Lieber, Nature, **421** (2003) 241.
[2] M. T. Björk, B. J. Ohlsson, T. Sass, A. I. Persson, C. Thelander, M. H. Magnusson, K. Deppert, L. R. Wallenberg and L. Samuelson, Appl. Phys. Lett., **50** (2002) 1058.

Figures:

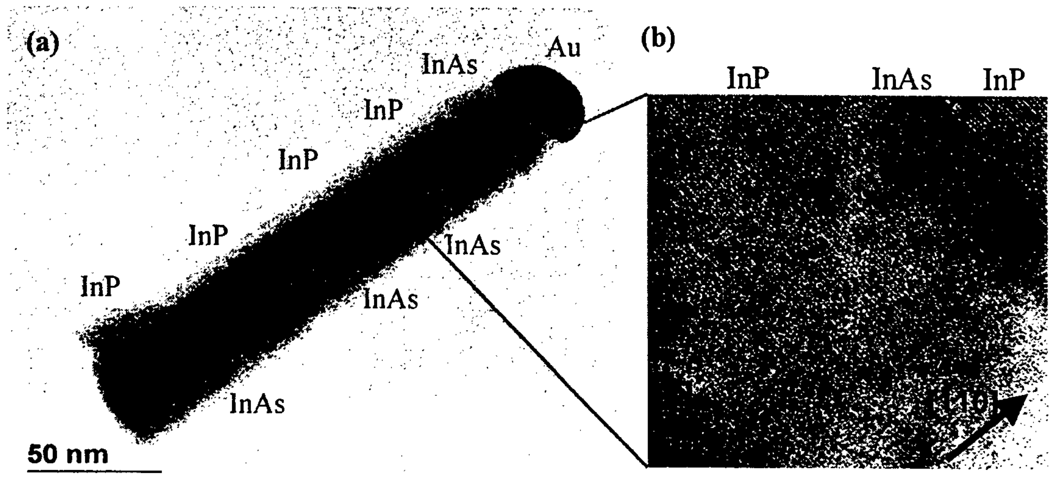

Fig. 1. InP/InAs/ InP one dimensional heterostructure. (a) TEM image of the one dimensional heretostructure, showing the contrast between the InP layers (grey) and InAs layers (dark). (b) High resolution TEM image of one section of the heterostructure.

MOLECULAR CONFINEMENT AND SHEAR OF THIN FILMS STUDIED BY ABSORPTION SPECTROSCOPY

Delphine Gourdon, Anna R. Godfrey and Jacob Israelachvili

Department of Chemical Engineering, University of California Santa Barbara
Santa Barbara, CA 93106, USA
Email: delph@engineering.ucsb.edu

We are investigating the effects of confinement and shear on the optical properties of dye molecules trapped in nm-gap films using the Surface Forces Apparatus (SFA) technique and absorption spectroscopy [1,2]. The absorption spectrum of Rhodamine B, a highly absorbing dye, has been studied under different pressures of confinement (hence different gaps), as a function of shear rate and external temperature.

The behavior of the absorption spectra under confinement (Fig.1) and shear has been compared with bulk absorption measurements performed as a function of temperature as well as of concentration, and revealed that the dye tends to form dimers under confinement and crystallizes rapidly under shear. In addition, freeze-fracture AFM of single surfaces (after they have been sheared), provides information on both the temperature changes of the molecules at the shearing interface and the eventual molecular shear-induced alignment. Ultimately, these correlations should allow us to use various dye molecules as in situ *molecular-level* temperature, pressure and structural *probes* at both static and shearing junctions.

References:

[1] Enhanced absorption within a cavity: a study of thin dye layers with the Surface Forces Apparatus, C. Müller, P. Mächtle and C. A. Helm, J. Phys. Chem. **98** (1994) 11119-11125.

[2] A thin absorbing layer at the center of a Fabry-Pérot interferometer, P. Mächtle, C. Müller and C. A. Helm, J. Phys. II France **4** (1994) 481-500.

Figures:

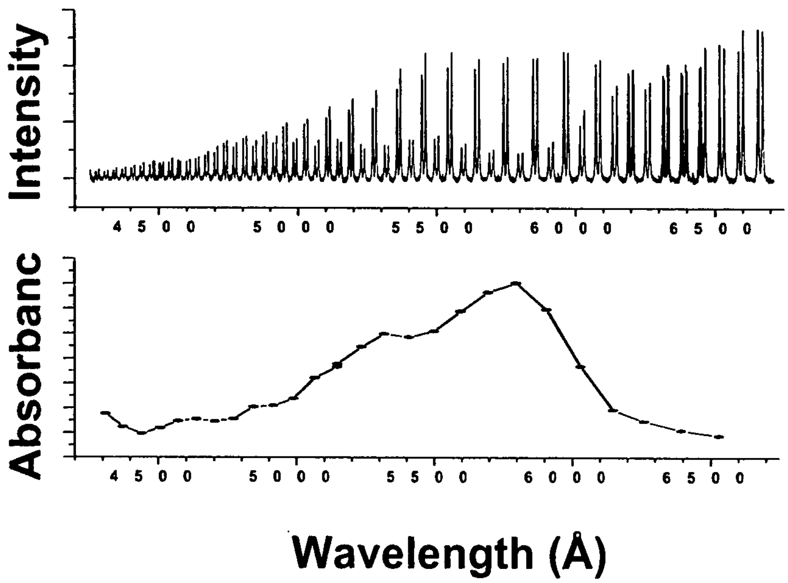

Fig 1: Measured transmitted intensity (top) and resulting absorbing spectrum (bottom) of two contacting atomically smooth mica sheets confining a 10 nm-thick Rhodamine B dye film.

INVESTIGATION OF CHROMOPHORIC NANOWIRES BY SINGLE MOLECULE FLUORESCENCE AND ATOMIC FORCE MICROSCOPY

J. Hernando[1], P.A.J. de Witte[2], E.M.H.P van Dijk[1], J. Korterik[1], E.E. Neuteboom[3], S.C.J. Meskers[3], R.A. J. Janssen[3], R.J.M. Nolte[2], A.E. Rowan[2], M.F. García-Parajó[1], N.F. van Hulst[1]

[1] Applied Optics Group, Faculty of Science Technology & MESA+ Research Institute, University of Twente, P.O. Box 217, 7500 AE Enschede (The Netherlands)

[2] Department of Organic Chemistry, NSRIM Center, University of Nijmegen, Toernooiveld 1, 6525 ED Nijmegen (The Netherlands)

[3] Macromolecular and Organic Chemistry, Faculty of Chemical Technology, University of Eindhoven, P.O. Box 513, 5600 MB Eindhoven (The Netherlands)

E-mail: j.hernando@tnw.utwente.nl

Multichromophoric systems display valuable optical properties due to excitonic interactions between close-by dye units. This is the case of light-harvesting antennas in photosynthetic complexes, which allow for efficient light absorption and unidirectional transfer of energy to the reaction center during the photosynthesis process. The design of artificial multichromophoric systems that mimic those properties can be envisaged with the ultimate goal of building molecular photonic devices. In this work, a rigid rod-like multichromophoric polymer intended to act as such a synthetic antenna has been investigated at the single molecule level by means of fluorescence and atomic force microscopy (AFM). Combined single molecule fluorescence and force measurements have provided with a unique insight into the complex optical behavior of this system.

To attain optimal excitonic behavior, a controlled close-packing of the chromophores in the aggregate is required. Recently, we have demonstrated that polyisocyanides, intrinsically rigid helical polymers [1], are an ideal scaffold to achieve such degree of chromophoric organization over large distances. Long well-ordered porphyrin [2] and perylene arrays have been synthesized in this way. The resulting polymers have a chiral backbone to which the chromophores are attached in four parallel stacks, as depicted in Figure 1a. The distances between consecutive chromophoric units in one stack are short enough to allow for strong excitonic coupling between them.

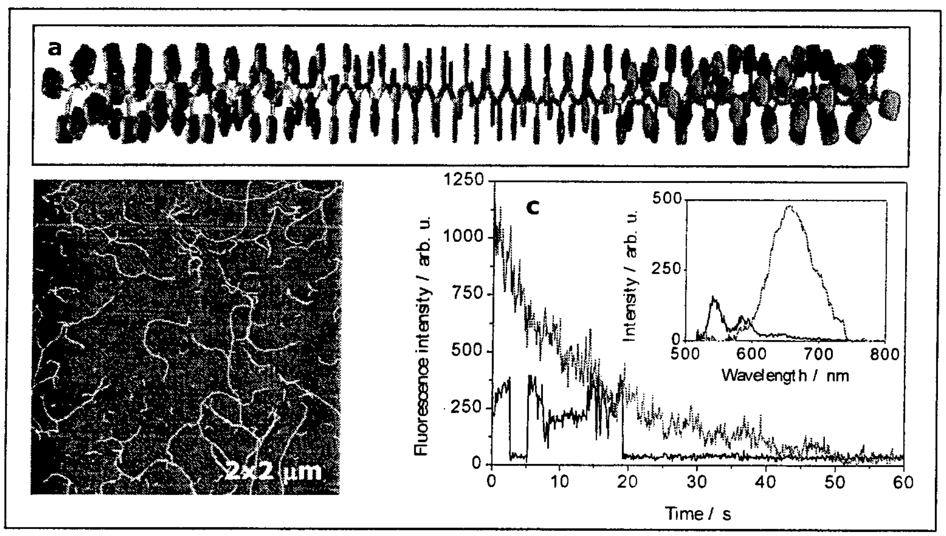

(a) Structure of the perylene polymer; (b) AFM image of the polymer fibers on mica; (c) fluorescence intensity trajectories for two different single molecules in a perylene polymer sample, including their emission spectra in the inset.

Single molecule techniques have recently proved to be a powerful tool to cope with the understanding of exciton dynamics in multichromophoric systems [3]. Fluorescence and atomic force microscopy (AFM) have been used in this work to thoroughly investigate the perylene polyisocyanide polymers. AFM measurements have shown rigid chromophoric fibers up to micrometers long and containing up to ten thousand perylene dye units (Figure 1b). The optical behavior of single polymer fibers has been investigated using a fluorescence confocal microscope with polarization and spectrum sensitivity [4]. Two different emissive behaviors arising from single entities in the polymer sample have been found, as shown in Figure 1c. Thus, steps in the fluorescence intensity trajectory correlate with a monomer-like spectrum, while continuously decaying intensity emission shows excimer-like spectrum. Combined AFM and confocal measurements have been performed to unravel this behavior: the monomer-like emission has been proved to arise from monomer molecules left in the sample and short perylene oligomers without helical structure, while the excimer-like emission has been shown to correspond to the long helical perylene arrays. For those arrays, excimer species are formed after excitation by interaction between few face-to-face perylene units. These species trap the electronic energy and prevent its fully delocalization throughout the polymer.

As already mentioned, the multichromophoric polymers studied here may be of interest as a synthetic antenna. To goal this, they must be further optimized and equipped with an energy gradient that acts as a driving force for the electronic energy flow. As demonstrated in this work, the combination of single molecule fluorescence and atomic force microscopy would then be an ideal technique to deal with the characterization of such system.

References:

[1] J. J. L. M. Cornelissen, J. J. J. M. Donners, R. de Gelder, W. S. Graswinckel, G. A. Metselaar, A. E. Rowan, N. A. J. M. Sommerdijk, R. J. M. Nolte, Science, **293** (2001) 676.

[2] P. A. J. de Witte, M. Castriciano, J. J. L. M. Cornelissen, L. Monsù Scolaro, R. J. M. Nolte, A. E. Rowan, Chemistry, **9** (2003) 1775.

[3] See e.g. A.M. van Oijen, M. Katelaars, J. Kohler, T.J. Aartsma, J. Schmidt, Science **285** (1999) 400.

[4] J.Hernando, M. van der Schaaf, E.M.H.P. van Dijk, M. Sauer, M.F. García-Parajó, N.F. van Hulst, J. Phys. Chem. A, **107** (2003) 43.

Can self assembled Ge quantum dots be defect free?

A. P. Jacob[1], Q. X. Zhao[1], M. Willander[1], L. Vescan[2]

1. Laboratory of Physical Electronics and Photonics,
Department of Physics and Engineering Physics, Gothenburg University/
Chalmers University of Technology, Goteborg, SE-41296, Sweden
2. Institute for Thin Films and Interfaces (ISG), Forschungszentrum Juelich,52425
Juelich, Germany

Silicon based devices had been the major thrust to the semiconductor industry. Integrating Germanium with Silicon gives the advantage of better device performance while maintaining the cost reduction for the industry. The exploitation of silicon/germanium based devices for optoelectronic application is still difficult due to the presence of indirect band gap characteristics in these materials. This problem could be solved with a zero dimensional structure. One could expect higher performance with zero dimensional Ge quantum dots because QD's exhibit increased exciton binding energy and oscillator strength over quantum well and quantum wire structures. The superior optical properties of Si/Ge quantum dots could be exploited for cheaper photonic devices. Thus great effort is currently underway to fabricate nm scale QD's.

In this report, we have extensively studied the effect of deuterium on self assembled Ge quantum dot structures using photoluminescence technique. The quantum dot samples used for this study included both molecular beam epitaxy (MBE) and chemical vapour deposition (CVD) grown structures. Deuterium was incorporated into the sample (i) by annealing them in deuterium atmosphere for 3 hours (ii) by exposing the sample into deuterium plasma for 2 hour at 1.8 mbar pressure. The PL spectroscopy was recorded at various temperatures (4.2 K, 15 K, 45 K, 200 K and 250 K). To our knowledge, this is the first attempt to learn the passivation effect on Ge quantum dots.

Our studies show that the recombination peaks does not have any significant effect even after passivation. Experiments on similarly grown sample from different growth chambers have also shown no significant passivation effect. The results are compared with those results obtained by annealing these samples in Argon atmosphere. These results are extremely interesting because non-radiative recombination centres could be passivated in the Ge quantum dots, in comparison with InAs quantum dots grown on GaAs, which shows a strong passivation effect of non-radiative channels [1].

The possible reasons for this result could be that Stranski-Krastanov Growth of Ge on Si (100) might be free of defects induced by dislocation [2].

Reference:

1. A. P. Jacob, Q. X. Zhao, M. Willander, F. Ferdos, M. Sadeghi and S.M. Wang, Journal of Applied Physics 92, 1 (2002).
2. D. J. Eaglesham and M. Cerullo, Physical Review Letters **64**, 1943 (1990).

Figure Caption:

1. Figure shows the low temperature PL spectra from one set of samples. This sample is grown by CVD. It is seen that there is no significant change in the QDs emission intensity observed in Ge QDs. Similar results are obtained for annealing in an Ar atmosphere.

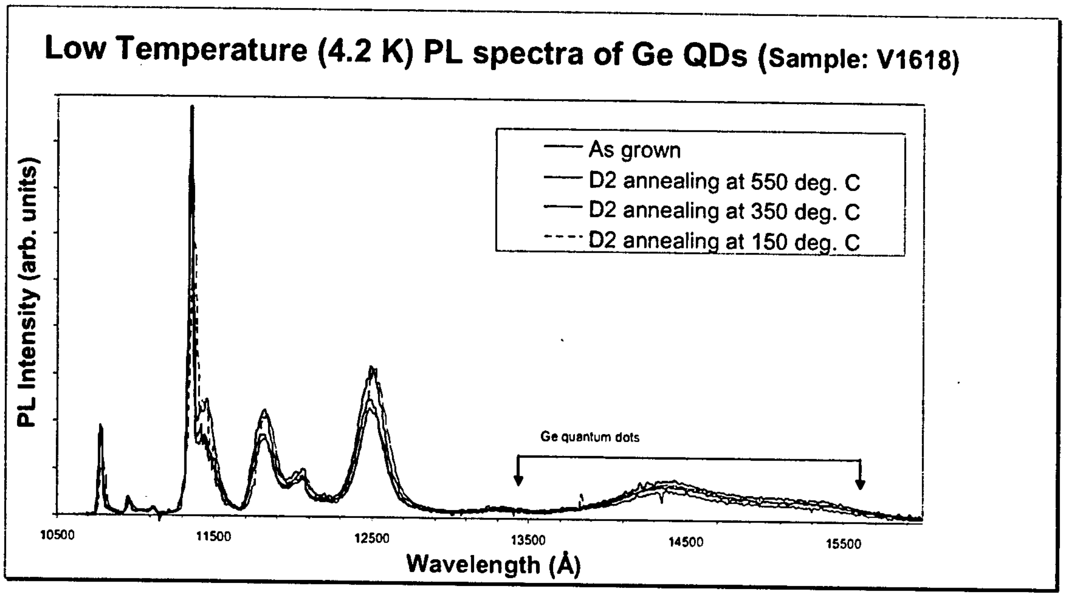

PHYSICS-BASED MODEL FOR THE SIMULATION OF BALLISTIC QUANTUM WIRE AND QUANTUM WELL MOSFETS

D. Jiménez[a*], J. J. Sáenz[b], B. Iñíguez[c], J. Suñé[a], L. F. Marsal[c], and J. Pallarès[c]

[a]Departament d'Enginyeria Electrònica (Universitat Autònoma de Barcelona), Spain
[b]Departamento de Física de la Materia Condensada (Universidad Autónoma de Madrid), Spain
[c]Departament d'Enginyeria Electrònica, Elèctrica i Automàtica (Universitat Rovira i Virgili), Spain
[*]Corresponding author: david.jimenez@uab.es

The control of short-channel effects is more difficult with the progressive scaling of MOSFETs. The double-gate MOSFET has emerged as an excellent device to provide the electrostatic integrity needed to scale down transistors to minimal channel lengths. In addition to a better electrostatics than the single-gate MOSFET, the use of this device has advantages relative to the electronic transport, mainly due to (i) the higher mobility of electrons and (ii) the reduction of the Coulomb scattering because the film is made of undoped silicon. Moreover, the introduction of new materials as the strained silicon to enhance the mobility, can result in electronic transport approaching the ballistic regime. The International Roadmap for Semiconductors (ITRS-2001)[1] has identified a series of challenges that must be solved before this device can enter the manufacturing of CMOS-based integrated circuits. Among them, a complete compact modeling of this structure remains an issue. In an attempt to contribute to this field, we propose a physical compact model of the ballistic double-gate MOSFET operation, based on the Landauer electronic transmission theory[2,3,4]. It captures the static current-voltage characteristics in all the operation regimes, below and above the threshold voltage, and provides a general framework to account for the electronic transport in MOSFETs, being adaptable to gate structures as the surrounding-gate or single-gate by changing the details of the electrostatics. The main novelty that we introduce is the extension of existing models, only formulated for quantum well double-gate MOSFETs, to structures of lower dimensionality, such as the quantum wire MOSFET. We introduce other contributions to the state-of-the-art: (i) the proposed model incorporates effects of multi-subband conduction, (ii) takes into account the band structure of silicon and (iii) the transition between subthreshold and above threshold is well modeled, where other compact models fail[5]. As an illustrative example of the capability of this compact model we show in Figure 1 the simulated transconductance and conductance of a quantum wire MOSFET with a gate oxide of 1.5 nm, a silicon film thickness of 2 nm and silicon width of 3 nm. To validate our approach, numerical simulations based on this compact model have been compared with experiments and quantum mechanical self-consistent simulations[6], with good agreement.

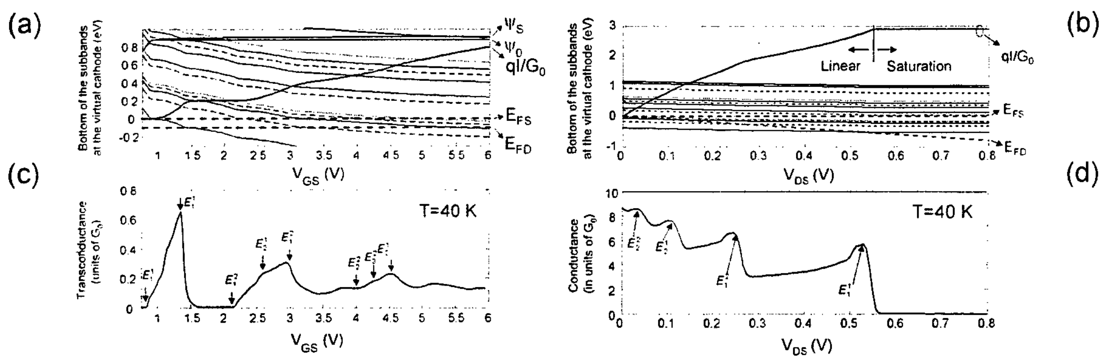

Figure 1. (a)-(b) Bottom of the subbands at the beginning of the channel versus the gate (drain) voltage. The operation temperature is 40 K, and the drain (source) voltage is 0.1 V (0.6 V). The thin solid, dashed and dotted lines represent the bottom of the subbands from the first, second and third set of valleys, respectively. The Fermi level at the source (E_{FS}) is taken as a reference. The normalized current (qI/G_0), the surface (ψ_S), and center (ψ_0) potentials are also represented. In (c)-(d) we plot the simulated transconductance (conductance), showing a clear structure of peaks and valleys at the positions where subbands cross the source and drain Fermi levels.

[1] The International Technology Roadmap for Semiconductors. Available: http://public.itrs.net
[2] M. Lundstrom, IEEE Electron Dev. Lett. **18**, 361 (1997).
[3] S. Datta, F. Assad, and M. S. Lundstrom, Superlatt. Microstruct. **23**, 771 (1998).
[4] D. Jiménez, J. J. Sáenz, B. Iñíguez, J. Suñé, L. F. Marsal, and J. Pallarès, J. Appl. Phys. (in press).
[5] A. Rahman, and M. S. Lundstrom, IEEE Trans. Electron Devices **49**, 481 (2002).
[6] Z. Ren, R. Venugopal, S. Datta, M. S. Lundstrom, D. Jovanovic, and J. G. Fossum, IEDM Tech. Dig., 715 (2000).

FABRICATION OF NANOARRAYS OF $SrZrO_3$ BY PULSED LASER DEPOSITION

S. Karthäuser, E. Vasco, R. Dittmann and R. Waser
Institut für Festkörperforschung, Forschungszentrum Jülich, D-52425 Jülich, Germany.

Nanoarrays of lateral confined structures (wires) of $SrZrO_3$ (SZO) have been fabricated on $SrRuO_3$-buffered $SrTiO_3$ (STO) by pulsed laser deposition. Commercial available STO substrates were chemically treated in order to prepare a TiO_2-finished regular vicinal surface, which promotes the ordered growth of the $SrRuO_3$ (SRO) buffer layer. On this template, SZO was deposited in different oxygen pressures ($P_{O_2}=10^{-4}$-0.5 mbar) at deposition temperatures of 700-800 °C by using a KrF laser emitting 20 ns-pulses at λ=248 nm (fluence of 5 J/cm^2). The deposited samples were studied by atomic force microscopy (AFM), x-ray diffraction and Rutherford backscattering spectroscopy (RBS). AFM-measurements with a conducting tip allow to identify SZO during its first growth stages (previous to the film completion regime, i.e. <30 nm) on basis of the difference between the electrical conductivities of SZO and SRO. Thus, the correlation between the topographic and conducting images corresponding to a same area (Fig. 1) allows to recognize the SZO wires (black area) separated by deep and narrow boundaries that extend up to the conductive buffer layer (light area).

The scaling analysis carried out from the deposition-time dependences of film roughness (σ) and surface correlation length (ξ), $\sigma \propto t^{0.93}$ and $\xi \propto t^{0.40}$, suggests that SZO grows with a 3D habit, which is induced by the geometric shadowing of the incident particles [1]. The study of the angular distribution of the evaporated particles confirms the presence and influence of this phenomenon on the SZO morphology evolution. Thus, the high oxygen pressures produce an increase of the particle scattering by collisions [2] spreading out the average incidence angle from 4° for $P_{O_2}=10^{-4}$ mbar up to 32° for $P_{O_2}=0.5$ mbar. The non-perpendicular incidence on a vicinal surface gives rise to a shadowing effect of the terraces edges on the steps. This effect in combination with an insufficient diffusion due to the high surface energy of SZO may be the reason for inhabitation of the coalescence among SZO wires so that the SRO steps correspond to the wire boundary areas.

Finally, the x-ray and RBS measurements demonstrate that the nano-patterned SZO films grow highly textured (with a channeling signal χ=9%) and stoichiometric.

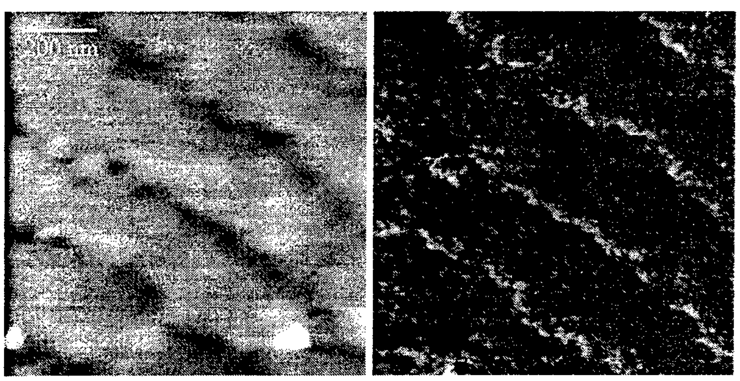

Fig 1. Correlation between topographic (left) and conducting (rigth) AFM images of 5nm-SZO deposited on SRO/STO

[1] C. Roland and H. Guo, Phys. Rev. Lett. **66**, 2104 (1991)
[2] *Pulsed Laser Deposition of Thin Films*, Ed. D. B. Chrisey and G. K. Hubler (John Wiley and Sons, New York, 1994)

A CARBON-NANOTUBE-BASED NANORELAY

Magnus Jonsson[1], Tomas Nord[1], Susanne Viefers[2], and Jari Kinaret[1]
[1]Department of Applied Physics, Chalmers University of Technology and Göteborg University, SE-41296 Gothenburg, SWEDEN
[2]Department of Physics, University of Oslo, Postboks 1048 – Blindern, N-0316 Oslo, NORWAY
E-mail: kinaret@fy.chalmers.se

We perform a theoretical investigation of the operational characteristics of a nanorelay based on a carbon nanotube. A conducting multi-walled nanotube (MWNT) is placed on a terrace in a silicon dioxide substrate connected to a source electrode. Two additional electrodes (gate and drain) are placed on the substrate below the terrace (Fig. 1). By applying a voltage between the tube and gate and/or drain electrodes, an excess charge is induced in the nanotube and hence a capacitive force acts to bend the tube towards the drain electrode. If the deflection is large enough a tunnel current can flow from the tube to the drain electrode. We model the mechanical properties of the nanotube by classical continuum theory and use experimentally measured values values for the Young's modulus. The charge transport between the tube and the drain electrode is treated using the orthodox theory of Coulomb blockade.

The system acts as three-terminal switch that operates in the GHz regime and has been studied by Kinaret *et al.* [1]. A related two-terminal structure has been studied by Dequesnes *et al.* [2]. Due to the exponential dependence of the tunneling conductance on the tube-drain separation there is a sharp transition between the conducting and the non-conducting states. Surface phenomena are important for the operational characteristics and in this work we have refined our previous treatment of short range forces such as the van der Waals and adhesion forces. The short range forces influence the geometry that is optimal for particular applications.

In this work we also analyze the application of the nanorelay as a memory element taking into account the effects of the surface forces. Other possible applications include logic devices, pulse generators and amplifiers.

References:

[1] J.M. Kinaret, T. Nord and S. Viefers, Applied Physics Letters **82**, 1287 (2003).
[2] M. Dequesnes, S.V. Rotkin and N.R. Aluru, Nanotechnology **13**, 129 (2002)

Figures:

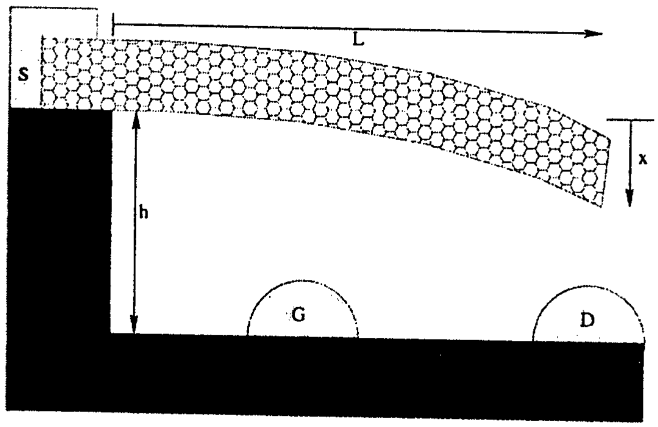

Figure 1

DETERMINATION OF HYDROPHILIC-HYDROPHOBIC PROPERTIES OF MULTIWALL CARBON NANOTUBES BY BINARY MIXTURE ADSORPTION

T. Kanyó[1], Z. Kónya[1], F. Berger[2], I. Dékány[2], I. Kiricsi[1]

[1]Applied and Environmental Chemistry Department, University of Szeged, Hungary
[2]Colloid Chemistry Department, University of Szeged, H-6720 Szeged, Hungary
E-mail: kiricsi@chem.u-szeged.hu

The nanoscience is a quite new branch of the material science. Besides, since their discovery[1] carbon nanotubes are one of the most widely studied nanomaterials. Several techniques have been developed for production both for singlewall (SWNT) and multiwall (MWNT) carbon nanotubes[2] which methods are commercially available nowadays. A quite large number of laboratories are working on their application as field emitters[3], nanoelectronic devices[4], hydrogen storage[5], polymer fillers[6], etc. A significant part of these applications require nanotubes of different hydrophilic/hydrophobic properties. To satisfy the demand of these potential users, samples of a given hydrophilic and/or hydrophobic character should be produced; however, the determination of hydrophilic or hydrophobic properties seems to be a quite hard task.

Several experimental techniques are used for characterization of carbon nanotubes. TEM is suitable for visualizing the walls and for statistical evaluation. HRTEM is generally applied for the observation of wall structure. The STM is a rather indirect tool for monitoring the shape and dimensions of carbon nanotubes. AFM sheds somewhat different light to the tube morphology. These methods render the easy investigation of a macroscopic amount of carbon nanotubes. The Raman spectroscopy gives a so called average result on the diameter of singlewall nanotubes. For SWNTs this measurement allows the classification of the tubes by diameter distribution. This parameter is regarded as one of the most important in characterization of nanotube products. XPS study gives the value of binding energies due to the bonds in different (=C=O, ≡C-OH, -COOH) groups generated by opening and/or purification-functionalization of nanotubes. Building functional groups on the outer surface particularly on the ends of the opened nanotubes may lead to product more appropriate in polymer chemistry since the tubes have opportunity to make chemical bonds with the polymer.

Generally the determination of functional group mentioned above is rather complex. Their concentration depends on the treatment to which nanotubes are subjected. After an acidic or oxidative treatment the product nanotubes are heat treated at different temperatures. Depending on this more or less functional groups remained intact since the carboxyl groups may decompose, the OH ones may release as water generated from two OH. It has also been reported that high temperature treatment in an inert atmosphere results in the decrease of structural imperfections of outer shells of MWNTs[7]. In some cases small contraction of nanotube diameter was also reported. The decreased number of functional groups and the structural imperfections leads to a sample of less hydrophilic and increased hydrophobic character. This should be evidenced experimentally with a higher amount of MWNT that is impossible using TEM, STM, AFM. However, it is also hard task using Raman, IR or XPS spectroscopy. What sort of technique can we use to determine the change in the hydrophilic and/or hydrophobic properties of carbon nanotubes subjected a treatment may modify this characteristics?

The determination of the lost functional groups may be performed by titration method. This technique is inaccurate at low concentration levels. The loss of oxygen containing functional groups changes the hydrophilic character of the nanotubes. On the basis of this observation we report details in this communication on how the adsorption isotherms of ethanol-cyclohexane binary solvent is used to show the change of hydrophilic-hydrophobic character of the nanotubes. This is the first time when binary solvent adsorption isotherms for carbon nanotubes have been investigated.

Multiwall carbon nanotubes were synthesized using the CCVD procedure as described elsewhere[8]. After removing the catalyst support, a treatment in concentrated HNO_3-H_2SO_4 solution was proceeded in order to remove the metal particles and the amorphous carbon matter. Upon this treatment the ends of the nanotubes became opened. It is also probable that the structural imperfections in the outer shells of MWNTs were closed by hydroxyl, carboxyl or carbonyl groups. A portion of this product was then heat treated at different temperatures for several hours in order to anneal the oxygen containing groups and to enhance the graphitization of the shells.

The TEM images reveal the presence of carbon nanotubes. There was no significant difference between the samples. The XRD patterns of the samples show substantial changes. Heat treated nanotube samples have a more intense reflection than that of the original sample.

The binary solvent adsorption isotherm of the original sample is characteristic of a material having rather hydrophilic character. The adsorption excess of ethanol is in the positive range and only a small hydrophobic part is seen at high ethanol concentrations, near to 1 mole fraction of ethanol. Oppositely, the isotherms of heat treated matters show much broader concentration range where the line goes into negative range indicating that the hydrophobic surface portion has been increased.

In our study a report is given on the binary solvent mixture adsorption on MWNTs in order to determine the hydrophilic/hydrophobic ratio. Furthermore, the samples were analyzed by infrared (IR) spectroscopy, XPS and X-ray diffraction (XRD) as well. The developed method is able to determine the hydrophilic/hydrophobic ratio of bulk nanotube samples which ratio correlates with other easily measurable physical properties.

References

[1] S. Iijima, Nature 354 (1991) 56.

[2] P.M. Ajayan, Chem. Rev. 99, 1787 (1999); C. Journet and P. Bernier, Appl. Phys. A-Mater. 67, 1 (1998)

[3] J.-M. Bonard, H. Kind, T. Stöckli, L.-O. Nilsson, Solid State Electron. 45 (2001) 893.

[4] S. Roth, M. Burghard, V. Krstic, K. Liu, J. Muster, G. Philipp, G. T. Kim, J. G. Park, Y. W. Park, Curr. Appl. Phys. 1 (2001) 56.

[5] M. Hirscher, M. Becher, M. Haluska, A. Quintel, V. Skakalova, Y. -M. Choi, U. Dettlaff-Weglikowska, S. Roth, I. Stepanek, P. Bernier, A. Leonhardt, J. Fink, J. Alloys Compd. 330-332 (2002) 654.

[6] P. Ajayan, L. Schalder, C. Giannaris, A. Rubio, Adv. Mater. 12 (2000) 750.

[7] X. Li, H. Zhu, L. Ci, C. Xu, Z. Mao, B. Wei, J. Liang, D. Wu, Carbon 39 (2001) 2077–2088

[8] A. Kukovecz, Z. Kónya, N. Nagaraju, I. Willems, A. Tamasi, A. Fonseca, J. B.Nagy and I. Kiricsi, Phys. Chem. Chem. Phys. 2, 3071 (2000)

PRODUCTION OF CARBON NANOTUBE JUNCTIONS BY CHEMICAL METHOD

Zoltán Kónya[1]*, Imre Kiricsi[1], Krisztián Niesz[1], Antal A. Koos[2], László P. Biró[2]

[1]Applied and Environmental Chemistry Department, University of Szeged, Rerrich Béla tér 1, H-6720 Szeged, Hungary

[2]Research Institute for Technical Physics and Materials Science, H-1525 Budapest, P.O.Box 49, Hungary

The preparation of carbon nanotube junctions was achieved. Carboxyl groups were generated onto the outermost wall of multiwall carbon nanotubes and converted to carbonyl chloride groups by reaction with $SOCl_2$ at room temperature. The formed COCl groups are very reactive on the outer surface and can be reacted easily with various amines, particularly diamines resulting in the formation of amide bonding. When two functionalized carbon nanotubes react with such a diamine molecule interconnection of tubes is generated. The resulted carbon nanotube junctions have been investigated by TEM and AFM.

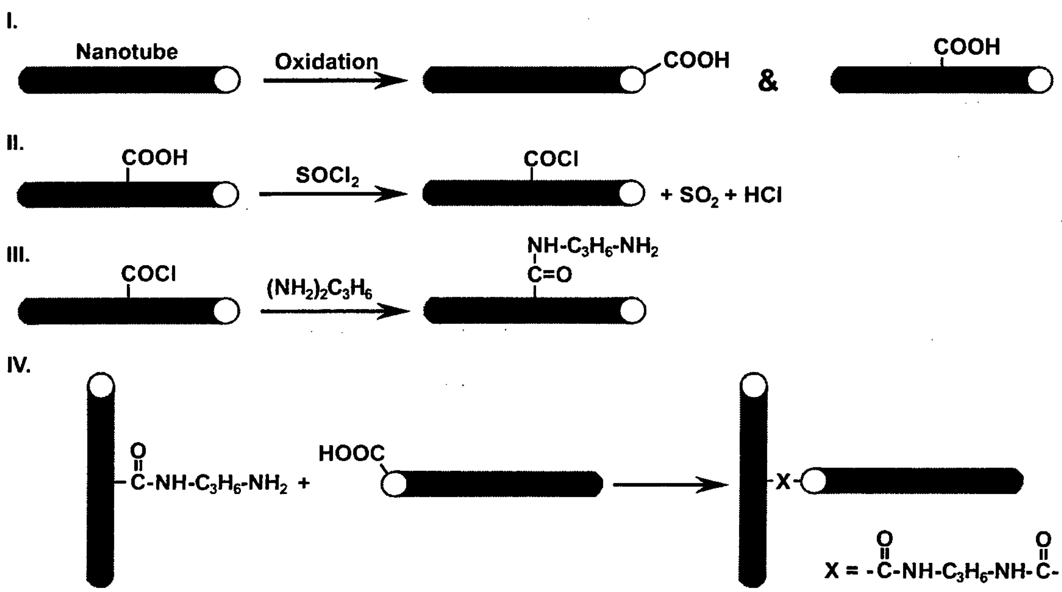

Figure 1 Formation mechanism of nanotube junctions

The basic reactions depicted above in Figure 1 while in Figure 2 the real nanotube junctions can be seen.

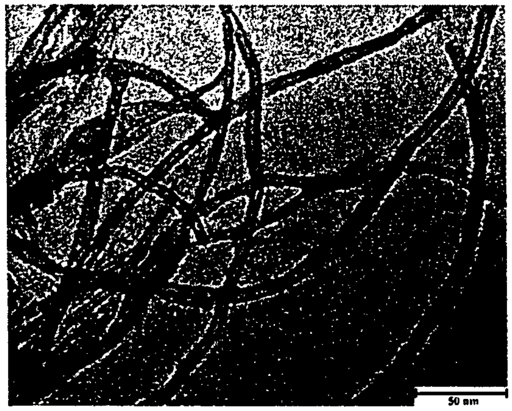

Figure 1: Nanotube junctions and overlying sections

We describe a procedure for preparation of multiwall carbon nanotube junctions applying chemical reactions where well graphitised carbon nanotube junctions were obtained.

Authors thank the financial help to the European Commission and the National Science Foundation of Hungary (RTN Program, NANOCOMP network, RTN1-1999-00013, OTKA T037952). KZ acknowledges support from the Bolyai fellowship and the Hungarian Ministry of Education (FKFP 216/2001, OTKA F038249).

ANODIC OXIDATION OF Si AND 3d-METAL COMPOUND THIN FILMS

H. Kuramochi[1,2], T. Tokizaki[1,3], T. Manago[1,3], M. Mizuguchi[1,3], J. Okabayashi[1,4], K. Ando[1,2], M. Yasutake[1,2], F. Perez-Murano[1,5], J. A. Dagata[1,6], H. Akinaga[1,3] and H. Yokoyama[1,3]

[1]Research Consortium for Synthetic Nano-Function Materials Project (SYNAF), National Institute of Advanced Industrial Science and Technology (AIST), 1-1-1 Higashi, Tsukuba, Ibaraki 305-8562, Japan

[2]Seiko Instruments Inc., 36-1 Takenoshita, Oyama-cho, Sunto-gun, Shizuoka 410-1393, Japan

[3] Nanotechnology Research Institute, AIST, 1-1-1 Umezono, Tsukuba, Ibaraki 305-8568, Japan

[4] The University of Tokyo, 7-3-1 Hongo, Bunkyo-ku, Tokyo 113-8656, Japan

[5]Universitat Autonoma de Barcelona, E-08193 Bellaterra, Spain

[6]National Institute of Standards and Technology, Gaithersburg MD20899-8214, USA

E-mail: hiromi.kuramochi@aist.go.jp

Nanometer-scale structures were fabricated by anodic oxidation using atomic force microscope (AFM) on Si and various 3d-metal compounds. Recently we reported the results of direct current monitoring during oxidation process [1,2] and humidity effects on nano-oxidation [3], which are necessary for achieving further understanding of kinetics and precise control. Faradaic current during anodic oxidation is detected in the pA order for an H-passivated Si(001) sample in the sample bias voltage range of 5-10 V and humidity range of 40-70 %. Fig. 1 shows detected current during applying a sample bias voltage of 10 V for 10 s at various RH. It flew immediately after applying voltage of 5 V and above and decreased with time according to the progress of oxidation. The total current flow by means of integration the current-time curve agrees well to the estimation current from the volume of fabricated dot (Fig. 2). The detected current curves well reflect the essential oxidation reaction. Additionally, current detection experiments were carried out in parallel with force curve measurement and in non-contact mode. These experiments are useful to know the behaviour of meniscus and results will be discussed as well.

As one possible direction of progress in anodic oxidation, variation of subject material means an expansion toward new possibilities on nanodevices [4]. Ferromagnetic 3d-metal compounds and alloys are good candidates as samples since these materials have potential of technological applications in spin-polarized electron transport devices. Local anodic oxidation will fabricate nano-dots and nano-structures with required size and shape at target points on such materials. It suggests realizable possibility of ultra high density storage devices. The suitable anodic oxidation

processing conditions depend on subject materials. Especially the suitable tip speed and humidity varied strongly according to materials. These parameters directly reflected the stability of meniscus between the tip and the sample, which due to roughness and hydrophilicity of each surface. Change of magnetism after nano-processing will be discussed based on MFM observation.

This work was partly supported by NEDO under the Nanotechnology Materials Program.

References

[1] F. Perez-Murano *et al.*, Appl. Phys. Lett., in press.

[2] H. Kuramochi *et al.*, Jpn. J. Appl. Phys., in press.

[3] H. Kuramochi *et al.*, Surf. Sci., submitted.

[4] recent examples; K. Matsumoto, *et al.*, Appl. Phys. Lett. **76**, 239 (2000); E. S. Snow, *et al.*, Appl. Phys. Lett. **79**, 110 (2001); T. Onuki *et al.*, Jpn. J. Appl. Phys. **41**, 6256 (2002).

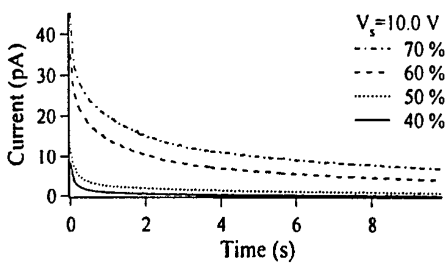

Fig. 1: Current during dot fabrication on H-Si(001) at 10 V for 10 s with various humidity.

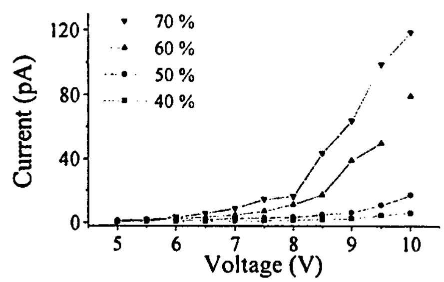

Fig. 2: Detected current during 10 s dot fabrication at various RH and Vs.

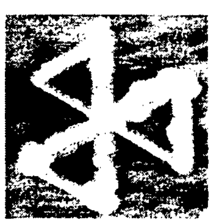

2x2 μm²

Fig. 3: AFM image of nano triangles fabricated on Chromium Oxide.

EXCHANGE COUPLING IN Ni/NiO NANOCOMPOSITES OBTAINED BY REACTIVE MILLING

V. Langlais[1], S. Doppiu[1], J. Sort[2], B. Dieny[2], S. Suriñach[1], J.S. Muñoz[1], M.D. Baró[1], J. Nogués[3]

[1]Departament de Física, Universitat Autònoma de Barcelona, 08193 Bellaterra, Barcelona, Spain
E-Mail: Veronique.Langlais@uab.es
[2]SPINTEC/CEA-Grenoble, 17 Avenue des Martyrs, 38054 Grenoble Cedex 9, France
[3]Institució Catalana de Recerca i Estudis Avançats (ICREA) and Departament de Física, Universitat Autònoma de Barcelona, 08193 Bellaterra, Barcelona, Spain

Magnetic nanoparticles are the subject of extensive research due to their potential (and present) applications in a variety of fields ranging from medicine to high density magnetic recording [1,2]. Magnetic nanoparticles have been traditionally obtained using classical chemical routes, such as gas condensation, electrodeposition, or microemulsion [2]. In this study, we have used reactive ball milling under hydrogen atmosphere in order to prepare Ni / NiO nanocomposites by the partial reduction of a NiO precursor. By varying the milling conditions, namely, the number of balls, the milling time, or the milling charge, we are able to obtain a complete set of samples with different Ni contents. Their structural and magnetic properties have been studied by X-ray diffraction (XRD) and vibrating sample magnetometer (VSM). The structural parameters such as crystallite size, microstrain and phase percentages present in each sample, are determined using quantitative Rietveld analysis. Independently, from VSM measurements, using saturation magnetization, the percentages of Ni have also been evaluated, providing values in very good agreement with the structural analysis.

As can be seen in fig. 1, the amount of Ni increases for larger milling energies. Moreover, the Ni crystallite size increases with total milling energy, attaining a value of around 7 nm, while the NiO crystallites size decreases by 40% for the particles obtained with the highest milling energy with respect to the ones obtained with the lowest milling energy (fig. 1).

This system, consisting of ferromagnetic (FM) Ni nanoparticles embedded in an antiferromagnetic (AFM) NiO matrix provides an ideal structure for the study of AFM/FM exchange coupling effects, i.e. exchange bias [3]. The main effects of exchange bias are a shift of the hysteresis loops in the field axis and a coercivity enhancement after field cooling the system from above the Néel temperature of the AFM [3]. Hence, the as-milled powders have been field cooled, under vacuum, from 620 K (i.e. above the Néel temperature of NiO) to room temperature under a magnetic field of 6kOe. As can be seen in fig. 2, the exchange bias, H_E, is found to be larger for the samples with a smaller amount of Ni while the coercivity enhancement, ΔH_C, is larger for Ni-rich samples. These observations can be correlated to the structural parameters of the composites such as size of the crystallites, which plays an important role in the anisotropy energy of the particles.

Acknowledgment: Partial financial support from NEXBIAS (HPRN-CT 2002-00296), CICYT (MAT2001-2555) and DGR (2001SGR00189) is acknowledged. VL and JS thank the NEXBIAS European Research Training Network for its financial support.

References:

[1] J.L. Dormann, D. Fiorani and E. Tronc, Adv. Chem. Phys. **XCVIII**, 283 (1997).

[2] J.I. Martín, J. Nogués, K.Liu, J.L. Vicent, I.K. Schuller, J. Magn. Magn. Mater. **256**, 449 (2003).

[3] J. Nogués and I.K. Schuller, J. Magn. Magn. Mater. **192**, 203 (1999).

Figures:

Fig. 1: Ni percentages (Δ) and crystallite sizes (Ni (•) and NiO (○)) as a function of the total energy transferred to the powder during milling.

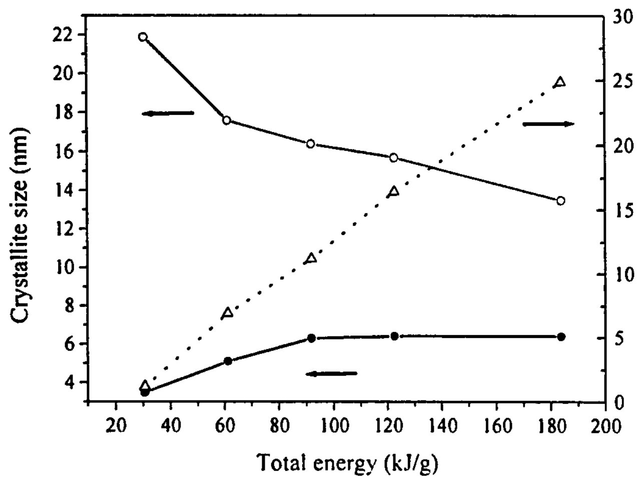

Fig. 2: Coercivity, H_C, and absolute value of the exchange bias, $|H_E|$, as a function of the Ni percentage.

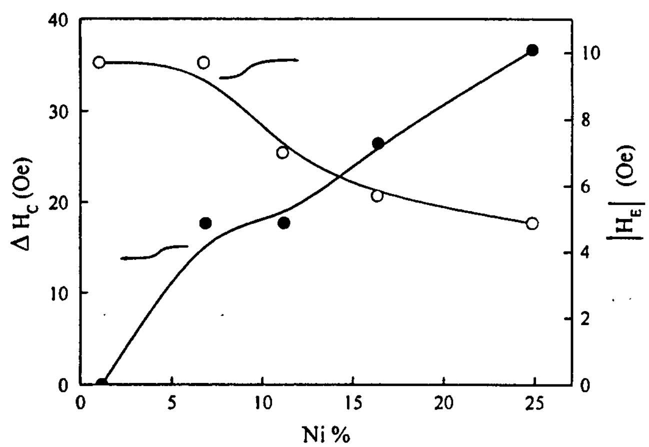

EXCHANGE COUPLING EFFECTS IN Fe NANOPARTICLES EMBEDDED IN A Cr_2O_3 MATRIX

J. Sort[1], V. Langlais[2], S. Doppiu[2], B. Dieny[1], S. Suriñach[2], J.S. Muñoz[2], M.D. Baró[2], Ch. Laurent[3], J. Nogués[4]

[1]SPINTEC/CEA-Grenoble, 17 Avenue des Martyrs, 38054 Grenoble Cedex 9, France
E-Mail: jordi.sort@uab.es

[2]Departament de Física, Universitat Autònoma de Barcelona, 08193 Bellaterra, Barcelona, Spain

[3]Centre Interuniversitaire de Recherche et d'Ingénierie des Matériaux, Bat. 2R1, Université Paul-Sabatier, 31062 Toulouse cedex 4, France

[4]Institució Catalana de Recerca i Estudis Avançats (ICREA) and Departament de Física, Universitat Autònoma de Barcelona, 08193 Bellaterra, Barcelona, Spain

Over the last decades, fine-particle magnetic systems have attracted attention due to the appealing properties, e.g. coercivity enhancement or tunneling of magnetization, arising from their reduced size and inter-particle coupling [1]. Moreover, nanoparticles consisting of ferromagnetic (FM) - antiferromagnetic (AFM) phases are also being studied due to their novel magnetic properties, e.g. exchange bias [2]. However, in this case, the AFM phases are usually obtained by oxidation or sulphuration of the FM particles, i.e. they are derived from the same transition metal as the FM (e.g. Fe-FeS, Ni-NiO or Co-CoO). This severely limits the types of systems that can be studied. In this study, a new approach to synthesize FM/AFM composites, in which the FM and AFM are **not** derived from the *same* transition metal, has been carried out. High temperature reduction under hydrogen atmosphere of mixed oxides (i.e. oxides of two different transition metals) can result in the selective reduction of one of the transition metals leaving the other in the oxidized state. Hence, microstructures consisting of metal nanoparticles embedded in oxide matrices can be obtained. In particular, $Cr_{1.8}Fe_{0.2}O_3$ powder was used to obtain FM iron nanoparticles embedded in an AFM Cr_2O_3 matrix. Structural and magnetic studies were carried out by transmission electron microscope (TEM), X-ray diffraction (XRD) and vibrating sample magnetometer (VSM), respectively.

Shown in figure 1 is a TEM micrograph of the as-obtained particles. It can be seen that the particles are around 200 nm in size and they host darker spots with sizes ~10 nm, which correspond to the iron nanoparticles, that are embedded in the AFM oxide matrix. Remarkably, the size distribution of the Fe nanoparticles is quite narrow.

The particles were field cooled from room temperature to 10 K under a field of 5 T to induce AFM/FM coupling [2]. Hysteresis loops were then recorded at different temperatures (10 K < T < 300 K). Figure 2 shows the evolution of exchange bias, H_E, with-temperature. At low temperatures, H_E is about 9 Oe and it decreases progressively with temperature becoming practically zero at room temperature, indicating a blocking temperature around 300 K, i.e. close to the Néel temperature of Cr_2O_3. Moreover, this was accompanied by a coercivity enhancement at low temperatures of about 70 Oe, which is another fingerprint of the FM/AFM exchange coupling.

Acknowledgment: Partial financial support from NEXBIAS (HPRN-CT 2002-00296), CICYT (MAT2001-2555), DGR (2001SGR00189), the Generalitat de Catalunya (ITT2000-14) and Midi Pyrénées Council (CTP Grant). VL and JS thank the NEXBIAS European Research Training Network for its financial support.

References:

[1] J.L. Dormann, D. Fiorani and E. Tronc, Adv. Chem. Phys. **XCVIII**, 283 (1997).
[2] J. Nogués and I.K. Schuller, J. Magn. Magn. Mater. **192**, 203 (1999).

Figures:

Fig. 1: TEM micrograph of Fe nanoparticles embedded in a Cr_2O_3 matrix

Fig. 2: Temperature dependence of exchange bias, H_E.

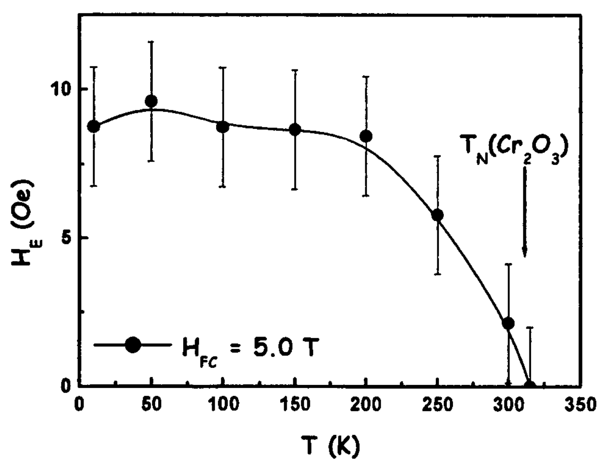

PROTEIN LIKE GOLD NANOPARTICLES

Raphael Levy[+□], David G. Spiller[+], Mike White[+], Mathias Brust[□], Richard J. Nichols[□], David J. Schiffrin[□], Dave G. Fernig[+]

[+] The University of Liverpool, School of Biological Sciences, Crown Street, Liverpool, L69 7ZD, United Kingdom
[□] The University of Liverpool, Department of Chemistry, Donnan Laboratories, Oxford Street, Liverpool, L69 7ZD, United Kingdom

Noble metals nanoparticles display fascinating electronic and optical properties and deserves a growing attention. They have been proposed as ultra sensitive new reporters in biological assays [1], as building blocks for bottom-up construction of nanodevices [2] and complex nanoassemblies [3].

Based on an original surface chemistry, we have obtained a new class of gold nanoparticles (GNP) with particularly useful properties. These GNP have been characterised by dark field microscopy, optical and infrared spectroscopy. They are stable in biological buffers and in a wide range of pH and NaCl concentrations. We have shown that it's possible to use classic biochemical tools for protein modification on these particles; including size exclusion chromatography and standard coupling chemistry. This opens the route for new applications in biological sciences and nanoengineering. As an example, we present preliminary results on a new GNP based biosensor allowing easy measurement of the adsorption of molecules onto a model membrane.

[1]. D. A. Schultz, Current Opinion in Biotechnology, **14**, (2003) 13-22.
[2]. D. I. Gittins, D. Bethell, D. J. Schiffrin and R. J. Nichols, Nature, **408**, (2000) 67-69.
[3]. A. G. Kanaras, Z. X. Wang, A. D. Bates, R. Cosstick and M. Brust, Angewandte Chemie-International Edition, **42**, (2003) 191-+.

Shot noise in strongly correlated double quantum dots

Rosa López[1], Ramón Aguado[2], and Gloria Platero[2]

[2] Départment de Physique Théorique, Université de Genève, CH-1211 Genève 4, Switzerland.

[2] Teoría de la Materia Condensada, Instituto de Ciencia de Materiales de Madrid, (CSIC) Cantoblanco,28049 Madrid, Spain.

Rosa.Lopez@physics.unige.ch

Abstract

We have investigated theoretically the shot noise of strongly correlated double quantum dot systems in the regime where the Kondo effect and the interdot antiferromagnetic exchange do compete [1]. Our calculations are based on a generalization to nonequilibrium transport of the two-impurity Anderson Hamiltonian which is solved by the slave boson mean field theory [2]. This mean field approach together with nonequilibrium Green's function techniques allow us to obtain closed formulae for the shot noise in the strong coupling regime. This mean field approach has already proven to be a good starting point to study shot noise of Kondo quantum dots in the strong coupling regime [3]. Here two configurations are considered for the double quantum dot: series and parallel. When the two quantum dots are in series, we obtain at low voltages, a non-monotonic behavior of the Fano factor, as a function of the interdot tunneling coupling. When the competition between the Kondo effect and the interdot antiferromagnetic exchange starts to play a role this picture is strongly modified. In a parallel configuration, the functional form of the Fano factor as a function of the applied voltage V_{dc} changes abruptly, depending on whether the ratio between the antiferromagnetic exchange constant J and the Kondo temperature T_K is below or above $(J/T_K)_c \simeq 2.5$. Below $(J/T_K)_c$, the Fano factor behaves as in the single quantum dot case (monotonic dependence which saturates at large voltages). Above $(J/T_K)_c$, the Fano factor exhibits a nonmonotonic dependence on voltage, with a kink at $eV_{dc} = J$.

References

[1] B.A. Jones, B.G. Kotliar, and A.J. Millis, Phys. Rev. B **39**, 3415 (1989);

[2] R. Lopez, R. Aguado, and G. Platero Phys. Rev. Lett. **89**, 136802 (2002).

[3] R. López and D. Sánchez, Phys. Rev. Lett. **90**, 116602 (2003): Y. Avishai, A. Golub, and A.D. Zaikin, Phys. Rev. B **67**, 041301 (2003).

THE PREPARATION OF MnZn-FERRITE NANOPARTICLES IN WATER-CTAB-HEXANOL MICROEMULSIONS

D. Makovec[1] A. Košak[1], and M. Drofenik[2]
[1]Jožef Stefan Institute, Jamova 39, SI-1000 Ljubljana, Slovenia,
[2]Faculty of Chemistry and Chemical Engineering, SI-2000 Maribor, Slovenia
E-mail: Darko.Makovec@ijs.si

Magnetic materials in the form of nanoparticles have received special attention because of their unique magnetic properties, which are dominated by superparamagnetism. Superparamagnetic nanoparticles with a particle size of the order of 10 nm and with a narrow size distribution can be colloidally dispersed in a carrier liquid to form magnetic fluids. These magnetic fluids have the potential to be used in a variety of modern technologies: from medicine and pharmacy to electronics and mechanics.

Precipitation in a water-in-oil microemulsion has been shown to be a very promising technique for preparing monodispersed, ultrafine particles of controlled size and morphology. In this method, coprecipitation occurs in tiny droplets of water embedded with a surfactant, so-called reverse micelles, which are distributed in an oil phase. Water pools of reverse micelles act as micro-reactors for the synthesis of the particles, in which the particle size of the product is controlled by the size of these pools. The size of the reverse micelles is thermodynamically determined, in particular by the water-to-surfactant molar ratio. The chemical reactions, which are very fast in water solutions and therefore hard to control, are controlled by a much slower reaction between the micro micelles carrying different reactants in the microemulsions. The control of chemical reactions in microemulsions enables multiple-step reactions and the synthesis of composite particles.

In this study, nanosized, superparamagnetic MnZn-ferrite ($Mn_{0.5}Zn_{0.5}Fe_2O_4$) nanoparticles were prepared using synthesis in the water pools of reverse micelles in a microemulsion system consisting of hexanol as the oil phase, n-hexadecil trimethylammonium bromide (CTAB) as the surfactant, and an aqueous phase of metal ions: Fe^{2+}, Mn^{2+} and Zn^{2+}. The synthesis of the magnetic MnZn ferrite occurred *in-situ* in a two-step process. In the first step, the corresponding hydroxides were precipitated by a microemulsion containing a water solution of the precipitation agent

tetra-methyl-ammonium hydroxide ($(CH_3)_4NOH$). In this step, special attention has to be paid to prevent the reoxidation of Fe^{2+}. In the second step, Fe^{2+} hydroxide was oxidized, resulting in the formation of the spinel MnZn-ferrite product (Fig. 1). The oxidation was performed by a microemulsion containing hydrogen peroxide (H_2O_2) or simply by oxygen gas. The morphology and magnetic properties of the synthesized particles were followed as a function of the processing parameters: concentration of the corresponding ions or precipitation agent in the aqueous solution, pH value after precipitation, temperature and time of reaction and type of oxidation agent. Special attention was paid to the evaluation of the stability of the water – CTAB – hexanol microemulsions as a function of temperature and the concentrations of the corresponding ions or precipitation agent.

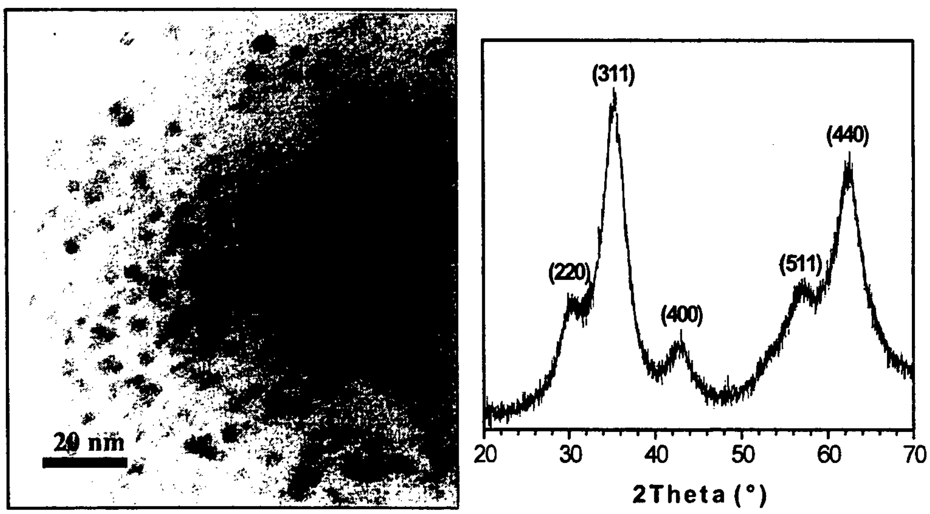

Fig. 1: TEM micrograph (a) and X-ray diffractogram (b) of the MnZn-ferrite nanopowder, prepared in the water – CTAB – hexanol microemulsion.

MONITORING METAL-INSULATOR TRANSITION ON A ONE-DIMENSIONAL LATTICE WITH NONRANDOM LONG-RANGE INTERACTION; A UNIVERSAL PARAMETER AT THE TRANSITION

A. V. Malyshev[*,2], V. A. Malyshev[1,3] and F. Domínguez-Adame[1]

[*]Area de Optica, Universidad de Salamanca, Salamanca, Spain
E-mail: a.malyshev@usal.es
[1]Departamento de Física de Materiales, Universidad Complutense, Madrid, Spain
[2]Ioffe Physico-Technical Institute, Saint-Petersburg, Russia
[3]"S. I. Vavilov State Optical Institute", Saint-Petersburg, Russia

We argue that the ratio of the standard deviation to the mean of the participation number distribution is a universal parameter at a metal-insulator transition. This finding allows for monitoring the transition by studying scalings of the participation number relative fluctuation. The family of curves of the relative fluctuation dependence on disorder, parametrized by the system size, has a joint intersection point at the critical magnitude of disorder Δ_c. Determining such point, we study the nature of quasi-particle states of one-dimensional tight-binding Hamiltonians with nonrandom power-law inter-site coupling, $J_{mn}=J/|m-n|^{\mu}$. The disorder is due to random on-site energies (uncorrelated diagonal disorder). At moderate magnitudes of disorder (smaller than the band width), the quasiparticle states are extended, provided that the interaction exponent satisfies the inequalities: $1<\mu<3/2$. The system undergoes a localization-delocalization transition at one of the band edges upon increasing the magnitude of disorder. In particular, analyzing very large systems (up to about 6×10^4) we found that the transition occurs at $\Delta_c=11.0\pm0.5J$ for $\mu=4/3$. For $\mu=3/2$, the only joint intersection point is located at $\Delta_c=0$, implying localization of all quasi-particle states. These results support previous findings obtained by the supersymmetric method for disorder averaging combined with a renormalization group analysis [1].

We discuss also the mapping of localization problems in higher dimensions onto the considered 1D two parameter model. This mapping is based on the appropriate choice of the interaction exponent μ. In particular, the one-dimensional model at $\mu=3/2$ is equivalent (from the viewpoint of the localization properties) to the standard two-dimensional Anderson model in which the quasi-particle states are localized weakly [2]. Our calculation is therefore the first direct numerical proof of the localized nature of the quasi-particle states in 2D.

[1]A. Rodríguez, V. A. Malyshev, G. Sierra, M. A. Martín-Delgado, J. Rodríguez-Laguna, and F. Domínguez-Adame, Phys. Rev. Lett. **90,** 27404:1-4 (2003).
[2] E. Abrahams, P. W. Anderson, D. C. Licciardello and T. V. Ramakrishnan, Phys. Rev. Lett. **42**, 673 (1979).

LOW-TEMPERATURE DIFFUSION OF FRENKEL EXCITONS IN LINEAR MOLECULAR AGGREGATES

A. V. Malyshev[*,2], V. A. Malyshev[1,3] and F. Domínguez-Adame[1]

[*]Area de Optica, Universidad de Salamanca, Salamanca, Spain
E-mail: a.malyshev@usal.es
[1]Departamento de Física de Materiales, Universidad Complutense, Madrid, Spain
[2]Ioffe Physico-Technical Institute, Saint-Petersburg, Russia
[3]"S. I. Vavilov State Optical Institute", Saint-Petersburg, Russia

We report the results of a theoretical study of Frenkel excitons diffusion in J-aggregates at low temperatures (smaller or of the order of the J-band width). We model an aggregate as an open linear chain with uncorrelated on-site disorder that localizes the exciton at chain segments of size small compared to the chain length. Exciton diffusion over the localized states is considered as an incoherent hopping process; the hopping rates being proportional to the overlap integrals of the squared exciton wave functions. The efficiency of diffusion is probed by the exciton fluorescence quenching that is due to point traps. The trapping rate is taken to be proportional to the probability of finding an exciton at the sites with traps. We use the rate equation to calculate the temperature dependence of the exciton quenching.

It is shown that there exist two regimes of the exciton diffusion. At low temperatures, those smaller than $T_1 \approx 0.25 \times$ J-band width, the exciton diffuses mostly over weakly overlapped states of the tail of the density of states, which determine the optical response and form the J-band. At higher temperatures, the diffusion begins to build up due to the two-step hops via higher states. This accelerates the exciton diffusion drastically, so that the exciton can diffuse over large distances during its lifetime. The higher states begin to contribute to the diffusion at temperatures higher than about T_1. However, the diffusion becomes really fast (in the sense that the quenching rate becomes comparable to the spontaneous emission rate of the aggregate) only at temperatures of the order of the J-band width.

On the basis of our study, we discuss the experimental data on the ultra fast low-temperature exciton-exciton annihilation reported recently [1].

References:

[1] I. G. Scheblykin, O. Yu. Sliusarenko, L. S. Lepnev, A. G. Vitukhnovsky, and M. Van der Auweraer, J. Phys. Chem. B **104**, 10949 (2000); **105**, 4636 (2001).

THERMAL STABILITY OF C_{60} FULLERENE DOPED WITH SUBSTITUTIONAL SILICON ATOMS

Pedro A. Marcos[1], María J. López[2] and Julio A. Alonso[2]
[1]Dpto. de Física, Universidad de Burgos, EPS, C/ Villadiego, s/n, 09001 Burgos, Spain
[2]Dpto. de Física Teórica, Universidad de Valladolid, 47011 Valladolid, Spain
E-mail: pamarcos@ubu.es

Since the discovery of fullerenes in 1985 [1], many researchers have focus their interest on the possibilities which these molecules offers from their chemistry point of view. In principle it was assumed that these molecules were electronically neutral, however it is well known their capacity to react with different elements due to their electrophile character. For this reason, many new materials of relevant technological interest have been synthesized, based on doping carbon structures using atoms of different species. One of the natural candidates used for doping is silicon, essentially due to its similar valence electronic structure with carbon, and one might expect an easy replacement of carbon atoms by silicon in the fullerene cage. On the other hand, silicon exhibits different hybridization capabilities, which prevent from the formation of fullerene-like structures with a few number of atoms. Moreover, there is large size mismatch between carbon and silicon, which plays against a easy replacement of carbon by silicon. Despite of these mismatches, silicon doped fullerenes have been extensively produced in a experimentally way [2, 3].

The study of the thermal stability of substitutional doped C_{60} with silicon atoms arises from the question of, how many silicon atoms are necessary to incorporate in a substitutional framework to destabilize the C_{60} cage? In order to give an insight about the stability of fullerenes doped with substitutional silicon atoms, we have simulated the thermal evolution of a variety of C_{60} molecules, replacing several carbon atoms by silicon. We have performed extensive molecular dynamics simulations, heating $C_{60-m}Si_m$ (m = 1-12) aggregates from 0 K, up to the thermal decomposition (fragmentation) occurs. The calculations have been performed using a Density Functional Tight Binding model (DFTB) due to Porezag and coworkers [4], which has been extensively used for the simulation of condensed matter systems, as well as for clusters and nanostructures.

Results obtained have shown that there is a clear correlation between the cohesive energy and thermal stability in these clusters. Stability decreases as larger the number of doping atoms is. Localized liquid-like behavior is also observed in these heterofullerenes, developed when silicon occupies segregated positions at the structure, weakening the cage. At the end of simulation, fragmentation, controlled by an autocatalysis process, occurs in several channels, giving rise to monomers, dimers or trimers emerging from the whole structure. It is necessary to mention, on the contrary one might suspect, that up to twelve silicon atoms, the fullerene cage remains intact at low temperatures.

References:

[1] H.W. Kroto, J.R. Heath, S.C. O'Brien, R.F. Curl, and R.E. Smalley, Nature, **318** (1985) 162.
[2] M. Pellarin, C. Ray, J.L. Lermé, J.L. Vialle, M. Broyer, X. Blase, P. Kéghélian, P. Mélinon, and A. Perez, J. Chem. Phys., **110** (1999) 6927.
[3] I.M.L. Billas, F. Tast, W. Branz, N. Malinowski, M. Heinebrodt, T.P. Martin, M. Boero, C. Massobrio, and M. Parrinello, Eur. Phys. J. D, **9** (1999) 337.
[4] D. Porezag, T. Frauenheim, T. Köhler, G. Seifert, and R. Kashner, Phys. Rev. B, **51** (1995) 12947.

ARRAYS OF SUB-MICRONIC PYRAMIDS AND HUT CLUSTERS SELF-ORGANIZED IN THE EPITAXIAL GROWTH OF $CoCr_2O_4$ FILMS

Ulrike Lüders, Florencio Sánchez, Benjamín Martínez, and Josep Fontcuberta
Institut de Ciència de Materials de Barcelona - CSIC, Campus UAB,
Bellaterra 08193, Catalunya. Spain
E-mail: fontcuberta@icmab.es

Self-organized growth of semiconductors has attracted much attention in the last decade due to its interest for nanoscience as well as promises of technological applications. However, the self-ordered growth of oxides has not been yet much explored, in spite of the renewed interest of these materials in science and technology. We have recently reported [1] the formation of pyramids and hut clusters in epitaxial ferrimagnetic $CoCr_2O_4$ (CCO) films deposited by sputtering on $MgAl_2O_4$(001). The scanning electron microscopy (SEM) image shown in Figure 1a illustrates that the islands are perfectly aligned (according their position and orientation) along the <110> crystal directions. The pyramidal shape, square or hut-cluster type) is confirmed with the atomic force microscopy (AFM) images shown in Figures 1b and 1c. Measurement of the island dimensions evidenced the existence of two island families according with their size, the first family with base dimensions of some hundred nanometers, the other one having a smaller size but the same pyramidal shape. The bimodal size distribution is confirmed with both island base width and length dimensions, and also with the island heights. The fact that the islands do not undergo a shape transition with size (even when dimensions are above the micron) is an outstanding result, and clearly distinctive to the widely studied semiconductor pyramids and hut clusters.

The measured angle between the lateral surfaces of the morphological structures and the (001) surface is $\Theta \approx 50$-$55°$, which implies that the pyramids and hut clusters can be considered as true three-dimensional objects because of their high aspect ratio. The measured angle also strongly suggests that their surfaces are the spinel {111} facets. Because the {111} surfaces are of lowest energy in spinels, anisotropic surface energy is proposed as the origin of this unusual morphology. Such thermodynamic reason favors the growth of CCO pyramids and hut cluster to be highly reproducible, as confirmed by obtaining them under a broad range of substrate temperature and also on other substrates [2]. We finally discuss on the possibility of tunability of island density and size.

References:

[1] U. Lüder, F. Sánchez, and J. Fontcuberta, Appl. Phys. Lett., submitted
[2] U. Lüder, F. Sánchez, and J. Fontcuberta, in preparation

Figures:

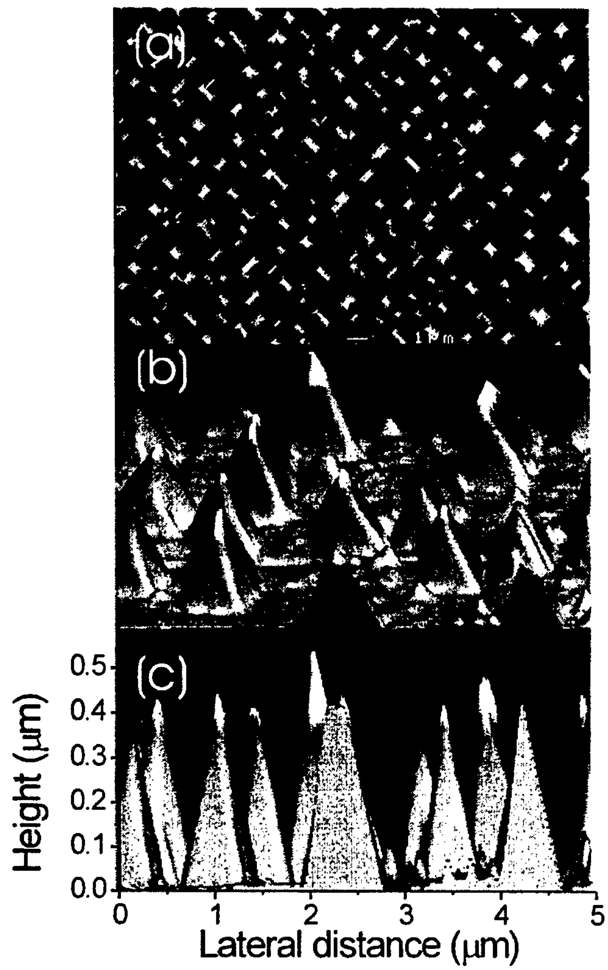

Figure 1: Topographic images of a $CoCr_2O_4$ film: (a) 0° view SEM image, (b) 60° view AFM image, and (c) 90° view AFM image of the same area with a height profile superposed.

PRESSURE INFLUENCE ON HYDROGEN ADSORPTION IN SINGLE WALL CARBON NANOTUBES

[a]A.Ansón, [a]M.A.Callejas, [a]A.M.Benito, [a]W.K.Maser, [a]M.T.Martínez*.

[a]Instituto de Carboquímica, CSIC, C/ Miguel Luesma Castán, 4, 50018 Zaragoza, Spain.

None of the existing technologies for hydrogen storage fulfil the requirements for mobile applications and nanostructured carbons are being investigated as potential hydrogen adsorbents. Hydrogen adsorption in Carbon Nanotubes (CNTs) has been object of huge interest since they are light, hollow and porous systems that seem ideal candidates for hydrogen storage. Nevertheless there is a big controversy due to the dispersion of both theoretical and experimental studies

In this paper, hydrogen adsorption data on as-grown and modified Single Walled Nanotubes in a volumetric equipment (Quantachrome Autosorb-1), and two gravimetric equipments, (IGA-001 and CAHN TG-2151) are reported. A range of hydrogen pressure from 100 to 50000 mbar is covered and the adsorption data show increasing hydrogen adsorption at increasing pressure, the adsorption data being far from the DOE target of 6.5 wt.%. Processes for modifying CNTs or/and for improving CNTs yields and production control have to be developed to reach higher hydrogen storage capacity.

Due to the discrepancies in the results from different laboratories and different techniques, it is interesting to note that the results from the three techniques are compatible.

FIELD EFFECT TRANSISTORS BASED ON ORGANIC POLYMERS

Marta Mas-Torrent, Murat Durkut, Peter Hadley
Department of NanoScience, Technical University of Delft, Lorentzweg 1, 2628 CJ Delft, The Netherlands
E-mail: marta@qt.tn.tudelft.nl
http://www.qt.tn.tudelft.nl

Conducting polymers offer potential applications for building cheap and flexible electronic devices such as field effect transistors (FETs) and light emitting diodes (LEDs). However, a full understanding of their electrical properties is complicated by their semi-crystalline nature. Our work is focused on obtaining well-ordered polymers in a FET configuration in order to improve the resulting mobilities and to further understand the transport mechanisms.

The fabrication of the contacts was carried out using electron-beam lithography and a double resist layer of PMMA on a silicon wafer. Using a shadow evaporation technique the spacing between the electrodes can be adjusted between 5 and 100 nm (Fig.1). The polymers were then deposited or grown between the source/drain electrodes and the current was modulated by applying a gate voltage (SiO_2, back gate).

Herein, we present different strategies used to place the polymers on FET devices. First, the transport properties of drop-cast regioregular poly(3-hexylthiophene) are studied at different length-scales as it is known that this polymer self-organises into a lamellar structure showing high mobility [1]. Another approach considered consists on growing polymers between the source and drain electrodes by electropolymerisation.

References:

[1] H. Sirrinhaus, P. J. Brown, R. H. Friend, M. M. Nielsen, K. Bechgaard, B. M. W. Langeveld-Voss, A. J. H. Spiering, R. A. J. Janssen, E. W. Meijer, P. Herwig, D. M. Leeuw, Nature, **401** (1999) 685.

Figures:

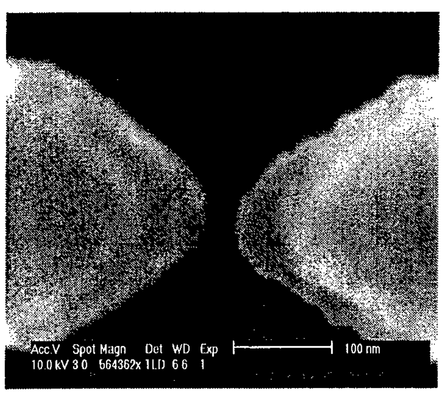

Fig. 1. SEM image of gold electrodes separated by 20 nm.

FABRICATION OF ELECTRON WAVEGUIDE DEVICES IN GaInAs/InP 2DEG USING NANOIMPRINT LITHOGRAPHY

P. Carlberg, D. Wallin, I. Maximov, H. Q. Xu, W. Seifert, L. Montelius and L. Samuelson

Division of Solid State Physics & The Nanometer Consortium,
Lund University, Box 118, Lund, S-221 00, Sweden
E-mail: ivan.maximov@ftf.lth.se
http://www.ftf.lth.se

We present fabrication technology of quantum point contact (QPC) and three-terminal ballistic junction (TBJ) devices in GaInAs/InP heterostructures using nanoimprint lithography (NIL). The TBJ is a novel nanoelectronic device with non-linear electrical properties [1,2], which can be used both for realization of logic functions and in analogue applications [3]. Logic functions, e.g. "NAND" or inverter, can easily be implemented by interconnecting QPCs and TBJs in a one lithography step. Previously we have demonstrated a functioning single GaInAs/InP TBJ-device made by NIL [4,5].

In the present work, we have used NIL for fabrication of both single QPC and TBJ devices and complex TBJ-based circuits in a high mobility $Ga_{0.25}In_{0.75}As/InP$ two-dimensional electron gas (2DEG). The NIL stamps with QPC and TBJ structures are fabricated from SiO_2/Si wafers using high-resolution electron beam lithography and reactive ion etching of SiO_2. The sub-150 nm stamp features are replicated into a polymer (PMMA or ZEP 520 resist), which is used as a mask during wet etching. Polymer residues are removed by plasma ashing prior to the etching process. We report on optimization of the nanoimprint technology for making QPCs and TBJs in GaInAs/InP as well as electrical characterization of the fabricated devices.

References:

[1] H. Q. Xu, *Appl. Phys. Lett.* **78**, 2064 (2001)
[2] H. Q. Xu, *Physica*, **E 13**, 942 (2002)
[3] I. Shorubalko, H. Q. Xu, I. Maximov, D. Nilsson, P. Omling, L. Samuelson, W. Seifert, *IEEE Electron Device Letters*, **23**, 377 (2002)
[4] I. Maximov, P. Carlberg, D. Wallin, I. Shorubalko, W. Seifert, H. Q. Xu, L. Montelius and L. Samuelson, *Nanotechnology*, **13**, 666 (2002)
[5] I. Maximov, P. Carlberg, I. Shorubalko, D. Wallin, E-L. Sarwe, M. Beck, M. Graczyk, W. Seifert, H. Q. Xu, L. Montelius and L. Samuelson, *Microelectronic Engineering*, **67-68**, 196 (2003)

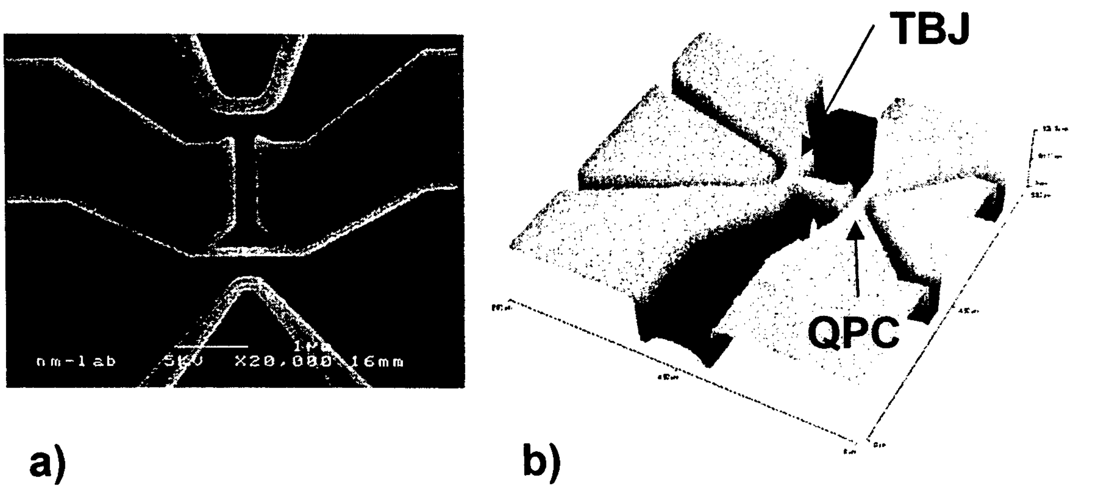

Fig. 1 (a): SEM image of a nanoimprint stamp with a TBJ device and QPC. The TBJ and QPC are electrostatically coupled together. Fig. 1(b): a corresponding circuit in GaInAs/InP high mobility 2DEG after NIL and wet etching. The lateral features of the stamp of about 150 nm are well-reproduced after NIL and etching.

ELECTROCHEMICAL SYNTHESIS OF GOLD-POLYTHIOPHENE NANOWIRES

F. Plumier, R. Flamant, J. Delhalle and Z. Mekhalif*

Facultés Universitaires Notre-Dame de la Paix, Département de Chimie, Laboratoire LISE, Rue de Bruxelles, 61, B-5000 Namur, Belgium
zineb.mekhalif@fundp.ac.be

Current miniaturization trends in electronics have stimulated the development of new approaches for fabricating electronic nanostructures. A major problem is in the integration of classical lithographic structures with chemically synthesized nanoscale components (molecules, polymers, nanoparticles,...). A more specific challenge is in the making of appropriate connections between the components. As a contribution to this goal, we report in this work the elctrochemical synthesis of gold nanowires end-capped with polythiophene bundles. For this purpose, we have used polycarbonates and alumina membranes as templates. Several characterization techniques such as X-ray Photoelectron Spectroscopy, and Scanning Electron Microscopy are used in this study.

Part of the Work has been supported by 'la Région Wallonne, SYNATEC convention N°: 0014526'

COMPARATIVE STUDY OF SELF-ASSEMBLED MONOLAYERS OF DODECANETHIOL AND DODECYL-TRICHLOROSILANE ON REDUCED AND OXIDISED COBALT

R . Flamant, C. Tondeur, Z. Mekhalif, J. Delhalle

Facultés Universitaires Notre-Dame de la Paix, Département de Chimie
Laboratoire LISE
Rue de Bruxelles, 61, B-5000 Namur - Belgium

The spontaneous ordering of adsorbates to form self-assembled monolayers (SAMs) is a phenomenon with great technological potential. Through the deposition of molecules with specific symmetry or functionality, surfaces can be tailored for particular applications such as electrodes, chemical sensors, or corrosion protection.

The presence of a dense organic film at the surface of an oxidizable metal can significantly decrease its corrosion rate. This corrosion inhibition depends more upon the coating's composition and structure and chemical bonds at the polymer/metal interface than upon its thickness.

In this contribution we will focuss on the preparation and the characterisation of self-assembled monolayers (SAMs) formed by chemisorption of dodécanethiol on active metals such as cobalt. The effect of several preparation conditions of the surface upon the monolayer properties will be shown. We will also show how the various steps involved in the surface preparation influence the monolayer properties. We will particularly insist upon the influence of:

- the electrochemical reduction of the native oxide,
- the solvent.

Comparative study will be done with the elaboration of monolayer with the same chain length on oxidised cobalt using the dodécyl-triclorosilane.

Stability of theses different monolayers will also be discussed.

X-ray Photoelectron Spectroscopy (XPS), cyclovoltammetry, polarisation curves, contact angle measurements and PM-IRRAS are used for surface characterisation.

Protection of silver using self-assembled monolayers for archaeological objects preservation

F. Laffineur, D. Auguste, F. Plumier, L. Hevesi[+], J. Delhalle, Z. Mekhalif

FUNDP,Départ. de Chimie, LISE and [+]CMO, 61 rue de Bruxelles, 5000 Namur, Belgium

Silver was highly valued in antiquity because of its lustrous surface and put to many decorative uses. Most of these archaeological objects are in good conservation state because of the protecting effect of the medium when buried. In fact, they reach equilibrium with the surrounding sediment and, if conditions are favourable, they are more or less preserved until their discovery. Once extracted from their burial environment, this equilibrium is disturbed and corrosion can occur causing rapid damages until destruction. In the particular case of silver, the airborne gases responsible for tarnishing are hydrogen sulphite and carbonyl sulphide [1]. Several ways are easily applicable to protect such objects :

- treat the metal to render its corrosion resistance by removing the element, which can catalyse the corrosion restart
- treat the environment to suppress the corroding element by controlling the atmosphere of the museum cases of by storing under vacuum
- isolate the object from the environment with a protective coating

All these solutions have some disadvantages : the first solution needs regular treatment of the surface and could be damageable for some metals, the second is very efficient but needs sophisticated infrastructures. The last point concern especially organic coating but application of such coating is still under investigation and not completely controlled. Such treatment has to fulfil several requests to be used on archaeological objects : the coating must be as invisible as possible and must be easily removable without damaging the object. Until now, research in this domain is still important and plasma polymerisation and electropolymerisation are two of the most studied technique for the formation of an organic protective coating [2, 3]. Such techniques needs sophisticate materials that is not easily accessible. An other approach of the problem consist to use self-assembled monolayers (SAM's) as protective coating. In fact, formation of SAM's is widely studied on gold, platinum but also on copper and silver [4, 5] and these thin films have shown very interesting properties : they could form a very compact and dense structure that protect the surface from air oxidation but also from aggressive environment such chloride or sulphite containing solutions.

The self-assembling of monolayers can be used easily, the process is very simple : after a cleaning and activation step of the surface, the sample is dipped in an appropriate solvent containing organothiol molecules. The thiol functionality is particularly reactive with several metals such as gold, copper, platinum and silver and a chemical bound is formed. Intermolecular interaction promote the self-organisation of the assembly leading to a dense structure, pinhole free in the more effective cases.

In this paper, two monolayers of different organothiols are studied and compared. These are a fully hydrogenated molecule : *n*-hexadecanethiol (CH_3-$(CH_2)_{15}$-SH : C_{16}) and a partially perfluorinated molecules (CF_3-$(CF_2)_3$-$(CH_2)_{11}$-SH : F_4H_{11}). Both monolayers have been self-assembled on electroreduced silver surface from a 10^{-2}M ethanolic solution for 2 hours. X-ray photoelectron spectroscopy, infrared spectroscopy, contact angle allow to investigate the composition and the structure of the monolayers. Electrochemical impedance spectroscopy and polarisation curves gives information on the protective properties. A tarnishing test has also been performed in NaCl (0.5 M) solution containing Na_2S (20mM). The substrates have been dipped form 30 min in the solution and then let react with atmosphere for 5 minutes before observation. It appears that introducing a fluorinated segment introduce a small disorganisation within the monolayer but nevertheless, good protection has been observed. Tarnishing of silver is suppress by the presence of the monolayer in both cases as observed in the following pictures.

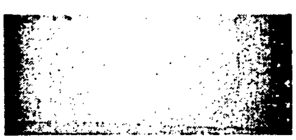

C_{16} coated silver

Uncoated silver

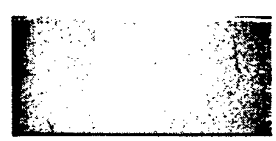

F_4H_{11} coated silver

References

[1] K. Hallet, D. Thickett, D.S. McPhail, R.J. Chater, Appl. Surf. Sci. 203 (2003) 789

[2] L.Favre-Quattropani, P. Groening, D. Ramseyer, L. Schalpbach, Surf. Cot. Techn. 125 (2000) 377

[3] M. Evesque, M. Keddam, L. Klein, H. Takenouti, B. Trachli, Paper on the EMCR 2003 Conference at Nieuwpoort (Belgium)

[4] LAIBINIS P.E., WHITESIDES G.M., ALLARA D.L., TAO Y.-T., PARIKH A.N., NUZZO R.G., J. Am. Chem. Soc. 113 (1991) 7152

[5] T.D. Burleigh, C. Shi, S. Kilic, S. Kovacik, T. Thompson, R.M. Enick, Corr. Sc. 58 (2002) 49

MODELLING THE ELECTRONIC PROPERTIES OF FUNCTIONALIZED CARBON NANOTUBES

Manuel Melle-Franco and Francesco Zerbetto
Dipartimento di Chimica G. Ciamician
Universita' degli Studi di Bologna
Italy

In order to increase their processibility in solution, carbon nanotubes must be functionalized. The process, however, saturates a number of trivalent carbon atoms and therefore affects the electronic properties of these systems. Here we combine Density Functional Theory and Tight Binding calculations to investigate which functionalization conditions minimize or maximize the alteration of the electronic properties.

STM/STS ON SELF-ORGANIZING 3D HYBRID NANOSTRUCTURES

Elena Mena-Osteritz and Peter Bäuerle
Dept. Organic Chemistry II, University of Ulm, 89081-Ulm, Germany
E-mail: elena.mena-osteritz@chemie.uni-ulm.de

The well-defined molecular structure of π-conjugated linear and macrocyclic Thiophenes [1] allows their self-organization on substrates. Moreover the semi conducting properties of such a family of organic compounds make possible their employment as components for coming nanoelectronic devices and as modular building blocks for the assembly of new materials and supramolecular chemistry. However, the assembly of molecular materials in nanoscale architectures will be a crucial step for the future molecular scale electronics. [2] The toroidal structure that such macrocycles show can represent intriguing "molecular circuits" which would additionally include sites for recognition and selective complexation.

In this contribution we will present the different 2D-arrangements of the macrocycles at the liquid/HOPG interface revealed by in-situ scanning tunneling microscopy (STM). The construction of well-ordered hybrid nanostructures (organic/inorganic and organic/metallic) in the third dimension will be presented. The constructed nanostructures will be analyzed with the help of theoretical calculations and MO analyses. By means of STM, we also investigated epitaxy and interactions of some of these hybrid superstructures, like C60/Cyclo[*12*]thiophene, in a perfect 2D and 3D crystalline "complex"-monolayer. STM and STS-analyses of the specificity, dynamics and electric properties of the 3D nanostructures will be also discussed.

References:

[1] a) E. Mena-Osteritz Adv. Mater. **2001**, 13, 243. b) J. Krömer, I. Rios-Carreras, G. Fuhrmann, Ch. Musch, M. Wunderlin, T.Debaerdemaeker, E. Mena-Osteritz, P. Bäuerle, Angew. Chem. Int. Ed. **2000**, 39, 3481.
[2] H. Engelkamp, S. Middelbeek, R.J.M. Nolte, Science **1999**, 284, 785.

CHARACTERISATION AND CHEMICAL PATTERNING OF NO_2-TERMINATED SELF-ASSEMBLY MONOLAYERS ON Si/SiO_2

Paula Mendes,[†] Susanne Jacke,[§] Jose Plaza,[§] Kevin Critchley,[‡] Stephen Evans,[‡] Yu Chen,[§] Richard Palmer,[§] Jon A. Preece[†*]

[†] School of Chemical Sciences, University of Birmingham, Edgbaston, Birmingham B15 2TT, U.K.
[§] Nanoscale Physics Research Laboratory, School of Physics and Astronomy, University of Birmingham, Edgbaston, Birmingham B15 2TT, U.K.
[‡] Department of Physics and Astronomy, University of Leeds, Leeds LS2 9JT, U.K.
[*]E-mail: j.a.preece@bham.ac.uk .

The development of easy, rapid and efficient techniques for the two-dimensional patterning of materials on surfaces is of great importance in modern science and technology [1]. Furthermore, many emerging nanotechnological applications rely on the development of well-defined surfaces functionalised with submonolayer coverages of complex organic molecules [2]. A particularly promising trend is the exploitation of self-assembled monolayers (SAMs) as ultrathin resists in combination with electron-beam lithography [3-5].

In this study, we have investigated the formation of SAMs of 3-(4-nitrophenoxy)-propyltrimethoxysilane (NPPTMS) on silicon (Si/SiO_2) wafers and whether they can produce uniform and thin monolayers. Important aspects concerning the experimental conditions of SAM formation, including effects of solvent, time and the environmental conditions were analysed. Our results are documented by contact angle measurements, ellipsometry, atomic force microscopy (AFM) and X-ray photoelectron spectroscopy (XPS). After formation of nitro-terminated SAMs on Si/SiO_2, scanning electron microscopy (SEM) can be used to induce the conversion of the NO_2 moiety to the NH_2 functionality in order to pattern the sample, using either a mask or direct e-beam writing.

References:

[1] Y. Xia and M. Whitesides, Angew. Chem. Int. Ed., **37** (1998) 550.
[2] J. J. Gooding, F. Mearns, W. Yang and J. Liu, Electroanalysis, **15** (2003) 81.
[3] W. Eck, V. Stadler, W. Geyer, M. Zharnikov, A. Gölzhäuser and M. Grunze, Adv. Mater., **12** (2000) 805.
[4] C. K. Harnett, K. M. Satyalakshmi and H. G. Craighead, Langmuir, **17** (2001) 178.
[5] Y. J. Jung, Y.-H. La, H. J. Kim, T.-H. Kang, K. Ihm, K.-J. Kim, B. Kim and J. W. Park, Langmuir, **19** (2003) 4512.

LARGE AREA INEXPENSIVE COLD CATHODES BASED ON DOPED CARBON NANOTUBES – POLYSTYRENE COMPOSITES

E. Mendoza, C.H.P. Poa, G.Y. Chen, W. K. Hsu[†], S. R. P. Silva
Advanced Technology Institute, University of Surrey, Guildford, Surrey, GU2 7XH, United Kingdom
[†] School of Chemistry, Physics and Environmental Science, University of Sussex , Brighton, BN1 9QJ, United Kingdom

E-mail: e.mendoza@surrey.ac.uk

The presence of a high chemical stability, good mechanical properties and high aspect ratio (>1000 for 10 – 50nm carbon nanotubes) have made carbon nanotubes (CNTs) a strong candidate as an electron field emitter[1]. Although, the physical attributes of CNTs are ideally suited for field emission applications, its incorporation into a three terminal structure has technologically been challenging. This is exacerbated by the need of pre-defined pixilated cathodes fabricated over large areas. In this paper we introduce a methodology that avails itself to screen printing and even spray coating, with the little effects to the detriment of the cathode properties.

There are many techniques that can be used to produce single walled carbon nanotube (SWCNTs) or mutiwalled carbon nanotubes (MWCNTs). Arc discharge, laser ablation and chemical vapor deposition (CVD) are well established to produce a wide varity of CNTs [2-5]. These techniques provide independent control of the size, height and density of MWCNTs by means of transition catalyst on the substrates [6,7]. However, these methods do not produce the large area deposits needed for cold cathodes for displays, and fabrication can be time consuming and expensive. One cheap and efficient method is by mixing CNTs with polymer to produce field emission devices.

In this work, the preparation and field emission characteristics of nonaligned MWCNTs – polymer matrix composites will be discussed. The MWCNTs are produced by arc discharge technique. After the synthesis and purification, the MWCNTs were mixed in polystyrene and toluene to produce the polymer composites. The resulting composites have been characterized by electron microscopy showing an homogeneous distribution on non-aligned MWCNTs.

Electron field emission properties of these composites will be presented for different concentration of MWCNTs in the polymer matrix, and the effect of different dopants such as Boron and Nitrogen will be discussed. These results show that the geometrical screening effects are the key issue on field emission from these types of composites.

References:

[1] W. Zhu, C. Bower, O. Zhou, G. Kochanski and S. Jin, Appl. Phys. Lett.. **75**, 873 (1999).
[2] S. Ijima, Nature **354**, 56 (1991).
[3] T. W. Ebbesen and P.M. Ajayan, Nature **358**, 220 (1992).
[4] A. Thess, R. Lee, P. Nikolaev, H.J. Dai, P. Petit, J. Robert, C.H. Xu, Y.H. Lee, S.G. Kim, A.G. Rinzler, D.T. Collbert, G.E. Scuseria, D. Tomanek, J.E. Fischer and R.E. Smalley, Science **273**, 483 (1996).
[5] M. Terrones, N. Grobert, J. Olivares, J.P. Zhang, H. Terrones, K. Kordatos, W.K. Hsu, J.P. Hare, P.D. Townsend, K. Prassides, A.K. Cheetham, H.W. Kroto and D.R.M. Walton, Nature **388**, 52 (1997).
[6] M. Chhowalla, K.B.K. Teo, C. Ducati, N.L. Rupensinghe, G.A.J. Amaratunga, A.C. Ferrari, D. Roy, J. Robertson and W.I. Milne, J. Appl. Phys **90**, 5308 (2001)
[7] Z.F. Ren, Z.P. Huang, J.W. Xu, J.H. Wang, P. Bush, M.P. Siegal and P.N. Provencio, Science **282**, 1105 (1998)

Figures:

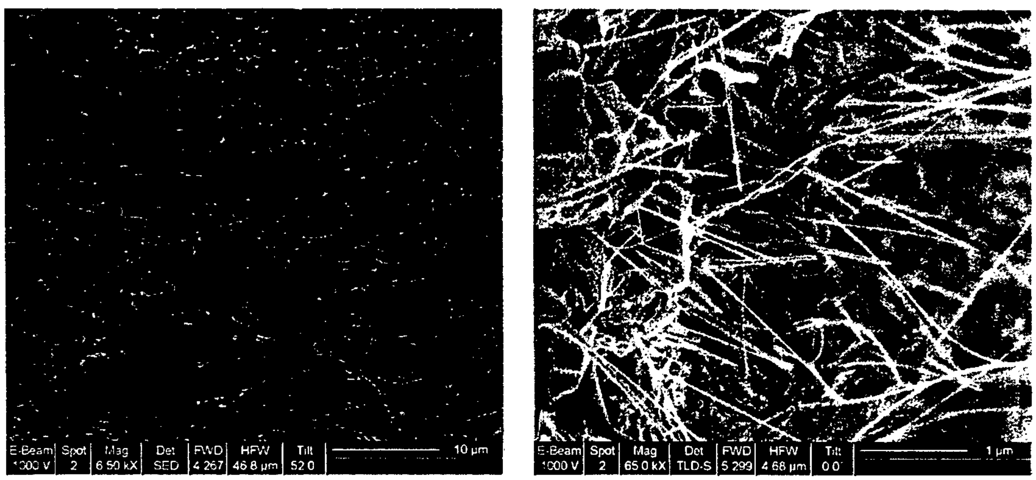

Figure 1. SEM images of the nanotube composite film. (a) Top view of the sample showing nanotubes protruding from the film. (b) Cross-sectional view of the nanotube composite film.

ULTRA HIGH SPEED SCANNING PROBE MICROSCOPY

A.D.L. Humphris, J.K. Hobbs and M.J. Miles
H.H. Wills Physics Laboratory, University of Bristol, Tyndall Avenue, Bristol, BS8 1TL, United Kingdom
http://spm.phy.bris.ac.uk

The ability to follow processes at the nanometre scale *in situ* in air and liquid in real time is one of the major advantages of scanning probe microscopy (SPM). However, unlike far field imaging methods that collect data in a parallel fashion, due to the scanning nature of SPM, it is necessary for the image to be collected one pixel at a time, line by line in series, thus severely limiting the rate at which an image can be obtained. Typically, a conventional atomic force microscope (AFM) will take from 10 seconds to a few minutes to acquire an image, much slower than the millisecond timescales typical of macromolecular processes, due to the relaxation time of the molecules. Other applications of SPM are limited by low acquisition rates including data storage and nanolithography. The burgeoning area of nanotechnology and nano length scale devices requires a scanning probe instrument that can address a surface at significantly increased rates compared to existing methods.

In an attempt to significantly increase image acquisition rates, efforts have recently focused on increasing the response time of an atomic force microscope (AFM) cantilever by decreasing its mass and incorporating a separate z-piezo transducer on the cantilever. Optimisation of these approaches has achieved scan times of considerably less then one second and now the ultimate image acquisition rate is limited by the rate at which the probe can mechanically address the surface of interest.

In this presentation, a new form of scanner that enables the probe to address the surface using a mechanical resonance of the scan system will be described. Using this Resonant Scanner, we have developed a scanning near field optical microscope (SNOM) that is capable of scan speeds of 150 mm/second producing images of an area 20μm^2 in less than 10ms, i.e. over 100 frames/second. Information to construct each image is collected at a rate of ~0.5GB/second and processed using a field programmable gate array (FPGA) enabling a real time presentation of the image to the operator.

Recently the Resonant Scanner has been implemented in an atomic force microscope and similar capabilities to those of the SNOM describe above demonstrated.

The presented microscopes are over 1000 times faster than a commercial SNOM and approximately 10 times faster than the highest frame rate previously achieved using any SPM technique. This is the first time a mechanical resonance has been used to scan a surface and demonstrates the step like improvement in the acquisition rate of SPM necessary if these techniques are to deliver the capabilities sought by the advancing fields of biotechnology and nanotechnology
.

ZnO NANOPARTICLES OF CONTROLLED SIZE AND SHAPE THROUGH A NOVEL ORGANOMETALLIC METHOD

Miguel Monge, Myrtil L. Kahn, André Maisonnat, Bruno Chaudret

Laboratoire de Chimie de Coordination du CNRS, 205, route de Narbonne, 31077 Toulouse Cedex 04, France.

ZnO is a wide band gap semiconductor (3.37 eV) that also displays interesting photoluminescent properties. In the past few years, the seek of well controlled ZnO nanomaterials [1] has prompted the researchers to the development of new methods for the synthesis of such kind of nanostructures involving physical [2] or chemical [3] techniques. Thus, among the chemical methods for the synthesis of nanoparticles, the organometallic route used in our research group presents several advantages as (i) the mild reaction conditions that allows the control of size and dispersity and (ii) the clean reaction conditions that lead to uncontaminated surface.

Going further, previous synthetic strategies for the synthesis of metal oxides from organometallic precursors involved a two-step approach: (i) formation of metal nanoparticles from the organometallic precursor and (ii) oxidation of the metallic nanoparticles.[4,5] In these sense we have developed a new one-step method for the preparation of metal oxides taking into account that most organometallic complexes are air-sensitive and decompose exothermically in air. Indeed, in the presence of stabilizing long alkyl chain amine ligands we can control the size and shape of the metal oxide nanoparticles when the organometallic precursor [$ZnCy_2$] (Cy = Cyclohexyl) is exposed to O_2.

Depending on the nature and concentration of the stabilizing ligand in solution, the overall concentration, the oxidation/evaporation rate, the solvent and the temperature (mostly room temperature) we have been able to achieve crystalline ZnO nanoparticles of small size (from 2.5 to 35 nm) with different shapes as regular disks or rod-like. In Figure 1 we show some examples of ZnO amine capped nanostructures.

References:

[1] a) M.H. Huang, S. Mao, H. Feick, H. Yan, Y. Wu, H. Kind, E. Weber, R. Russo, P. Yang, *Science* **2001**, 292, 1897. b) J. Johnson, H. Yan, R. Schaller, L. Haber, R. Saykally, P. Yang *J. Phys. Chem. B*, **2001**, *105*, 11387.

[2] a) P. Yang, H. Yan, S. Mao, R. Russo, J. Johnson, R. Saykally, N. Morris, J. Pham, R. He, H. Choi, *Adv. Funct. Mater.*, **2002**, *12*,323. b) W.I. Park, G. Yi, M. Kim, S.L. Pennycock, *Adv. Mater.*, **2002**, *14*, 1841.

[3] a) L. Vayssieres, K. Keis, A. Hagfeldt, S. Lindquist, *Chem. Mater.*, **2001**, *13*, 4395. b) L. Vayssieres, *Adv. Mater.*, **2003**, *15*, 464. c) C. Pacholski, A. Kornowski, H. Weller, *Angew. Chem.Int. Ed.*, **2002**, *41*, 1188.

[4] a) C. Nayral, E. Viala, P. Fau, F. Senocq, J.-C. Jumas, A. Maisonnat, B. Chaudret, *Chem. Eur. J.* **2000**, *6*, 4082. b) K. Soulantica, L. Erades, M. Sauvan, F. Senocq, A. Maisonnat, B. Chaudret, *Adv. Funct. Mater.*, **2003**, *13*, in press.

[5] F. Rataboul, C. Nayral, M.-J. Casanove, A. Maisonnat, B. Chaudret, *J. Organometal. Chem.* **2002**, *643-644*, 311.

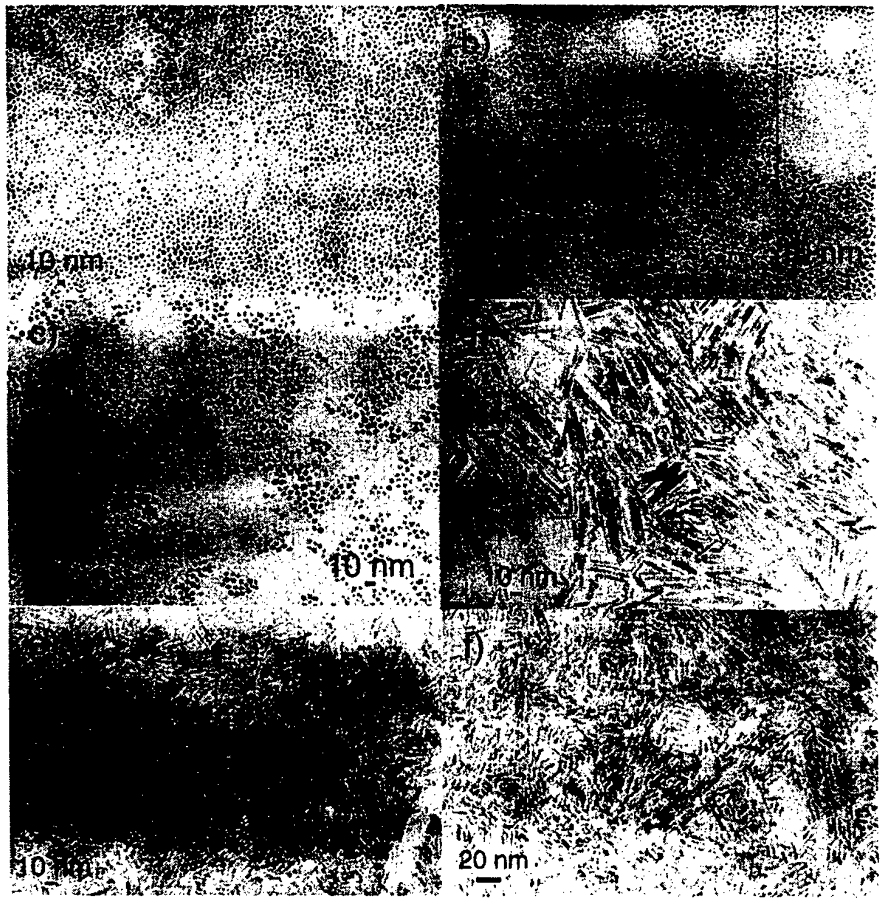

Figure 1. Some TEM micrographs of different ZnO amine capped nanostructures obtained from the oxidation of the organometallic precursor [$ZnCy_2$]: a) very slow oxidation (2 weeks) in Tetrahydrofurane (THF) as solvent with 1 equivalent of Hexadecylamine (HDA) as stabilizing amine. b) oxidation in Heptane as solvent with 1 equivalent of HDA as ligand. c) oxidation in THF with 1 equivalent of Octylamine (OA) as ligand. d) oxidation without solvent using 2 equivalents of OA as stabilizing ligand. e) oxidation without solvent using 2 equivalents of Dodecylamine (DDA) as ligand. f) oxidation without solvent using 1 equivalent of HDA as ligand.

CHARGE AND DISCHARGE DYNAMICS IN SILICON NANO-CRYSTALS : A DIRECT CONSTANT CAPACITANCE APPROACH

Mikaël Tihy, Laurent Montès, Xavier Mescot, Stéphane Ferraton, Jacques Zimmermann.
Institut de Microélectronique, Electromagnétisme et Photonique
UMR CNRS 5130, 23 rue des Martyrs, BP 257, 38016 Grenoble Cedex 1, France

With the recent development of a new generation of non volatile memories (NVM) using floating gates made of silicon nano-crystals (Si-nc) in place of a compact poly-Si layer embedded in the MOS gate oxide [1], the problem of how to control charge and discharge Si-nc, the voltage required to do so, the write/erase speeds (or times), the retention time and the control of the subsequent sub-threshold MOS leakage current controlled by the registered charges in the Si-nc layer, are prominent factors to be determined with accuracy [2,3]. Below, we describe and apply a new method for evaluating the charge retention dynamic properties of Si-nc embedded in the gate oxide of MOS capacitors (MOSC). The method is applicable to MOS transistors gate capacitances, as well.

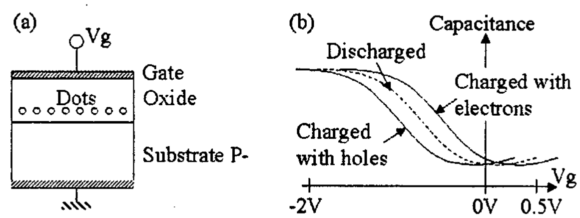

Fig. 1 : (a) NVM-MOSC structure and (b) C(V)

The MOSC studied here is sketched Fig. 1a. The detailed structures were described in a previous paper [4]. The principle of operation is based on the fact that when the MOSC is subjected to a large positive (or negative) voltage stress for sufficient time, electrons (or holes) from the oxide/substrate interface are injected into the Si-nc layer and remain there until stress is removed. The result of this is a shift *without deformation* of the MOSC capacitance along the voltage scale towards positive (or negative) voltages, as illustrated in Fig. 1b. We chose a capacitance C_0 (preferably close to the flat band voltage capacitance in order to maximise the effect of the Si-nc charge) and as Si-nc begin to release their charges in the substrate (after stress removal), we adjust the voltage to be applied to the MOSC in order to maintain the measured capacitance at C_0. This was performed with a home-made code used in a LabVIEW™ environment. It monitors the voltage versus time and performs capacitance measurements with a HP 4284A LCR metre. The way in which the voltage shift is extracted from the voltage change is illustrated in Fig. 2. It takes in account the fact that during the acquisition and treatment times of registered data, discharge continues and voltage slightly changes. A formula based on the recorded V_{start} and V_{stop} voltages enables voltage correction. In order to do so, a file containing the uncharged MOSC reference capacitance C(V) is required before the initial stress session, while the other part of the code monitors the applied voltage so that the measured capacitance $C_{meas}(t)$ approaches C_0 at each step. Let V_0 be the voltage at which $C(V_0)=C_0$, we have $V_{stop}=V_{start}+(V_0-V_{aux})$, where V_{aux} is just the voltage at which we have $C_{start}=C(V_{aux})$, and $C(V_{stop})=C_0$ of course.

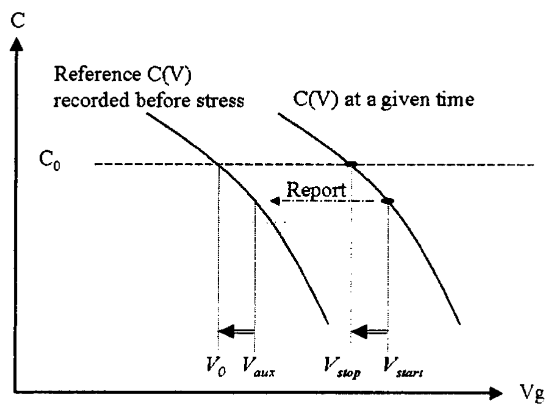

Fig. 2 : Voltage correction

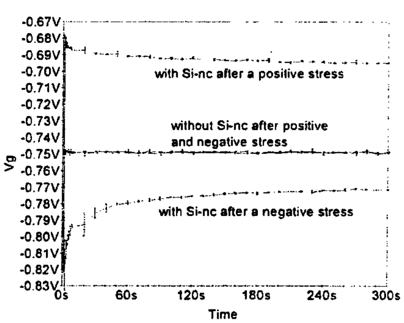

Fig. 3 : Vg(t) with error bars transferred from the $C_{meas}(t)$-C_0.

Voltage is monitored with a constant step. Three steps are currently needed for sufficient accuracy of the voltage shift. The three stages of the process are: i) a C(V) recording; ii) a stress phase; iii) a monitoring phase where measurement is performed.

Fig. 3 compares the results obtained during the discharging of two MOSC, one with Si-nc and another without Si-nc, used as a reference. The case with Si-nc clearly shows that the amount of charges stored in the Si-nc has a great influence over the discharging speed. Indeed, discharging is initially faster, and tends to slow down for longer times. This can be explained by the configuration of the electric field in the tunnelling oxide, as it evolves with the discharging of the Si-nc, and the fact that tunnelling controls the movement of the charges across the dielectric barrier in both directions.

Curves fits with y0+A1.exp(-t/t1)+A2.exp(-t/t2) are shown in Fig.4. The presence of a different constant value y0 and different time constants for a positive or a negative stress voltage proves that the implied charges are not the same : electrons for a positive stress and holes for a negative one.

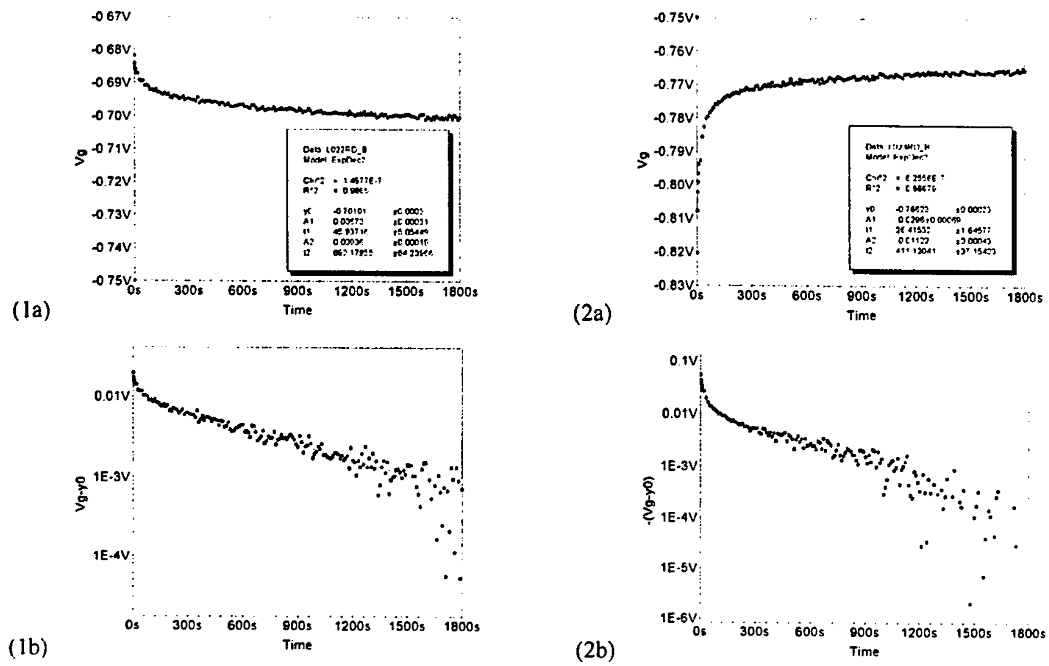

Fig. 4 : Fits of positive (1) and negative (2) stress in linear scale (a) and logarithm scale (b)

In this paper we will further explain this specific constant capacitance measurement method we have developed. We will show the advantages it gives to have a better understanding on the storage properties and on the charge and discharge mechanisms of devices that include silicon nanodots as an active part. A physical model will be proposed to explain the observed phenomena.

Acknowledgements : This work was performed on devices provided by LETI/PLATO in the framework of CPMA. Financial support from Région Rhône-Alpes is also acknowledged.

[1] Baron T., Martin F., Mur P., Wyon C., Dupuy M., 2000, Silicon quantum dot nucleation on Si_3N_4, SiO_2 and SiO_xN_y substrates for nano-electronic devices. J. of Crystal Growth, 209, p. 1004.

[2] De Salvo B., Ghibaudo G., Pananakakis G., Masson P., Baron T., Buffet N., Fernandes A.,Guillaumot B., 2001, Experimental and theoretical investigation of nano-crystal and nitride-trap memory devices, IEEE Trans. Electron Devices, 48, p. 1789.

[3] Tiwari S., Rana F., Chan K., Shi L. Hanafi H., 1996, Single charge and confinement in nano-crystal memories. Appl. Phys. Lett., 69, p 1232.

[4] Ferraton S., Montès L., Souifi A., Zimmermann J., 2003, Evidence of charging effect in silicon nano-crystals using feedback charge method with MOS capacitors, Nanotechnology, 14, p. 630.

GROWTH OF CARBON NANOTUBES BY LOW- AND HIGH-PRESSURE CHEMICAL VAPOR DEPOSITION

Stanislav A. Moshkalyov[1**]; Antonio C. S. Ramos[2]; José L. Gonçalves[1]; Jacobus W. Swart[1]

[1] Centro de Componentes Semicondutores- CCS, UNICAMP, C.P. 6061, CEP 13083-970, Campinas, SP

[2] Laboratório de Pesquisa em Dispositivos – LPD, IFGW, UNICAMP, CEP 13083-970, Campinas, SP

**E-mail: stanisla@led.unicamp.br

Carbon nanotubes (CNTs) attract much attention since their discovery in 1991 [1] due to exceptional mechanical, electrical and optical properties and potential applications [2,3]. For the CNTs growth, a number of methods was developed, including arc-discharge, laser ablation and different versions of chemical vapor deposition (CVD). CVD methods have certain advantages over other ones as they provide a way for controlled, directional growth of both single-walled and multi-walled CNTs. In the present work, preliminary results of CNTs synthesis using two different catalytic CVD techniques (plasma-enhanced low-pressure CVD and atmospheric-pressure thermal CVD) are presented. Multi-walled CNTs with tube diameters ranging from about 10 to 100 of nanometers were obtained and analyzed using high-resolution scanning electron microscopy.

In the present work, thin Ni films (1-40 nm thick) were used as a catalyst material. For the film growth, high-vacuum electron-beam thermal deposition was employed. After deposition, the films were thermally treated (~700° C) in a nitrogen or hydrogen atmosphere to provide formation of separate catalyst nanoparticles. As substrates, Si wafers were used previously covered by thin (50 nm) oxide films. The oxide films are necessary to avoid the catalyst diffusion into the Si substrate during high-temperature processing. CTNs synthesis was realized in two different reactors. The first one uses a low-pressure microwave plasma source, with low-pressure (~1Torr) nitrogen-acetylene gas mixtures. Samples are heated up to ~550-700 ° C by a halogen lamp heater. In the second reactor, the flowing gas mixture and samples are heated in a resistive heating oven to temperatures up to 900° C. Atmospheric pressure methane-hydrogen based mixtures were used in this case. After synthesis, the samples were examined using high-resolution scanning electron microscopes JSM-5900LV and JSM-6330F of the LME/LNLS, Campinas.

Fast CNT growth was obtained in both reactors. The process appears to depends critically on the catalyst film thickness. For thicker Ni films, large diameter (up to 100 nanometers) tubes, apparently with high content of amorphous carbon were deposited. For thin catalyst films, it was possible to grow long (up to 30 μm, with the growth rate up to 1 - 2 μm/min) CNTs. The CNTs with diameters as small as ~10 nm were obtained. In many cases, small catalyst particles were detected at the tip of the tubes. This suggests that the tip growth mechanism is likely to be responsible for the CNTs synthesis under the present conditions. In the high-pressure CVD, higher temperatures were needed to obtain CNTs. For higher temperatures, it was possible to obtain longer and straighter CNTs. The future work will focus on the optimization of the growth processes, in particular, in order to achieve directional CNTs growth.

References:

[1] S. Iijima, *Nature*, **354**, 56 (1991).
[2] H. Dai, *Surface Science*, **500**, 218 (2002).
[3] A. Huczko, *Appl. Phys.* A **74**, 617 (2002).

Acknowledgements

This work was supported by CNPq, FAPESP and FINEP.

LITHIUM STORAGE IN HYDROGEN-RICH CARBON NANOSTRUCTURES: A QUANTUM-CHEMICAL STUDY BASED ON MODEL PAHs

Fabrizia Negri and Giorgia Brancolini
Dipartimento di Chimica"G. Ciamician", via Selmi 2, I-40126 Bologna
e-mail:fabry@ciam.unibo.it

Rechargeable batteries, in particular "lithium-ion" batteries, are one of the most important commercialized energy storage devices. In recent years several theoretical and experimental investigations have been directed toward the development of new materials for high-density energy storage.

The most common negative electrodes in lithium-ion batteries are made by carbonaceous insertion compounds such as synthetic graphite, carbon fibres, etc. [1]. At ambient temperature, there is a limit to the amount of lithium that can intercalate pure graphite: one lithium per six carbon atoms to form the LiC_6 compound. However, in carbonaceous materials containing substantial hydrogen (soft carbon), the amount of lithium that can be stored is larger and lithium appears to reversibly bind near hydrogen atoms [1].

The binding mechanism in "soft" carbon materials, has been investigated by several authors by considering small aromatic hydrocarbons [2,3].

In this work we model the hydrogen-rich carbon material with polycyclic aromatic hydrocarbons (PAH) and investigate the interaction of lithium atoms with hexa-*peri*-hexabenzocoronene (HBC), $C_{42}H_{18}$ (Fig.1). To this end we have carried out quantum chemical calculations using the hybrid B3LYP functional with the 6-31G* basis set, a level of theory that has been shown to provide results comparable to MP2. We considered, initially, the interaction of two lithium atoms with the PAH and explored a large number of interaction sites both above or above and below the HBC molecule.

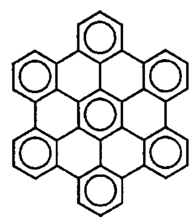

Fig.1. Chemical formula of hexa-*peri*-hexabenzocoronene

Binding energies were computed and corrected for the basis set superposition error. From the computed equilibrium structures and binding energies, the most favorable sites for lithium doping were identified. It is shown that the most stable structures correspond to lithium bound to the periphery of the hydrocarbon, as suggested by previous experimental studies [1]. It is concluded that the remarkable stability of peripheral interaction sites might be at the origin of the large lithium storage capacity recently measured for HBC [4] as well as for soft carbons compared with graphite. The details of the structural and energetic characteristics of the Li_2-HBC complexes will be discussed.

[1] J. R. Dahn, T. Zheng, Y. Liu, J. S. Xue, Science, 270, (1995), 590.
[2] S. Ishikawa, G. Madjarova, T. Yamabe, J. Phys. Chem. B, 105, (2001), 11986.
[3] J. M. Vollmer, A. K. Kandalam, L. A. Curtiss, J. Phys. Chem. A., 106, (2002), 9533.
[4] M. Keil, P. Samorì, D. A. dos Santos, J. Birgerson, R. Friedlein, A. Dkhissi, M. Watson, K. Mullen, J. L. Bredas, J. P. Rabe, W. R. Salaneck, J. Chem. Phys., 116, (2002), 10854.

HYDROGEN STORAGE IN AMORPHOUS AGGREGATES OF 3D POLYCONJUGATED DENDRIMERS: A MOLECULAR DYNAMICS STUDY

Fabrizia Negri

Universita' di Bologna, Dipartimento di Chimica 'G. Ciamician',
Via F. Selmi, 2, 40126 Bologna, Italy
e-mail:fabry@ciam.unibo.it

The study of the hydrogen storage capacity in carbon based materials is an active research field since alternatives to the use of metal hydrides, cryotechniques, or high pressure tanks, for the use of hydrogen as a pollution-free energy carrier in mobile applications are not yet available [1]. Among various carbon based materials, in this work we selected the class of polyphenylene dendrimers recently synthesized in Mainz [2]. These materials form amorphous phases that can contain voids owing to the semi-rigid structure imposed by the polyphenyl chains. The physisorption of gas molecules inside the cavities of the amorphous material might then result in a gas storage capacity attractive for practical applications. In this work we present a computational study, carried out at atomistic level, with the help of molecular mechanics and molecular dynamics simulations, of gas diffusion and physisorption in aggregates of first generation polyphenylene dendrimers (see Figure 1). Our aim is to assess whether the peculiar three dimensional structure of this material offers advantages compared to other carbon based materials, as regard hydrogen storage.
The simulations were carried out with periodic boundary conditions and the MM3 potential [3] was selected because it is particularly well suited to describe through-space interactions between aromatic rings.

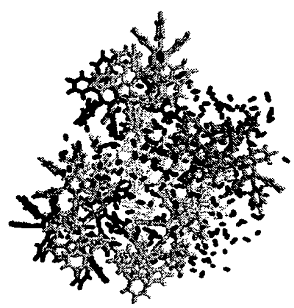

Figure 1: Structure of the simulated aggregate of polyphenylene dendrimers with molecules of H_2 filling the voids

From the molecular dynamics simulations, the parameters that characterize the hydrogen storage capacity were extracted. It is shown that polyphenylene dendrimers should perform, at liquid nitrogen temperatures, comparably to the best carbon based materials known, thanks to the considerable specific surface offered to incoming hydrogen molecules. The comparison between predicted storage capacities and available measurements will be discussed.

References

[1] L. Schlapbach, and A. Züttel, Nature, **414**, 353-358 (2001).
[2] A. J. Berresheim, M. Müller, K. Müllen, Chem. Rev., 99, 1747-1785 (1999); M. Schlupp, T. Weil, A. J. Berresheim, U. M. Wiesler, J. Bargon, K. Müllen, Angew. Chem. Int. Ed., **40**, 4011-4015 (2001).
[3] N. L. Allinger, H. Y. Yuh, J.-H. Lii, J. Am. Chem. Soc., **111**, 8551-8566 (1989).

ELECTROCHEMICAL PRODUCTION OF NANOCRYSTALLINE LAYERS CONTAINING MOLYBDENUM

Jolanta Niedbała
University of Silesia, Institute of Physics & Chemistry of Metals
Bankowa 12, 40-007 Katowice, Poland
E-mail: jniedbal@us.edu.pl

Electrolytic nickel alloys are characterized by good corrosion resistance and electrochemical activity towards cathodic hydrogen evolution and anodic oxygen evolution. They are also used as protection covers for elements working in an aggressive environments [1-5].

The purpose of this work was to determine the structure of Ni-Mo, Ni-Mo-P and Ni+Mo layers, their chemical composition and also surface morphology. Scanning microscopy, X-ray methods and electrochemical studies were used for characterization of the layers.

The Ni-Mo alloy were deposited from nickel-molybdenum bath and Ni-Mo-P layers from the same bath containing additionally sodium hypophosphite under galvanostatic conditions. Ni+Mo layers were electrodeposited from nickel bath containing molybdenum powder suspension. The carbon steel (St3S) with a surface of 4 cm^2 was used as a substrate material.

The phase composition of the layers depends on the composition of galvanic bath. It was stated that Ni-Mo-P alloys are amorphous (Fig. 1a). Ni-Mo alloys obtained by induced codeposition from nickel-molybdenum bath are Mo(Ni) solid solution characterized by nonocrystalline structure (Fig. 1b). Ni+Mo composite layers obtained from the bath containing dispersed molybdenum powder have a crystalline structure (Fig. 1c).

The Ni-Mo-P layer contain 75%Ni, 10%Mo and 15%P, Ni-Mo and Ni+Mo layers contain about 90% of nickel and about 10% of molybdenum. All layers show good adhesion to the substrate. The surface of Ni-Mo and Ni-Mo-P alloys was compact, smooth, mat and grey (Fig. 2a, b). The analysis of Ni-Mo-P surface indicates the presence of phosphorus solid solution in molybdenum and nickel (Fig. 2a). On the surface of this layer there are microcracks. The surface of Ni-Mo layer characterized by island structure (Fig. 2b). The surface of Ni+Mo composite layers was porous, mat and light-grey. On the surface of a nickel grains the smaller molybdenum grains are clearly visible (Fig. 2c).

All layers were subjected to electrochemical investigations included chronovoltammetric studies and corrosion resistance tests by Stern method in alkaline environment (Fig. 3). It was stated that the lowest corrosion rate exibit Ni-Mo alloy, next Ni-Mo-P alloy and Ni+Mo composite layer.

References:

1. J. Niedbała, K. Wykpis, A. Budniok, and E. Łągiewka, Archives of Material Science, **23** 2 (2002) 123-136.
2. E. Łągiewka, A. Budniok and J. Niedbała, Archives of Material Science, **23** 2 (2002) 137-150.
3. E. Bełtowska-Lehman, E. Chassaing, J. Applied Electrochemistry, Iss 5, **27** (1997), 568-572.
4. Y. Zeng, SW Yao, XQ Cao, HX Huang, ZY Zhong, HT Guo, Chinese Journal of Chemistry, Iss3, **15** (1997), 193-200.
5. D. Landolt, E. J. Podlaha, N. Zech, Zeitschrift fur Physikalische Chemie, **208**, no. 1-2 (1999), 167-182.

Figures:

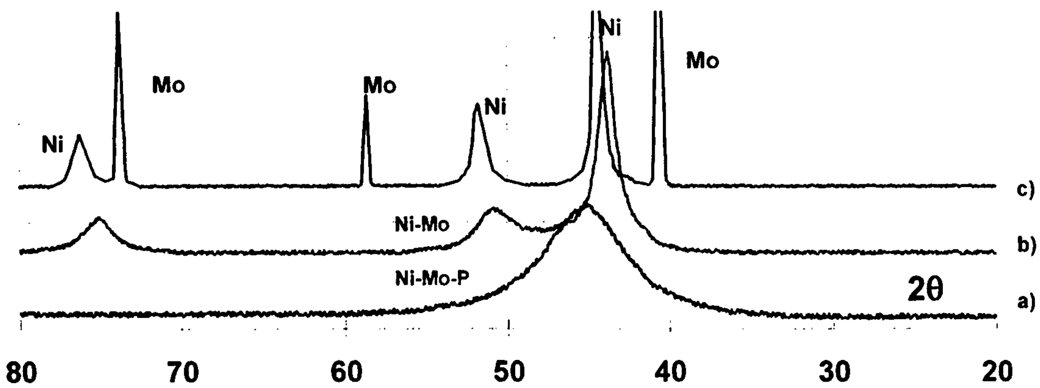

Fig. 1. X-ray diffraction pattern of amorphous Ni-Mo-P alloy (a), nanocrystalline Ni-Mo alloy (b), and Ni+Mo composite layer (c).

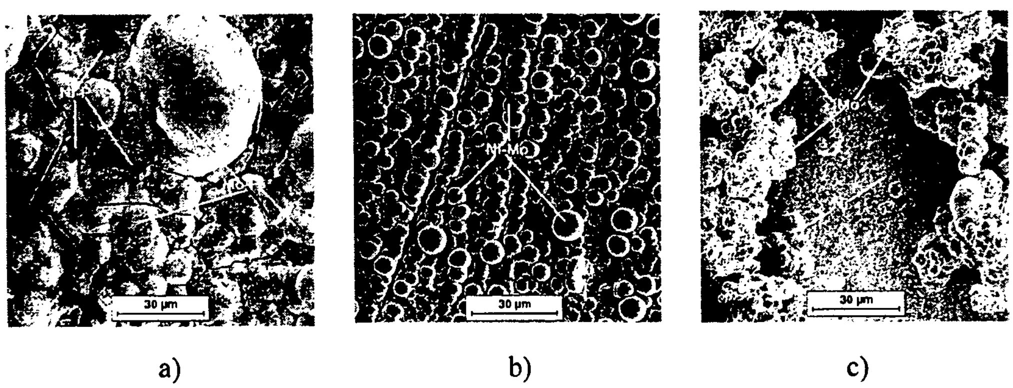

Fig. 2. Surface morphology of amorphous Ni-Mo-P alloy (a), nanocrystalline Ni-Mo alloy (b), and Ni+Mo composite layer (c).

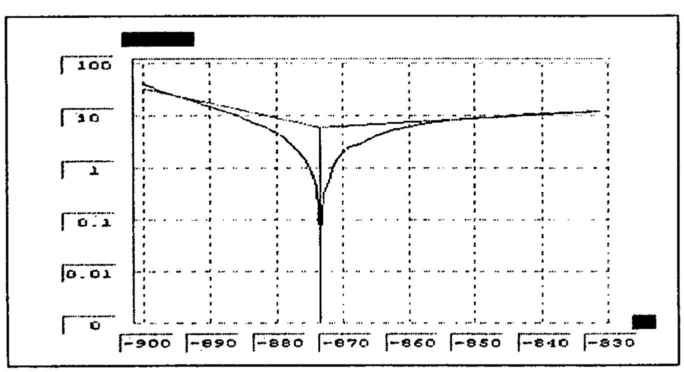

Fig. 3. Corrosion resistance parameters for Ni+Mo composite layer determined by Stern method.

SELF-ASSEMBLED NANOPARTICLE ARRAYS ON MICROCRYSTALS: STRUCTURAL INVESTIGATIONS

K. Nikolic[1], D. Crawley[1], M. Forshaw[1],

D. Cunningham[2], J.-L. Martinez-Albertos[2], B.D. Moore[2]

[1]Department of Physics and Astronomy, University College London, Gower Street, London WC1E 6BT, UK. e-mail: k.nikolic@ucl.ac.uk

[2]Department of Pure and Applied Chemistry, University of Strathclyde, 295 Cathedral St, Glasgow G1 1XL, UK . e-mail: b.d.moore@strath.ac.uk.

The self-assembly of nanostructures is currently very much at the focus of many research groups. It recently has been discovered by the University of Strathclyde group that with a suitable combination of nanoparticle suspensions and ionic salt solutions, it is possible to coprecipitate microcrystals that are coated with nanoparticles [1]. Careful process control provides nanoparticle-coated crystals (NCCs) of relatively uniform size and shape on a gram scale. The self-assembly process of coating microcrystals with nanoparticles (NP) is mediated simply by the crystal lattice and appears generic. If a sub-monolayer of NP is deposited and viewed by TEM a further interesting self-assembling process is observed: the NP seem to form a network of parallel lines, see Fig.1. The periodicity of the parallel lines is approximately 5-6nm. The average size of the nanoparticles is about 3-4nm.

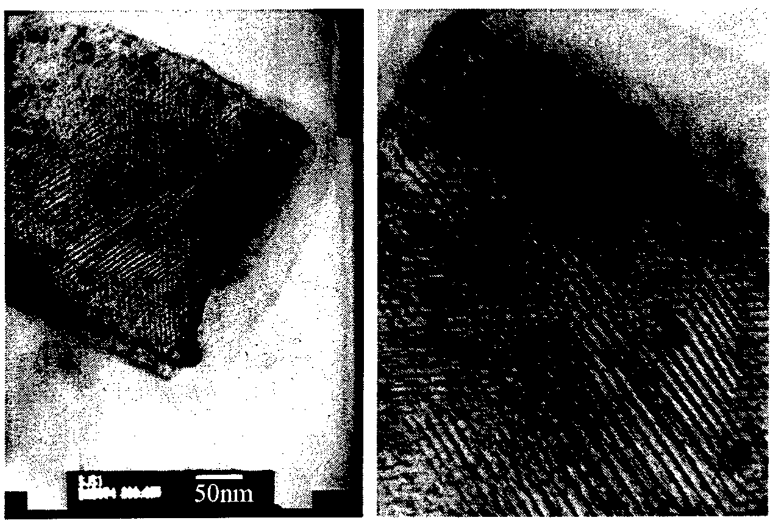

Figure 1. *A transmission electron microscope (TEM) image of K_2SO_4 microcrystal (crystal size is approximately 300nm x 500nm) coated with gold nanoparticles. A possible explanation for the black lines seen in the images is that nanoparticles are forming arrays on the crystal surface, which blend into more uniform regions, probably containing multiple layers of gold nanoparticles.*

The reason for this apparent spontaneous alignment is not yet known and is currently under investigation. In this paper we try to investigate possible reasons for this phenomenon. The first step is to conduct a detailed structural investigation of the NP arrays. For that purpose we have performed a series of (TEM) observations on various samples of NCCs. Immediately apparent is that the electron microscope beam provides a way for simultaneous heating and imaging of

crystals and the effects of such a heating process, are shown in Fig.2. These pictures first confirmed that the black lines on the surface are actually chains of NP. In Figure 2(b) one can clearly see the individual NP separated by the peptide tiopronin molecules (which were used as ligand stabilisers in the process of formation of NP).

(a) (b)

Figure 2. These images illustrate several phenomena that seem to occur when a nanoparticle covered crystal of K_2SO_4 is heated by the electron beam of a transmission electron microscope. Due to partial melting or subliming, the crystal no longer has a regular rectangular-shaped structure. (a) A 'skin' of gold nanoparticles (with tiopronin coating) is retracting, leaving parts of the crystal surface almost uncovered. The image contrast has been increased near the centre to show parallel lines of gold NP. In picture (b) is shown the same crystal but at a later stage in the heating and at a higher magnification. Some Au NP can be seen as small dark spots (about 3-4nm in diameter). The parallel lines of Au NP have disappeared. Instead, spherical clumps of Au NP are forming. NP in clumps are separated by ligand shells (white gaps in the figure). The crystals are eventually destroyed in this process.

The K_2SO_4 crystal structure is orthorhombic, with the largest lattice constant of 1nm, hence the periodicity of NP lines on the crystal surface is not a direct consequence of the underlying lattice structure. There are some indications that lines are formed only when the crystals are heated, because similar line structures emerge on the TEM pictures of pure K_2SO_4 microcrystals when heated. Since K_2SO_4 is a dielectric there is a possibility that a charge distribution on the surface creates a pattern for initiating the formation of nanorods. Crystals grown at room temperature from aqueous solution incorporate OH_3^+ ions in small concentration [2], which might influence the surface potential distribution. These ions undergo recombination in the temperature region 573-723K. K_2SO_4 is also known to undergo a crystallographic phase change at about 850K.

[1] D. Cunningham, J.-L. Martínez-Albertos and B.D. Moore: "Generic route for organisation of nanoparticles on microcrystals", *Trends in Nanotechnology TNT02 Conference* (Santiago de Compostela, Spain, 2002), http://www.phantomsnet.com/html/abstracts.php

[2] H. Arnold et. al.: "The Phase Transition of K_2SO_4 at about 850K", *Acta Cryst.* **B37**, pp.1643-51 (1981).

NANOFOCUSING PROBE FOR A NEAR-FIELD OPTICAL HEAD

Ivan D. Nikolov[1], Kenya Goto[2] and Takayuki Kurigaya[2]

[1] Optics and Spectroscopy Dept., University of Sofia, 5 James Bourcher Blvd., Sofia BG-1164, Bulgaria

[2] Information and Communication Technology Dept., Tokai University, Numazu, Shizuoka 410-0395, Japan

[1] E-mail: ivandn@intech.bg

1. Introduction

Nanophotonics is defined as nanoscale optical science, research and technology. Nanophotonics field offers challenging opportunities for the design of novel nano-structural optical materials and devices such as ultra-high density optical memories, near-field nano-probes, nanoscale switches and scanning micro-stations. Nanometrology secures nanoscale measurements and nano-topographic inspection of the microstructures, MEMS, optical memory modules, integrated arrays and photonic devices.

Nanofocusing is determined as light collecting into a spot size under 200 nm. The conventional microlens systems can focus laser beams into spot diameters from 1 μm to 0.4 μm. Nanofocusing research is a part of the field of nanophotonics directed to nanoscale light-matter interaction and nano-fabrication of optics. The production accuracy of the existing optical technology is from 1/10 to /20 that is from 60 nm to 30 nm during the precise optical surface diagnostics.

For a successful modeling and design of the new optoelectronic devices, the optical functions of each component should be known [1]. The theories and applications of nano-optics are discussed in Ref. [2, 3]. The concept of writing heads in the array system has been reported in a previous publication [4]. It is very important to focus the vertical cavity surface emitting laser (VCSEL) output energy on the optical disk photosensitive structure. The nanofocusing effect is possible [5]. The design and fabrication of microlens array (MLA) intended for a near-field optical head has been proved experimentally [6]. The total internal reflection in the MLA causes a significant ray and wave vignetting [7].

The aim of this research is to improve the design and fabrication of a nanofocusing probe for a near-field optical head. The main ultra-high density optical storage (UHDOS) requirements are to design free of aberrations nanofocusing recording modules applied in arrayed memory heads and to fabricate nanophotonics integrated structures. We discuss the design characteristics and further methods for the amendments of the optical performance of the nanofocusing probe realized for a UHDOS system.

In this paper, we report on the obtained results for a nanofocusing probe optimization. The balancing of the residual aberrations and technological errors is also evaluated for the developed near-field optical head. This research focuses on the nano-probe configurations with the possible aberration solutions, the recording specifications and theoretical background, the MLA shape and calculation formulae, the ray and wave-front analysis, the nano-spots' energy distribution and finite-difference time-domain (FDTD) optical power density computing.

2. Results and discussion

The micrometre-scale refractive lens can focus a micro-laser beam into a light spot under 1 μm. The flat surface of the MLA is covered with anti-reflection coating (ARC) system or with sandwiched photosensitive layers as shown in Fig. 1. The VCSEL matrix forms a number of micro-beams having a ray-divergence of about 12 degrees. The lens elements of the RIE-fabricated MLA collect the VCSEL light on the infra-red (IR) sensitive film. The MLA focuses the VCSEL beams forming a set of nano-spots into the IR film. One can obtain an array of tiny black disks after the developing of the exposed IR photosensitive film. The IR recording VCSEL wavelength is 850 nm. The optical integration technology continues with the photoresist layer exposition using a ultra-violet source. The array of the IR film's black disks produces a patterned structure on the photoresist for the next nano-probe array fabrication into the GaP wafer. In this way the MLA nanofocused points can be adjusted into the nano-probe apertures.

The most important nano-polishing technology must guarantee the coincidence of the MLA focal points with the rear exit plane surface of the MLA. The only MLA refractive surface focuses the VCSEL beams on the MLA exit plane surface. The MLA module is corrected for transversal aberrations on its back focal plane. The axially symmetric MLA optical surface can be fabricated as spherical or aspherical. The exact MLA surface is ellipsoidal for this developed near-field optical head. The nano-asphERization of the MLA convex surfaces is fulfilled using the RIE technology during the super-polishing process. The maximal nano-polishing value is about 150 nm on the periphery area of the MLA surfaces fabricated with a diameter of 13 μm. Our proposed near-field optical head is presented in Fig. 2. Every one micro-laser beam of about 8 μm diameter emitted from the VCSEL array is collected by the MLA to the GaP micro-probe array's tip. The obtained nanofocusing array produces near-field recordings into the optical disk structure. The fabricated memory head is required to have a high energy throughput and small optical power distribution.

3. Conclusion

The obtained nanofocusing module is practically an aberration-free optical system. The designed nanofocusing probe has an enlarged numerical aperture (NA) over 2.15. This NA value is about three times larger than the previous published result. Using an ARC optimization one can realize an energy throughput about 4.80-fold than the output of the MLA without optical coatings. The optimized arrayed probe has nanofocusing energy efficiency about 45 times higher than the values published in previous reports. The computed nanofocused spots are from 23 nm at the geometrical MLA limit and up to 130 nm at the diffraction FWHM size applying experimental ARC systems and using FDTD modeling for electromagnetic waves' analysis.

References

1. Jahns J. and Lee S. H. (ed) 1994 *Optical Computing Hardware* (London: Academic)
2. Ohtsu M. 1997 *Near-Field Nano/Atom Optics and Technology* (Heidelberg: Springer)
3. Kawata S. et al. (ed) 2001 *Nano-Optics* (Springer Series in Optical Sciences, vol. 84)
4. Goto K. 2000 Two-dimensional near-field optical memory head, *US Patent Specification 6,084,848*
5. Nikolov I. D., Goto K., Mitsugi S., Kim Y. J. And Kavardjikov V. I. 2002 *Nanotechnology* **13** 471-7
6. Kurihara K., Nikolov I. D., Mitsugi S., Nanri K. And Goto K. 2003 *Optical Review* **10** 89-95
7. Nikolov I. D., Kurihara K. And Goto K. 2003 *Nanotechnology* **14** 945-54.

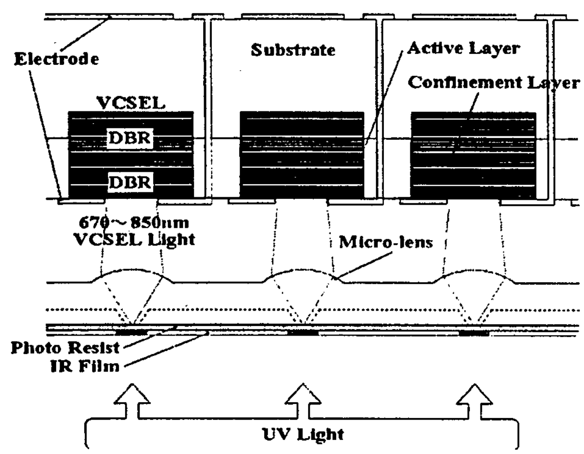

Figure 1. Schematic diagram of the optical integration technology for the MLA to nano-probe array axis adjustment with the aid of a VCSEL matrix.

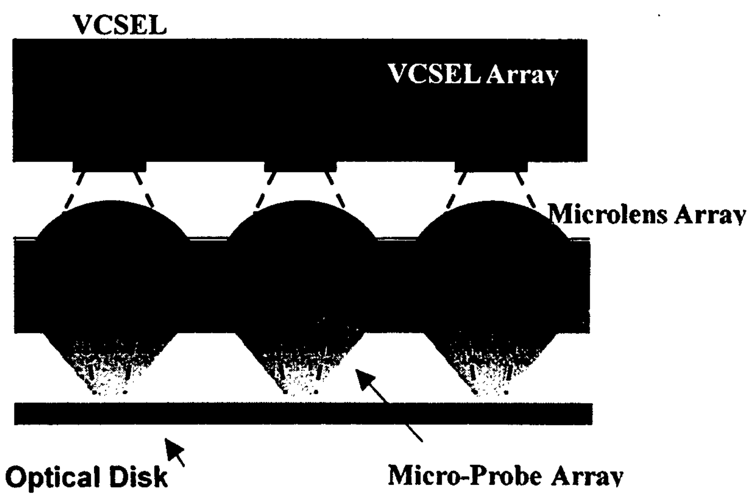

Figure 2. Proposed near-field optical head comprising a VCSEL matrix integrated with a module of GaP microlens array and micro-probe array intended for nano-recordings on a UHDOS disk system

THE INFLUENCE OF THE SUBSTRATE ANISOTROPY ON THE LASER-FOCUSED ATOM DEPOSITION STUDIED BY 2D MONTE CARLO SIMULATION

Florin Nita [1,2] and Alberto Pimpinelli [1]
[1] LASMEA, UMR 6602 CNRS / Blaise Pascal University, Clermont 2, 63177 Aubiére Cedex, France
[2] Institute of Physical Chemistry, Romanian Academy, Spl. Independentei 202, Bucharest, Romania
E-mail: nita@lasmea.univ-bpclermont.fr
http://wwwlasmea.univ-bpclermont.fr/

If a laser beam is directed parallel to a crystal surface and retroflected, a standing wave region will be create in the proximity of the surface[1-4]. This standing wave region acts like an array of cylindrical lenses for an incoming neutral atoms beam. The distance between these lenses is $\lambda/2$ where λ is the optical wave length (Fig. 1).

We study the role of the surface diffusion anisotropy in the fabrication of nanostructures by laser-focused ("cold") atom lithography, and on the stability of nanostructures using 2D kinetic Monte Carlo simulations. The simulations were performed using one- and two-dimensional standing wave fields (using two different wave profiles) and two different difusion models (limited and total diffusion model) on anisotropic surfaces, such as (110) surfaces of CFC crystals, or reconstructed surfaces such as Si(100). The simulations were made with and without Schwoebel barriers. Our diffusion-deposition models reproduce both qualitative and quantitative experimental results[5] (Fig. 2).

Figure 3 shows the time evolution of the heights of profiles obtained using an one-dimensional standing wave field and a wave profile corresponding to Fig. 2b. The results for diffusion models and for different orientations of the standing wave field direction relatively to the easy diffusion direction for the ad-atoms on the substrate, parallel ($\|$) and perpendicular ($\perp$), are shown in this figure.

References:

[1] J.P. Gordon, A. Ashkin, Phys. Rev. A, **21** 5 (1980) 1606.
[2] G. Timp, R.E. Behringer, D.M. Tennant, J.E. Cunningham, M. Prentiss, K.K. Berggren, Phys. Rev. Lett., **69** 11 (1992) 1636.
[3] C.C. Bradley, W.R. Anderson, J.J. McClelland, R.J. Celotta, Appl. Surf. Sci., **141** (1999) 210.
[4] R.E. Behringer, Vasant Natarajan, G. Timp, Appl. Surf. Sci., **104/105** (1996) 291.
[5] Florin Nita and Alberto Pimpinelli, Shedding light on the Nanoworld: Diffusion-limited nanostructures from laser-focused atom deposition, submited to Comptes rendus Physique.

Figures:

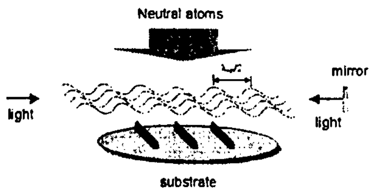

Figure 1.

a) 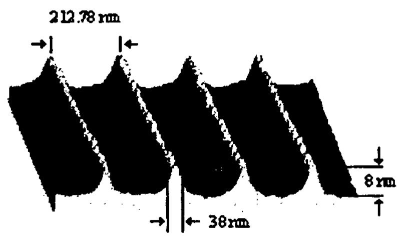

b) 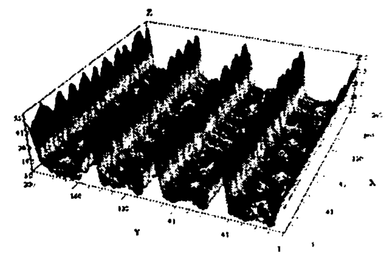

Figure 2. A comparison between experimental and simulation results:
a) one-dimensional array of Cr features obtained by laser focused atomic deposition (NIST Electron Physics Group)
b) simulated surface obtained using one-dimensional standing wave field and limited diffusion model

	limited diffusion model	total diffusion model
∥	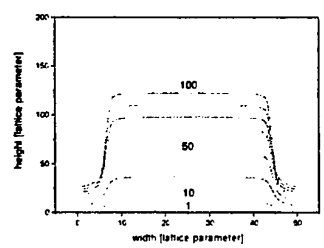	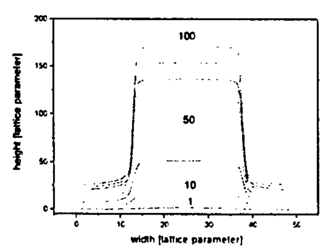
⊥	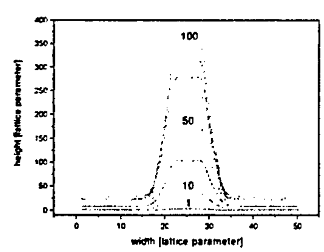	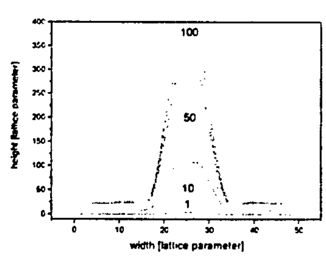

Figure 3. A comparison between the time evolution of profiles height obtained using a standing wave field corresponding to the surface shown in Fig. 2b for both orientations of the standing wave field to the easy diffusion direction of the adatoms on the surface: parallel (∥) and perpendicular (⊥), respectively.

ATOMIC FORCE MICROSCOPY AND ELECTRIC FORCE MICROSCOPY OF SYNTHETIC MELANIN THIN FILMS

M. I. N. da Silva[1], S. N. Dezidério[2], J. C. Gonzalez[3], C. F. O. Graeff[2], and M. A. Cotta[1].
[1]Universidade Estadual de Campinas, Instituto de Física Gleb Wataghin, Departamento de Física Aplicada, Laboratório de Pesquisa em Dispositivos, CP 6165, 13083-970, Campinas, SP, Brazil.
[2]Faculdade de Filosofia, Ciências e Letras, Universidade de São Paulo, Ribeirão Preto, SP, Brazil.
[3]Laboratório Nacional de Luz Síncrontron, Campinas, SP, Brazil.

Melanins are important photoprotective pigments found in many organisms and tissues. They have attracted great attention due to their role in photo protection and technological applications. In this work we will study the effect of hydration on the structural and electrical properties of synthetic melanin samples using Atomic Force Microscopy (AFM), Electrical Force Gradient Microscopy (EFM), and Conductive Atomic Force Microscopy (C-AFM).

Two thin film synthetic melanin samples were prepared by evaporating (casting) a solution of melanin powder in a mixture of DMSO (Dimethyl Sulfoxide) and acetone on 1cm x 1 cm crystalline silicon substrates. After dried out, one of the samples was hydrated in a humid chamber. The experiments were carried out in both hydrated and no-hydrated samples.

All the experiments were done in air using a Digital Instrument MultiMode Scanning Probe Microscope, with a Nanoscope III controller and an extender electronic box, and an AutoProbe CP from ThermoMicroscopes. TappingMode ultra sharp Si tips were used in all the experiments.

AFM was used to study the morphology of the synthetic melanin thin films. Flat terraces with small round depressions were observed on both samples, as is shown in figure 1. The root mean square roughness (Rq) of the flat terraces was of approximately 0.4 nm and 0.3 nm for the no-hydrated and hydrated samples, respectively. The hydrated melanin sample also exhibits agglomerates in the center of the depressions with height of aproximately1 to 3 nm and lateral dimension in the 100-200nm range (figure 1 (b)).

EFM (figure 2) and C-AFM were used to study the electrical properties of the samples in correlation with their morphology. An increment of the EFM signal was observed in both samples at the edges of the flat terraces. However, a lower EFM signal was found in the agglomerates present in the hydrated sample. The decrease of the EFM signal indicates a lowering of the free radical density produced by hydration of the sample.

These results show a strong modification of the structural and local electrical properties of melanin thin films caused by hydration. The formation of non-planar agglomerates on the hydrated sample is associated to a decrease of free radicals density on the samples and consequently to the different electrical transport properties observed by C-AFM. This behavior reveals the potentiality of this material for sensor applications.

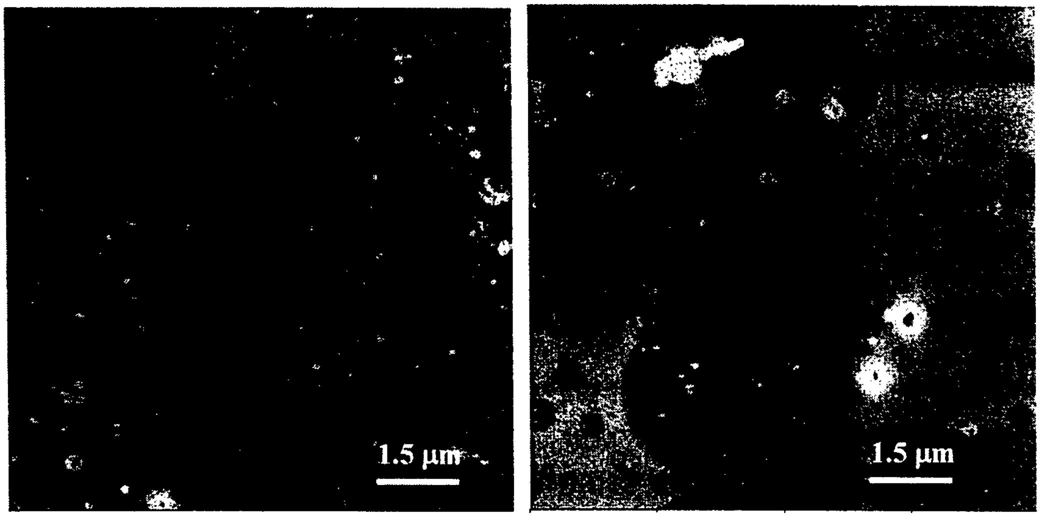

Figure 1- Tapping Mode topographic images of synthetic melanin thin films deposited on Si substrates. (a) no-hydrated sample and (b) hydrated sample. Z scale is 60 nm in both images.

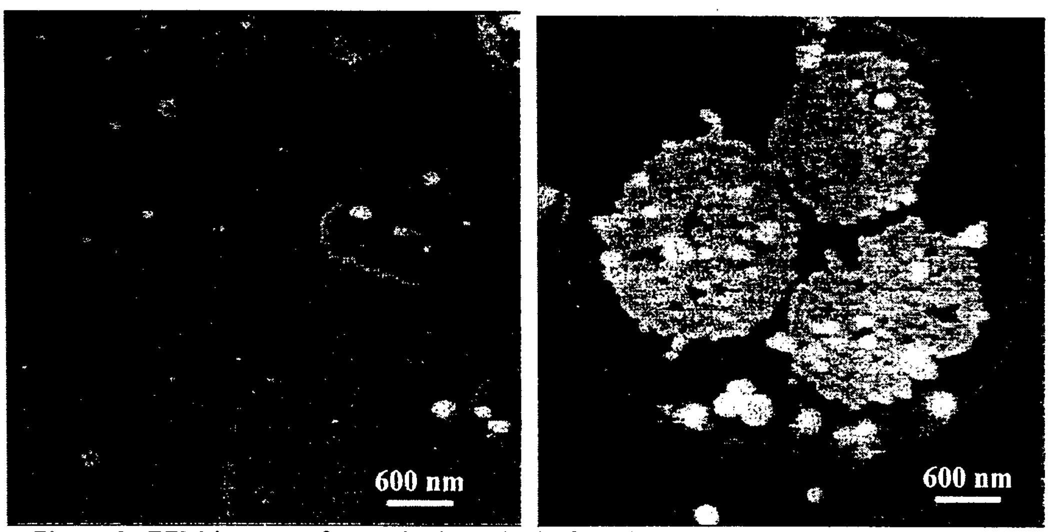

Figure 2- EFM images of a synthetic melanin film deposited on a Si substrate. (a) no-hydrated, and (b) hydrated melanin. Z scale is 100 Hz in both images.

Co GROWTH ON NANOSTRUCTURED Ag/Cu INTERFACES

Javier Cordón[1,2,*] and Enrique Ortega[2,3]

[1]Dpto. de Física de Materiales, Universidad del País Vasco, Manuel Lardizabal 3, 20018-San Sebastian, Spain

[2] Donostia International Physics Center & Centro Mixto CSIC-UPV, Manuel Lardizabal 4, San Sebastian,Spain

[3]Dpto. de Física Aplicada, Universidad del País Vasco, Plaza de Oñate 2, 20018-San Sebastian, Spain

*E-mail: waacovej@scsx03.sc.ehu.es

http://scsx01.sc.ehu.es/waporcoj/nanolab/nanolab.html

The Ag/Cu system can be used to tailor growth, and hence electronic and magnetic properties of Co nanostructures. Ag grows on Cu surfaces with little or negligible intermixing, leading to flat layers with sharp interfaces on Cu(111). On the other hand, periodic, striped Ag/Cu phases are induced by growing submonolayer amounts of Ag on Cu vicinal substrates [1]. Since Co and Ag also display little tendency to form mixed compounds, the idea is using Ag buffer layers and nanostructured templates to modify Co growth on Cu(111).

On flat Cu(111) Ag grows in a perfect layer-by-layer mode with very minor Ag/Cu mixing. Up to 4-5 layers, the Ag(111) surface is characterized by a quasi 10x10 Moiré superstructure, which is explained by a perfect Cu(111) substrate wetting. Ag adlayers display discrete, quantum well states in the perpendicular direction [2], as well as an almost linear decrease in the density of surface electrons [3]. Since both surface potential (Moiré corrugation) and electronic states are Ag-thickness-dependent and differ from Cu(111) or Ag(111) bulk crystals, we expect both Co nucleation and growth to proceed also in a different way. Thus our aim is studying the diffusion and aggregation behavior of two-dimensional Co clusters on Ag layers on Cu(111) by means of in-situ variable temperature STM measurements.

In Fig. 1 we show the STM image for 0.05 ML Co/0.5 Ag ML/Cu(111). Small Co dots nucleate on Ag covered areas, where the Moiré pattern is preserved. As shown in Fig. 2, from 1 ML to 2 ML cluster sizes double (from 28 to 47 Å, and from 3 to 5 Å height) and densities reduce to one half, suggesting faster adatom diffusion for 2 ML. Clusters nucleate at hollow places in the Moiré reconstruction, which are in turn nicely observed in the background. Images suggest very little Ag layer disruption, since there is a minor presence of point defects and superlattice distortions in the 1 ML buffer. Such defects are mostly suppressed at very low Co coverages. We do not observe any special cluster arrangement, discarding long range elastic or electronic interactions at this coverage and temperature [4].

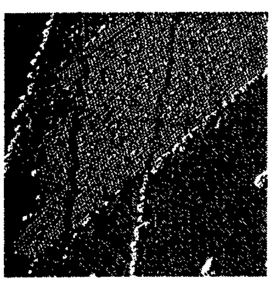

Fig. 1. *0.05 ML Co on 0.5 ML Ag covering Cu(111). Co forms tiny dots on top of the Ag Moiré, by contrast to step edge decoration and large triangular bilayer islands on Cu(111). (Image derivate, 200 nm, 1.5 V)*

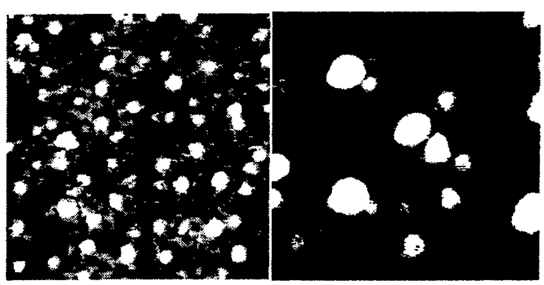

Fig. 2. *0.1 ML Co on 1 ML (left) and 2 ML (right) thick Ag buffer deposited on Cu(111) at 300K. Co cluster size doubles and the density reduces to one halffor2 ML, revealing lower adatom diffusion barrier in this case. (Image 50 nm, 1.5 V).*

In contrast to flat Cu(111), Ag evaporation on stepped Cu(111) surfaces induces periodic faceting of the surface, i.e. phase separation of Ag-covered facets and clean Cu stripes [1]. The driving force is the lattice matching of Ag packed layers with different Cu planes, leading to a hierarchy among the different orientation of the Ag-covered facets observed, and hence to a rich morphology that depends on step density, step type and Ag coverage. Fig. 3 shows an example of such Ag/Cu periodic structure obtained in the particular case of Cu(775), with 8.5° miscut towards [11-2], and 0.4 ML of Ag. Current images or topographic derivatives along the horizontal show strong contrast between [773]-oriented Ag-covered facets (105 Å wide) and Cu(111) terraces (130 Å wide). The inset shows the details of the Ag covered facet, with its characteristic Moiré.

Varying substrate miscut and Ag coverage we have examined the stability of such nanostructure upon Co adsorption. The aim is keeping the striped morphology, thereby inducing one-dimensional magnetic behavior. Co adsorption follows the general rule found in infinite systems, i.e., bilayer islands decorating Cu steps and stripe edges while small Co dots nucleate across Ag facets. The topography still shows periodic facets, but the Moiré quickly vanishes and the derivate images loose their contrast. The Moiré and the derivative contrast is generally preserved at low coverage, as shown in Fig. 4 (a) for 0.3 ML. In this case, Co nucleates preferently at Cu stripe edges, and only minor amounts incorporate to Ag stripes. The homogeneity of the array is even improved with respect to Fig. 3, such that stripes are as long as 1 micron. Fig. 4 (b) shows the surface after additional adsorption of 0.4 ML Ag and 1.9 ML Co. We observe the same overall morphology and contrast, strongly suggesting that the Co content periodically changes across the striped structure. The magnetic properties of this Co stripe array are unknown.

Fig. 3. *Ag/Cu striped nanostructure grown on Cu(775). Cu(111) terraces alternate with Ag covered [773] facets (inset) (200nm, 1.5 V, image derivate along the horizontal direction).*

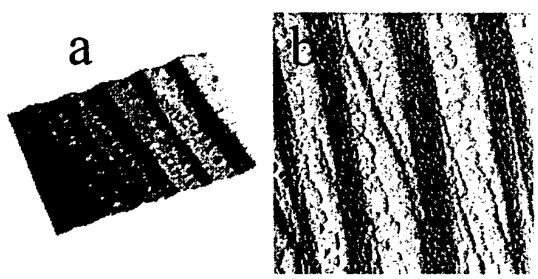

Fig. 4. (a) 0.3 ML *Co evaporation on the striped structure of Fig. 1. Co sticks preferently to steps and Ag stripe edges in Cu terraces (100nm). (b) The same surface after 0.8 ML of Ag and 2.2 ML of Co. The faceted structure and the contrast of Fig.1 is maintained, suggesting the presence of alternating stripes with different Co content (200nm, image derivate along the horizontal direction).*

References:

[1] A. Bachmann et al., Phys. Rev. B **64**, 153409 (2001); A Bachmann et al., Surf. Sci. **526**, L143 (2003).
[2] M. A. Mueller, T. Miller, and T.-C. Chiang, Phys. Rev. B **41**, 5214 (1990).
[3] A. P. Shapiro et al., Solid State Commun., **58**, 121 (1986).
[4] N. Knorr et al., Phys. Rev. B **65**, 115420 (2002).

MAGNETIC BEAD DETECTION USING GMR SENSING

Lena Lui, Sow Chorng Haur and Sean O'Shea

Institute of Materials Research and Engineering (IMRE), 3 Research Link, 117602 Singapore.
Department of Physics, National University of Singapore, 10 Kent Ridge Crescent, 119260 Singapore.

There is increasing research in magnetically tagged bio-molecules for sensor applications in addition to their more common usage in separation. We have constructed simple giant magneto-resistance (GMR) strips for the detection of magnetic beads with an aim to use such devices in micro-fluidic applications. In order to understand the interactions between the bead and the GMR strip we attach the beads to an AFM tip and vary the relative position between bead and tip whilst measuring the GMR response. The basic theory behind the expected response is outlined and compared to the data. If time permits we will also outline our approach to the problem of bead-GMR interaction using the optical tweezers technique.

Forcing the assembly of the building blocks of a molecular wire with a nanopatterned Cu(110) template

[1]Y. Naitoh, [1]R. Otero, [1]F. Rosei, [2]P. Jiang, [1]M. Schunack,[2]A. Gourdon, [1]E. Lægsgaard, [1]I. Stensgaard, [2]C. Joachim & [1]F. Besenbacher

[1] *Department of Physics and Astronomy and Interdisciplinary Nanoscience Center (iNANO), University of Aarhus, 8000 Aarhus C, Denmark*

[2] *CEMES – CNRS, 29 rue J. Marvig, P.O. Box 4347, F – 31055 Toulouse Cedex, France*

Large organic molecules are promising building blocks for nanoscale molecular electronic devices [1], but new approaches are required to order them with atomic precision on surfaces. This goal comprises two different aspects: the adsorption sites must be arranged in a suitable pattern, and the adsorption geometry must facilitate the interconnection with the other elements of the circuit. Here we show that the nanopatterning of a Cu(110) surface with a sub-monolayer of oxygen [2] not only creates a suitable template for the selective adsorption of two related molecular wires into ultra clean 1 D nanostructures, but also can force their orientation to align along the structure. This can be considered as one step towards the parallel fabrication of long molecular wires on surfaces starting from its molecular building blocks.

The template is created by exposing the clean Cu(110) surface to 4 – 6 Langmuir (1 L = 10^{-6} torrs) of oxygen at 625 K. Under these conditions, the surface is patterned into 1D alternating bare Cu stripes running parallel to the [001] direction, and (2×1)-O reconstructed regions (Fig. 1), consisting of Cu-O added rows aligned parallel to the [001] surface direction [2]

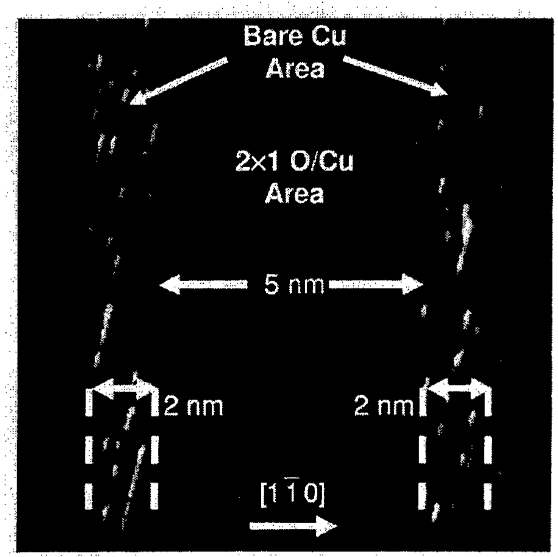

Fig 1. Nanotemplate created by a controlled oxidation of the Cu(110) surface. Bare Cu stripes running along [001] separate 2×1 oxidized areas

Onto this template, we have deposited first the molecule known as Single Lander [3] (SL, $C_{90}H_{98}$). It is composed of a polyaromatic hydrocarbon main board with four lateral 3,5-di-*tert*-butylphenyl substituents acting as "spacer legs" (Fig. 2-a). The aromatic central board has been designed so as to act as a conductive molecular wire because of its extended π system. When deposited on a metal surface, high-resolution scanning tunneling microscopy (STM) images in ultrahigh vacuum reveal the SL as four lobes (Fig. 2-b). On Cu(110), SL adsorbs always with its board aligned along the $[1\bar{1}0]$

crystallographic direction of the substrate, and no order is observed even at high coverage. When deposited on the periodic template obtained by the partial oxidation of Cu(110), the SL molecules adsorb exclusively on bare Cu regions, forming well ordered long molecular chains (Fig 2 c). However, the direction of the board turns out to be aligned along $[1\bar{1}0]$ and, thus, perpendicular to the direction of the chain.

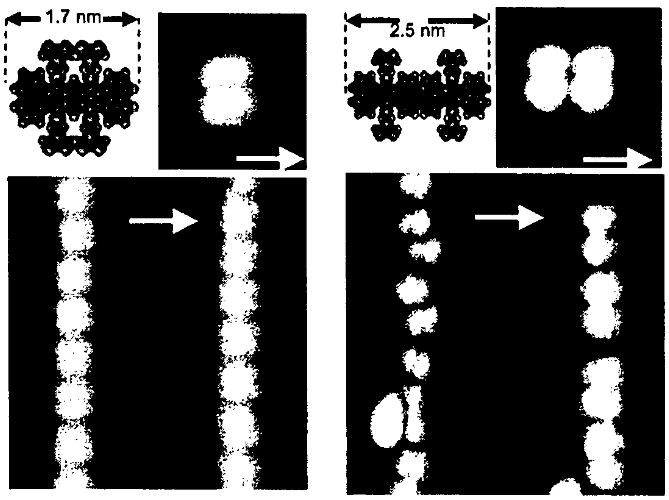

Fig 2. a) Filled-Space Model f the SL. b) Typical STM image of a SL on Cu(110). c) Ordering of the SL on the templated surface. d) Filled space representation of the VL. e) Typical STM image of the VL. f) Rotation of the VL on the templated surface. The white arrow marks the close packed direction.

Figure 2-d shows a filled-space model of the Violet Lander molecule (VL, $C_{108}H_{104}$). The difference between the VL and SL molecules is the length of the board, being 2.5 nm long in the VL and only 1.7 nm in the SL. When deposited on Cu(110) the VL is also imaged as four lobes (Fig. 2-e). On the nanotemplated surface, it only adsorbs on the bare Cu stripes (Fig 3-c). The difference now is that *the direction of the board is no longer perpendicular to the direction of the stripes*. Figure 2-f shows the two types of orientations most commonly found: with the board rotated 70° and 90° with respect to the $[1\bar{1}0]$ direction. Therefore, we can conclude that *the template not only acts by providing specific adsorption sites, but it also affects the adsorption geometry.*

Using a pre-patterned template we succeeded in controlling the formation of long one-dimensional molecular nanostructures. Furthermore, we have shown that the template is able to force the molecule to align in the right direction. This type of directed forced-assembly using appropriate periodic superstructures on the nanoscale opens a variety of new possibilities for the ordered deposition of organic molecules on surfaces, and for guiding the growth of nanostructures in general.

References.

1. Joachim, C., Gimzewski, J.K., Aviram, A., *Nature* **408**, 541 (2000).
2. Kern, K. Niehus, H., Schatz, A., Zeppenfeld, P., Goerge, J., Comsa, G., *Phys. Rev. Lett.* **67**, 855 (1991).
3. Langlais, V. L., Schlittler, R. R., Tang, H., Gourdon, A., Joachim, C., Gimsewski, J. K., *Phys. Rev. Lett.* **83**, 2809 (1999).
4. Zambelli, T., Tang, H., Lagoute, J., Gauthier, S., Gourdon, A., Joachim, C., *Chem. Phys. Lett.* **348**, 1 (2001).

GRAIN BOUNDARIES OF NANOCRYSTALS INVESTIGATED BY ELECTRON TRANSPORT

K. Pękała[1], L. Łukaszuk[2]

[1]Faculty of Physics, Warsaw University of Technology, Koszykowa 75, 00-662 Warsaw,
[2] Andrzej Sołtan Institute for Nuclear Studies, Theory Division, Hoża 69, 00-682 Warsaw, Poland

We present a new approach to investigate an influence of grain boundaries of nanocrystals embedded in amorphous matrix on electron transport processes. This method is applied to analyse an evolution of electrical resistivity during nanocrystallization of $Al_{90}Y_{10}$ alloy. The temprature variation of resistivity is measured for amorphous and partially nanocrystalline alloys obtained by heating amorphous alloy up to several temperatures exceeding nanocrystallization threshold. The Maxwell - Garnett equation is used to calculate resistivity of precipitating fcc Al nanocrystals covered with the grain boundaries enriched in Y atoms. The resistivity of nanocrystals rises with a progress of nanocrystallization and is several time larger than a resistivity of polycrystalline Al. This can be due to the grain boundary containing layers enriched in Y atoms, which exhibit a relatively high resistivity. Finally a mean thickness of grain boundaries is evaluated. This thickness rises with increasing annealing temperature and saturates at a level of 4 nm.

ELECTRICAL RESISTIVITY OF NANOCRYSTALLINE FeNbCrBCu ALLOYS

K. Pekala[1], M. Pekala[2], I. Škorvánek[3]

[1] Department of Physics, Warsaw University of Technology, PL-02-524 Warsaw, Poland
[2]Department of Chemistry, Warsaw University, PL-02-089 Warsaw, Poland
[3]Institute of Experimental Physics, Slovak Academy of Sciences, SK-04353 Košice, Slovakia

Amorphous alloys of $Fe_{73.5}Nb_{4.5}Cr_5Cu_1B_{16}$ produced by planar flow casting are thermally stable up to 750 K, when the primary crystallization of bcc-Fe starts. After a partial crystallization controlled by temperature and annealing time, the resulting microstructure consists of bcc-Fe grains embedded in a residual amorphous matrix. The amorphous/crystalline transformation is accompanied by changes in chemical composition of the amorphous matrix. Due to the limited solubility of Cr, Nb, Cu and B in bcc-Fe, these atoms are rejected from the growing grains. The typical sizes of the grains are about 4-8 nm and 5-10 nm for the samples annealed for 1 hour at 783 K and 863 K, respectively. The volume fraction of crystalline phase in the samples annealed for 1 hour at 783 K and is estimated to be 31% and it increased to 46% after annealing for 1 hour at 863 K. The electrical resistivity is measured by a four probe method. For the as quenched alloy the negative temperature coefficient of resistivity (TCR) is observed up to 210 K. Values of TCR increase gradually with an increasing crystalline fraction. Electrical resistivity of nanocrystalline phase is calculated and and the thickness of grain boundaries is analysed.

MONTE CARLO ANALYSIS OF NANO-SCALE SCHOTTKY DIODES FOR TERAHERTZ GENERATION

S. Pérez[1], T. González[1], E. Starikov[2], P. Shiktorov[2], V. Gruzinskis[2], L. Reggiani[3], L. Varani[4] and J.C. Vaissiere[4]

[1]Departamento de Física Aplicada, Universidad de Salamanca, Plaza de la Merced s/n, 37008 Salamanca, Spain

[2]Semiconductor Physics Institute Goshtauto 11, LT2600 Vilnius, Lithuania

[3]INFM – National Nanotechnology Laboratory. Universitá di Lecce, Dipartimento di Ingegneria dell'Innovazione Via Arnesano, 73100 Lecce, Italy

[4]Centre d'Electronique et de Micro-optoelectronique de Montpellier (CNRS UMR 5507) Université Montpellier II, 34095 Montpellier, France

The increasing importance of telecommunications in the high-microwave region (above the millimeter range) demands new high power generators within the submillimeter wavelength or THz frequency ranges. Schottky-barrier diodes are commonly used to this purpose as multipliers and mixers of time-varying signals because of their strongly nonlinear current-voltage (I-V) and capacitance-voltage (C-V) characteristics. Since high capability to generate high-order harmonics and good feasibility for their power extraction (that is, low level of noise) are prerequisites to use these devices as THz generators, high technology and accurate design are mandatory. In particular, Schottky diodes for THz generation require extremely short sizes, usually in the nano-scale range or beyond [1], and very high dopings at the limit of degeneracy.

The improvement in the fabrication processes during the last years has made possible the production of nano-scale Schottky diodes with active layer thickness below 50 nm, making these structures promising devices for THz generators [2]. However, little work has been done on the modeling of the effects that the downscaling of conventional Schottky diodes have on the noise and dynamic behavior of these devices operating under cyclostationary conditions (periodic, large-signal excitation). Simulations have mainly focused on the study of the static behavior of nano-scale Schottky contacts when they are formed at the interfaces between semiconductors and metal inclusions in more complex devices as MOSFETs and HEMTs [3].

The aim of this paper is to present a theoretical investigation of the electronic properties of GaAs Schottky-barrier nano-diodes as THz generators. In particular, the intensity of the fundamental and higher order harmonics of the current response, the intrinsic noise and the signal-to-noise ratio as a function of the amplitude and frequency of the excitation are analyzed. For the calculations we use an ensemble Monte Carlo simulator coupled with a self-consistent Poisson solver, which includes intrinsically all the effects at the origin of nonlinearities and noise in these devices (hot carriers, velocity overshoot, etc.) [4,5,6].

We have found that, in the frequency range where the C-V nonlinearities dominate the diode response, the intensity of the high order harmonics grows with the increase of the excitation frequency. Due to the short length of the devices, this behavior takes place at frequencies high enough (above 500 GHz) to achieve efficient harmonic generation in the THz frequency range.

As concerns the noise behavior of the diode, the current noise spectra $S_{\delta I}(f)$ obtained under cyclostationary operation are found to be similar to those obtained under static excitations, showing the following main features.

i) a low-frequency plateau that essentially coincides with the full shot-noise level associated with the average value of the cyclostationary current response $<I>$. This level of noise increases with the excitation frequency due to the mixing of the different harmonics, that leads to higher values of $<I>$. This result indicates that special attention must be paid to the ratio between the amplitude of the harmonic and noise level when trying to extract an harmonic of given order.

ii) a first high-frequency peak related to the returning carriers (which disappears at voltages when flat-band conditions are approached).

iii) a second high-frequency peak due to spontaneous plasma oscillations.

This increase of noise at high frequencies could prevent the detection of the harmonics. However, our results show that both high-frequency peaks are displaced to the high THz region for short and heavily doped GaAs Schottky diodes, thus allowing harmonics extraction in the frequency range of interest.

As concerns voltage noise, all the spectra contain the peaks corresponding to the frequencies of the plasma oscillations associated with the doping level of the n and n^+ regions, with a magnitude that is practically independent of the excitation. By contrast, the level of the low-frequency plateau is very sensitive to the amplitude of the driving current, with the peculiarity of exhibiting a cutoff related to the value of the excitation frequency.

References

[1] A. Jelenski, A. Grub, V. Krozer and H.L. Hartnagel, IEEE Trans. Microwave Theory Techn. **41** (1993) 549.
[2] B. Gelmont, D. Woolard, J. Hesler and T. Crowe, IEEE Trans. Electron Devices **45** (1998) 2521.
[3] M. Achermann, U. Siegner, L.E. Wernersson and U. Keller, Applied Surface Science **190** (2002) 513.
[4] J. Mateos, T. González and D. Pardo, Appl. Phys. Lett. **67** (1995) 685.
[5] T. González, D. Pardo, L. Varani and L. Reggiani, J. Appl. Phys. **82** (1997) 2349.
[6] P. Shiktorov, E. Starikov, V. Gruzinskis, S. Pérez, T. González, L. Reggiani, L. Varani and J.C. Vaissière, IEEE Trans. Electron Devices (to be published).

MOTT CONSTANT IN TWO DIMENSIONAL METAL-INSULATOR TRANSITION

A. John Peter
Faculty Member in Physics, Dept. of Basic Sciences,
Arulmigu Kalasalingam college of Engineering, Anand Nagar,
Krishnankovil, Srivilliputhur.626 190
Viruthunagar Dt.India

It is a review of scaling theory of metal-insulator transition in two dimensions.The recent developments of scaling theory is elicited in a good manner. Metal –Insulator transition using exact two dimensional dielectric function is investigated for a shallow donor in an isolated well of GaAs/Ga1-xAlsAs superlattice system within the effective mass approximation. Vanishing of the donor ionization energy as a function of well width and the donor concentration suggests that the phase transition is not possible even below awell width of 10Ǻ supporting the scaling theory of localization. The effects of Anderson localization, exchange and correlation in the Hubbard model are included in a simple way. The relationship between the present model and the Mott criterion in terms of Hubbard model is also brought out.A simple expression for a Mott constant in 2D, a* Nc1/2 exp (-9.86exp(-L/a*)) = 0.123, where Nc is the critical concentration per area,is derived . The critical concentration is enhanced when a random distribution of impurities is considered. The limiting behaviour of well width for a quantum 2D is brought out. The results are compared with the existing data available.

FABRICATION OF NANO-BALLISTIC DEVICES USING HIGH RESOLUTION PROCESS

E. Pichonat[(1)], J.S. Galloo[(1)], S. Bollaert[(1)], Y. Roelens[(1)], X. Wallart[(1)], A. Cappy[(1)], J.Mateos[(2)], T. Gonzales[(2)], H. Boutry[(3)], B. Hackens[(3)], V. Bayot[(3)], L. Berdnarz[(3)], I. Huynen[(3)]

[(1)] IEMN-DHS, CNRS UMR 8520
Avenue Poincaré, BP 69, 59652 Villeneuve d'Ascq, France
E-mail: emmanuelle.pichonat@iemn.univ-lille1.fr
[(2)] Dpto Fisica Aplicad, Universitad de Salamanca, Salamanca, Spain,
[(3)] Université Catholique de Louvain, Louvain-La-Neuve, Belgium

In semiconductor device with dimensions smaller than the mean free path, ballistic behavior of electron can lead to novel effects. Ballistic rectifiers, switch and logic gate working at room temperature have been proposed [1-4]. Dimension of few ten nanometers and use of high mobility material are necessary to obtain ballistic operation. In this paper, we propose technological process based on negative e-beam resist to define these nano-dimensions. InAlAs/InGaAs heterostructure on InP substrate has been used for its technological compatibility with high frequency HEMTs [5]. To defined active zone of the device, dry and wet etchings are proposed and compared.

Figure 1 presents cross section of the heterostructure grown by Molecular Beam Epitaxy. In this heterostructure, Indium content in the channel has been fixed at 70% to achieve high electron mobility. Epilayers with spacer layer thickness at 5, 10 and 20 nanometers have been fabricated, to reduce coulomb scattering with the delta-doped. The delta-doped level has been fixed to obtain high 2DEG densities and to avoid free electron in the delta. Hall measurements are reported in table 1. High hall mobility is obtained with large spacer thickness. However electron density is lower due to a poor transfer of electron from the delta.

Wires, T- and Y-branches, rectifiers with dimension of few ten nanometers, have been fabricated. The process begins by alignment marks, mesa isolation to define the active zone, and Ni/Ge/Au/Ni/Au ohmic contact formation. Finaly, Ti/Au bonding pads are defined. All the levels, except bonding pads, have been made by e-beam lithography using a high resolution machine (LEICA EBPG5000+). Mesa isolation is a delicate step of the technological process. Indeed nano-dimension of the device is defined by this step. To reduce e-beam exposure time, high resolution negative resist has been used. It consists on HSQ (Hydrogen SilsesQuioxane) resist. Figure 2 gives an electron microscopy of an Y-branch junction defined in HSQ resist. Width is 20 nanometers. Wires of 15nm have been also obtained. After the lithography process, etching of active layers have been made by dry and wet etching. For wet etching, $H_3PO_4/H_2O_2/H_2O$ solution has been used. On figure 3, a SEM of 150nm width T-branch is given. As a result of undercut etching, final width is only 80nm. Moreover, shape is strongly rough. This will affect transport properties in the channel. To reduce undercut etching and improve roughness, dry etching with $CH_4/H_2/Ar$ gases has been used. Figure 4 presents a SEM of 150nm T-branch width. The measured width is 100nm and the roughness is improved. Wires, T- and Y-branches, rectifiers with several dimensions have been realized using both etching. Comparisons by electrical measurements are in progress and will be presented at the conference.

References:

[1] A. M. Song et al, Applied Physic Letters, vol 79, n°9, August 2001.
[2] K. Hieke et al, Physical Review B, vol. 62, n°24, Dec 2000.
[3] I. Shorubalko et al, Applied Physic Letters, vol 79, n°9, August 2001.
[4] S. Reitzenstein et al, Electronic Letters, vol. 38, n°17, Aug 2002.
[5] Y. Yamashita et al, IEEE Electron device Letters, vol. 23, n°10, Aug 2002.

Figures:

Contact InGaAs 6 $10^{18}/cm^2$	100 Å
Barrier LM InAlAs nid	150 Å
Delta doping plane Si	
Spacer LM InAlAs nid	
Channel $In_{70}Ga_{30}As$ nid	150 Å
Buffer InAlAs nid	4000 Å
InP SI substrate	

Figure 1 Cross section of layers structures on InP substrate

Spacer (nm)	Nh ($/cm^2$)	μh (cm^2/Vs)
5	5.2	10000
10	2.7	14000
20	1.8	15000

Table 1 Hall measurements at room temperature

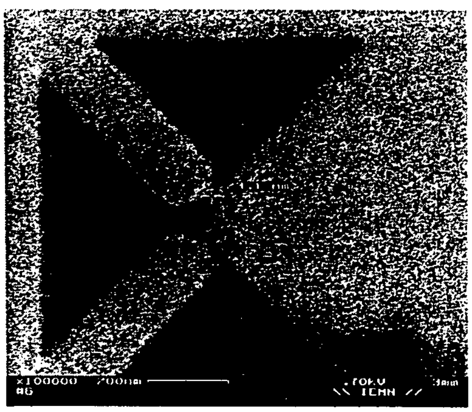

Figure 2 SEM of Y-branch defined in HSQ resist

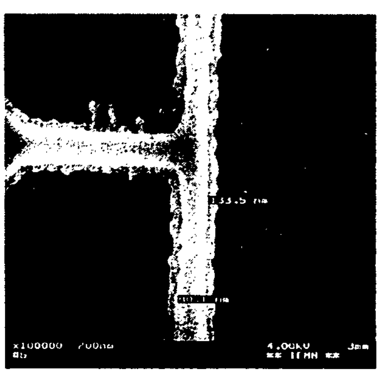

Figure 3 SEM of T-branch using wet etching process

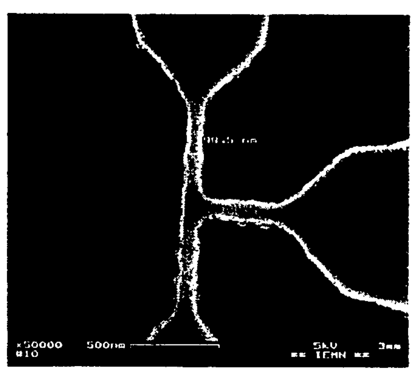

Figure 4 SEM of T-branch using dry etching process

TIP-WRITING-INDUCED CHEMICAL MODIFICATION OF SELF-ASSEMBLED MONOLAYERS INSPECTED BY MASS RESOLVED ToF-SIMS IMAGING

B. Pignataro, A. Licciardello, G. Marletta

Dipartimento di Scienze Chimiche, Università degli Studi di Catania, V.le A. Doria 6, 95125-Catania, Italy
e-mail: bpignataro@unict.it

Modification of molecular surfaces by employing a biased conductive Atomic Force Microscopy (AFM) tip has been shown to be a feasible route to nanofabrication. In this work alkyl self-assembled monolayers (SAMs) obtained on hydrogenated silicon surfaces via radical-initiated reactions of 1-octadecene have been modified with such method employed in presence of water vapors carried by a nitrogen stream. AFM showed that the modification of the organic layer depends on the magnitude of biases applied to the tip, with a threshold value for detectable modification. The extent of modification is observed in terms of increase in tip/sample friction force, in agreement with the formation of hydrophilic moieties at the surface of the organic monolayer. Depending on the experimental conditions, the increase in friction can be accompanied by a significant raise of the surface height, suggesting the occurrence, in the most drastic conditions, of a concomitant growth of silicon oxide underneath the organic layer.

In order to get a more detailed idea on the chemistry involved in the observed modifications, TOF-SIMS imaging measurements have been carried out on patterns of the size of some microns, tip written on purpose on the alkyl SAM by using different applied biases. Retrospective spectra, obtained from the modified regions, display the presence of CxHyO and CxHyN type peaks having intensity increasing with the tip bias. Simultaneously, an intensity reduction of the SiCxHy signals, compared to those arising from the unmodified regions, was observed. This allowed to outline the chemical mechanism involved in the process.

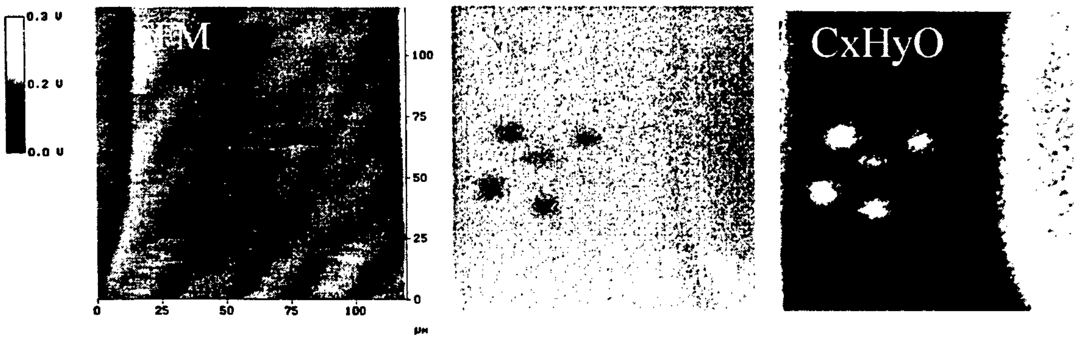

a) b) c)

a) Retrace Friction Force Microscopy (FFM) image of a tip-written pattern on a 1-octadecene monolayer self-assembled on silicon; b) and c) ToF-SIMS chemical maps obtained in the same region for the silicon and CxHyO-type peaks, respectively.

ELECTRODEPOSITION OF Ni-Co-P AND Ni-W-P LAYERS BASED ON AMORPHOUS Ni-P MATRIX

Magdalena Popczyk, Antoni Budniok, Henryk Scholl*, Tadeusz Blaszczyk*
University of Silesia, Institute of Physics & Chemistry of Metals
Bankowa 12, 40-007 Katowice, Poland
*University of Lodz, Institute of Chemistry
Narutowicza 68, 90-136 Lodz, Poland

Properties of nickel coatings are well known. Their wide application is a result of specific properties of nickel, which exhibit good corrosion resistance in aggressive solutions and also high catalytic activity for many electrochemical processes, in particular for the hydrogen evolution reaction. In order to improve the utilization of these materials and to enhance their electrocatalytic activity, various methods of their modifications could be applied, allowing to obtain materials with very developed, rough or porous electrode surface [1-11]. This study was undertaken in order to obtain the Ni-P layers, containing an additional alloying component (cobalt or tungsten) in an amount of ensuring obtained amorphous structure.

The purpose of this work was to determine structure of Ni-P, Ni-Co-P and Ni-W-P layers, their chemical composition and also surface morphology. X-ray diffractometer, stereoscopic and tunneling microscope, Form Talysurf-type profilograph and atomic absorption spectroscope were used for characterization of the layers.

The electrodeposition process was conducted in galvanostatic conditions at the current density 0.200 A cm^{-2}. The layers were deposited on a copper plate with a surface area of 1 cm^2 [6-7].

All Ni-P, Ni-Co-P and Ni-W-P layers electrolytically deposited, show good adhesion to the substrate. For comparison, in work presented surface topography in the scale of nano- and millimetric. In the both cases the Ni-Co-P layer was characterized by higher elevations on the surface in comparison to the Ni-W-P and Ni-P layers. It was found that the presence of cobalt or tungsten into the Ni-P matrix distinctly enlarges the real surface of the layers, in particular in the case of the Ni-Co-P layer (Fig.1).

The Ni-P layer contains about 80% of nickel and about 20% of phosphorus. XRD investigations show that the Ni-P layer is an amorphous. This may be concluded from the presence of wide reflex on the diffraction pattern of this layer in the range of diffraction angles characteristic for (111) and (200) reflexes of nickel. The Ni-Co-P layer contains about 45% of nickel, about 11% of phosphorus and about 44% of cobalt. The Ni-W-P layer contains about 68% of nickel, about 12% of phosphorus and about 20% of tungsten. XRD investigations show that the Ni-Co-P and Ni-W-P layers are an amorphous structure like the Ni-P layer. The absence of sharp reflexes of cobalt or tungsten does not prove unequivocally that this phase is absent in the layer. This component may be built in the layer but in the amorphous form (Fig.2).

It was ascertained that, introduction of cobalt or tungsten into Ni-P matrix, lead to obtain the layers about very developed surface. Thus obtained layers may be useful in application as electrode materials in electrochemistry [6,11].

References:

[1] C. Fan, D. L. Piron, P. Paradis, Electrochim. Acta, **39** (1994) 2716.
[2] I. Paseka, Electrochim. Acta, **40** (1995) 1633.
[3] I. Paseka, J. Velicka, Electrochim. Acta, **42** (1997) 237.
[4] A. Lasia, Curr. Top. Electrochem., **2** (1993) 239.
[5] A. Budniok, B. Losiewicz, M. Popczyk, A. Serek, Meeting Abstracts No. 1209, The Electrochemical Society, Toronto (2000).
[6] M. Popczyk, W. Bajdur, Galvanotechnik, **3(90)** (1999) 662.

[7] M. Popczyk, A. Budniok, Archiwum nauki o materialach, **4(22)** (2001) 261.
[8] M. Popczyk, A. Budniok, Abstracts No. A236, International Conference Materiais'2001, University of Coimbra, Portugal (2001).
[9] R. Karimi - Shervedani, A. Lasia, J. Electrochem. Soc., **145** (1998) 2219.
[10] R. Karimi - Shervedani, A. Lasia, J. Electrochem. Soc., **144** (1997) 2652.
[11] G. Lu, P. Evans, G. Zangari, J. Electrochem. Soc., **150(5)** (2003) A551.

Figures:

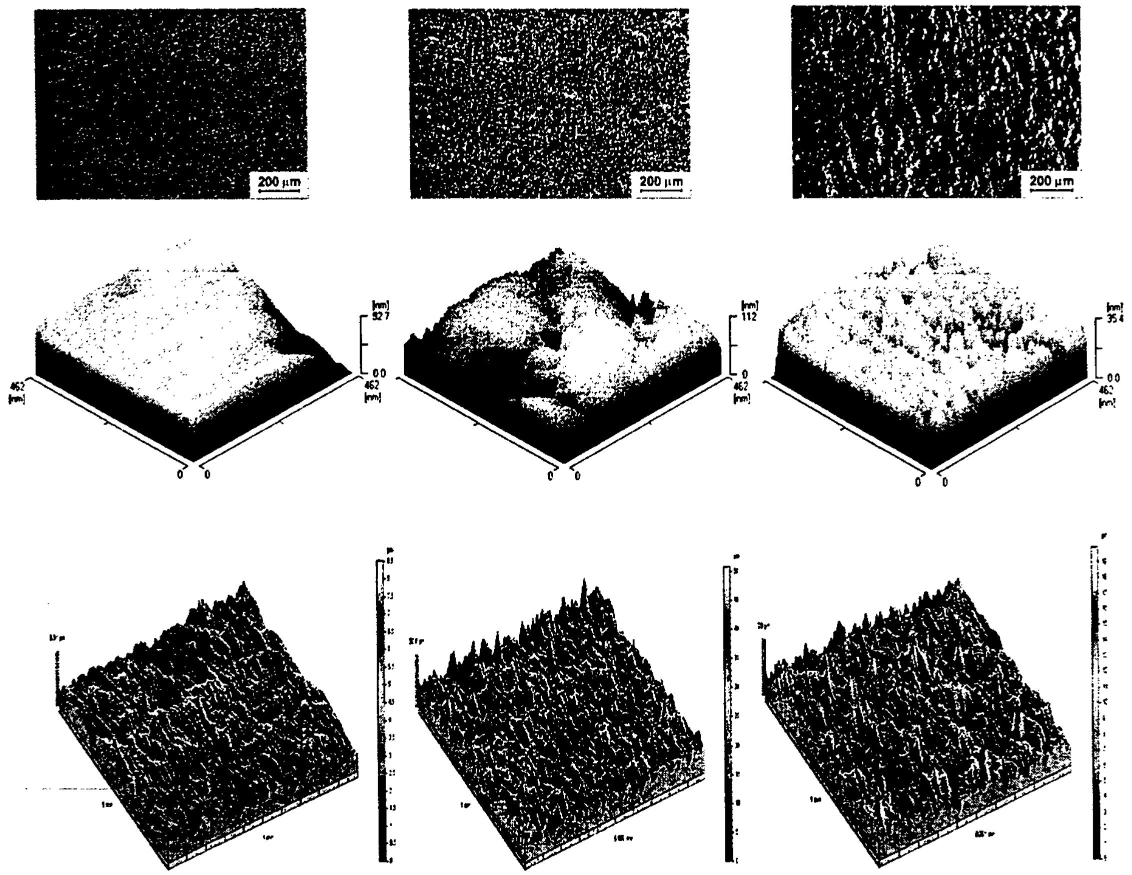

a) b) c)

Figure 1. Surface morphology and surface topography in the scale of nano- and millimetric of Ni-P (a), Ni-Co-P (b) and Ni-W-P (c) layers.

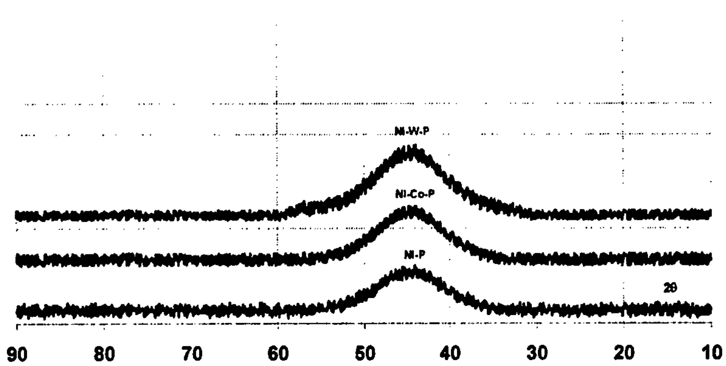

Figure 2. X-ray diffraction pattern for the Ni-P, Ni-Co-P and Ni-W-P layers.

LOCALIZATION AND FIR ABSORPTION IN QUASI-1D TWO ELECTRON QUANTUM DOT MOLECULES

Antonio Puente and Llorenç Serra

Dept. de Física, Universitat de les Illes Balears, E-07122 Palma de Mallorca, Spain

E-mail: dfsapf8@clust.uib.es

In this work we study the dynamical behaviour of two electrons confined in a double quantum dot nanostructure under the influence of an external electric field. The electrons are strongly confined both in the vertical and one lateral direction, thus giving rise to an effective quasi-1D system with a corresponding effective Coulomb interaction. As already discussed in [1], localization in one of the two potential wells can be achieved for certain values of the applied electric field. At these field values the characteristic time oscillations lead to a periodic maximum probability of double occupancy in one of the two wells $P_{LL}(t)$. It is our aim here to interpret this effect in terms of the spatial structure of the concomitant wave functions and to relate the localization phenomena to peculiarities in the absorption properties of the system.

References:

[1] P. I. Tamborenea and H. Metiu, Europhys. Lett. **53**, 776 (2001).

TOWARDS THE NANO-SCALE: INFLUENCE OF SCALING ON THE ELECTRONIC TRANSPORT AND SMALL-SIGNAL BEHAVIOUR OF MOSFETS

Raúl Rengel, Daniel Pardo and María Jesús Martín

Departamento de Física Aplicada, Universidad de Salamanca

Pza de la Merced s/n, 37008 Salamanca, Spain
E-mail: raulr@usal.es

As the dimensions of bulk CMOS transistors approach the nano-scale, many benefits are obtained both in digital and analog applications: as an example, faster switching speeds, higher current drive, a reduced power consumption and the smaller size of the integrated circuits have allowed to boost the market of mobile communications based on Silicon devices [1]. Nevertheless, in return for these advantages, serious problems raise associated to the small size of the transistors, such as severe short channel effects, tunnel current leakage at the gate, lithographic constraints, etc. [1]. These inconveniencies represent an important restriction to the scaling roadmap for Silicon technologies because of the degradation in the figures of merit of the devices as compared to the ideal predictions. Moreover, in a moment when the physical limits of many important technological parameters are about to be reached [2], it becomes critical to analyze the phenomena that set off a worse-than-expected performance in nano-scaled CMOS transistors.

In this work, the consequences of downscaling bulk MOSFET devices below the 100 nm range are investigated by means of a 2D bipolar Ensemble Monte Carlo (EMC) simulator [3]. Taking a 250 nm gate length MOSFET structure as the starting point, the ideal rules of scaling [4] are considered, and progressively smaller structures corresponding to actual technology nodes (130 nm, 90 nm and 60 nm) are studied in depth. The huge amount of information provided by the EMC simulator allows to give a microscopic insight of the quantities of interest associated to electron transport inside the devices, such as electric fields, potential, scattering mechanisms, velocity, energy and concentration of carriers, etc. In this way, it is possible to check the progressive importance of two-dimensional effects when the dimensions of the transistors are shrunk, and to give a physical explanation to the discrepancies obtained with the ideal predictions in the static characteristics.

We have also evaluated the dynamic behaviour of the devices by means of the analysis of a non-quasistatic small-signal equivalent circuit (SSEC). It has been found that some of the SSEC parameters (such as gate-to-source capacitance or transconductance) differ significantly from the scaling predictions when reaching dimensions below 100 nm. By examining the relationship between the SSEC parameters and the internal magnitudes previously studied, we have checked that the onset of strong two-dimensional effects in the electric field and the carrier concentration profiles corresponding to the active region (that takes place for the device with 130 nm gate-length and below) has a strong influence on the deviation from the ideal behaviour of the dynamic figures of merit. To overcome this problem, and to minimize short channel and hot carrier effects, special care must be considered in the design of the devices (including topology modifications from the scaling rules if necessary) in order to maintain the shape of the potential as similar as possible to the one observed in long-channel devices.

References:

[1] H. Iwai, "Downsizing of silicon MOSFETs beyond 0.1 μm," *Microelectr. Journal*, **29** (1998) 671.

[2] Semiconductor Industry Association, *International Technology Road Map for Semiconductors in 2002 Edition*: SIA (2002).

[3] R. Rengel *et al.*, "Numerical and experimental study of a 0.25 μm fully-depleted silicon-on-insulator MOSFET: static and dynamic radio-frequency behaviour," *Semicond. Sci. Technol.*, **17** (2002) 1149.

[4] R. H. Dennard *et al.*, "Design of ion-implanted MOSFETs with very small physical dimensions," *IEEE J. Solid-State Circuits*, **9** (1974) 256.

CURRENT CHANGES IN ELECTROOSMOTICALLY PUMPED MICRO AND NANO FLUIDIC DEVICES

Kambiz Ansari [1], Chandrasekhar Natarajan[2], Jeroen A. van Kan[1] and Isabel Rodríguez[2]*,

[1]Centre for Ion Beam Applications, Department of Physics, National University of Singapore. Lower Kent Ridge Road, Singapore 119260
[2] Institute of Materials Research and Engineering (IMRE), 3 Research Link, Singapore 117602.
*E-mail: i-rodriguez@imre.a-star.edu.sg
http://www.imre.a-star.edu.sg

Electrokinetic forces have been the mechanism most widely used for the transport of molecules and flows in microfluidic applications such as miniaturized analysis systems or so called "Labs on a Chip". With further downscaling towards the sub-micron domain, understanding of the electrokinetic effects and associated phenomena becomes a critical issue as these effects are expected to be enhanced. Because electrokinetic field forces originate at the very channel surface, it is one of the few pumping mechanisms that can be effectively applied at nano scale.

We have used proton beam writing to machine fluidic channels in the micrometer and nanometer scale. In our work, we use current measurements to determine two phenomena. The first is the study the interfacial electrical properties of the machined substrates. The second is the estimation of the electroosmotic flow (EOF) characteristics. Observation of an increase on the ionic current in the system indicates that in small volumes, the electrolysis process dominate the fluid transport giving rise to changes in concentrations of ionic species in the system. As result, thickness of the Debye layer changes thus, the EOF. EOF anomalies are undesirable during analytical separations and consequently, this problem need to be addressed for these applications.

The results of the current monitoring studies are presented and the mechanisms for current changes evaluated.

Characterising Nanoscale Heterogeneity: Switching between imaging regimes in tapping-mode AFM

ANDY ROUND and Mervyn Miles
Interdisciplinary Research Collaboration in Nanotechnology,
HH Wills Physics Lab, University of Bristol, Tyndall Avenue, Bristol BS8 1TL, UK
andy.round@bristol.ac.uk

It is a goal of imaging technologies in the field of nanoscale science and technology to accurately and reproducibly image sub-nanometre, intramolecular structural heterogeneity in materials such as polymers, particularly in the case of complex biological polymers such as proteins and glycoconjugates. Such resolution is now achievable with various modes of AFM, but the underlying mechanisms which describe the complexities of operation of one of the most commonly used modes, tapping mode AFM (TM-AFM) in air, are only now being elucidated [1,2].

A major result of this theoretical work has been the prediction and demonstration [3,4] of the existence of two imaging 'regimes'- the one dominated by an attractive, non-contact interaction and the other by a repulsive, contact interaction. This emerging theoretical description can explain a number of hitherto puzzling effects commonly seen during TM-AFM imaging.

In this poster we present an investigation of the criteria required for accessing the two imaging regimes, a simple method for controlling the transition between them in situ, and preliminary results of a systematic study of their topographic and phase-contrast consequences for DNA. We also assess the effect of the cantilever's quality factor on accessing the two regimes using active resonance control.

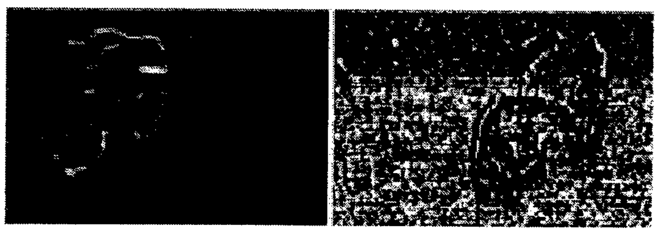

Figure 1: Simultaneously acquired topography (left) and phase (right) images of plasmid DNA on mica imaged by TM-AFM in air. The images depict a spontaneous transition from the attractive imaging regime (top) to the repulsive regime (bottom). Scans approx. 750 nm x 500 nm.

References

[1] R. Garcia and R. Perez, Surface Science Reports 47 (2002) 197-301
[2] A. San Paulo and R. Garcia, Physical Review B 66 (2002) 041406(R)
[3] A. San Paulo and R. Garcia, Biophysical Journal 78 (2000) 1599-1605
[4] B. Pignataro et al., Applied Physics A 74 (2002) 447-452

KINETIC STUDIES OF CNT'S FORMATION BY DECOMPOSITION OF METHANE ON A $Ni/(MgO)_{0.4}(Al_2O_3)$ CATALYST

N. Latorre, T. Ubieto, C. Royo, E. Romeo, A. Monzón*
Dept. of Chemical and Environmental Engineering, University of Zaragoza, E50009 Zaragoza, Spain.
amonzon@posta.unizar.es

Hydrogen is predicted to become a major source of energy in the future [1]. It is an important raw material in the chemical and petroleum industries; large quantities are used in the manufacture of ammonia and methanol and in a variety of petroleum hydrotreatment processes. A growing demand is forecast in all sectors, mainly for petroleum refining where the increasing need to process heavy and high-sulphur content crudes is accompanied with the lowering of hydrogen co-product in the catalytic reforming process [2]. Hydrogen is a clean fuel that emits no CO_2 when burned or used in H_2-O_2 fuel cells, can be stored as a liquid or gas, is distributed via pipelines, and has been described as a long-term replacement for natural gas [1]. Given that catalytic processes produce the main fraction of the hydrogen needed in industry, involving multiple steps with different types of catalyst, it is clear that catalysis plays a critical role in the production of H_2 [1]. Steam reforming of methane and other hydrocarbon feedstocks has been the most widely used and usually the most economical technology for the production of hydrogen [1]. However, this route makes hydrogen an indirect source of CO_2. In addition, the co-product of steam reforming, CO, must be removed by two subsequent steps: water-gas shift and methanation. The complete removal of CO is not economical and therefore, the hydrogen thus produced is not suitable for low-temperature fuel cells given that the catalyst is poisoned by CO [2].
The reaction of direct cracking of methane over nickel catalysts has recently been receiving attention as an alternative route to the production of hydrogen from natural gas [3-5].
With this reaction, the direct formation of CO_2 is avoided and the subsequent steps for CO removal are not needed.

In addition to the production of H_2, the cracking of methane produces nanocarbonaceous materials like carbon nanofibres (CNF's) or carbon nanotubes (CNT's). These nanocarbonaceous materials have been known for a long time as a nuisance that often appears during catalytic conversion of carbon containing gases. The recent outburst of interest in these graphitic materials originates from their potential for unique applications as well as their chemical similarity to fullerenes and carbon nanotubes [6]. Carbon nanofibers have potential utilisation as gas (e.g. hydrogen) storage, polymer additives, and as catalyst supports [7].
Carbon formation during catalytic methane decomposition mainly occurs in the form of CNF's and CNT's [7-9]. This mode of carbon accumulation allows the catalyst to maintain its activity for an extended period of time without deactivation [7]. Catalyst deactivation eventually occurs through the formation of encapsulating carbon on the nickel particles [8], or is due to the limitations imposed by the free space available in the reactor [3]. The mechanism of carbon filament formation resulting from the decomposition of hydrocarbons on catalyst metal particles has been extensively studied in the past [8-10], but few kinetic studies have been reported [5,8].
In the present paper we report the results of characterisation and catalytic behaviour of a coprecipitated Ni-$MgO.Al_2O_3$ catalyst during the reaction of methane cracking. A complete kinetic study has been made of the main operating variables of this process. It is worth noting that most kinetic studies presented in the literature only consider the period of constant carbon formation rate [8,9]. However, our experiments indicate that the rate of carbon formation is not constant and follows a quite complex pattern [5]. In Figure 1, it is shown that the duration

of the induction period, ascribed to *CNF* nucleation, depends of temperature and H_2 content. The rate of *CNF* growth follows a complex pattern with respect p_{H_2} and this must be taken into account in the developing of accurate kinetic models.

For this reason, the evolution of the carbon formation rate over time has been measured during the complete duration of each experiment. The influence of the operating temperature and feed composition on the methane conversion, hydrogen production as well as the carbon formation rate, has been studied. The effects of the regeneration step on activity and carbon formation are also investigated. A kinetic model has been developed for the prediction of CNT's and H_2 production. The proposed model takes into account the stages of carbon formation: nucleation, filament growth and catalyst deactivation.

Acknowledgments. The authors acknowledge financial support from MCyT (Grant PPQ2001-2479)

Referencias

[1] J.N. Armor, Appl. Catal. A, **176**, 159 (1999).
[2] N.Z. Muradov, Int. J. Hydrogen Energy, **18**, 211 (1993).
[3] T. Zhang and M.D. Amiridis, Appl. Catal. A, **167**, 1161 (1998).
[4] K. Otsuka, T. Seino, S. Kobayashi and S. Takenaka, Chem. Letters, **11**, 1179 (1999).
[5] J.I. Villacampa, C. Royo, E. Romeo, J.A. Montoya, P. del Angel and A. Monzón, Appl. Catal. In press, 2003.
[6] P.M. Ajayan, Chem. Rev., **99**, 1787 (1999).
[7] K.P. de Jong and J. W. Geus, Catal. Rev.–Sci and Eng., **42**, 481 (2000).
[8] J.-W. Snoeck, G.F. Froment and M. Fowles, J. Catal., **169**, 240 (1997); Ibid, **169**, 250 (1997).
[9] I. Alstrup and M.T. Tavares; J. Catal., 135 (1992) 147; Ibid, **139**, 513 (1993).

Figure 1:

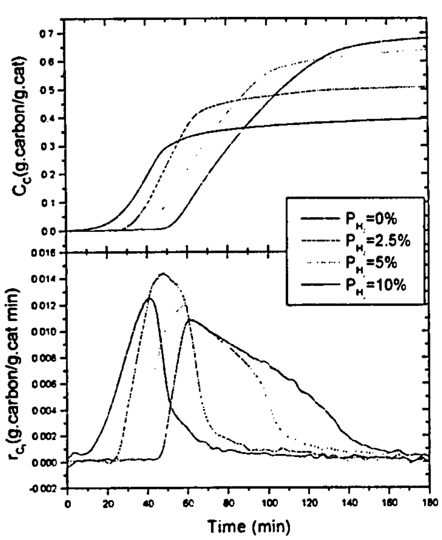

Figure 1a. Influence of p_{H2} and time on carbon content and carbon formation rate.

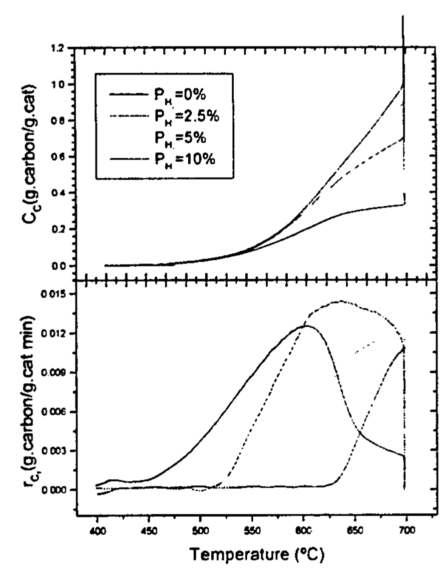

Figure 1b. Influence of p_{H2} and Temperature on carbon content and carbon formation rate

MOLECULAR TECTONICS AND SELECTED APPLICATIONS IN NANOSCIENCE

Catalina Ruiz-Pérez

Laboratorio de Rayos X y Materiales Moleculares, Departamento de Física Fundamental II, Universidad de La Laguna, Avda. Astrofísico Francisco Sánchez s/n, 38204 La Laguna, Tenerife, España.. *E-mail: caruiz@ull.es

The development of concepts and strategies allowing the design of molecular networks with predicted and programmed structures is currently under active investigations. The engineering of molecular networks involves modelling, synthesis and exploitation of crystalline solids with predefined connectivity patterns between molecules or ions. This approach is at the intersection of supramolecular and materials chemistry.

Molecular networks are defined as hyper structures possessing translational symmetry. Whereas molecules are described as assemblies of atoms interconnected by covalent bonds, by analogy, molecular networks may be described as hypermolecules for which the connectivity between the elementary molecular components (tectons) is ensured by non-covalent and/or reversible interactions. The formation of these molecular solids results from the chemical and physical nature of the molecular components comprising the solid. The design and formation of molecular networks may be achieved through iterative self-assembling processes by using programmed tectons which contain both recognition and iteration information.

The use of coordination chemistry in the synthesis of nanoscale molecules represents an emerging area of research with enormous potential. In this approach, metal complexes with fixed coordination geometries and featuring one or more labile ligands are combined with bridging ligands to generate a range of soluble molecular units. In many cases, reversible bond formation enables repair defects, leading to pure molecular compounds obtained in high yield. Combining the knowledge of the coordination preferences of the metal ions and the bridging modes of ligands utilized, it is possible to direct the formation of specific structures (particularly, polygons and polyhedra bearing well-defined internal cavities), thereby permitting the design of species with a variety of recognition properties. Nanoclusters possessing cavities of tunable dimensions, shape, chirality, and functionality (e.g. hydrophobicity, or metal or anion binding capability) could yield applications in sensing, catalysis, and separations. While significant progress is being made along these fronts, it is clear that much work is needed to advance beyond the ~2 nm.

Among a number of ligands used as building blocks, the two end functional groups of dicarboxylic acids could yield a variety of crystal structures of coordination compounds even with close chemical formulae, depending of the conformation of the carbon chains and the end functional groups. In order to check the ability of dicarboxylate ligands to lead high dimensional materials, we have thus undertaken a study of the metal transition malonate complexes (where malonate stands for the dianion of the propanedioic acid, H_2mal). This ligand has, indeed a great ability to form infinite connections with metal ions and remarkable versatility in adopting several different modes of bonding, ranging from unidentate, chelating and bridging, sometimes in more than one way in the same compound. Also malonic acid is widely used in many important fields as a result of its excellent coordination ability. The malonic acid complexes with lanthanide and transition elements have been used in the fluorescent probe technique, solid fluorescent materials, biological active materials and modifiers of polyethylene. Therefore, studies of the new complexes with malonic acid are quite valuable in theory and application.

Figure 1. Relationship between structure and magnetic property

As anticipated from the malonate structural relationship, the magnetic properties of these complexes were in general easily rationalized on the basis of the combined electronic and molecular structural data. Most importantly, through these investigations we

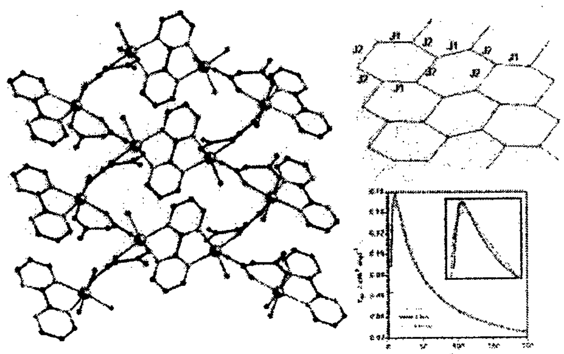

were able to demonstrate a degree of rational structural control over the property of interest—magnetism—in metal-malonate complexes (Fig. 1). The level of control over the structure and magnetic properties in metal-malonate coordination complexes cannot be as easily achieved with any other metal-carboxylate ligand systems under study.

From these studies, an entirely new set of building blocks has been developed that clearly demonstrate the enormous potential offered by these units for magnetic materials. The metal-malonate relationships between structure and property gained through this study are invaluable for future rational synthetic investigations using new malonate ligands. The groundwork has been laid for the pursuit of unique polymeric arrays containing malonates and metals, and it is expected that bulk magnetism in these molecular based materials can soon be achieved.

COMPARISON OF FFM AND SFA FRICTION MEASUREMENTS UNDER CONDITIONS OF LOW ADHESION

Marina Ruths
Department of Physical Chemistry, Åbo Akademi University
Porthansgatan 3-5, FIN-20500 Åbo, Finland
E-mail: mruths@abo.fi

The boundary friction between aromatic thiol and silane monolayers was measured with friction force microscopy (FFM) and the surface forces apparatus (SFA). Under conditions of low adhesion (in a solvent), the dependence of the friction force on the contact area was significantly reduced, and good agreement was found between friction coefficients μ measured with the two techniques despite the large differences in the contact areas, forces and pressures. The radius of curvature R of the single asperity contact in these two techniques differs by a factor 10^6.

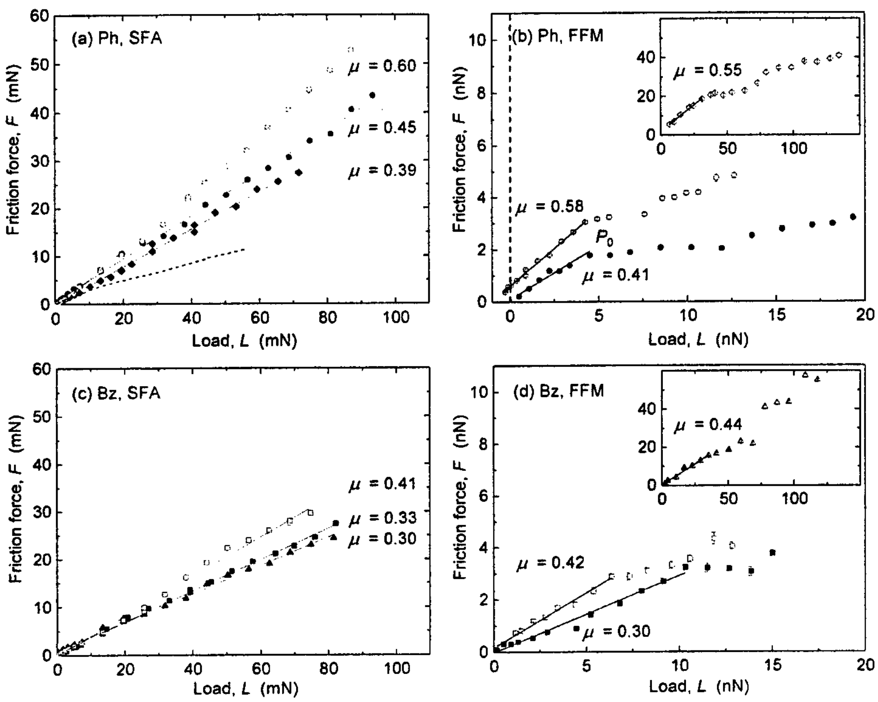

Figure. Load-dependence of the friction forces of monolayers of phenyltricholorsilane (Ph) and benzyltrichlorosilane (Bz) monolayers measured in ethanol with the SFA at sliding velocities of 0.15–0.5 μm/s, and with FFM at 0.15 μm/s. Open symbols denote sliding of a monolayer against a bare glass surface in the SFA (R = 0.2–2.8 cm) or unfunctionalized Si (R = 11 or 33 nm) in the FFM experiments. Filled symbols show results from systems with both surfaces covered with the respective silane monolayer (using tips with R = 16 nm and 11 nm in (b) and (d), respectively). The insets in (b) and (d) show FFM data obtained with an unfunctionalized Si tip (R = 33 nm) that was stiffer than the other cantilevers. The dashed curve in (a) shows the friction force between two bare glass surfaces in ethanol.

The friction forces were generally found to be lower when both sliding surfaces were covered with a monolayer, and plateaus in the friction force as a function of velocity found in the FFM experiments appeared at higher velocity, suggesting a more fluid-like sliding.

Kondo Effect in Quantum Dots Coupled to Ferromagnetic Leads

David Sánchez[1], Rosa López[1], and Mahn-Soo Choi[2]

[1]Département de Physique Théorique, Université de Genève, CH-1211 Genève 4, Switzerland
[2]Department of Physics, Korea University, Seoul 136-701 Korea

David.Sanchez@physics.unige.ch

Abstract

A single spin-1/2 confined in a discrete level represents the ultimate degree of miniaturization in semiconductor physics. Thus, it is crucial to understand the properties of spintronic transport in quantum dots (QD's). In particular, one might ask to what extent the Kondo effect in QD's is sensitive to the presence of ferromagnetic leads or spin flip processes.

Using a slave-boson mean-field theory, we have shown that the combined influence of ferromagnetic electrodes and spin flip transitions manifests itself in the nonequilibirium properties of a quantum dot. We find a splitting of the differential conductance when the spin flip scattering amplitude is of the order of the Kondo temperature. We discuss how the relative orientation of the lead magnetizations strongly influences the electronic current and its fluctuations at zero temperature (shot noise) in a nontrivial way [1].

Furthermore, we present a numerical renormalization group analysis showing that the Kondo effect is not necessarily suppressed by the lead polarization: While the Kondo effect is quenched for the asymmetric Anderson model, it survives even for finite polarizations in the regime where charge fluctuations are negligible [2].

References

[1] R. López and D. Sánchez, Phys. Rev. Lett. **90**, 116602 (2003).

[2] M.-S. Choi, D. Sánchez and R. López, cond-mat/0305107 (unpublished).

Andreev Drag Effect in Ferromagnetic Hybrid Systems

David Sánchez, **Rosa López, Peter Samuelsson and M. Büttiker**

[1]Département de Physique Théorique, Université de Genève, CH-1211 Genève 4, Switzerland

David.Sanchez@physics.unige.ch

Abstract

In the Andreev effect, an electron with spin up, incoming toward a normal-superconducting interface, is reflected as a hole with spin down. This may lead to exciting consequences in spintronic transport based devices, where the current-carrying quasiparticles are spin polarized and the transport properties are strongly sensitive to the relative orientation of the ordered moments of ferromagnetic electrodes [1]. In particular, a dc biased ferromagnetic lead coupled to a superconductor can induce a reversal of the electronic flow in a nearby, grounded lead with antiparallel magnetic moment due to crossed Andreev scattering [2].

We propose a readily feasible experimental setup that uses a chaotic (normal) dot to greatly increase the transmission probability. Moreover, the sources of the competing phenomena—superconductitivity and ferromagnetism—are spatially separated, thereby avoiding unwanted modifications of the local properties of the superconductivity and ferromagnetism. Within a semiclassical model, we present the conditions for the Andreev drag effect in terms of the degree of polarization, contact conductances and spin-flip relaxation time in the normal conductor. Remarkably, we find that both equilibrium and nonequilibrium zero-frequency current–current correlations at different probes become positive even in the presence of spin flip scattering [3].

References

[1] See, e.g., S.A. Wolf *et al.*, Science **294**, 1488 (2001) and references therein.

[2] G. Deutscher and D. Feinberg, Appl. Phys. Lett. **76**, 487 (2000).

[3] D. Sánchez, R. López, P. Samuelsson and M. Büttiker, preprint (2003).

TIME DEPENDENT DENSITY FUNCTIONAL THEORY CALCULATION OF THE DIELECTRIC RESPONSE OF CARBON NANOTUBES

Daniel Sánchez-Portal

Centro Mixto CSIC-UPV/EHU and Donostia International Physics Center (DIPC),
Paseo Manuel de Lardizabal 4, 20018 Donostia, Spain
Email: sqbsapod@sc.ehu.es

I have performed an *ab initio* study of the optical absorption and dielectric properties of small-diameter carbon nanotubes using time dependent density functional theory (TDDFT) [1,2]. The calculations have been performed using the SIESTA program [3]. This code performs standard pseudopotential density functional calculations using a linear combination of atomic orbitals as a flexible basis set. It has been specially optimised for the treatment of very large systems, being an ideal tool to calculate systems like large surface reconstructions or nanotubes. The implementation of TDDFT in this program was recently performed [4]. The scheme to calculate the optical response in this implementation follows closely the method proposed by Yabana and Bertsch [5]. The idea is to apply an external perturbation to the system at time equal zero. The system is then allowed to evolve by solving the time dependent Kohn-Sham equations. The solution of the coupled equations is performed making an unitary Crank-Nicholson-type approximation for the time evolution operator for small time durations dt [4]. We then can obtain the new Kohn-Sham orbitals for time $(t+dt)$ from the wavefunctions at the previous time step t. The Hamiltonian, according to what the system evolves, is taken constant for this evolution during time dt. It is, however, updated in each time step once the new electronic density has been calculated [4]. The Hamiltonian includes the both the Hartree potential and the exchange-correlation potential calculated within the local density approximation in each time step, this is known as the *adiabatic* local density approximation.

From the computed time evolution of the density it is possible to obtain information about the dielectric response of the system. For example, from the Fourier transform of the time evolution of the electric dipole it is possible to obtain information about the linear [3] and non-linear [4] dynamical polarizabilities of clusters or molecules. Unfortunately, this scheme as described to this point presents an important short coming: it cannot be directly applied for the calculation of the optical response of bulk systems. In the present study, since we are dealing with one-dimensional systems, i.e. infinite along the axial direction, we have extended the implementation of TDDFT in SIESTA to deal with infinite, crystalline systems. We have used for that the prescription given by Bertsch *et al.* in Ref. [6], in which the perturbing electric field is introduced in the form of a vector potential, consistent with the crystal periodicity, via a gauge transformation. The response properties are now not only calculated from the density evolution, but from the currents created in the system.

I will present results for several carbon nanotubes of small diameter with different chiralities. As a benchmark we include results for the tubes (3,3), (5,0) and (4,2) tube that, being recently synthesized inside zeolite channels, have attracted much attention[7] and, to the best of our knowledge, are the sole carbon nanotubes for which TDDFT studies of the optical response exist [8]. The main outcome of the calculations is that, while for electric fields directed along the axis of the tube the TDDFT dieletric function only differs slightly from those obtained by classical time-dependent perturbation theory based on dipolar transitions between Kohn-Sham states[7], in the case of electric fields perpendicular to the tube axis the full description of the screening provided by the TDDFT calculations is crucial. For the perpendicular fields, therefore, the optical absorption is extraordinarily reduce in accordance with the experimental information and the previous TDDFT results reported by Wirtz *et al.* for the (3,3) tube.

References:

[1] E. K. U. Gross, C. A. Ulrich and U. J. Grossman, in *Density Functional Theory*, edited by E. K. U. Gross and R. M. Dreizler (Plenum Press, New York, 1995), and references therein.
[2] E. K. U. Gross, J. F. Dobson, and M. Petersilka, in *Topics in Current Chemistry*, edited by R. F. Nalewajski (Springer-Verlag, Berlin Heidelberg, 1996), Vol. 181.
[3] J. M. Soler *et al., J. of Phys.: Cond. Matter* **14**, (2002) 2745, and references therein.
[4] A. Tsolakidis, D. Sánchez-Portal, and R. M. Martin, *Phys. Rev. B* **66**, (2002) 235416.
[5] K. Yabana and G. F. Bertsch, *Phys. Rev. B* **54**, 4484 (1996).
[6] G. F. Bertsch, J.-I. Iwata, A. Rubio, and K. Yabana, *Phys. Rev. B* **62**, (2000) 7998.
[7] M. Machón *et al., Phys. Rev. B* **66**, (2002) 155410 ; H. J. Liu and C. T. Chan, Phys. Rev. B **66**, (2002) 115416
[8] L. Wirtz, *et al. Electronic Properties of Novel Materials: XVIIth International Winterschool*, Ed. H. Kuzmany, J. Fink, M. Mehring and S. Roth, World Scientific, Singapure (2003)

Figures:

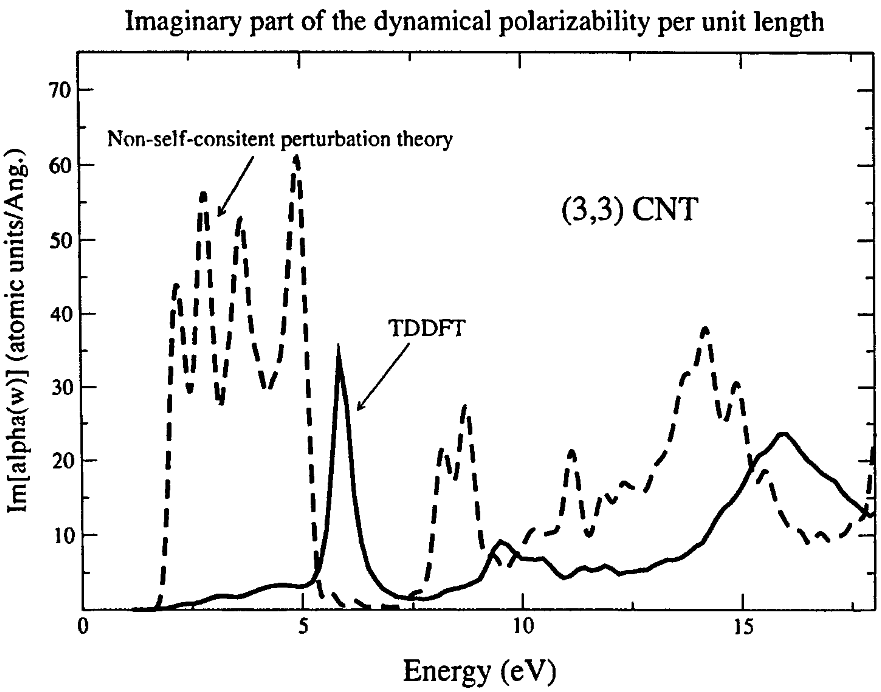

Figure 1 : Optical absorption of a (3,3) carbon nanotube for a field polarization perpendicular to the tube axis. The TDDFT calculation is shown together with a calculation based standard non-self-consistent time dependent perturbation theory. The suppression of the response for low energies is evident. The results are in very good agreement with the calculation of Ref. [8]

CONTROLLING NANOTUBE SIZE AND PLACEMENT

D. Sarangi and A. Karimi

Institut de Physique de la Matière Complexe (IPMC-FSB),
Ecole Polytechnique Fédérale de Lausanne (EPFL), CH-1015 Lausanne, Switzerland.
E-mail: Debajyoti.Sarangi@epfl.ch
http://ipmc.epfl.ch/akarimi

The fascination of the use of carbon nanotubes in the field emission based devices has opened a new era and offers a lot of challenges and opportunities in this field. Control placement of the nanotubes over the substrate with uniform density and the size of the nanotubes are the key issues for these kinds of devices. In the present investigation, carbon nanotube was grown over catalyst supported metallic wire by a very simple technique called as Cold Plasma Chemical Vapor Deposition [1]. The simplicity of this growth technique allows one to control the nanotube growth in better fashion. The main emphasizes in the present paper has been given over catalyst. It is well established that the catalyst particle size determines the diameter of the nanotube. Liquid catalyst has much more added advantage than the catalyst deposited by sputtering or the electro-deposition. Liquid catalyst preparation using iron nitrate, nickel nitrate etc with different concentrations leads to well control growth of the nanotubes. Bur the effect of inert metal with catalyst has dramatic effect. Aluminum nitrate was mixed with iron nitrate or nickel nitrate with a variety of fashion while prepare the liquid catalyst solution. The inert matrix inside the metal catalyst matrix leads to very thin and sparse growth of carbon nanotube. Figure 1 shows spare growth of nanotube over the metal using iron and aluminum nitrate solution. A systematic studies have presented.

References:

[1] D. Sarangi and A. Karimi, Nanotechnology, **14** (2003) 109.

Figures:

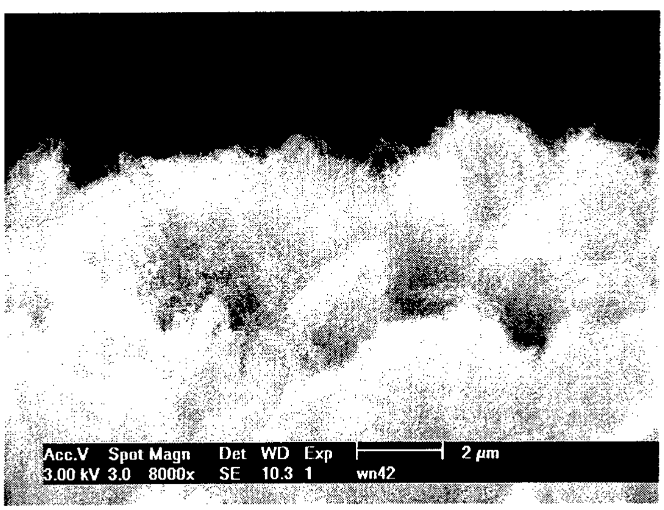

Fig. 1. Spares growth of carbon nanotube over the metallic wire

SUPER HARDENING IN SUPERLATTICE THIN FILMS: BASIC MECHANISM TO PRACTICAL REALIZATION

D. Sarangi, T. Vasco Boutoand A. Karimi

Institut de Physique de la Matière Complexe (IPMC-FSB),
Ecole Polytechnique Fédérale de Lausanne (EPFL), CH-1015 Lausanne, Switzerland.
E-mail: Debajyoti.Sarangi@epfl.ch
http://ipmc.epfl.ch/akarimi

The search for superhard materials is motivated by the researchers as well as by the great potential of such materials for industrial applications. Superlattice thin film consisting of many alternative layers in nanometer range demonstrates very good hardness [1]. In the present investigation first we have made a detailed review study regarding the basic mechanism involved for the increase of hardness in the superlattice film. We have made also some studies of hardening behavior using AlN and TiN multilayer. The multilayer films were grown using reactive RF sputtering of Al and Ti targets alternatively. The Si substrate was kept around 400°C and an additional DC bias was applied to the substrate. Nanoindentation was used to study the mechanical behavior of this film. The affect of bilayer period was the main scope. XRD was also employed to investigate their crystalline behavior.

References:

[1] S. A. Barnett, A. Madanm I. Kim and K. Martin, MRS Bulletin, 28 (2003) 169.

CHARACTERISATION OF LASER-DERIVED MWNT/SiO_2-COMPOSITES

T. Seeger, W.K. Maser, J. Galindo, M.A. Callejas and M. T. Martínez
Instituto Carboquimica, CSIC; Miguel Luesma Castán 4; E-50018, Zaragoza Spain

G. de la Fuente[b]
ICMA, CSIC Universidad de Zaragoza; Maria de Luna 3; E-50018, Zaragoza (Spain)

J.-L. Sauvajol, A. Righi,
Groupe de Dynamique des Phases Condensées, UMR CNRS 5581,
Université,Montpellier II, France

Carbon nanotubes are interesting candidates for the reinforcement in robust composites [1] and for conducting fillers in polymers [2-3] due to their fascinating electronic and mechanical properties. However, a sufficient fibre-matrix bonding must be achieved for the observation reinforcement effect introduced by the CNT. For an inorganic matrix of SiO_2 a fibre-matrix bonding via Si – C bridges has been proposed by Seeger et al. [4,5].

One of the possible reasons is that the iniciation of a controlled interface-reaction requires precisely defined conditions in the fibre-matrix interface. This would permit the esablishment of bonds without destroying the CNT. Laser treatment allows the precise control of reaction in a very short time scale. Recently the authors reported the incorporation of MWNTs into glass surfaces by using a silica gel/MWNT precursor [6]. Here we report a similar effect by the simple deposition of pristine MWNT on a glass surface and subsequent laser treatment. The surface composites have been characterised using scanning electron microscopy (SEM), Raman spectroscopy, atomic force microscopy (AFM) and high resolution transmission electron microscopy (HRTEM).

Before the laser treatment, arc-discharge MWNTs were dispersed in ethanol using ultrasonic treatment. From this dispersion the MWNTs were then deposited on the surface of a light-microscopy sample-support of silica-lime-glass. The laser beam was focused on the MWNTs on the glass-surface with an energy density of 3.1 J/mm^{-2}.

Fig 1a) shows the surface of a laser treated glass surface as reported in [6]: MWNTs incorporated in the surface are bridging a crack. Note that the glass surface exhibits a distinct relief exactly where a MWNT is incorporated (arrows). Fig. 1b) depicts the surface of pristine MWNT deposited on the glass surface after laser treatment as described. Besides agglomerated of MWNTs and polyhedradral particles a very similiar relief in the glass surface is shown.

From this observation we conclude that the incorporation of MWNT occures due to the direct interactions between the MWNTs and the glass surface. AFM measurements (not shown here) of the treated glass surface reveal a relief hight of ca 10 nm and a width of ca. 100 to 150 nm. Raman Spectroscopy (not shown here) revealed a strong reaction MWNT with Silica gel. An interaction of the surface incorporated MWNT with the glass matrix could not be observed

Figure 1:

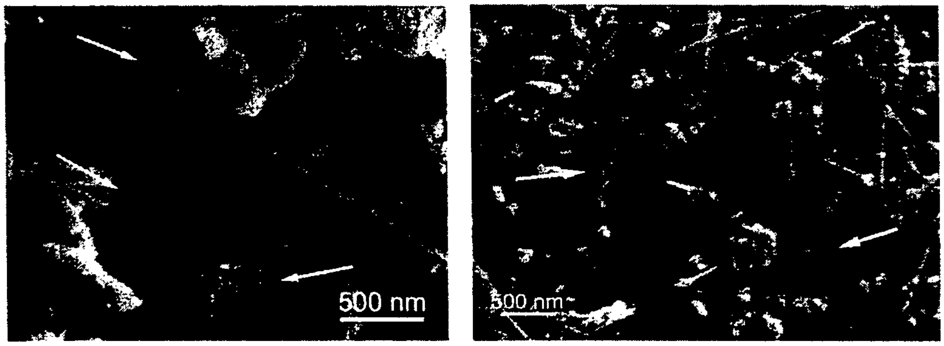

Fig. 1: Laser treated glass surfaces: a) silica-gel/MWNT composite fixed between two glass plates, b) pristine MWNT deposited on the surface

References:

[1] M. Terrones, W. K. Hsu, H. W. Kroto, D. R. M. Walton Fullerenes and Related Structures; Topics in Chemistry Series, Ed. A. Hirsch (Springer-Verlag) **199** (1998) 189.

[2] I. Musa, M. Baxendale, G. A. J. Amaratunga, W. Eccleston, Synthetic Metals **102** (1999) 1250.

[3] K. Yoshino, H. Kajii, H. Araki, T. Sonoda, H. Take, S. Lee, Full. Sci. & Tech. **7** (1999) 695.

[4] T. Seeger, T. Köhler, T. Frauenheim, N. Grobert, M. Rühle, M. Terrones, G. Seifert; Chem. Comm. **1** (2002) 34.

[5] T. Seeger, T. Köhler, T. Frauenheim, N. Grobert, M. Terrones, G. Seifert, M. Rühle, Zeitschrift fur Metallkunde **93** (2002) 455.

[6] T. Seeger, G. de la Fuente, A. M. Benito, M. A. Callejas and W. K. Maser , M. T. Martínez, Nanotechnology, **14** (2003) 184.

ELECTRONIC STRUCTURE AND MAGNETIC PROPERTIES OF DOPED SILICON CARBIDE

V.L. Shaposhnikov[1,2], N.A. Sobolev[1,3]
[1]Department of Physics, University of Aveiro, 3810-193 Aveiro, Portugal
[2]Belarusian State University of Informatics and Radioelectronics, 220013 Minsk, Belarus
[3]Institute of Solid State and Semiconductor Physics, 220072 Minsk, Belarus
E-mail: victor@fis.ua.pt
http://www.fis.ua.pt

The introduction of magnetic or spin-related functions into semiconductor materials is a new challenge for researchers in the fields of solid-state physics [1-3]. One of the most important issues is the development of ferromagnet/semiconductor hybrid structures, in which the spin degree of freedom can be used. One of the possible solutions comes from the diluted magnetic semiconductors (DMS), i.e. semiconductor compounds in which a fraction of the constituent ions is replaced by magnetic ions. Several types of DMSs based on III–V and II-VI semiconductors are well investigated, both theoretically and experimentally [4]. Very little attention has been paid to potential dilute magnetic semiconductor behavior in SiC, which is at a relatively mature state of development for high-power, high-temperature electronics. With its wide bandgap (3.0 eV for the 6H polytype), excellent transport properties and dopability, it would be a good candidate for spintronic applications. Recently, some promising experiments have been made on this compound, implanted with different transition metals for which the high values of the Curie temperature were obtained [5].

In this work we present a theoretical study of the electronic structure and magnetic properties of different SiC polytypes, doped with $3d$ transition metals. The spin-polarized calculations have been performed by the full potential linearized augmented plane waves within the generalized gradient approximation. Two phases were considered: cubic 3C and hexagonal 6H, which are most often used in microelectronic technology. Cr, Mn and Fe were chosen as doping impurities. The influence of the dopant concentration has been studied by the creation of a $2\times2\times2$ supercell and replacement of one or more silicon or carbon sites with $3d$ metal atom.

The most distinctive features between the different polytypes are the calculated magnetic moments of the supercell. In 3C-SiC, light magnetic atoms (Cr, Mn) are found to produce a ferromagnetic phase. However, the magnetic moment differs when a dopant atom substitutes the C or Si sites. When an iron atom is used as a dopant, nonmagnetic solution occurs for both substitutional sites. These results are rather stable; neither relaxation effects nor any parameter variation can produce nonzero magnetic moments for the iron dopant. This is confirmed by the practically similar densities of states (DOS), calculated for the spin-up and spin-down configurations.

The picture changes for the hexagonal 6H polytype. The Fe-doped system remains non-magnetic if Fe substitutes the C-site, while it becomes ferromagnetic when the silicon site is replaced. This fact confirms the latest experimental results [5], where ferromagnetism was observed in Fe-implanted SiC.

Substitution of the silicon sites with chromium also leads to a ferromagnetic phase, while a non-magnetic solution is observed for carbon. This situation practically does not depend on the location of the dopant site in the crystal. Manganese provides a ferromagnetic solution for

both types of substitution. However, replacements of Si atoms lead to higher values of magnetic moment of the system.

The decomposed DOS analysis of the states near the band gap shows that the valence band edge of the doped compound consists mainly of 3*d* metal atom orbitals hybridized with *p* states of the neighbors.

The influence of the relaxation of the crystal structure and of the atomic positions on the resulting magnetic properties of doped silicon carbide is discussed too.

References:

[1] G. A. Prinz, Science, **282** (1998) 1660.

[2]. S. A. Wolf *et al.*, Science, **294** (2001) 1488.

[3] M. Oestreich, Nature, **402** (1999) 735.

[4] T. Dietl, H. Ohno, F. Matsakura, *et al.*, Science, **287** (2000) 1019.

[5] N. Theodoropoulou, *et al.,* J. Vac. Sci. Technol. A, **20** (2002) 579.

RADIATION-INDUCED DEFECTS IN QUANTUM-SIZE SEMICONDUCTOR STRUCTURES AND DEVICES

Nikolai Sobolev
Departamento de Física, Universidade de Aveiro, 3810-193 Aveiro, Portugal
E-mail: sobolev@fis.ua.pt
http://www.fis.ua.pt

The tolerance of materials and devices to radiation-induced defects (RDs) is of crucial importance in atomic energy and space applications. Moreover, the creation of RDs is an inevitable collateral effect in the ion implantation that is a well-established technique of materials modification. The electrical, optical and mechanical properties of implanted layers strongly depend not only on the implanted species but also on the implantation and annealing conditions. And finally, there is a possibility of using RDs themselves in the device technology. With the onrushing advent of quantum-size semiconductor structures (QSSS), the studies of RDs in them rapidly grow in importance.

The paper reports studies on electron and proton irradiation and ion implantation in semiconductor quantum wells (QW), quantum dots (QD) and superlattices (SL).

What can we learn from the RD studies?

- Influence of the defects on the electronic properties of quantum size structures and on the corresponding device parameters;
- Role of heterointerfaces in the defect evolution and defect reactions;
- Elucidation of the electronic structure of quantum semiconductor structures using defects as microprobes;
- Modification of the structure and properties of local defects, well known from the bulk semiconductors, through the influence of the quantum confinement;
- Novel technological processes of micro-, nano- and optoelectronics.

Radiation hardness. An enhanced radiation hardness of the photoluminescence (PL) and electroluminescence (EL) in thin-layer Si/Ge superlattices (SLs) as compared to Si/Ge quantum wells (QWs) and to bulk Si has been found [1] (see Fig. 1). The effect has been explained by the trapping of mobile Frenkel pair components at Si/Ge interfaces, which is more probable than that at impurity atom sites, even at doping levels as high as 10^{19} cm^{-3}.

For In(Ga)As/GaAs QDs, irradiation with electrons or protons has been found to quench the PL intensity about one order of magnitude more slowly than for comparable QWs [2]. The improved radiation hardness is reflected in a superior performance of irradiated QD lasers [3] (see Fig. 2). This effect is in the first line due to a reduced interaction of charge carriers localized in the QDs with non-radiative defects. Moreover, PL excitation and time resolved PL experiments have shown that the ground state of the exciton localized in a QD is unaffected by defects, at least at moderate irradiation doses [4]. Very recently, an enhanced radiation hardness of the electrical properties of the QD structures upon ion implantation has been shown, too [5].

SL amorphization. The ion doses needed for the amorphization of various crystalline materials differ by orders of magnitude. Hence, a selective amorphization of (rather thick) individual layers is usually observed upon ion implantation into multilayer structures. A quite opposite result has been obtained by the Rutherford backscattering/channeling (RBS) and high-resolution cross-sectional transmission electron microscopy (HR XTEM) on short-period Si/Ge SLs: the Si and Ge layers in the SL are amorphized simultaneously at one and the same

dose [6,7]. The importance of the relation between the projected range of recoil atoms and the individual layer thickness in the SL has been emphasized and proven in subsequent experiments with AlAs/GaAs SLs [8]. The role of intermixing still is a matter of debate. Ion-induced intermixing is particularly important in the QW laser fabrication (e.g. GRINSCH: graded-index separate confinement heterostructure). It seems that mixing in the collision cascades is rather weak. As shown by the Raman scattering and PL, the mixing during the post-irradiation heat treatment is strong and occurs due to the defect-enhanced diffusion [9].

References:

[1] N.A. Sobolev, F.P. Korshunov, R. Sauer, K. Thonke, U. König, and H. Presting. J. Cryst. Growth **167** (1996) 502.
[2] N.A. Sobolev, A. Cavaco, M.C. Carmo, M. Grundmann, F. Heinrichsdorff, and D. Bimberg. Phys. Stat. Solidi (b) **224** (2001) 93.
[3] Ch. Ribbat, R. Sellin, M. Grundmann, D. Bimberg, N.A. Sobolev, and M.C. Carmo. Electronics Letters **37** (2001) 174.
[4] F. Guffarth, R. Heitz, M. Geller, C.M.A. Kapteyn, H. Born, R. Sellin, A. Hoffmann, D. Bimberg, N.A. Sobolev and M.C. Carmo. Appl. Phys. Lett. **82** (2003) 1941.
[5] N.V. Baidus, B.N. Zvonkov, V.V. Ovchinnikov, and N.A. Sobolev (to be published).
[6] N.A. Sobolev, K. Gärtner, U. Kaiser, U. König, H. Presting, B. Weber, E. Wendler, and W. Wesch. Materials Science Forum **248-249** (1997) 289.
[7] N.A. Sobolev, U. Kaiser, I.I. Khodos, H. Presting, and U. König. Mat. Res. Soc. Symp. Proc., Warrendale, PA, USA, 1999, Vol. **540**, p. 91.
[8] N.A. Sobolev, B. Breeger, E. Wendler, W. Wesch, I.I. Khodos, R. Hey, H.T. Grahn (to be published).
[9] N.A. Sobolev, J. Gerster, G. Mauckner, M. Wolpert, W. Limmer, K. Thonke, R. Sauer, H. Presting, and U. König. Nucl. Instr. and Methods B, Vols. **136-138** (1998) 1057.

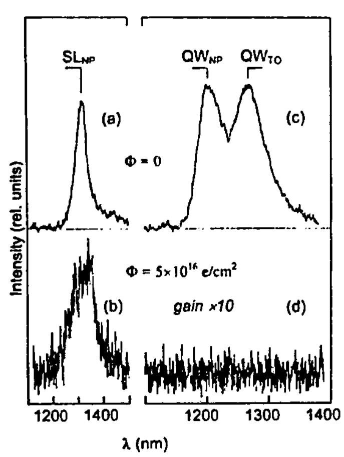

Figure 1. EL spectra of a Si_6Ge_4 SL and a $Ge_2Si_{20}Ge_2$ QW prior to and after irradiation with 5×10^{16} cm^{-2} of 3-4 MeV electrons. $T_{meas} = 4.2$ K.

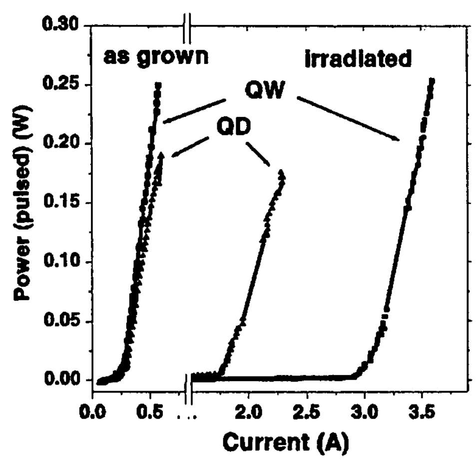

Figure 2. Optical output power against current in pulsed operation for same QW and QD lasers before and after irradiation with 2×10^{13} cm^{-2} of 2.4 MeV protons [5].

STUDY OF THE DISSIPATIVE SYSTEMS OF FERMIONS (DSF) IN OPTICAL AND NUCLEAR ENGINEERING

Eliade Ştefănescu, Andreea Rodica Sterian, Paul Sterian

Academic Center for Optical Engineering and Photonics, Bucharest Polytechnics University, Bucharest, Romania, sterian@physics.pub.ro

The systems of fermions are essential for describing some very important phenomena as nuclear giant resonances, fusion and fission reactions semiconductor nano-structures and high temperature superconductibility.

In such systems, the dissipative coupling mechanism in very important describing the studied system coupled with another system having a large state density, that is the environment.

Generally, the dissipative dynamics of a quantum system is described by a master equation of Lindblad type:

$$\frac{d}{dt}q(t) = -\frac{i}{\hbar}[H,\rho(t)] + \frac{1}{2}\sum_{i,j} a_{ij}\left([s_i\rho(t), s_j^+] + [s_i, \rho(t)s_j^+]\right) \qquad (1)$$

where H is the system hamiltonian, s_i are the system operators and $a_{ij} = a_{ij}^*$ are complex dissipative coefficients.

Their number is N^2-1 for a system with N energy levels, that is a big number for a complex system of particles.

To avoid this difficulty, explicit expressions of the dissipative coefficients, depending of the two-body interaction and the environment properties are necessary.

Using a method proposed by Ford, Lewis and O'Connell, we have obtained a master equation for a fermions system in a dissipative environment of a particles:

$$\dot{\rho}(t) = -\frac{i}{\hbar}[H,\rho(t)] + \sum_{i,j=0}^{N-1}\frac{1}{\hbar}\int d\varepsilon_\beta \frac{\tilde{\lambda}_{ij}}{e^{(\varepsilon_\beta - F)/kT} \pm 1}\left([c_i^+c_j\rho(t), c_j^+c_i] + [c_i^+c_j, \rho(t)c_j^+c_i]\right) \quad (2)$$

where H is the system hamiltonian, c_i^+, c_i are the creation and annihilation operators and λ_{ij} are real dissipative coefficients.

We have evaluated these coefficients describing the N^2-N-1 induced transitions by the environment in a system of N uniparticle states.

The coefficients $\tilde{\lambda}_{ij}$ are dependent of three dissipative parameters: the temperature *T*, the Thomas-Fermi coefficient Λ and the radius r_ε which depends of the dissipative potential.

In this description a transition $|j\rangle - |i\rangle$ induced by the environment is characterized as a probability flux reflected on a potential surfaces Σ from one state $|j\rangle$ to another one $|i\rangle$.

The properties of the dissipative matrix (λ_{ij}), for the case of a complex model having six energy levels of a rectangular potential were illustrated and their dependence on dissipative parameter was discussed. The results have a direct physical interpretation. We have found that the dissipative matrix elements λ_{ij} are essentially dependent on the population distribution of the environment states. For a normal distribution of these states, the relaxation coefficients are bigger than those of relaxation, the states occupied by the system being the lower one.

For a reverse distribution of the environment states, the system moves preponderantly toward an excited state. This state corresponds to a stable configuration of excited fermions on higher levels, forming a cluster which finally is emitted by a process of dissipative tunneling. This mechanism is proposed to describe the population distribution in the clustering process.

We established a weak dependence of temperature of this distribution.

Another two parameters, Λ and r_ε are important in the transition rate magnitude but not in the spectrum of the transition probabilities so that for a steady state, their influence can be neglected.

PREPARATION AND SOME PROPERTIES OF Cu-Te-S THIN FILMS ON THE POLYAMIDE(PA) SURFACE

Vida Judita Šukytė, Remigijus Ivanauskas, Vitalijus Janickis
Department of Inorganic Chemistry,Kaunas University of Technology

The semiconductor gas sensors market generated 11.5percent of revenues in the European industrial gas sensors market in 1997.Manufacturers of semiconductor gas sensors have continuously found new applications and markets for their products, which are some of the lowest cost gas sensors to be found.

This work was basically inspired by an increasing interest in new semiconductor as a material for an application in flexible and efficient gas sensors production. Applications as solar control coatings and as a conductive base for opt electronic device structures are among the possibilities for these new Cu-Te-S films on modified PA. To our knowledge the formation of semi conductive containing tellurium thin films of chalcogenides such as Cu_xTe_y and Cu_xS_y by sorption-diffusion processes on modified polymeric substrate-polyamide PA, has so far not been reported. The research has been undertaken for clarifying the kinetics of the diffusion of chalcogens into PA surface and some structural and electrical properties of such films has been investigated also.

. The diffusion- sorption of chalcogens and Cu into PA are concentration of initial $Na_2TeS_4O_6$ solution, as a source of chalcogens, an exposure time and temperature dependent The concentrations of sulfur, diffused per gramme of PA,are significantly lower than concentrations of tellurium and copper. The stoichiometry of prepared Cu-Te-S films was established by UV-Visible and AA spectrometry analysis and confirmed by X-ray diffraction, corresponding to Cu_xTe_y or Cu_xS_y formula. X-ray diffraction measurements were performed at low and medium diffraction angles using CuK_α radiation (voltage 30 kV) in a DRON-3 diffract meter provided with a special device for beam limitation and a graphite monochromator in the diffracted beam.

Samples of prepared Cu-Te-S thin films of different compositions are polycrystalline and many of them have some binary phases such as Cu_2Te, $Cu_{3-\delta}Te_2$,$Cu_{2-\delta}S$.The phases of tetragonal copper telluride $Cu_{2.72}Te_2$(43-1401) and orthorhombic vulcanite CuTe (13-258) were found in the thin films on the PA surface, among them orthorhombic aniliteCu_7S_4 (72-617) and copper sulfide$Cu_{1.8}S$ (75-2241) phases. The variation in grain size of the crystallites for various films composition is a function of non-molecularity, δ, which shows the position of a sample of any stoichiometry on the Cu_xS_y-Cu_xTe_y pseudo-binary tie –line. (The midpoint on this line is stoichiometric Cu_2Te, Cu_3Te_2, Cu_2S.$\delta < 0$ represents Cu-rich material while$\delta > 0$ is for Te –rich one). Our data also clearly points out that the crystallinity of the films increases as the copper content in the film goes up.

The resistance to constant current of Cu-Te-S thin layers with different composition was measured on an E7-8 numerical measuring device with special electrodes. The electrical properties of investigated films are very sensitive to variations in the films composition. Cu-Te-S polymer composites indicate p-type electricity conductive properties and have electrical resistance in the range of 1.5×10^{-3}-$4.0\times10^{-3}\Omega/\square$ to 3-5$\Omega/\square$ after to 2-3 hours of an exposure in 0.05-0.1mol.dm^{-3}solutions of $Na_2TeS_4O_6$, and 1.0-1.5 $\Omega/\square$ after 24-72 hours of exposure

ELECTRICAL MEASUREMENTS ON SINGLE NANOWIRES FABRICATED IN ETCHED ION-TRACK MEMBRANES

M.E. Toimil Molares[1], N. Chtanko[1], Th. Cornelius[1], D. Dobrev[1], I. Enculescu[1], E. M. Höhberger[2], Ch. Schaeflein[2], R.H. Blick[2], R. Neumann[1]

[1]Gesellschaft für Schwerionenforschung (GSI),
Planckstr. 1, D-64291 Darmstadt, Germany.
[2] Center for Nanoscience and Sektion Physik, Ludwig-Maximilians-Universität, Geschwister-Scholl-Platz 1, D-80539 Munich, Germany.
E-mail: e.toimil@gsi.de

Electrical properties of nanowires are being intensively studied due to their potential applications in the nanotechnology industry [1]. Besides, they are considered excellent objects to study how the properties of solids deviate from the macroscopic behavior when their dimensions are comparable to the characteristic length scales. To gain insight in electron transport mechanisms, it is necessary to measure absolute values of the resistance of single nanowires. This requires contacting single nanowires individually [2]. Several techniques have been reported in literature, which enable to contact single nanowires individually, however usually only transport measurements on wires with a maximum aspect ratio (length over diameter) of up to 10 have been described. In this paper, we will report about two different methods to contact single nanowires: optical lithography and electrochemical deposition in etched *single*-ion track membranes. The latter, allows the study of the transport properties of single nanowires, with a maximum aspect ratio of 1000.

We have created copper and bismuth nanowires with diameters as small as 30 nm by electrochemical deposition in polymeric etched ion-track membranes [3,4]. After dissolution of the polymeric membrane, gold contacts have been fabricated by optical lithography on top of single nanowires on a SiO_2 substrate. Current-voltage characteristics display an ohmic behaviour. Oxidation of the wire was evidenced by a dramatic resistance increase. Since Cu_2O is a p-type semiconductor, the I-U curve after oxidation of the wire was non-linear and resembled such from two Schottky diodes in a back-to-back configuration [5].

Alternatively, single nanowires have been created by electrochemical deposition in etched *single*-ion track membranes. Similar to the process used for fabricating many pore membranes, the worldwide unique single-ion irradiation facility existing at GSI, enables us to create polymer foils (diameter up to 5 cm) with a single pore placed at the center. The geometry of the pore is determined by the etching conditions, being possible to fabricate cylindrical or conical wires [6]. After the growth of the wire, a thin gold layer is sputtered on top. The wire, embedded in the membrane, is thus contacted with a very low contact resistance. Absolute values of the resistance of single bismuth nanowires with diameters ranging between 80 nm and 1 μm have been successfully measured. Up to our knowledge, electrical contacts on single bismuth nanowires had been performed before only by a combination of electron beam lithography and focused ion beam, and difficulties due to oxidation had been reported [7]. With our method, the wire remains embedded in the polymeric membrane, and is covered by gold on both sides, being protected except for several minutes from direct contact with air. The resistance value measured for these single wires was constant over several months (less than 8% change), even when measuring continuously during several days. Finally, this method also allows the transport measurements on nanowires embedded in different matrixes (e.g. Polycarbonate, Polyimide, PET, Mica, SiO_2). Results obtained for single copper and bismuth nanowires will be presented. Advantages and disadvantages of both contacting methods will be discussed.

References:

[1] Y. Xia, P. Yang, Y. Sun, Y. Wu, B. Mayers, B. Gates, Y. Yin, F. Kim, H. Yan, Adv. Mater., **15** (2003) 353.
[2] C. Durham, M.E. Welland, Phys. Rev. B, **61** (2000) 4215.
[3] M.E. Toimil Molares, V. Buschmann, D. Dobrev, R. Neumann, R. Scholz, I.U. Schuchert, J. Vetter, Adv. Mater., **13** (2001) 62.
[4] M.E. Toimil Molares, J. Brötz, V. Buschmann, D. Dobrev, R. Neumann, R. Scholz, I.U. Schuchert, C. Trautmann, J. Vetter, Nucl. Instr. and Meth. in Phys. Res. B **185** (2001) 192.
[5] M.E. Toimil Molares, E.M. Höhberger, Ch. Schaeflein, R.H. Blick, R. Neumann, C. Trautmann, Appl. Phys. Lett., **82** (2003) 2139.
[6] I. Enculescu, Z. Siwy, D. Dobrev, C. Trautmann, M.E. Toimil Molares, R. Neumann, K. Hjort, L. Westerberg, and R. Spohr, Appl. Phys. A, 77 (2003) 751.
[7] S.B. Cronin, Y.-M. Lin, O. Rabin, M.R. Black, J.Y. Ying, M.S. Dresselhaus, P.L. Gai, J.-P. Minet and J.P. Issi, Nanotechnology, **13** (2002) 653.

CALCULATED MOLECULAR PROPERTIES OF CARBON NANOTUBE MODELS

Francisco Torrens
Institut Universitari de Ciència Molecular, Universitat de València, Dr. Moliner 50, E-46100 Burjassot (València), Spain
E-mail: Francisco.Torrens@uv.es
http://www.uv.es/~icmol

The interacting induced dipole polarization model implemented in our program POLAR is used for the calculation of the dipole–dipole polarizability $\boldsymbol{\alpha}$ [1]. The method is tested with zigzag $(n,0)$ $(7 \le n \le 12)$ single-wall carbon nanotube models as a function of nanotube radius and elliptical deformation [2–8]. The results for the polarizability follow the same trend as reference calculations carried out with our version of program PAPID [9].

For the zigzag tubes [10–12], the polarizability is found to follow a remarkably simple law, *i.e.*, varies as the inverse of the radius (Fig. 1). An effect is also found with elliptical deformation. It is found that the polarizability and related properties can be modified continuously and reversibly by the external radial deformation. The effects of curvature and radial deformation depend on the chirality of the tube. The results suggest an interesting technology, in which mechanical deformation can control chemical properties of the carbon nanotubes. This remarkable and significant tunable adsorption can have important implications for metal coverage, and selective adsorption and desorption of foreign atoms and molecules on nanotubes, and can lead to a wide variety of technological applications, such as catalysts, hydrogen storage, magnetic tubes, *etc.*

A graph-theoretical study of the zigzag nanotube models has also been performed. For the nanotube models, the Kekulé structure count $K = 2$ is constant and smaller than for the corresponding planar acenes (heptacene to dodecacene linear polybenzenoid hydrocarbons, K in the range 8–13). This suggests a smaller stability for the former. Moreover, for the nanotube models the permanent of the adjacency matrix of the hydrogen-suppressed graph per($\mathbf{A}$) = 16 is constant and smaller than for the corresponding acenes, per($\mathbf{A}$) in the range 64–169. Since the quotient per($\mathbf{A}$)/ln$K$ is 2 for alternant hydrocarbons (*e.g.*, benzene) or >~2 for rather conjugated hydrocarbons (*e.g.*, buckminsterfullerene per($\mathbf{A}$)/ln$K$ = 2.0986), this ratio for the nanotube models (per($\mathbf{A}$)/ln$K$ = 4) is constant and smaller than for the corresponding acenes (per($\mathbf{A}$)/ln$K$ = 2). This confirms the smaller stability for the former.

The results of the graph-theoretical study are in agreement with the standard heats of formation per C atom calculated with MOPAC-AM1 (Fig. 2). While nanotube models are strongly stabilized with increasing number of C atoms v, planar acenes are slightly destabilized for greater v. The value extrapolated for $n \rightarrow \infty$ results 25.08 and 27.70kJ·mol^{-1} for nanotube models and planar acenenes, respectively.

Provisional conclusions follow.

1. Due to the differences between POLAR and PAPID results, it may become necessary to recalibrate POLAR. The results of good quality *ab initio* calculations might be suitable as primary standards for such a calibration. Work is in progress on the recalibration of POLAR.

2. The polarizability of a zigzag SWNT model can be modified reversibly and variably by the radial deformation. PAPID differentiates more effectively than POLAR among SWNT models with increasing radial deformation.

3. Different effective polarizabilities are calculated for the atoms at the sharp and flat sites. POLAR discriminates more efficiently than PAPID between α^{eff} of the sharp and flat sites.

4. The physics and chemistry of SWNT models permit a difference for undeformed and elliptically deformed SWNTs. While all positions in the undeformed SWNT are identical, a variation of C atoms is found in deformed SWNTs. The different atoms display different chemical reactivities. These different reactivities were observed in the chemistry of fullerenes C_{60} and C_{70}.

References:

[1] F. Torrens, J. Sánchez-Marín and I. Nebot-Gil, J. Mol. Struct. (Theochem), **463** (1999) 27.
[2] A. Bezryadin, A. R. M. Verschueren, S. J. Tans and C. Dekker, Phys. Rev. Lett., **80** (1998) 4036.
[3] J. P. Lu and J. Han, Int. J. High Electron. Syst., **9** (1998) 101.
[4] A. Rochefort, D. R. Salahub and P. Avouris, Chem. Phys. Lett., **297** (1998) 45.
[5] Ç. K□l□ç, S. Ciraci, O. Gülseren and T. Yildirim, Phys. Rev. B, **62** (2000) R16345.
[6] O. Gülseren, T. Yildirim, S. Ciraci and Ç. K□l□ç, Phys. Rev. B, **65** (2002) 155410.
[7] O. Gülseren, T. Yildirim and S. Ciraci, Phys. Rev. B, **65** (2002) 153405.
[8] O. Gülseren, T. Yildirim and S. Ciraci, Phys. Rev. Lett., **87** (2001) 116802.
[9] C. Voisin, A. Cartier and J.-L. Rivail, J. Phys. Chem., **96** (1992) 7966.
[10] F. Torrens, J. Nanosci. Nanotech., in press.
[11] F. Torrens, Microelectron. Eng., submitted for publication.
[12] F. Torrens, J. Phys. Chem. Solids, submitted for publication.

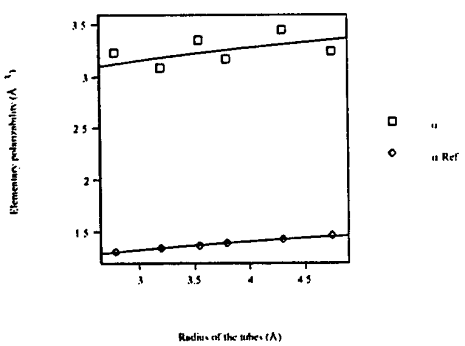

(a)

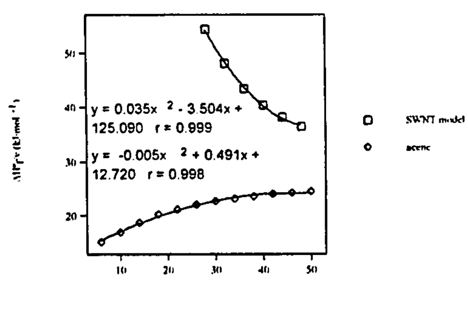

(b)

Fig. 1. Elementary polarizability per atom of the zigzag $(n,0)$ $(7 \leq n \leq 12)$ SWNT models *vs.* the radius of tubes.

Fig. 2. Standard heat of formation per C atom calculated with MOPAC-AM1.

GATE VOLTAGE DEPENDENCE OF TRANSMISSION AND SCATTERING IN NANOTUBE-BASED FIELD EFFECT TRANSISTORS

François Triozon (1), Stephan Roche (1), Angel Rubio (2), and Didier Mayou (3)

(1) Commissariat a l'Energie Atomique, DSM/DRFMC/SPSMS,
17 avenue des Martyrs, 38054 Grenoble Cedex 9, France
(2) DIPC, San Sebastián, Spain
(3) LEPES-CNRS, Grenoble, France

Understanding the precise conduction mechanisms in carbon nanotubes together with the coupling effect with nanoelectrodes is of crucial importance for the further developement of carbon based nanodevices. Today's experiments bring controversial interpretation of field effect on nanotube-based transistors, with a major role played either by the Schottky barrier in between a semiconducting nanotube and metallic contact, or by intrinsic electronic mobilities in the framework of conventional theory of CMOS devices. To investigate simultaneously both scenario it is necessary to employ efficient numerical order N methods that enable both an atomistic description of metal/nanotube contacts, together with a proper accounting of intrinsic scattering within the nanotubes due to the presence of defects, substitutional dopants, or chemisorbed molecular entities. We have developed such a method based on real space calculations and recursion approaches [1]. In this presentation we will first investigate the propagation of electrons in single-wall and multi-wall carbon nanotubes. We analyze how the scattering by structural defects, as well as the inter-tube coupling, both depend on the position of the Fermi level. Second, we consider the effect of a varying electrostatic potential along the nanotube due, for instance, to a potential drop close to the electrodes, or to an applied gate voltage. The transmission coefficients through different potential profiles, in perfect or disordered nanotubes, are compared. Finally a study of transmission in presence of a Schottky barrier in a real nanotube based device is performed, and the main operating regimes outlined. The combination of these transmission and scattering properties provide us with important informations to understand the behaviors of nanotube-based field effect transistors.

References:

[1] F. Triozon, S. Roche, A. Rubio, D. Mayou,
Transport length scales in carbon nanotubes
submitted to Physical Review Letters

S. Roche and R. Saito,
Magnetoresistance in carbon nanotubes : from molecular to mesoscopic fingerprints
Physical Review Letters 87, 246803 (2001).

S. Roche, F. Triozon, A. Rubio, D. Mayou,
Conduction mechanisms in multiwalled carbon nanotubes
Physical Review B 64, 121401(R) (2001).

S. Roche, F. Triozon, A. Rubio, D. Mayou,
Electronic conduction in multiwalled carbon nanotubes: role of intershell
coupling and incommensurability
Physics Letters A 285, 94 (2001).

VISCOELASTIC PROPERTIES OF MULTIWALLED CARBON NANOTUBE SOLUTIONS

Isabel Echeverría

Department of Chemistry, University of Wisconsin,
1101 University Avenue, Madison WI 53706, USA

<u>Antonio Urbina</u>

Departamento de Electrónica, Universidad Politécnica de Cartagena,
C/Doctor Fleming s/n, 30202 Cartagena, Spain

We have prepared solutions of multiwalled carbon nanotubes in very low pressure vapor solvents (a mixture of polychlorinated biphenyls). The solutions are very stable and have shown no sign of precipitation for months. Rheological measurements using anular and Sogel-Pochetino geometries have been performed.

We obtained the real and imaginary part of the complex viscosity coefficient in a frequency range covering eight orders of magnitud and a temperature range form 5 to 50°C. The data shows unexpected changes in the solution with temperature: for T below 20°C there appears to be substantial reorganization or clustering, suggesting incipient formation of a liquid crystalline phase (the solution concentration is at least 1000 times the overlap concentration of the nanotubes). This self-organization could result in a useful technique to improve the electronic properties of polymer/carbon nanotubes composites used in electronic devices, specially organic photovoltaic cells.

ROLE OF SUBSTRATE GEOMETRY IN SLIDING FRICTION

Andrea Vanossi[1], Alan R. Bishop[2], and Virginio Bortolani[1]
(1) INFM-S3 e Dipartimento di Fisica, Università di Modena e Reggio Emilia,
Via Campi 213/A, 41100 Modena, Italy
(2) Theoretical Division and Center for Nonlinear Studies, Los Alamos National Laboratory,
Los Alamos, New Mexico 87545
E-mail: vanossi.andrea@unimo.it

Especially in the emerging discipline of nanosciences, understanding the atomic processes occurring at the interface of two interacting systems in relative motion is central to many technological applications [1].

In the context of solid friction phenomena, we study, via a Frenkel-Kontorova (FK) model approach [2], the role of the substrate potential geometry on the underdamped dynamics of a chain of interacting atoms. The choice of an on-site potential defined by the sum of two sinusoidal functions with different periodicity allows us to simulate microscopic sliding over *simply periodic*, *multiple-well periodic* [3] and *quasiperiodic* substrates [4].

We comment on the nature of the particle dynamics in the vicinity of the *pinning-depinning transition* point and consider the role played by the *coverage variable* on the depinning mechanism. We also investigate on the different *nonlinear excitations* forming during sliding and characterizing the dynamical states observed at different strengths of the imposed driving. The dependence of the *static friction* on the ratio of the model interaction strengths is analyzed in detail and compared to the well-known case of the standard FK model.

Even though an analysis in the presence of a thermal bath would be more exhaustive (Langevin equation approach), we also examine the *hysteretic behaviour* (see, e.g., Fig. 1.) of the chain mobility as a function of the adiabatically varying force at zero temperature.

References:

[1] B. Brushan, J.N. Israelachvili, and U. Landman, Nature (London) **374**, 607 (1995); B. N. J. Persson, *Sliding Friction: Physical Principles and Applications*, Springer-Verlag, Berlin, 2000.
[2] See, e.g., O.M. Braun and Y.S. Kivshar, Phys. Rep. **306**, 1 (1998) and references therein.
[3] A. Vanossi, J. Röder, A.R. Bishop, and V. Bortolani, Phys. Rev. E **67**, 016605 (2003).
[4] A. Vanossi, J. Röder, A.R. Bishop, and V. Bortolani, Phys. Rev. E **63**, 017203 (2001); T.S. van Erp, A. Fasolino, O. Radulescu, and T. Janssen., Phys. Rev. B **60**, 6522 (1999).

Figures:

Fig. 1.

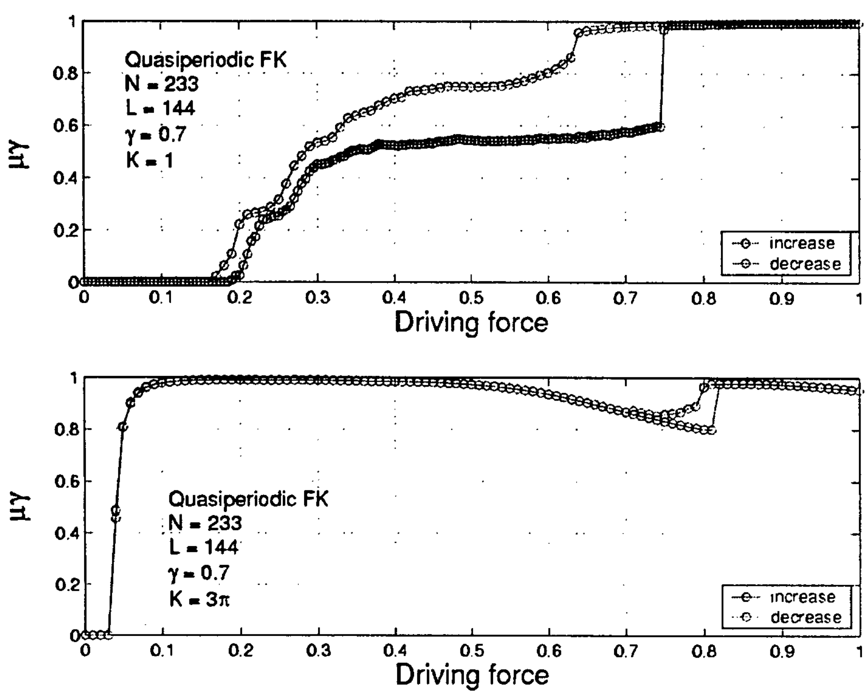

Fig. 1. Dependence of the chain mobility μ on the driving force F for two different values of the interparticle interaction strength K. In this quasiperiodic FK model, the system length and the number of particles in the chain are, respectively, L=144 and N=233 (*golden mean* case). The value of the damping coefficient γ (=0.7) is chosen in the underdamped regime. The colours blue (increasing F) and red (decreasing F) show the hysteretic behaviour of the mobility.

INTERACTION OF INTRINSIC LOCALIZED MODES IN THE GAP OF DOPED SEMICONDUCTORS WITH PLASMONS

A. Franchini[1], V. Bortolani[1], A. Vanossi[1] and R. F. Wallis [2]

(1) INFM-S3 e Dipartimento di Fisica, Università di Modena e Reggio Emilia, Via Campi 213/A, 41100 Modena, Italy
(2) Institute for Surface and Interface Science and Department of Physics and Astronomy, University of California, Irvine, CA 92697 (USA)
E-mail: vanossi.andrea@unimo.it

A theoretical investigation has been made of the interaction of intrinsic localized modes with plasmons. The existence of highly localized modes in anharmonic crystals is by now well established [1]. These modes have been termed intrinsic localized modes (ILMs), reflecting the fact that no external defects are needed for their creation.

In a diatomic chain with realistic potentials, however, Kiselev et al. [2] showed that ILMs arise in the gap between the acoustic and the optical branches. The above treatments are based on the rotating wave approximation (RWA) in which the atomic displacements contain a static part and a vibrational part proportional to $\cos(\omega t)$, where ω is the frequency of the stationary localized mode. Localized vibrational states have been measured in $PtCl_2$ [3].

The anharmonic localized modes for one-dimensional diatomic lattice have been determined in this investigation using a two-body potential which describe the interactions among particles in a zinc-blende structure material. Calculations have been performed for GaN, because of its large gap. A typical displacement pattern of the gap ILM [4] is shown in Fig. 1a.

To study the coupling we have added to the equation of motion of atoms an electric field to produce the plasmon. Solving the system we obtain the dynamical displacements pattern from which we determine the microscopic polarization. The displacement pattern of the ILM coupled with the plasmon is shown in Fig.1b.

Evaluating the macroscopic polarization we can determine the frequency of the combined system for which the dielectric function is zero. In this case a longitudinal disturbance which does not couple to the electric field is possible.

Keywords:
Theoretical methods, models and techniques: Semiempirical models and model calculations, models of nonlinear phenomena

References:

[1] A. J. Sievers and S. Takeno , Phys. Rev. Lett. **61**, 97 (1988); A. Franchini, V. Bortolani and R.F. Wallis, Phys. Rev. B **53**, 5420 (1996).
[2] S.A. Kiselev and A.J. Sievers, Phys. Rev. B **55**, 5755 (1997).
[3] B.I. Swanson et al, Phys. Rev. Lett. **82**, 3288 (1999).
[4] A. Franchini, V. Bortolani and R.F. Wallis, J. Phys. Cond. Matter **12**, 5629 (2000).

Figures:

Fig. 1.

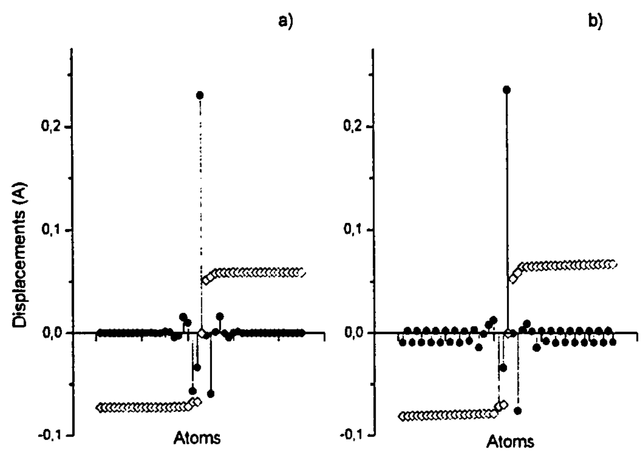

Fig. 1. Panel a) gap ILM at ? = 558 cm^{-1}. The diamonds indicate the static diplacements; panel b) ILM coupled with the plasma oscillation.

SYNTHESIS, PHOTOPHYSICAL PROPERTIES AND NANO-CRYSTAL FORMATION OF A NEW CLASS OF TETRA-N-SUBSTITUTED PERYLENES*

René M. Williams, Lutz H. Gade, Christian H. Galka,
Luisa De Cola, Mary McPartlin, Bin Dong and Lifeng Chi

Prof. L. H. Gade, Dr. C. H. Galka, Laboratoire de Chimie Organométallique et de Catalyse (UMR 7513), Institut Le Bel, Université Louis Pasteur, 4, rue Blaise Pascal, 67070 Strasbourg (France)

Prof. L. De Cola, Dr. R. M. Williams, Molecular Photonic Materials, Institute of Molecular Chemistry, Universiteit van Amsterdam, Nwe Achtergracht 166, 1018 WV Amsterdam (The Netherlands)

Prof. M. McPartlin, School of Applied Chemistry, University of North London, Holloway Road, London N7 8DB (U.K.)

Priv.-Doz. Dr. L. Chi, B. Dong, Physikalisches Institut,, Westfälische-Wilhelms-Universität Münster, Wilhelm Klemm Str 10, D-48149 Münster (Germany)

* This work will appear in Angewandte Chemie 23, 2003

A new class of perylene-derived dyes, tetra(carboxamido)perylenes has been obtained by a generally applicable synthetic method. Derivative **A** is shown to form nano-crystalline aggregates in DMSO which display significantly modified photophysical behaviour with respect to the monomer and which were studied using AFM techniques.

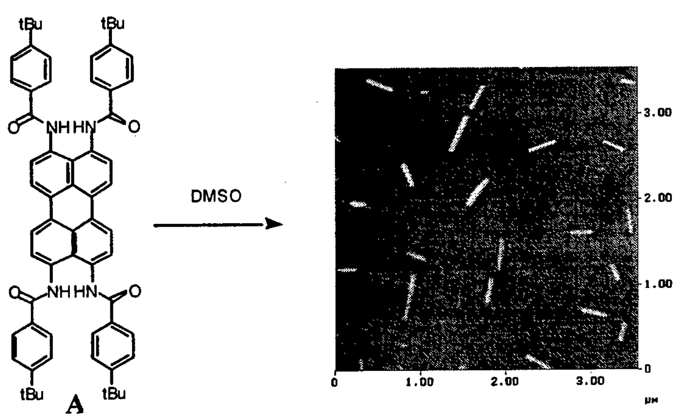

Perylenes as pigments and fluorescent dyes have found wide ranging applications in very diverse fields of current research.[1-3] There are very few examples of tetra-N-substituted perylenes to be found in the literature to date which is due to the cumbersome nature of the established preparative methodes.[4] We recently discovered a novel and efficient route to 4,9-diaminoperylenequinone-3,10,-diimines[5] and showed that it is possible to convert these quinoidal systems to the reduced 3,4,9,10-tetraaminoperylenes,[6] a class of compounds which has very recently been cited in the patent literature of photovoltaic devices.[7]

The UV-vis absorption spectra of compound **B** in dichloromethane turned out to be virtually concentration independent. However, whereas compound **A** is only sparingly soluble

in dichloromethane, its behaviour in dimethylsulfoxide (DMSO) is very different and at high concentrations (10^{-2} M) gives rise to magenta solutions which display significantly changed photophysics. The absorption is strongly red-shifted and broadened relative to the monomer, with a maximum at 574 nm while the emission of the aggregated form is located at 690 nm, and has much lower quantum yield (10^{-2}).

A fresh magenta solution of the compound at high concentration (10^{-2} M) was studied with scanning probe microscopy (AFM-tapping mode) (see Figure).[8]

The sample consists of long rod type structures with a length between 100 and 400 nm, a width of approximately 40 nm and a height of only 2 nm. The observed structures can best be described as nano-crystals.[9] Related structures have been studied[9] which were made by the reprecipitation method (involving injection of perylene-solutions into hot water). They can be considered a special form of "Scheibe" or *J* aggregates because of their linear rod type shape even though we do not have a direct spectroscopic evidence of their nature. It is worth to notice however that the solvent, DMSO, plays a major role in the formation of the rods and it is the only solvent in which was possible to grow such nanocrystals.

[1] H. Zollinger, *Color Chemistry*, 2nd ed., VCH, Weinheim, **1991**;

[2] H. Langhals, H. Jaschke, U. Ring, P. von Unold, *Angew. Chem.* **1999**, *111*, 143; *Angew. Chem. Int. Ed.* **1999**, *38*, 201;

[3] C. W. Struijk, A. B. Sieval, J. E. J. Dakhorst, M. van Dijk, P. Kimkes, R. B. M. Koehorst, H. Donker, T. J. Schaafsma, S. J. Picken, A. M. van de Craats, J. M. Warman, H. Zuilhof, E. J. R. Sudhölter, *J. Am. Chem. Soc.* **2000**, *122*, 11057

[4] A. Zinke, E. Unterkreuter, *Monatsh. f. Chem.* **1919**, *40*, 405; b) A. Zinke, W. Hirsch, E. Brozek, *Monatsh. f. Chem.* **1929**, *51*, 205.

[5] K. W. Hellmann, C. H. Galka, I. Rüdenauer, L. H. Gade, I. J. Scowen, M. McPartlin, *Angew. Chem.* **1998**, *110*, 2053; *Angew. Chem. Int. Ed.* **1998**, *37*, 1948; b) K. W. Hellmann, C. H. Galka, L. H. Gade, A. Steiner, D. S. Wright, T. Kottke, D. Stalke, *Chem. Commun.* **1998**, 549.

[6] L. H. Gade, C. H. Galka, K. W. Hellmann, R. M. Williams, L. De Cola, I. J. Scowen, M. McPartlin, *Chem. Eur. J.* **2002**, *8*, 3732.

[7] a) M. Tamano, S. Maki (Toyo Ink MFG Co., Ltd), EP 0965629A, **1999**; b) S. Onikubo, M. Tamano (Toyo Ink MFG Co., Ltd), JP 2000150152A, **2000**; c) S. Onikubo, M. Tamano (Toyo Ink MFG Co., Ltd), JP 2000150161A, **2000**; d) M. Tamano, S. Onikubo (Toyo Ink MFG Co., Ltd), JP 2000068058A, **2000**.

[8] For SFM investigations, the substance was dissolved in DMSO and dropped onto freshly cleaved mica surfaces. SFM inspections were performed with a commercial instrument (Digital Instruments. Nanoscope IIIa, Dimension 3000, Santa Barbara, CA) running in tapping mode. Silicon cantilevers (Nanosensors) with a resonant frequency of 250-350 kHz were used for the experiments. AFM images obtained under identical conditions with compound **3** from a saturated dichloromethane only displaed featureless aggregation which indicates that this phenomenon is directly associated with the incorporation of the solvent.

[9] a) T. Onodera, T. Oshikiri, H. Katagi, H. Kasai, S. Okada, H. Oikawa, M. Terauchi, M. Tanaka, and H. Nakanishi, *J. Cryst. Growth*, **2001**, *229*, 586-590; b) J. I. Niitsuma, T. Fujimura, T. Itoh, H. Kasai, S. Okada, H. Oikawa, and H. Nakanishi, *Int. J. Mod. Phys. B*, **2001**, *15*, 3901-3903; c) H. Kasai, H. S. Nalwa, H. Oikawa, S. Okada, H. Matsuda, N. Minami, A. Kakuta, K. Ono, A. Mukoh, and H. Nakanishi, *Jpn. J. Appl. Phys. Part 2 - Lett.*, **1992**, *31*, L1132-L1134; d) D. A. Higgins and P. F. Barbara, *J. Phys. Chem.*, **1995**, *99*, 3-7; e) D. A. Higgins, J. Kerimo, D. A. VandenBout, and P. F. Barbara, *J. Am. Chem. Soc.*, **1996**, *118*, 4049-4058; f) H. Yao, S. Sugiyama, R. Kawabata, H. Ikeda, O. Matsuoka, S. Yamamoto, and N. Kitamura, *J. Phys. Chem. B*, **1999**, *103*, 4452-4456; g) J. A. Tuszynski, M. F. Jorgensen, and D. Mobius, *Phys. Rev. E*, **1999**, *59*, 4374-4383.

ELECTRONIC STRUCTURE OF DOUBLE BARRIER InAs/InP NANOWIRES

Matthew Zervos and Lou-Fe′ Feiner.

Philips Research Laboratories , Prof.Holstlaan 4, 5656 AA, Eindhoven, The Netherlands.
e-mail : zervos@natlab.research.philips.com

We study in the effective mass approximation the electronic structure of an n-type InAs quantum wire (QWire) with built-in InAs/InP heterojunctions via self consistent Poisson-Schrödinger (SCPS) calculations in cylindrical coordinates. Rapid convergence and efficiency are achieved by (i) a suitable transformation of the radial part of the Hamiltonian matrix thereby maintaining symmetry (ii) using quantum mechanical perturbation theory to derive an expression for the change in electron density with electrostatic potential.

We calculate the energy levels in a 150Å long InAs QDot surrounded by 50Å strained InP barriers within an InAs QWire of radius 200Å having a doping level of 1×10^{16} cm^{-3} and conduction band discontinuities of $\delta E_C = 0.6$ eV. In equilibrium there are two QDot states at 15 meV and 110 meV above the Fermi level. We find that upon variation of the applied source-drain voltage V_{sd}, the entire structure gets into resonance at $V_{sd} = 88$ mV. This is in good agreement with an experimental study of resonant tunnelling in a nominally un-doped InAs/InP QWire of similar dimensions, grown in the [111] direction, where resonance was detected at 80 mV, and a small shift (< 5mV) in its position occurred upon inverting the voltage polarity. We rule-out barrier asymmetry, band-bending due to impurities or defects and contact effects as being the origin of the current asymmetry and attribute it to the strain induced piezoelectric charges at the InP/InAs interfaces.

EXPLORING THE ELECTRIC PROPERTIES OF METALLOPROTEIN AT MOLECULAR LEVEL

Jianwei Zhao and Jason J. Davis*

Inorganic Chemistry Laboratory South Parks Road, Oxford, OX1 3QR;
Bionanotechnology IRC, Clarendon Laboratory, Parks Road,Oxford OX1 3PU UK

Understanding how electrons transfer through protein is of essential importance in life science and exploiting new molecular electronic devices.

In order to reveal intrinsic electron transfer properties, one requires providing a versatile technique at molecular level.

In present work, the electron transfer through metalloprotein was investigated using conducting atomic force microscopy by assembling the protein molecules on the gold-coated conducting tip, which was then in contact with highly oriented pyrolytic graphite (HOPG). The electric stability was studied at a force load less than 2 nN. Dielectric breakdown took place at a bias higher than a critical value at either positive or negative polarization. Obvious current flow at small bias can be observed when the force is beyond 5 nN. Current-bias (I-V) curves recorded under various tip force loads were used to estimate the resistance of protein at molecular level.

A theoretical interpretation of the results, based on a force modulation of protein electric and mechanical properties will be presented.

PATENTING NANOTECHNOLOGY INVENTIONS IN THE US

Raj Bawa, Ph.D., Patent Agent[1]

President, Bawa Biotechnology Consulting, LLC, Arlington, VA and Adjunct Assistant Professor, Rensselaer Polytechnic Institute, Troy, NY, USA

Obtaining and protecting intellectual property rights is economically critical to any research enterprise interested in commercialization. Patents are the strongest form of intellectual property protection and are essential to the growth of a nanotechnology company. As in the case of biotechnology and information technology, patents will also play a critical role in the success of the global nanotechnology revolution. As companies develop the products and processes of nanotechnology, and begin to seek commercial applications for their inventions, securing valid and defensible patent protection will be vital to their long-term survival. Nanotechnology is in its infancy. Not only is it an emerging technology, it is multidisciplinary in nature. Therefore, patenting in this field poses unique opportunities as well as challenges. The full-length paper will present key patent strategies for a small tech inventor. Examples are derived from nanobiotechnology, pharmaceutical sciences, and biotechnology. The paper will also address the role of the US Patent and Trademark Office, as this federal agency struggles with evaluating nanoscience-related patent applications.

[1] **Address for Correspondence:** Bawa Biotechnology Consulting, LLC, 1801 Crystal Drive, Suite 907, Arlington, VA 22202
E-mail: doctorhockey@aol.com
Tel.: 703-271-1240; 703-582-1745
FAX: 703-271-8588
Key Words: patent, nanotechnology, invention, commercialization, small tech

TNT 2003
Trends in Nanotechnology

INDEX

ALPHABETICAL ORDER

Presenting Author		Country		Page
Abdel Mottaleb	Mohamed	Germany	Poster PB1	281
Acharya	Somobrata	Israel	Poster PB2	283
Agulo	Ian Jasper	Sweden	Poster PA1	1
Akiba	Uichi	Japan	Poster PB3	285
Alonso	Julio A.	Spain	Poster PB4	287
Alonso Cotta	Monica	Brazil	Poster PB5	289
			Poster PB6	291
Alvarez-Sanchez	Ruben	Spain	Poster PA2	3
Ambrosio	Antonio	Italy	Poster PA3	5
Arbiol	Jordi	Spain	Poster PB7	293
Arnold	Walter	Germany	Poster PB8	295
Artiaga	Ramón	Spain	Poster PB9	297
Asenjo	Agustina	Spain	Poster PB10	299
Auguste	Denis	Belgium	Poster PA4	7
Auvray	Stephane	France	Poster PA5	9
Avram	Marioara	Romania	Poster PA6	11
Axelrod	Eikaterina	Israel	Poster PA7	13
Axmann	Yvonne	Switzerland	Poster PA8	15
Ayuela	Andres	Spain	Poster PA9	17
Azzaroni	Omar	Spain	Poster PA10	19
Babarada	Florin	Romania	Poster PB11	301
Baciu	Anca Mihaela	Romania	Poster PA11	21
Balcells	Lluis	Spain	Poster PB12	303
Balocco	Claudio	UK	Poster PA12	23
Barberan	Nuria	Spain	Poster PB13	305
Bautista	Mª Carmen	Spain	Poster PB14	307
Bawa	Raj	US	Poster PB123	525
Bednarz	Lukasz	Belgium	Poster PA13	25
Beecher	Paul	Ireland	Poster PA14	27
Bengochea	Ana	Spain	Poster PA15	29
Berman	Amir	Israel	Poster PB15	309
Betancourt Riera	Ricardo	Mexico	Poster PA16	31
Bhusal	Leknath	USA	Poster PA17	33
Bini	Simone	Italy	Poster PA18	35
Blasi	Laura	Italy	Poster PB16	311
Borondo	Florentino	Spain	Poster PB17	313
Brummer	Maya	Israel	Poster PA19	37
Burke	Sarah	Canada	Poster PA20	39
Burns	Scott	USA	Poster PA21	41
Callejas	Alicia	Spain	Poster PB18	315
Castro-Couceiro	Ada	Spain	Poster PA22	43
Casuso	Ignacio	Spain	Poster PA23	45

Cerqueira	Fatima	Portugal	Poster PB19	317
Ciobanu	Gabriela	Romania	Poster PB22	323
Ciuparu	Dragos	USA	Poster PB23	325
Clavijo	Celio	Germany	Poster PA26	51
Cohen	Yehezkel	Israel	Poster PA27	53
Cohen	Jacob	Israel	Poster PB24	327
Conoci	Sabrina	Italy	Poster PB25	329
Cordon	Javier	Spain	Poster PA28	55
Coronas	Joaquin	Spain	Poster PB26	331
			Poster PB27	333
Costa	Manuel	Portugal	Poster PB28	335
Crittenden	Scott	USA	Poster PA29	57
Cui	Hai-Ning	Portugal	Poster PA30	59
Cwilich	Gabriel	USA	Poster PB29	337
Chastellain	Mathieu	Switzerland	Poster PA24	47
Choi	Seong	Korea	Poster PB20	319
Chubykalo	Oksana	Spain	Poster PB21	321
Chun	Ai Lin	USA	Poster PA25	49
De La Fuente	Cesar	Spain	Poster PB30	339
De Toro	Jose Angel	Spain	Poster PB31	341
Dickey	Michael	USA	Poster PA31	61
Dimaki	Maria	Denmark	Poster PA32	63
Docter	Margreet W.	Netherlands	Poster PA33	65
Domingues	Gilberto	France	Poster PA34	67
Doppiu	Stefania	Spain	Poster PB32	343
Duque Calvo	Fernando	Spain	Poster PA35	69
Efrima	Shlomo	Israel	Poster PB33	345
Eisenmenger	Johannes	Germany	Poster PA36	71
Elbaile	Laura	Spain	Poster PA37	73
Elizalde	Eduardo	Spain	Poster PB34	347
Engström	Olof	Sweden	Poster PB35	349
Feiner	Louis F.	Netherlands	Poster PB36	351
Forsberg	Erik	Sweden	Poster PB37	353
Froufe	Luis	Spain	Poster PA38	75
			Poster PA39	76
Fuentes Garcia	Manuel	Spain	Poster PA40	79
Gabriel Buguña	Gemma	Spain	Poster PA41	81
Galvao	Douglas	Brazil	Poster PB38	355
			Poster PB39	357
Galloo	Jean-Sebastien	France	Poster PA42	83
Garcia	Miguel Angel	Spain	Poster PB40	359
Garcia Martin	Antonio	Spain	Poster PB41	361
Garcia Martinez	Yamila	Spain	Poster PA43	85
Garcia Prieto	Ana	Spain	Poster PA44	87

Garcia Sanchez	Felipe	Spain	Poster PA45	89
Garcia Suarez	Victor Manuel	Spain	Poster PA46	91
			Poster PA47	93
Ge	Xin	Germany	Poster PA48	95
Gerber	Andreas	Germany	Poster PA49	97
Golan	Yuval	Israel	Poster PB42	363
Gomez Cuesta	Ignacio	Spain	Poster PB43	365
Gomez Medina	Raquel	Spain	Poster PA50	99
Gomez Moñivas	Sacha	Spain	Poster PB44	367
Gomez Navarro	Cristina	Spain	Poster PA51	101
Gomila	Gabriel	Spain	Poster PB45	369
Gonzalez Ferez	Rosario	Germany	Poster PB46	371
Gonzalez Perez	Juan Carlos	Brazil	Poster PB47	373
Gourdon	Delphine	USA	Poster PB48	375
Graf	Herbert	Germany	Poster PA52	103
Granados Ruiz	Daniel	Spain	Poster PA53	105
Grigoriev	Anton	Sweden	Poster PA54	107
Guzman de Villoria	Roberto	Spain	Poster PA55	109
			Poster PA56	111
Hackens	Benoit	Belgium	Poster PA57	113
Han	Jie	Netherlands	Poster PA58	115
Hernando Campos	Jordi	Netherlands	Poster PB49	377
Herranz	Gervasi	Spain	Poster PA59	117
Hofmann	Stephan	UK	Poster PA60	119
Horansky	Robert	USA	Poster PA61	121
Jacob	David	Spain	Poster PA62	123
Jacob	Ajey	Sweden	Poster PB50	379
Jimenez	David	Spain	Poster PB51	381
Kabir	Mohammad	Sweden	Poster PA63	125
Karthäuser	Silvia	Germany	Poster PB52	383
Kinaret	Jari	Sweden	Poster PB53	385
Kipferl	Wolfgang	Germany	Poster PA64	127
Kiricsi	Imre	Hungary	Poster PB54	387
Konya	Zoltan	Hungary	Poster PB55	389
Kuramochi	Hiromi	Japan	Poster PB56	391
Langlais	Veronique	Spain	Poster PB57	393
			Poster PB58	395
Ledenyov	Viktor	Ukraine	Poster PA65	129
Lemme	Max	Germany	Poster PA66	131
Levy	Raphael	UK	Poster PB59	397
Liang	Gengchiau	USA	Poster PA67	133
Lisenkov	Sergei	Russia	Poster PA68	135
Liu	Yi	Canada	Poster PA69	137
Lopez	Rosa	Switzerland	Poster PB60	399

Luna	Carlos	Spain	Poster PA70	139
Machado	Eduardo	Spain	Poster PA71	141
Makovec	Darko	Slovenia	Poster PB61	401
Malyvshev	Andrei	Spain	Poster PB62	403
Malyvshev	Andrei	Spain	Poster PB63	405
Marcos Villa	Pedro Angel	Spain	Poster PB64	407
Marliere	Sylvain	France	Poster PA72	143
			Poster PA73	145
Marsal Berenguel	Roser	Spain	Poster PA74	147
Martinez	Benjamin	Spain	Poster PB65	409
Martinez	Maria Teresa	Spain	Poster PB66	411
Mas Torrent	Marta	Netherlands	Poster PB67	413
Maury	Pascale	Netherlands	Poster PA75	149
Maximov	Ivan	Sweden	Poster PB68	415
Mekhalif	Zineb	Belgium	Poster PB69	417
			Poster PB70	419
			Poster PB71	421
Melle-Franco	Manuel	Italy	Poster PB72	423
Mena-Osteritz	Elena	germany	Poster PB73	425
Mendes	Paula	UK	Poster PB74	427
Mendoza	Raquel	Spain	Poster PA76	151
Mendoza	Ernest	UK	Poster PB75	429
Miles	Mervyn	UK	Poster PB76	431
Minoux	Eric	France	Poster PA77	153
Molhave	Kristian	Denmark	Poster PA78	155
Monge	Miguel	France	Poster PB77	433
Montes	Laurent	France	Poster PB78	435
Moshkalyov	Stanislav	Brazil	Poster PB79	437
Murillo	Nieves	Spain	Poster PA79	157
			Poster PA80	159
			Poster PA81	161
Nascov	Victor	Romania	Poster PA82	163
Negri	Fabrizia	Italy	Poster PB80	439
			Poster PB81	441
Niedbala	Jolanta	Poland	Poster PB82	443
Nikolic	Konstantin	UK	Poster PB83	445
Nikolov	Ivan	Bulgaria	Poster PB84	447
Nita	Florin	France	Poster PB85	449
Nogueira da Silva	Maria Ivonete	Brazil	Poster PB86	451
O'Brien	Garret	Ireland	Poster PA83	165
Ogando	Eduardo	Spain	Poster PA84	167
Ortega	Enrique	Spain	Poster PB87	453
O'Shea	Sean	Singapore	Poster PB88	455
Otero	Roberto	Denmark	Poster PB89	457

Pegaz	Bernadette	Switzerland	Poster PA85	169
Pekala	Krystina	Poland	Poster PB90	459
Pekala	Marek	Poland	Poster PB91	461
Perales Eceiza	Alvaro	Spain	Poster PA86	171
Perea	Jose Ignacio	Spain	Poster PA87	173
Perez Fernandez	Mª Jose	Spain	Poster PA88	175
Perez Junquera	Alejandro	Spain	Poster PA89	177
Perez Santos	Susana	Spain	Poster PB92	463
Persano	Luana	Italy	Poster PA90	179
Peter	Amal John	India	Poster PB93	465
Pichonat	Emmanuelle	France	Poster PB94	467
Pignataro	Bruno	Italy	Poster PB95	469
Pisignano	Dario	Italy	Poster PA91	181
Pita	Marcos	Spain	Poster PA92	183
Pomerantz	Richard	USA	Poster PA93	185
Ponomareva	Inna	Russia	Poster PA94	187
Popczyk	Magdalena	Poland	Poster PB96	471
Portinha	Anibal	Portugal	Poster PA95	189
Pozas Bravos	Raul	Spain	Poster PA96	191
Puente	Antonio	Spain	Poster PB97	473
Rakshit	Titash	USA	Poster PA97	193
Ranchal	Rocio	Spain	Poster PA98	195
Ratera	Imma	USA	Poster PA99	197
Rendon	Otto	Venezuela	Poster PA100	199
Rengel Estevez	Raul	Spain	Poster PB98	475
Restrepo	Alexandre	Spain	Poster PA101	201
Riikonen	Sampsa	Spain	Poster PA102	203
Robinson	Luke	UK	Poster PA103	205
Rodriguez	Isabel	Singapore	Poster PB99	477
Rodriguez Contreras	Julio	Germany	Poster PA104	207
Round	Andy	UK	Poster PB100	479
Royo Pascual	Carlos	Spain	Poster PB101	481
Ruiz Perez	Catalina	Spain	Poster PB102	483
Ruths	Marina	Finland	Poster PB103	485
Saal	Kristjan	Estonia	Poster PA105	209
Sanchez	David	Switzerland	Poster PB104	487
			Poster PB105	489
Sanchez Lotero	Pedro Nel	Spain	Poster PA106	211
Sanchez Portal	Daniel	Spain	Poster PB106	491
Santalla Arribas	Silvia Noemi	Spain	Poster PA107	213
			Poster PA108	215
Sarangi	Debajyoti	Switzerland	Poster PB107	493
			Poster PB108	495

Sato	Fuminobu	Japan	Poster PA109	217
Seeger	Torsten	Spain	Poster PB109	497
Semenova	Elizaveta	Russia	Poster PA110	219
Sergueev	Nikolai	Canada	Poster PA111	221
Shaposnikov	Victor Manuel	Portugal	Poster PB110	499
Sinapi	Fabrice	Belgium	Poster PA112	223
			Poster PA113	225
Sobolev	Nikolai	Portugal	Poster PB111	501
Solomon	Gemma	Australia	Poster PA114	227
Sterian	Andrea Rodica	Romania	Poster PA115	229
Sterian	Paul	Romania	Poster PB112	503
Stires	John	USA	Poster PA116	231
Subramanian	Kavasseri	UK	Poster PA117	233
Sukyte	Judita	Lithuania	Poster PB113	505
Tamborra	Michaela	Italy	Poster PA118	235
Tanasa	Gheorghe	Netherlands	Poster PA119	237
Tantussi	Francesco	Italy	Poster PA120	239
Tarrazo Antelo	Teresa	Spain	Poster PA121	241
Tätte	Tanel	Estonia	Poster PA122	243
Taylor	Laura	USA	Poster PA123	245
Teobaldi	Gilberto	Italy	Poster PA124	247
Teva Meroño	Jordi	Spain	Poster PA125	249
Thomas	Marjorie	France	Poster PA126	251
Tirosh	Shay	Israel	Poster PA127	253
Toimil Molares	Maria Eugenia	Germany	Poster PB114	507
Tombolini	Francesca	Italy	Poster PA128	255
Torrens	Francisco	Spain	Poster PB115	509
Triozon	Francois	France	Poster PB116	511
Urbina	Antonio	Spain	Poster PB117	513
Van Bruggen	Martin	Netherlands	Poster PA129	257
Vanossi	Andrea	Italy	Poster PB118	515
			Poster PB119	517
Vasallo	Beatriz G.	Spain	Poster PA130	259
Vasilyev	Alexey	Russia	Poster PA131	261
Vast	Laurence	Belgium	Poster PA132	263
Vicary	James	UK	Poster PA133	265
Villarroya	Maria	Spain	Poster PA134	267
Wakamatsu	Satoshi	Japan	Poster PA135	269
Welter	Steve	Netherlands	Poster PA136	271
Williams	Rene M.	Netherlands	Poster PB120	519
Wouters	Daniel	Netherlands	Poster PA137	273
Yamada	Toyokazu	Netherlands	Poster PA138	275
Yang	Heesun	USA	Poster PA139	277
Yang	Ming-Hsun	UK	Poster PA140	279

Zervos	Matthew	Netherlands	Poster PB121	521
Zhao	Jianwei	UK	Poster PB122	523

TNT 2003
Trends in Nanotechnology

INDEX

SESSION A / SESSION B

Presenting Author		Country		Page
Agulo	Ian Jasper	Sweden	Poster PA1	1
Alvarez-Sanchez	Ruben	Spain	Poster PA2	3
Ambrosio	Antonio	Italy	Poster PA3	5
Auguste	Denis	Belgium	Poster PA4	7
Auvray	Stephane	France	Poster PA5	9
Avram	Marioara	Romania	Poster PA6	11
Axelrod	Eikaterina	Israel	Poster PA7	13
Axmann	Yvonne	Switzerland	Poster PA8	15
Ayuela	Andres	Spain	Poster PA9	17
Azzaroni	Omar	Spain	Poster PA10	19
Baciu	Anca Mihaela	Romania	Poster PA11	21
Balocco	Claudio	UK	Poster PA12	23
Bednarz	Lukasz	Belgium	Poster PA13	25
Beecher	Paul	Ireland	Poster PA14	27
Bengochea	Ana	Spain	Poster PA15	29
Betancourt Riera	Ricardo	Mexico	Poster PA16	31
Bhusal	Leknath	USA	Poster PA17	33
Bini	Simone	Italy	Poster PA18	35
Brummer	Maya	Israel	Poster PA19	37
Burke	Sarah	Canada	Poster PA20	39
Burns	Scott	USA	Poster PA21	41
Castro-Couceiro	Ada	Spain	Poster PA22	43
Casuso	Ignacio	Spain	Poster PA23	45
Chastellain	Mathieu	Switzerland	Poster PA24	47
Chun	Ai Lin	USA	Poster PA25	49
Clavijo	Celio	Germany	Poster PA26	51
Cohen	Yehezkel	Israel	Poster PA27	53
Cordon	Javier	Spain	Poster PA28	55
Crittenden	Scott	USA	Poster PA29	57
Cui	Hai-Ning	Portugal	Poster PA30	59
Dickey	Michael	USA	Poster PA31	61
Dimaki	Maria	Denmark	Poster PA32	63
Docter	Margreet W.	Netherlands	Poster PA33	65
Domingues	Gilberto	France	Poster PA34	67
Duque Calvo	Fernando	Spain	Poster PA35	69
Eisenmenger	Johannes	Germany	Poster PA36	71
Elbaile	Laura	Spain	Poster PA37	73
Froufe	Luis	Spain	Poster PA38	75
			Poster PA39	77
Fuentes Garcia	Manuel	Spain	Poster PA40	79
Gabriel Buguña	Gemma	Spain	Poster PA41	81
Galloo	Jean-Sebastien	France	Poster PA42	83
Garcia Martinez	Yamila	Spain	Poster PA43	85
Garcia Prieto	Ana	Spain	Poster PA44	87

Garcia Sanchez	Felipe	Spain	Poster PA45	89
Garcia Suarez	Victor Manuel	Spain	Poster PA46	91
			Poster PA47	93
Ge	Xin	Germany	Poster PA48	95
Gerber	Andreas	Germany	Poster PA49	97
Gomez Medina	Raquel	Spain	Poster PA50	99
Gomez Navarro	Cristina	Spain	Poster PA51	101
Graf	Herbert	Germany	Poster PA52	103
Granados Ruiz	Daniel	Spain	Poster PA53	105
Grigoriev	Anton	Sweden	Poster PA54	107
Guzman de Villoria	Roberto	Spain	Poster PA55	109
			Poster PA56	111
Hackens	Benoit	Belgium	Poster PA57	113
Han	Jie	Netherlands	Poster PA58	115
Herranz	Gervasi	Spain	Poster PA59	117
Hofmann	Stephan	UK	Poster PA60	119
Horansky	Robert	USA	Poster PA61	121
Jacob	David	Spain	Poster PA62	123
Kabir	Mohammad	Sweden	Poster PA63	125
Kipferl	Wolfgang	Germany	Poster PA64	127
Ledenyov	Viktor	Ukraine	Poster PA65	129
Lemme	Max	Germany	Poster PA66	131
Liang	Gengchiau	USA	Poster PA67	133
Lisenkov	Sergei	Russia	Poster PA68	135
Liu	Yi	Canada	Poster PA69	137
Luna	Carlos	Spain	Poster PA70	139
Machado	Eduardo	Spain	Poster PA71	141
Marliere	Sylvain	France	Poster PA72	143
			Poster PA73	145
Marsal Berenguel	Roser	Spain	Poster PA74	147
Maury	Pascale	Netherlands	Poster PA75	149
Mendoza	Raquel	Spain	Poster PA76	151
Minoux	Eric	France	Poster PA77	153
Molhave	Kristian	Denmark	Poster PA78	155
Murillo	Nieves	Spain	Poster PA79	157
			Poster PA80	159
			Poster PA81	161
Nascov	Victor	Romania	Poster PA82	163
O'Brien	Garret	Ireland	Poster PA83	165
Ogando	Eduardo	Spain	Poster PA84	167
Pegaz	Bernadette	Switzerland	Poster PA85	169
Perales Eceiza	Alvaro	Spain	Poster PA86	171
Perea	Jose Ignacio	Spain	Poster PA87	173
Perez Fernandez	Mª Jose	Spain	Poster PA88	175
Perez Junquera	Alejandro	Spain	Poster PA89	177
Persano	Luana	Italy	Poster PA90	179

Pisignano	Dario	Italy	Poster PA91	181
Pita	Marcos	Spain	Poster PA92	183
Pomerantz	Richard	USA	Poster PA93	185
Ponomareva	Inna	Russia	Poster PA94	187
Portinha	Anibal	Portugal	Poster PA95	189
Pozas Bravos	Raul	Spain	Poster PA96	191
Rakshit	Titash	USA	Poster PA97	193
Ranchal	Rocio	Spain	Poster PA98	195
Ratera	Imma	USA	Poster PA99	197
Rendon	Otto	Venezuela	Poster PA100	199
Restrepo	Alexandre	Spain	Poster PA101	201
Riikonen	Sampsa	Spain	Poster PA102	203
Robinson	Luke	UK	Poster PA103	205
Rodriguez Contreras	Julio	Germany	Poster PA104	207
Saal	Kristjan	Estonia	Poster PA105	209
Sanchez Lotero	Pedro Nel	Spain	Poster PA106	211
Santalla Arribas	Silvia Noemi	Spain	Poster PA107	213
			Poster PA108	215
Sato	Fuminobu	Japan	Poster PA109	217
Semenova	Elizaveta	Russia	Poster PA110	219
Sergueev	Nikolai	Canada	Poster PA111	221
Sinapi	Fabrice	Belgium	Poster PA112	223
			Poster PA113	225
Solomon	Gemma	Australia	Poster PA114	227
Sterian	Andrea Rodica	Romania	Poster PA115	229
Stires	John	USA	Poster PA116	231
Subramanian	Kavasseri	UK	Poster PA117	233
Tamborra	Michaela	Italy	Poster PA118	235
Tanasa	Gheorghe	Netherlands	Poster PA119	237
Tantussi	Francesco	Italy	Poster PA120	239
Tarrazo Antelo	Teresa	Spain	Poster PA121	241
Tätte	Tanel	Estonia	Poster PA122	243
Taylor	Laura	USA	Poster PA123	245
Teobaldi	Gilberto	Italy	Poster PA124	247
Teva Meroño	Jordi	Spain	Poster PA125	249
Thomas	Marjorie	France	Poster PA126	251
Tirosh	Shay	Israel	Poster PA127	253
Tombolini	Francesca	Italy	Poster PA128	255
Van Bruggen	Martin	Netherlands	Poster PA129	257
Vasallo	Beatriz G.	Spain	Poster PA130	259
Vasilyev	Alexey	Russia	Poster PA131	261
Vast	Laurence	Belgium	Poster PA132	263
Vicary	James	UK	Poster PA133	265
Villarroya	Maria	Spain	Poster PA134	267
Wakamatsu	Satoshi	Japan	Poster PA135	269
Welter	Steve	Netherlands	Poster PA136	271

Wouters	Daniel	Netherlands	Poster PA137	273
Yamada	Toyo Kazu	Netherlands	Poster PA138	275
Yang	Heesun	USA	Poster PA139	277
Yang	Ming-Hsun	UK	Poster PA140	279

Presenting Author		Country		Page
Abdel Mottaleb	Mohamed	Germany	Poster PB1	281
Acharya	Somobrata	Israel	Poster PB2	283
Akiba	Uichi	Japan	Poster PB3	285
Alonso	Julio A.	Spain	Poster PB4	287
Alonso Cotta	Monica	Brazil	Poster PB5	289
			Poster PB6	291
Arbiol	Jordi	Spain	Poster PB7	293
Arnold	Walter	Germany	Poster PB8	295
Artiaga	Ramón	Spain	Poster PB9	297
Asenjo	Agustina	Spain	Poster PB10	299
Babarada	Florin	Romania	Poster PB11	301
Balcells	Lluis	Spain	Poster PB12	303
Barberan	Nuria	Spain	Poster PB13	305
Bautista	Mª Carmen	Spain	Poster PB14	307
Berman	Amir	Israel	Poster PB15	309
Blasi	Laura	Italy	Poster PB16	311
Borondo	Florentino	Spain	Poster PB17	313
Callejas	Alicia	Spain	Poster PB18	315
Cerqueira	Fatima	Portugal	Poster PB19	317
Choi	Seong	Korea	Poster PB20	319
Chubykalo	Oksana	Spain	Poster PB21	321
Ciobanu	Gabriela	Romania	Poster PB22	323
Ciuparu	Dragos	USA	Poster PB23	325
Cohen	Jacob	Israel	Poster PB24	327
Conoci	Sabrina	Italy	Poster PB25	329
Coronas	Joaquin	Spain	Poster PB26	331
			Poster PB27	333
Costa	Manuel	Portugal	Poster PB28	335
Cwilich	Gabriel	USA	Poster PB29	337
De La Fuente	Cesar	Spain	Poster PB30	339
De Toro	Jose Angel	Spain	Poster PB31	341
Doppiu	Stefania	Spain	Poster PB32	343
Efrima	Shlomo	Israel	Poster PB33	345
Elizalde	Eduardo	Spain	Poster PB34	347
Engström	Olof	Sweden	Poster PB35	349
Feiner	Louis F.	Netherlands	Poster PB36	351
Forsberg	Erik	Sweden	Poster PB37	353
Galvao	Douglas	Brazil	Poster PB38	355
			Poster PB39	357
Garcia	Miguel Angel	Spain	Poster PB40	359
Garcia Martin	Antonio	Spain	Poster PB41	361

Golan	Yuval	Israel	Poster PB42	363
Gomez Cuesta	Ignacio	Spain	Poster PB43	365
Gomez Moñivas	Sacha	Spain	Poster PB44	367
Gomila	Gabriel	Spain	Poster PB45	369
Gonzalez Ferez	Rosario	Germany	Poster PB46	371
Gonzalez Perez	Juan Carlos	Brazil	Poster PB47	373
Gourdon	Delphine	USA	Poster PB48	375
Hernando Campos	Jordi	Netherlands	Poster PB49	377
Jacob	Ajey	Sweden	Poster PB50	379
Jimenez	David	Spain	Poster PB51	381
Karthäuser	Silvia	Germany	Poster PB52	383
Kinaret	Jari	Sweden	Poster PB53	385
Kiricsi	Imre	Hungary	Poster PB54	387
Konya	Zoltan	Hungary	Poster PB55	389
Kuramochi	Hiromi	Japan	Poster PB56	391
Langlais	Veronique	Spain	Poster PB57	393
			Poster PB58	395
Levy	Raphael	UK	Poster PB59	397
Lopez	Rosa	Switzerland	Poster PB60	399
Makovec	Darko	Slovenia	Poster PB61	401
Malyvshev	Andrei	Spain	Poster PB62	403
			Poster PB63	405
Marcos Villa	Pedro Angel	Spain	Poster PB64	407
Martinez	Benjamin	Spain	Poster PB65	409
Martinez	Maria Teresa	Spain	Poster PB66	411
Mas Torrent	Marta	Netherlands	Poster PB67	413
Maximov	Ivan	Sweden	Poster PB68	415
Mekhalif	Zineb	Belgium	Poster PB69	417
			Poster PB70	419
			Poster PB71	421
Melle-Franco	Manuel	Italy	Poster PB72	423
Mena-Osteritz	Elena	Germany	Poster PB73	425
Mendes	Paula	UK	Poster PB74	427
Mendoza	Ernest	UK	Poster PB75	429
Miles	Mervyn	UK	Poster PB76	431
Monge	Miguel	France	Poster PB77	433
Montes	Laurent	France	Poster PB78	435
Moshkalyov	Stanislav	Brazil	Poster PB79	437
Negri	Fabrizia	Italy	Poster PB80	439
			Poster PB81	441
Niedbala	Jolanta	Poland	Poster PB82	443
Nikolic	Konstantin	UK	Poster PB83	445
Nikolov	Ivan	Bulgaria	Poster PB84	447
Nita	Florin	France	Poster PB85	449

Nogueira da Silva	Maria Ivonete	Brazil	Poster PB86	451
Ortega	Enrique	Spain	Poster PB87	453
O'Shea	Sean	Singapore	Poster PB88	455
Otero	Roberto	Denmark	Poster PB89	457
Pekala	Krystina	Poland	Poster PB90	459
Pekala	Marek	Poland	Poster PB91	461
Perez Santos	Susana	Spain	Poster PB92	463
Peter	Amal John	India	Poster PB93	465
Pichonat	Emmanuelle	France	Poster PB94	467
Pignataro	Bruno	Italy	Poster PB95	469
Popczyk	Magdalena	Poland	Poster PB96	471
Puente	Antonio	Spain	Poster PB97	473
Rengel Estevez	Raul	Spain	Poster PB98	475
Rodriguez	Isabel	Singapore	Poster PB99	477
Round	Andy	UK	Poster PB100	479
Royo Pascual	Carlos	Spain	Poster PB101	481
Ruiz Perez	Catalina	Spain	Poster PB102	483
Ruths	Marina	Finland	Poster PB103	485
Sanchez	David	Switzerland	Poster PB104	487
			Poster PB105	489
Sanchez Portal	Daniel	Spain	Poster PB106	491
Sarangi	Debajyoti	Switzerland	Poster PB107	493
			Poster PB108	495
Seeger	Torsten	Spain	Poster PB109	497
Shaposnikov	Victor Manuel	Portugal	Poster PB110	499
Sobolev	Nikolai	Portugal	Poster PB111	501
Sterian	Paul	Romania	Poster PB112	503
Sukyte	Judita	Lithuania	Poster PB113	505
Toimil Molares	Maria Eugenia	Germany	Poster PB114	507
Torrens	Francisco	Spain	Poster PB115	509
Triozon	Francois	France	Poster PB116	511
Urbina	Antonio	Spain	Poster PB117	513
Vanossi	Andrea	Italy	Poster PB118	515
			Poster PB119	517
Williams	Rene M.	Netherlands	Poster PB120	519
Zervos	Matthew	Netherlands	Poster PB121	521
Zhao	Jianwei	UK	Poster PB122	523
Bawa	Raj	US	Poster PB123	525

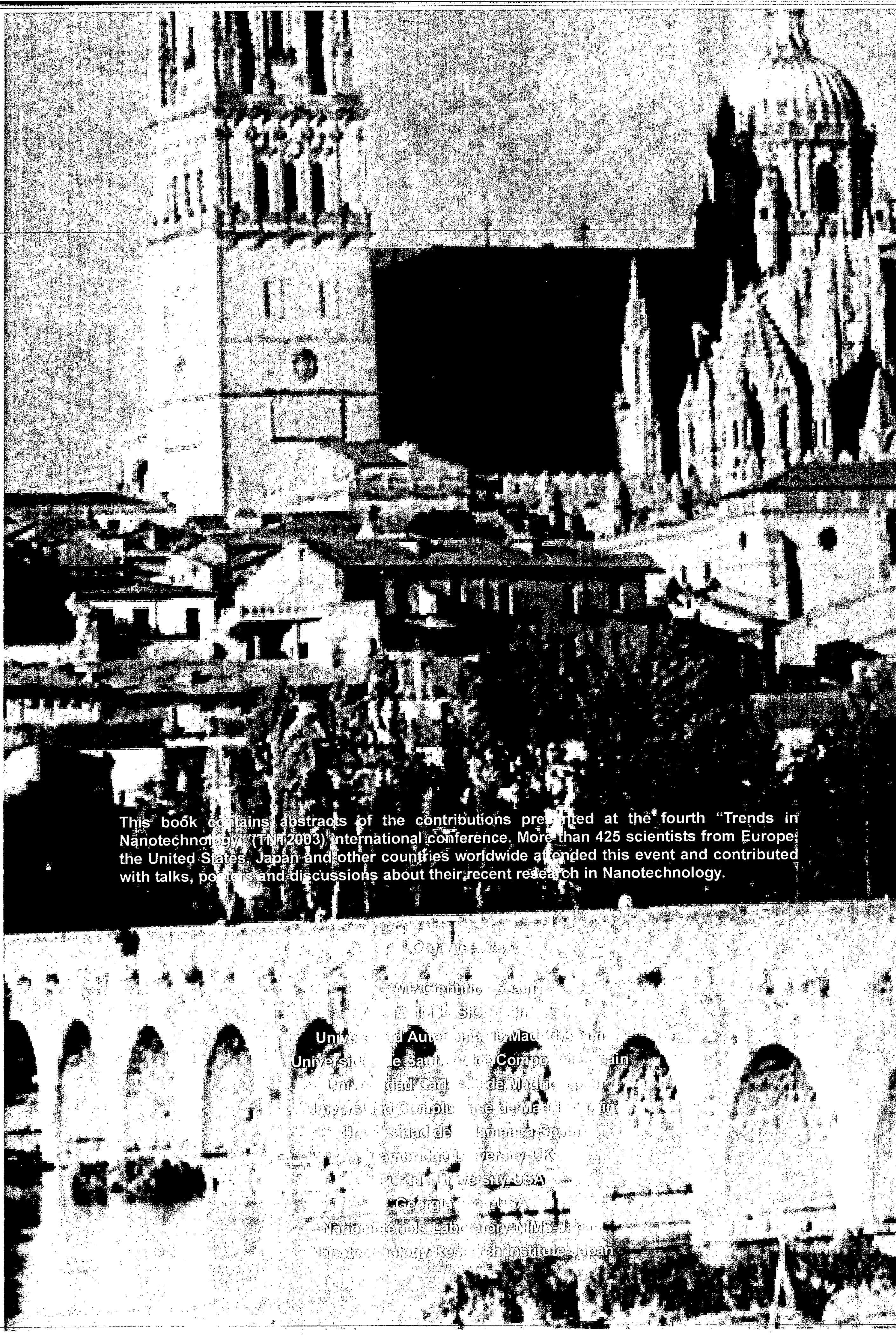

This book contains abstracts of the contributions presented at the fourth "Trends in Nanotechnology" (TNT2003) international conference. More than 425 scientists from Europe, the United States, Japan and other countries worldwide attended this event and contributed with talks, posters and discussions about their recent research in Nanotechnology.